TMS 2006 ELECTRONIC MATERIALS CONFERENCE

and Exhibition

June 28-30, 2006
Pennsylvania State University
University Park, PA

FINAL PROGRAM

TMS

Sponsored by the
Electronic, Magnetic & Photonic
Materials Division

www.tms.org/EMC.html

Welcome to

TMS 2006 ELECTRONIC MATERIALS CONFERENCE

The Premier Annual Forum on the Preparation and Characterization of Electronic Materials

As an attendee, you may take full advantage of the following events included as part of your registration fee:

- Technical Sessions
- Exhibition
- Welcoming Reception
- Coffee Breaks
- Thursday Banquet*

  (One Day registration does not include Thursday banquet.)

Value for Your Cost

The Electronic Materials Conference (EMC) is being coordinated with the Device Research Conference, also held at the Penn Stater Conference Center, June 26-28. Badges will be accepted by both conferences on Wednesday, June 28.

Technical Sessions

Technical sessions are held at the Penn Stater Conference Center beginning at 8:20 a.m. on Wednesday, June 28; the conference plenary session is located in Presidents Hall 3 & 4.

Table of Contents

About TMS

The Minerals, Metals & Materials Society (TMS) is the professional organization encompassing the entire range of materials science and engineering, from minerals processing and primary metals production to basic research and the advanced applications of materials.

Included among its professional and student members are metallurgical and materials engineers, scientists, researchers, educators and administrators from more than 70 countries on six continents.

TMS' mission is to promote the global science and engineering professions concerned with minerals, metals and materials. To learn more, visit **www.tms.org.**

About the Location

Parking

Parking at the Penn Stater Conference Center is complimentary. Overnight parking at the campus residence halls is $21 for the week. Parking passes for the residence halls can be purchased at the EMC registration desk at the Penn Stater Conference Center.

Shuttle

Penn State residence halls and dining facilities are not located within walking distance to the session meeting rooms, which are located at the Penn Stater Conference Center. A daily shuttle will be provided for those staying in the residence halls.

Computer/Network Facilities

The Penn Stater Conference Center has complimentary wireless Internet access throughout the facility. Ethernet connections in the Penn Stater sleeping rooms are also complimentary; Ethernet cables are located at the front desk. Additionally, there are a limited number of computers available on the first level to check e-mail on a complimentary basis.

Messages

A message board located near the EMC registration desk on the first level of the conference center will be available for use throughout the conference.

Dress

Casual clothing is in order with a sweater or light jacket occasionally needed for the evenings. Layered clothing is recommended for cooler days or in air-conditioned buildings. The average afternoon temperatures in June in the Nittany Valley reach the middle 80s ºF (22-25ºC); nighttime temperatures drop to between 55 and 65ºF (13-15ºC).

Commuter Lunch Package

A three-day box lunch plan at the Penn Stater Conference Center is available but must be purchased at the EMC registration desk. The lunches will be available in the exhibition area, located in Presidents Hall 1 & 2. The deadline to purchase tickets is 10 a.m. on Wednesday, June 28.

On-Campus Dining Hours

Pollock Commons Dining Hall
Breakfast .....7 to 8 a.m. *(cost included in on-campus housing plan)*
Dinner .....5:30 to 7 p.m. *($10.50 per person)*

Food facilities on campus close at 7 p.m.; no refunds are made for late arrivals, early departures or missed meals.

For evening dinner options, visit www. lionsmenu.com to find local restaurants, which are only a short walk from the residence halls.

Networking & Social Events

Welcoming Reception for Attendees

Wednesday, June 28, 6 to 8 p.m.

Penn Stater Conference Center, Presidents Hall 1 & 2

Evening at Beaver Stadium for Attendees and Guests

Thursday, June 29, 6 to 9 p.m.

Beaver Stadium

Enjoy a catered dinner and complimentary access to the sports museum located within Beaver Stadium.

Cost: Free to full conference and student registrants
$65 for one-day registrants and adult guests
$30 for children age 12 and under

Tickets: A limited number of tickets are available for purchase at the EMC registration desk. Deadline for ticket sales is 5 p.m. Wednesday, June 28.

Transportation: Complimentary shuttle service is available to and from Beaver Stadium. Board shuttles at the exit to the Penn Stater Conference Center by Presidents Hall 4.

Informal Coffee Breaks for Attendees

Intermission of morning and afternoon sessions
Presidents Hall 1 & 2, first and second level break areas

Light Fare and Beverages Served

Policies

Campus Smoking Policy

Pennsylvania State University prohibits smoking in all buildings, including residence halls. Smoking is permitted in designated areas outside.

Americans With Disabilities Act

TMS strongly supports the federal Americans with Disabilities Act (ADA) which prohibits discrimination against, and promotes public accessibility for, those with disabilities. In support of, and in compliance with, ADA, we ask those requiring specific equipment or services to notify an individual at the conference registration desk.

Audio/Video Recording Policy

TMS reserves the right to all audio and video reproductions of presentations at TMS sponsored meetings. Recording of sessions (audio, video, still photography, etc.) intended for personal use, distribution, publication, or copyright without the express written consent of TMS and the individual authors is strictly prohibited.

Refund Policy

The deadline for refunds was June 12, 2006. No refunds are issued at the meeting. All fees and tickets are nonrefundable after the June 12 deadline.

UNIVERSITY PARK

Campus Guide

2005 - 06

1 Academic Activities **G8**
2 Academic Projects **G8**
3 Agricultural Administration **E6**
4 Agricultural Arena **C12**
5 Agricultural Engineering **E5**
6 Agricultural Science & Industries **E6**
7 All-Sports Museum **D10**
8 Almquist Research Center **B11**
9 Althouse Lab **F5**
10 Applied Research Lab (ARL) **H2**
11 Applied Science **G1**
12 Armsby **F5**
13 Arts (Playhouse Theatre) **E4**
14 Arts Cottage **F5**
15 Bag House **H3**
16 Beam Business Administration **D4**
17 Beaver Stadium **D10**
18 Beecher-Dock House **H8**
19 Benedict House **H8**
20 Bennett Family Center **G8**
21 Blue Band Facility **B8**
22 Bookstore **G5**
23 Borland Lab **E5**
24 Boucke **F5**
25 Breazeale Nuclear Reactor **G9**
26 Buckhout Lab **F5**
27 Burrowes **F4**
28 Bus Station **G2**
29 Business Administration I **D3**
30 Business Administration II **D4**
31 Butler (Ag Engineering)
32 Butler Farm
33 Calder Square II **H4**
34 Carnegie **G4**
35 Carpenter **E3**
36 CEDAR **E4**
37 Central Biological Lab **H11**
38 Central Milk Testing Lab **A12**
39 Centre County-Penn State Visitors Center **C12**
40 Chambers **E3**
41 Chandlee Lab **G4**
42 Chemistry **F5**
43 Coal Utilization Lab **G8**
44 Computer Building **E7**
45 Corn Breeding Lab **B11**
46 Creamery **E5**
47 Dairy Complex **A9**
48 Davey Lab **F5**
49 Daybridge Child Development Center **inset**
50 Deike **G3**
51 Earth-Engineering Sciences **G1**
52 East Area Locker Room **F8**
53 East Campus Heating Plant **G12**
54 Eisenhower Auditorium **F6**
55 Eisenhower Chapel **E4**
56 Eisenhower Parking Deck **F6**
57 Electrical Engineering East **G3**
58 Electrical Engineering West **G3**
59 Engineering Services **G1**
60 Engineering Units (A-D) **H3**
61 Executive Education **E2**
62 Farms Department **B11**
63 Fenske Lab **F5**
64 Ferguson **E5**
65 Fleet Operations **B10**
66 Flower Test Gardens **C7**
67 Food Science **E6**
68 Forest Resource Lab **G9**
69 Forest Resources **D6**
70 Forum **E4**
71 Fraternity House **F3, G3**
72 Frear North **F5**
73 Frear South **F5**
74 Gardner House **H8**
75 General Stores **B10**
76 Golf Courses **E1**
77 Grange **G6**
78 Greenberg (Ice Pavillion) **F8**
79 Gypsy Moth Research Lab **A12**
80 Hallowell **G2**
81 Hammond **H3**
82 Headhouse I **E6**
83 Headhouse II **E6**
84 Headhouse III **E6**
85 Health & Human Development **H5**
86 Henderson **G5**
87 Henderson South **H5**
88 Henning **E6**
89 Hetzel Union Building (HUB) **G5**
90 High Pressure Gas Laboratory **A7**
91 Hintz Family Alumni Center **H3**
92 Holuba Hall **F9**
93 Horse Barn **A11**
94 Hosler **G3**
95 Hostetter (Business Services) **B7**
96 Housing & Food Services **B6**
97 HUB Parking Deck **G6**
98 Ihlseng **F3**
99 Information Sciences & Technology **G2**
100 Intramural **D9**
101 Intramural Fields **C8, D8, D9**
102 James **H3**
103 Jeffrey Field **C9**
104 Jordan Center **E9**
105 Keller **E3**
106 Kern **E3**
107 Land & Water Research **G11**
108 Lasch Football Building **F9**
109 Laundry **B10**
110 Leonhard **G1**
111 Life Sciences **F6**
112 Livestock Testing Lab **B12**
113 Lubert **inset**
114 Mateer **E3**
115 Materials Research Institute **inset**
116 Materials Research Lab **G10**
117 MBNA Career Services **F7**
118 McAllister **G5**
119 McCoy Natatorium **E7**
120 Meats Lab **D11**
121 Merkle **A12**
122 Moore **E3**
123 Mueller Lab **F5**
124 Multisport Indoor Facility **F10**
125 Mushroom Research Center **A7**
126 Music I **E4**
127 Music II **E4**
128 Nittany Lion Inn **E2**
129 Nittany Lion Shrine **E3**
130 Nittany Parking Deck **E3**
131 Noll Lab **F2**
132 Old Botany **G4**
133 Old Main **G4**
134 Osmond Lab **F5**
135 Oswald Tower **F4**
136 Palmer Museum of Art **E5**
137 Parking Deck - East **E6**
138 Pasquerilla Spiritual Center **E4**
139 Pasture Research Lab **E6**
140 Paterno Library **F4**
141 Pattee Library **F4**
142 Patterson **E5**
143 Pavilion Theatre **E5**
144 Penn State Downtown Theatre Center **H4**
★ 145 Penn Stater Conference Center Hotel **inset**
146 Pesticide Research Lab **A12**
147 Physical Plant **C10**
148 Pine Cottage **F5**
149 Pond Lab **F4**
150 Post Office **G5**
151 Power Plant **H3**
152 Procurement Services **B7**
153 Rackley **E3**
154 Reber **H3**
155 Recreation (Rec Hall) **F2**
156 Research Center **G10**
157 Research East **G9**
158 Research West **G1**
159 Rider House **H3**
160 Rider I **H3**
161 Rider II **H4**
162 Ritenour **F6**
163 Robeson Cultural Center **G5**
164 Sackett **H4**
165 SALA **E5**
166 Salvage Warehouse **B7**
167 Sarni Tennis Facility **F7**
168 Schreyer House **B5**
169 Schwab Auditorium **G4**
170 Scott **H4**
171 Service Depot East **G8**
172 Shields **E8**
173 Smeal Business **D5**
174 Sparks **F4**
175 Spruce Cottage **F5**
176 Steidle **G3**
177 Swimming Pool (outdoor) **F7**
178 Swine Research **G12**
179 Technology Center **inset**
180 Telecommunications **F5**
181 Tennis **F8**
182 Thomas **F6**
183 Track & Field Stadium **F11**
184 Transportation Research **G10**
185 Turfgrass Museum **A8**
186 Tyson **E6**
187 Undergrad. (Pollock) Library **G7**
188 University Club **H2**
189 University Support I **A7**
190 University Support II **A7**
191 Valentine Turfgrass Res. Cntr. **B8**
192 Visual Arts **E5**
193 Wagner **E8**
194 Walker **G2**
195 Wartik Lab **F5**
196 Water Tunnel (G. Thomas) **G2**
197 Weaver **F5**
198 White **G6**
199 White North **G6**
200 Whitmore Lab **F5**
201 Willard **G3**

East Residence Halls

202 Bigler Hall **E7**
203 Brumbaugh Hall **D7**
204 Curtin Hall **E7**
205 Findlay Commons **D7**
206 Fisher Hall **D7**
207 Geary Hall **D7**
208 Hastings Hall **D8**
209 Johnston Commons **D7**
210 McKean Hall **D8**
211 Packer Hall **D7**
212 Pennypacker Hall **E8**
213 Pinchot Hall **D7**
214 Snyder Hall **D8**
215 Sproul Hall **D7**
216 Stone Hall **D8**
217 Stuart Hall **D7**
218 Tener Hall **D7**

North Residence Halls

219 Holmes Hall **D5**
220 Leete Hall **D5**
221 Runkle Hall **D5**
222 Warnock Commons **D5**

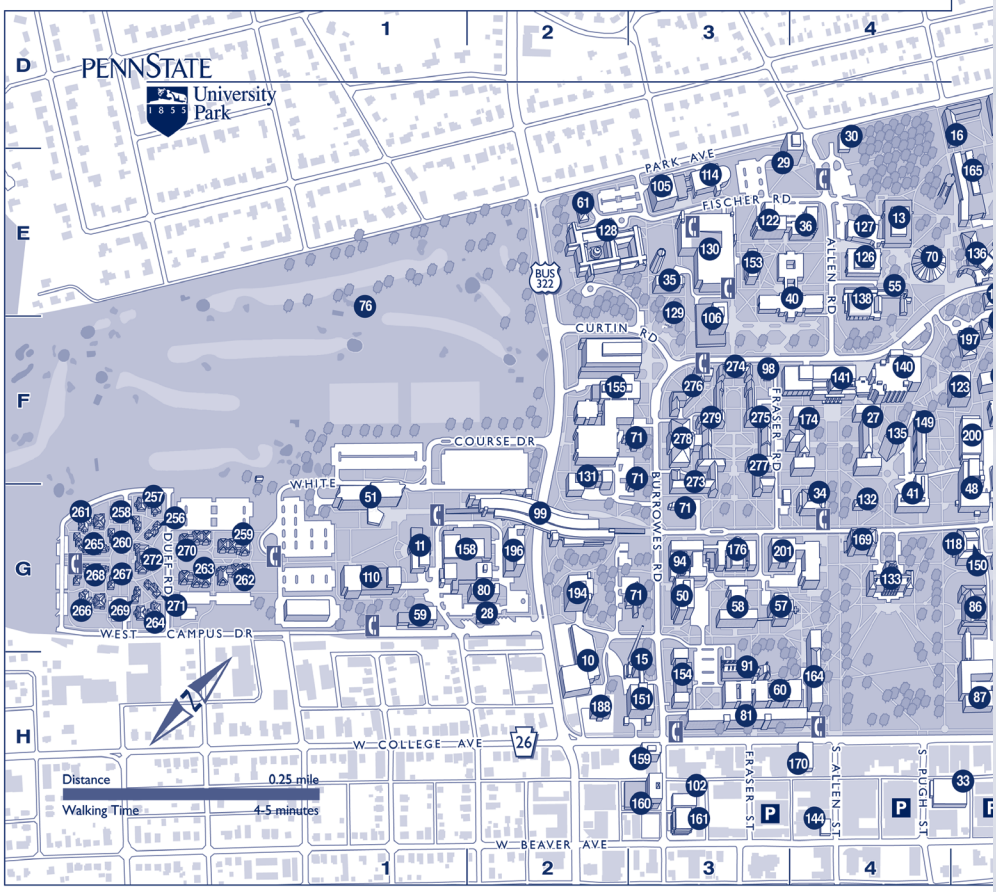

Pollock Residence Halls

223 Beaver Hall **G7**
224 Hartranft Hall **G6**
225 Hiester Hall **G7**
226 Mifflin Hall **G6**
227 Pollock Commons **G7**
228 Porter Hall **G7**
229 Ritner Hall **G7**
230 Shulze Hall **G7**
231 Shunk Hall **G7**
232 Wolf Hall **G7**

South Residence Halls

233 Atherton Hall **G6**
234 Cooper Hall **H7**
235 Cross Hall **H7**
236 Ewing Hall **H7**
237 Haller Hall **H6**
238 Hibbs Hall **H6**
239 Hoyt Hall **H7**
240 Lyons Hall **H7**
241 McElwain Hall **H7**
242 Redifer Commons **H7**
243 Simmons Hall **G6**
244 Stephens Hall **H6**

University Apartments

Eastview Terrace

245 Brill Hall **G8**
246 Curry Hall **G8**
247 Harris Hall **G8**
248 Miller Hall **H8**
249 Nelson Hall **H8**
250 Panofsky Hall **H8**
251 Young Hall **H7**
252 Graduate Circle **H9**
253 Nittany Apartments **F8**
254 Nittany Community Center **F7**
255 Nittany Hall **G8**

White Course Apartments

256 Bernreuter Hall **G1**
257 Cunningham Hall **G1**
258 Donkin Hall **G1**
259 Dunham Hall **G1**
260 Farrell Hall **G1**
261 Ferguson Hall **G1**
262 Garban Hall **G1**
263 Grubb Hall **G1**
264 Haffner Hall **G1**
265 Holderman Hall **G1**
266 Ikenberry Hall **G1**
267 Lovejoy Hall **G1**
268 Osborn Hall **G1**
269 Palladino Hall **G1**
270 Patterson Hall **G1**
271 Ray Hall **G1**
272 Weston Community Center **G1**

West Residence Halls

273 Hamilton Hall **F3**
274 Irvin Hall **F3**
275 Jordan Hall **F3**
276 McKee Hall **F3**
277 Thompson Hall **F3**
278 Waring Commons **F3**
279 Watts Hall **F3**

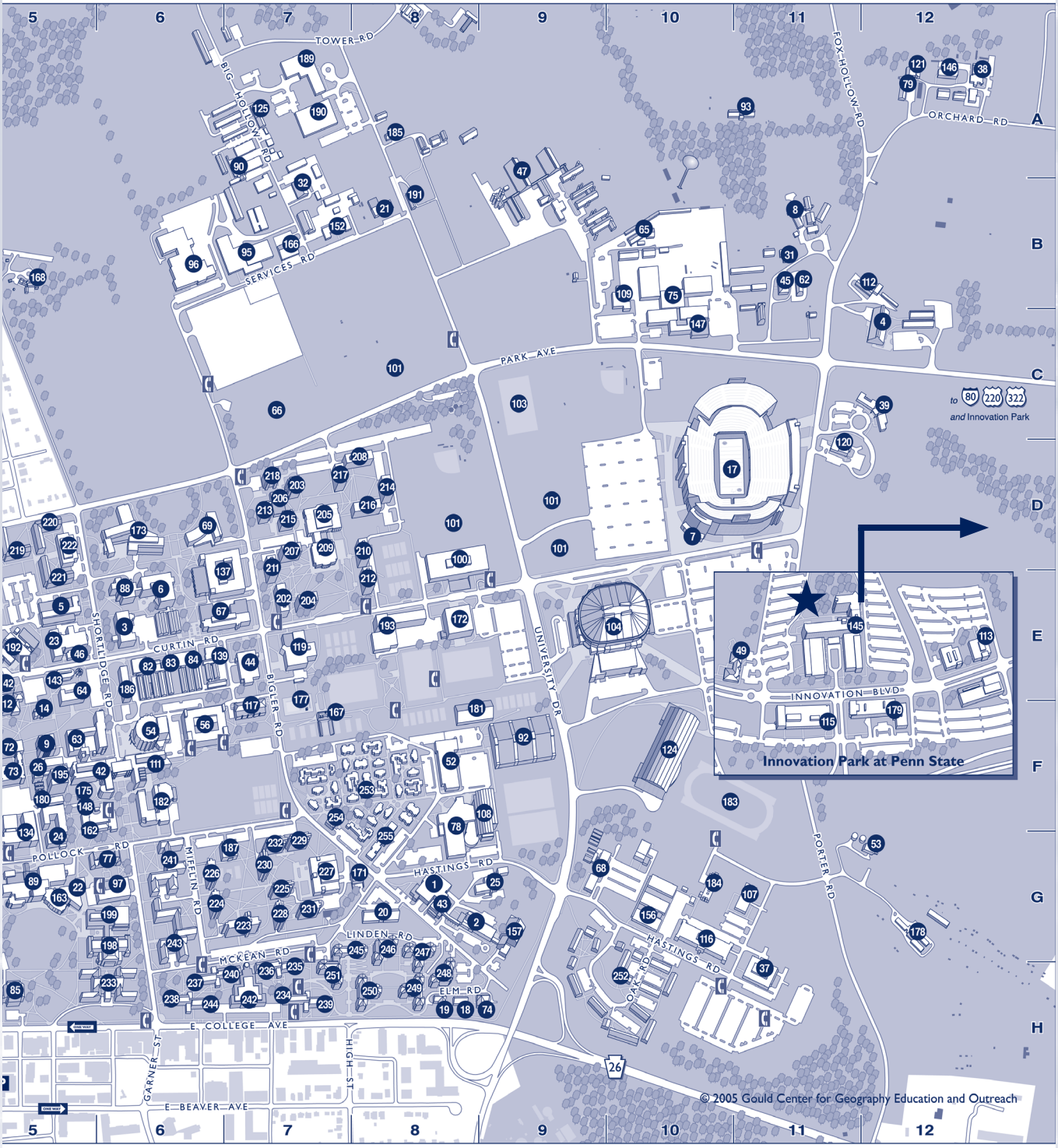

Awards

John Bardeen Award

Established in 1994, this award recognizes an individual who has made outstanding contributions, and is a leader, in the electronic materials field.

2006 Recipient: Isamu Akasaki

Citation: For his pioneering work and key discoveries in the field of GaN and related materials which has enabled their widespread development and use

About the Recipient: Isamu Akasaki is a professor at Meijo and Nagoya universities in Japan, where his research over the past 25 years has surrounded compound semiconductor materials and devices, with special emphasis on nitride semiconductors. He has published more than 580 scientific papers, edited nine books and received a total of 133 patents, including 65 for Group III Nitrides. Dr. Akasaki has also received numerous awards including selection by the Japanese government as a "Person of Cultural Merits" in 2004.

"Dr. John Bardeen is a great scientist with outstanding achievements in two fields of electronic materials in the last century, whom I highly respect. I deem it indeed a great honor to be selected as a recipient of the TMS John Bardeen Award. Moreover, all of the past recipients of this prestigious award have made significant achievements and are excellent leaders in the field of electronic materials; they have helped promote the importance of this award. It is a real honor for me to be among these distinguished scientists."

Student Paper Awards

Awards of $500 are given to the authors of the top five percent of student papers presented at the 2005 EMC. Student papers are judged on both scientific content and oral presentation. Awards are funded by the Electronic Materials Committee and presented during the plenary session on Wednesday, June 28.

Award Winners

1. **Siddharth Rajan,** *University of California, Santa Barbara*
   "Structural and Electrical Characterization of N-Face GaN Grown on C-Face SiC by MBE"
   Umesh Mishra, Advisor
2. **Nate Quitoriano,** *Massachusetts Institute of Technology*
   "Defect Behavior in Metamorphic Buffer Layers on Lattice Constants Near InP Grown by Metal Organic Chemical Vapor Deposition (MOCVD) on GaAs"
   Eugene Fitzgerald, Advisor
3. **Christiane Poblenz,** *University of California, Santa Barbara*
   "Effect of AlN Nucleation Layer Growth Conditions on Buffer Leakage in AlGaN/GaN High Electron Mobility Transistors Grown by Molecular Beam Epitaxy (MBE)"
   James Speck, Advisor
4. **Eric Krauland,** *Massachusetts Institute of Technology*
   "Composition and Contextual Influence of Peptide Specificity for Inorganic Material Surfaces"
   Angela Belcher, Advisor

Nominate a Deserving Colleague for the TMS 2008 John Bardeen Award!

This award recognizes an individual who has made an outstanding contribution, and is a leader, in the field of electronic materials.

Who was John Bardeen?

John Bardeen's career of theoretical and experimental research set the foundation for the current state of understanding of electronic materials. Two areas where Bardeen had great impact were the invention and development of the solid-state transistor and the theory that developed greater understanding of superconductivity.

For Award Criteria and Additional Information

Pick up a nomination form at the EMC registration desk, or visit the TMS Web site at www.tms.org/Society/honors.html.

Exhibition

Visit the exhibition for solutions in the preparation and characterization of electronic materials!

Exhibit Dates and Hours

Presidents Hall 1 & 2

Wednesday, June 28..... 9:20 a.m. to 4 p.m.
Welcoming Reception.....6 to 8 p.m.

Thursday, June 29 ..... 10 a.m. to 4 p.m.

Exhibiting Companies (as of 6/6/06)

Accent Optical Technologies
Akzo Nobel Polymer Chemicals LLC
Allied High Tech Products Inc.
Andeen - Hagerling Inc.
Applied Surface Technologies
Epichem Group
EXAKT Technologies Inc.
INTRINSIC Semiconductor
k-Space Associates Inc.
Kurt J. Lesker Company
Lake Shore Cryotronics Inc.
Lehighton Electronics Inc.
MMR Technologies Inc.
NOVOCONTROL America Inc.
Omicron Nanotechnology USA
Oxford Applied Research
Pennsylvania State University
Riber Inc.
RJM Semiconductor
Springer
Structured Materials Ind. Inc.
SVT Associates Inc.
United Mineral & Chemical Corporation
Vacuum Barrier Corporation
Veeco Instruments Inc.
Wafer Technology Ltd.
WEP - Dage EEV

Recreation

Visit these attractions on Penn State's campus!

Old Main

Founded in 1855, Penn State is Pennsylvania's land-grant institution. Old Main, the chief administrative building, contains frescoes by artist Henry Varnam Poor showing the growth of the university.

University Creamery

Penn State retains its leadership in agricultural sciences. Many visitors stop by the University Creamery for ice cream made on-site.

Museums

Matson Museum of Anthropology
Earth and Mineral Sciences Museum
Frost Entomological Museum
Palmer Museum of Art

Sporting Facilities (on campus)

Blue and White Golf Course (36 holes)
Tennis Courts
Indoor Tracks
Exercise and Fitness Centers (also located at hotels)
Indoor Ice Skating Rink
Swimming Pools

Hiking and Bird Watching

Shaver's Creek Environmental Center
Stone Valley Recreation Area

Nittany Lion Shrine

Located near the Nittany Lion Inn, the shrine was a gift of the Class of 1940 and is the university's most photographed landmark.

Or travel to these nearby sites!

Penn's Cave

Take a one-mile boat tour through America's only all-water cavern and visit the animal preserve.

Bellefonte Historical Railroad

Enjoy a leisurely trip through the Nittany Valley.

Pennsylvania Military Museum in Boalsburg

The history of America's citizen soldiers is preserved in this museum, surrounded by quaint shops and antique emporiums in Boalsburg, Lemont, and Centre Hall. These shops feature the works of local artists and craftspeople.

Proceedings/Publications

EMC does not publish formal conference proceedings; however, conference abstracts are published in the *Journal of Electronic Materials* (*JEM*) throughout the year. *JEM* encourages both presenters and attendees to submit manuscripts of their work.

A special issue on Group III Nitrides, SiC and ZnO is planned for early 2007. Papers are due August 1, 2006, and may be submitted through the *JEM* Web site at http://jem.msubmit.net.

About JEM

JEM is a monthly archival journal of TMS and the Institute of Electrical and Electronics Engineers (IEEE). Articles are reviewed, selected and edited by peers who serve as voluntary members of the editorial board, the board of associate editors, or section editors.

JEM's Content

JEM is a forum for the rapid circulation of the results of original research. It contains technical papers detailing critical new developments in the electronics field, as well as invited and contributed review papers on topics of current interest. The journal focuses on electronic memory and logic structures, magnetic-optical recording media, superlattices, packaging, detectors, emitters, metallization technology, superconductors, and low thermal-budget processing and includes general papers on electronic materials for device application, structure making, reliability and yield. Articles on methods for preparing and evaluating the chemical, physical and electronic properties of electronic materials are also included.

JEM Subscription for Attendees

If you did not choose to include a 2007 subscription in your registration fee, you may subscribe to JEM through the online TMS Document Center at http://doc.tms.org. The 2007 journals will include papers presented at this conference. TMS and IEEE members receive an 85% discount!

Manuscript Submission

JEM employs an online manuscript submission and review system. To be considered for publication, authors must submit manuscripts electronically. Detailed submission guidelines are available from the *JEM* Web site at http://jem.msubmit.net.

Look for these electronic materials related publications in the TMS Document Center!

Arsenic Metallurgy

Metal Matrix Composites

Surface Engineering: Science and Technology II

Surfaces and Interfaces in Nanostructured Materials and Trends in LIGA, Miniaturization, and Nanoscale Materials

***TMS Letters* (2004)**

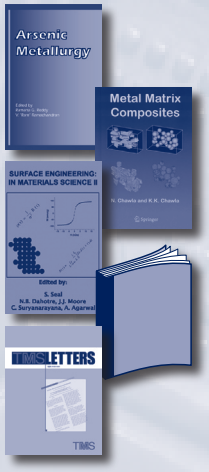

Special Issues of Journal of Electronic Materials:

- Microstructures and Textures of Films and Coatings in Electronic Applications (December 2005)
- 2004 U.S. Workshop on the Physics and Chemistry of II-VI Materials (June 2005)
- Challenges in Advanced Thin Films: Microstructures, Interfaces and Reactions (May 2005)
- SiC and the Group III Nitride Semiconductors (April 2005)
- Lead-Free Solders and Processing Issues Relevant to Microelectronic Packaging (December 2004)
- Nanostructured Magnetic Materials: Recent Progress in Magnetic Nanostructures (November 2004)
- Phase Stability, Phase Transformations and Reactive Phase Formation in Electronic Materials III (October 2004)
- III-V Nitrides and Silicon Carbide (May 2004)

For other publications or to order:

Visit the TMS Document Center online at http://doc.tms.org, e-mail publications@tms.org or telephone (800) 759-4TMS, ext. 251.

Conference Organizers

Electronic Materials Committee

Officers

Edward Yu
Chairman
University of California, San Diego

Robert Biefeld
Vice Chairman
Sandia National Laboratories

Mark Goorsky
Secretary
University of California, Los Angeles

Patrice Turchi
Director/Chair
TMS Electronic, Magnetic & Photonic Materials Division
Lawrence Livermore National Laboratory

April Brown
Past Chairman
Duke University

Chris Palmstrom
Treasurer
University of Minnesota

Ted Harman
Editor-*JEM*
Massachusetts Institute of Technology

Members

Andrew A. Allerman
Sandia National Laboratories

Brian Bennett
Naval Research Laboratory

Leonard J. Brillson
Ohio State University

Michael A. Capano
Purdue University

L. Ralph Dawson
University of New Mexico

Kurt Eyink
Wright Patterson Air Force Base

Eugene A. Fitzgerald
Massachusetts Institute of Technology

Rachel S. Goldman
University of Michigan

Karl Hobart
Naval Research Laboratory

Archie Holmes
University of Texas

Julia W.P. Hsu
Sandia National Laboratories

Diana Huffaker
University of New Mexico

David B. Janes
Purdue University

Thomas F. Kuech
University of Wisconsin

Theresa Mayer
Pennsylvania State University

James L. Merz
University of Notre Dame

Mark S. Miller
University of Utah

Suzanne E. Mohney
Pennsylvania State University

Thomas H. Myers
West Virginia University

Lisa M. Porter
Carnegie Mellon University

Laura S. Rea
US Air Force

Joan M. Redwing
Pennsylvania State University

Timothy D. Sands
Purdue University

Akio Sasaki
Osaka Electro-Communication University

William Schaff
Cornell University

Glenn Solomon
Stanford University

James S. Speck
University of California

Susanne Stemmer
University of California

Charles W. Tu
University of California

Christine Wang
Massachusetts Institute of Technology

Christian M. Wetzel
Uniroyal Optoelectronics

Jerry M. Woodall
Purdue University

Conference Organizers

Invited Organizers

EMC thanks the following invited organizers for their support and contribution to this year's technical program:

Shigefusa Chichibu
University of Tsukuba

Russell Dupuis
Georgia Institute of Technology

Randy Feenstra
Carnegie Mellon University

David Gundlach
ETH-Zurich

Evgeni Gusev
IBM Corporation

Douglas Hall
University of Notre Dame

Jung Han
Yale University

Mark Hersam
Northwestern University

Andrew Hoff
University of South Florida

Thomas Jackson
Pennsylvania State University

Debdeep Jena
University of Notre Dame

Kei-May Lau
Hong Kong University of Science & Technology

Pat Lenahan
Pennsylvania State University

Gregory Lopinski
Steacie Institute for Molecular Sciences

Maria Losurdo
Institute of Inorganic Methodologies and Plasmas

Yicheng Lu
Rutgers University

Charles Lutz
Kopin Corporation

Michael Manfra
Bell Labs, Lucent Technologies

Peter Moran
Michigan Technological University

Hubert Moriceau
CEA Leti

Yasushi Nanishi
Ritsumeikan University

Hou T. Ng
NASA Ames Research Center

David Norton
University of Florida

Robert Okojie
NASA Glenn Research Center

Sarah Olsen
University of Newcastle-Upon-Tyne

Jamie Phillips
University of Michigan

Klaus Ploog
Paul Drude Institute for Solid State Electronics

Steve Ringel
Ohio State University

Alberto Salleo
Palo Alto Research Center

Nitin Samarth
Pennsylvania State University

Tae-Yeon Seong
Kwangju Institute of Science & Technology

Ben Shanabrook
Naval Research Laboratory

Max Shtein
University of Michigan

Robert Stahlbush
Naval Research Laboratory

Alec Talin
Sandia National Laboratories

Masaaki Tanaka
University of Tokyo

Michael Tischler
Ocis Technologies

Raymond Tsui
Motorola

Lloyd Whitman
Naval Research Laboratory

David Wilt
NASA Glenn Research Center

Shalom Wind
Columbia University

William Wong
Palo Alto Research Center

Michael Wraback
US Army Research Laboratory

Ya-Hong Xie
University of California

Grace Huili Xing
University of Notre Dame

Wednesday AM, June 28

8:20 AM	EMC PLENARY LECTURE/STUDENT AWARDS
Room:	Presidents Hall III/Presidents Hall IV
Plenary Speaker:	Arthur C. Gossard, University of California, Santa Barbara
Topic:	"Growth and Uses of Metal/Semiconductor Heterostructures"
Break:	9:20 AM–10:00 AM

Session A: ZnO Nanomaterials Room: Presidents Hall III		**Session B: III-Nitride Optoelectronic Devices** Room: Presidents Hall IV		**Session C: Narrow Bandgap Semiconductors** Room: Conference Room 106	
10:00 AM	A1, (Student), Undoped and Doped ZnO Nanorods ……..…… Jinkyoung Yoo	10:00 AM	B1, (Student), Growth and Characterization of High-Performance III-N Avalanche Photodiodes Grown on Bulk GaN Substrates ……..…… Jae Limb	10:00 AM	C1, Carrier Recombination Kinetics in 2.3-2.4 μM InGaAsSb/AlGaAsSb QW Laser Heterostructures ……Dmitri Donetsky
10:20 AM	A2, (Student), Spatially-Dependent Optical Emission from ZnO Nanotips on Al_2O_33 and Si Substrates ……..…… Lei Fang	10:20 AM	B2, (Student), MOCVD Growth of AlGaN Heterostructures and UV LEDs on Bulk AlN Substrates …….. Zaiyuan Ren	10:20 AM	C2, Electron and Hole Energy Relaxation in InGaAsSb/InAs/InGaSb Type-II QW Laser Heterostructures …….. Dmitri Donetsky
10:40 AM	A3, (Student), Selective Growth of Zinc Oxide Nanowires Grown from Thin Film Multilayer Structure for Shadow Lithography ……..…… Bruce J. Hinds	10:40 AM	B3, (Student), Characterization of Green LED Structures with p-InGaN and p-GaN Layers …….. Wonseok Lee	10:40 AM	C3, Improved Properties of MOCVD Grown InAs/GaSb Superlattices on (001) GaSb Substrate by Introducing an InAsSb Layer at the Interfaces …… Xue-Bing Zhang
11:00 AM	A4, Piezoelectric and Electrical Properties of Solution Grown ZnO Nanorods …….. David Scrymgeour	11:00 AM	B4, (Student), High Light-Extraction Efficiency in GaInN Light-Emitting Diode with Pyramid Reflector ……..…… J.-Q. Xi	11:00 AM	C4, (Student), Effects of Ga and Sb Precursor Chemistry on the Alloy Composition in Pseudomorphically Strained GaAsSb Films Grown via Metalorganic Vapor Phase Epitaxy …..…… A. A. Khandekar
11:20 AM	A5, ZnO/ZnMgO Quantum Wells Embedded in Nanorods ……..…… Andrey Bakin	11:20 AM	B5, (Student), Temperature Dependence of the Quantum Efficiency in Green and Deep Green GaInN/GaN Light Emitting Diodes ……..…… Yufeng Li	11:20 AM	C5, (Student), Island Size and Development of Systematic Crystallographic Tilt during Growth of InAs on (100) GaAs Substrates …….. Suryanarayanan Ganesan
11:40 AM	A6, Catalyst-Free Two-Step Growth of Quasi-Aligned ZnMgO Nanorods and Their Properties …….. Liping Zhu	11:40 AM	B6, (Student), Nitride-Based Type-II InGaN-GaNAs 'W' Quantum Well Gain Media at 420-550 nm ……..…….Ronald A. Arif	11:40 AM	C6, (Student), Growth Mechanisms for InAs Deposition on Low Index GaAs Substrates by Metalorganic Vapor Phase Epitaxy …….. A. A. Khandekar

Wednesday AM, June 28

Wednesday Afternoon Begins

Session D: Fun with Nanostructures Room: Conference Room 208		Session E: Nitride and Oxide Nanowires Room: Conference Room 207		Session F: Directed Assembly of Nanostructures Room: Presidents Hall III	
10:00 AM	D1, Structural and Optical Studies of Quantum Dot Molecules …… Valeria G. Stoleru	10:00 AM	E1, Polarization-Resolved Photoluminescence Study of Isolated GaN Nanowires Grown by Catalyst-Free MBE …… John B. Schlager	1:30 PM	F1, (Student), Selective Growth and Characterization of GaAs Quantum Dots on Patterned Substrate by Utilizing Diblock Copolymer Template ……. Joo Hyung Park
10:20 AM	D2, (Student), Fluorescence Intermittency of Localized Excitons in CdSe Nanowires …… Vladimir Protasenko	10:20 AM	E2, Structural Control and Characterization of GaN Nanowires ……. Blake S. Simpkins	1:50 PM	F2, (Student), Simulation of Thermal-Field Directed Self-Assembly of Epitaxial Quantum Dots ……..…. Chandan Kumar
10:40 AM	D3, Discrimination of Isoelectronic Centers and Type-II Quantum Dots with ZnTe Embedded in ZnSe …….. Masafumi Jo	10:40 AM	E3, (Student), Experimental and Computational Modeling Studies of MOCVD Growth of GaN Nanowires ……Robert A. Burke	2:10 PM	F3, (Student), Real-Time Studies of Ga Droplet Formation for the Directed Seeding of Semiconductor Nanopillars ……... Weifeng Ye
11:00 AM	D4, Thermoelectric Properties of Vertically Aligned InAs/GaAs Quantum Dot Superlattices …… Abhishek Yadav	11:00 AM	E4, Epitaxial Growth and Applications of Aligned GaN Nanowires …….. Kyungkon Kim	2:30 PM	F4, Self-Assembly of Heterojunction Quantum Dots(HeQuaDs) ……..… Kurt G. Eyink
11:20 AM	D5, (Student), Fabrication of High Frequency Ultrasound Transducers …… Hyunsoo Kim	11:20 AM	E5, Growth and Characterization of Vanadium Oxide Nanowires …….. Jongsun Maeng	2:50 PM	F5, Fabrication of Nanometer-Period Gratings on Si Using HSQ Etching Mask …… Niu Jin
11:40 AM	D6, Electron Energy Levels in ZnSe:Mn Quantum Dots ……Shailaja Mahamuni	11:40 AM	E6, (Student), Integration and Characterization of High Aspect Ratio Ferroelectric Microtubes Fabricated by Vacuum Infiltration of Macroporous Silicon Templates …….. Xin Li	3:10 PM	Break

Wednesday PM, June 28

Session G: Quantum Dot Growth Room: Presidents Hall III		Session H: III-Nitride Electronic Devices Room: Presidents Hall IV		Session I: Materials Integration: Wafer Bonding and Alternative Substrates Room: Conference Room 106	
		1:30 PM	H1, Growth and Characterization of Graded InGaN Heterojunction Bipolar Transistors ……. Jae-Hyun Ryou	1:30 PM	I1, Exfoliation Temperature Dependence on Hydrogen Exfoliated Layer Properties …….. Sumiko L. Hayashi
		1:50 PM	H2, (Student), Device Performance of Full-Vertical GaN p-i-n Rectifiers Using Conducting Buffer Layers on SiC Substrates …… Dongwon Yoo	1:50 PM	I2, (Student), Interfacial Chemistry of InP/GaAs Bonded Pairs …… Ning Liu
		2:10 PM	H3, (Student), EBIC and XPS Study of Post-Annealing Process on AlGaN/GaN Schottky Diodes ……. Hyeongnam Kim	2:10 PM	I3, (Student), Dislocation-Gettering in Hydrogen-Induced Exfoliation of Metamorphic InAs Epilayers…… Atif M. Noori
		2:30 PM	H4, Gate Dielectric Considerations for Scaleable III-V MOS Structures …… Mark Johnson	2:30 PM	I4, Ultra-High Vacuum-Wafer Direct Bonding of III-V Compounds Semiconductors to Si-Wafer Using Low Energy (300 eV) Hydrogen Ion Beam Surface Cleaning …… N. Razek
		2:50 PM	H5, (Student), Fabrication and Characterization of Enhancement-Mode n-Channel GaN MOSFETs …… Weixiao Huang	2:50 PM	I5, (Student), Stress Analysis of Transferred Thin-GaN Light Emitting Diode by Au-Si Wafer Bonding…… Shih-Chieh Hsu
		3:10 PM	Break	3:10 PM	Break
3:30 PM	G1, (Student), Growth of High Quality Stransky-Krastanov GaSb Quantum Dots on a GaAs Substrate ……. Ganesh Balakrishnan	3:30 PM	H6, Spin-Orbit Quantum Interference and Dephasing in High Mobility GaN/AlGaN Heterostructures ……. …… Michael Manfra	3:30 PM	I6, Copper Interconnect Bonding for Polymer Pillar I/O Interconnects and Three-Dimensional (3D) Integration Application …… Kuan-Neng Chen
3:50 PM	G2, (Student), Characteristics of InGaAs/GaAs(P) Quantum Dot Stacks Grown by MOCVD …….. Nam-Heon Kim	3:50 PM	H7, Transport Characterization of AlGaN/AlN/GaN Heterostructures Grown on SiC …….. Said Elhamri	3:50 PM	I7, (Student), Fabrication of Poly-Silicon TFT on Flexible Thin Glass Substrate …….. Yoochul Jung
4:10 PM	G3, Influence of Strain Modulations in Capping Layers of InAs Quantum Dots with Compressive-InGaAs and Tensile-GaAsN Layer Structures.. Ikuo Suemune	4:10 PM	H8, (Student), High Voltage AlGaN/GaN HFETs with Fe-Doped GaN Buffer on Silicon Substrate …… Young Chul Choi	4:10 PM	I8, (Student), Built-In Strain in Silicon Nitride Films on Polymer Foils …….. Alex Z. Kattamis
4:30 PM	G4, (Student), Growth of High Density InAs Quantum Dots by Metalorganic Chemical Vapor Deposition with Periodic Interruption of AsH_3…… Youngsoo Lee	4:30 PM	H9, (Student), Effects of UHV Surface Preparation and Gate Deposition on AlGaN/GaN HEMT Device Performance …….. Dennis E. Walker, Jr.	4:30 PM	I9, Digital Lithographically Patterned Fine-Features for Flexible Thin-Film Transistor Array Backplanes …….. William S. Wong
4:50 PM	G5, Late News	4:50 PM	H10, (Student), Growth and Characterization of $(AlN)_x(Si_3N_4)_{1-x}$ Thin Films for the Passivation of AlGaN/GaN HEMT Structures …….. Richard J. Brown	4:50 PM	I10, Late News

Wednesday PM, June 28

Session J: Nanotubes Room: Conference Room 208		Session K: Chemical and Biological Sensors I Room: Conference Room 207		Session L: Contacts to Organic Thin Film Transistors Room: Conference Room 207	
1:30 PM	J1, Thin Film Transistors from Transparent Conducting Single-Wall Carbon Nanotube Networks …….. G. Fanchini	1:30 PM	K1, Large Area, Dense Si Nanowire Array Chemical Sensors……..… Alec Talin		
1:50 PM	J2, Carbon Nanotube Single-Electron Transistors Fabricated with Focused-Ion-Beam Technique ……. Kenzo Maehashi	1:50 PM	K2, A Self-Assembling Semiconductor Nanowire-Based Pathogen Detection System - Thin ALD-HfO_2 Gate Dielectrics …….. Debdeep Jena		
2:10 PM	J3, Contact Metallization Process for Vertical Carbon Nanotube Arrays Templated in Porous Anodic Alumina …….. Aaron Franklin	2:10 PM	K3, Trace Chemical Detection Using Single-Walled Carbon Nanotubes …….. Joshua A. Robinson		
2:30 PM	J4, Field Emission Induced UV Electroluminescence from Atomic Layer Deposition ZnO Coated Carbon Nanotubes …….…… John F. Conley	2:30 PM	K4, (Student), High-Sensitive Detection of Immunoglobulin E Using Aptamer-Modified Carbon Nanotube Field-Effect Transistors ……..…….. Taiji Katsura		
2:50 PM	J5, (Student), Characterization and Application of Transparent and Conductive Single Walled Carbon Nanotube Thin Films ……..…… Husnu Unalan	2:50 PM	K5, Real-Time Sensing of Proteins by Using a Top-Gate CNT-FET Biosensor ……..…. Masuhiro Abe		
3:10 PM	Break	3:10 PM	Break		
3:30 PM	J6, (Student), Precise Control of Number of Carbon Nanotube Growth by Digital Growth Process ……..….. Masatoshi Maeda			3:30 PM	L1, Surface Chemistry Modifications to Contact Resistances in Organic Field-Effect Transistors ……..……..… Douglas Natelson
3:50 PM	J7, (Student), Assemblies of Single Wall Carbon Nanotubes and Unencapsulated Sub-10 nm Gold Nanoparticles ……. Qingling Hang			3:50 PM	L2, (Student), Chemical Doping Modified Contacts to Organic Thin Film Transistors ……..…… Bo Bai
4:10 PM	J8, (Student), Characterization of the Field Emission Properties of Carbon Nanotube Films Formed on Silicon Carbide Substrates by Surface Decomposition …… Michael C. Pochet			4:10 PM	L3, Characterization of Top-Contact Pentacene Thin Film Transistors with Submicron-Length Channel …….. Kazuhito Tsukagoshi
4:30 PM	J9, Oxygen Effects on Formation of Carbon Nanotube Structure in SiC Decomposition …….. Senthil N. Sambandam			4:30 PM	L4, (Student), Electrical Contacts and Patterning Technique in n-Channel Organic Transistors …….. Byungwook Yoo
4:50 PM	J10, Late News			4:50 PM	L5, Late News

Wednesday PM, June 28

Session M: Oxide Thin Film Integration I Room: Conference Room 206		Session N: GaN Processing Room: Conference Room 108		Session O: Semiconductors: Processing and Oxidation Room: Conference Room 108	
1:30 PM	M1, (Student), Growth and Structural Characterization of TiO2 Thin Films Deposited on SrTiO3, LaAlO3, and Al2O3 Substrates Using Reactive Molecular Beam Epitaxy ……. Patrick Fisher	1:30 PM	N1, Substantial Advantages of Cat-CVD SiN Surface Passivation over PECVD in Electrical Properties of AlGaN/GaN Heterostructure …….. Norio Onojima		
1:50 PM	M2, (Student), Microwave Characterization of Thin Film Titanium Dioxide …….. Lance Haney	1:50 PM	N2, (Student), Oxygen Induced Gate Leakage in AlGaN/GaN HFETs and Its Suppression by a Novel Surface Control Process ……..…… Junji Kotani		
2:10 PM	M3, Lattice Dynamics and Ferroelectric Phase Transitions in $BaTiO_3/SrTiO_3$ Superlattices Studied by Ultraviolet Raman Spectroscopy Photodetector Applications … Dmitri A. Tenne	2:10 PM	N3, (Student), SF_6/O_2 Plasma Effects on AlGaN/GaN Heterojunction Field Effect Transistors ……..….. David J. Meyer		
2:30 PM	M4, Epitaxial Lanthanum Lutetium Oxide Thin Films Prepared by Pulsed Laser Deposition… Juergen Schubert	2:30 PM	N4, Processing of LiAlO2 Substrates for m-Plane GaN Epitaxy…….. Maria Losurdo		
2:50 PM	M5, Rare-Earth Scandate Multi-Layer Thin Films ……..…. Tassilo Heeg	2:50 PM	N5, (Student), Matrix-Addressable III-Nitride LED Arrays on Si Substrates by Flip-Chip Technology..……..… Chi Wing Keung		
3:10 PM	Break	3:10 PM	Break		
3:30 PM	M6, (Student), Atomic Layer Deposition of Cubic Tantalum Nitride Thin Films for Gate Electrode Application Raghavasimhan Sreenivasan			3:30 PM	O1, (Student), The Electrical and Physical Analysis of $Co_xNi_{1-x}Si_2$ Gate/SiO_2/p-Si (100) with Dual Work Function for Deep Submicron Complementary Metal-Oxide-Semiconductor Device……..… Jun Liu
3:50 PM	M7, (Student), Resistive Switching Behavior in Cr-Doped SrZrO3 Heterostructures: The Affects of Metal Electrode, Oxide Thickness, and Cr-Doping Levels…..…….. Sukwon Choi			3:50 PM	O2, (Student), Studies of Surface Wetting Phenomena during Thin Film Formation by Mist Deposition…….Karthikeyan Shanmugasundaram
4:10 PM	M8, Comparative Investigation of Epitaxial Gd2O3 Thin Films Grown on Si Substrates with Different Orientations for High-K Application…… Apurba Laha			4:10 PM	O3, (Student), Dry Etching of PbSrSe Epitaxial Layers toward Distributed Bragg Reflectors …….…… An Cheng
4:30 PM	M9, (Student), Epitaxial $BaTiO_3/SrTiO_3$ Superlattices for Phonon Bragg Mirrors and Cavities.… Arsen Soukiassian			4:30 PM	O4, (Student), A Novel Masking Technology for Deep Glass Wet Etching……. Ying-Ming Huang
4:50 PM	M10, Epitaxial and Amorphous Lu_2O_3 and $LaLuO_3$ on Si for Alternative Gate Dielectrics Applications…..…… Wei Tian			4:50 PM	O5, Late News

Thursday AM, June 29

Session P: Device Aspects for ZnO Room: Deans Hall I		Session Q: III-Nitride MOCVD Growth Room: Deans Hall II		Session R: Lattice Engineered Epitaxy of III-V and IV Semiconductors Room: Conference Room 106	
8:20 AM	P1, (Student), Electrical and Optical Properties of ZnO Thin Films for Transparent Electrodes and Antireflection Coatings in Optoelectronic Devices ……. J. H. Yun	8:20 AM	Q1, Pulsed Lateral over Growth (PLOG) of $Al_xGa_{1-x}N$ ……..…… Qhalid Fareed	8:20 AM	R1, (Student), Materials Optimization for High Indium Content (In,Ga)As Channel HEMTs ……..…….. Mike Morse
8:40 AM	P2, Switchable Interface Charges in Zinkoxide-Barium-titanite Heterostructures: Concepts for New Oxide-Based Electronic Device Structures ……..… Mathias M. Schubert	8:40 AM	Q2, (Student), MOCVD Growth of Nonpolar M-Plane AlN on (1-100) 6H-SiC Substrate …..…….. Qian Sun	8:40 AM	R2, (Student), High-Mobility 2DEG in InAlAs/InAs Hetero-structures Grown on InP Using Metamorphic $InAs_yP_{1-y}$ Graded Buffers …… Yong Lin
9:00 AM	P3, (Student), Metal-Ferroelec-tric-Semiconductor Capacitors Based on PZT/ZnO Heterostructures ……... Emine Cagin	9:00 AM	Q3, Halide Chemical Vapor Deposition of AlN …….... Timothy E. Bogart	9:00 AM	R3, (Student), High-Quality InP on GaAs Using Graded Buffers Grown by MOVPE (Metal Organic Vapor Phase Epitaxy): …….. Nate Quitoriano
9:20 AM	P4, (Student), ZnO Schottky Diode Performance as a Function of Contact Metal and Surface Polarity …… Martin W. Allen	9:20 AM	Q4, Extremely High Quality AlN Grown on (0001) Sapphire by Using Metal-Organic Vapor Phase Epitaxy……..….. Yangang A. Xi	9:20 AM	R4, Optical and Electrical Defect Characterization of $In_{0.49}Ga_{0.51}P$ Grown on Metamorphic SiGe Substrates …… Maria Gonzalez
9:40 AM	P5, (Student), Zinc Oxide Thin Films Deposited by Reactive RF Sputtering for Metal-Semiconductor-Metal Photodectors and Solar Cells …….. Meiya Li	9:40 AM	Q5, Late News	9:40 AM	R5, (Student), Lattice-Engineering for Monolithic Visible Yellow-Green Light Emitters …….. Michael J. Mori
10:00 AM	Break	10:00 AM	Break	10:00 AM	Break
10:20 AM	P6, Hybrid II-VI and III-V Compound Double Heterostruc-tures and Their Properties ……. Yahya Alivov	10:20 AM	Q6, Effects of Compositionally Graded $Al_{1-x}Ga_xN$ Buffer Layers on the Threading Dislocation Evolution in GaN Films Grown on (111) Si Substrate…….. X. Weng	10:20 AM	R6, (Student), The Fabrication of Misfit Dislocation-Free Strained Si Thin Films Using Porous Si Substrates ……..…… Jeehwan Kim
10:40 AM	P7, (Student), Investigation of ZnO Dry Etching in Inductively Coupled CH_4/H_2- and C_2H_6/H_2-Based Plasmas ……..…… Wantae Lim	10:40 AM	Q7, (Student), Crack Free GaN Grown on Patterned Si(111) Substrates by Metal-Organic Chemical Vapor Deposition …….. Hu Liang	10:40 AM	R7, Novel Fabrication Process for Multi SOI Layers Using Selective Etching of SiGe in Multi Si/SiGe Layers ……..…… Shun-Ichiro Ohmi
11:00 AM	P8, (Student), Magnetic Properties and Observation of Anomalous Hall Effect in Cobalt-Doped ZnO ……. Mathew Ivill	11:00 AM	Q8, (Student), Defect Reduction in Nonpolar A-Plane GaN Films Using In-Situ SiNx Nano-Mask ..…….. Kwang-Choong Kim	11:00 AM	R8, Perimeter-Limited Strain in Patterned Structures of SSOI …… Albert J. Paul
11:20 AM	P9, (Student), Growth and Physical Properties of N-Al or Cu Co-Doped (Zn,Co)O Dilute Magnetic Semiconductors ……..…. Govind Mundada	11:20 AM	Q9, Maskless Epitaxial Lateral Overgrowth of GaN Using Dimethylhydrazine as a Nitrogen Precursor …….. Toshiyuki Takizawa	11:20 AM	R9, FET Mobilities in Layers Grown by Ultra-High Growth Rate CVD with High-Order Silane Precursor …….. Keith H. Chung
11:40 AM	P10, Optical and Magnetic Properties of ZnVo Prepared by Ion Implantation ……..Vitaliy Avrutin	11:40 AM	Q10, Room Temperature Layer-by-Layer Epitaxial Growth of GaN on Lattice-Matched Hf (0001) ……..……Hiroshi Fujioka	11:40 AM	R10, Late News

Thursday AM, June 29

Session S: SiC: Growth and Interface Studies Room: Conference Room 208		Session T: Materials and Processing for Organic Transistors Room: Conference Room 207		Session U: Oxide Thin Film Integration II Room: Conference Room 206	
8:20 AM	S1, Effects of Hydrogen on Physical Vapor Transport Growth and Deep Trap Concentrations in 6H SiC …….. Mark Fanton	8:20 AM	T1, (Invited), Solution-Processable Organic Conductors and Semiconductors: Viable Materials for Thin Film Electronics ……. …….. Lynn Loo	8:20 AM	U1, Photocurrent-Voltage Measurements for Characterizing Oxide Charge in HfO_2 Gate Dielectrics …… Daniel Felnhofer
8:40 AM	S2, (Student), Surface Morphology, Doping and Oxide Field of 4H-SiC C-Face Epitaxial Layer Grown by Horizontal Hot-Wall Chemical Vapor Deposition…….. Kung-Yen Lee			8:40 AM	U2, Internal Photoemission Studies of TaSiN and TaCN Metal Gates on SiO_2 and HfO_2 …….. Nhan V. Nguyen
9:00 AM	S3, Chemical Vapor Deposition of Silcon Carbide Epitaxial Films and Their Characterization ……..…… Govindhan Dhanaraj	9:00 AM	T2, Acene-Based Materials for Thin-Film Transistors …….. John E. Anthony	9:00 AM	U3, (Student), Electron Spin Resonance and Spin Dependent Recombination Study of Deep Levels within the near Si/Dielectric Interfacial Layer of HfO2 Based Metal Oxide Silicon Field Effect Transistors …….. Jason T. Ryan
9:20 AM	S4, Structural and Electrical Characterization of Carbon Nanotubes Formed on Silicon Carbide Materials by Surface Decomposition …….. John Boeckl	9:20 AM	T3, (Student), Pentacene Devices Fabricated by Organic Vapor Phase Deposition ……..…….. Cédric Rolin	9:20 AM	U4, Photoemission and Inverse Photoemission Studies of Band Offsets in Alternative High-k Metal Oxide Semiconductor (MOS) Stacks …… Eric Bersch
9:40 AM	S5, Late News	9:40 AM	T4, (Student), Molecular Ordering of Solution Processed TIPS-Pentacene ……..…….. Sungkyu Park	9:40 AM	U5, Growth and Characterization of Epitaxial Sc_2O_3 on Silicon by Molecular Beam Epitaxy for Alternative Gate Dielectric Applications …… Darrell G. Schlom
10:00 AM	Break	10:00 AM	Break	10:00 AM	Break
10:20 AM	S6, Role of Interface Layers and Localized States in TiAl-Based Ohmic Contacts to P-Type 4H-SiC ……..…….. Min Gao	10:20 AM	T5, (Student), Zinc Tetrabenzoporphyrin Organic Field-Effect Transistors …… Patrick Shea	10:20 AM	U6, Medium Energy Ion Scattering Study of Oxygen Diffusion-Reactions in High-k Dielectrics on Si ..…….. Lyudmila Goncharova
10:40 AM	S7, As-Deposited Ohmic Contacts Using Ti on InN on SiC …… Lisa M. Porter	10:40 AM	T6, (Student), Modeling and Experiments of Organic Material Patterning by Stamping in the Fabrication of Organic Electronic Devices…….. Yifang Cao	10:40 AM	U7, (Student), Characterization of n-MISFETs with Ultrathin HfO_xN_y Gate Insulator Formed by ECR-Ar/N_2 Plasma Nitridation ……..… Masaki Satoh
11:00 AM	S8, (Student), Electronic States of Chemically Treated and/or Oxidized SiC Surfaces …….. Shu Nie	11:00 AM	T7, (Student), Pentacene OTFTs with Parylene Active Layer Patterning and Passivation …….. Dalong Zhao	11:00 AM	U8, Late News
11:20 AM	S9, (Student), Effect of Oxide Deposition Temperature on Interface Properties of SiC/SiO_2…… Tahir A. Khan	11:20 AM	T8, All Organic Non-Volatile Switching Device Fabricated by Using Conducting Polymer Micropores…… Oleg Kirillov	11:20 AM	U9, Late News
11:40 AM	S10, Late News	11:40 AM	T9, Late News	11:40 AM	U10, Late News

Thursday AM, June 29

Thursday Afternoon Begins

Session V: Non-Destructive Testing and In-Situ Monitoring and Control Room: Conference Room 108		Session W: ZnO Growth Room: Deans Hall I		Session X: MBE Growth of Group III-Nitrides Room: Deans Hall II	
8:20 AM	V1, (Student), Surface Plasmon Resonance of Ga and In Nanoparticles Measured by In-Situ Spectroscopic Ellipsometry …….. Pae C. Wu	1:30 PM	W1, (Student), Zinc Oxide Thin Films Deposited by Laser Assisted Molecular Beam Deposition…….. Meiya Li	1:30 PM	X1, Optical Investigation of the Dependence of Luminescence Efficiency on Stokes Shift in Nanoscale Compositionally Inhomogeneous AlGaN …….. Gregory A. Garrett
8:40 AM	V2, (Student), Kinetics of Ga Adlayer Formation on Gallium Nitride (0001) Surface …….. Soojeong Choi	1:50 PM	W2, (Student), The Effect of Substrate Material and Post-Annealing on DC Sputtered ZnO …….. Leo P. Schuler	1:50 PM	X2, (Student), The Use of Cathodoluminescence in Gallium Nitride during Growth to Determine Substrate Temperature …… Kyoungnae Lee
9:00 AM	V3, (Student), Spectroscopic Ellipsometric Characterization of Metal-Free Carbon Nanotube Formation by SiC Surface Decomposition …….. Jeremy Harrison	2:10 PM	W3, Effect of Substrate Surface Structure and Chemistry on Microstructure and Properties of Epitaxial ZnO Thin Films Grown on Sapphire and ZnO Substrates …… Xiaoqing Pan	2:10 PM	X3, (Student), A New Mechanism for the Tilting of Dislocations in Oxygen Doped Gallium Nitride Layers Grown by Molecular Beam Epitaxy …….. Michael E. Hawkridge
9:20 AM	V4, Reduced Interference Photoreflectance for Measurement of HBTs …… Eric Rehder	2:30 PM	W4, Plasma-Assisted MOCVD Growth of Highly Oriented ZnO Thin Films…… Maria Losurdo	2:30 PM	X4, Unintentional Si Incorporation in GaN/AlN Interface Grown on SiC by PAMBE…T.-H. Kim
9:40 AM	V5, (Student), AlGaAs/GaAs Interface States by Surface Photovoltage Studies …… Clara Vargas	2:50 PM	W5, (Student), Surface and Interface Characterization of A-Plane ZnO and $Mg_XZn_{1-X}O$ Films…….. Gaurav Saraf	2:50 PM	X5, High-Quality Nonpolar 4H-AlN Grown on 4H-SiC by Molecular-Beam Epitaxy……. M. Horita
10:00 AM	Break	3:10 PM	Break	3:10 PM	Break
10:20 AM	V6, Quantification of Ultra-Thin Indium MBE Layers by Low Energy X-Ray Emission Spectroscopy (LEXES).... K. G. Eyink	3:30 PM	W6, Three Step Growth as a Novel Approach for the Growth of ZnO on Si(111) by MOVPE …… Takumi Moriyama	3:30 PM	X6, (Student), Physical Processes during Growth of InN on GaN (0001) by Plasma-Assisted Molecular Beam Epitaxy….. Emmanouil Dimakis
10:40 AM	V7, (Student), In-Situ Investigation of Surface Stoichiometry during $YMnO_3$, InGaN and GaN Growth by Plasma-Assisted Molecular Beam Epitaxy Using RHEED-TRAXS …….. Randy P. Tompkins	3:50 PM	W7, (Student), Growth of ZnO on Cubic Substrates by Molecular Beam Epitaxy ……. Emine Cagin	3:50 PM	X7, Study of PA-MBE Growth of In- and N-Polar InN on SiC Substrates …….. Maria Losurdo
11:00 AM	V8, Composition Driven Surface Transition and Electronic Transport in $LaSrMnO_3$ …..… Maitri P. Warusawithana	4:10 PM	W8, (Student), ZnO Thin Films Produced via Reactive Pulsed Arc Molecular Beam Deposition …….. Chi-Tung Chiang	4:10 PM	X8, (Student), Direct Write Composition Patterning of InGaN during Molecular Beam Epitaxy…….. Xiaodong Chen
11:20 AM	V9, (Student), Structural Transformations Underlying the Refractive Index Contrast for Optical Waveguides in He-Implanted Single Crystal PZN-PT…… Peter Moran	4:30 PM	W9, (Student), Low Temperature Highly Conducting Boron-Doped ZnO Films by Plasma Enhanced Chemical Vapor Deposition …….. Jie Sun	4:30 PM	X9, Growth of In-Rich $in_XAl_{1-X}N$ Films on (0001) Sapphire by RF-MBE and Their Properties …….. Hiroyuki Naoi
11:40 AM	V10, (Student), Pre-Oxidation Iron Contamination of Silicon and 4H-SiC Substrates …….. Helen Benjamin	4:50 AM	W10, Late News	4:50 PM	X10, (Student), Structural, Optical and Electronic Properties of InN Grown on GaN Substrate by Molecular Beam Epitaxy ….. Kejia (Albert) Wang

Thursday PM, June 29

Session Y: Epitaxy for Devices Room: Conference Room 106		Session Z: SiC: Characterization Room: Conference Room 208		Session AA: Organic/Inorganic Hybrid Photovoltaics Room: Conference Room 207	
1:30 PM	Y1, Selective MBE Growth of Hexagonal Networks of GaAs Triangular Nanowires on (111)B Patterned Substrates ……. Hideki Hasegawa	1:30 PM	Z1, Optical Characterization of Stacking Faults in 4H-SiC PiN Diodes …..... Joshua D. Caldwell	1:30 PM	AA1, (Invited), Metal Nanostructure Enhanced Organic Solar Cells ……..…..Peter Peumans
1:50 PM	Y2, (Student), Structural and Electronic Characterization of Homoepitaxial $SrTiO_3$ Films Prepared by Molecular Beam Epitaxy …… Charles M. Brooks	1:50 PM	Z2, A 180 A/4.5 kV 4H-SiC PiN Diode for High Current Power Modules…… Brett A. Hull		
2:10 PM	Y3, (Student), Asymmetric Relaxation of Semiconductor Grade $SrTiO_3$ Films ……. Michael D. Biegalski	2:10 PM	Z3, Improvement of PMOS Channel Properties for 4H-SiC P-IGBTs …..…….. Mrinal K. Das	2:10 PM	AA2, (Student), Organic Photovoltaic Cells with External Antennas …….. Jonathan K. Mapel
2:30 PM	Y4, (Student), Structural and Magnetic Properties of MBE Grown Single Crystal Co_2MnGe on $SrTiO_3$(001), $BaTiO_3$ (001) and MgO (001) Substrates.….S. K. Srivastava	2:30 PM	Z4, Photo and Electro Luminescence Imaging of Carrot Defect in 4H-SiC Epitaxy …….. Kendrick X. Liu	2:30 PM	AA3, (Student), A Quantum Dot Photovoltaic Device Fabricated via Microcontact Printing ……..…… Alexi Arango
2:50 PM	Y5, (Student), Fabrication and Optical Modulation of Silicon-Filled Capillary Fiber …..…….. Dong-Jin Won	2:50 PM	Z5, Identification of a Three-Site Defect in SI 4H-SiC …… Nelson Y. Garces	2:50 PM	AA4, Late News
3:10 PM	Break	3:10 PM	Break	3:10 PM	Break
3:30 PM	Y6, (Student), MBE-Grown $Zn_xCd_{(1-x)}Se/Zn_{x'}Cd_{y'}Mg_{(1-x'-y')}Se$ Multi-Quantum Wells for Intersubband Devices …….. Hong Lu	3:30 PM	Z6, EPR Characterization of Halide CVD 4H SiC …… Mary Ellen Zvanut	3:30 PM	AA5, Transparent Conducting SWNT Electrodes for Plastic Solar Cells ……..…… Aurelien Du Pasquier
3:50 PM	Y7, (Student), Effectiveness of SiGe Buffer Layers in Reducing Dark Current in Ge-on-Si Photodetectors ……. Zhihong Huang	3:50 PM	Z7, Effect of Electron-Irradiation on Deep Centers in High-Purity Semi-Insulating 6H-SiC …….. Zhaoqiang Fang	3:50 PM	AA6, (Student), Hybrid Conjugated Polymer/Nano-structured ZnO Photovoltaic Devices …….. Dana C. Olson
4:10 PM	Y8, (Student), Accurate Carbon Doping System for Low-Voltage and Low-Loss VCSELs ……. Yu-Chia Chang	4:10 PM	Z8, (Student), Deep Level Defects which Limit Current Gain in 4H SiC Bipolar Junction Transistors ….. Corey Cochrane	4:10 PM	AA7, (Student), Nanostructured Hybrid Solar Cells ……. Vignesh Gowrishankar
4:30 PM	Y9, (Student), Optically Pumped GaSb Based "Arsenic Free" Mid IR Vertical Cavity Surface Emitting Laser Design …… Ravi Kalyanam	4:30 PM	Z9, Performance of SiC Field-Effect Devices at Elevated Temperature during Several Months of Continuous Operation …….. Ruby N. Ghosh	4:30 PM	AA8, (Student), Investigating Charge Dynamics of Small Molecule Organic Heterojunction Interfaces in Lateral Photocon-ductor Devices ……. John Ho
4:50 PM	Y10, (Student), Monolithic GaSb-Based VCSEL on Si …… Ganesh Balakrishnan	4:50 PM	Z10, Late News	4:50 PM	AA9, Late News

Thursday PM, June 29

Session BB: Oxide Thin Film Integration III Room: Conference Room 206		Session CC: Dilute Nitride Semiconductors Room: Conference Room 108		NOTES:
1:30 PM	BB1, (Student), GaN MOSFET with ALD High-k Gate Dielectric ……. Yanqing Wu	1:30 PM	CC1, Effect of Strain on the Nitrogen Incorporation in InGaAsN Quantum Wells Grown on GaAs and InP Substrates by Metalorganic Vapor Phase Epitaxy …….…….. Nelson Tansu	
1:50 PM	BB2, (Student), CV Studies on ALD Al_2O_3/GaAs and Al_2O_3/InGaAs Interfaces for Enhancement-Mode GaAs MOSFET Application …… H. C. Lin	1:50 PM	CC2, (Student), TEM Analysis of GaInNAsSb Quantum Wells Grown and Annealed at Varied Temperatures ……..…. Evan R. Pickett	
2:10 PM	BB3, (Student), GaAs Growth on Silicon Substrates Using a Thin (~80 Nm) Si_XGe_{1-X} Step-Graded Buffer Layer for High-k III-V MOSFET Applications ……..…. Michael M. Oye	2:10 PM	CC3, (Student), Relative Speed and Temperature Dependence of Constituent Processes in the Annealing of GaInNAs(Sb) and Their Implications on Device Growth and Annealing …….. H. P. Bae	
2:30 PM	BB4, Passivation of Ge Surface Using Ceria …… Y. A. Panayiotatos	2:30 PM	CC4, (Student), The Role of Bismuth as a Surfactant during Beryllium Doping of GaAsN Grown by Molecular Beam Epitaxy …… Ting Liu	
2:50 PM	BB5, Late News	2:50 PM	CC5, (Student), Strong Luminescence Enhancement in GaInNAsSb Quantum Wells through Variation of the Group-V Fluxes …..S. R. Bank	
3:10 PM	Break	3:10 PM	Break	
3:30 PM	BB6, (Student), Nonlinear Optical Probing of Polarization Dynamics in Strained Ferroelectric $SrTiO_3$ Films ……. Aravind Vasudeva Rao	3:30 PM	CC6, (Student), Influence of Nitrogen Incorporation on Electron Transport in Selectively Doped GaAsN/AlGaAs Heterostructures ……. Yu Jin	
3:50 PM	BB7, (Student), Epitaxial $BiMnO_3$ Films with Reduced Twinning and the Effect of Film Composition on Ferromagnetism …… June Hyuk Lee	3:50 PM	CC7, (Student), Growth and Fabrication of InGaNP Quantum Well Based Yellow-Red Light-Emitting Diodes ……. Vladimir A. Odnoblyudov	
4:10 PM	BB8, Single Nanoparticle Transistors: A New Thin Film Device ……. Steve Campbell	4:10 PM	CC8, Electrical and Luminescence Properties of n- and p-Type GaPN ……..…….. Yuzo Furukawa	
4:30 PM	BB9, Late News	4:30 PM	CC9, The Role of Kinetic Effects in Radiative and Non-Radiative Recombination of Optical Excitations in Dilute Nitride Heterostructures: Theory and Experiment …….. Oleg Rubel	
4:50 PM	BB10, Late News	4:50 PM	CC10, (Student), Bandgap Reduction and Lattice Matching in Dilute Nitride Antimonide Alloys ……..…….. Paul Jefferson	

Friday AM, June 30

Session DD: P-Type Doping and Electroluminescence in ZnO Room: Deans Hall I		Session EE: Contacts to III-Nitrides Room: Deans Hall II		Session FF: Indium Nitride Room: Conference Room 106	
8:20 AM	DD1, (Student), Band-Edge Electroluminescence from N^+-Implanted Bulk ZnO …….. Hung-Ta Wang	8:20 AM	EE1, (Student), Comparison of Thermally Stable TiB_2, CrB_2 and W_2B_5 Based Ohmic Contacts on n-GaN ……..…..…. Rohit Khanna	8:20 AM	FF1, Origin of the N-Type Conductivity of InN – The Role of Positively Charged Nitrogen Vacancies along Threading Dislocations - Quality ZnO Layers on Sapphire …….. Tim Veal
8:40 AM	DD2, (Student), Photoluminescence and Electroluminescence Properties of ZnO Nanotips Grown on p-Type GaN…….. Jian Zhong	8:40 AM	EE2, (Student), Reduction of Metal/GaN Barrier Height Using Nanopatterning …… Ho Gyoung Kim	8:40 AM	FF2, Optical Properties of the In-Polarity InN/$In_{0.7}Ga_{0.3}N$ MQWs Grown by RF-MBE …….. Song-Bek Che
9:00 AM	DD3, Changes in Electrical Characteristics of p-Type Zinc Oxide Thin Films Due to Light and Gas Ambient ……..…… Bruce Claflin	9:00 AM	EE3, (Student), Investigation of a Low-Temperature Cu_3Ge Ohmic Contact to N-GaN …….…… Michael L. Schuette	9:00 AM	FF3, In-Polar InN: Evidence of a Possible Hole Accumulation Layer ……. Steven M. Durbin
9:20 AM	DD4, (Student), Bi-Doped ZnO Films Grown by Molecular-Beam Epitaxy …….. Faxian Xiu	9:20 AM	EE4, Formation of High-Quality Ag Ohmic Contacts for Flip-Chip LEDs by Using Transparent Conducting Oxide Interlayers…….. T.-Y. Seong	9:20 AM	FF4, Anisotropy of the Γ-Point Electron Effective Mass in Hexagonal InN ……..…….. Tino Hofmann
9:40 AM	DD5, (Student), Phosphorus Bipolar Doping of ZnO Thin Films Fabricated by Pulsed Laser Deposition ……..…… Arnold Allenic	9:40 AM	EE5, Late News	9:40 AM	FF5, (Student), Structural and Optical Properties of InN Layers Grown by HPCVD …… Mustafa Alevli
10:00 AM	Break	10:00 AM	Break	10:00 AM	Break
10:20 AM	DD6, ZnO Light-Emitting Diode Fabricated by Plasma-Assisted Metalorganic Chemical Vapor Deposition ……..…..….. Zhizhen Ye	10:20 AM	EE6, (Student), Analytical Transmission Electron Microscopy (TEM) Investigation of the Structural Evolution of Ti-Based Ohmic Contacts on GaN and AlGaN/GaN at Different Annealing Temperatures ……..…… Liang Wang	10:20 AM	FF6, Effect of the Growth Mode and Substrate Properties on the Biaxial Strain in InN (0001) Epilayers …..…… Eleftherios Iliopoulos
10:40 AM	DD7, MOCVD Growth of ZnO and p-Type Doping ……..…….. Ming Pan	10:40 AM	EE7, (Student), Low-Temperature-Annealed Mo-Based Ohmic Contacts for AlGaN/GaN Heterostructures ……. Anirban Basu	10:40 AM	FF7, Study of Graded InGaN Buffer Layers for MOCVD Growth of Indium Nitride Thin Films…….. Abhishek Jain
11:00 AM	DD8, Characterization of Defects in Zinc Oxide Single Crystals …… Govindhan Dhanaraj	11:00 AM	EE8, (Student), Si and Ge Incorporation in Ti/Al/Mo/Au for AlGaN/GaN HEMTs: Effects on Electrical and Microstructural Properties ….. Fitih M. Mohammed	11:00 AM	FF8, (Student), Optical Properties of InN Epilayer and Self-Organized InN Quantum Dots Grown by Flow-Rate Modulated Epitaxy… C.-P. Fu
11:20 AM	DD9, Late News	11:20 AM	EE9, (Student), Comparison of V- and Ti-Based Ohmic Contacts to High Al-Fraction n-$Al_xGa_{1-x}N$ ……..…… Mary A. Horsey	11:20 AM	FF9, Low Temperature Epitaxial Growth of InN on Substrates with Small Lattice Mismatches… Hiroshi Fujioka
11:40 AM	DD10, Late News	11:40 AM	EE10, Late News	11:40 AM	FF10, Ammonothermal Growth and Characterization of Indium Nitride Crystals ……..…… Buguo Wang

Friday AM, June 30

Session GG: Silicon and Germanium Nanowires Room: Conference Room 208		Session HH: Molecular Electronics: Devices, Materials and Contacts Room: Conference Room 207		Session II: Trapping and Charge Transport in Organic Transistors Room: Conference Room 206	
8:20 AM	GG1, (Student), RF Dielectric Properties of Silicon Nanowire Networks …….. Theresa S. Mayer	8:20 AM	HH1, (Student), Ordered Molecular Films on Semiconductors: Characterization of Ordered Organothiolate Monolayers on GaAs (100) and (110) for Molecular Electronic Applications……C. McGuiness	8:20 AM	II1, (Invited) Trapping of Majority and Minority Carriers at the Insulator-Polymer Semiconductor Interface …… David M. Taylor
8:40 AM	GG2, (Student), Nanowire Bandgap Engineering through Highly Strained Si/Ge Heterostructures …… T. J. Clement	8:40 AM	HH2, (Student), Investigating the Stability of Organic Molecules Bound to Semiconductor Surfaces with Low Temperature UHV-STM …….. Nathan L. Yoder		
9:00 AM	GG3, (Student), Unintentional Background Doping of Vapor-Liquid-Solid Synthesized SiNWs .....…. ……..…Tsung-Ta Ho	9:00 AM	HH3, (Student), High Resolution Inelastic Electron Tunneling Spectroscopy of Nanoscale Crossed-Wire Molecular Junctions …….. Heayoung Yoon	9:00 AM	II2, (Student), Trap Energy Determination by Analysis of Isothermal Gated Space-Charge-Limited Current in Organic Thin Film Transistors……. R. Yang
9:20 AM	GG4, (Student), Synthesis and X-Ray Diffraction Characterization of Heteroepitaxially Grown Germanium Nanowires …….. Irene A. Goldthorpe	9:20 AM	HH4, Single-Molecule Transistors to Characterize Bistability in Molecular Conduction ……..……Douglas Natelson	9:20 AM	II3, (Student), Measurement of Drift Velocity and Mobility of Carriers in a Polymer Thin-Film Transistor ….. Debarshi Basu
9:40 AM	GG5, (Student), Structural and Field-Effect Properties of Thermally-Oxidized Silicon Nanowires ……. Yanfeng Wang	9:40 AM	HH5, (Student), Criteria for Statistical Determination of Working Devices of Microscale Via-Hole Molecular Structures ……T.-W. Kim	9:40 AM	II4, Influence of Charged Dielectrics and Adsorbed Dipoles on Organic Semiconductors in Transistor Architectures…..… Howard E. Katz
10:00 AM	Break	10:00 AM	Break	10:00 AM	Break
10:20 AM	GG6, (Student), Growth and Passivation of Vertically Aligned Germanium Nanowires for Three Dimensional Nanoelectronics …….. Hemant Adhikari	10:20 AM	HH6, Fundamental Studies of Vapor Deposited Metal Contacts for Molecular Electronics Devices …….. Thomas A. Daniel	10:20 AM	II5, (Student), Charge Transport as a Function of Gate Voltage and Temperature in N,N'-bis(n-octyl)-Dicyano-perylene-3,4:9,10-bis-(Dicarboximide) [PDI-8CN2] …….. Y. T. Jeong
10:40 AM	GG7, (Student), Integrated Silicon Nanowire Diodes ……..…… Justin B. Jackson	10:40 AM	HH7, (Student), Electrical and Structural Characterization of Evaporated Contacts in Au/Molecule/GaAs Devices……. P. D. Carpenter	10:40 AM	II6, Using High-Sensitivity Electric Force Microscopy to Probe Charge Trapping in Pentacene Thin-Film Transistors…… Michael J. Jaquith
11:00 AM	GG8, Silicidation of Silicon Nanowires ……. Bangzhi Liu	11:00 AM	HH8, (Student), Molecule-Electrode Contact Effect on the Conductance of Single Alkanedithiols ……..…… Xiulan Li	11:00 AM	II7, (Student), Charge Transport at Very High Carrier Densities in Organic Semiconductor Thin Films and Single Crystals …….. M. J. Panzer
11:20 AM	GG9, (Student), Self-Assembled Nickel Silicide Nanowire Contacts and Direct Electrical Measurement ...……..… Joondong Kim	11:20 AM	HH9, (Student), Scalable Molecular Electrodes at the Paterned Edge of a Metal/Insulator/Metal Junction …… Pawan Tyagi	11:20 AM	II8, Building Blocks for Single-Component Organic Electronics: Electrostatic Modulation and Majority Carrier Sign Inversion of Organic Semiconductors via Polarized Gates …….. Cheng Huang
11:40 AM	GG10, Late News	11:40 AM	HH10, (Student), From Quantum Chemistry to Molecular Electronic Circuits……..… Yuhui Lu	11:40 AM	II9, High-Mobility Charge Transport in Laminated Rubrene Crystal/Polymer Field-Effect Transistors ……. Jun Takeya

Friday AM, June 30

Friday Afternoon Begins

Session JJ: Spintronic Materials Room: Conference Room 108		Session KK: GaN Characterization Room: Deans Hall II		Session LL: Compound Semiconductor Nanowires Room: Conference Room 208	
8:20 AM	JJ1, Magnetoresistance and Insulator-Metal Transition of EuO_{1-x} Thin Films Grown on (110) $YAlO_3$ and (001) Si Substrates ……. A. Schmehl	1:30 PM	KK1, A Dynamic Micro-Analysis of Temperature Distribution and Electric Potential Distribution of AlGaN/GaN HFETs Using Micro-Raman Spectroscopy and Kelvin-Force Microscopy……. A. Suzuki	1:30 PM	LL1, InAs Nanowire Transistors Using Solution-Grown Nanowires with Acceptor Doping …….. Qingling Hang
8:40 AM	JJ2, (Student), High Field Magnetoresistance and Hall Effect Studies of Nonmagnetic Al- and Cu-Doped (Zn,Mn)O Dilute Magnetic Semiconductors …… Theodore W. Kehl	1:50 PM	KK2, (Student), Selective Quantification of AlGaN-Related Deep Levels in AlGaN/GaN Heterostructures Using Capacitance-Mode Deep Level Optical Spectroscopy…… Andrew Armstrong	1:50 PM	LL2 , Photocurrent Spectroscopy of Solution-Synthesized Nanowire-Based Photodetectors … Huili (Grace)Xing
9:00 AM	JJ3, Conduction-Band Electron Effective Mass in $Zn_{0.87}Mn_{0.13}Se$ Measured by Terahertz and Far-Infrared Magnetooptic Ellipsometry …….. Tino Hofmann	2:10 PM	KK3, Anisotropic Strain in GaN Films Grown on a-Plane and r-Plane Sapphire: Effect on GaN Phonons …….. V. Darakchieva	2:10 PM	LL3, (Student), Growth Mechanism and Optimization of InAs Nanowires Synthesized by OMVPE ……..…… Shadi A. Dayeh
9:20 AM	JJ4, (Student), Ferromagnetism in Fe-Implanted ZnO Films and Nanotips …….. Pan Wu	2:30 PM	KK4, (Student), Phase Separation and Defects in Quaternary $In_XAl_YGa_{1-X-Y}N$ Layers ……. Fanyu Meng	2:30 PM	LL4, III-V Nanostructures Formed from GaP Nanowires/ on Si(111) Substrates ……..…..…… Kouta Tateno
9:40 AM	JJ5, (Student), Dilute Magnetic MnGe Semiconductor Using Ion Implantation of Mn into Nano-Patterned Ge .... J. Chen	2:50 PM	KK5, Consequences of Polarity and Related Defects on the Electrical Properties of GaN Grown by MOVPE ……. Ramon Collazo	2:50 PM	LL5, The Fabrication of Extreme Aspect Ratio Semicon-ductor and Metal Wires within Photonic Crystal Fibers……..… Neil Baril
10:00 AM	Break	3:10 PM	Break	3:10 PM	Break
10:20 AM	JJ6, Direct Imaging of Photo-Induced Changes in Magnetization Orientation in (Ga,Mn)As by a Scanning Magneto-Optical Microscope….. Tsuyoshi Kondo	3:30 PM	KK6, (Student), Defect Reduction in GaN through Formation of 'Dislocation Clusters' at the Nanoheteroepitaxial Interface …… Mohammad Ferdous	3:30 PM	LL6, In Situ Electrical Annealing of Bio-Templated Nanowires ……..……..…….. Yan Gao
10:40 AM	JJ7, (Student), Electroluminescence Studies of (Ga,Mn)As-Based p-i-n Structures ……..…… Zhiguo Ge	3:50 PM	KK7, (Student), Influence of Arsenic Isova-lent Co-Doping on the Electronic Properties of N-Type and P-Type GaN Grown by Metal-Organic Chemical Vapor Deposition ……..…….. David Gray	3:50 PM	LL7, (Student), Contacts to Gold Nanowires in Porous Anodic Alumina Templates …… Kalapi Biswas
11:00 AM	JJ8, (Student), Ferromagnetic Co_2MnGe Contacts for GaAs: Growth, Characterization, and Interface Stability …….. J. L. Hilton	4:10 PM	KK8, Strong Light-Matter Coupling a Room Temperature in GaN Microcavities …….. Ian R. Sellers	4:10 PM	LL8, Three-Dimensional Nano-scale Composition Mapping of Semiconductor Nanowires ……..…. Lincoln J. Lauhon
11:20 AM	JJ9, Magnetic Characterization of Fe/Tb Superlattice Grown on InAs as a Vertically Magnetized Spin Injector……..…… Kanji Yoh	4:30PM	KK9, (Student), Microstructural Investigation of AlN Re-Growth by MOCVD ……..…… Xianglin Li	4:30PM	LL9, (Student), Photoluminescent Properties of $ZnO/Mg_{0.2}Zn_{0.8}O$ Coaxial Nanorod Quantum Structures ……..…. Jinkyoung Yoo
11:40 AM	JJ10, (Student), Thickness Determination of Ultra-Thin Oxide Films and the Application in Magnetic Tunnel Junctions ..… Jianhua J. Yang	4:50 PM	KK10, Late News	4:50 PM	LL10, (Student), Transport Properties of Solution Grown Thin Film Nanowire Solids ……Amol K. Singh

Friday PM, June 30

Session MM: Chemical and Biological Sensors II

Room: Conference Room 207

1:30 PM	MM1, Modification of Nano-particle-Organic Composite Electronic Materials for Improved Chemical Sensors ……. Stephen W. Howell
1:50 PM	MM2, Conductance Sensor Based on Polyion Stabilized and Thiol Functionalized Double Stranded DNA Molecules …….. Ajit K. Mahapatro
2:10 PM	MM3, (Student) AFM Study of Current Transport through Porphyrin Based Molecules …….. Raghu Ramachandran
2:30 PM	MM4, (Student), Surface Plasmon Resonance: Sensing Chips and Applications …….. Kyle Foley
2:50 PM	MM5, Late News
3:10 PM	Break
3:30 PM	MM6, (Student), The Functionalization of GaN and AlGaN Surfaces with Hemin for Nitric Oxide Detection …….. Michael A. Garcia
3:50 PM	MM7, BioFETs Based on GaN/AlGaN Devices …… Kendra McCoy
4:10 PM	MM8, Sensing Characteristics and Mechanism of Liquid-Phase and Gas-Phase Sensors Using AlGaN/GaN Heterostructure …….. Hideki Hasegawa
4:30PM	MM9, (Student), Scalable Dope-Coded Biosensing Particles for Protein Detection …… Nguyen H. Ly
4:50 PM	MM10, Electric Field Dependence of Photoluminescence of Silica Coated CdSe/CdS Quantum Dots …… Yang Xu

NOTES:

EMC Plenary Lecture/Student Awards

Wednesday AM Room: Presidents Hall III/Presidents Hall IV
June 28, 2006 Location: Pennsylvania State University

8:20 AM: Ceremony

Plenary Speaker: *Arthur C. Gossard*[1]; [1]University of California, Santa Barbara

Topic: Growth and Uses of Metal/Semiconductor Heterostructures

Dozens of metallic compounds exist that potentially can be grown epitaxially on and in semiconductors. The rare-earth group III-V metallic compounds are particularly noteworthy. We illustrate the growth and uses of such compounds by studies of the molecular beam epitaxy of erbium-based III-V metallic compounds with simple rock-salt crystal structure on and in III-V semiconductors. 1) All-epitaxial metal/semiconductor microwave detector diodes, 2) time-domain Terahertz sources and detectors based on embedded metal nanoparticles, 3) thermo-electric power generators based on embedded nanoparticles, and 4) tandem solar cells coupled by monolayers of metallic epitaxial nanoparticles are all showing record-breaking performance. It is apparent that the epitaxial metal/semiconductor heterostructure is joining the semiconductor/semiconductor heterostructure as a key element in enhanced-performance electronic and optoelectronic devices.

9:20 AM Break

Session A: ZnO Nanomaterials

Wednesday AM Room: Presidents Hall III
June 28, 2006 Location: Pennsylvania State University

Session Chairs: Yicheng Lu, Rutgers University; David P. Norton, University of Florida

10:00 AM Student

A1, Undoped and Doped ZnO Nanorods: *Jinkyoung Yoo*[1]; Gyu-Chul Yi[1]; [1]POSTECH

One-dimensional (1D) semiconductor nanostructures have been considered as promising building blocks for electronic and photonic devices in nanometer scales due to their interesting properties and high aspect ratio. Although preliminary research has shown that 1D semiconductor nanostructures may be used as building blocks for nanodevices, several fundamental issues on nanodevice fabrications based on the semiconductor nanostructures still remain. In particular, doping in nanostructures is scientifically interesting because doping behavior in nanomaterials may be different from that in bulk materials. Furthermore, an accurate control of doping concentration in a wide range is technically very important for many device fabrications as already proven in microelectronics. Nevertheless, dopings in 1D semiconductor nanostructures have rarely been reported. The difficulties of dopings in nanomaterials may be originated from difficulty in preparation of high purity nanomaterials as well as insufficient understandings on behavior of dopants in nanomaterials. Here we present on high purity nanorod preparation and doping of ZnO nanorods. In addition, structural, optical, and electrical characteristics of the doped nanomaterials were also investigated. High quality ZnO nanorods were prepared on Si substrates using catalyst-free metal-organic chemical vapor deposition. As one of the n-type dopants in ZnO nanorods, Al was employed. Structural properties of the undoped and doped ZnO nanorods were investigated using electron microscopies. Electrical characteristics of Al-doped ZnO nanorods were characterized by four probe current-voltage (I-V) measurements using electron beam lithography. From I-V characteristic curves of Al-doped ZnO nanorods, we observed that electrical conductivity of Al-doped ZnO nanorods can be controlled by change of doping process condition. In addition, optical properties of Al-doped ZnO nanorods were investigated by photoluminescence (PL) spectroscopy. Low temperature PL spectra of Al-doped ZnO nanorods exhibited strong excitonic emission peaks and negligibly weak deep level emission. Through a series of analytic characterizations of the doped, n-type ZnO nanorods, we demonstrate that Al doping is very useful for controlling electrical properties of ZnO nanorods without significant morphology change.

10:20 AM Student

A2, Spatially-Dependent Optical Emission from ZnO Nanotips on $Al_2O_3$3 and Si Substrates: *Lei Fang*[1]; Yuri Strzhemechny[2]; Michael J. Hetzer[1]; Leonard J. Brillson[1]; H. Chen[3]; Yicheng Lu[3]; [1]Ohio State University; [2]Texas Christian University; [3]Rutgers University

ZnO nanostructures have attracted considerable attention for applications in nanometer-scale opto- and microelectronics. However, device applications require understanding the effect of sample morphology, alignment, and growth conditions on electronic properties. We have used depth-resolved cathodoluminescence spectroscopy (DRCLS) at low incident beam energies Eb to measure the optical emission from ZnO nanotips on sapphire vs. silicon substrates as a function of distance from the base of the nanotip. The nanotips were grown by a vertical flow, rotating disk MOCVD reactor with diethylzinc and oxygen used as the Zn source and oxidizer, respectively. We found that ZnO nanotips grown on $Al_2O_3$3 exhibit low temperature (10 K) optical emissions resembling those of very high quality bulk ZnO single crystals in terms of energies, phonon replicas and phonon broadening as well as absence of significant deep level defect emissions. Bound exciton emissions appear at 3.369 eV for $Al_2O_3$3 and at 3.363 eV for Si along with multiple phonon replicas. By orienting the incident electron beam normal to the densely packed 400 nm long, 50 nm diameter nanotips and varying Eb from 1 keV to 25 keV, we could excite preferentially from within 10 nm of the nanotip (1 keV) down to the base (25 keV). The DRCLS features exhibited pronounced changes with depth, indicating highest crystal quality near the tip and, using shifts of the phonon replicas, lower quality near the base due to strains in excess of 6 GPa. Nanotips grown on Si also show an improvement in crystal quality with increasing distance from the substrate. However, exciton and phonon replicas peaks are closer in energy with closer phonon energy shifts, more phonon replicas and lower peak broadening for nanotips on $Al_2O_3$3 vs. ZnO on Si as compared with bulk ZnO. This is consistent with the better (hexagonal) lattice match with $Al_2O_3$3 vs. Si. For the c-$Al_2O_3$3 substrate nanotips, peak differences of the phonon replicas yield phonon energies that increase as beam excites deeper. The first phonon (1LO) replicas at different depths are all ~73 meV, corresponding to the E1 LO phonon frequency of 588 cm-1. The 2LO phonon replica spacing increases with increasing depth/base proximity by up to 23 meV, increasing further for higher order. For the nanotips grown on Si, only two phonon replicas are evident and only for near-tip excitation. 1LO phonon replicas are also 73 meV, but 2LO phonon replica spacings decrease with increasing depth by >11 meV. We propose that these changes are due to strain-induced distortions of the phonon dispersion curves. Overall, these are the first measurements of crystal quality inside a nanotip. They show that crystal quality can vary with distance from the substrate and that substrates can introduce large strains that degrade crystal quality locally.

10:40 AM Student

A3, Selective Growth of Zinc Oxide Nanowires Grown from Thin Film Multilayer Structure for Shadow Lithography: Bing Hu[1]; Pawan Tyagi[1]; *Bruce J. Hinds*[1]; [1]University of Kentucky

High aspect ratio and rigid structure of oxide nanowires (NWs) make them useful for nanoscale circuits, interconnects, NEMs, and sensing. There are many literature examples of ZnO NWs being grown from the Al2O3 substrate. Critical to their application is the location and diameter control of these 1-D nanostructures. Our research focuses on the growth of ZnO NWs from an exposed edge of a Si/Al2O3 (10-30 nm)/Si thin film multilayer structure patterned on a silicon substrate. The Al2O3 film acts as a grown area for ZnO NWs in a VLS growth process. Such thin film patterning eliminates the necessity for e-beam lithography as the film thickness determines nm-scale line dimension. The growth is performed at 700°C in a high temperature furnace with an Ar flow of 130-150 sccm and O2 flow of 8-10 sccm. The vapor pressure of the Zinc source is controlled by the flow of

gases and the source temperature. ZnO NWs were observed to grow from the cleaved/etched face of the multilayer structure in the selective area via VLS growth process. The NWs exhibited diameters between 10 to 30 nm and an aspect ratio over 20. The NWs were characterized by SEM, TEM and EDS studies. The diameter of ZnO nanowires can be adjusted by changing the thickness of Al2O3 thin film. Such an approach to control nanowire diameter and its selective growth can be the basis for the development of bottom-up growth of architectures and cast nm-scale lines in a shadow lithography process.

11:00 AM

A4, Piezoelectric and Electrical Properties of Solution Grown ZnO Nanorods: *David Scrymgeour*[1]; Thomas L. Sounart[1]; Neil C. Simmons[1]; Yun-Ju Lee[1]; Paul G. Clem[1]; Julia W. P. Hsu[1]; [1]Sandia National Laboratory

Zinc oxide is a technologically important material because it can be grown in a variety of methods and it possesses a wide range of interesting optoelectronic, pyroelectric, and piezoelectric properties. Because of these properties and the high surface to volume ratio, zinc oxide nanostructures are of great interest for the next generation applications in UV lasers, solar energy conversion, gas and biological sensors, and actuator materials. Piezoelectric zinc oxide nanocrystals are grown by solution techniques on highly textured Ag (111) films in patterned arrays. These ZnO nanocrystals form hexagonal crystal rods with diameters of 100-600 nm and heights of 400-1200 nm with their <0001> polar axis perpendicular to the substrate. The crystal polarity, which has an effect on the incorporation of impurities, the optical and electrical properties, and the reactivity to chemicals, was determined to be oriented [0001] by piezoelectric force microscopy studies. The strength of the piezoelectric response of individual nanorods was also examined and compared to measured values on thin films and single crystals. The nanorods were measured to have ~3 times larger piezoelectric response than a single crystal of ZnO with a resistivity of 266 ohm-cm and carrier concentration of 1.57×10^{14} cm^{-3}. It was found that the amplitudes varied from rod to rod and are not strongly correlated to nanorod height, radius, or embedding depth, which indicate another factor is responsible for the variation. Since the conductivity can strongly affect the measured piezoelectric coefficient, parallel measurements of the transport properties of the ZnO nanorods have been examined by conductive atomic force microscopy, and comparisons are made with thin film and single crystal ZnO. Additionally, dielectric spectroscopy investigations of arrays of oriented nanorods will be presented. The correlations between measured piezoelectric response and conductive properties of individual rods will be discussed. We thank D. C. Look for the ZnO single crystals and Hall measurements. Sandia is a multiprogram laboratory operated by Sandia Corporation, a Lockheed Martin Company for the United States Department of Energy's National Nuclear Security Administration under contract DE-AC04-94AL85000.

11:20 AM

A5, ZnO/ZnMgO Quantum Wells Embedded in Nanorods: *Andrey Bakin*[1]; Abdel-Hamid El Shaer[1]; Augustine Che Mofor[1]; Muhamed Aid Mansur Al-Suleiman[1]; Sergey Ivanov[2]; Johannis Stoimenos[3]; Andreas Waag[1]; [1]Technical University Braunschweig; [2]Ioffe Physico-Technical Institute of RAS; [3]Aristotele University

We present results on further improvements of the radical source molecular beam epitaxy (MBE) and vapour phase transport (VPT) for fabrication of ZnO and ZnMgO layers, nanorods and quantum wells. ZnO and ZnMgO layers have been grown using MBE on high-quality ZnO buffer layers and MgO buffer layers grown on (0001) sapphire substrates in a modified Varian Gen II MBE system. In-situ Reflection High-Energy Electron Diffraction (RHEED) was employed for the optimization of the ZnO and ZnMgO growth. We have also developed a novel advanced VPT approach. Sapphire, SiC and ZnO epiwafers were implemented as substrates for ZnO growth. Growth temperatures ranged from 600°C to 900°C. Reactor pressures were from 10 mbar to atmospheric pressure. We employed X-ray diffractometry, optical microscopy, scanning electron microscopy, atomic force microscopy, PL measurements and transmission electron microscopy to investigate the obtained samples. The influence of different growth parameters on the ZnO and ZnMgO growth and the evaluation of the set of growth parameters either for manufacturing of epitaxial layers or of nanostructures will be discussed. Finally we report on ZnO/ZnMgO quantum wells fabricated both on MBE grown epitaxial layers and embedded in the high quality VPT grown nanorods.

11:40 AM

A6, Catalyst-Free Two-Step Growth of Quasi-Aligned ZnMgO Nanorods and Their Properties: *Liping Zhu*[1]; Mingjia Zhi[1]; Zhizhen Ye[1]; [1]Zhejiang University

Recently, much work has been done to realize ZnO nanowires nanotubes, and nanorods. And as we known, doping in semiconductor materials with selective elements will offer an effective way to adjust their electrical, optical, and magnetic properties, which is important for practical applications. And by doping Mg in ZnO, the bandgap can be modulated for the realization of light-emitting devices operating in a wider wavelength region. ZnMgO alloy is also an important material to construct the heterojunction or superlattice to obtain high-performance LD and LED devices. In this work,Quasi-aligned ZnMgO ternary nanorods with sharp single-crystal tips were prepared by using thermal evaporation without catalyst. The growth progress included two steps, the formation of ZnO droplets firstly and then the formation of ZnMgO nanorods. XRD, FESEM, HRTEM and room temperature PL measurement were used to determine the structure and optical properties of the obtained products.The obtained ZnMgO nanorods with abruptly sharpened tips crystallized well as hexagonal with preferred orientation along c-axis and the Mg content is to be 5%. The nanorods are about 200 nm in diameter and the tips are 50 nm. A 190 mev blue shift of NBE emission has been achieved, which probably affords a valuable way in current effort to realize the ZnO-based optoelectronic and field emission nano devices.

Session B: III-Nitride Optoelectronic Devices

Wednesday AM Room: Presidents Hall IV
June 28, 2006 Location: Pennsylvania State University

Session Chairs: Russell Dupuis, Georgia Institute of Technology; Andrew Allerman, Sandia National Laboratories

10:00 AM Student

B1, Growth and Characterization of High-Performance III-N Avalanche Photodiodes Grown on Bulk GaN Substrates: *Jae Limb*[1]; Dongwon Yoo[1]; Jae-Hyun Ryou[1]; Wonseok Lee[1]; Shyh-Chiang Shen[1]; Meredith Reed[2]; Charles J. Collins[2]; Michael Wraback[2]; Drew Hanser[3]; Edward Preble[3]; N. Mark Williams[3]; Keith Evans[3]; Russell Dupuis[1]; [1]Georgia Institute of Technology; [2]US Army Research Laboratory; [3]Kyma Technologies, Inc.

GaN based PIN avalanche photodiodes (APDs) are prime candidates for high-sensitivity ultraviolet (UV) photodetection in a wide variety of critical applications. The development of GaN based APDs, however, has been hampered by high dislocation densities in the epitaxial layers grown on lattice-mismatched substrates and only a few reports have been made of true avalanche gain in GaN-based APDs. For these cases, device yield was extremely low. The high density of defects and dislocations commonly observed in heteroepitaxial III-N PINs can lead to a premature microplasma breakdown in the active region of the detector before the electric field in the depletion region can reach the bulk avalanche breakdown field. In order to minimize the dislocation density of the devices, we have grown GaN and AlGaN PIN avalanche photodiodes by metalorganic chemical vapor deposition on low-dislocation density (<10^5 cm^{-3}) "bulk" GaN *n*-type substrates (manufactured by Kyma Technologies). The structures were grown using EpiPure TMGa, TMAl, and NH3 and consisted of a 2-µm thick, Si-doped ([Si] = 10^{19} cm^{-3}) *n*-type layer, followed by a 0.2~0.3-µm thick, unintentionally doped ($n = 5\times10^{16}$ cm^{-3}) drift region topped with a 0.1-µm GaN:Mg ([Mg] = 5×10^{19} cm^{-3}) *p*-layer. The linewidth of X-ray rocking curve peak of the epitaxial layer had a tendency to replicate the linewidth of GaN substrates. AFM surface morphology showed smooth surface containing parallel aligned atomic steps. The RMS roughness of the APD structures was less than 0.2~0.3nm for 1x1 µm^2 scans. The devices were processed into 30µm diameter circular mesas by ICP etching using Cl_2/He carrier gases,

followed by SiO_2 passivation by PECVD. Ti/Al/Ti/Au and Pd/Au ohmic contacts were evaporated on *n*-layer and *p*-layer respectively. Typically, the breakdown voltage was between 80V and 90V. The reverse bias *I-V* characteristics of the devices measured in the dark exhibited a dark current and current density of $2x10^{-11}$A and $3.5x10^{-6}$A/cm^2, respectively, at ~82V, just before breakdown (~83V). To confirm avalanche breakdown, temperature dependent *I-V* measurements were carried out and the breakdown showed a clear positive shift with the increase of temperature from 313K to 353K to yield a temperature coefficient of 0.05 V/K. The sharp breakdown and temperature dependence confirms that the breakdown is by avalanche ionization. Finally, photocurrent and dark-current characteristics were compared at room temperature. The typical 50 µm device in the wavelength of 280 nm < λ < 370 nm exhibits a gain >80 at onset of breakdown. During the testing, no microplasma was visually observed and devices rolled into breakdown consistently over all wavelengths tested, suggesting no microplasma formation for the breakdown. Various characteristics related to APDs will be measured and reported.

10:20 AM Student

B2, MOCVD Growth of AlGaN Heterostructures and UV LEDs on Bulk AlN Substrates: *Zaiyuan Ren*[1]; Qian Sun[1]; Soon-Yong Kwon[1]; Jung Han[1]; Kristina Davitt[2]; Yoon-Kyu Song[2]; Arto Nurmikko[2]; Wayne Liu[3]; Joseph A. Smart[3]; Leo Schowalter[3]; [1]Yale University; [2]Brown University; [3]Crystal IS Inc.

Low dislocation (<1e4 cm^{-2}) bulk AlN substrate is promising in supporting closely-matched epitaxy of high-Al content AlGaN alloys for ultraviolet optoelectronics. In this paper we will present our study of MOCVD growth of AlN and AlGaN (Al>50%) on c-plane AlN substrates. Unlike the growth of AlGaN on sapphire substrates where surface kinetics is strongly mediated by the presence of a high density of dislocations, we observed more intrinsic behavior of heteroepitaxial growth. Homoepitaxial growth of AlN by MOCVD leads to atomically smooth surface with straight (over several microns), parallel monolayer steps separated according to off-axis angles. Heteroepitaxy of high-Al content AlGaN (down to 75%) on AlN leads to mostly coherent growth. Depending on the direction of miscut axis, we have also seen alternating atomic steps with saw-tooth like steps due to the difference of growth kinetics between the two adjacent manolayer edges. AFMs taken successively, in conjunction with in-situ reflectance study, suggest that three-dimensional island formation occurs as the Al content decreases below 60%. Symmetric x-ray rocking curve scans of 50% AlGaN indicate a reduction of around ten times in full-width at half maximum, from about 0.3° on sapphire to 0.036° on AlN. (The FWHM of AlN substrates is typically below 0.01°). Both compositionally graded superlattice and linear grading have been tested and the details of strain relaxation and its impact on structural quality will be presented. AlGaN MQWs were grown on both sapphire and AlN substrates to ascertain the optical quality. Room temperature photoluminescence measurement indicates, under identical excitation geometry, a typical improvement in PL intensity (at 290 nm) of five to ten times. Quantitative optical studies using time-resolved PL are under way and will be presented. Deep UV LEDs with emission wavelengths at 295 nm were grown on both AlN and sapphire substrates. Mesa structures were formed by dry etching and front contacts were made to n- and p-type AlGaN. I-V measurement indicates a distinct improvement in the turn-on behavior for devices on AlN substrates with a reduction in device impedance by a factor of three. Preliminary measurement of optical output of UV LEDs with bottom-emitting configuration, indicate that devices on AlN outperforms those on sapphire; the exact magnitude of improvement is under study given an absorption (more than a factor of 2) of AlN substrates in the 290 nm range. Unlike devices on sapphire where L-I curves normally saturate and slump with current injection (due to heating), the devices on AlN exhibit straight L-I behavior within the range (up to 1kA/cm^2) measured. We believe the improvement of device performance can be attributed to the low dislocation density and higher thermal conductivity of AlN substrates. The partial support from the DARPA SUVOS program is acknowledged.

10:40 AM Student

B3, Characterization of Green LED Structures with *p*-InGaN and *p*-GaN Layers: *Wonseok Lee*[1]; Jae Limb[1]; Jae-Hyun Ryou[1]; Dongwon Yoo[1]; Michael Stevens[2]; Sridhar Srinivasan[2]; Fernando Ponce[2]; Russell Dupuis[1]; [1]Georgia Institute of Technology; [2]Arizona State University

High-efficiency "true" green LEDs (emitting at ~550nm) are one of the key elements in realizing high-brightness RGB-based white-lighting systems. LEDs emitting at true green wavelengths have suffered from a low internal quantum efficiency (IQE) compared to blue- (InGaN) and red-emitting (InAlGaP) LEDs. This deficiency is believed to be related to the epitaxial materials quality and the fundamental structure of green LEDs. Because the InGaN quantum-well active region contains a high composition of indium, the active region has a reduced material quality and a larger accumulated strain. Fundamental effects also play a role in this reduced IQE, e.g., a reduced overlap of the electron-hole wave functions due to higher degree of piezoelectric-charge-induced field effects, etc. In addition, other effects can strongly impact InGaN materials with high indium content, e.g., detrimental annealing of the MQW active region during the growth of the *p*-type layers. In this study, the optoelectronic and structural characteristics of green LED and related structures employing *p*-GaN and *p*-InGaN layers were compared. Also, the microstructure and electronic structure of green LED MQW active regions with *p*-GaN and *p*-InGaN were characterized by novel characterization techniques. The growth conditions were calibrated to improve LED performance characteristics. Hall-effect measurements on *p*-type GaN and InGaN layers revealed a 300K free-hole concentration of ~$2x10^{18}$ cm^{-3} with mobility of ~7 cm^2/Vs for *p*-$In_{0.04}Ga_{0.96}N$:Mg layer grown at 840°C in nitrogen ambient, while a free-hole concentration of ~$5x10^{17}$ cm^{-3} with mobility of ~7cm^2/Vs for *p*-GaN:Mg layer grown at 930°C in hydrogen ambient. For the *p*-type layers employed in green LEDs, thermal annealing effects on the active region during the growth needs to be considered as well as the structural and electrical properties of the layer itself. For the LEDs with *p*-InGaN, only slight decrease in PL intensity was observed compared to similar structures grown without a *p*-layer. The EL spectra of the LEDs with *p*-InGaN show a peak longer than 590 nm (depending on the current level) at relatively lower current levels. Such peaks were not observed in the LEDs with *p*-GaN. The possible origin of this long-wavelength peak will be discussed. At higher current levels, the EL intensity of the LEDs with *p*-InGaN was much better than that of similar LEDs with *p*-GaN layers. The *I-V* characteristics of the diodes showed that the turn-on voltages of the LEDs with *p*-GaN and with *p*-InGaN were 2.5 and 2.8 V; however, the series resistance of the LEDs with *p*-InGaN is lower than that of ones with *p*-GaN. To study structural and optoelectronic characteristics of active region and related structures of green LEDs with *p*-InGaN and *p*-GaN layers, CL, XRD, TEM, and EH characterization were used and the results will be described in detail.

11:00 AM Student

B4, High Light-Extraction Efficiency in GaInN Light-Emitting Diode with Pyramid Reflector: *J.-Q. Xi*[1]; Alyssa J. Pasquale[1]; Jong Kyu Kim[1]; Hong Luo[1]; E. F. Schubert[1]; [1]Rensselaer Polytechnic Institute

The light-extraction efficiency of a light-emitting diode (LED) can be limited by total internal reflection inside the semiconductor particularly for devices with a planar structure. Light rays lying outside the escape cone are trapped inside the device. This strongly limits the light-extraction efficiency in LEDs. In this work, a pyramid-patterned reflector is used to increase the light-extraction efficiency of an LED by changing the propagation direction of the light reflected back from the reflector. The pyramid patterned reflector can enable light rays lying outside the escape cone to be extracted out from the device into free space. The device used in this work is a GaInN LED with emission wavelength 400 nm. An array of SiO2 pyramid is fabricated on p-type GaInN by wet chemical etching of a thick SiO2 layer. Each SiO2 pyramid has a base width of 3.5 µm and a height of ~ 1.0 µm. The spacing between pyramids is 2.5 µm. Silver is used as a reflective layer. A reference GaInN LED with planer Ag reflector is fabricated too. The GaInN LED employing the pyramid-patterned Ag reflector is demonstrated to have 14% light-output improvement compared with the LED with planar Ag reflector. The higher light output of the pyramid-patterned LED is attributed to enhanced light-extraction efficiency enabled by the 3-dimensional structure of the pyramid reflector.

11:20 AM Student

B5, Temperature Dependence of the Quantum Efficiency in Green and Deep Green GaInN/GaN Light Emitting Diodes: *Yufeng Li*[1]; W. Zhao[1]; Y. Xia[1]; M. Zhu[1]; T. Detchprohm[1]; E. F. Schubert[1]; C. Wetzel[1]; [1]Rensselaer Polytechnic Institute

The radiative recombination processes in group-III nitride heterostructures remain the subject of continued investigation in order to increase performance of high brightness light emitting diodes (LEDs). In particular, green LEDs employing active regions of GaInN/GaN quantum wells (QWs) reveal a strong drop in emission power performance when the emission wavelength is being extended beyond 500 nm. Also the external quantum efficiency (EQE) shows a strong dependence on the drive current. It is found that for typical operation current, EQE is only a fraction of its maximum value at low current. A detailed spectroscopic analysis is therefore warranted to identify the limiting mechanism and to enhance performance in next generation solid state lighting. Here we present a comparative study of EQE in three nominally identical green LED dies emitting near 520 nm. The samples exhibit distinctively different behavior of EQE as a function of current density. By help of a spectroscopic electroluminescence study at variable low temperature we analyze the diodes distinctive behavior. As the temperature is reduced from 297 K to 77 K, the spectra of all three samples follow the same trend: The peak intensity of the 520 nm emission increases until it reaches a maximum near 158 K. EQE here reaches its overall maximum. For lower temperatures, the intensity drops again significantly. For temperatures below 136 K, we find a strong secondary emission band at 390 nm. As a function of temperature, we observe further revealing features in the behavior of EQE. In all three samples, as the temperature decreases, the current of maximum EQE shifts to lower values. In parallel, the distinction of the samples in their high current performance gradually disappears and all perform very similar at the lowest measured temperatures. These findings lead us to conclude the following: The observation of a decrease of EQE with higher current density cannot be the consequence of a raised junction temperature. In such a case, EQE should reach its maximum at higher current densities, when the temperature is lowered. This is the opposite of the observation. The distinction of performance primarily at room temperature suggests that the loss mechanism is a temperature activated process that is not controlled by the primary parameters of the sample structure and the general growth conditions. Examples for such processes include carrier spillovers and hopping conduction into non-radiative recombination paths. Our findings will furthermore be complemented with low temperature cathodo-luminescence data. From this detailed analysis we anticipate to reveal further insights into the optimization needs of green and deep green LEDs.

11:40 AM Student

B6, Nitride-Based Type-II InGaN-GaNAs 'W' Quantum Well Gain Media at 420-550 nm: *Ronald A. Arif*[1]; Yik-Khoon Ee[1]; Nelson Tansu[1]; [1]Lehigh University

Here we present and analyze a novel III-Nitride gain media for LEDs and lasers capable of emission from ~ 450-nm up to ~ 550-nm with significantly improved electron-holes wavefunctions overlap (Γ_{e_hh} > 65-70%) by utilizing a novel type-II InGaN-GaNAs 'W' quantum well. The proposed type-II QW allows polarization engineering of the band lineup which suppresses charge separation in the active region, which in turn leads to significantly-improved transition matrix element and optical gain of the QW. Dilute-As (~2-8%) GaNAs materials, grown by MOCVD, exhibit a significant bandgap reduction resulting from dilute-As addition (2-8%) in the GaN lattice. Dilute As in the N-rich GaNAs leads to valence band hybridization, which significantly increases valence band offset, while leaving the conduction band unchanged. Type-II InGaN-GaNAs 'W' quantum well configuration can be formed by inserting a thin layer (~10-15 Å) of dilute-As (2-8 %) GaNAs between two InGaN QW layers (~25 Å and ~5-10 Å). Numerical model has been developed to study and optimize the type-II InGaN-GaNAs QW structure by employing Kane's model and k.p method for strained wurtzite semiconductors taking into account the polarization effect. For the case of gain media emitting at ~456-nm, thin $GaN_{0.98}As_{0.02}$ layer with thickness of 10-Å can be inserted between 25-Å $In_{0.18}Ga_{0.82}N$ QW and 5-Å $In_{0.18}Ga_{0.82}N$ QW layers to form type-II $In_{0.18}Ga_{0.82}N$-$GaN_{0.98}As_{0.02}$ QW with GaN barriers. The insertion of the thin GaNAs in the type-II QW structure causes heavy holes wavefunction to be primarily confined in the GaNAs layer, giving rise to a large overlap of ~ 69% with the electron wavefunction. In comparison, the type-I 30-Å $In_{0.18}Ga_{0.82}N$-GaN QW emitting at 465-nm has an overlap of Γ_{e_hh} < 24%. For gain media emitting at ~530-nm, an optimized type-II InGaN-GaNAs QW employing a graded In-content in the lower InGaN layers leads to a large Γ_{e_hh} overlap of ~ 69.9 %. As a comparison purpose, conventional type-I 30-Å $In_{0.26}Ga_{0.74}N$-GaN QW emitting at ~530-nm has a low Γ_{e_hh} overlap of only ~18%. In summary, the proposed type-II InGaN-GaNAs 'W' quantum well allows polarization field engineering of the electron and holes wavefunctions resulting in large Γ_{e_hh} overlap (> 65-70 %), which leads to significantly improved transition matrix element and optical gain of the QW in the 420-550 nm regime.

Session C: Narrow Bandgap Semiconductors

Wednesday AM Room: Conference Room 106
June 28, 2006 Location: Pennsylvania State University

Session Chairs: Brian R. Bennett, Naval Research Laboratory; L. Ralph Dawson, University of New Mexico

10:00 AM

C1, Carrier Recombination Kinetics in 2.3-2.4 μM InGaAsSb/AlGaAsSb QW Laser Heterostructures: *Dmitri Donetsky*[1]; Leon Shterengas[1]; George Kim[2]; Gregory Belenky[1]; Alex Gourevitch[1]; David Westerfeld[3]; Ray Martinelli[2]; [1]Stony Brook University; [2]Sarnoff Corporation; [3]Power Photonic Corporation

Development of Type–I GaSb-based diode lasers with wavelengths up to 2.8-μm with hundreds of mW output power at room temperature was reported recently[1]. This result encourages optimization of heterostructure growth and study of carrier recombination processes for better understanding phenomena limiting the device output parameters. This work presents the carrier lifetime data obtained by time-resolved photoluminescence in sets of 2.3-2.4-μm laser heterostructures grown with different amount of compressive strain in the multiple-quantum-well regions. The PL decays were measured with sub-ps time resolution obtained by wavelength up-conversion. The excess carrier generation and optical gating were performed by a 150-fs mode-locked Nd: glass solid-state laser (SSL) with the emission spectrum centered at 1058 nm. Pumping at ~ 1 μm provides the optimal matching of the laser photon energy to the absorber bandgap resulting in excess carriers with low initial energy. Besides the SSL wavelength lays outside of the photomultiplier tube sensitivity range providing a low dark count rate. We have designed and fabricated type-I InGaAsSb QW lasers with two and four QWs located in the middle of the broadened waveguide. Laser 1 had two 11.5-nm thick 1.2% compressively-strained QWs spaced by 200-nm. Laser 2 had had two 12-nm thick 1.7% compressively-strained QWs spaced by 45 nm. Laser 3 had had four 12-nm thick 1.6 % compressively strained QWs spaced by 45-nm. The QWs were enclosed in a 800-nm-thick $Al_{0.25}Ga_{0.75}As_{0.02}Sb_{0.98}$ waveguides. The cladding layers were 2-μm-thick $Al_{0.9}Ga_{0.1}As_{0.07}Sb_{0.93}$ doped with Te (n~$2x10^{17}cm^{-3}$) and Be (p~$1\text{-}5x10^{18}cm^{-3}$). The wafers were processed into oxide-confined gain-guided lasers and cleaved into 1-mm-long cavity devices. The effect of compressive strain on laser differential gain have been studied previously and was associated with decrease of the heavy hole in-plane effective mass. The latter brings quasi-Fermi levels closer to band edges decreasing threshold carrier concentration. Change of the heavy hole dispersion associated with different compressive strain can affect the Auger recombination coefficient. The initial carrier relaxation rate in heavily strained QWs was found to be slower than that in moderately strained QW. As carrier concentration decreases the difference in relaxation rates for two structures tends to vanish. This observation allows speculating that in heavily strained laser heterostructures the Auger recombination coefficient is lower. We demonstrated that increase of the InGaAsSb QW compressive strain from 1.2 to 1.7% improves carrier lifetime and device differential gain and thus decreases laser threshold current. Nearly two-fold decrease in the threshold current was demonstrated. This work was supported by the United States Air Force Office of Scientific Research, Grants No. FA95500410372 and

FA955004C0021 and NY State Center for Advanced Technology (Sensor CAT). [1]L.Shterengas, G.L.Belenky, J.G.Kim, R.U.Martinelli, "Design of high-power room-temperature continuous-wave GaSb-based type-I quantum-well lasers with λ>2.5μm," Semicond. Sci.Tech., 19, 655 (2004).

10:20 AM

C2, Electron and Hole Energy Relaxation in InGaAsSb/InAs/InGaSb Type-II QW Laser Heterostructures: Leon Shterengas[1]; Andrew Ongstad[2]; Ron Kaspi[2]; Serge Suchalkin[1]; Gregory Belenky[1]; Michail Kisin[1]; *Dmitri Donetsky*[1]; [1]Stony Brook University; [2]Air Force Research Laboratory

High-power semiconductor lasers operating within spectral range from 3 to 5 μm are of special importance for a variety of military and civilian applications including systems for infrared countermeasures. Optically-pumped Type-II GaSb-based lasers with integrated absorber (IA) are within the most promising candidates for development of devices with advanced operating characteristics.[1] IA W-QW GaSb-based lasers with present design of the active region suffer from excessive temperature sensitivity of the device operating parameters precluding their high-power continuous-wave room-temperature operation. It is often assumed that the reduced value of optical matrix element associated with spatially indirect optical transition decreases the device differential gain thus leading to the high threshold carrier concentration and, hence, high Auger recombination rate. However, we recently performed direct comparison of the absorption spectra of type-I and type-II structures and found no significant difference in saturation gain for these two systems.[2] The source of temperature sensitivity of the type-II laser performance can indeed be related to some strong nonradiative recombination process though its nature and exact mechanism of its triggering at high temperatures still remains unclear. The plausible scenario includes temperature degradation of the device differential gain due to thermal population of the lower hole subbands with large density of states. In this work, we performed direct measurement of the electron and hole capture efficiency in IA W-QW laser heterostructures. We studied W-QW (6 InAs/InGaSb/InAs QWs) samples as well as samples with only electron QWs (6 InAs QWs) and only hole QWs (14 InGaSb QWs). In all samples the active QWs were separated by 100 nm of $In_{0.2}Ga_{0.8}As_{0.18}Sb_{0.82}$ IA layers. The capture efficiency was experimentally characterized by measurement of the time resolved photoluminescence (PL) from InGaAsSb IA layers. PL relaxation in picosecond range was studied by ultrafast photoluminescence up-conversion technique. Difference between electron and hole relaxation rates will be discussed. This work was supported by the United States Air Force Office of Scientific Research, Grant No. FA95500410372, Army Research Office, Grant No. DAAD190310259 and NY State Center for Advanced Technology (Sensor CAT). [1]R. Kaspi, A. Ongstad, G. C. Dente, J. Chavez, M. L. Tilton, and D. Gianardi, "High power and high brightness from an optically pumped InAs/InGaSb Type II midinfrared laser with low confinement", Appl. Phys. Lett. 81, 406 (2002). [2]S. Suchalkin, L. Shterengas, M. Kisin, S. Luryi, G. Belenky, R. Kaspi, A. Ongstad, J.G. Kim, R.U. Martinelli, "Mechanism of the temperature sensitivity of mid-IR GaSb based semiconductor lasers," Appl. Phys. Lett. 87, 041102 (2005).

10:40 AM

C3, Improved Properties of MOCVD Grown InAs/GaSb Superlattices on (001) GaSb Substrate by Introducing an InAsSb Layer at the Interfaces: *Xue-Bing Zhang*[1]; C. Xu[2]; Shin Mou[2]; Jae-Hyun Ryou[1]; K. C. Hsieh[2]; Shun-Lien Chuang[2]; Russell Dupuis[1]; [1]Georgia Institute of Technology; [2]University of Illinois at Urbana-Champaign

InAs/GaInSb superlattices (SLs) have been considered as the next generation mid-infrared (IR) photodetector because of their superior properties in comparison with the conventional HgCdTe and the intersubband quantum-well IR photodetectors. Due to the Type-II band alignment nature in this system, the Auger recombination coefficient can be significantly reduced and this is especially important for realizing the high performance IR detectors at room temperature. Also, the band-to-band tunneling current is intrinsically small due to the smaller electron effective mass. Furthermore, the InAs/GaSb SLs have the flexibility in bandgap engineering, which enables one to design the bandgap over a wide IR range. When properly designed, these Type-II SLs are predicted to have absorption coefficients comparable to that of HgCdTe materials. So far, the InAs/GaAs type II SL photodetectors reported were mainly grown by molecular beam epitaxial (MBE). Reports on the metalorganic chemical vapor deposition (MOCVD) growth of InAs/GaSb detector structures are quite scarce in the literature. We have recently investigated the MOCVD growth of InAs/GaSb SLs on GaAs substrates by introducing a low-temperature GaSb buffer layer. By using this technique and though optimizing the growth condition, we have realized 100-period SLs with optical and structural properties comparable to those high quality SLs grown by MBE. Due to the large lattice mismatch between GaAs/GaSb, threading dislocation with a density as high as $1x10^8$ cm^{-2} are found in the SL structures. These dislocations are detrimental to the device performances. Therefore, we consider GaSb as the substrate for the InAs/GaSb SLs growth. However, the build-up of the tensile stress which deteriorates the quality of the SLs is found when the number of layer in the SL increases. Using a monolayer-thick compressively strained InSb layer at the InAs/GaSb interface has been found successful in improving the structural quality of the SLs in MBE growth but not successful in our MOCVD growth, and we have attributed this to the higher growth temperature for InAs/GaSb SLs in MOCVD growth. Here, we report on the growth of InAs/GaSb SLs on (001) GaSb substrates by introducing a thin compressively strained InAsSb layer at the interfaces to counterbalance the tensile strain in the InAs layers. Atomic force microscopy (AFM), X-ray diffraction (XRD), and transmission electron microscopy (TEM) are used to characterize the grown structures. Effects of interface layer thickness, composition, and V/III ratio on the morphology, structural and optical properties of the SLs are systematically investigated. Generally, a cross-hatch structure is observed on the surface of SLs wafers grown without the InAsSb interface layers; however, with these layers, the surface becomes very smooth, also the structural properties are greatly improved when the interface layer is optimized.

11:00 AM Student

C4, Effects of Ga and Sb Precursor Chemistry on the Alloy Composition in Pseudomorphically Strained GaAsSb Films Grown via Metalorganic Vapor Phase Epitaxy: *A. A. Khandekar*[1]; J. Yeh[1]; L. J. Mawst[1]; Xueyan Song[1]; S. E. Babcock[1]; T. F. Kuech[1]; [1]University of Wisconsin

GaAs-based heterostructures comprised of $GaAs_{(1-x)}N_x$-$GaAs_{(1-y)}Sb_y$ ($x \leq 0.03$, $y \leq 0.35$) multiple quantum wells (MQW), utilizing 'W'-shaped type II transitions, have potential for realizing high-performance monolithic VCSELs and low temperature-sensitivity edge-emitting lasers in the 1.55 μm wavelength region. For long emission wavelengths, a high Sb content is desired in the thin GaAsSb layers. However, 'lattice latching' effects, in principle, limit the Sb concentration in growth of pseudomorphic GaAsSb layers on GaAs. MOVPE growth of GaAsSb is further complicated by the kinetic effects arising due to incomplete thermal decomposition of methyl- and hydride precursors at lower growth temperatures. Hence, a study was conducted to determine the effect of Ga and Sb precursor chemistry on Sb incorporation efficiencies in relaxed and strained GaAsSb films. Relaxed GaAsSb films and four-period pseudomorphic GaAsSb/GaAs superlattice (SL) samples were grown via MOVPE at 530°C. Both trimethyl- and triethyl-gallium (TMGa and TEGa) and trimethyl- and triethyl- antimony (TMSb and TESb) were used as Ga and Sb precursors, in a variety of combinations. Sb/Ga precursor ratios of 1.54, 4.64 and 4 were used for the TMGa-TMSb, TEGa-TMSb and TEGa-TESb chemistries, respectively. Sb content in relaxed and strained GaAsSb films was determined as a function of the gas-phase AsH_3/III ratio using x-ray diffraction θ-2θ scans coupled with dynamical simulation models. Sb incorporation efficiencies for relaxed GaAsSb films increased with decreasing AsH_3/III ratio, and films with Sb content of 63% were grown using TEGa-TMSb chemistry at AsH_3/III ratio of 1.65. Sb incorporation efficiencies for strained films were always lower compared to the relaxed films under identical growth conditions. In the case of TMGa-TMSb chemistry, AsH_3/III of 0.79 resulted in 33 and 21% Sb incorporation in relaxed and strained films, respectively. For the TEGa-TESb chemistry, Sb content in strained films was held constant either at 29 or 12% for AsH_3/III ratio variation between 2 and 6, while the relaxed film Sb content increased monotonically from 17 to 53%. This difference in Sb content between the strained and relaxed films, along with the observed compositional pinning of the GaAsSb thin films could be explained by the strain-induced lattice latching of growing crystal. The precursor chemistry can influence Sb incorporation via the site-blocking or steric effects for specific surface species produced by different precursors. Ethyl-based precursors with relatively low decomposition temperatures produce elemental species on the growth

surface resulting into higher Sb incorporation. For example, the TEGa-TESb chemistry allowed lowering of the growth temperature to 485°C resulting in a 48% Sb incorporation in strained layers. Such changes in the growth chemistry allow for a good control on the Sb content in strained layers and hence an extended range of wavelength in type II MQW structures.

11:20 AM Student
C5, Island Size and Development of Systematic Crystallographic Tilt during Growth of InAs on (100) GaAs Substrates: *Suryanarayanan Ganesan*[1]; Anish A. Khandekar[1]; Manish Rathi[1]; Joshua Webb[1]; Thomas F. Kuech[1]; Susan E. Babcock[1]; [1]University of Wisconsin-Madison

The development of devices based on InAs, GaSb and AlSb, semiconductors that possess narrow band gaps and 0.61nm lattice parameters, has been limited by the defects that ensue in epitaxial films that typically are grown on commercial semi-insulating, but 7% lattice-mismatched, GaAs substrates. This study explores the development of microstructure during the transition from the pseudomorphic growth exhibited in quantum dots to strain-relaxed film growth using InAs on GaAs as a model. For a range of growth conditions, InAs films on GaAs substrates exhibit not only the threading dislocations characteristic of largely mismatched epitaxial films, but also systematic tilting within micron-scale InAs domains. Alteration of the pattern and magnitude of the tilt achieved by varying the growth conditions and/or introducing mask-patterned substrates suggest that not only chemical and kinetic, but also physical, constraints can direct microstructural evolution during growth. Back scattered electron Kikuchi pattern analysis, SEM imaging, and atomic force microscopy were used to characterize the shape of and local tilt within InAs islands as a function of the island size. Islands showed characteristic morphology and tilt behavior associated with three different island size regimes. Islands ≤ 1μm in lateral extent were equiaxed, either pyramidal or dome-shaped, bound by combinations of (111) and (110) facets, and aligned crystallographically with the substrate. Isolated islands 1μm–2μm in lateral extent developed diamond shaped footprints elongated along [0-11], irregularly stepped surfaces, and a width to height ratio of order 4. They also developed sub-sections, each tilted approximately 3° to the GaAs about the four in-plane <110> directions in a pattern that repeated from island to island. Isolated islands with lateral dimensions of > 2μm retained the morphology of diamond shaped islands, albeit with larger aspect ratio and additional surface roughness that outlined six distinct volumes within the island. The InAs [100] in each of these six subsections was tilted approximately 4° away from the surface normal and toward the nearest edge of the island. A model proposed by Spencer and Tersoff for introduction of 60° misfit dislocation with specific [100] components at the edges of larger islands is in quantitative agreement with the observed pattern of tilt observed in both island size ranges.[1,2] The tilt pattern observed in islands grown on mask patterned (lateral epitaxial overgrowth, LEO) substrates that constrain growth in one or more directions further support the conclusion that tilt is caused by compressive stresses that amass as the island size increases. These stresses cause a non-zero [100] component of net burgers vector of the mismatch array develop as the island grows, and, consequently, tilt, as described by Spencer and Tersoff. [1]B.J. Spencer and J. Tersoff, Appl. Phys. Lett. 77, 2533 (1997).[2]B.J. Spencer and J. Tersoff, Phys. Rev. B63, 205424 (2001).

11:40 AM Student
C6, Growth Mechanisms for InAs Deposition on Low Index GaAs Substrates by Metalorganic Vapor Phase Epitaxy: *A. A. Khandekar*[1]; J. Webb[1]; G. Suryanarayanan[1]; M. Rathi[1]; S. E. Babcock[1]; T. F. Kuech[1]; [1]University of Wisconsin-Madison

InAs is a narrow band gap semiconductor with applications in high-speed electronic and infrared optoelectronic devices. Due to the lack of lattice-matched, high resistivity substrates, InAs films are often deposited on semi-insulating (100) GaAs. The large lattice mismatch between two materials leads formation of 3D InAs islands very early during the growth. High densities of misfit-related defects are observed in InAs films grown on (100) GaAs. Growth on non-(100) substrates has been explored as a means to reduce the defect density. InAs surface morphology, strain relaxation and resultant defect microstructure is dependent on the orientation of the growth plane. Hence, studying InAs growth mechanisms on alternative, low index planes is important for development of new device structures. InAs films were grown via MOVPE on six GaAs substrate orientations: (100), (111)A, (111)B, (110), (211)A and (211)B. The dependence of InAs growth rate and surface morphology on the growth temperature and the trimethyl indium and arsine gas phase concentrations was determined. The growth rate increased linearly by ~50% for (100) planes between 400 and 800°C; the growth rate on other planes increased by ~20% over the same temperature range. The slow increase in growth rate with temperature indicates a reactant-transport limited growth mechanism. The highest growth rate was observed on the (100) plane. Growth was slowest on the (111)A plane, indicating some effect of the plane-specific growth chemistry. The growth rate increased linearly with TMIn concentration at a constant arsine flux, and was independent of arsine flux. The morphology and root-mean-square (RMS) roughness of InAs films showed a strong dependence on the substrate orientation and growth temperature. Low growth temperatures (<500°C) and low V/III ratios, which promote coalescence of small-sized islands gave rise to smooth InAs films with RMS roughness ~20nm for the (100)-growth. InAs growth on (111)A GaAs proceeds via layer-by-layer mode and smooth films with RMS roughness of ~5nm were obtained for all growth conditions. Film morphology for (110) substrates changed from a cross-hatch pattern at low growth temperatures to an elongated step-like grain structure at 600°C. The grain size increased with growth temperature, leading to smoothening of films at 800°C. InAs films on (111)B substrates also showed a crosshatch morphology transitioning to a triangular grain structure with increasing growth temperature. The individual (111)B 'grains' had smooth top surfaces with RMS roughness of ~6nm. These changes in morphology are attributed to variations in the bonding arrangements, diffusivities and coverages of surface adatoms with temperature. Arsine decomposition to elemental arsenic is known to be partially complete up to 650°C, which coincides with the morphology transitions. The findings of this study could translate into newer growth strategies on non-(100) GaAs substrates for making low defect density InAs films.

Session D: Fun with Nanostructures

Wednesday AM — Room: Conference Room 208
June 28, 2006 — Location: Pennsylvania State University

Session Chairs: Glenn S. Solomon, National Institute of Standards and Technology; Ben Shanabrook, Naval Research Laboratory

10:00 AM
D1, Structural and Optical Studies of Quantum Dot Molecules: *Valeria G. Stoleru*[1]; Anup Pancholi[1]; William Kerr[1]; Hassan Shah[1]; [1]University of Delaware

InAs/GaAs quantum dot molecules formed by pairs of electronically coupled quantum dots have been identified as suitable candidates for a number of applications in the Terahertz regime by using their intraband carrier transitions. By adjusting the dot size, shape, and composition under appropriate growth conditions, the atomic-like optical and electronic properties of the dots can be tailored. Drastic modifications of the basic features of single layer dot assemblies occur in both the growth patterns and physical properties as soon as the thickness of the GaAs barrier layer is reduced to a few nm, so as to induce a strong coupling between vertically adjacent dots.We provide here a detailed theoretical and experimental structural and optical analysis of the coupling effects in InAs/GaAs quantum dot molecules in which the GaAs barrier thickness is varied between 2 and 10 nm. In the end, we propose a quantum cascade structure consisting of InAs/GaAs quantum dot molecules embedded in InGaAs quantum wells. The underlying rationale for our studies is to provide a basis for the development of a new type of quantum cascade emitters based on intraband electron transitions within the conduction band in quantum dot molecules.

10:20 AM Student
D2, Fluorescence Intermittency of Localized Excitons in CdSe Nanowires: *Vladimir Protasenko*[1]; Masaru K. Kuno[1]; [1]University of Notre Dame

Quantum-confined CdSe nanowires have been synthesized using solution-liquid-solid growth with Au/Bi core/shell nanoparticles as seeds. Transmission electron microscopy of chemically grown CdSe nanowires (NWs) reveals their a) high quality/crystallinity, b) narrow diameters (5 to 10 nm) leading to weak/intermediate exciton confinement (~5.6 nm bulk exciton Bohr radius, CdSe), and c) zinc-blende/wurtzite sectioning along the NW length suggesting a Type II electronic potential as well as strong spontaneous polarization within wurtzite segments. These properties begin to rationalize fluorescence intensity/spectral heterogeneity along the length of a single NW as well as the fluorescence intermittency observed in both confocal and epi-fluorescence experiments. A qualitative model which explains these phenomena includes the effect of exciton localization in Type II disordered potentials, variations in the exciton binding energy caused by fluctuations of the local dielectric constant, interactions of localized excitons with trapped and free electrons/holes, and the electron passivation of surface defects.

10:40 AM

D3, Discrimination of Isoelectronic Centers and Type-II Quantum Dots with ZnTe Embedded in ZnSe: *Masafumi Jo*[1]; Michiaki Endo[1]; Hidekazu Kumano[1]; Ikuo Suemune[1]; [1]Hokkaido University

Recently semiconductor-based single photon sources have been intensively studied due to the long-term stability and compatibility with integrated devices. Self-assembled quantum dots (QDs) are one of the most investigated solid-state systems with their narrow emission line close to the Fourier-limit at low temperature. Each single photon emitted from QDs, however, has a unique emission wavelength and radiative lifetime due to size variation of QDs, which makes it difficult to use more than two single photon sources together. In the context of emission wavelength the impurity-bound excitons in semiconductors have superior property to the QDs. The emission wavelength of excitons localized at impurities is identified as the combination of the impurity species and the host semiconductor. Ten isoelectronic centers (ICs) in ZnSe are such well-known radiative defects emitting around 470 nm. Interestingly, an increase in Te deposition will lead to formation of type-II ZnTe QDs, which offers a unique possibility of controlling the nature of emitted single photons in a unitary solid-state system. In this work we studied variation of Photoluminescence (PL) origin from isoelectronic traps to type-II quantum dots with growth conditions. A smooth shift of PL peak dominance from 470 nm to 510 nm was observed with increasing ZnTe layer thickness, implying the evolution from ICs to QDs.

11:00 AM

D4, Thermoelectric Properties of Vertically Aligned InAs/GaAs Quantum Dot Superlattices: *Abhishek Yadav*[1]; Kevin Pipe[1]; Weifeng Ye[1]; Rachel S. Goldman[1]; [1]University of Michigan

It has been shown that 1D quantum confinement in structures such as nanowires and nanowire superlattices can lead to better thermoelectric figure of merit (ZT) than bulk materials. However, nanowires are difficult to implement in practical devices due to issues with electrical contacts, structural weakness, and alignment. Quantum-Dot Superlattices (QDS), on the other hand, do not suffer from these difficulties because the quantum-confined dots are fabricated within a matrix that provides structural support. The aim of this work is to show that QDS that are grown such that the dots are vertically or laterally aligned to form QD "chains" can have greatly enhanced thermoelectric properties due to 1D carrier transport along the QD chains, analogous to transport in nanowire superlattices[1]. Here we investigate the effects of quantum confinement and miniband transport on thermoelectric performance in aligned InAs/GaAs QDS. For a large thermoelectric figure of merit ($ZT=S^2\sigma/k$, where k is the thermal conducivity), we want a large number of minibands (for high electrical conductivity σ) distributed asymmetrically around the Fermi level (for high Seebeck coefficient S). Perpendicular to the chain, the dots are modeled as a finite quantum well, giving rise to energy subbands. This 1D model is then coupled to a 1D model for transport along the chain, using these subbands to calculate miniband dispersion using Kronig-Penny model. In nanowires, due to the infinite quantum well potential perpendicular to the wire, the number of subbands remains constant. On the other hand, for QD chains, the finite quantum well potential leads to a QD size-dependent number of subbands. As a first approximation, we assume negligible doping of the matrix and consider only miniband transport. We find a general trend of a large increase in thermoelectric power factor $S^2\sigma$ in the direction of alignment as the dot size decreases. This size decrease causes decreased electrical conductivity due to a decrease in the number of subbands and a shift in the minibands to higher energy levels. However, this effect is outweighed by a large increase in the Seebeck coefficient due to an increase in the asymmetry of the density of states about the Fermi level. In addition, oscillations in ZT are observed with decrease in lateral dot size due to interplay between inter-miniband spacing, density of states, miniband width, and number of subbands. A maximum increase of a factor of 2.5 in ZT over bulk GaAs and a factor of 4 in $S^2\sigma$ over bulk InAs is predicted. [1]Lin Y. M., Dresselhaus M. S., "Thermoelectric properties of superlattice nanowires", Physical Review B, 68, 075304, (2003).

11:20 AM Student

D5, Fabrication of High Frequency Ultrasound Transducers: *Hyunsoo Kim*[1]; Sungkyu Park[1]; Ioanna Mina[2]; Insoo Kim[3]; S. Bharadwaja[2]; X. Li[4]; Kyusun Choi[3]; Susan Trolier-McKinstry[2]; Richard Tutwiler[5]; Theresa S. Mayer[4]; Thomas N. Jackson[1]; [1]Pennsylvania State/Center for Thin Film Devices and Materials Research Institute; [2]Pennsylvania State/Material Science and Engineering; [3]Pennsylvania State/Computer Science and Engineering; [4]Pennsylvania State/Electrical Engineering; [5]Pennsylvania State/Applied Research Laboratory

Ultrasound transducers are widely used in biomedical imaging and acoustic microscopy. For these applications, sound waves are both generated and detected by piezoelectric transducers. Focusing of the acoustic wave can be accomplished electrically if arrays of piezoelectric elements spaced at half the acoustic wavelength can be addressed individually. The ultimate resolution of the imaging system is a function of frequency, with higher frequency devices yielding better resolution. At present, the frequency range of single element transducers for imaging skin or eye ailments is 30 ~ 50 MHz; most abdominal and cardiac transducer arrays are still in ~5MHz range. Arrays of fine-pitch piezoelectric elements can raise the frequency of the device and provide improved image resolution for medical applications. However, as transducer size decreases, close-coupling of the electronics is necessary. The work reported here is focused on the fabrication of high frequency (>50 MHz) piezoelectric transducer arrays using micromachining and thin film processing. Essential to the development is the need to prepare closely spaced, high aspect ratio piezoelectric structures. Lead zirconate titanate (PZT) was chosen as the piezoelectric due to its high sensitivity and wide achievable bandwidth. We demonstrate two different approaches for making PZT transducer arrays. The first approach uses vacuum infiltration of pre-patterned Si molds using chemical solutions. Vertically aligned LaNiO3/PZT/Pd microtubes (diameters <2 μm) have been prepared via sequential deposition of the individual layers with LaNiO3 used as a conducting oxide electrode for electrical interconnections.[1] After infiltration of all of the layers, the Si template is removed by XeF2 etching. Alternatively, tall metal post arrays are first prepared by electroplating in SU8 photoresist templates and then coated with the piezoelectric PZT layer by mist deposition. This approach has the advantage that the electroplated post, typically Ni, can also be used as a transducer electrode. Typical post diameter and height are 10 μm and 50 μm with deposited PZT thickness typically <1 μm. The thin PZT section obtained by either infiltration or post coating allows low voltage operation of the piezoelectric transducer, typically < 5 V and compatible with standard CMOS circuits. [1]Fabrication of high aspect ratio ferroelectric microtubes by vacuum infiltration of macroporous silicon templates,S. S. N. Bharadwaja et al, Journal of the american ceramic society, 2005.

11:40 AM

D6, Electron Energy Levels in ZnSe:Mn Quantum Dots: *Shailaja Mahamuni*[1]; Amit D. Lad[1]; Shashikant P. Patole[1]; [1]University of Pune

The electron energy levels of transition metal Mn^{2+} in variety of semiconductors constitute a new class of materials called as diluted magnetic semiconductors (DMS). DMS quantum dots have received special attention due to unique set of properties such as high photoluminescence, substantially faster luminescence decay etc. Here, we report our investigations on ZnSe quantum dots doped with Mn emphasizing the variation in Mn related electron energy levels in ZnSe quantum dot matrix. ZnSe quantum dots doped with Mn were prepared by wet chemical route using tetra-octyl phosphine (TOP) and hexa-decyl amine (HDA) as capping agents and with size distribution less than 10%. Detailed optical studies were carried out for Mn doped ZnSe

quantum dots with size of about 2.7 nm. The blue shifted optical absorption appears at about 400 nm. Phase of the quantum dots was zinc blende as monitored by x-ray diffraction. Size distribution of Mn doped ZnSe quantum dots is found to be narrower compared to that of undoped ZnSe nanoparticles as revealed from the sharper optical features. Photoluminescence emission (PL) and photoluminescence excitation (PLE) spectra were recorded at 10 K. Studies were also carried out with the temperature variation within a range from 300 K to 10 K. Band edge luminescence was blue shifted from 430 nm to 420 nm while Mn orange luminescence was red shifted from 579 nm to 583 nm for 5% Mn doped ZnSe quantum dots with decrease in temperature. For all other concentrations, similar effect was observed. PL intensity increases for band edge as well as orange luminescence as temperature decreases. Variation in relative intensity of band edge luminescence and Mn luminescence with change in concentration indicate that both the processes are competing in PL spectra. Moreover with increase in concentration of Mn in ZnSe causes redshift in $^4T_1$—>$^6A_1$ due to enhanced exchange interaction effects. However, ferromagnetism was not observed for ZnSe:Mn quantum dots at any doping level. Photoluminescence excitation recorded at Mn related emission of 580 nm showed four different absorption features attributable to Mn $^6A_1$—>$^4T_1$, $^6A_1$—>$^4T_2$, $^6A_1$—>$^4A_1$, and $^6A_1$—>^{4}E. Transitions $^6A_1$—>$^4T_1$ and $^6A_1$—>$^4T_2$ show red shift in ZnSe:Mn quantum dots as compared to the bulk material. This fact was attributed to a small increase of p-d hybridization in Mn doped ZnSe quantum dots. Furthermore, absence of ferromagnetism also indicates rather weak p-d hybridization.

Session E: Nitride and Oxide Nanowires

Wednesday AM — Room: Conference Room 207
June 28, 2006 — Location: Pennsylvania State University

Session Chair: Joan M. Redwing, Pennsylvania State University

10:00 AM

E1, Polarization-Resolved Photoluminescence Study of Isolated GaN Nanowires Grown by Catalyst-Free MBE: *John B. Schlager*[1]; Norman A. Sanford[1]; Kris A. Bertness[1]; Joy M. Barker[1]; Alexana Roshko[1]; Paul T. Blanchard[1]; [1]National Institute of Standards and Technology

Polarization- and temperature-dependent photoluminescence (PL) measurements were performed on individual GaN nanowires grown by catalyst-free molecular beam epitaxy on Si(111) substrates. The c-axis lattice constant (0.518 46 ± 0.000 05 nm) for these wires, measured with x-ray diffraction, matched that of strain-free bulk GaN. The wires were typically 5-10 mm in length, c-axis oriented, and 30 - 100 nm in diameter. Mostly wire diameters were uniform over the entire length with cross sections displaying a hexagonal growth habit with sides conforming to the prismatic planes. These wires were ultrasonically removed from the growth substrate and dispersed onto sapphire substrates to enable PL measurements on individual wires with a *k* (pump light) perpendicular to *c* (wire axis) geometry. Polarized and unpolarized PL spectra were collected from several dispersed nanowire samples. Strong near-band-edge emission occurred within 1 meV of energy peaks associated with both free and bound excitons of strain-free GaN at low temperatures (< 5 K). For a typical sample, the donor-bound exciton D^0X_A peak dominated the spectrum at the stress-free position of 3.472 eV. Free exciton peaks X_A and X_B were evident and respectively located at 3.478 eV and 3.483 eV. The first phonon replicas of these dominant peaks occured over the spectral range of 3.38 eV to 3.39 eV. Evidence of the second phonon replicas appeared above the noise floor at around 3.29 eV. Other weaker peaks observed at 3.41 eV, 3.34 eV, and 3.21 eV may indicate excitons bound to surface or other structural defects. A peak at 3.43 eV was not yet assigned but was also observed in nanowire samples taken from separate growth runs. Broad blue luminescence centered around 2.9 eV was observed in PL spectra taken from the as-grown material, while no such emission was observed in the dispersed nanowires. This broad blue emission therefore is associated with the highly defective GaN "matrix" layer portion of the growth. No yellow luminescence (YL), which is widely reported to be associated with vacancy and structural defects in GaN films, was observed in the PL of individual nanowires. Polarized PL spectra differed for the σ (*E* perp. *c*, *k* perp. *c*) and π (*E*||*c*, *k* perp. *c*) polarization cases, illustrating the polarization anisotropy of the exciton emission associated with high-quality wurtzite GaN. This anisotropy in PL emission persisted even up to room temperature (4 K to 296 K). To the best of our knowledge, this is the first time such exitonic-polaritron anisotropy has been observed at room temperature for any type of wurtzite GaN. Additionally, the nanowire PL varied with excitation intensity and with (325 nm) pump exposure time. Further work is planned to isolate the effects of excitation intensity, light exposure, and nanowire sample preparation.

10:20 AM

E2, Structural Control and Characterization of GaN Nanowires: *Blake S. Simpkins*[1]; Pehr E. Pehrsson[1]; [1]Naval Research Laboratory

Our recent attention has focused on controlling nanowire (NW) structural properties (geometry and crystallinity) and NW assembly. These issues have been addressed through the use of electron beam lithography (EBL). EBL allows catalyst particles, and therefore the wires that will eventually grow from them, to be fabricated with position and size control with resolution of tens of nanometers. Although the size of EBL-defined dots has a lower limit of tens of nanometers, deposited film thickness may be controlled with sub-nm resolution. We have utilized this control, along with surface tension forces acting on the catalyst particles, to predictably control NW size. Structural characterization of these size-controlled NWs has been carried out using Raman microscopy. Results of this approach are described as follows and are further illustrated in the extended abstract material. Catalyst metal (Ni) is patterned with EBL resulting in metallic discs. Surface tension drives these discs to form spheres at the growth temperature where they catalyze the growth of GaN NWs through the vapor-liquid-solid mechanism. The thickness and radius of the initial catalyst disc are related to the radius of the final sphere through simple conservation of volume. This analytical prediction of final NW size and our experimental results are plotted in the supplementary material and show excellent agreement.We are currently studying the relationship between wire size and Raman signature. Bulk Raman spectra result from crystal symmetries. However, certain Raman mode selection rules are modified for nanoscale structures and may depend strongly on crystal properties such as NW radius and axial orientation. Initial Raman spectra, presented in the supplementary material, have been recorded and exhibit typical GaN signatures as well as peaks that are significantly shifted with respect to their bulk positions.

10:40 AM Student

E3, Experimental and Computational Modeling Studies of MOCVD Growth of GaN Nanowires: *Robert A. Burke*[1]; Daniel R. Lamborn[1]; Trevor E. Clark[1]; Elizabeth C. Dickey[1]; Joan M. Redwing[1]; [1]Pennsylvania State University

Single crystal GaN nanowires show promise as key components in future nanoscale devices including sensors and light emitters. GaN nanowires have been synthesized by metal-mediated vapor-liquid-solid (VLS) growth using techniques such as laser ablation, vapor transport, hydride vapor epitaxy, and most recently metalorganic chemical vapor deposition (MOCVD). MOCVD offers several advantages over other methods including the ability to control gas phase concentrations directly via precursor flow rates and the fabrication of heterostructures through the addition of Al and In metalorganic sources. However, thin film deposition of GaN can occur simultaneously with VLS growth resulting in the formation of tapered nanowires. A detailed understanding of the VLS growth process using metalorganic sources is required in order to identify conditions that maximize the nanowire growth rate over the thin film deposition. In this study, we have utilized a combination of experimental and computational fluid dynamics based reactor modeling studies to explore the effects of growth conditions on nanowire formation. The studies were carried out using an isothermal quartz tube reactor to provide a simplified computational geometry and enable direct comparison with prior experimental reports. GaN nanowires were grown by the VLS method utilizing a nickel thin film (1.25-5 nm) deposited on c-plane sapphire substrates. Trimethylgallium (TMG) and NH_3 were used as precursors with H_2 or N_2 as the carrier gas. A concentric tube inlet geometry was used to minimize pre-reactions between the TMG and NH_3. GaN nanowire growth

was obtained over a furnace temperature range of 800-900°C. Due to adduct formation and the extensive gas phase reactions that occur between TMG and NH_3, nanowire growth was found to be strongly dependent on the position of the substrate relative to the TMG inlet tube and the precursor flow rates in the reactor. Computational fluid dynamics modeling was used to simulate the thermal fluid conditions and gas phase concentration profiles in the reactor as a function of position under the experimental conditions. The modeling results demonstrated a maximum in the gas phase concentration of Ga and N-containing species which corresponded to the position in the reactor where nanowire growth was observed. Furthermore, by varying the NH_3 flow rate and carrier gas, the reaction zone broadens and is shifted further away from the gas inlet, consistent with the experimental observations of nanowire growth. Transmission electron microscopy was used to characterize GaN nanowires released from the substrate by ultrasonic agitation. The GaN nanowires varied in length (5-25 μm) and degree of tapering depending on the growth conditions. A nickel tip and triangular wire cross-section were typically observed at the end of the nanowires, consistent with the VLS mechanism.

11:00 AM

E4, Epitaxial Growth and Applications of Aligned GaN Nanowires: *Kyungkon Kim*[1]; Tania Henry[1]; George Cui[1]; Jung Han[1]; Yoon-Kyu Song[2]; Arto V. Nurmikko[2]; [1]Yale University; [2]Brown University

Nanowires are typically processed into nanodevices through solution dispersion and electrically accessed after contact metallization. This process presents inherent challenges in controlling the spatial ordering of final devices. While very promising results of FETs, LEDs, and sensors based on single nanowire devices have been reported, the lack of reliable means in bridging the gap between nanoscale active region and microscale physical interface remains a great hurdle for practical applications. In this paper we will discuss the possibility of using crystallographic alignment of nanowires, in conjunction with patterned surface and/or specially orientated substrates, to achieve spatial alignment of nanowires with enhanced functionality. Crystallographic information forms the basis in designing and selecting an epitaxial system. To test the idea of crystallographic alignment of nanowires epitaxially, we obtained a set of bulk AlN substrates that were sliced and polished with c-, a-, and m-plane orientations. These single crystalline substrates with a wurtzite structure provide a useful test concerning the role of substrate in nanosynthesis. Aligned GaN nanorods were found on both a- and m-planes with the catalyst tips clearly visible under SEM observation. Upon close examination, it was found that nanorods grown on a-plane AlN have mixed characters of a-axis and m-axis, while the majority (~90%) of the nanorods on m-plane were vertically aligned. Growth on c-plane AlN, on the other hand, showed the appearance of catalyst droplets and one-dimensional features (tails) confined to the in-plane directions, suggesting that anisotropic growth is preferred in directions perpendicular to c-axis. Analysis of the free energy of several low-index surfaces suggest that the presence of pyramidal side facets for a- and m-axis nanowires, in contrast to the need of prism facets for c-axis wires, help to stabilize the nanowire formation under catalytic synthesis. Having demonstrated the possibility of crystallographic alignment and established the preferential, non-polar growth directions for nanowires, we tested two different approaches in extending such ordered nanosynthesis toward useful applications. In the first example, we combined the technique of epitaxial lateral overgrowth (ELO) with nanowire epitaxy. ELO is known to form well-defined stripes or hexagons that can serve as electrically conducting bases upon which horizontally aligned nanowires emanate and interconnect with one another. Comb-like and hexagonal network of nanowires have been observed in which the number/density and location of the nanowires can be tailored conceivably by lithographical patterning of catalyst thin films. In the second example of exploring electrical pathways into nanotextured GaN nanowires, we have explored the possibility of conformal deposition of conducting polymer for a hybrid inorganic/organic structure. The optoelectronic properties of such a hybrid nanostructures will also be presented. This work was supported by Department of Energy (DOE) under Grant No. DE-FC26-03NT41941.

11:20 AM

E5, Growth and Characterization of Vanadium Oxide Nanowires: *Jongsun Maeng*[1]; Takhee Lee[1]; [1]Gwangju Institute of Science and Technology

Vanadium dioxide (VO_2) material shows a Mott metal-insulator transition (MIT) around 340K. Drastic change of resistance and optical properties from the MIT effect can be applied to electrical or optical switching device. Recently VO_2 materials have been grown as nanowire form by a simple vapor transport method[1]. In our study, VO_2 nanowires are fabricated at 900-1000°, a few sccm with Ar gas flow, and ~ 10 Torr for 5 hours by simply heating VO_2 powder without any metal catalysts. Growth of VO_2 nanowires depends on substrate type, silicon nitride or oxide layer. Although the growth mechanism is not yet clear, silicon nitride layer may act as a seeding material for VO_2 nanowire growth and some VO_2 nanowires are grown embedded in silicon nitride layer. The structural properties of the grown VO_2 nanowires were characterized by scanning electron microscopy (SEM), transmission electron microscopy (TEM), X-ray diffraction (XRD), X-ray photoelectron spectroscopy (XPS), etc. SEM images show that VO_2 nanowires were successfully grown with a diameter of 10's to 100's nanometers and a length up to ~ 10 μm. The nanowires are rectangular shapes from SEM images. TEM images and electron diffraction patterns show that VO_2 nanowires are single crystalline. XRD data shows that VO_2 nanowires are monoclinic and main peaks are (011) and (022), which suggests these nanowires have a preferential axial growth direction of [100]. To characterize the electrical properties of the VO_2 nanowires, we fabricated VO_2 nanowire field effect transistors by optical lithographies. The temperature-variable current-voltage characterization was performed to investigate the MIT effect of VO_2 nanowires. VO_2 nanowires in our study showed a gradual metal-insulator-transition at around 320-360°. It has been reported that the gradual transition effect may be attributed to the deviation of oxygen composition from VO_2 materials[2]. The gate-dependent field effects of VO_2 nanowires will be presented. [1]B. S. Guiton et al, J. Am. Chem. Soc. 127, 498-499 (2005).[2]X. Wu et al, Materials Research Bulletin, 40, 315-321 (2005).

11:40 AM Student

E6, Integration and Characterization of High Aspect Ratio Ferroelectric Microtubes Fabricated by Vacuum Infiltration of Macroporous Silicon Templates: *Xin Li*[1]; S. S. N. Bharadwaja[1]; N. Bassiri Gharb[1]; E. Hong[1]; M. Olszta[1]; F. Roozeboom[1]; Theresa S. Mayer[1]; Susan Trolier McKinstry[1]; [1]Pennsylvania State University

The ability to predict and control the behavior of ferroelectric devices as they are scaled down in dimension depends on quantifying the impact of mechanical constraints on the dielectric (eij) and piezoelectric response (dijk) of ferroelectric thin films. It has been shown that domain wall motion typically contributes more than 50% of the dijk and eij at 25°C in bulk perovskite ferroelectrics and dominates the field and frequency dependence of these properties. However, recent work shows that domain wall motion contributes far less in substrate-clamped thin films, and that a new non-ferroelastic mechanism of domain wall motion dominates the net piezoelectric response of these films. In this talk, we will discuss the fabrication, integration, and electrical characterization of high aspect ratio ferroelectric Pb(Zr0.52Ti0.48)O3 (PZT) microtubes that are processed by vacuum infiltration of macroporous silicon (Si) templates using a 2 methoxyethanol-based sol-gel precursor. These microtubes with 1 – 2 mm diameter, 20 – 50 mm length, and 100 – 200 nm wall thickness will allow us for the first time to investigate the response of mechanically unconstrained thin films. Two fabrication methods were investigated to prevent a chemical reaction between the Pb and Si during high temperature crystallization of the microtubes. The first method involved partially releasing the microtubes from the Si template after low temperature pyrolysis at 300°C, and then crystallizing the tubes by rapid thermal annealing at 750°C for 1-3 min. The second method incorporated a barrier layer (e.g. MgO) prior to infiltration and high temperature crystallization of the microtubes. X-ray diffraction and transmission electron microscopy was used to confirm perovskite phase formation of both types of microtubes. Following fabrication, the microtubes were released by reactive ion etching of the template and suspended in isopropyl alcohol for on-chip integration and electrical characterization. Dielectrophoretic assembly was used to integrate parallel arrays of microtubes on which interdigitated electrode arrays were patterned using sputtered TiW metal. This interdigitated test structure is being used to collect the first electrical measurements of mechanically unconstrained PZT thin films. The results of these measurements will be compared to those collected on substrate clamped thin films of comparable thickness.

Session F:
Directed Assembly of Nanostructures

Wednesday PM Room: Presidents Hall III
June 28, 2006 Location: Pennsylvania State University

Session Chairs: Diana Huffaker, University of New Mexico; Ben Shanabrook, Naval Research Laboratory

1:30 PM Student
F1, Selective Growth and Characterization of GaAs Quantum Dots on Patterned Substrate by Utilizing Diblock Copolymer Template: *Joo Hyung Park*[1]; Anish Arun Khandekar[1]; Sang-Min Park[1]; Luke J. Mawst[1]; Thomas F. Kuech[1]; Paul F. Nealey[1]; [1]University of Wisconsin-Madison

The theoretical advantages of ideal Quantum Dots(QDs) for diodes lasers are well established, including ultra-low transparency current density, low linewidth enhancement factors, and temperature insensitive device performance. Self-assembled QDs have been widely studied as a means to achieve the theoretical advantages. Issues such as QD size variations and the existence of a wetting layer have inhibited device performance of self-assembled QDs. One key issue which significantly impacts the performance of optoelectronic devices is thermionic emission of carriers to the large density of wetting layer states. This carrier leakage acts as a source of highly temperature-dependent current which does not contribute to the lasing. However, the wetting layers are inevitably produced in the fabrication process of self-assembled QDs. An alternate approach for QD formation is the use of nanopatterning combined with selective MOCVD growth. Using the technique of diblock copolymer lithography followed by selective MOCVD growth of the QDs, a higher degree of control of QD shape, size uniformity, and composition is expected. Higher growth temperatures compared with the self-assembled growth can be employed, resulting in improved QD material quality. In addition, the problematic wetting layer states can be eliminated, and improved optical gain is expected. Control of the QD height, shape, and strain, also allows for the design of increased energy spacing between ground and excited QD states and hence the control of the emission wavelengths. The diblock copolymer lithography technique consists of a series of pattern transfers from a dense nanoscale diblock copolymer pattern to a template mask (SiO_2 or Si_3N_4) and from the template mask to the GaAs substrate. As the first step, an annealing study to improve the template mask adhesion was performed. Annealing the dielectric mask at 700°C in hydrogen with an Arsenic overpressure prior to nanopatterning was found to be critical for preventing template mask cracks and detachment during the selective MOCVD growth. The annealing step is followed by a cylindrically oriented copolymer(PS-b-PMMA) coating, leading to a hexagonally arranged patterning. The advantage of using cylindrically oriented PS-b-PMMA rather than other spherically oriented diblock copolymers is to preserve the hole size through the pattern transfer procedures. Patterns with 30-40nm-scale holes are then transferred to the template mask using reactive ion etching. GaAs QDs are selectively grown on the patterned GaAs substrate. SEM and AFM measurements are used to characterize the shape and size distribution of the selectively grown QDs. By measuring XRD with a large area detector, we confirmed single crystal GaAs QDs were formed on the patterned substrate. This QD fabrication method holds potential for producing dense, large area QD distributions with an economically favorable process. Further studies are needed on the selective growth conditions to optimize the uniformity and size control of the QDs.

1:50 PM Student
F2, Simulation of Thermal-Field Directed Self-Assembly of Epitaxial Quantum Dots: *Chandan Kumar*[1]; Lawrence H. Friedman[1]; [1]Pennsylvania State University

Self-assembly of quantum dots represents an important step in the advancement of semiconductor fabrication at the nanoscale that will allow breakthroughs in electronics and optoelectronics. The two most studied systems are Ge_xSi_{1-x} dots grown on a Si substrate and $In_xGa_{1-x}As$ dots grown on a GaAs substrate. The former being most interesting for electronic applications and possibly even optoelectronic applications, and the latter being most useful for optoelectronic applications. An important step in developing Self-Assembled Quantum Dot (SAQD) technology is to control randomness and disorder in SAQD size and SAQD position. One would like to direct self-assembly to either a) generate large arrays of regularly spaced and/or regularly sized SAQDs or b) be able to place SAQDs in desired locations. Three previous examples of directed self-assembly of quantum dots are the preferential nucleation of SAQDs above intersection points of an array of misfit dislocations (Shiryaev, *et al.,* 1997), nucleation of quantum dots on etched mesas (S. Krishna, *et al.,* 1999), and the ability to nucleate SAQD clusters using a FIB (focused ion beam). (R. Hull, *et al.,* 2003). Here, thermal-field directed self-assembly is investigated using a finite element based simulation. Thermal-field direct self-assembly proposes to use spatially varying surface temperatures to enhance order and control placement of self-assembled quantum dots. (L.H. Friedman and J. Xu, in press). To further assess the effectiveness of thermal-field directed self-assembly and motivate appropriate experimental trials, three cases of spatially varying heating have been studied via simple 2D computational simulations. First, a spatially flat temperature profile is used as a baseline simulation. In the second case, a spatially varying periodic temperature distribution was applied. Such a profile might be created using a laser interference pattern. Finite element simulations of the growth process show that one can obtain an array of nearly uniform quantum dots compared with the first case. A third studied case is localized heating with a spot size of a few 100 nm in attempt to control precise placement of a single dot or dot cluster. Simulations are carried out under these conditions for temperature profiles with different minimum and maximum temperatures and examine how quantum dot statistics evolve during growth and evolution. The success of spatially varying heating to produce ordered or controlled quantum dots has not yet been confirmed experimentally, and it should be followed up by both more detailed, more sophisticated modeling and experimental trials.

2:10 PM Student
F3, Real-Time Studies of Ga Droplet Formation for the Directed Seeding of Semiconductor Nanopillars: *Weifeng Ye*[1]; Ben L. Cardozo[1]; Xiaojun Weng[2]; John F. Mansfield[1]; Rachel S. Goldman[1]; [1]University of Michigan; [2]Pennsylvania State University

The directed self-assembly of low-dimensional semiconductor structures has been achieved using a variety of approaches to producing topographical patterns. However, an approach for achieving highly ordered arrangements of nanostructures with well-controlled shapes and size distributions has yet to be developed. Therefore, we are exploring the formation mechanisms of Ga droplet "seeds" for the directed seeding of semiconductor nanopillars. Using a Ga focused-ion-beam, we have investigated the formation and ordering of Ga droplets on GaAs surfaces.To investigate the Ga droplet formation mechanisms, we studied the effects of ion beam doses and scan directions using static and real-time measurements, both with the incident ion beam perpendicular to the sample surface. For doses > 4×10^{16} ions/cm^2, randomly distributed Ga droplets are observed. Subsequent ion beam irradiation at a fast scan rate results in growth, diffusion, and coalescence of the Ga droplets, all of which are independent of the scan direction. As the dose increases, the droplet size and density remain constant, presumably limited by the balance between sputtering and implantation/diffusion. For fluxes >1×10^{15} ions/cm^2/s, motion of the droplets becomes apparent. The droplet motion velocity increases with the ion flux, presumably due to ion-induced temperature gradients, in turn leading to surface tension gradients[1]. However, for slow scan rates, the size and position of the Ga droplets has a distinct directional dependence. The droplet size is observed to increase along the slow scan direction. Additionally, at very high dose and slow scan rate, the droplets align preferentially along the [1-10] direction. These results point to a droplet formation mechanism based on ion-assisted Ga diffusion. To obtain ordered Ga droplets, we have milled ordered arrays of holes with nearly uniform sizes and shapes. By controlling the ion beam energy, current, and position, hole arrays with various sizes, depths, and periodicities may be produced. After scanning the ion beam over the patterned area, Ga atoms diffuse to the holes and agglomerate, leading to the formation of ordered arrays of nearly uniformly-sized Ga "seeds". As the dwell time increases, the average droplet size increases while the droplet size uniformity decreases along the scan direction. Thus, to maintain a uniform distribution of droplet size, the

scan direction must be cycled. We have examined the interaction of Ga droplets with various N-source gases. Exposure of Ga droplets to NH_3 vapor has resulted in the fabrication of GaN-rich nanocrystals. We will discuss the crystallinity and composition gradient in the GaN-rich nanocrystal layers. We will also discuss the use of Ga droplets as catalysts for the vapor-liquid-solid growth of variety of semiconductor nanopillars. [1]J. Thomson, Philios. Mag. Ser. 4(10), 330 (1855); C. Marangoni, Nuovo Cimento Ser. 2(5/6), 239 (1872).

2:30 PM

F4, Self-Assembly of Heterojunction Quantum Dots(HeQuaDs): *Kurt G. Eyink*[1]; David H. Tomich[1]; Jeremey J. Pitz[1]; Krishnamurthy Mahalingam[2]; J. M. Shank[3]; S. Munshi[1]; Bruno Ulrich[4]; Wally Rice[5]; [1]Air Force Research Laboratory; [2]Universal Technology Corporation; [3]Southwestern Ohio Council for Higher Education; [4]Bowling Green University; [5]Wright State University

Quantum dots (QDs) have been receiving considerable attention due to the unique properties, which arise due to the confinement of the electron and holes in a lower band gap material. The InAs on GaAs material system is one of the most studied combinations in which quantum dots form during epitaxy. These QDs form in a Stranski Krastanov manner via a self-assembly process in which the dots nucleate at a critical adatom coverage on a wetting layer of InAs. QDs may be vertically aligned by using the residual strain above a buried dot layer to enhance the nucleation of the second layer of dots. In this work, we show the formation of QDs, which are composed of multiple materials, can be formed through a marriage of these two concepts. In this particular demonstration, we formed InAs dots on GaAs and crowned the QDs with GaSb and encapsulated the entire structure with GaAs. Atomic Force Microscopy shows additional nucleation between the InAs layers has been minimized and cross-sectional transmission electron microscopy shows the formation the composite structure. Transmission electron microscopy indicated a clear boundary between the GaSb and InAs regions. AFM analysis of the HeQuaD structure shows that GaSb material grows mainly on the two (1 1 0) inclined facets. Thus, the HeQuaD is elongated along the (1 1 0) direction. We have also obtained preliminary photoluminescence (PL) from a 3 layer GaS/InAs HeQuaD structure with a peak around 1.3 microns.

2:50 PM

F5, Fabrication of Nanometer-Period Gratings on Si Using HSQ Etching Mask: *Niu Jin*[1]; Vipan Kumar[1]; Sookyung Choi[1]; Mark Shannon[1]; Ilesanmi Adesida[1]; [1]University of Illinois

Hydrogen Silsesquioxane (HSQ) has been utilized as a high resolution negative-tone inorganic resist for electron beam lithography. In this abstract, we report our work on writing HSQ 1:1 line/space gratings with periodicity of 27 nm using electron beam lithography and pattern transferring on Si wafer by inductively-coupled-plasma reactive ion etching (ICP-RIE). An HSQ solution (Fox-14) obtained from Dow Corning was diluted with methylisobutylketone (MIBK) with a ratio of 1:7. The solution was then spun on Si wafer and followed by oven baking at 90°C. The thickness of the resulting HSQ film was measured as ~ 20 nm using a Rudolph FE-III Focus Ellipsometer. The sample was then exposed in a JEOL JBX-6000FS/E electron beam nanowriter with beam parameters of 50 kV acceleration voltage and a spot size of ~ 5 nm. Gratings with periodicity varying from 50 nm to 20 nm were written using a double-pass technique at 20 pA beam current. After exposures, the sample was developed in tetramethyl ammonium hydroxide (TMAH) developer at 22°C for 60 s followed by a bath in 1:9 TMAH:DI for 60 s and then rinsed in pure de-ionzied water. After development, the sample was annealed at 450°C for 1 hour in N2 atmosphere to ensure the complete dissociation of the Si-H with a resulting harder HSQ etching mask. The etching of Si was performed in an inductively-coupled-plasma reactive ion etch (ICP-RIE) system using a $Cl_2/BCl_3/Ar/O_2$ plasma at 3 mT and – 110 V bias. The etch rate of Si under these conditions was about 600 A/min. The addition of O_2 increased the selectivity of etching HSQ over Si from ~ 1.5 to ~ 6.0. The sample was then inspected using a Hitachi S-4800 scanning electron microscope. The results showed that 1:1 line/space gratings with periodicity down to 27 nm on Si wafer were written and transferred. Anisotropic etch profiles for the etched Si were obtained. Detailed variations of linewidth versus periodicity in various thicknesses of HSQ and strategies to obtain ultra-short period gratings will be described.

3:10 PM Break

Session G: Quantum Dot Growth

Wednesday PM
June 28, 2006

Room: Presidents Hall III
Location: Pennsylvania State University

Session Chairs: Ben Shanabrook, Naval Research Laboratory; Diana Huffaker, University of New Mexico

3:30 PM Student

G1, Growth of High Quality Stransky-Krastanov GaSb Quantum Dots on a GaAs Substrate: *Ganesh Balakrishnan*[1]; Shenghong Huang[1]; Arezou Khoshakhlagh[1]; Anitha Jallipalli[1]; Jun Tatebayashi[1]; L. R. Dawson[1]; D. L. Huffaker[1]; [1]University of New Mexico

The Sb-bearing compounds offer a wide range of electronic bandgaps, bandgap offsets and electronic barriers. Extremely high electron mobility enables a variety of extremely fast, low power electronic devices and infrared light sources. The ability to grow high quality Sb-bearing quantum dots (QDs) on GaAs would provide an excellent alternative to the existing In(Ga)As QD technology and may extend the accessible wavelength of QD emitters. The growth of GaSb QDs however has not been as straightforward as that of InAs QDs since the GaSb QD formation by Stransky-Krastanov (SK) modes requires non-standard molecular beam epitaxy recipes, i.e. a very low III-V ratio (III/V ratio ~ 1:1). As a result, there has been no report of fully quantized SK QDs. Under standard recipes involving higher III/V ratio, interfacial misfit array formation (IMF) occurs forming strain-relaxed GaSb islands on GaAs. In this presentation, we demonstrate GaSb SK QDs on a GaAs substrate. Furthermore, we demonstrate growth mode control via gallium to antimony (III/V) ratio. We report that high III:V ratio of 1:10 produces IMF and a low ratio of 1:1 favors the SK growth mode. The IMF growth mode produces strain-relaxed QDs, where the SK QDs remain highly strained. Both ensembles demonstrate strong room temperature photoluminescence with the SK QDs emitting at 1180 nm and the IMF QDs emitting at 1375 nm. Under cryogenic temperatures, the PL from both QDs blue shifts with increased pump power, thus indicating a type II band alignment between the GaSb QDs and the surrounding GaAs matrix. Quantized energy levels are observed in 77 K PL spectra, with the SK QDs showing two excited states with intersubband energy spacing of 117.8 meV and 67.9 meV. Transmission electron microscope images identify the array of misfit dislocations in the IMF dots with the dislocations spaced ~5 nm apart. The crystallographic shapes for both types of QD formation and associated strain patterns have also been observed. The QDs have been further characterized by AFM and RHEED.

3:50 PM Student

G2, Characteristics of InGaAs/GaAs(P) Quantum Dot Stacks Grown by MOCVD: *Nam-Heon Kim*[1]; Gene Tsvid[1]; Anish A. Khandekar[1]; Luke J. Mawst[1]; Thomas F. Kuech[1]; Manoj Kanskar[2]; [1]University of Wisconsin-Madison; [2]Alfalight Inc.

Self-assembled In(Ga)As quantum dots(QD) have been intensively studied for device applications such as 1.3-μm edge emitting and vertical cavity surface emitting lasers(VCSELs). The use of a low-dimensional QD active region holds potential for realizing extremely low threshold current density lasers that are temperature insensitive. Carrier leakage out of the QD is one of the underlying causes for the observed low modal QD ground state gain and the relatively high temperature sensitivity of QD lasers. Carriers which are thermally excited into the excited QD states and wetting layers surrounding the QD, lead to gain saturation at values significantly lower than achievable if saturation occurs due to full population inversion in the dot states. As a result, many stacked layers of QDs are needed to achieve typical threshold gain requirements in diode-laser application. However, the multi-stacked QD layers exhibit different characteristics from the single QD layer for MOCVD grown structures. The upper QD layers are found to have a different QD size distribution from the 1st QD layer, although

the growth conditions are maintained the same for each QD layer and the QD layer separation is as large as 50 nm(vertically uncoupled). Broad area laser structures with varying number of QD layers have been fabricated and characterized to extract the material gain coefficient or gain/per QD layer and the current injection efficiency. A single-QD layer and 3-stack-QD structures with GaAs barrier materials samples were grown to compare QD size and distribution within the stacked structure using low pressure MOCVD. We find, the 3rd stack of QDs exhibits a higher fraction of large(possibly strain relaxed) QDs compared with the first QD layer. This correlates well with 3- and 5-stacked InGaAs QD(with GaAsP barriers) active region laser characteristics, which indicate that a larger number of QD stacks results in lower gain/per QD layer. The impact of the QD growth temperature, InGaAs thickness, and GaAs spacer V/III ratio on the number of large QDs in the stack has been determined. The optimized QD stack growth condition is found to improve photoluminescence(PL) intensity. Atomic-force-microscopy(AFM) studies show the number of large "optically dead" QDs can be reduced in the 3rd-stack when the upper stack InGaAs is 10-15% thinner or grown at higher growth temperature than the 1st-QD layer in the stack. Room temperature PL measurements indicates that higher growth temperature for the 3rd-QD layer results in ~50% higher PL intensity than the 3-stacked standard structure (i.e. same growth condition of each QD layer), which is correlated with AFM measurements. Employing the optimized QD stack growth conditions for the diode laser active region is expected to lead to a reduction in nonradiative recombination outside of the QDs, thereby improving the current injection efficiency and material gain parameter.

4:10 PM
G3, Influence of Strain Modulations in Capping Layers of InAs Quantum Dots with Compressive-InGaAs and Tensile-GaAsN Layer Structures: Wei Zhang[1]; Katsuhiro Uesugi[1]; *Ikuo Suemune*[1]; [1]Hokkaido University

Quantum dots (QDs) have been attracting intensive attention in basic research and device applications, and long-wavelength QDs offer excellent active regions for high-performance optical devices in the optical-fibre communication window. For InAs QDs grown on GaAs substrates, use of an InGaAs capping layer reduces the interface mismatch and is an effective way to extend the emission wavelength up to 1.55 um. However, the optical quality of QDs capped with In-rich InGaAs layers frequently shows serious degradations of luminescence efficiencies due to highly accumulated compressive strain in both QDs and capping layers. In this paper, we propose an application of InGaAs/GaAsN strain-compensated superlattice (SCSL) as a capping layer of InAs QDs. Each pair of such SCSLs consists of a thin compressively strained InGaAs layer with high In concentration which is strain-compensated with a thin tensile-strained GaAsN layer. In our measurements, an InGaAs(37.5% of In) capping layer exhibited extended red-shift of the emission wavelength by ~70nm. However the thickness of the InGaAs capping layer over 1.6nm substantially degraded the luminescence efficiency. Replacement of the single InGaAs layer with two periods of 1.1-nm-thick InGaAs(37.5% of In)/2-nm-thick GaAsN(2.2% of N) SCSL exhibited the similar red-shift of the QD emission wavelength with much improved luminescence efficiency. The red-shift is extended with the the increase of the periods of the InGaAs/GaAsN SCSL. Another problem during capping process of InAs QDs is the In segregation/diffusion and the related flattening of InAs QDs. It is shown that such phenomenon can be suppressed with the application of the InGaAs/GaAsN SCSL.

4:30 PM Student
G4, Growth of High Density InAs Quantum Dots by Metalorganic Chemical Vapor Deposition with Periodic Interruption of AsH_3: *Youngsoo Lee*[1]; Eungjin Ahn[1]; Jungsub Kim[1]; Pilkyung Moon[1]; Euijoon Yoon[1]; [1]Seoul National University

The formation of self-assembled quantum dots (QDs) by Stranski-Krastanow growth mode has attracted a lot of interest as a viable technique to create nano-scale structures without the need of any lithography. The research activities range from studies on QD growth and their fundamental electronic properties to technological application such as QD laser diode, photodetector and other optoelectronic devices. In particular, GaAs-based semiconductor lasers using InAs QDs as an active material have attracted more attention because of the fact that these structures offer the prospect of high characteristic temperature, low threshold current density and light emission at 1.3 μm. To realize such device applications, it is essential to control the size, density and size uniformity of InAs islands. More importantly, the uncontrolled coalesced dots or defects associated with coalescence are very detrimental since they provide non-radiative recombination centers. It is well known that the surface adatom diffusivity of group III elements increases with V/III ratio. Thus, the low V/III ratio is one of the key parameters to obtain high quality defects-free InAs QD with high density and uniformity. We grew InAs QDs on Si-doped GaAs (001) substrates with a horizontal MOCVD reactor at 76 Torr using TMGa, TMIn and AsH_3 as source materials for gallium, indium and arsenic, respectively. Before the InAs QD growth, we grew a 4 ML $In_xGa_{1-x}As$ strained buffer layer to reduce the strain between GaAs and InAs and to form a dot-in-a-well structure. In order to lower the V/III ratio during the InAs QD growth, we introduced a novel method. In conventional InAs QD growth by MOCVD, the source gases (TMIn, AsH_3) are introduced into the reactor simultaneously. However, in this experiment, we interrupted the AsH_3 flow periodically, *i.e.*, run and vent in turn, while TMIn was introduced into the reactor continuously. This method allowed the effective V/III ratio to be lowered during the InAs QD growth. In an environment with abundant As atoms on surface, In atoms can easily bond with each other via As intermediary and InAs dots would easily coalesce. By interrupting the AsH_3 flow periodically, we could suppress the QD coalescence process, resulting in the formation of highly dense ($8\times10^{10}/cm^2$) and uniform array of InAs QDs. Moreover, it was found that the aspect ratio of QDs increased from 0.28 to 0.38 when the number of AsH_3 interruption increased from 3 to 4. Detailed results on the effect of growth variables will be presented.

4:50 PM
G5, Late News

Session H: III-Nitride Electronic Devices

Wednesday PM Room: Presidents Hall IV
June 28, 2006 Location: Pennsylvania State University

Session Chairs: Russell Dupuis, Georgia Institute of Technology; April S. Brown, Duke University

1:30 PM
H1, Growth and Characterization of Graded InGaN Heterojunction Bipolar Transistors: Theodore Chung[1]; David Keogh[2]; Dongwon Yoo[1]; *Jae-Hyun Ryou*[1]; Jae Limb[1]; Wonseok Lee[1]; Shyh-Chiang Shen[1]; Peter Asbeck[2]; Russell Dupuis[1]; [1]Georgia Institute of Technology; [2]University of California, San Diego

The device operation of GaN/InGaN heterojunction bipolar transistors (HBTs) employing graded-alloy-composition $In_xGa_{1-x}N$ layers grown by metalorganic chemical vapor deposition (MOCVD) on sapphire and SiC substrates are demonstrated. InGaN was proposed to be employed in the base layer in III-nitride based *NpN* HBTs; however, the growth of a highly strained InGaN base sandwiched between the wider-bandgap GaN emitter and collector introduces material defects, which is believed to be a major factor that hinders transistor operation of GaN/InGaN HBTs. The grading in the emitter and the base serves to improve the crystalline quality at the interface between GaN and the InGaN emitter-base and base-collector as well as in the emitter and base layers caused by lattice mismatch. The HBT structure employed in this study consists of a 70 nm n^{++}-GaN:Si emitter cap, a 30 nm n^{++}-InGaN:Si graded emitter, a 100 nm p^+-$In_xGa_{1-x}N$:Mg graded base (p=2×10^{18} cm^{-3}, x=0.03-0.06), a 30 nm $In_xGa_{1-x}N$:Si graded collector (x=0-0.03), a 0.2 μm n-GaN:Si collector, and 0.5 μm n^+-GaN:Si subcollector. The growth challenges lie in suppressing the formation of defects. While maintaining a high V/III ratio and a suitable growth temperature are important, the growth temperature ramp and the ramping gradient have a dramatic impact on the device performance and yield. The indium composition in the base layer has a reverse grading that helps to produce a smooth high-quality indium base layer; however, this grading also counteracts the electron diffusion

flow from the emitter to the collector to some degree. Also, piezoelectric effect modifications by employing a graded InGaN and doping concentration gradient originating from a higher doping efficiency toward emitter interface in the base needs to be considered in the band structure of HBTs. Band structure modification by these effects is believed to be beneficial to the diffusion of injected electrons across the base. The device performance is optimized by a study of the epitaxial design parameters related to a trade-off between the improved material quality and the beneficial field distribution in the InGaN base layer and the reverse electric field produced by the indium graded-composition profile in the base. A hole concentration of $p \geq 2x10^{18}$ cm^{-3} in the $In_xGa_{1-x}N$:Mg, x~5-6% base layer is one of the critical factors in obtaining transistor action. Devices grown on sapphire substrates show a common-emitter (CE) DC current gain as high as β~25, while those on SiC substrates have values in the range of β~30-40. The CE family curves show the collector-base breakdown voltage for these devices is larger than 85 V in the common emitter configuration. Devices have been operated as transistors at temperatures up to 300°C. We will describe the growth and performance of III-N HBTs employing InGaN graded layers.

1:50 PM Student

H2, Device Performance of Full-Vertical GaN *p-i-n* Rectifiers Using Conducting Buffer Layers on SiC Substrates: *Dongwon Yoo*[1]; Jae Boum Limb[1]; Jae-Hyun Ryou[1]; Wonseok Lee[1]; Russell Dupuis[1]; [1]Georgia Institute of Technology

The epitaxial structure, growth parameters, and device design for full-vertical GaN *p-i-n* rectifiers grown on *n*-type 6H-SiC substrates employing AlGaN:Si conducting buffer layers have been studied. The conventional rectifier structure, utilizing a mesa-defined *p*- and *n*-contacts on top which is an inevitable choice due to the insulating AlN buffer layer commonly employed for the growth of GaN on SiC substrates, introduces excessive current crowding at the bottom of *i*-region as well as an increase in the leakage current due to damaged sidewalls. However, a full-vertical device configuration enables the structural design of rectifiers without a deep mesa-etch. The growth conditions for the $Al_{0.1}Ga_{0.9}N$:Si conducting buffer layer are calibrated to achieve improved crystalline and structural quality by altering the growth parameters and the epitaxial designs. The $Al_{0.1}Ga_{0.9}N$:Si layer is also demonstrated to provide excellent electrical properties while acting as a good buffer layer for subsequent GaN heteroepitaxial growth. Full-vertical rectifiers consist of the following layers: p^{++}-GaN:Mg (p= $1.2x10^{20}$ cm^{-3}), p-GaN:Mg (p = $1x10^{18}$ cm^{-3}), a 2.5 μm GaN *i*-layer, *n*-GaN:Si, and $Al_{0.1}Ga_{0.9}N$:Si as a conducting buffer. AFM images reveal the atomically smooth surface with no visible nano-pits. RMS roughness values are 0.22 nm and 0.26 nm for 1x1 μm^2 and 5x5 μm^2 scans, respectively. FWHM values of GaN-related peaks were 181 arc-s and 320 arc-s for (002) and (102) scans respectively, which are comparable to those of GaN *p-i-n* rectifiers employing a conventional AlN buffer layer on SiC substrates. Ni/Au and Pd/Au ohmic contacts were applied to the *n*-SiC and *p*-GaN, respectively. The top *p*-type contact was a circular pattern while the *n*-type contact covered most of backside of the SiC substrate. Two configurations of devices were compared: one does not have any current guiding scheme and the other has current guiding only in *p*-layer. To provide the current guiding in p-layer, the layer was shallow-etched by ICP etching and passivated by SiO_2. Performance characteristics are compared. Both configurations show a low on-resistance of $7.5x10^{-3}$ Ω•cm^2. The reverse breakdown voltage for rectifiers without p-current guiding was over -330V, while one with *p*-current guiding was over -400V. The devices with *p*-current guiding exhibit much reduced reverse leakage current, indicating that the current guiding even in relatively thin *p*-layer facilitates the reduction of the reverse leakage current and improves the device performance characteristics. Another method for current guiding has been achieved by the proton implantation. The dose and the implantation depth are calculated to be $1.5x10^{16}$ cm^2 and 1.3 μm, respectively. The device characteristics of full-vertical rectifiers employing proton implantation will be reported.

2:10 PM Student

H3, EBIC and XPS Study of Post-Annealing Process on AlGaN/GaN Schottky Diodes: *Hyeongnam Kim*[1]; Michael L. Schuette[1]; Hyunchul Jung[1]; Junghui Song[1]; Jaesun Lee[1]; Wu Lu[1]; James C. Mabon[2]; [1]Ohio State University; [2]Material Research Laboratory

Control of surface states is an important issue in AlGaN/GaN high electron mobility transistors (HEMTs) for high power, high speed, and high temperature applications. Many efforts have been made to suppress radio frequency current dispersion and thermal/electrical stress-induced degradation, or/and to improve the breakdown voltage performance, which are directly related electron trapping behavior due to surface states in AlGaN/GaN heterostructures. Thermal annealing after Schottky gate formation has been used as one of the techniques to engineer surface/interface states in AlGaN/GaN HEMTs[1]. However, the mechanism of the thermal annealing effects is not still completely understood. In this presentation, we report impacts of post-annealing on Ni/AlGaN interface and free AlGaN surface to investigate physical origin of post-annealing effects in AlGaN/GaN heterostructures. Ni/AlGaN/GaN Schottky diodes were examined before and after annealing at 400 °C for 20, 50, and 170 min using current-voltage (I-V) characteristics and electron beam induced current (EBIC) analysis. Annealed Schottky diodes exhibited smaller area of dark spots in EBIC images than as-deposited ones, indicating that the post-annealing process reduced electrically active states at Ni/AlGaN interface. Reverse leakage current densities of a Schottky diode before annealing, and after 20-min, 50-min, and 170-min annealing at 400 °C were 6.89×10^{-2}, -1.29×10^{-2}, -2.25×10^{-3}, and -1.34×10^{-3} A/cm^2, respectively, at $V_{applied\ bias}$ = -5 V. Saturation current density (J_S), ideality factor (n) and Schottky barrier (ϕ_B) were extracted from the forward-biased I-V curves. ϕ_B increased from ~0.74 eV to 0.82 eV, and J_S decreased from 9.85×10^{-7} A/cm^2 to 6.1×10^{-8} A/cm^2 before and after 170-min annealing, respectively. n decreased from ~2.0 to 1.65 after 50-min annealing but increased after 170-min annealing. Thus, we suggest that the thermal reaction near Ni/AlGaN interface due to the post-annealing induced passivation effect, leading to decrease in reverse leakage current and saturation current and increase in the Schottky barrier height. R_S initially decreased after 20-min annealing as explained by removal of a native oxide layer due to thermal reaction at metal/AlGaN interface. Further annealing increased R_S owing to formation of highly resistive layer at metal/AlGaN interface or unintentional oxidation of metal. Using X-ray photoelectron spectroscopy, it was observed that the post-annealing unintentionally oxidized the free AlGaN surface between the Schottky gate and ohmic contacts, which also contributes to preventing electron trapping onto surface states near the Schottky contact edge under reverse biased conditions. In conclusion, the post-annealing process removed electrically-active states at Ni/AlGaN interface and oxidized free AlGaN surface. The modification of surface and interface states is directly related to improvement of AlGaN/GaN device performance. We suggest that the post-annealing process is an effective way to passivate the AlGaN/GaN heterojunction field effect transistors. [1]J. lee, D. Liu, H. Kim, and W. Lu, Appl. Phys. Lett. 85, 2631 (2004).

2:30 PM

H4, Gate Dielectric Considerations for Scaleable III-V MOS Structures: *Mark Johnson*[1]; J. A. Grenko[1]; Y. N. Saripalli[1]; D. W. Barlage[1]; Y. Jin[1]; Dave Braddock[2]; [1]North Carolina State University; [2]OSEMI, Inc.

The use of a suitable dielectric-semiconductor interface for the fabrication of a stable gate dielectric has been a long-standing challenge for the compound semiconductor industry. Recent advances in the deposition of oxides by molecular beam epitaxy have resulted in dielectric-semiconductor structures which exhibit interface fixed-charge state densities low enough to be fabricated into useful device structures. For example, the recent demonstration of epitaxial Ga2O3/Gd2O3 on GaAs has resulted in viable enhancement mode devices for potential microwave communications. The gate dielectrics to III-N present a special opportunity as the volatility of competing phases at the III-N-O interface provide a process mechanism for low interface state density structures. With appropriate source-drain contact design, such III-Nitride MOS structures have been show to develop accumulation channel charge densities of >2x1013/cm2, exceeding the charge density typically observed in strain-polarization doped III-N HFETs. As the accumulation channel exists at the III-N/dielectric interface, rather than at an offset by a fixed depth of AlGaN thickness to induce strain, III-N MOSFET structures have the potential to be scaled to nanoscale dimensions. To achieve this scaling, several issues need to be addressed including: thermodynamic stability for metal-oxide/Ga2O3/GaN in appropriate anion and cation sub-lattice interfaces; conduction and valence band-offsets; lattice mismatch minimization to reduce structurally induced strain; the influence of GaN polarity on threshold voltage and band

alignment, and thicknesses of the Ga2O3 intermediate layer to avoid phase transformations. In our current work, we have deposited Ga2O3/Gd2O3 structures by molecular beam epitaxy on undoped GaN channel structures. The undoped channels incorporate selective-area regrowth of n-GaN for source-drain contact formation. These GaN MOS structures have been investigated structurally by cross-sectional TEM and AFM and exhibit a high degree of structural coherence. Fabricated devices exhibit enhancement mode behavior for an electron accumulation channel exceeding 2x1013/cm2, and were measured electrically with current gain at mm-wave frequencies for Lg=150nm devices. The corresponding interface state density was estimated to be Dit=1011/cm2. These GaN MOSFET devices are used as a guide for on-going dielectric interface development. From these results, we project that GaN MOSFET structures may be further reduced to nanoscaled dimensions and device simulations for scaled GaN MOSFETs down to 10nm gatelengths will be presented. At such size ranges, high-field electron and hole transport behavior dominate and the high saturated electron velocity of is beneficial for high-frequency operation.

2:50 PM Student

H5, Fabrication and Characterization of Enhancement-Mode n-Channel GaN MOSFETs: *Weixiao Huang*[1]; Tahir A. Khan[1]; T. Paul Chow[1]; [1]Rensselaer Polytechnic Institute

GaN is promising material for high power and high temperature electronics due to its wide energy band gap and large critical electric field. With high quality Oxide/GaN interface,[1] proper design and fabrication, GaN MOSFETs can be demonstrated with high field-effect mobility and high blocking voltages.[2] We have fabricated GaN MOSFETs on both p and n^- GaN epilayer on sapphire substrate. The SiO_2/GaN interface achieved a mid-bandgap low interface-state density around 10^{10} $cm^{-2}eV^{-1}$ with optimized annealing conditions.[1] The polysilicon gate material was sputtered to a thickness of 650 nm and doped at 900°C with $POCl_3$ to achieve a gate sheet resistance of 1 kΩ/square. The source and drain regions were selectively implanted with silicon dose of 3×10^{15} cm^{-2}. More than 30% dopant activation was achieved by annealing at 1100°C for 5 min. in N_2 with 600 nm field oxide as capping layer. Ti-Al (35 nm/115 nm) was deposited and annealed at 700°C for 30s for n^+ ohmic contacts and for p or n^- epilayer contacts. A specific contact resistivity of 4×10^{-5} Ωcm^2 was achieved. Ti-Mo metal was used for probe contact pads. Threshold voltage of 3.3 V for p GaN and 1.5 V for n- GaN was determined from the linear transfer characteristic of circular device with channel length 20 μm and channel width 800 μm. The subthreshold slope of 490 mV/decade n-channel MOSFETs on p GaN and 170 mV/decade on n- GaN was extracted. A maximum field-effect mobility of 167 $cm^2V^{-1}s^{-1}$ for both p GaN and n^- GaN was extracted on long channel (L_{ch}=100 μm) circular MOSFETs to minimize the effect of Source/Drain resistance. This is about 19% of the bulk mobility (900 $cm^2V^{-1}s^{-1}$) and a record achievement for GaN MOSFETs, to the best of our knowledge. The gate leakage is below 100 pA in all the measurements. Specific on-resistance with different channel lengths was characterized. A channel sheet resistance of 9 kΩ/square. and 160 Ωmm series resistance can be derived for p GaN while channel sheet resistance and series resistance are 6 kΩ/square. and 90 Ωmm for n^- GaN respectively. Furthermore, short-channel (2 μm) GaN MOSFETs have yielded transconductance of 20-30 mS/mm.

In summary, we have demonstrated the high performance enhancement-mode n-channel MOSFETs with the use of PECVD SiO_2 for the gate oxide and ion implantation processing. This process is also fully compatible with the commercial lateral silicon MOSFETs technology. [1]W. Huang, T. Khan, T.P. Chow, "Comparison of MOS capacitors on N an P type GaN", later news paper, DRC/EMC(2005), Accepted by J. Electronic Material, 2006; [2]W. Huang, T.Khan, and T.P. Chow, "Enhancement-mode n-channel GaN MOSFETs on p and n^- GaN/Sapphire substrate", accepted by ISPSD, June, 2006.

3:10 PM Break

3:30 PM

H6, Spin-Orbit Quantum Interference and Dephasing in High Mobility GaN/AlGaN Heterostructures: *Michael Manfra*[1]; Stefan Schmult[1]; Alex Punnoose[1]; Richard Molnar[2]; [1]Bell Laboratories; [2]Massachusetts Institute of Technology, Lincoln Laboratory

Manipulation of spin via the Rashba spin-orbit (SO) interaction in quantum confined structures with structural inversion asymmetry is necessary for such device concepts as the spin field-effect transistor. To this end, much experimental effort has been devoted to narrow bandgap material systems (InAs, InGaAs, GaAs, etc) as spin-orbit coupling is expected to be strong in these systems. Conversely, far less experimental effort has been directed toward wide bandgap systems, e.g. GaN, in which spin-orbit effects are predicted to be suppressed by the large fundamental bandgap, E_g, and reduced the spin-orbit splitting, Δ_0, of the valence band at zone center. Indeed, in the k*p formalism, the bare Rashba spin-orbit coupling constant for electrons, α_0, scales as: $\alpha_0 \approx \Delta_0/E_g^2$. As the value of Δ_0 for GaAs exceeds in GaN by at least a factor of ten, it is reasonable to suspect that spin splitting of the conduction band in GaN-based heterostructures would be insignificant compared to GaAs and other narrow gap heterostructures. We present low temperature magnetoconductivity measurements of a density-tunable high mobility two-dimensional electron gas confined in the wide bandgap GaN/AlGaN system. Experiments are conducted with gated Hall bars that allow access to a previously inaccessable range of low density $5x10^{15}m^{-2}<n_e<2x10^{16}m^{-2}$ and very high mobilities $1.4m^2/Vs<\mu<8.5m^2/Vs$. We observed pronounced anti-localization minima in the low-field conductivity, indicating the presence of significant spin-orbit coupling. Density dependent measurements of magnetoconductivity indicate that the coupling is mainly due to the Bychkov-Rashba mechanism. Using a recently derived, closed-form, expression for the magnetoconductivity, we are able to extract reliable transport parameters for our devices. The Rashba spin-orbit coupling constant is $\alpha_{SO} \approx 6x10^{-13}eVm$, while the conduction band spin-orbit splitting energy amounts to $\Delta_0 \approx 0.3meV$ at $n_e=1x10^{16}m^{-2}$.

3:50 PM

H7, Transport Characterization of AlGaN/AlN/GaN Heterostructures Grown on SiC: *Said Elhamri*[1]; William C. Mitchel[2]; William D. Mitchell[2]; Rex Berney[1]; Adam Saxler[3]; [1]University of Dayton; [2]Air Force Research Laboratory; [3]Cree, Inc.

Transport measurements were used to characterize AlGaN/AlN/GaN heterostructures grown on a 3" high-purity semi-insulating 4H-SiC substrate. The thickness of the AlN layer was 8 Å and that of the $Al_xGa_{1-x}N$ was 240 Å with an Al mole fraction x = 0.25. The room-temperature sheet resistivity map indicated an average resistivity of 280 ohms/square with a standard deviation of 0.45% over the wafer. Hall effect measurements returned an electron concentration of roughly 1 x 10^{13} cm^{-2} and a mobility that was slightly over 2000 cm^2/Vs, which is one of the highest mobilities ever reported for an AlGaN/GaN structure for that high a carrier concentration, at room temperature. At low temperatures, the electron concentration remained relatively unchanged while the mobility increased to over 3 x 10^4 cm^2/Vs at 1.2 K. Despite the high carrier density, mobility spectrum analysis at low temperatures indicated single-carrier transport and negligible parallel conduction. Magnetoresistance measurements in field ups to 8 T revealed the presence of well defined Shubnikov-de Haas (SdH) oscillations that were clearly visible in fields lower than 2 T. The electron concentrations determined from the frequency of the Shubnikov-de Haas oscillation were in good agreement with the Hall data. Because of the high carrier density and the high mobility more than 90 peaks in the SdH oscillations were clearly visible. Compared to an AlGaN/GaN heterostructure with similar AlGaN growth parameters, the AlGaN/AlN/GaN exhibited higher electron density and mobility. The observed increase is attributed to an increase in the conduction band offset. A reduction in alloy disorder scattering contributes to a further increase in the mobility. Exposing this structure to illumination resulted in a persistent photocurrent at low temperatures. Extended exposure to UV illumination (λ =395 nm) increased the carrier density to a saturated value of 1.3 $x10^{13}$ cm^{-2} and decreased the mobility to about 2.4 x 10^4 cm^2/Vs.

4:10 PM Student

H8, High Voltage AlGaN/GaN HFETs with Fe-Doped GaN Buffer on Silicon Substrate: *Young Chul Choi*[1]; Milan Pophristic[2]; Ho-Young Cha[3]; Boris Peres[2]; Michael G. Spencer[1]; Lester F. Eastman[1]; [1]Cornell University; [2]Velox Semiconductor Company; [3]GE Global Research

We report on high voltage AlGaN/GaN heterostructure field-effect transistors (HFETs) with a Fe-doped GaN buffer on a silicon substrate. In order to investigate the effects of a Fe-doped GaN buffer, devices with and without a Fe-doped GaN buffer on a silicon substrate were fabricated

alongside and their characteristics were compared. It was shown that the AlGaN/GaN HFET structure without a Fe-doped GaN buffer on a silicon substrate was not suitable for high power switching operation because of the unstable breakdown voltage (BV) characteristics. On the other hand, the AlGaN/GaN HFET structure with a Fe-doped GaN buffer on a silicon substrate showed much more stable and higher BVs by suppressing the premature failure caused by silicon breakdown, i.e. BV of 295 V and specific on-resistance (ARDS(ON)) of 2.44 mO–cm2. In addition, it was shown that the SiO2 isolation layer placed on the region of the mesa isolation suppressed pad-to-pad leakage currents associated with the conduction through the unintentionally doped (UID) GaN buffer.

4:30 PM Student

H9, Effects of UHV Surface Preparation and Gate Deposition on AlGaN/GaN HEMT Device Performance: *Dennis E. Walker, Jr.*[1]; Robert C. Fitch[2]; James K. Gillespie[2]; Gregg H. Jessen[2]; Leonard J. Brillson[1]; [1]Ohio State University; [2]Air Force Research Laboratory

We have used low-energy cathodoluminescence spectroscopy (CLS) and Auger electron spectroscopy (AES) to correlate chemical and electronic properties with device performance for AlGaN/GaN high electron mobility transistors (HEMTs) as a function of UHV-controlled surface preparation. We used surface science techniques to prepare cleaned AlGaN surfaces by annealing, Ga reflux, or N ion sputtering of current generation AlGaN/GaN HEMTs prior to their final optical gate metallization. Device fabrication in a cleanroom using standard techniques produced low-resistance Ohmic contacts (~ 4e-6 ohm-cm^2). A dual-layer mask consisting of SiO2/Si3N4 formed using low-power reactive ion etch (RIE) techniques allowed ultra-high vacuum (UHV) analysis and surface cleaning of the gate region prior to gate metal deposition.[1] Once metallized in UHV, final gate lift-off device processing was performed in a standard cleanroom. Four samples from the same quarter wafer were prepared allowing an investigation of a control sample and three different surface preparations: thermal desorption at 800 C, Ga deposition and desorption (Ga reflux) at 800 C, and N2-ion sputter cleaning at 1-3.5 kV energies with 800 C anneal. AES measurements indicate surface C and O reduction for all three sample cleaning methods and an increase in overall N signature. Ion sputtering produced the cleanest surface as determined by AES. However, CLS measurements reveal defect emissions that indicate damage of the surface layers. This damage is partially restored after annealing. The Ga reflux step produced defect emission near the GaN band edge due to excess Ga incorporation in the AlGaN layer as well as defect formation below the band edge. Preliminary device characteristics for the unpassivated devices show working HEMTs in all four samples with an average cutoff frequency at gm-peak ~ 4 GHz for the standard process, ~ 5 GHz for N2-ion sputter-cleaned, ~ 7 GHz for annealed, and ~ 9 GHz for Ga reflux transistors. However, RIE damage increased gate leakage in the annealed portion of the sample by nearly 1000x compared to the standard process sample. Gate leakage current increases an additional 10x for the Ga-reflux treated sample indicating a possible mechanism for device failure. Overall, these UHV device results show the importance of surface preparation both on defects and device performance – affecting both the final frequency performance and the gate leakage currents. [1]G. Jessen, "Investigation and characterization of AlGaN/GaN device structures and the effects of material defects and processing on device performance," Ph.D. thesis, The Ohio State University, Columbus, OH, 2002.

4:50 PM Student

H10, Growth and Characterization of $(AlN)_x(Si_3N_4)_{1-x}$ Thin Films for the Passivation of AlGaN/GaN HEMT Structures: *Richard J. Brown*[1]; James R. Shealy[1]; [1]Cornell University

Low Pressure Chemical Vapor Deposition (LPCVD) of mixed solutions of AlN and Si_3N_4 are reported for the first time. These films structural and optical properties were investigated as well as their passivation behavior when deposited on AlGaN HEMT structures. Etch rates were determined, using both wet chemistry and reactive ion etching. The films were deposited on both Si substrates and AlGaN/GaN High Electron Mobility Transistor (HEMT) structures in a hot-wall LPCVD furnace at 800°C. The precursors used were NH_3 (ammonia), SiH_2Cl_2 (dichlorosilane), and TMAl (trimethylaluminum) transported in a nitrogen carrier gas at 2 torr. As determined by Rutherford Backscattering (RBS) analysis, varying the ratio of the TMAl mole fraction to that of the SiH_2Cl_2 allowed a range of the aluminum nitride content (x) to be realized in the mixed solution. A significant growth rate enhancement was observed (a factor of 6) for films containing roughly 50% of AlN. The RBS data also demonstrates the lack of both chlorine and oxygen contamination, while the hydrogen content was roughly 2%. These films were applied to AlGaN/GaN HEMTs to examine their passivating properties by capacitance-voltage (CV) measurements. Note that the direct deposition of AlN films on the HEMT surface destroyed the two dimensional electron gas (2DEG) by cracking the AlGaN barrier layer. This can be avoided by the insertion of a thin silicon nitride layer (40 angstroms) underneath the AlN. For LPCVD silicon nitride films, if the dielectric is of sufficient thickness, the surface related depletion of the (2DEG) can be completely removed. The sheet electron density is increased (depending on the AlGaN barrier thickness) after passivation, and the 2DEG can be fully depleted through the insulator. Analysis of the CV data indicates that the LPCVD silicon nitride provides a fixed interface charge on the AlGaN surface which is equal and opposite of the AlGaN surface polarization charge[1] which explains the removal of the surface depletion. However, when LPCVD films containing AlN mixtures are used, a distributed fixed negative charge is present which allows controlled depletion of the 2DEG (depending on both film composition and thickness). These films are of particular interest for transistor passivation with reduced gate leakage, and for the application of metal-insulator-semiconductor (MIS) field plates in high power HEMTs[2]. The authors wish to acknowledge the support of Northrup Grumman, Raytheon and ONR. [1]"Growth and Passivation of AlGaN/GaN Heterostructures," J.R. Shealy, T.R. Prunty, E.M. Chumbes and B.K. Ridley, J. Crystal Growth, 250 (2003) 7-13. [2]"Performance of the AlGaN HEMT Structure With a Gate Extension," R. Thompson, T. Prunty, V. Kaper and J.R. Shealy, IEEE Trans. Electron Devices, 51, No.2 (2004) 292-295.

Session I: Materials Integration: Wafer Bonding and Alternative Substrates

Wednesday PM — Room: Conference Room 106
June 28, 2006 — Location: Pennsylvania State University

Session Chairs: Peter D. Moran, Michigan Technological University; Karl D. Hobart, Naval Research Laboratory

1:30 PM

I1, Exfoliation Temperature Dependence on Hydrogen Exfoliated Layer Properties: *Sumiko L. Hayashi*[1]; Rajinder Sandhu[2]; Mark S. Goorsky[1]; [1]University of California, Los Angeles; [2]Northrop Grumman Space Technology

The effect of thermal processing during the exfoliation of a thin InP layer onto a GaAs substrate is investigated. Before bonding, the InP is implanted with $5x10^{16} H_2^+/cm^2$ at 150 keV. This wafer is then bonded to a GaAs substrate using SiN intermediate layers. Both wafers are annealed for 3 hours at 150°C to strengthen the bond. Following our previously published approach (S. Hayashi, et al, J. Appl. Phys. 98, 093526 (2005)), the InP layer is exfoliated from the rest of the wafer by increasing the temperature to 300°C. The exfoliation typically occurs within a few seconds at this temperature. The second approach discussed here continued the annealing at 150°C until exfoliation occurred. This typically requires 48 hours. The extended annealing at lower temperature produced smoother surfaces, 2.8 nm RMS roughness, compared to the sample exfoliated at 300°C, 8.5 nm RMS roughness. This change in surface morphology exhibits a much larger impact than the effect of implantation energy (i.e. straggle) on the surface morphology. The difference is attributed to the ability to trap hydrogen and form extended defects parallel to the surface at the lower temperature, which is confirmed by cross sectional transmission electron microscope images of the exfoliated layer. This allows the surface morphology to be controlled regardless of the desired layer thickness, i.e. it is not determined solely by the implantation straggle. Additionally, the exfoliation depth

of the lower temperature specimen is slightly deeper (~50 nm) than the specimen exfoliated at 300°C. The "cut" location for the low temperature sample coincides with the depth of maximum hydrogen concentration after ion implantation. However, for the higher temperature exfoliation the layer is severed closer to the location of maximum lattice damage, as simulated by SRIM. The exfoliation at lower temperatures inhibits the diffusion of hydrogen producing exfoliation where the majority of the hydrogen resides in the as-implanted state. Conversely, for exfoliation at higher temperatures the implanted hydrogen is allowed to diffuse and preferentially agglomerates where the crystal is highly damaged, inducing the cut at this location. These conclusions are supported with transmission electron microscopy and high resolution x-ray scattering measurements.

1:50 PM Student

I2, Interfacial Chemistry of InP/GaAs Bonded Pairs: *Ning Liu*[1]; Thomas F. Kuech[1]; [1]University of Wisconsin-Madison

The integration of III-V materials, through wafer bonding, provides extra freedom and flexibility in the device design and fabrication processes. Combined GaAs and InP –based material systems has attracted considerable attention in order to take advantage of both of the electrical and photonic properties in optoelectronic devices. In these applications, an increase in initial bonding strength allows for more aggressive post-bonding processing. Many efforts have directed to increasing the bonding strength and improve the bonding quality by activating the surfaces during wafer bonding processes. In this study, InP (100)-GaAs (100) bonded pairs were prepared using both 5% HF in DI water and HF:ethanol (1:9) wet chemical treatments for InP combined with HCl:H_2O(1:1) rinsing for GaAs. The bond strength was quantitatively determined using the crack-opening method. Bonded surfaces were characterized using IR transmission imaging combined with MIT-FTIR measurements. For as-bonded InP/GaAs pairs, the bonding energies were 115±16 mJ/m_2, 116±17 mJ/m_2, and 103±12 mJ/m_2, corresponding to InP wafers without any treatments, 5% HF in DI water and HF:ethanol (1:9) chemical treatments, respectively. The bonding energies were increased to 469±99 mJ/m_2, 438±90 mJ/m_2, and 228±35 mJ/m_2, respectively, after annealing to 300°C for 8h in N_2. However, the bonding energies are too high to be measured after annealing to 400°C for 1h for all three cases using a simple crack-opening technique. The interfacial bonding energy is affected by the intermediate species on the prebonded surfaces which is determined by the specific chemical treatment. The surfaces of InP and GaAs wafers are initially covered by the native oxide, consisting of In_2O_3, or In_2O_3 with a very small amount of $InPO_3$ and or $InPO_4$ for InP, and a complex mixture of Ga and As oxides, as well as their respective suboxides, and potentially some free As for GaAs. The chemical pretreatment can remove this native oxide and leads to the formation of hydroxyl groups on the surface. The concentration of adventitious water and the areal density of hydroxyl groups are affected by the specific treatment. IR spectra were obtained as a function of pretreatment, anneal time and temperature and the evolution of the chemical composition of the bonding interface determined. Similar to GaAs-GaAs bonding, previous studies have shown that the room temperature bond is formed by hydrogen-bonded H_2O/OH groups with the areal concentration of these groups being directly correlated to the initial bonding strength. For InP-GaAs bonding, the use of ethanol leads to further interactions with the presence and reaction of hydrocarbons at the interface that affect the interfacial chemical composition and bond strength.

2:10 PM Student

I3, Dislocation-Gettering in Hydrogen-Induced Exfoliation of Metamorphic InAs Epilayers: *Atif M. Noori*[1]; Sumiko L. Hayashi[1]; Rajinder Sandhu[2]; Abdullah Cavus[2]; Vincent Gambin[2]; Augusto Gutierrez-Aitken[2]; Mark S. Goorsky[1]; [1]University of California, Los Angeles; [2]Northrop Grumman Space Technology

Hydrogen exfoliation and wafer bonding of epixatially grown semiconductors is demonstrated with the successful blistering of hydrogen implanted MBE-grown InAs on InP. The role of dislocations in this process is addressed by controlling the threading dislocation (TD) density in the InAs epitaxial layer. A 1 µm layer of InAs was grown directly on InP; the 3.2% lattice mismatch strain results in a threading dislocation density of 4×10^8 cm^{-2}, and a surface RMS roughness of 1.1 nm. A compositionally graded InAlAs buffer layer is used to produce an InAs epilayer with a lower TD density of 5×10^6 cm^{-2}, however a characteristic crosshatch morphology arises with an RMS roughness of 6.0 nm. This sample was chemical-mechanically polished to reduce the RMS roughness to less than 2.2 nm. All samples were subsequently implanted with a 1.5×10^{16} cm^{-2} dose of H_2^+ at an implant energy of 150 KeV resulting in an implantation depth of approximately 600 nm. High resolution x-ray diffraction demonstrated the strain evolution in the InAs with annealing time and temperature. This study confirmed that hydrogen is significantly more mobile in InAs than in InP. Blistering experiments were conducted to investigate the optimal exfoliation conditions. From previous studies in this laboratory, the kinetic nature of blistering was identified as occurring in two regimes - A high temperature regime characterized by the diffusion of hydrogen, and a low temperature regime that creates hydrogen trapping defects followed by the agglomeration of hydrogen around these defects. Annealing at 150°C for 10 minutes caused interstitial hydrogen to diffuse away from the implanted region towards lower energy sites - tensile strained regions around dislocations. Hydrogen agglomeration at dislocations sites was characterized by AFM and XTEM. Annealing at 75°C for 5 hours produced uniform surface blistering for both samples at the implantation depth.

2:30 PM

I4, Ultra-High Vacuum-Wafer Direct Bonding of III-V Compounds Semiconductors to Si-Wafer Using Low Energy (300 eV) Hydrogen Ion Beam Surface Cleaning: *N. Razek*[1]; A. Schindler[1]; B. Rauschenbach[1]; [1]Leibniz-Institut für Oberflächenmodifizierung

UHV-wafer direct bonding is becoming an important method to join different semiconductor materials with each other. Wafer surfaces must be prepared to be mirror-polished, flat, and clean from foreign contamination and dust for successful joining by forming chemical bonds at the interface. For applications of this bonding technique in MOEMS technology the bonding of III-V compounds and Si is very interesting. We performed a study of GaAs- to-Si bonding under UHV conditions. The wafers were cleaned using low energy (<500eV) hydrogen ion beam bombardment at low temperatures (<300°C) in order to achieve an oxygen and carbon contaminant as well as near damage free surface. The cleaned wafers are transported and brought together in contact for bonding at room temperature and finally annealed at low temperature(<150°C) in UHV to increase the bonding strength. In-situ and ex-situ infrared imaging of the as-bonded wafers show directly the bonding behaviour. High-resolution transmission electron microscopy images reveal that the wafers are bonded without damage of the crystal lattice or intermediate layer and that the interface is smooth. Current-voltage measurements are used for the electrical characterization of the bonding interface of heterotype (p-Si and n-GaAs) material bonding.

2:50 PM Student

I5, Stress Analysis of Transferred Thin-GaN Light Emitting Diode by Au-Si Wafer Bonding: *Shih-Chieh Hsu*[1]; Cheng-Yi Liu[1]; [1]National Central University

For the past decade, wide band gaps GaN-based semiconductors have attracted serious attention due to the application of high brightness light emitting diodes (LEDs). The GaN film is usually grown on sapphire. Yet, the relatively poor thermal conductivity of the sapphire substrate has been recognized to be the main limitation for the application of high-brightness LED. Many researchers start to replace sapphire substrate with a thermal conductive one by wafer bonding technique and Laser Lift-Off (LLO) process. This substrate substitution technology, which is called "thin-GaN device", has been proven that it can promote the electrical and optical properties. Comparing to the conventional wire-bonding LED, thin-GaN LED performs better results in the output lighting performance. The major advantages of thin-GaN LED are better current spreading and thermal dissipation. In this experiment, the thin-GaN LED devices are fabricated by Au-Si eutectic wafer bonding and LLO process. Au-Si eutectic bonding has been widely used for the Si die attachment and MEMS packaging as well. It can achieve a bonding layer with a high melting point (over 650°C) under a relatively low processing temperature (400°C). Besides, Au also has the best ductility of all the metal elements. The Au bonding layer will absorb the thermal stress induced during the wafer bonding and the LLO processes. This means that a low residual stress level can be obtained in the transferred GaN epi-layer. Wafer bonder (EVGroup, model 501) was used to

perform Au-Si bonding. The bonding temperature and pressure were 420°C and 5MPa, respectively. The bonding time was 30 minutes. After the wafer bonding process, KrF excimer laser (LPX210, 248nm, 25ns) was used to separate the GaN epi-layer from the sapphire substrate. The energy of a single laser pulse was 250 mJ/cm^2 and the irradiation size was 5×20mm. The relaxation process of the thermal strain in the transferred GaN films onto Si substrate is studied by varying the bonding film thickness of Au in a wide range from 0.7 μm to 50 μm. The transferred GaN thin films on Si substrates are characterized by Raman spectroscopy measurement and the residual stress state are also calculated. The transferred GaN thin films are found to be strained by the biaxial compressive stress. From the measured strain and the shift of Raman peak, 20μm Au bonding layer thickness is proven the least residual compressive stress and the maximum deformation potential of InGaN quantum well is found to be ~65meV. The complete compressive stress variation at whole thin-GaN fabrication process is discussed.

3:10 PM Break

3:30 PM

I6, Copper Interconnect Bonding for Polymer Pillar I/O Interconnects and Three-Dimensional (3D) Integration Application: *Kuan-Neng Chen*[1]; Muhannad S. Bakir[2]; James D. Meindl[2]; Rafael Reif[1]; [1]Massachusetts Institute of Technology; [2]Georgia Institute of Technology

Novel interconnect technologies and design methodologies are essential for the semiconductor industry to transcend known-limits in interconnects. The performance of a nanosystem is constrained by a hierarchy of interconnects. Three-dimensional (3D) integration, in which multiple layers of devices are stacked with high density of interconnects between layers, offers solutions for problems when the critical dimensions in integrated circuits keep shrinking. Copper interconnect bonding has been considered as an attractive candidate for fabrication of three-dimensional integrated circuits (3D ICs) since copper bonding medium acts as an electrical current path to connect two active device layers and a mechanical bond to offer a reliable strength for bonding structure. The bonding strength, interfacial morphology, and electrical property of bonded copper interconnects are demonstrated. The bonding qualities of different interconnect sizes and densities have been investigated. In addition to increasing the bonding temperature and duration, options such as larger interconnect sizes, total bonding area, or use of dummy pads for bonding in the unused area improve the quality of bonded interconnects. In addition, using metal-clad polymer pillars, simultaneous electrical and optical chip-to-substrate interconnection has been described. Copper was prepared in a ring-like pattern to receive the copper cladding on the polymer pillar. Since the polymer pillars were metallized only on their sidewall, light may be transmitted through the polymer core of the pillar. Beneath the metallized ring-shape pads, optical devices such as micromirrors or grating couplers are fabricated.In order to demonstrate this concept, three types of samples were prepared to experimentally study low-temperature Cu-Cu bonding of electrical/optical metal-clad polymer pillars: (a) two Si wafers coated with Cu films, (b) structures similar to (a) with the exception that the upper wafer was coated with a polymer film and cured prior to metal deposition, and (c) structures similar (b) with the exception that polymer film was patterned into polymer pillars prior to curing and metal deposition. The bonded wafers were diced into square pieces to mechanically characterize the bond strength. The microstructure morphologies of the bonded structures were examined using an SEM. A greater than 90% yield was achieved for all three samples, while the proper bonding time durations at the peak temperature were applied. Using the dicing test and SEM observation, the polymer pillars coated with Cu films are successfully bonded with Cu wafers without damage of the structure at desired temperature. This demonstrates that in addition to three-dimensional integration, Cu bonding can be also applied to polymer pillar I/O applications.

3:50 PM Student

I7, Fabrication of Poly-Silicon TFT on Flexible Thin Glass Substrate: *Yoochul Jung*[1]; Sunghwan Won[1]; Dieter G. Ast[1]; [1]Cornell University

Currently, most of the flexible displays use amorphous Si:H as an active layer, deposited at temperatures below 300° on a variety of plastics substrates. However, these substrates are not a suitable material for low cost poly silicon (poly-Si) thin film transistors, TFT's, since the thermal expansion (CTE) of plastic substrates exceeds by more than an order of magnitude the CTE of semiconductors and insulators. Consequently, severe thermal stresses are induced the management of which requires time consuming and expensive steps, including the deposition of "dummy" layers on the backside of the plastic foil. As an alternative, we use thin flexible glass of 75 um average thickness (Corning 00 microsheet) as a substrate to fabricate poly-Si TFT's. These glass substrates are so thin that they can be bent to radius of curvature as small as 3 inch and have a CTE within a factor 2 of silicon. A barrier layers, SiNx, followed by a SiO2 layer, is first deposited on both sides of glass substrate to suppress the out-migration of unwanted glass constituents from the glass into the semiconductor during processing and to minimize back channel leakage. To process these TFT's on glass in conventional semiconductor equipment is not trivial and after exploring several approaches (including In-Ga alloy bonding) we settled on the use Si wafers that contains "pockets" in which the thin glass substrates can be inserted. These "pocket carriers" were fabricated using a by combination of micro-machining and electrostatic bonding of Si to Si via a pyrex "glue" layer. The flexible glass can easily be removed from the carrier for wet etching, but is mechanically supported by the Si wafer during high temperature processing steps such as poly-Si deposition, LTO (low temperature oxide) deposition, and implant activation anneal. After fabrication of the TFT, the transistors are passivated using a hydrogen plasma. Results obtained will be presented at the meeting.

4:10 PM Student

I8, Built-In Strain in Silicon Nitride Films on Polymer Foils: *Alex Z. Kattamis*[1]; I-Chun Cheng[1]; Ke Long[1]; James C. Sturm[1]; Sigurd Wagner[1]; [1]Princeton University

We studied the built-in strain in silicon nitride (SiN_x) thin films on Kapton® E foil substrates as a function of radio frequency (RF) deposition power and film thickness. Our study was motivated by the prospective use of silicon thin-film transistor (TFT) arrays on polymer foil substrates for flexible active-matrix backplanes. In such applications the TFT layers and the polymer substrate typically have comparable mechanical strengths, expressed as the product of thickness and biaxial elastic modulus. Earlier we showed that the dimensions of the substrate change noticeably as the strain in SiN_x layers of constant thickness is varied by varying the RF power in PE-CVD[1]. These changes induce substrate curvature. Subsequent changes in the substrate dimensions lead to feature misalignments between patterning steps in the TFT process. We now conducted a study of the effects of varying the thickness of SiN_x films, in addition to the RF power. Our goal was to determine if the built-in strain at a given RF power varies with SiN_x film thickness, either because of a change in film structure or because of the continuous change in size of the substrate as the film grows in thickness. The SiN_x was deposited at room temperature to eliminate thermal stress, and thereby isolate the built-in stress. The thickness was varied from 50nm to 1050nm and the RF power density from 66mW/cm^2 to 155mW/cm^2. This range of power density is known to produce SiN_x with tensile strain at low power and compressive strain at high power. Substrates were held flat but not clamped during film growth. The radii of curvature of the samples were measured after removal from the deposition system. The curvature is defined positive for inward bending (tensile strain in the film) and negative for outward bending (compressive strain), with the growth surface up. To extract accurate values for the built-in strain[2], we separately measured the stress-strain curve of a SiN_x/Kapton® E sample in a tensile tester and extracted the biaxial elastic modulus of the SiN_x. Our preliminary conclusion is that the built-in strain is a function only of RF deposition power, and does not vary with film thickness. Thus the changes in substrate dimensions results only from the changes in the relative strengths of film and substrate. This also changes the SiN_x/Kapton® E interfacial strain. At present we are working on defining the admissible film thicknesses that do not exceed the critical interface strain. [1]I-C. Cheng, A. Z. Kattamis, K. Long, J. C. Sturm, and S. Wagner, J. Soc. Info. Disp. (SID), 13.7, p. 536, 2005. [2]Z. Suo, E. Y. Ma, H. Gleskova, and S. Wagner, Appl. Phys. Lett. 74, p. 1177, 1999.

4:30 PM
I9, Digital Lithographically Patterned Fine-Features for Flexible Thin-Film Transistor Array Backplanes: *William S. Wong*[1]; Scott Limb[1]; Eugene Chow[1]; Michael Chabinyc[1]; Rene Lujan[1]; Beverly Russo[1]; [1]Palo Alto Research Center

Digital lithographic methods for patterning thin-film transistor devices, in which an electronically generated and digitally aligned etch mask is jet-printed onto a substrate surface, have been demonstrated as a viable alternative technology for low-cost, large-area electronics. Combining this electronic imaging and patterning technology with low-melting point flexible substrates, would further lower materials and fabrication cost for large-area electronics in display, sensor, and evolving electric paper applications. The spatial resolution and small drop volume of jet-printing methods present opportunities to simplify and reduce the cost for conventional large-area electronic device fabrication and has been demonstrated with a-Si:H thin-film transistor (TFT) array backplanes for reflective display applications. In some cases, the minimum drop size of jet-printed features may be too large for high-performance and high-resolution display and image sensor applications. The digital lithographic process, having minimum printed features of ~40 microns, allows for very accurate and precise drop placement control. By using this spatial control, fine-feature gaps (10-15 microns) can be patterned over large areas. In this talk we will describe the fabrication of fine-feature TFT devices using a jet-printed etch mask process with conventional a-Si:H and polymeric semiconductor materials. Channel lengths as short as 10 microns were fabricated using the digital lithographic process. In combination with digital lithography, a low temperature a-Si:H based TFT deposition process (T<150°C) was used to fabricate TFT devices having threshold voltages of 2-3 V and on/off ratios of 10^8, and field effect mobilities of 1 cm^2/Vs, comparable to conventionally processed a-Si:H TFT devices. Polymeric thin-film transistors were also fabricated using the digital lithographic fine-feature patterning process. Pixel design using digital lithography and integration of the flexible TFT array backplane with display media will be discussed.

4:50 PM
I10, Late News

Session J: Nanotubes

Wednesday PM Room: Conference Room 208
June 28, 2006 Location: Pennsylvania State University

Session Chairs: Ray Tsui, Motorola Laboratories; Alec Talin, Sandia National Laboratories

1:30 PM
J1, Thin Film Transistors from Transparent Conducting Single-Wall Carbon Nanotube Networks: *Giovanni Fanchini*[1]; Husnu Emrah Unalan[1]; Manish Chhowalla[1]; [1]Rutgers University

Transparent conducting nanotube thin films are promising materials formed by low density networks of single-walled carbon nanotubes (SWNT)[1]. They find applications in transistors due to their semiconducting properties. However only 67% of the SWNT are semiconducting, the complementary fraction being metallic and this requires special cares in order to use SWNT films in electronic devices. We recently developed an optimization process[2] to determine the optimum properties for SWNT thin film to be used as semiconducting layers in thin film transistors. Devices have been fabricated in order to validate our model. We show that crucial roles are played by the percolation threshold of the metallic nanotubes and by the percolation threshold of the whole network. Optimum SWNT transistors are made by thin films above the network percolation threshold but much below the percolation threshold of the metallic tubes. Indeed, even below the metallic percolation threshold, the transistor performances, especially the on/off ratio, still suffer severe limitations by the tunneling current between isolated metallic SWNT or bundles. Such device limitations have been partially overcome by thin films where SWNT are functionalized by bromine in the form of acyl bromide (COBr) radicals, leading to doping from chemically bonded species. Transistor mobility rises from 4.10^{-2} cm^2/Vs to 5 cm^2/V/s, with on/off ratio increasing from 10 to 200. Indeed, the role of the Br functionals is not only in moving the Fermi level but also in passivating the free electrons in metallic SWNT. [[1]L Hu et al Nano Letters 4 (2004) 2513. [2]HE Unalan et al Nano Letters (in press, 2006).

1:50 PM
J2, Carbon Nanotube Single-Electron Transistors Fabricated with Focused-Ion-Beam Technique: *Kenzo Maehashi*[1]; Hirokazu Ozaki[1]; Yasuhide Ohno[1]; Koichi Inoue[1]; Kazuhiko Matsumoto[1]; Shu Seki[1]; Seiichi Tagawa[1]; [1]Osaka University

Single-walled carbon nanotubes (SWNTs) behave as quasi one-dimensional electronic systems, because they have inherently small diameter (typically 1–2 nm). SWNTs are one of the promising candidates for the nano-scale devices. It is possible to operate single electron transistors (SETs) at room temperature if the charging energy of a quantum dot sufficiently exceeds the thermal energy at room temperature. Chemical process succeeded in fabricating room-temperature SETs by introducing defects on the SWNT channel. However, the channel has multi-dot structures with multi-energy levels. Then, it is impossible to precisely control the size and number of dots on the SWNT channel with this method. In this study, we have fabricated carbon nanotube SETs using focused-ion-beam (FIB) technique. The FIB has been used for nano-fabrication processes. For SETs, the tunnel barriers can be fabricated on the SWNT channel by FIB etching. Therefore, we will control the size and number of dots on the SWNT channel. A p-type Si wafer with thermally oxidized SiO2 was used as a substrate. First, Co as a metal catalyst was patterned on the substrate using conventional photolithography and liftoff processes. Next, the SWNTs were synthesized by thermal chemical vapor deposition using C2H5OH as a carbon source. Following this, Ti/Au electrodes were formed, both on the patterned catalysts and on the backside of the substrate. The distance for the source and drain was 5 μm. Finally, we introduced two defects on the SWNT channel by irradiating two ion-beam lines to fabricate one ultrasmall island. The acceleration voltage and diameter of the Ga ion beam were 30 kV and 5 nm, respectively. The electrical properties of the device were all measured at room temperature. Before FIB processes, typical p-type characteristics are obtained for CNTFETs. However, after introduction of two defects with the distance of 50 nm on the SWNT channel by FIB process, the source-drain current oscillation is clearly observed at room temperature, resulting from the Coulomb blockade effect. The charging energy of the island on the SWNT channel is estimated to be 270 meV, which is more than ten times higher than thermal energy at room temperature. Moreover, the gate capacitance dependence of the distance of two defects is also obtained. These results indicate that the room-temperature operating SETs can be fabricated by controlling the size and number of defects using FIB techniques.

2:10 PM
J3, Contact Metallization Process for Vertical Carbon Nanotube Arrays Templated in Porous Anodic Alumina: *Aaron Franklin*[1]; Matthew R. Maschmann[1]; Manuel DaSilva[1]; Timothy D. Sands[1]; Timothy S. Fisher[1]; David B. Janes[1]; [1]Purdue University

While interest in nanowire and nanotube device research continues to increase, efficient and repeatable fabrication of devices on pre-functionalized substrates remains a challenge. Porous anodic alumina (PAA), with its high-density nanoporous structure, has provided a template for the synthesis of nanowires and nanotubes for over a decade. One of the most pervasive challenges for using PAA to create devices on pre-functionalized substrates is the presence of an oxide barrier that forms at pore bottoms as part of the anodization process. Previous methods used to remove the oxide barrier utilized an electrochemical step in either a KCl solution[1] or the anodization electrolyte[2] with a polarity opposite that used to anodize the sample. Use of a KCl solution selectively oxidizes the underlying titanium, impeding the deposition of nanowires into some pores. The reverse bias step in the anodization electrolyte generates large voids at the bottom of the PAA template, thus hindering the ability to control the length of the deposited nanowire array. In the present study, a microwave-generated hydrogen plasma is used to penetrate the bottom oxide barrier in PAA fabricated by anodization of aluminum films deposited on silicon substrates. A titanium layer between

the aluminum film and the silicon substrate is incorporated to promote adhesion and to provide a conductive layer for subsequent electrodeposition of palladium (Pd) nanowires. Using pores of various diameters, the Pd nanowires were deposited and imaged using a field-emission scanning electron microscope (FESEM), revealing nanowires with uniform length and diameter. The length variation of the nanowires is approximately 12%, and the average yield of Pd in the pores is approximately 80%. Uniform deposition of Pd nanowires suggests that the hydrogen plasma etches the bottom oxide barrier, without leaving voids in the PAA film. Using the Pd nanowires in the pores as a patterned catalyst, carbon nanotubes (CNTs) have been synthesized using plasma-enhanced chemical vapor deposition (PECVD). The resulting multi-wall CNTs demonstrate a diameter dependence on the Pd nanowire (PAA pore) diameter. Simple electrical characterization of the as-grown CNTs reveals that electrical contact exists between the Ti electrode at the bottom of the PAA template and the CNT bundles on the top PAA surface. Furthermore, the Pd nanowires have been used to achieve electrical contact to single-wall CNTs (SWCNTs) synthesized using a buried iron catalyst about 200nm from the top surface of a PAA template[3]. The SWCNT growth proceeds with generally no more than one SWCNT growing from a single pore. Pd nanowires are subsequently electrodeposited, filling the pores to a level that contacts the SWCNT. A top contact is currently being implemented to create a two terminal SWCNT device, and further processing will lead to a vertical three terminal field-effect transistor.

2:30 PM

J4, Field Emission Induced UV Electroluminescence from Atomic Layer Deposition ZnO Coated Carbon Nanotubes: *John F. Conley*[1]; Joshua M. Greene[2]; Lifeng Dong[2]; Jun Jiao[2]; Yoshi Ono[1]; [1]Sharp Laboratories of America; [2]Portland State University

Atomic layer deposition (ALD) is a pulsed chemical vapor deposition technique in which a substrate is alternately exposed to purge separated pulses of the individual precursors required for a complete reaction. Because reactions take place on the substrate surface and are self limiting, ALD offers inherent high conformality deposition of thin films. This high conformality makes ALD an ideal technique for surface treatment of nanostructures. In this work, ALD was used to coat multiwall carbon nanotubes (CNTs) with a thin conformal layer of ZnO. Scanning and transmission electron microscopy revealed that subsequent annealing of the ZnO coated CNTs resulted in the agglomeration of the ZnO film into ball-shaped single crystalline nanoparticles attached to the sidewalls of the CNTs with no significant changes in the internal structure of the CNTs. The diameter of these ZnO nanoparticles is approximately equal to the diameter of the multiwall CNTs. CNTs are well known to be excellent field emitters. Electron field emission measurements of annealed ZnO coated CNTs revealed an enhancement of field emission properties by a factor of approximately 3x or over uncoated CNTs. It is proposed that the ZnO nanoparticles serve as additional emission sites. ZnO is a well known UV photoluminescent material with an intrinsic emission at 380nm as well as an often observed defect emission in the visible range (~515-530nm). Although UV electroluminescence would have many optoelectronics applications, despite much effort, it has proven very difficult to generate UV EL from ZnO planar thin films. By applying a very high voltage (>1000 V) to a sharp tip (anode) positioned within 150-200 µm from the ZnO coated CNT surface (cathode), a strong EL spectra consisting of a 382nm visible peak and a slightly shifted visible peak at about 515nm. Field emission and UV EL are observed simultaneously. These field emission induced EL peaks were not observed in uncoated CNTs or in ZnO nanowires. A comparison to PL spectra of the ZnO coated CNT film demonstrates that the EL arises from the ZnO film. A likely mechanism for the EL is impact ionization in the ZnO. These results demonstrate a novel way to improve the field emission properties of CNTs and to generate UV EL from ZnO. This work also demonstrates the utility of ALD as a tool to engineer the surface properties of nanostructures.

2:50 PM Student

J5, Characterization and Application of Transparent and Conductive Single Walled Carbon Nanotube Thin Films: *Husnu Unalan*[1]; Aurelien Du Pasquier[1]; Giovanni Fanchini[1]; Manish Chhowalla[1]; [1]Rutgers University

Single walled carbon nanotube (SWNT) thin film devices provide an alternative to individual SWNT devices. Uniform and reproducible SWNT thin films can be deposited over several centimeters, allowing fabrication of devices over large areas. Several methods are being employed for the fabrication of SWNT films, including the recently reported vacuum filtration method[1]. Although the device characteristics of the SWNT thin films have been characterized[2], no detailed investigation of the film properties has been reported. In this work, we will present a detailed analysis of the SWNT thin film properties using the vacuum filtration method. We will present the variation of the SWNT thin film properties as a function of the film thickness and the nanotube concentration in the filtrated solution. The SWNT thin films were found to be highly transparent and conducting with values comparable to indium tin oxide (ITO)[3]. Specifically, at the lowest nanotube concentration, the transmission of the SWNT thin films exceeded the values of ITO. The SWNT thin films were always found to be more transparent in the UV in comparison to ITO. The transmission and sheet resistance of the SWNT thin films were found to decrease with the film thickness and SWNT concentration in the filtrated solution. The SWNT thin films have a highly porous structure which can be used to explain the optical and electrical properties. We will also present our thin film transistor characteristics[4]. [1]Z. Wu, Z. Chen, X. Du, J.M. Logan, J. Sippel, M. Nikolou, K. Kamaras, J.R.Reynolds, D.B. Tanner, A.F. Hebard, A.G. Rinzler, Science 305 (2004) 1273. [1]E. Artukovic, M. Kaempgen, D.S. Hecht, S. Roth, G. Gruner, Nanoletters, 5(4) (2005) 757. [1]A. Du.Pasquier, H.E. Unalan, A. Kanwal, M. Chhowalla, Appl. Phys. Lett. 87 (2005) 203511.[1]H. E. Unalan, G. Fanchini, A. Kanwal, A. Du Pasquier, M. Chhowalla, Nanoletters (accepted 2005).

3:10 PM Break

3:30 PM Student

J6, Precise Control of Number of Carbon Nanotube Growth by Digital Growth Process: *Masatoshi Maeda*[1]; Takafumi Kamimura[2]; Kazuhiko Matsumoto[2]; [1]University of Tsukuba; [2]Osaka University

Carbon nanotube (CNT) is the useful element for the future nanodevices. For example, semi-conducting nanotubes can be electrically switched as field effect transistors. In addition, CNTs have been demonstrated as biological sensors with high sensitivity. The control of the number of CNT between electrodes is quite important technology for the electronic device applications. However, it is quite difficult and has not been realized yet. It is therefore, indispensable to control it for the future applications of CNT. In the present study, we have established the new technology to control the number of the CNT one by one during the growth of CNT by monitoring the electrical current between electrodes, which is named as “Digital Growth Process”. The sample was then, set in an electric furnace and two electrodes were connected to the bias source. During the heat-up process of furnace, Ar gas of 1000 sccm was supplied. At a growth temperature of 900°C, ethanol vapor bubbled by Ar gas of 750 sccm was supplied with hydrogen gas of 500 sccm. During the growth of the CNT for 600 to 650 sec, DC bias of 500mV was applied between two electrodes and the current was monitored. After the growth of CNT, the furnace was cooled down to room temperature with a 1000 sccm flow of Ar gas. In the monitoring current during the growth of CNT, the step-like increase of the current was observed. The clear two step increase of current was observed. These step-like current supposed to be strongly related to the one by one increase of the number of the CNTs which make bridges between electrodes. In order to confirm this assumption, the electrical breakdown process was applied to these devices. CNTs were cut using the electrical breakdown process and the current was monitored. In this process, two step-like decrease of the current was observed. These results mean that we have two CNTs between electrodes. The number of steps of the current in the electrical breakdown process coincided with that of the monitoring current during the growth of CNT. Therefore, each step of increase current in this figure during the growth of CNT corresponds to each bridging CNT between electrodes. So, by monitoring the current during the growth of CNT, you could know now many CNTs are bridging between electrodes. We have first succeeded in one by one control of the number of CNT by monitoring the number of the step like current during the growth of CNT. We named this process as “Digital Growth Process”. The number of CNTs between two electrodes can be made an arbitrary number using this process. This technique is useful for the application of the future CNT devices.

3:50 PM Student
J7, Assemblies of Single Wall Carbon Nanotubes and Unencapsulated Sub-10 nm Gold Nanoparticles: *Qingling Hang*[1]; Matt R. Maschmann[1]; Timothy S. Fisher[1]; David B. Janes[1]; [1]Purdue University

Single-wall carbon nanotube (SWNT) based devices are of interest for both electronic and sensing applications. This interest derives from the exceptional electrical performance of CNT-transistors and the high reported sensitivity of CNT-based sensors. Various approaches to contacting and functionalizing CNTs have been reported. These approaches include forming assemblies of encapsulated Au nanoparticles with CNTs, which have been reported to increase selectivity in sensing applications. The use of unencapsulated Au nanoparticles on individual SWNTs should provide much stronger electronic coupling between the Au and the CNT. This feature in turn, could provide much stronger responses in sensor applications and better contacts in electronic devices. We report a technique for forming assemblies consisting of unencapsulated, sub-10 nm Au nanoparticles that are stably bound to individual, bare, single-wall CNTs. The SWNTs were grown by plasma-enhanced chemical vapor deposition on porous anodized alumina surfaces using embedded catalyst particles. The gold particles are formed on the SWNTs by an indirect evaporation technique in which the gold is first evaporated on adjacent sections of the alumina surface and then coalesces into nanoscale particles. The gold nanoparticles then diffuse along the surface and adhere to the SWNTs. Scanning electron microscope images indicate that isolated Au nanoparticles are attached to the SWNTs, with sufficiently strong binding that they are stable over free-standing sections of the SWNTs and can move along with the SWNTs. An estimate of the van der Waals binding energy confirms that a nanoscale Au particle should bind stably to a CNT surface. The close coupling of Au nanoparticles may eliminate the need to chemically modify carbon nanotubes in order to provide adequate binding sites. In addition, the assemblies are of interest as potential electrical contacts to SWNTs.

4:10 PM Student
J8, Characterization of the Field Emission Properties of Carbon Nanotube Films Formed on Silicon Carbide Substrates by Surface Decomposition: *Michael C. Pochet*[1]; James A. Fellows[1]; John Boeckl[2]; [1]Air Force Institute of Technology; [2]Air Force Research Laboratory/Materials and Manufacturing Directorate

Numerous works found in the literature report that carbon nanotubes have excellent field emission properties, emitting high current densities at low electric fields. Recent work by the Air Force Research Laboratory Materials and Manufacturing Directorate has shown that dense arrays of vertically aligned carbon nanotubes form on the surface of silicon carbide wafers during high temperature (1400-1700°C) anneals under moderate vacuum conditions (10^{-3} – 10^{-5} Torr). The novelty of this growth method is that the carbon nanotubes form without the aid of a metal catalyst, allowing for potentially defect free carbon nanotubes to form. In this paper, carbon nanotube films were grown through the surface decomposition of silicon carbide substrates and the associated field emission characteristics were investigated to determine if films grown using this method possessed advantages over films grown using metal catalyzed methods. The parameters of the growth conditions, such as anneal time and vacuum conditions, were varied to determine the optimal conditions necessary for fabricating an effective emission surface. Scanning electron microscopy, transmission electron microscopy, and atomic force microscopy have been used to characterize the surface properties of the fabricated films. The associated turn-on voltage, threshold voltage, and maximum current density exhibited by the films were measured using the standard diode-type test configuration. The stability of the CNT films' emission current was recorded over finite lengths of time. The presence of adsorbed molecules altered the field emission performance of samples in a manner that was not fully understood. In some instances, the application of high strength electric fields (ranging from 7.0 – 13.0 V/μm) resulted in improved field emission characteristics; while in other cases, the field emission performances drastically deteriorated. Although the samples tested did not demonstrate improved field emission characteristics when compared to values found in the literature, the data collected shows that further investigation is warranted regarding their emission capabilities. From the collected data, the lowest turn-on electric field was found to be lower than 3.0 V/μm, while exhibiting a high maximum current density of 4.25 mA/cm^2, at 6.7 V/μm.

4:30 PM
J9, Oxygen Effects on Formation of Carbon Nanotube Structure in SiC Decomposition: Weijie Lu[1]; *Senthil N. Sambandam*[1]; John Rigueur[1]; Warren E. Collins[1]; John Boeckl[2]; William C. Mitchel[2]; [1]Fisk University; [2]Air Force Research Laboratory

Metal-free carbon nanotubes (CNTs) by SiC thermal decomposition are well-aligned and have minimal structural defects. The metal-free aligned CNTs/SiC structures have great potentials for various electronic device applications. Importantly, the metal-free CNTs growth process provides an excellent platform to investigate the fundamental issues such as the mechanism of CNT formation at the atomic scale. In this study, the effects of oxygen pressure on CNT growth by SiC thermal decomposition are investigated in high vacuum ($10e^{-5}$ torr) and ultra-high vacuum ($10e^{-8}$ torr). Oxygen in the UHV chamber is not detective by mass spectrometer, and in the high vacuum furnace, the oxygen pressure is at about $10e^{-7}$ torr. Using transmission electron microscopy (TEM), CNTs are formed in the high vacuum condition in the temperature range from 1400 to 1700°C, and are well-aligned vertically on the SiC surface. In the ultra-high vacuum, no CNTs structural features are found in the cross-section TEM images, and only some amorphous carbon thin film structures are found on the SiC surface. Therefore, metal-free CNTs can be formed only the presence of a low pressure of oxygen. Raman scattering provide additional evidence that CNTs are formed only on the samples grown in the high vacuum. Graphitic features co-exist with CNTs on the samples grown in the high vacuum. The results in this work are consistent with our previous results that a thermal oxygen-carbon compound is the intermediate compound in the process of CNTs formation. The study provides additional evidence that low-pressure oxygen atoms interact with carbon atoms in the hexagonal network structures to form CNT structures at high temperatures, and oxygen acts as a graphitization catalyst in the CNT growth. An oxygen catalytic growth model at the atomic scale is presented.

4:50 PM
J10, Late News

Session K: Chemical and Biological Sensors I

Wednesday PM — Room: Conference Room 207
June 28, 2006 — Location: Pennsylvania State University

Session Chairs: Stephen W. Howell, Sandia National Laboratories; David B. Janes, Purdue University

---

1:30 PM
K1, Large Area, Dense Si Nanowire Array Chemical Sensors: *Alec Talin*[1]; Luke Hunter[1]; Francois Leonard[1]; Rokad Bhavin[2]; Blake Simmons[1]; [1]Sandia National Laboratories; [2]Cornell University

Si nanowires (SiNWs) have been demonstrated as excellent chemical and biological sensors. However, most nanowire-based sensor devices to date have been fabricated by first synthesizing, then harvesting, and finally disbursing the nanowires over substrates to create devices. While these methods are acceptable for demonstrating a sensing effect, their practical implementation remains challenging. Furthermore, non-uniformity in as-synthesized nanowire dimensions, coupled with a small number of devices leads to poor statistics and lack of reproducibility in sensing results (particularly among different research groups). Here, we demonstrate a simple, 'top-down' technique for defining SiNWs over large areas, with high density and uniformity, and illustrate their application for chemical sensing. To fabricate large arrays of SiNWs with uniform dimensions we rely on nanoimprint lithography (NIL), a technique based on direct replication of a master template in a suitable organic polymer. Using a 4" diameter Si template with a 200 nm pitch grating (100 nm line/space) and 2:1 aspect ratio, we replicate the grating pattern in PMMA resist spun over a SOI substrate. Using reactive ion etching, we then transfer the grating pattern into the 100 nm thick device layer, resulting in 60 nm wide nanowires that span the entire area

of the wafer. Arrays of interdigitated, individually addressable Al electrodes that serve as source and drain contacts are defined over the SiNWs using optical lithography. The resulting devices consist each of 900 Si nanowires that span pairs of Al electrodes separated by 1 um - 4 um. These devices exhibit clear and reproducible transistor characteristics. We demonstrate the chemical sensing properties of the SiNW arrays by applying solutions of different concentration of nitrobenzene in cyclohexane and measuring changes in source-drain current versus gate voltage characteristics. Sandia is a multiprogram laboratory operated by Sandia Corporation, a Lockheed Martin Company for the United States Department of Energy's National Nuclear Security Administration under contract DE-AC04-94AL85000.

1:50 PM

K2, A Self-Assembling Semiconductor Nanowire-Based Pathogen Detection System: *Debdeep Jena*[1]; Ronghui Zhou[1]; Hsueh-Chia Chang[1]; Masaru K. Kuno[1]; [1]University of Notre Dame

The rapid detection of pathogens like bacteria, viruses and parasites on a portable device would be invaluable for medical diagnostics, water supply monitoring, food safety and homeland security. As a typical example, detecting and identifying the proper antibiotics for TB bacteria is still carried out with the century-old technique of culturing, which takes days, and requires laboratory equipment and monitoring by trained technicians. Nanowires and carbon nanotubes (CNT) are among the best examples of novel nanostructures. They exhibit a range of extraordinary physical properties, such as extremely small sizes, high aspect ratios (>1000), and a rich spectrum of electrical and optical properties. In addition, they can be physically moved around in a liquid environment with electric fields. These unique features can be exploited to improve biosensors, bioelectronics and circuitries. Biosensor applications which exploit the sensitive conductance change (or field-gating effects) of SWNT/nanowires with respect to bioparticle docking events all suffer from the extremely slow process of directing a low concentration of pathogens to the electrodes due to the intrinsically low diffusivity of bacteria and viruses. For example, given a typical bioparticle diffusivity of 10^{-7} cm^2/s, it requires the bioparticle hours to diffuse across a realistic diffusion length of 0.1 cm to reach the sensor given a typical pathogen concentration of one thousand bacteria per cc. To tackle the technical hurdle of enhancing the pathogen transport rate across a 1 mm length within minutes, we have exploited the giant positive ac dielectrophoresis (DEP) of solution-grown (~10nm diameter, ~few microns long) semiconducting CdSe nanowires. The pathogen-sensing device we demonstrate exploits the propensity of highly polar semiconductor nanowires to dock with pathogens in an ac electric field through dipole-dipole interaction. The CdSe nanowires + bacterial cell composites are observed to self-assemble within 30 seconds between electrodes between which an ac voltage (10 V peak-peak, 1 MHz) is applied. Both nanowires and nanotubes are observed to capture bacterial cells from a solution, and are attracted by the DEP force to form a bridge across the electrodes, where their fluorescence is directly read out. The electronic and optical properties of the CdSe nanowires have been studied in detail; a 2-3 order of magnitude increase in current is achieved either by electrostatic field-gating, or by exposure to visible light. The high dielectrophoretic (DEP) mobility of the nanowires and nanotubes, and the high sensitivity of their fluorescence, electrical conductivity, and photoconductivity to docked pathogens offer additional readout mechanisms for identification of the pathogens, and elimination of false alarms. The nanowire/pathogen bridge formed between electrodes in a very short time scale provides the first step towards realization of a portable electronic single bacteria/virus detection from very dilute solutions.

2:10 PM

K3, Trace Chemical Detection Using Single-Walled Carbon Nanotubes: *Joshua A. Robinson*[1]; Eric Snow[1]; F. Keith Perkins[1]; [1]Naval Research Laboratory

In this presentation I will describe our effort at NRL to develop a chemical detection technology based on single-walled carbon nanotubes (SWNTs). SWNTs possess many unique properties that make them well suited for the direct electronic detection of trace chemical vapors. These properties include the structure of SWNTs in which every atom is a surface atom. This infinite surface-to-volume ratio produces a high sensitivity to its local chemical environment. SWNTs also exhibit near-ballistic electron transport along the nanotube axis. This high-quality transport provides an efficient electrical conduit to transmit changes in electrical properties caused by the presence of a chemical adsorbate. Finally, the graphitic surface of SWNTs is almost chemically inert, which allows reliable operation in harsh environments. However, in order to utilize these properties there are a number of issues that must be addressed before SWNTs can be incorporated into a commercial detection system. These issues include the development of an inexpensive, high-yield fabrication procedure, reduction of the 1/f noise, optimization of the sensor transduction mechanism and providing chemical specificity. In this presentation I will describe our approach to addressing each of these issues and will report on our progress toward developing a SWNT-based trace chemical detection system for toxic industrial chemicals, chemical warfare agents, and explosives.

2:30 PM Student

K4, High-Sensitive Detection of Immunoglobulin E Using Aptamer-Modified Carbon Nanotube Field-Effect Transistors: *Taiji Katsura*[1]; Kenzo Maehashi[1]; Kazuhiko Matsumoto[1]; Kagan Kerman[2]; Yuzuru Takamura[2]; Eiichi Tamiya[2]; [1]Osaka University; [2]Japan Advanced Institute of Science and Technology

Carbon nanotube field-effect transistors (CNT-FETs) are promising candidates for the high-sensitive label-free biosensors due to their excellent electrical transport properties. However, conventional FET biosensors based on antigen-antibody reactions, using antibodies as probes, have an inevitable problem on the size of probes. Since the size of antibodies is larger than that of the Debye length in buffer solutions, most of the protein charges will be canceled in buffer solutions. As a result, proteins may not be detected easily with such FET biosensors. In this study, we have detected Immunoglobulin E (IgE) with CNT-FETs, in which aptamers are used as probes. Aptamers are artificial oligonucleotides that have the ability to recognize specific ligands by forming binding pockets. The aptamers are smaller in size than the Debye length. They have also demonstrated stronger and more selective affinity for their target proteins than the corresponding antibodies. Recently various aptamers, which can bind to nucleic acids, proteins or small organic compounds, have been found. IgE is the type of antibody and most instrumental in allergic reactions. Hence, detection of IgE is very important in terms of immunology. Moreover, IgE exists only low amount in human blood. Therefore, high-sensitive detection is required in medical scene. In this abstract, we have fabricated the aptamer-modified CNT-FETs, and the electrical properties of the CNT-FETs have been measured after introduction of IgE at various concentrations.CNTs were synthesized with alcohol chemical vapor deposition method, and were employed as channels in CNT-FETs. First, the side-walls of CNT channels were modified with linkers (1-pyrenebutanoic acid succinimidyl ester). Next, the 5'- amino modified aptamers were covalently immobilized on the CNTs. Then, unreacted linkers were blocked by ethanolamine. Afterwards the aptamer-modified channels in the CNT-FETs were incubated into 10mM phosphate buffer solutions. A reference electrode (Ag/AgCl) was used as a gate electrode. The different concentrated IgE solutions were introduced into the samples, and the electrical properties were measured in real time. After introduction of IgE, source-drain current sharply decreased, and gradually saturated at lower values. This indicates that the changes in conductance of CNTs after aptamer-IgE binding on channel were detected by CNT-FETs. Therefore, IgE at 0.25 nmol/L could be detected by CNT-FETs. Consequently, IgE can be high-sensitively detected with the aptamer-modified CNT-FETs. Our aptamer-based CNT-FETs are promising for future generations of biosensors which are compact and realize easily real time detection in medical, forensic and environmental diagnostics.

2:50 PM

K5, Real-Time Sensing of Proteins by Using a Top-Gate CNT-FET Biosensor: *Masuhiro Abe*[1]; Katsuyuki Murata[2]; Atsuhiko Kojima[3]; Yasuo Ifuku[4]; Mitsuaki Shimizu[5]; Tatsuaki Ataka[1]; Kazuhiko Matsumoto[6]; [1]Olympus Corporation, NEDO; [2]Olympus Corporation, NEDO, CREST-JST; [3]CREST-JST, Mitsubishi Kagaku; [4]Mitsubishi Kagaku Iatron; [5]AIST; [6]AIST, Osaka University, CREST-JST

The development of compact and inexpensive biosensors is indispensable for improving medical care facilities in distant places. We developed a carbon nanotube field effect transistor (CNT-FET) that can be used as a

biosensor; CNT functions as the channel. This CNT-FET biosensor was used for real-time sensing of pig serum albumin (PSA), and the results are reported here. PSA was measured by an antigen-antibody reaction. For PSA sensing, immobilized anti-PSA (a-PSA) by physical adsorption on the top gate of the CNT-FET. PSA was dissolved in buffer (pH = 8.0) and reacted with immobilized a-PSA on the top gate of the biosensor. A silicon rubber wall was placed around the top gate to retain the PSA test solutions there. FET characteristics were determined before and after pouring the PSA test solutions into the biosensors, and variations in the FET characteristics were compared. Drain current-top gate voltage characteristic curves of the CNT-FET biosensor were obtained before and after pouring PSA into the pool that was fixed on the biosensor. The threshold voltage shifted toward the positive direction (+0.2 V) in comparison with that of preparative CNT-FET. It is considered that PSA reacted with immobilized a-PSA and generated a charge at the top gate. In conclusion, real-time sensing of PSA was successfully realized based on the changing in FET characteristic before and after pouring the PSA test solutions into the biosensor.

3:10 PM Break

Session L: Contacts to Organic Thin Film Transistors

Wednesday PM Room: Conference Room 207
June 28, 2006 Location: Pennsylvania State University

Session Chairs: Max Shtein, University of Michigan; Alberto Salleo, Stanford University

3:30 PM

L1, Surface Chemistry Modifications to Contact Resistances in Organic Field-Effect Transistors: Behrang H. Hamadani[1]; David A. Corley[1]; Jacob W. Ciszek[1]; James M. Tour[1]; *Douglas Natelson*[1]; [1]Rice University

To enhance field-effect transistor (FET) performance, it is desirable to minimize contact resistance contributions to the total device resistance. In inorganic FETs this is often achieved by enhanced doping in the contact regions, but this is difficult in organic FETs. We report measurements on bottom-contact poly(3-hexylthiophene) FETs made with Au source and drain electrodes and SiO_2 gate dielectric. Via the transmission line method we extract both contact resistance and channel mobility as a function of temperature and gate voltage in these devices. We find that surface treatment of the Au source and drain electrodes via self-assembled monolayers (SAMs) can significantly modify the injection process and the contact resistance. SAMs with intrinsic dipole moments designed to increase the Au work function are found to decrease contact resistance, and vice-versa. We discuss our latest results and compare with untreated Au electrode devices.

3:50 PM Student

L2, Chemical Doping Modified Contacts to Organic Thin Film Transistors: *Bo Bai*[1]; Thomas N. Jackson[1]; [1]Pennsylvania State University

Impressive progress has been made in improved organic semiconductor materials and devices over the last several years. However, device limitations may still limit the use of organic devices, especially organic thin film transistors (OTFTs), in practical applications. One such limitation is the lack of detailed knowledge of the metal contact to the organic semiconductor. For low current density organic devices such as OLEDs, contacts may present only minor problems. However, for high current density devices such as high mobility OTFTs, contacts can significantly limit both device performance and stability. Large carrier injection barriers may be present at metal-organic contacts and can lead to a voltage drop comparable to or even greater than the normal FET channel voltage drop[1]. In conventional inorganic semiconductor devices such contact problems are avoided by the use of heavy doping of the semiconductor at contact area. Even for contacts with a significant barrier, heavy doping can reduce the barrier thickness sufficiently that carrier tunneling results in negligible or small contact voltage drop. Contact doping has also been used for organic thin film transistors[2, 3]. Undoped, ungated, vaccum-deposited thin films of pentacene are typically p-type with resistivity > 10^11 ohm-cm. By doping pentacene with materials such as ferric chloride we have been able to reduce the pentacene resistivity by five or six orders of magnitude; however, this doping level is still too low for effective use in organic ohmic contacts. By using alloys of pentacene and the organic electron acceptors 7,7',8,8'-tetracyanoquinodimethane(TCNQ), or dichlorodicyanoquinone (DDQ) we have been able to deposit organic semiconductor layers with resistivity < 100 ohm-cm. Using such alloys we have fabricated simple TFTs with doped contacts. Masked selective-doping of the pentacene TFT contact edge shows improved effective carrier mobilities, with only small changes in the sub-threshold regions and off-currents. Devices with only a single doped contact have asymmetric characteristics when the source and drain is interchanged. This indicates that contact doping may be useful for OTFTs. [1]Nichols, J.A., D.J. Gundlach, and T.N. Jackson, Potential imaging of pentacene organic thin-film transistors. App. Phys. Lett., 83, p. 2366-2368 (2003). [2]Schroeder, R., L.A. Majewski, and M. Grell, Improving organic transistor performance with Schottky contacts. App. Phys. Lett., 84, p. 1004-1006 (2004). [3]Abe, Y., et al., Control of threshold voltage in pentacene thin-film transistors using carrier doping at the charge-transfer interface with organic acceptors. App. Phys. Lett., 87 (2005).

4:10 PM

L3, Characterization of Top-Contact Pentacene Thin Film Transistors with Submicron-Length Channel: *Kazuhito Tsukagoshi*[1]; Kunji Shigeto[1]; Fumihiro Fujimori[1]; Tetze Hamano[1]; Takeo Minari[1]; Iwao Yagi[1]; Yoshinobu Aoyagi[1]; [1]RIKEN

We have systematically characterized organic thin film transistors (OTFTs) with submicron-length channel. The OTFTs were formed by alignment-free method[1] in which metallic electrode can be formed directly on the organic thin film channel in top-contact (TC) configuration. The organic channel and the electrode can be formed in-situ formation without exposing air. We drastically improved the operation of the short channel TC-OTFT by controlling both the interface between the channel and the gate insulator, and the interface between the channel and the contact. The fabrication method of the OTFT requires a prefabricated insulating structure. The structure has two cavities with undercut edges, and they are connected under a suspended bridge. Oblique evaporation of organic semiconductor (Pentacene) and normal evaporation of metal electrodes (Au) onto the prefabricated insulating structure are continuously performed in vacuum. The area under the suspended bridge is the channel of the TC-OTFT. In this experiment, the prefabricated structures were prepared by electron beam lithography. The short channel TC-OTFT with various channel length (L) from 0.18 μm to 0.41 μm was systematically characterized. Typical field-effect mobility of the short channel OTFT is 0.01-0.03 cm^2/Vs. The field-effect mobility decreased when the channel length became shorter than 0.3 μm. This originates in an exponential off-current increase with decreasing L below 0.3 μm while on-current is almost constant. By inserting the charge transfer molecules TCNQ into interface between the electrode and the pentacene channel, the field-effect mobility was improved up to 0.1 cm2/Vs. Even though the TC-OTFT with short channel length of 0.4 μm showed typical output and transfer characteristics, the OTFT without any treatment of substrate-surface behaved as unstable operation for gate voltage cycles. The operation stability was obtained by covering the substrate surface through the prefabricated insulating structure with a thin poly-para-xylylene (diX-C) layer of 10 nm. These improvements indicate that the operation characteristic in the chart channel TC-OTFT strongly governed by the interface conditions in the transistor. The interface effects and the above controlling method will be discussed. [1]I. Yagi, K. Shigeto, K. Tsukagoshi, and Y. Aoyagi, Jpn. J. Appl. Phys. 44 (2005) L479.

4:30 PM Student

L4, Electrical Contacts and Patterning Technique in n-Channel Organic Transistors: *Byungwook Yoo*[1]; Taeho Jung[1]; Brooks A. Jones[2]; Antonio Facchetti[2]; Tobin J. Marks[2]; Ananth Dodabalapur[1]; [1]University of Texas at Austin; [2]Northwestern University

Organic field effect transistors (OFETs) have attracted considerable interest for use in applications such as display drivers and sensor arrays. In particular, high performance n-channel organic semiconductors are crucial for the fabrication of complimentary circuits and the Marks' group has successfully synthesized the first air-stable n-type perylene diimide (PDI)

derivative, N,N'-bis(n-octyl)-dicyanoperylene-3,4:9,10-bis(dicarboximide) (PDI-8CN_2). Among a number of device parameters, electrical contacts between the organic semiconductor and the electrodes is an important issue for high resolution/small channel bottom-contact OFETs. Most bottom-contact OFETs exhibit degradation of the electrical properties upon operation compared to top-contact devices. This result has been mainly ascribed to morphological changes of the semiconductor material due to surface energy mismatch between the metal contact electrodes and the organic semiconductor. To investigate this problem, bottom-contact OFETs were fabricated with poly(3,4-ethylenedioxythiophene) poly(stylene sulfonate) (PEDOT:PSS) and the electrical properties compared to those of metal electrodes. The conventional approach to realize bottom-contact OFETs is using photolithography followed by lift-off with organic solvents such as acetone. However, this approach is not favorable for PEDOT:PSS pattern. Here we present a new patterning technique to prevent the photographically-defined PEDOT:PSS pattern from coming into contact with the organic solvent. In the present approach, a double photoresist layer was used, in which the upper layer was patterned to serve as the mask before oxygen plasma etching. The saturation mobility of OFETs with conventional lithography was 2.8×10^{-3} cm^2/Vs and the saturation mobility with this technique was 6.4×10^{-3} cm^2/Vs. It is known that conductivity enhancement by more than two orders is observed by immersing a dried PEDOT:PSS film into ethylene glycol (EG) due to the conformational change of PEDOT chains in the film. We applied this process to the OFETs fabricated by the conventional lift-off process. The mobility was 1.3×10^{-2} cm^2/Vs and the I_{on} / I_{off} ratio was 1.1×10^2. We also employed gold source-drain electrodes that were treated with 1-octadecanethiol (ODT) to facilitate charge carrier injection. Hexamethyldisilazane (HMDS) have been characterized for modifying the surface energy of gate dielectrics. These surface treatments are compared for the n-channel bottom-contact OFETs. The samples treated with ODT showed an increase in mobility of one order of magnitude in comparison with untreated samples. The best OFET performace were achieved by using both HMDS and ODT treated dielectric surface and metal, respectively. The saturation mobility, threshold voltage, and I_{on} / I_{off} ratio (V_{DS} = 40 V, V_G = 0 ~ 40 V) of these PDI-8CN_2 devices were 0.14 cm^2/Vs, 1.6 V, and 1.2×10^3, respectively.

4:50 PM
L5, Late News

Session M:
Oxide Thin Film Integration I

Wednesday PM — Room: Conference Room 206
June 28, 2006 — Location: Pennsylvania State University

Session Chairs: Michael Lanagan, Pennsylvania State University; Darrell G. Schlom, Pennsylvania State University

---

1:30 PM Student
M1, Growth and Structural Characterization of TiO2 Thin Films Deposited on SrTiO3, LaAlO3, and Al2O3 Substrates Using Reactive Molecular Beam Epitaxy: *Patrick Fisher*[1]; Oleg Maksimov[2]; Hui Du[1]; Marek Skowronski[1]; Paul A. Salvador[1]; [1]Carnegie Mellon University; [2]Electro-Optics Center

There is broad technological interest in TiO2 owing to its interesting physical and chemical properties, such as high refractive index, excellent optical transmittance in the visible and near-infrared regions, high dielectric constant, and significant photocatalytic activity. A number of reports have discussed the growth of TiO2 on various substrates, including Al2O3, LaAlO3, (La, Sr)(Al, Ta)O3, MgO, SrTiO3, and (Zr, Y)O2. Depending on the substrate and the deposition conditions, both rutile and anatase TiO2 have been grown. Most films were grown by pulsed laser deposition, metal organic chemical vapor deposition, or sputtering, while reports of TiO2 growth by molecular beam epitaxy (MBE) have been limited to LaAlO3 and SrTiO3. In general, these reports discussed only the optimal growth conditions. In this paper, we will present a detailed study of the reactive MBE growth of TiO2 on various substrates and over a range of deposition conditions. Films were deposited on SrTiO3 (001) and (011), Al2O3 (0001) and (1-102), and LaAlO3 (001) substrates by reactive MBE, in which high-temperature effusion cells were used to evaporate Ti and an ozone source was used to introduce pure ozone into the chamber. Crystalline quality of the films was observed in-situ by RHEED and ex-situ by XRD, TEM, and AFM. Growth mode and structural characteristics were investigated as a function of substrate material, substrate temperature, O3 flux, and titanium effusion cell temperature (which corresponds to the growth rate). We will present growth maps for films grown on LaAlO3 (001). Owing to the good lattice-matching, (001) anatase grows on LaAlO3 (001) and on SrTiO3 (001). Using XRD, AFM, TEM, and HREM it was observed that well-oriented, epitaxial, and atomically smooth films of pure anatase can be grown, but that all of the growth parameters influence the overall quality of the films. At higher substrate temperatures large inclusions were observed, which become more prevalent with increasing temperature and which lead to rough surface morphologies; at lower temperatures films had a relatively smooth surface morphology, although the growth mode was a function of ozone flux. At higher ozone fluxes, more two-dimensional growth was observed. Furthermore, as the growth rate increased, the growth mode was observed to change from a layer-by-layer growth mode to an island-like growth mode. On the remaining substrates, rutile films were observed and they exhibited the following orientations: (100) rutile on (0001) Al2O3, (101) rutile on (01-12) Al2O3, and (001) rutile on SrTiO3 (011). Compared to the anatase films, the crystalline qualities of all rutile films were inferior and the surfaces were rougher, which is a result of the large lattice mismatch between rutile and these substrates. This work was supported by Dr. Colin Wood, ONR under Contract No. N00014-05-1-0238.

1:50 PM Student
M2, Microwave Characterization of Thin Film Titanium Dioxide: *Lance Haney*[1]; Michael T. Lanagan[1]; Mark W. Horn[1]; [1]Pennsylvania State University

To obtain the dielectric properties of thin film titanium dioxide (TiO_2), the research utilized a parallel plate capacitor with short standards device specifically designed for operation in the microwave frequency range. Next, a comparison of the data occurred with measurements from the split cavity technique in order to validate the results. The deposition of the TiO_2 thin film occurred through pulsed DC sputtering and produced an anatase/rutile crystal structure. The measurements from the capacitor and short standards of the TiO_2 thin film indicate that the average permittivity value is 67.2 in the frequency range of 1 to 3 GHz. The permittivity value has a percent difference of 6.79% when compared to the permittivity measured with the split cavity of 62.9. The Q of the capacitor device ranged from 27 down to 4 over the 1 to 3 GHz freqency range. The split cavity measurements indicate that the loss of the TiO_2 thin film is only 0.68% in the microwave frequency range.

2:10 PM
M3, Lattice Dynamics and Ferroelectric Phase Transitions in $BaTiO_3$/$SrTiO_3$ Superlattices Studied by Ultraviolet Raman Spectroscopy: *Dmitri A. Tenne*[1]; A. Bruchhausen[2]; A. Fainstein[2]; R. S. Katiyar[3]; A. Cantarero[4]; A. Soukiassian[1]; V. Vaithyanathan[1]; W. Tian[1]; D. G. Schlom[1]; Y. L. Li[1]; L. Q. Chen[1]; S. M. Nakhmanson[5]; K. M. Rabe[5]; C. B. Eom[6]; H. P. Sun[7]; X. Q. Pan[7]; X. X. Xi[1]; [1]Pennsylvania State University; [2]Centro Atomico Bariloche and Instituto Balseiro; [3]University of Puerto Rico; [4]University of Valencia; [5]Rutgers University; [6]University of Wisconsin; [7]University of Michigan

Recent advances in epitaxial technology made possible the growth of multilayer oxide structures with monolayer-precision control of thicknesses and atomically flat interfaces, opening a way for synthesis of new materials, such as periodic multilayer ferroelectric structures – superlattices (SLs). These artificially engineered nanostructures were predicted by theoretical investigations to possess essentially new properties compared to their bulk constituents, and provide an opportunity to manipulate and enhance the ferroelectric properties of these materials. Vibrational (Raman and infrared) spectroscopies can provide valuable information for understanding the behavior of nanoscale ferroelectrics, as the lattice dynamics determines the fundamental ferroelectric properties. However, conventional Raman or infrared spectroscopies fail to measure the phonon spectra of nanoscale ferroelectric heterostructures because of extremely weak signals from

nanometer-thick films and the overwhelming substrate signals. Here we present the first experimental study of short-period $BaTiO_3/SrTiO_3$ SLs by ultraviolet (UV) Raman spectroscopy. SLs were grown by molecular beam epitaxy on (001)-oriented $SrTiO_3$ substrates. Using the UV excitation allowed us to overcome the problem of overwhelming substrate contributions in Raman spectra and made possible the observation of phonons in superlattices having the ferroelectric $BaTiO_3$ layers as thin as 1 unit cell. The ferroelectric-paraelectric phase transitions have been observed. Depending on the thickness of the $BaTiO_3$ layers and strain, the phase transition temperature T_c varies by hundreds of degrees from ~140 K to 640 K, i.e from over 250° below to over 200° above the T_c in bulk $BaTiO_3$. Below the T_c, the superlattices remain in the single (tetragonal) ferroelectric phase down to 7 K, i.e. the low-temperature phases characteristic for bulk $BaTiO_3$, are suppressed by strain. The experimental data are in good agreement with the results of the thermodynamic calculations of polarization in superlattices as a function of temperature. This work was supported in part by DOE, NSF, and ONR.

2:30 PM

M4, Epitaxial Lanthanum Lutetium Oxide Thin Films Prepared by Pulsed Laser Deposition: *Juergen Schubert*[1]; O. Trithaveesak[1]; M. Wagner[1]; T. Heeg[1]; H. Y. Chen[1]; C. L. Jia[1]; Y. Jia[2]; D. G. Schlom[2]; [1]Forschungszentrum Jülich GmbH; [2]Pennsylvania State University

A large number of alternative gate oxides are in discussion to replace silicon dioxide as the gate dielectric in a future MOSFET-structure. For the moment HfO_2 is the favorite material with a k = 25 and an optical bandgap of E_g = 5.5 eV. One of the drawbacks of this material is the low recrystallization temperature (600°C) of amorphous films which is below the thermal budget needed for a CMOS process. Several other materials are investigated and one of them, $LaLuO_3$, was proposed by Schlom et al.[1]. They measured a permittivity of 22 and an optical bandgap of E_g = 5.6 eV on single crystal material. These values are comparable to that of HfO_2. Furthermore $LaLuO_3$ has a high melting temperature of 2120°C and has been shown to be stable against reduction while heated up in vacuum or hydrogen atmosphere. $LaLuO_3$ in its crystalline form has the orthorhombic crystal structure Pbnm (62) with lattice parameters of a = 5.8259 Å, b = 6.0218 Å and c = 8.3804 Å. To investigate the properties of epitaxial thin films, $LaLuO_3$ was deposited by means of pulsed laser deposition in an oxygen ambient of 1 to $5*10^{-3}$ mbar at a substrate temperature of 500°C to 1000°C. A pellet made from a stoichiometric mixture of the metal oxides sintered at 1600°C formed the target. $SrTiO_3$(100) were used as substrate as well as epitaxially grown films of $SrRuO_3$ on $SrTiO_3$(100). The latter were used as the bottom electrode for the electrical characterization of the $LaLuO_3$ thin films. The layers were investigated with respect to their morphology and chemical composition by means of Rutherford backscattering spectrometry, x-ray diffraction, transmission electron microscopy, and atomic force microscopy. For the electrical characterization of the films capacitor stacks were prepared by evaporation of gold through a shadow mask. The capacitor stacks were investigated on a measuring station equipped with an impedance analyzer (HP 4192A) for recording of the C-V-curves. A constant voltage was applied to determine the break down field of the films. Summarizing the results, epitaxial $LaLuO_3$ thin films prepared by pulsed laser deposition reveal the same stoichiometry as the target material and have low minimum yield values (3%). They are smooth and the crystalline orientation is (001) perpendicular to the substrate surface. A permittivity of 45, higher than the values measured on single crystals, could be achieved on samples grown at a substrate temperature higher than 600°C. A break down voltage of 2 MV/cm was determined at a 80 nm thin film. These results are very promising for $LaLuO_3$ in possible future high-k applications.[1]D.G. Schlom, J.H. Haeni, MRS Bulletin V. 27, No. 3 (2002).

2:50 PM

M5, Rare-Earth Scandate Multi-Layer Thin Films: *Tassilo Heeg*[1]; Jürgen Schubert[1]; Christoph Buchal[1]; Markus Boese[2]; Martina Luysberg[2]; [1]Research Centre Juelich, ISG1-IT/CNI; [2]Research Centre Juelich, ER-C/CNI

The rare-earth scandates ($RE ScO_3$, *RE* denoting a rare earth element) have gained considerable attention as candidate materials for the replacement of SiO_2 in silicon MOSFETs in either amorphous or epitaxial form[1]. In this work, amorphous as well as epitaxial multi-layer systems consisting of scandate and titanate layers were grown in situ on different substrates using pulsed laser deposition (PLD)[2]. $BaTiO_3$ was used in combination with $GdScO_3$, and $SrTiO_3$ was combined with $DyScO_3$. The thickness ratio, bi-layer thickness and the total number of layers were varied. Rutherford backscattering spectrometry (RBS) and channeling were used to investigate the stoichiometry and crystal quality of the films. X-ray diffraction measurements were performed to analyze the crystal structure. HRTEM was used to get detailed information on the orientation relationship between scandate and titanate layers as well as on the strain present in the layers. To determine the electrical properties of the amorphous multi-layer films on silicon substrates, the results of several samples with a thickness from 26 nm to 100 nm have been evaluated using an EOT plot. To investigate the dielectric properties of the epitaxial films, $SrRuO_3$ covered $SrTiO_3$(100)-substrates were used for the electrical characterization. E.g., amorphous $BaTiO_3/GdScO_3$ films with a 2:1 thickness ratio exhibit a dielectric constant of 35, whereas the epitaxial films show a higher value of 60. *This work was supported by the Deutsche Forschungsgemeinschaft (Graduiertenkolleg GRK 549 „Non-centrosymmetric crystals").* [1]D. G. Schlom and Jeffrey H. Haeni, MRS Bulletin 27, 198 (2002)[2]L. Beckers, J. Schubert, W. Zander, J. Ziesmann, A. Eckau, P. Leinenbach, and Ch. Buchal, J. Appl. Phys. 83, 3305 (1998).

3:10 PM Break

3:30 PM Student

M6, Atomic Layer Deposition of Cubic Tantalum Nitride Thin Films for Gate Electrode Application: *Raghavasimhan Sreenivasan*[1]; Krishna Saraswat[1]; Paul C. McIntyre[1]; [1]Stanford University

Metal gates are being extensively researched as a replacement for poly-Si gate electrodes for high performance transistors. Poly-Si gates suffer from gate depletion leading to an increase in equivalent oxide thickness and boron penetration into the channel resulting in V_T instability. Also, poly-Si electrodes on HfO_2 exhibit Fermi level pinning due to 1) the formation of Hf-Si bonds at the poly-Si/HfO_2 interface, 2) possible reduction of the HfO_2 film during poly-Si deposition to produce an oxygen vacancy defect band. Tantalum nitride has been extensively studied as a barrier liner for copper interconnects due to its excellent thermal stability, good diffusion barrier properties and outstanding adhesion characteristics. These attributes also make it an interesting candidate as a metal gate for front-end applications. Atomic Layer Deposition (ALD) is a layer-by-layer growth technique where complementary, self-limiting reactions occur at the substrate surface. This leads to the growth of highly uniform, conformal, stoichiometric films with excellent control over the film thickness. The ability to conformally deposit both dielectrics and metals using ALD provides a unique opportunity to enable novel 3-D devices like nanotubes and nanowires. Also, as the workfunction of surface can be modified by submonolayer segregation of surface species, ALD of ultrathin conductive layers may offer the opportunity of engineering gate workfunctions with precise control. Tantalum nitride films were grown on Si substrates at 250°C by a remote plasma-enhanced ALD (PEALD) method using a novel metal organic precursor – isopropylimino tris(ethylmethylamino) tantalum (IPTEMT). The plasma, generated by flowing an $Ar/N_2/H_2$ mixture through an ICP source, produces NH* free radicals that serves as the reducing agent. The as-deposited films were amorphous with a Ta:N ratio of 1:1.6. High resolution XPS scans for the Ta 4f feature revealed the Ta $4f_{5/2}$ and Ta $4f_{7/2}$ peaks to be positioned at 26.7eV and 24.8V consistent with a Ta_3N_5 phase. Angle resolved XPS studies showed a uniform nitrogen content in the bulk of the films. The carbon content in the bulk of the film was below the detection levels of the XPS. High temperature in-situ anneals performed in the TEM column at 850°C crystallized the ALD tantalum nitride films deposited on SiO_2/Si substrates. Electron diffraction studies revealed a cubic TaN phase. The Ta $4f_{5/2}$ and Ta $4f_{7/2}$ peaks in the annealed sample shifted to 25.0eV and 23.6eV consistent with reported values for cubic TaN. A systematic study of the effect of growth conditions on the nitrogen content of the films will be presented. High temperature anneals in vacuum and reducing atmospheres such as hydrogen will be analyzed. Electrical measurements made on capacitor structures fabricated on TaN/HfO_2 stacks will be discussed.

3:50 PM Student

M7, Resistive Switching Behavior in Cr-Doped SrZrO3 Heterostructures: The Affects of Metal Electrode, Oxide Thickness, and Cr-Doping Levels: *Sukwon Choi*[1]; Paul A. Salvador[1]; Hwansoo Lee[1]; James A. Bain[1]; Jeong-

Heon Park[1]; Marek Skowronski[1]; [1]Carnegie Mellon University

In recent years, many wide-band gap oxides— such as TiO2, SrTiO3, and SrZrO3— have been investigated as dielectrics in devices using oxide-semiconductor heterostructures. These same materials (and heterostructures) have been observed to exhibit reversible, bistable, electrically-controlled resistive switching behavior and, as such, are of interest as media in novel probe storage devices. Although the initial property reports indicate that this class of materials is attractive for information storage, very little is known about the true details of the switching mechanisms. There is debate as to what the fundamental mechanism is and whether it is a pure interface property, a pure bulk property, or a combination between the two. In our research, we have attempted to unravel the mechanism of resistance switching in Cr-doped SrZrO3 heterostructures. We have been depositing metal-insulator-metal (MIM) heterostructures using pulsed laser deposition. SrTiO3 (100) single crystals were used as substrates; SrRuO3(100) was deposited epitaxially as a bottom metal electrode; Cr-doped SrZrO3(100) was deposited as the epitaxial insulating layer; and various top metal electrodes were deposited to complete MIM structure. Film fabrication was done using lift-off masks to pattern the heterostructure for electrical measurement. After deposition, current-voltage characteristics were studied. Using such heterostructures, we previously showed that the type of upper metal electrode makes a significant difference in both the overall current-voltage characteristics, including the switching properties and the absolute resistance values. Therefore, we set out to better understand the role of the upper-metal/oxide interface on controlling the properties of these resistive switching heterostructures. In this paper, we present the dependence of the resistance switching properties on the Cr contents in SrZrO3 films. Pure (0.0% Cr), 0.2% Cr-doped, and 2% Cr-doped SrZrO3 targets were prepared by standard ceramic method and MIM were made using pulsed laser deposition. Three different thicknesses of the Cr-doped SrZrO3 layers were deposited for each doping level: 60 nm, 200 nm, and 500 nm. Finally, both Pt and Ag top electrodes were grown on each sample surface, since these two top electrodes have been observed to exhibit the biggest differences in behavior. Each of the heterostructures was investigated with respect to its switching behavior and to its current-voltage characteristics. In some case, further electrical property measurements were made, including capacitance-voltage measurements and electron-beam induced current measurements. Finally, a model of the switching behavior based on the evolution of Schottky-like tunnel barriers at the top metal-SrZrO3 interface was developed to explain the observed switching behavior. This model will be presented and compared to the observed switching behavior as a function of the heterostructure's characteristics.

4:10 PM

M8, Comparative Investigation of Epitaxial Gd2O3 Thin Films Grown on Si Substrates with Different Orientations for High-K Application: *Apurba Laha*[1]; Andreas Fissel[2]; Hans Jörg Osten[1]; [1]Institute of Electronic Materials and Devices; [2]Information Technology Laboratory

Complementary metal oxide semiconductor (CMOS) devices are normally fabricated on Si(100) wafer because of its technological advantages over other orientations such as Si(110) and Si(111). For instance, density of interface states was found to be minimum when SiO2 like dielectrics were grown on Si(100) for gate oxide application. However, there is no further need to focus only on Si(100) substrates since high-K oxides will replace the conventional amorphous silicon based dielectric in future CMOS devices. On Si(100) oriented surfaces, crystalline binary metal oxides grow as (110)-oriented domains, with two orthogonal in-plane orientations. On other Si orientations, we can expect perfect single crystalline growth of cubic lanthanide oxides. In the present work, we investigate and compare the growth and dielectric properties of epitaxial Gd2O3 thin films on different silicon substrates for high-K application. For the first time, we will demonstrate the successful growth of a high quality crystalline high-K oxide on Si(110) substrates. Epitaxial Gd2O3 thin films were deposited on 4" Si substrates using modified solid source molecular beam epitaxy technique. We found that the electrical properties of Pt/Gd2O3/Si(110) MOS heterostructures were as good as of Pt/Gd2O3/Si(100) structure. The equivalent oxide thickness estimated from the capacitance vs. voltage (C-V) characteristics was found to be 0.9 nm with a leakage current density of only 3 mA/cm^2 at 1V. The crystalline quality of the Gd2O3 thin films on different Si substrates was investigated using reflection high energy electron diffraction (RHEED) and transmission electron microscopy (TEM). X-ray photoelectron spectroscopy was used to study the chemical composition and interface properties. Finally, the structural and electrical properties of crystalline Gd2O3 thin films were compared for the growth on silicon substrates with different orientations.

4:30 PM Student

M9, Epitaxial $BaTiO_3/SrTiO_3$ Superlattices for Phonon Bragg Mirrors and Cavities: *Arsen Soukiassian*[1]; W. Tian[1]; D. A. Tenne[1]; X. X. Xi[1]; D. G. Schlom[1]; N. D. Lanzillotti Kimura[2]; A. Bruchhausen[2]; A. Fainstein[2]; H. P. Sun[3]; X. Q. Pan[3]; A. Cross[4]; A. Cantarero[4]; [1]Pennsylvania State University; [2]Centro Atómico Bariloche and Instituto Balseiro; [3]University of Michigan; [4]University of Valencia

We discuss the design and material parameters of $BaTiO_3/SrTiO_3$ heterostructures relevant for novel phonon devices, including mirrors, filters, and cavities for coherent phonon generation and control. The first step to phonon confinement structures is to grow a $\lambda/4$ thick planar periodic stack of two different materials with different acoustic impedance, which will work as a Bragg reflector with a stop band around λ and functions as a phonon mirror. The second step is the construction of a phonon cavity by enclosing a spacer of thickness $d_c = m\lambda_c/2$ between two phonon mirrors, where λ_c is the acoustical phonon wavelength at the center of the phonon minigap and *m* is an integer. The advantages of using these ferroelectric superlattices include that they have an enormous stop band compared to the GaAs/AlAs superlattices previously reported for this application and that due to their high photoelastic coefficient there can be greatly amplified light-sound interaction in these ferroelectric materials. We have used reactive molecular-beam epitaxy (MBE) for growth of $BaTiO_3/SrTiO_3$ superlattices on TiO_2-terminated (001) $SrTiO_3$, (110) $DyScO_3$, and (110) $GdScO_3$ substrates. With the aid of RHEED, precise one monolayer doses of BaO, SrO, and TiO_2 were deposited sequentially to create $BaTiO_3/SrTiO_3$ superlattices. Structural characterization by XRD and TEM revealed that the samples studied are of high quality with nearly atomically abrupt interfaces. A θ-2θ X-ray diffraction scan showed that nearly all superlattice peaks are present for $2\theta < 55°$ which is an indication of atomically sharp interfaces between the superlattice layers. This was confirmed by high-resolution TEM images. $BaTiO_3/SrTiO_3$ superlattices grown on (110) $DyScO_3$ and (110) $GdScO_3$ substrates demonstrate the highest structural perfection ever reported for oxide superlattices with rocking curve full widths at half maximum as narrow as 0.0028°. This is due to the higher structural perfection and smaller lattice mismatch of $GdScO_3$ and $DyScO_3$ substrates with $BaTiO_3/SrTiO_3$ superlattices compared to $SrTiO_3$ substrates. UV Raman results (the first ever reported for thin ferroelectric films) show that $BaTiO_3$ is tetragonal and $SrTiO_3$ is polar due to strain in these $BaTiO_3/SrTiO_3$ superlattices. Although the UV Raman resolution was insufficient to resolve the acoustic information, we have observed folded acoustic phonons at the expected energy with the expected selection rules. The observed results are in excellent agreement with theoretical predictions. This work was supported by NSF and DOE.

4:50 PM

M10, Epitaxial and Amorphous Lu_2O_3 and $LaLuO_3$ on Si for Alternative Gate Dielectrics Applications: *Wei Tian*[1]; L. F. Edge[1]; D. G. Schlom[1]; V. V. Afanas'ev[2]; A. Stesmans[2]; S. Shamuilia[2]; B. Holländer[3]; J. Schubert[3]; [1]Pennsylvania State University; [2]University of Leuven; [3]Research Centre Juelich

Appropriate gate dielectric oxides are needed to replace SiO_2 in metal—oxide—semiconductor field—effect transistors (MOSFETs) as the scaling of MOSFETs continues. Among many criteria for choosing satisfactory alternative gate dielectrics are relatively high dielectric constant (high—*K*), thermodynamic stability in contact with Si, and sufficient valence and conduction band offsets with respect to Si. Lu_2O_3 with a dielectric constant of 12-13 and an optical bandgap of 5.52 eV and $LaLuO_3$ with a dielectric constant of ~22 and an optical bandgap of 5.6 eV are promising candidates. $LaLuO_3$ is of particular interest due to its high melting point (2120°C) and excellent thermal expansion match with silicon. In this work, epitaxial and amorphous Lu_2O_3 and $LaLuO_3$ thin films were grown on (111) Si and (100) Si using molecular beam epitaxy to explore their applications for alternative high—*K* gate dielectrics. The structural quality and epitaxial orientation relationships with respect to the silicon substrate were characterized by four-circle x-ray diffraction. Epitaxial Lu_2O_3 films were grown on the (111) surface of Si with

two orientation relationships: (111)[1-10]Lu_2O_3 || (111)[-110] Si (*B*-type) and (111)[1-10]Lu_2O_3 || (111)[1-10]Si (*A*-type). The volume fraction of the *A*-type growth variant is less than 0.3%. The full widths at half maximum of the rocking curve of the 222 peak of the Lu_2O_3 films are 0.058°, indicating a high degree of structural perfection. $LaLuO_3$ grew epitaxially on the (111) surface of Si with an orientation relationship of (110)[1-10]$LaLuO_3$ || (111)[11-2] Si as well as two in-plane 120° rotational twin variants. The band alignment of epitaxial and amorphous Lu_2O_3 and $LaLuO_3$ with respect to Si were measured by internal photoemission and photoconductivity measurements. Epitaxial Lu_2O_3 thin films were found to have conduction and valence band offsets of 2.0 and 2.3 eV, respectively, sufficiently large to suppress electron and hole tunneling.

Session N: GaN Processing

Wednesday PM Room: Conference Room 108
June 28, 2006 Location: Pennsylvania State University

Session Chair: Michael Manfra, Bell Laboratories

1:30 PM

N1, Substantial Advantages of Cat-CVD SiN Surface Passivation over PECVD in Electrical Properties of AlGaN/GaN Heterostructure: *Norio Onojima*[1]; Masataka Higashiwaki[1]; Toshiaki Matsui[1]; Takashi Mimura[2]; [1]National Institute of Information and Communications Technology; [2]Fujitsu Laboratories

Recently we achieved AlGaN/GaN heterostructure field-effect transistors (HFETs) with an extremely high cut-off frequency of 163 GHz by using thin, high-Al-composition AlGaN barriers and surface passivation using SiN formed by catalytic chemical vapor deposition (Cat-CVD)[1]. Although the two-dimensional electron gas (2DEG) was depleted by thinning the AlGaN barrier less than 10 nm, Cat-CVD SiN passivation successfully induced a remarkable increase in the 2DEG density and improved the electrical properties of AlGaN/GaN HFETs. Cat-CVD is considered as a preferable method for surface passivation since it does not use plasma-excited high-energy species in contrast with widely used plasma-enhanced CVD (PECVD). Controlling the surface/interface properties of AlGaN/GaN HFETs by a more suitable passivation method is of the utmost importance. We report on comparative studies of Cat-CVD and PECVD SiN passivation, and demonstrate noteworthy impacts of Cat-CVD SiN passivation on the electrical properties of AlGaN/GaN heterostructure. Samples used in this study were grown on sapphire substrates by plasma-assisted molecular-beam epitaxy. The sample structure consisted of 30-nm-thick SiN passivation layer, nominally undoped $Al_{0.4}Ga_{0.6}N$ barrier (5, 20 nm), 1.3-nm-thick AlN spacer, and 1-µm-thick GaN. The 2DEG density at the AlN spacer/GaN interface was calculated using capacitance-voltage (*C*-*V*) and Hall measurements. For both AlGaN thicknesses the 2DEG density increased by SiN passivation, and more dramatically for the thinner AlGaN barrier. Noticeably, the increase for the 5-nm-thick AlGaN samples with Cat-CVD SiN was considerably larger than that with PECVD SiN (Cat-CVD: 1.9×10^{13} cm^{-2}, PECVD: 0.99×10^{13} cm^{-2}, without SiN: 0.62×10^{13} cm^{-2}). The 2DEG density can be modulated by the surface barrier height. The AlGaN surface barrier height was estimated based on *C*-*V* profiles, and the AlGaN surface passivated by Cat-CVD SiN was found to have a relatively lower barrier height than the AlGaN surface passivated by PECVD SiN or free AlGaN surfaces. This result indicates that Cat-CVD SiN can control the AlGaN surface barrier height more effectively, thereby leading to the pronounced increase in the 2DEG density. The SiN/AlGaN interface formed by PECVD presumably suffers from plasma-induced damages and/or disordering incurred during the initial deposition on the AlGaN surface. In contrast, Cat-CVD is expected to form a much better interface because of its plasma-free soft deposition. The large increase in the 2DEG density yielded a significant decrease in the sheet resistance. The sheet resistance value for samples with Cat-CVD SiN was 367 Ω/sq, whereas 491 Ω/sq for ones with PECVD SiN and 1800 Ω/sq without SiN. The larger reduction in the source and drain series resistance of AlGaN/GaN HFETs leads to a larger increase in the drain current density. Therefore, Cat-CVD SiN passivation is substantially advantageous over PECVD to improve the electrical properties of AlGaN/GaN HFETs. [1]M. Higashiwaki *et al.*, IEEE Electron Device Lett. 27, 16 (2006).

1:50 PM Student

N2, Oxygen Induced Gate Leakage in AlGaN/GaN HFETs and Its Suppression by a Novel Surface Control Process: *Junji Kotani*[1]; Masamitsu Kaneko[1]; Hideki Hasegawa[1]; Tamotsu Hashizume[1]; [1]Hokkaido University

One unsolved key issue in the AlGaN/GaN HFET is the large reverse leakage current of the Schottky gate. It is many orders of magnitude lager than that predicted by the thermionic emission theory. It increases with Al composition in spite of increase of Schottky barrier height. In this paper, we show that the oxygen shallow donor plays a very important role in increasing gate leakage in AlGaN/GaN HFETs. We also show that the gate leakage can be substantially reduced by applying a novel surface control process developed for oxygen gettering.Detailed temperature-dependent Schottky I-V measurements were made on nanometer length Ni/Au Schottky gates of Al0.3Ga0.7N/GaN HFETs as well as on large area Ni/n-AlxGa1-xN ($0.1<x<0.3$) Schottky diodes. It was found that reverse leakage currents were much larger, and their temperature dependences were much smaller, than those of GaN Schottky diodes. We analyzed these data on computer on the basis of our thin surface barrier (TSB) model[1] where presence of unintentional surface donors reduces the Schottky barrier width and cause thermionic field emission (TFE) transport. This model previously gave excellent computer fitting to measured I-V-T curves of GaN Schottky diodes[2] where presence of N-vacancy related deep donors was assumed. However, this was not the case for present AlGaN Schottky barriers. Excellent fitting could only be obtained by assuming high-density shallow donors near surface co-existent with N-vacancy related deep donors. The analysis also showed that, in HFET devices, the leakage current has a lateral tunneling injection component which most likely triggers the current collapse. Being consistent with many recent reports on large incorporation of oxygen in AlGaN layers, the most likely candidate for the shallow donor is the oxygen shallow donor at Ec-0.03eV. Based on the above result, we developed a novel surface control process which attempts to getter out oxygen from the near surface region of the AlGaN layer by covering the surface with an ultrathin Al film and performing annealing in ultrahigh vacuum. By this process, a remarkable reduction of reverse leakage current by 2-3 orders of magnitude took place in HFET samples, and that by 4-5 orders of magnitude in large area Schottky diodes. An in-situ XPS analysis indicated formation of AlOx layer during the surface control process. Oxygen atoms mostly come from the surface native oxide, but they partly come from the underlying AlGaN layer. Schottky C-V measurements indicated exponential increase of shallow donors toward the surface before application of the surface control process. After the surface control process, donor distributions became uniform. [1]H. Hasegawa and S. Oyama, J. Vac. Sci. Technol. B 20 1647(2002). [2]J. Kotani, T. Hashizume and H. HasegawaJ. Vac. Sci. Technol. B 22 2179(2004).

2:10 PM Student

N3, SF_6/O_2 Plasma Effects on AlGaN/GaN Heterojunction Field Effect Transistors: *David J. Meyer*[1]; Joseph R. Flemish[1]; Joan M. Redwing[1]; [1]Pennsylvania State University

The AlGaN/GaN Heterojunction Field-Effect Transistor (HFET) offers specific advantages over existing Silicon and GaAs based devices for high-power, high-frequency amplifiers. However, these devices remain prone to the phenomena of current collapse and RF dispersion. The literature suggests these problems are attributable to surface states or defects in the AlGaN layer. A variety of passivation techniques have been examined in the past as methods to mitigate current collapse. Silicon nitride passivation of the AlGaN surface has been shown to lessen electrical degradation, but not entirely remove the susceptibility to current collapse. Passivation with SiN_x can be performed either before or after defining the FET gate. The advantage of pre-gate passivation is that the device surface can be protected during subsequent processing. In this case, the gate contact must be made by plasma etching a window in the SiN_x film prior to metallization. In this study, we implement a pre-gate passivation methodology and determine what effects plasma processing will have on SiN_x etch characteristics and HFET

electrical properties. Specifically, the effects of process parameters associated with inductively-coupled plasma (ICP) etching using SF_6/O_2 chemistry on the SiN_x etch rate, profile, and selectivity, as well as the channel sheet resistance have been evaluated. By increasing the RF power to the substrate (independent of the ICP power) one can vary the etch profile from isotropic to nearly vertical sidewalls, even while employing an undercut liftoff resist layer between the photoresist and SiN_x. In the case of anisotropic etching, accurate dimensions are maintained and a subsequent O_2 plasma etch-back of the resist allows the fabrication of a gate field-plate in one lithography step. However, previous studies have reported that significant degradation to transistor channel conductivity can occur in ICP plasmas.[1] Therefore, the change in sheet resistance of the AlGaN/GaN heterostructure was measured as a function of plasma conditions. Exposure of the unpassivated surface to moderately aggressive plasma conditions (self-biasing up to 160V), which produces anisotropic SiN_x profiles, resulted in either no change or an anomalous reduction in sheet resistance. XPS inspection of HFET surfaces after plasma exposure revealed a large incorporation of fluorine (around 25 at %) which is bonded to both Al and Ga. In contrast, samples exposed to HF solutions had only a small concentration (around 3 at %) with no evidence of significant Al-F or Ga-F bonding, and no noticeable effect on channel resistance. These results suggest that the AlGaN surface can be passivated with fluorine by plasma exposure but not by typical HF wet-chemical treatment. Future work will investigate the effects of plasma passivation in conjunction with the SiN_x deposition on HFET characteristics including RF dispersion. [1]F.A. Khan, V. Kumar, and I. Adesida, Electrochemical and Solid-State Letters 5, 8-9 (2002).

2:30 PM

N4, Processing of LiAlO2 Substrates for m-Plane GaN Epitaxy: *Maria Losurdo*[1]; Tong-Ho Kim[2]; Soojeong Choi[2]; Pae C. Wu[2]; Maria Giangregorio[1]; Giovanni Bruno[1]; April S. Brown[2]; [1]IMIP-CNR; [2]Duke University

For several decades, polar c-axis oriented GaN has been used for optoelectronics and high-power electronics that, unfortunately, suffer from internal electric fields produced by discontinuities in the spontaneous and piezoelectric polarization along the [0001] direction. Previous work has demonstrated that non-polar (10-10) m-plane GaN is a promising material for implementing multifunctional optical and power electronic devices. m-plane GaN has been grown on m-plane sapphire, as well as 6H-SiC and LiAlO2. Indeed, the GaN/LiAlO2 system exhibits a lower lattice mismatch, GaN[000 1]llLiAlO2[010]~0.3%, in comparison to the GaN/sapphire and GaN/4H-SiC systems. However, the device performance of m-plane GaN on LiAlO2 has been limited by several factors, including Li segregation and interdiffusion, and decomposition of LiAlO2. Therefore, the understanding of the interfacial chemistry between GaN and LiAlO2 is indispensable for optimizing III-N epitaxy. Herein, we present pre-treatments to modify the chemistry of the LiAlO2 surface and improve GaN heteroepitaxial growth. Specifically, we investigate LiAlO2 surface modifications resulting from air annealing at high temperature, followed by nitridation performed using a N2 remote plasma source. Ellipsometric spectra of the pseudodielectric function have been acquired to determine the kinetics of the chemical and optical modifications, and the properties of the LiAlO2 surface. Complementary atomic force microscopy (AFM) and angle resolved X-ray photoelectron spectroscopy (XPS) measurements are also performed for analysis of the surface chemistry and morphology, respectively. It is shown that nitridation performed on the “as received” LiAlO2 substrate results in a disordered and rough layer leading to a variety of chemical products, such as Li3N, Li3AlN2, and NO that damage the LiAlO2 lattice, independent of the nitridation temperature. Furthermore, lithium nitride Li3N can desorb at high temperature, yielding further disruption of the LiAlO2. Conversely, a pre-annealing in air at 900°C of the LiAlO2 substrate results in a Li-depletion with formation of an Al-rich surface. The excess Al is subsequently converted to AlN by the nitridation process. This two-steps (annealing+nitridation) pre-treatment results in a smooth and very thin (2ML) AlN surface layer, which preserves the LiAlO2 lattice and acts also as a barrier for Li and O interdiffusion. The effectiveness of the air anneal followed by nitridation in improving GaN growth has been checked. GaN epitaxial layers have been grown by plasma assisted MBE under Ga-rich growth conditions on the LiAlO2 annealed in air at 900°C and then nitrided at the growth temperature, and the quality has been compared with that of GaN epitaxial layers grown on “as-received” LiAlO2. GaN films grown on the air-annealed and nitrided LiAlO2 shows a clear m-plane RHEED pattern during growth, high m-plane orientation with a FWHM of the XRD (200) Θ/2Θ of 140 arcsec and morphologies typical of the m-plane with RMS values as low as 0.63nm.

2:50 PM Student

N5, Matrix-Addressable III-Nitride LED Arrays on Si Substrates by Flip-Chip Technology: *Chi Wing Keung*[1]; Kei May Lau[1]; [1]Hong Kong University of Science and Technology

Matrix-addressable light emitting diode (LED) micro-arrays on sapphire substrates have been reported[1, 2]. In the fabrication process, complicated chemical-mechanical polishing after planarization with oxides, or conformal sputtering metallization process were needed to ensure smooth metal interconnections. The resistance of each individual device was reported to depend strongly on the n-GaN stripe length and distance of the die from the contact at the end of the column[2], leading to significantly larger turn-on voltages with great variation. We have developed a simpler and more reliable fabrication process with much improved performance using a flip-chip configuration on a silicon wafer. The p-contact aluminum bus lines were fabricated on the Si carrier under the solder bumps, with very simple steps. The contact pads of the matrix were formed on the silicon wafer, with light emitting from the sapphire side. Moreover, electronic control circuits can also be implemented on the silicon wafer before flipping the light emitting matrix onto it. Large pixels requiring high drive currents can also be accommodated as the flip-chip technology was developed for power devices and is advantageous in thermal management. Individual devices (pixels) within the same column were isolated from other columns by inductively coupled plasma (ICP) etching all the way to the sapphire substrate, using silicon dioxide as mask. Thin Ni/Au (50/50A) system was deposited on p-GaN as ohmic contact. Ti/Al/Ni/Au (300/1000/5000/300A) system was used for both p-GaN and n-GaN as flip-chip contacts. Various n-contact line designs were investigated to obtain the minimum contact resistance and uniform turn-on voltages. In the design without a side metal line, the average turn-on voltage was very large and varied significantly. Our optimum design showed an average turn-on voltage of the matrix fabricated on the same LED wafer not much higher from individual ones fabricated with conventional process. The variation was also small, from 3.75V to 3.96V. The matrix was flipped onto the silicon wafer afterward. We demonstrated that each LED on the matrix was addressed and lit up successfully. With this flip-chip system, variable pixel (die) size can be fabricated. We first demonstrated an 8x8 matrix with 300x300 µm die size. We also fabricated 8x8 matrixes with device sizes of 200 µm and 150 µm square. The limitation of the device size is the size of the solder bump on the silicon wafer. The smallest solder size we have available was 20 µm in diameter. The spacing between solders was 40 µm. [1]Jeon,C.W.;Choi,H.W.;Dawson,M.D., “Fabrication of matrix-addressable InGaN-based microdisplays of high array density;” Photonics Technology Letters, IEEE Volume 15,Issue 11,Nov. 2003 Page(s):1516 - 1518.[2]Chan-Wook Jeon;Hoi Wai Choi;Gu,E.;Dawson,M.D., “High-density matrix-addressable AlInGaN-based 368-nm microarray light-emitting diodes;” Photonics Technology Letters, IEEE Volume 16,Issue 11,Nov. 2004 Page(s):2421 - 2423.

3:10 PM Break

Session O: Semiconductors: Processing and Oxidation

Wednesday PM
June 28, 2006

Room: Conference Room 108
Location: Pennsylvania State University

Session Chairs: Douglas C. Hall, University of Notre Dame; Michael A. Capano, Purdue University

3:30 PM Student

O1, The Electrical and Physical Analysis of $Co_xNi_{1-x}Si_2$ Gate/SiO_2/p-Si (100) with Dual Work Function for Deep Submicron Complementary Metal-Oxide-Semiconductor Device: *Jun Liu*[1]; Dim Lee Kwong[1]; [1]University of Texas at Austin

Recently, fully silicidation of poly-silicon gates (FUSI) has demonstrated promising results in reductions of gate sheet resistance and poly-depletion. Co-Ni alloy silicide, $Co_xNi_{1-x}Si_2$, is reported to have low sheet resistance than $CoSi_2$ and better thermal stability than NiSi in a wide range of Ni concentration. In order to combine the advantages of both NiSi and $CoSi_2$, silicidation process, phase formation, sheet resistance, dopant segregation, and work function tuning behavior of undoped, As- and B- doped Co-Ni alloy FUSI are investigated with different Co:Ni ratios. SiO_2 with 2.5, 3.5, 6.5nm thicknesses were fabricated on p-type Si(100) substrates. 80nm thick Poly-Si were deposited above oxide and implanted with As, B or without doping, followed by spike activation anneal at 1050°C. Co/Ni bi-layers with different thickness ratio (Co:Ni=200Å:50Å, Co:Ni= 175Å:75Å, Co:Ni=125Å:125Å) were deposited on poly. FUSI process was performed using rapid thermal annealing (RTA) at 800°C 30sec in N2, followed by removal of unreacted metal. The Co-Ni silicides were then patterned to form capacitors with area of $5x10^{-5}cm^2$. NiSi and $CoSi_2$ gated capacitors were also fabricated as control samples. Cross-sectional transmission microscopy (XTEM) was used to confirm FUSI and examine the silicide/SiO_2 interface integrity. Phase formations were studied by using X-ray Diffraction (XRD). Dopant segregation and silicide formation were investigated by Secondary Ion Mass Spectroscopy (SIMS). XTEM images clearly show that all three $Co_xNi_{1-x}Si_2$ have been fully silicided to form a uniform silicide layer by 800°C 30sec anneal, while excellent SiO_2 quality and gate/oxide/substrate interface are observed. Sheet resistances of $Co_xNi_{1-x}Si_2$ are decreasing with higher Ni percentage in the silicides. Glancing-angle XRD shows that $CoNiSi_2$ (1 1 1), $CoNiSi_2$ (2 2 0), Co_2Si_3 (2 1 0) and Co_2Si_3 (2 1 2) are found in all samples. Intensity of $CoNiSi_2$ phases increase, while that of Co_2Si_3 phases decrease with higher Ni percentage in the silicides. As and B segregation at the interface are observed in all samples in SIMS. Boron has lower concentration at the gate/oxide interface than As due to smaller atom size and easier diffusion to the top surface of the silicides during the high temperature anneal. The extrapolated work function values of undoped $Co_xNi_{1-x}Si_2$ are between those of $CoSi_2$ and NiSi, and exhibit a linear relationship with the Ni percentage in the metal gates. The work functions of As- and B-doped $Co_xNi_{1-x}Si_2$ FUSI metal gates are nearly the same, indicating that in the doped metal gate samples, the dopant enrichment at the interface dominates the work function adjustments. In summary, impacts of the Co:Ni ratio on FUSI condition, sheet resistance, phase formation, dopant segregation and work function tuning in $Co_xNi_{1-x}Si_2$ are studied and dual work function metal gate are realized.

3:50 PM Student

O2, Studies of Surface Wetting Phenomena during Thin Film Formation by Mist Deposition: *Karthikeyan Shanmugasundaram*[1]; Matt Brubaker[2]; Kyuhwan Chang[1]; Jerzy Ruzyllo[1]; [1]Pennsylvania State University; [2]Symetrix Corporation

Mist deposition technology has been demonstrated in the deposition of ferroelectric materials, alternative gate dielectric materials for CMOS technology, and photoresist films. This technology offers an attractive alternative to current methods of thin film formation using liquid precursors, such as spin-on. The principle of mist deposition is to convert the liquid source material into a fine mist with droplet size in the order of 0.25 micron, which is then carried into the deposition chamber in a pressurized stream of N_2 gas and the droplets are allowed to coalesce on the substrate at room temperature. This forms a uniform film of liquid on the substrate, which can be thermally treated to burn off solvent and leave a thin film of solid on the surface. The deposition rate is controlled by accelerating the droplets under the influence of an electric field. At the same time, however, the way material from the mist is coalescing on the surface, degree of surface coverage, as well as morphology of mist deposited thin films is a strong function of the energy of the substrate surface, i.e. its chemical composition. The focus of this experiment was on the investigation of the kinetics of mist deposition on different and/or differently prepared surfaces and its main goal was an exploration of mist deposition as a method allowing selective deposition of thin films using liquid precursors. Precursors used included primarily ferroelectrics and organic semiconductors. Substrates used were hydrophobic and hydrophilic Si surfaces, aluminum, ITO and glass. Film morphology was evaluated by AFM while the degree of surface coverage was optically recorded and analyzed using image analysis software ImageJ. In this study the ability of mist deposition technique to selectively deposit ferroelectric materials is demonstrated. The results of our experiments indicate that the surface energy as well as the geometry of the structures on the substrate plays an important role in determining the selectivity of film formation. Moisture on the surface of oxidized Si substrates was found to impede deposition. An alternating series of SiO_2 and Si strips was defined on Si substrates by conventional lithography and the phenomenon mentioned earlier is utilized to deposit material selectively on the Si strips without subsequent lithographic processes. Similar dependence of deposition rate of polymeric semiconductors was observed with hydrophilic Si substrates and glass substrates with ITO coatings forming complete films while bare glass substrates were found to impede film formation. Furthermore, it was determined that the morphology of mist deposited films depends on the chemical composition of the substrate. For instance this effect was readily observed through AFM characteristic of organic semiconductor films deposited on glass and ITO. The results are discussed in the full account of this work.

4:10 PM Student

O3, Dry Etching of PbSrSe Epitaxial Layers toward Distributed Bragg Reflectors: *An Cheng*[1]; Jian Xu[1]; Edward Basgall[1]; Guy Lavallee[1]; Michael Gerhold[2]; Fanghai Zhao[3]; Zhengping Guan[3]; Dewali Ray[3]; Zhisheng Shi[3]; Anuj Dhawas[2]; [1]Pennsylvania State University; [2]North Carolina State University; [3]University of Oklahoma

Recently, Z. Shi et al reported the epitaxial growth of high quality PbSe/PbSrSe multiple-quantum-well (MQW) structures on less expensive (111) CaF2 substrate and demonstrated an optically pumped vertical-cavity surface-emitting-laser (VCSEL) based on the MQW's grown on (111) CaF2 substrate.[1] An edge emitting diode laser structure grown on (111) CaF2 substrate will be very promising for the development of low cost, high power, single mode, and wavelength tunable mid-infrared injection lasers with high CW operation temperature. Such a laser design needs lateral distributed-Bragg-reflectors at both ends of the waveguide for the optical feedback. Owing to short periods and high aspect ratio, the technological requirements for deeply etched DBR mirrors are quite challenging. In our study, the DBR mirror was dry etched in PbSe/PbSrSe multiple-quantum-well (MQW) structures. The mirrors were patterned using photo lithography and etched with a decoupled plasma source (DPS). The DPS design allows independent control of the plasma ion flux and ion acceleration energy, creating a wide processing window for the reactive ion etching. Ni lines were deposited on MQW structures as the hard mask. The influences of the rf power, the Cl2 percentage in Ar, and the chamber pressure on the etching profile were investigated. Increasing the bias rf power was found to reduce the etching selectivity between PbSe/PbSrSe and Ni mask, while decreasing bias rf power has led to more isotropic etching effects.[2] Increasing the Cl2 flow brought smoother side walls, but hindered the vertical etching process. In addition, the chamber pressure also played a key role on etching morphology. A low pressure was observed to help in achieving high aspect ratio in the fabricated DBR mirrors. Nevertheless, extreme low pressure could drastically increase the surface roughness. Good etching profile was observed with chamber pressure of ~3 mTorr. We will present an optimized etching condition that yields vertical etching profiles with smooth surface morphology and high selectivity to

the masking material. This work will be extended to the developing of real deeply etched DBR mirrors for the PbSe/PbSrSe mid-infrared semiconductor laser structures grown on CaF2 substrate.This work was supported by the U. S. Army Research Office under Contract No. DAAD19-02-D-0001. [1]H. Zhao, H. Wu, A. Majumdar and Z. Shi, "Continuous wave optically pumped lead-salt mid-infrared quantum well vertical-cavity surface-emitting lasers", Applied Physics Letters, 83, 2003, 5133. [2]E.W. Berg and S. W. Pang, "Low Pressure Etching of Nanostructures and Via Holes Using and Inductively Coupled Plasma Source", J. Electrochem. Soc. 146,775-779(1999).

4:30 PM Student

O4, A Novel Masking Technology for Deep Glass Wet Etching: *Ying-Ming Huang*[1]; Maruti Uppalapati[1]; William O. Hancock[1]; Thomas N. Jackson[1]; [1]Pennsylvania State University

Bulk micromachining of glass substrates is widely used for the fabrication of microfluidic structures such as fluid flow channels and thin diaphragms for pumps, active valves, and dispenser applications[1]. Wet glass etching with various concentrations of HF is widely used because the etching rate is fast (about 8 ~ 10 μm/min), and a large number of glass wafers can be processed simultaneously. However, the formation of pinholes through defects within the etch mask is a notorious problem that becomes especially severe when deep etching is required. Masks that have been employed for glass etching in HF include photoresist, Cr/Au photoresist combinations, SU-8, anodically bonded silicon, polysilicon, electroplated gold, and their combinations[2,3]. However, most reported processes are problematic for etch depths greater than 200μm. We have investigated a range of mask materials for deep glass etching. Based on our results, we have developed a modified masking material combination. First, we deposit a blanket Cr (100Å) /Au (1000Å) layer on the glass substrate to be etched. Second, the sample is laminated with a dry film photoresist (Riston®) at 110°C and the Riston layer is patterned by photolithography. Third, a 1.5μm thick gold layer is electroplated on top of the sample and the dry film photoresist is removed. Fourth, Cr and Au etchants are used to remove the unplated Cr/Au areas that were covered by Riston layer. Next black wax (Apiezon W) and a silicon wafer are applied to protect the backside and the edges of the sample during the HF etching process. Omnicoat and SU-8 (Microchem) are then spin-coated on top of electroplated gold layer, and patterned to open windows for 49% HF etching. After etching, the SU8 layer can be removed by piranha cleaning or the sample can be soaked in Cr etchant to lift off the whole Cr/Au/SU-8 combination. With this new masking material combination, 300μm etch depths are achieved with a pinhole free glass surface after 40 minutes wet etch in concentrated HF solution. This project was funded by the Penn State Center for Nanoscale Science (NSF MRSEC DMR0213623) and by an NSF Biophotonics Grant (0323024) to W.O.H. and T.N.J. funded jointly by NSF and NIH/NIBIB. [1]M. J. Madou, Fundamentals of Microfabrication, CRC-Press, 1998. [2]D. C. S. Bien, P. V. Rainey, S. J. N. Mitchell and H. S. Gamble "Characterization of masking materials for deep glass micromachining", J. Micromech. Microeng, 13, pp. S34–S40 (2003).[3]M. Bu, T. Melvin, G. J. Ensell, J. S. Wilkinson and A. G.R. Evans "A new masking technology for deep glass etching and its microfluidic application", Sensors and Actuators A, 115, pp.476-482 (2004).

4:50 PM
O5, Late News

NOTES

Session P:
Device Aspects for ZnO

Thursday AM
June 29, 2006

Room: Deans Hall I
Location: Pennsylvania State University

Session Chairs: Julia W.P. Hsu, Sandia National Laboratories; Jamie D. Phillips, University of Michigan

8:20 AM Student

P1, Electrical and Optical Properties of ZnO Thin Films for Transparent Electrodes and Antireflection Coatings in Optoelectronic Devices: *J. H. Yun*[1]; C. H. Lim[2]; J. H. Lim[1]; J. H. Jang[1]; S. J. Park[1]; [1]Gwangju Institute of Science and Technology; [2]Korea Institute of Energy Research

Transparent conducting oxide (TCO) thin films have been widely used as transparent electrodes for flat panel displays and solar cells. Although indium tin oxide (ITO) is the most popular TCO material, ZnO-based material is now under active investigation as an alternative of ITO because of low cost and high optical transmittance at short wavelength range (400~500 nm). Presently there have been few reports on ZnO thin film in the application area of antireflection (AR) coating material due to its low refractive index that is not suitable for single layer AR coating on top of optoelectronic devices such as light emitters and detectors. However, ZnO film is one of the promising AR coating material for solar cell applications where broadband characteristics are more important because whole visible light spectrum should reach to photon-absorbing material through AR coating material. The problem of refractive index mismatch between air/ZnO/semiconductors can also be alleviated by employing double layer AR coating scheme. In this study, aluminum-doped ZnO (AZO) thin films deposited by RF magnetron sputtering methods at room temperature because low temperature process is required in fabricating GaAs-based solar cells. AZO thin film on top of GaAs-based solar cell heterostructures functions as a transparent electrode as well as AR-coating material so that high transmittance at broadband spectral range and high electrical conductivity is required. Very thin AZO film (57 nm) was sputtered at room temperature and the electrical and optical characteristics were measured. The film exhibited excellent transparency higher than 95% at 600 nm-wavelength where the transparency of ITO film was 87%. The sheet resistance of this thin AZO layer was measured to be 422.3 Ω/square where ITO 47.3 Ω/square. The thermal stability of AZO film was also studied. The sputtered AZO films were post-annealed at various temperatures ranging from 200 to 600°C for 1 min. under high vacuum. The characteristics did not change and demonstrated very good thermal stability. Finally, AZO film was deposited on top of GaAs-based solar cells. By employing AZO as a top contact as well as AR coating material, the performance of solar cell was improved in terms of efficiency, fill factor, and current density. The detailed processing steps and performances of GaAs-solar cells with AZO top contact will be presented.

8:40 AM

P2, Switchable Interface Charges in Zinkoxide-Bariumtitanite Heterostructures: Concepts for New Oxide-Based Electronic Device Structures: *Mathias M. Schubert*[1]; Nurdin Ashkenov[2]; Rao Voora[2]; Holger Hochmuth[2]; Michael Lorenz[2]; Marius Grundmann[2]; [1]University of Nebraska-Lincoln; [2]University Leipzig

Many properties of ZnO (wurtzite structure) and BaTiO3 (perovskite structure) render both materials as interesting candidates for next generation micro- and optoelectronic devices. The spontaneous electric polarizations in both materials have received little attention so far, especially if combined in heterostructures. Whereas the spontaneous wurtzite-type polarisation is inherently tied to one distinct lattice direction and orientation, the spontaneous perovskite-type polarization can be reversed and switched by external electric fields within the perovskite lattice. Coupling between the fixed ionic wurtzite interface charges and the switchable ferroelectric interface charges should give rise to ferroelectric polarization exchange coupling phenomena. Switching of ferroelectric domains in ZnO-BaTiO3-ZnO heterostructures may allow for controllable free-charge-carrier accumulations at heterointerfaces, band-to-band transition characteristics or electro-optical properties, for example. We have successfully grown various ZnO-BTO- and ZnO-BTO-ZnO-type heterostructures by pulsed laser deposition on silicon and sapphire. Pt electrodes are used as bottom and top contacts, with ohmic properties on ZnO, and Schottky-characteristics on BaTiO3. We also employ electrically conductive ZnO layers as transparent top and bottom electrodes for electro-optical studies. The structural properties of the heterostructures are investigated by XRD, TEM, and micro-Raman scattering techniques. The interaction between the fixed ionic wurtzite interface charges of ZnO and the switchable ferroelectric interface charges of BaTiO3 gives rise to ferroelectric polarization exchange coupling phenomena, which were revealed by optical and electrical techniques. Electro-optical Spectroscopic Ellipsometry measurements display interesting index-of-refraction hysteresis loops, which may be used for optical transparent memory storage. Electro-optic temperature-dependent micro-Raman scattering prove the ferroelectric properties of the BTO layers inside the heterostructures. Temperature-dependent electric polarisation, current-voltage (I-V), and capacitance-voltage (C-V) studies result in interesting polarization hysteresis behaviour for various device structures. The I-V curve of Pt/ZnO/BaTiO3/Pt/Si structures is strongly asymmetric and reflects the rectifying nature of the BaTiO3/Pt interface. Additionally, for forward bias-voltages, the I-V curve exhibits a hysteresis, which we assign to the ferroelectric BTO polarization reversal, rendering resistive switching with tuneable threshold voltage. Temperature-controlled I-V measurements reveal that the resistive switching is induced by the ferroelectric domain reversal in the BTO layers, where the switching disappears above the paraelectric phase transition temperature. Electro-optic micro-Raman measurements performed simultaneously on the same structure provide further proof upon disappearance of the ferroelectric mode in conjunction with the disappearance of the hysteresis loop. Symmetric Pt/ZnO/BaTiO3/ZnO/Pt structures provide an asymmetric C-V hysteresis loop with bistable maxima occurring for negative bias-voltages. Depending upon the bias-voltage sweep direction, the capacitance of the structure switches between high and small values. The observed results suggest that the polarization exchange coupling in wurtzite-structure ZnO-alloys and ferroelectric oxides may find use in future transparent nano-optoelectronic device structures, which shall be discussed.

9:00 AM Student

P3, Metal-Ferroelectric-Semiconductor Capacitors Based on PZT/ZnO Heterostructures: *Emine Cagin*[1]; Ding-Yuan Chen[1]; Jeffrey Siddiqui[1]; Jamie D. Phillips[1]; [1]University of Michigan

Interfacing ferroelectric and semiconductor materials provides a means of coupling unique properties associated with ferroelectric materials to high performance semiconductor devices. The quality of the ferroelectric/semiconductor interface is critical for creating and maintaining a significant charge density. Chemical interactions between the two materials lead to a poor interface characterized by material defects degrading the charge density. Oxidation of the semiconductor is often a problem when using common semiconductors such as GaAs and Si in conjunction with ferroelectric oxides. We believe that a semiconducting oxide material such as ZnO would provide an excellent material for interfacing with ferroelectric oxides due to suppressed oxidation or reactivity at the ferroelectric/semiconductor interface. In this work, the electronic properties of ferroelectric/ZnO heterostructures are reported, where (Pb,Zr)TiO3 (PZT) is used as a prototypical ferroelectric oxide. PZT materials were deposited using the sol-gel technique. Platinum substrates were coated with a PZT solution through spin coating. PZT films were annealed using rapid thermal annealing (RTA) at 4800C and 7500C to improve crystallinity. ZnO layers were deposited using pulsed laser deposition or molecular beam epitaxy. X-ray diffraction studies showed that ZnO layers grown on sol-gel PZT aligned preferentially along the (001) direction. There was no preferential orientation observed in the PZT films. Capacitors were fabricated for metal-PZT-ZnO-metal and metal-PZT-metal structures using standard metal evaporation, photolithography, and wet etching techniques. Metal-PZT-metal structures demonstrate ferroelectric hysteresis with remanent polarization of 28uC/cm2 and coercive field of 75kV/cm for a loop of 15V. The metal-PZT-ZnO capacitor structures demonstrate a characteristic metal-insulator-semiconductor characteristic with a hysteretic memory window of approximately 2 V. Details of the structural and electronic properties, as well as applications of this technology will be presented. This

work is supported by the National Science Foundation under Grant ECS-0238108 and AFOSR under contract number FA9550-04-1-0390.

9:20 AM Student

P4, ZnO Schottky Diode Performance as a Function of Contact Metal and Surface Polarity: *Martin W. Allen*[1]; W. C. T. Lee[1]; P. Miller[1]; R. J. Reeves[1]; M. M. Alkaisi[1]; S. M. Durbin[1]; [1]University of Canterbury

Historically, Au, Ag, Pt and Pd have been used to fabricate ZnO Schottky contacts. However, few studies have reported good quality contacts for each of these metals on the same ZnO material and, to our knowledge, none have examined the effect of ZnO surface polarity on each of these metal contacts. We have investigated the performance of these four Schottky metals on the Zn-polar (0001) and O-polar (000bar1) faces of bulk, single crystal ZnO (n = 4×10^{16} cm^{-3}) and on O-polar ZnO thin films grown by plasma-assisted molecular beam epitaxy on (0001) sapphire (n = 6×10^{17} cm^{-3}). Lift-off photolithography was used to fabricate arrays of planar Schottky diodes on ZnO surfaces ultrasonically pre-cleaned using simple organic solvents. The diodes were characterised by room temperature I-V and C-V measurements. For the bulk material, no significant polarity effect was observed for either the Au or Ag diodes, in that similar barrier heights (ϕ_B) and ideality factors (n) were obtained on both the Zn-polar and [O-polar] faces; typically across an array of diodes, ϕ_B(Au) = 0.71 [0.69] eV, n = 1.4 [1.1] and ϕ_B(Ag) = 0.78 [0.77] eV, n = 1.2 [1.1]. A polarity effect was observed, however, for the Pt and Pd diodes, with higher quality diodes achieved on the O-polar face; ϕ_B(Pt) = 0.55 [0.68] eV, n = 2.0 [1.2] and ϕ_B(Pd) = 0.55 [0.60] eV, n = 2.0 [1.2]. For the O-polar PAMBE ZnO thin films, good quality Schottky diodes were only obtained with Ag as the Schottky metal; ϕ_B(Ag) = 0.79eV, n = 1.6. Interestingly, good quality Schottky contacts were achieved on bulk ZnO without the need for oxidation pre-treatments reported elsewhere. 4K photoluminescence measurements on the as-received bulk ZnO wafers revealed an almost complete absence of the I_4 line (thought to be due to shallow hydrogen donor impurities) and no observable green defect emission (often attributed to oxygen vacancies). Also, it is possible that the photolithography developer may clear surface contamination not removed by organic solvent cleaning. Surprisingly, Ag, the lowest work function metal, produced the highest Schottky barriers. To investigate this further, additional arrays of Ag diodes were fabricated on separate pieces of the same bulk Zn-polar and O-polar surfaces. These diodes showed excellent rectifying properties with barrier heights varying from 0.77 eV to 1.02 [0.88] eV, n = 1.2 [1.1]. Barriers in excess of 1 eV were achieved and these are thought to be the highest yet reported on ZnO. There is some evidence to suggest that this variation is due to varying degrees of oxidation of the Ag contacts which causes an increase in their effective work function; we are presently seeking to confirm this using X-ray photoelectron spectroscopy measurements.

9:40 AM Student

P5, Zinc Oxide Thin Films Deposited by Reactive RF Sputtering for Metal-Semiconductor-Metal Photodectors and Solar Cells: *Meiya Li*[1]; Nehal Chokshi[2]; Robert L. DeLeon[2]; Gary Tompa[2]; Wayne A. Anderson[1]; [1]State University of New York at Buffalo; [2]AMBP Tech Corporation

Zinc oxide (ZnO) thin films are of interest for UV detectors and low-cost heterojunction solar cells. We have utilized reactive RF magnetron sputtering to deposit ZnO with substrate heated or at room temperature. Thickness and refractive index, chemical composition, surface morphology and roughness of the thin films were analyzed by using ellipsometry, X-ray photoelectron spectroscopy (XPS), field emission scanning electron microscopy (FESEM), and atomic force microscopy (AFM). Photoluminescence and transmission measurements were employed for testing the device optical properties. The surface morphology appeared to be sensitive to the sputtering parameters for RF films deposited under various conditions. The size of grains became larger, and the structure changed from granular and nanoporous into elongated 3-D nanostructure as the growth temperature increased. The atomic structure was significantly modified by post-deposition annealing, and more crystals were formed uniformly and tightly with heat treatment under air ambient. Also, films deposited at high temperature (HT) were more close to 1:1 Zn: O stoichiometry with less carbon contamination. This indicates that the stoichiometric quality and crystallinity of ZnO films are improved with HT deposition. Furthermore, samples with and without post-deposition annealing showed near-band emission at ~3.3 eV, which indicates that the films are near perfectly stoichiometric. Metal-semiconductor-metal photodetectors (MSM-PD's) and heterojunction solar cells were fabricated on RF sputtered ZnO/Si films with different metals. The dark IV curves showed the current to be reduced with higher work metal function, which indicates that films deposited by RF sputtering are p-type. In some cases, the ZnO film was heat treated at 300 °C for 30 minutes before metal deposition. The dark current of the heat-treated ZnO MSM-PD was reduced from 3.06 μA to 96.5 nA at 5V when compared with that of as-deposited ZnO. Its magnitude was found to be at least two orders lower than that of the as-deposited sample. Both dark current and responsivities were improved for the heat-treated case. The value of responsivities for the heat-treated device was increased from 41.9 mA/W to 59.3 mA/W.

10:00 AM Break

10:20 AM

P6, Hybrid II-VI and III-V Compound Double Heterostructures and Their Properties: *Yahya Alivov*[1]; Ü. Özgür[1]; X. Gu[1]; C. Liu[1]; Y. Moon[1]; H. Morkoç[1]; O. Lopatiuk[2]; L. Chernyak[2]; [1]Virginia Commonwealth University; [2]University of Central Florida

Zinc oxide with its large exciton binding energy of 60 meV is considered a prospective material for low threshold ultraviolet light emitting devices. Because the growth of high quality, reproducible p-type ZnO films and crystals is still problematic, fabrication of ZnO based heterostructures is considered an alternative way for exploiting of ZnO unique properties. This has received a great deal of interest lately, and different heterostructures, both single and double, have been fabricated using different materials as the p-type layer. GaN and its alloys with AlN are good candidates for such heterostructures since they have the same crystal structure, close lattice constants, and other close physical properties. In this work n-GaN/n-ZnO/p-GaN double heterostructures (DHs) were grown employing molecular-beam epitaxy and metal-organic chemical vapor deposition methods, and their properties were studied by different techniques. Reflection high-energy electron diffraction (RHEED) and atomic force microscopy techniques showed streaky RHEED patterns, indicating 2D growth, and smooth film surface morphology with a rms roughness as low as 1.45 nm for ZnO, 5 nm for n-GaN, and 0.2 nm for p-GaN. Scanning electron microscopy in both secondary electron and cathodoluminescence modes revealed sharp boundaries of the interlayers and high optical quality of the layers that indicated no significant interduffusion of constituting elements. Also double mesa n-GaN/n-ZnO/p-GaN structures were fabricated and their current-voltage characteristics and electroluminescence properties are discussed in this report.

10:40 AM Student

P7, Investigation of ZnO Dry Etching in Inductively Coupled CH_4/H_2- and C_2H_6/H_2-Based Plasmas: *Wantae Lim*[1]; Lars Voss[1]; Rohit Khanna[1]; Brent P. Gila[1]; David P. Norton[1]; Stephen J. Pearton[1]; Fan Ren[1]; [1]University of Florida

We studied dry etching of bulk single-crystal ZnO in high density inductively coupled CH_4- and C_2H_6-based chemistries. Substitution of C_2H_6 for CH_4 in the methane/hydrogen plasma chemistry provides a strong enhancement in ZnO etch rate by approximation a factor 2. In addition, Ar mixing to C_2H_6/H_2 produced relatively high etch rate of ZnO, in sharp contrast to the case of CH_4/H_2. At this time, the value of E_{TH} for initiation of the etching is 42.4 eV for C_2H_6/H_2/Ar and 59.8 eV for CH_4/H_2/Ar. The etched surface of ZnO was smooth and clean. The band-edge PL intensity increased after etching while the deep emission intensity decreased from the bulk ZnO, due to possibly to removal of surface contamination layer. The near-surface of the etched samples shows no enrichment in Zn as a result of preferential removal of oxygen, at least within the experimental error. Therefore, the non-corrosive, non-toxic C_2H_6/H_2/Ar plasma chemistry appears to be a good choice for patterning of ZnO, providing a clean, smooth surface and reasonable etch rates for bulk, single-crystal substrates.

11:00 AM Student

P8, Magnetic Properties and Observation of Anomalous Hall Effect in Cobalt-Doped ZnO: *Mathew Ivill*[1]; Ryan Pate[1]; David P. Norton[1]; Arthur F. Hebard[1]; Ritesh Das[1]; [1]University of Florida

Transition-metal doped ZnO is a dilute magnetic semiconductor (DMS) that has been shown to exhibit room temperature ferromagnetism when

doped with Co or Mn. We have investigated the transport properties of cobalt-doped ZnO films using field-varying Hall-effect measurements. ZnO films were deposited onto (0001)-oriented sapphire substrates via pulsed laser deposition. Evidence for anomalous hall effect (AHE) up to 400K is found for films containing 30 atomic percent cobalt that were grown at 400°C in vacuum. The films are n-type, conducting, and have large carrier concentrations (~$1x10^{18}$ /cm^3). These films also display ferromagnetic hysteresis as measured by SQUID magnetometry. Ferromagnetism disappears in films grown at higher temperatures and higher partial pressures of oxygen. The origins of AHE and the possible role of magnetic impurity phases will be discussed.

11:20 AM Student

P9, Growth and Physical Properties of N-Al or Cu Co-Doped (Zn,Co)O Dilute Magnetic Semiconductors: *Govind Mundada*[1]; Craig J. Vera[1]; Damon E. Horst[1]; Theodore W. Kehl[1]; Srikanth Manchiraju[1]; Sandhya Pulugam[1]; Pawan K. Kahol[1]; Manivannan Kandiah[1]; Kartik Ghosh[1]; [1]Missouri State University

Dilute magnetic semiconductors (DMS) are promising materials which will combine the charge and spin degrees of freedom into a single substance. Oxide-based DMS have received much attention due to the possibility of ferromagnetism at room temperature and above. Based upon ab-initio calculations, II-IV group ZnO based DMS show high Curie temperature and a large saturation magnetization. Previous studies have shown that ZnO thin films can be made p type by co-doping such as N-Ga [1] ,N-Al [2], and N-In.ZnO doped with transition metal like Co and non magnetic materials like Cu and Al in N_2O-O_2 ambient is an interesting prospectus for spintronic device applications due to its unique electrical and magnetic properties. In this work, N-Al or Cu co-doped $Zn_{0.95}Co_{0.05}O$ thin films were grown on sapphire substrates by pulse laser deposition system in the temperature range from 350 to 600 C in N_2O-O_2 ambient. In these films, Nitrogen concentration varies with N_2O: O_2 pressure. The structural and magnetic properties of these thin films have been investigated using various characterization techniques such as X-ray diffraction, Raman spectroscopy, and Electron microscopy. Both XRD and Raman data show the strong orientation along c-axis without any secondary phase. Temperature dependent resistivity, Hall Effect and magnetization measurements were carried out to understand the electronic and magnetic properties. Preliminary results show both N- and P-type ferromagnetism in these compounds. Detailed results obtained in these films will be discussed in the presentation ahead. This work was supported by the Office of Naval Research (award number N00014-03-1-0893), National Science Foundation (award number DMR- 0321187), and Research Corporation (award number CC6166). [1]M.Joseph,H. Tabata, H.saeki, K.Ueda, and T.Kawai, Physica B 302/303, 140 (2001). [2]J. G. Lu, Z. Z. Ye, F. Zhuge, Y. J. Zeng, B. H. Zhao, and L. P. Zhu, Appl. Phys. Lett. 85, 3134 (2004).

11:40 AM

P10, Optical and Magnetic Properties of ZnVo Prepared by Ion Implantation: *Vitaliy Avrutin*[1]; Umit Ozgur[1]; Sergey Chevtchenko[1]; Hadis Morkoc[1]; Michael J. Callahan[2]; [1]Virginia Commonwealth University; [2]Air Force Research Laboratory

In the last decade, ZnO has attracted a great attention both due to its unique optical properties and as a promising material for applications exploiting spin manipulation. The room-temperature ferromagnetism was predicted for ZnO doped with various transition metal,[1] including vanadium (V). The latter has stimulated a high degree of interest in this material system. In this contribution, we report the optical and magnetic properties of magnetic semiconductor ZnVO fabricated by implantation of 195 keV 51V+ ions into bulk ZnO:Al samples grown by hydrothermal technique. Two sets of the samples, containing Nd – Na ~ 1015 and 1018 cm-3, were implanted to doses of 1 x 1015, 3 x 1015, and 1 x 1016 cm-2. The ion implantation was performed at an elevated temperature of 300°C in order to avoid possible amorphization effect and to enhance the probability of dynamic annealing of radiation damage. Using TRIM calculations, the implantation with the dose of 1 x 1016 ion/cm2 was chosen to reach a maximum vanadium concentration of about 5 at%. To remove irradiation-induced defects, the samples were annealed in air. The crystal structure of the layers was examined by high-resolution x-ray diffractometry (HRXRD) (CuKα radiation). Steady-state photoluminescence (PL) of ZnVO films were carried out both at room temperature and at 15K. The effect of implantation dose and free carrier concentration on the magnetic properties of ZnVO were studied using a commercial superconducting quantum interference device (SQUID) magnetometer (Quantum Design, MPMS). The magnetic field was applied perpendicular and parallel to the sample surface. Ferromagnetic ordering has been observed in highly conductive samples implanted to 1 x 1016 cm-2. PL studies of ZnO bulk samples implanted with V+ have revealed that thermal annealing at 800°C restores to a large extent the optical quality of the material. A new emission line centered at 3.307 eV has been found in the PL spectrum of the highly conductive samples implanted to the dose of 1 x 1016 cm-2, which is most probably due to complexes involving V ions. [1]K. Sato and H. Katyama-Yoshida, Jpn. J. Phys., Part 2 39, L555 (2000).

Session Q: III-Nitride MOCVD Growth

Thursday AM, June 29, 2006
Room: Deans Hall II
Location: Pennsylvania State University

Session Chairs: Andrew Allerman, Sandia National Laboratories; Jae-Hyun Ryou, Georgia Institute of Technology

8:20 AM

Q1, Pulsed Lateral over Growth (PLOG) of $Al_xGa_{1-x}N$: M. Asif Khan[1]; *Qhalid Fareed*[2]; Chen Zheng[1]; Mickael Gaevski[1]; Vinod Adivarahan[1]; Jinwei Yang[1]; [1]University of South Carolina; [2]Sensor Electronic Technology Inc.

The group III-nitride materials are key to applications in deep ultraviolet, blue and green emitters, visible-blind ultraviolet detectors and high frequency heterostructure field effect transistors. In recent years, epitaxial lateral overgrowth (ELOG) of GaN has been extensively used to reduce the threading dislocation densities in heteroepitaxy of GaN over sapphire and SiC resulting in a significant increase in the lifetime of blue laser diodes. AlN with its bandgap around 6.2eV and $Al_xGa_{1-x}N$ with $x > 0.5$ are ideal material for the active regions of deep ultraviolet light emitting diodes (UVLED). Such deep UV emitters are needed to build miniaturized modules for biological-chemical agents, detection, non-line-of-sight (NLOS) covert communications, water purification and polymer curing. Milliwatt power deep UVLEDs with emission from 250-360nm and efficiencies around 1-2% have been successfully demonstrated and are commercialized by Sensor Electronic Technology Inc. Increasing their efficiency and that of UV photodiodes requires $Al_xGa_{1-x}N$ ($0 < x < 1$) layers with dislocation density well below the current values of 10^9 cm^{-2}. However, conventional epitaxial overgrowth of AlGaN with typical masks such as SiO_2 and Si_3N_4 is not possible, due to the larger sticking coefficient for Al on the mask material. In this paper, we present the recent results on growth of low defect density $Al_xGa_{1-x}N$ ($0.1 > x > 1$) layers using a new pulsed lateral overgrowth procedure. First, 1.0 μm thick $Al_{0.6}Ga_{0.4}N$ was deposited on sapphire substrate using TMAl, TMGa and NH_3 as precursors. This template was then selectively etched to create periodic 2 μm wide pillars and 10 μm wide trenches using reactive ion etching. The AlGaN lateral growth was performed at 1100°C using the PLOG epitaxy. In this process, the precursors are pulsed at regular intervals to enhance the migration of adatoms and lateral overgrowth of AlGaN layers. Completely coalesced crack free AlGaN layers with Al composition more than 50% have been successfully grown. The films are characterized using scanning electron microscopy (SEM), cathodoluminescence (CL) and transmission electron microscopy (TEM). Plane view and cross section SEM images show coalesced AlGaN layers with thicknesses more than 10μm. Significant reduction in the dislocation density in the lateral overgrown area has been confirmed using TEM and CL data. Details of growth procedure and characterization results will be included in the presentation.

8:40 AM Student

Q2, MOCVD Growth of Nonpolar *M*-Plane AlN on (1-100) 6H-SiC Substrate: *Qian Sun*[1]; Zaiyuan Ren[1]; Soon-Yong Kwon[1]; Jung Han[1]; [1]Yale University

Growth of nonpolar III-nitride semiconductors has encountered at least two

major issues. Firstly, the density of extended defects in nonpolar GaN films, including threading dislocations and stacking faults, appears to be much higher than that in *c*-plane epitaxial GaN. At the same time, the nonpolar surface of III-nitrides (*a*- and *m*-planes) frequently exhibits striation morphology due to the anisotropy in growth kinetics along *c*- and nonpolar directions. The anisotropic surface kinetics may very well be responsible for the observed anisotropy, in terms of structural, electrical and optical characteristics, in nonpolar epitaxial thin films. AlN is commonly employed as a buffer layer for the epitaxy of III-nitrides on SiC substrates. The crystalline quality and surface roughness of AlN buffer significantly influence the subsequent growth of nitride layers and heterostructures. In spite of the worldwide pursuit of non-polar III-nitride devices, relatively little is known about the heteroepitaxial evolution and surface kinetics that profoundly impact the material microstructure and functionality. In this paper, we present a study of MOCVD growth of *m*-plane AlN on (1-100) 6H-SiC substrates. AlN layers with a nominal thickness ranging from 210 to 270 nm (determined by in-situ reflectance) were grown on *m*-plane SiC substrates with temperature, ammonia flow, and reactor pressure as three controlled variables. Under a low NH_3 flow (10 sccm), a condition that was determined favorable for producing atomically smooth *c*-plane AlN, *m*-plane AlN exhibits disconnected islands composed of parallel stripes. Increasing the NH_3 flow was found effective in improving the surface morphology and crystalline quality. Samples grown with a NH_3 flow of 1000 sccm exhibit a fairly smooth surface fully covered by elongated stripes interconnected with each other along the both planar directions. The full width at half maximum (2.28 arcmin) of the (1-100) symmetric x-ray rocking curve of the sample grown with 500 sccm NH_3 is more than three times narrower than that of the sample grown with 10 sccm NH_3. Temperature and pressure also play important roles in the *m*-plane AlN growth kinetics. As temperature increases from 1030 to 1150°C, the stripes get wider. The sample grown under 120 mbar shows rectangular shape rod-like plateaus, while the stripes of the sample grown under 60 mbar get much elongated and interconnected along the stripe direction. This evolution of surface morphology under various growth conditions indicates anisotropic island coalescence along *c*- and *a*-directions. Information of mosaic tilt and twist in the AlN layers along the two directions parallel and perpendicular to the stripes will be presented. A model combining Wulff theorem in predicting crystal shape near equilibrium with competitive growth based on kinetically-limited epitaxial lateral overgrowth will be used to explain the observed dependence on growth conditions.

9:00 AM

Q3, Halide Chemical Vapor Deposition of AlN: *Timothy E. Bogart*[1]; Mark Fanton[1]; Xiaojun Weng[2]; Ed Oslosky[1]; Brian Weiland[1]; Rodney Ray[1]; Adam Dilts[1]; David Snyder[1]; [1]Pennsylvania State Electro-Optics Center; [2]Pennsylvania State University

Aluminum nitride films up to 240 µm thick were grown on SiC and sapphire substrates by a novel halide chemical vapor deposition (HCVD) process. Growth took place in a vertical hot wall impinging jet reactor by flowing a mixture of $AlCl_3$ and NH_3 diluted in N_2 over the substrate at temperatures between 1100°C and 1500°C and pressures between 25 Torr and 400 Torr. Growth temperatures are significantly higher than those used in typical HVPE growth of AlN, yet well below the temperatures used for sublimation growth. The increased growth temperature allows CVD growth rates to be significantly increased. Growth rates as high as 120 µm/hr have been obtained for epitaxial growth of AlN on both sapphire and SiC substrates compared to 3 µm/hr to 60 µm/hr for typical HVPE growth rates suggesting that this process may provide an alternate route for bulk growth of AlN single crystals. In addition to increasing growth rate, the use of very high purity Al and N source materials in HCVD growth has the potential to significantly reduce the oxygen concentration in the resulting AlN compared to sublimation grown crystals. AlN films 3 µm to 200 µm thick were grown to study the effect of the growth conditions temperature, pressure, and gas flow to AlN growth rate and crystal quality. The trend of the growth rate with respect to the growth conditions from experimental data will be compared to the trend observed theoretically suggesting the ability to predict growth result trends theoretically. The crystal quality is characterized by x-ray rocking curve analyses, SIMS, and TEM.

9:20 AM

Q4, Extremely High Quality AlN Grown on (0001) Sapphire by Using Metal-Organic Vapor Phase Epitaxy: *Yangang A. Xi*[1]; Kaixuan Chen[1]; Frank W. Mont[1]; Xiaolu Li[1]; Jong Kyu Kim[1]; E. Fred Schubert[1]; Wayne Liu[2]; Joseph A. Smart[2]; [1]Rensselaer Polytechnic Institute; [2]Crystal IS

AlN has generated much interest due to its unique properties such as its very wide direct bandgap and its high thermal conductivity. High-quality AlN epitaxial layers are used in AlGaN-based ultra-violet (UV) light-emitting diodes (LEDs), which are strongly impacting applications such as fluorescence-based biological agent detection, water purification, sterilization, and decontamination, and non-line-of-sight communications. At the same time, deep UV photo detectors need extremely high quality AlN with low dislocation density for the reduction of the dark current. Nevertheless, the crystalline quality of AlN must be improved particularly when used as buffer layer in UV LEDs and photo detectors. We report on very high quality AlN epitaxial layers grown by low pressure metal-organic vapor phase epitaxy (MOVPE) using a single-wafer horizontal-flow Aixtron 200/4-RF S reactor with radio-frequency heating. The well-known two-step growth method is used to initiate the growth. A systematic study is presented on the low temperature (LT) AlN nucleation layer and a high temperature (HT) AlN layer. After optimization of growth parameters, AlN epitaxial layers are investigated by atomic force microscopy (AFM), x-ray diffraction (XRD), and photospectrometry. A clear and continuously linear step-flow pattern with saw-edge shaped feature is observed on 5 µm × 5 µm AFM images. The triple-axis x-ray rocking curve scans show a full-width at half-maximum (FWHM) of 11.5 arcsec for the (002) peak and 14.5 arcsec for the (004) peak. KOH etching reveals an etch-pit density (EPD) of 2×10^7 cm^{-2}. The optical transmission spectrum shows a very sharp drop of transmittance at 6.1 eV. AlN with such high crystalline quality has great potential in UV LEDs and UV photodetectors.

9:40 AM

Q5, Late News

10:00 AM Break

10:20 AM

Q6, Effects of Compositionally Graded $Al_{1-x}Ga_xN$ Buffer Layers on the Threading Dislocation Evolution in GaN Films Grown on (111) Si Substrates: *Xiaojun Weng*[1]; Srinivasan Raghavan[1]; Abhishek Jain[1]; Jeremy Acord[1]; Elizabeth C. Dickey[1]; Joan M. Redwing[1]; [1]Pennsylvania State University

Recently, growth of GaN on (111) Si substrates has attracted much attention due to the high quality, low cost, and large wafer size of Si and the potential integration of high-speed and high-power nitride devices with Si microelectronics. However, the large lattice mismatch between GaN and Si leads to a high density of threading dislocations (TDs) in the heteroepitaxial GaN films. Furthermore, in thick (>~250 nm) GaN films grown on Si using thin (~100 nm) AlN buffer layers, cracks develop during the post-growth cooling process due to the tensile coefficient of thermal expansion (CTE) mismatch stress and the additional tensile growth stress arising from island coalescence and lateral grain growth. By introducing compositionally graded $Al_{1-x}Ga_xN$ buffer layers, a compressive lattice mismatch stress can be induced to offset the tensile CTE mismatch stress and growth stress, thus suppressing the cracking of the GaN films.[1-4] To date, only limited studies have been carried out on the effects of $Al_{1-x}Ga_xN$ buffer layers on the TD evolution and contradicting results were obtained.[2,3] In one study, plan-view transmission electron microscopy (TEM) showed an increase in TD density in the GaN film grown on an $Al_{1-x}Ga_xN$ buffer layer, in comparison with those grown directly on AlN buffer layers.[2] However, etch pit counting suggested a decreased TD density in another study.[3] Thus, the effects of $Al_{1-x}Ga_xN$ buffer layers on TD evolution in GaN films on Si are not well understood. Using a combination of plan-view and cross-sectional TEM, we have studied the structural evolution of GaN films grown by metalorganic chemical vapor deposition on (111) Si substrates via compositionally graded $Al_{1-x}Ga_xN$ ($0 \le x \le 1$) buffer layers. Plan-view TEM shows a reduced TD density of 1.1×10^{10} cm^{-2} in GaN films grown on linearly graded $Al_{1-x}Ga_xN$ buffer layers, in comparison with 1.5×10^{10} cm^{-2} for those grown directly on AlN buffer layers. Cross-sectional TEM reveals significant bending and annihilation of TDs in the top half of the $Al_{1-x}Ga_xN$ buffer and the GaN/$Al_{1-x}Ga_xN$ interface, which subsequently lead to the

decrease of TD density of the GaN films. In addition, growing a thin high-temperature GaN base layer prior to growing the compositionally graded $Al_{1-x}Ga_xN$ buffer layer significantly reduces the TD density in the $Al_{1-x}Ga_xN$ buffer layer, which subsequently further reduces the TD density to $5.1x10^9$ cm^{-2} in the overgrown GaN film. The effects of step-graded $Al_{1-x}Ga_xN$ buffer layers and a variety of buffer combinations on TD and stress evolution and cracking suppression will also be discussed. [1]S. Raghavan et al., Appl. Phys. Lett. 88, 041904 (2006). [2]H. Marchand et al., J. Appl. Phys. 89, 7846 (2001). [3]A. Able et al., J. Cryst. Growth 276, 415 (2005). [4]M.-H. Kim et al., Appl. Phys. Lett. 79, 2713 (2001).

10:40 AM Student

Q7, Crack Free GaN Grown on Patterned Si(111) Substrates by Metal-Organic Chemical Vapor Deposition: *Hu Liang*[1]; Baoshun Zhang[1]; Kar Wei Ng[1]; Chi Wing Keung[1]; Kei May Lau[1]; [1]Photonics Technology Center

GaN growth on Si allows the use of low cost and large size substrates for manufacture of LEDs and high-temperature electronics. However, direct growth of high quality crack-free GaN films on whole silicon wafers is challenging. The grown layers usually suffer from cracking at layer thickness larger than 1 μm, because of the lattice mismatch and thermal mismatch between the Si substrate and GaN layer. Different growth techniques such as insertion of inter-layers were employed to increase material crystalline quality. Combined with silicon micromachining techniques, we have been developing technologies and devices by patterned growth of III-nitrides on Si substrates for HEMTs, microsensors, and LEDs. Choosing growth parameters to avoid lateral growth, isolated islands of GaN are not only crack-free, but also allow easier substrate removal, without the complication of laser lift-off[1]. Square islands with LED die size ranging from 340 x 340 μm^2 to 1.5 x 1.5 mm^2, separated by 20 μm trenches, were etched to a depth of 3 μm on Si (111) substrates by inductively coupled plasma (ICP) etching. 2 μm thick crack free GaN films were then grown with different growth conditions, particularly with and without insertion of SixNy interlayers. Low temperature AlN seed layers were used for the patterned growth on Si substrates. Inspection by optical microscopy clearly showed the morphology and crack density difference between growth on the plateaus and unpatterned areas. Spatial distribution of tensile stress in the GaN square islands were investigated by micro-Raman spectroscopy. The tensile stress relaxed symmetrically within 20 μm of the square edges and was constant elsewhere. The FWHM of the XRD spectra did not show much difference in terms of material crystalline quality on different size plateaus. Samples with and without the inter-layer exhibit (002) rocking curves (ω-scans) widths around 520 arcsec for all patterned regions. However, the rocking curves of asymmetric planes (102), which were sensitive to edge threading dislocations, showed FWHM around 993 arcsec and 1296 arcsec for the sample with SixNy interlayer and without SixNy interlayer, respectively. LED structures were deposited after optimization for the patterned growth. With insertion of an SixNy interlayer in the buffer, the room temperature photo-luminescence intensity was significantly enhanced, compared with one grown without the inter-layer, which is also crack-free on small and mid-size islands. [1]Z. Yang, R. N. Wang, S. Jia, D. Wang, B. S. Zhang, K. M. Lau, and K. J. Chen, "Mechanical characterization of suspended GaN microstructures fabricated by GaN-on-patterned-silicon technique," Appl. Phys. Lett. 88, 041913 (2006).

11:00 AM Student

Q8, Defect Reduction in Nonpolar A-Plane GaN Films Using In-Situ SiNx Nano-Mask: *Kwang-Choong Kim*[1]; Arpan Chakraborty[1]; Feng Wu[1]; James S. Speck[1]; Umesh K. Mishra[1]; Steven DenBaars[1]; [1]University of California, Santa Barbara

We report on the use of in-situ SiNx nano-mask for defect reduction in nonpolar a-plane GaN template. Significant improvement in the structural and optical quality of the GaN template was observed. Planar a-plane GaN templates are characterized by the presence of high defect density which limits the performance of devices grown on them. The use of in-situ SiN interlayer has proved to be an effective technique in defect reduction in conventional c-plane GaN. The simplicity of this technique over the more widely used lateral epitaxial overgrowth (LEO) makes this technique more attractive. Unlike traditional single-step LEO, the reduced feature size of the SiNx nanopores facilitates nanometer-scale lateral epitaxial overgrowth thereby resulting in defect reduction uniformly across the wafer. The sample structure, grown by metal-organic chemical vapor deposition consisted of a low temperature GaN nucleation layer grown on r-plane sapphire substrate, followed by the growth of ~0.7μm high temperature GaN. Then a thin layer of SiNx was inserted by flowing disilane and ammonia. The thickness of the SiNx was controlled by varying the growth time of the SiNx layer. The SiNx layer was followed by the growth of ~ 0.1μm unintentionally doped GaN and finally by 2μm Si-doped GaN. Following the growth, the sample was characterized by high-resolution x-ray diffraction (HRXRD), scanning electron microscopy, atomic force microscopy (AFM), transmission electron microscopy (TEM), room temperature photoluminescence (PL) and Hall-effect measurement. HRXRD analysis revealed that there was a monotonic reduction in the full-width-half-maximum (FWHM) numbers, both (110) on-axis and (100) and (102) off-axis, with the increase in the SiNx growth time. AFM images revealed a significant decrease in the density of sub-micron pits. RMS roughness reduced from 2.6nm (for 5×5 μm^2 scan) for a sample without the SiNx interlayer to 6Å for a sample with 120s of SiNx interlayer. An interrupted growth series, where the GaN thickness above the SiNx layer was increased, was carried out to study the microstructural evolution of the GaN islands on the SiNx layer. PL measurement revealed that the emission intensity of the band-edge increased with the insertion of the SiNx layer, which suggests reduction in the non-radiative recombination centers. Cross-section and plan-view TEM on the samples showed a decrease in the density of both stacking faults (SFs) and threading dislocations (TDs). SF density decreased from 8×105 to 3×105/cm whereas TD density decreased from 8×1010 to 9×109/cm^2. Hall measurement showed that the compensation decreased with the increase in the SiNx growth time and also the Hall mobility increased by a factor of 2-3. The detail of the growths, the optimization of the SiNx layer, the results of the characterization, and the evolution of the microstructures would be presented at the conference.

11:20 AM

Q9, Maskless Epitaxial Lateral Overgrowth of GaN Using Dimethylhydrazine as a Nitrogen Precursor: *Toshiyuki Takizawa*[1]; Jun Shimizu[1]; Tetsuzo Ueda[1]; [1]Matsushita Electric Industrial, Company, Ltd.

Epitaxial lateral overgrowth (ELO) technique has been investigated to reduce the dislocation density in III-V nitride materials[1]. The ELO leads to better device performance especially in III-V nitride optoelectronic devices such as blue lasers with longer lifetime. In order to increase the area of low dislocation density, lateral growth rate needs to be enhanced. In addition, suppression of the vertical growth is strongly desired to avoid unnecessary thick growth which would result in epitaxial cracks. In this paper, highly selective ELO, so-called "maskless" ELO, is presented. It is experimentally found that epitaxial growth occurs only from the sidewall of the mesa stripe without any dielectric masks by using dimethylhydrazine (DMHy) as a nitrogen precursor for the MOCVD (metalorganic chemical vapor deposition) growth. The DMHy can be decomposed at lower temperatures than conventional NH_3 precursor. Thus, DMHy is advantageous for high quality epitaxial growth at low temperatures with enhanced lateral growth rates. Striped mesa structures are formed on (0001) GaN layer on (0001) sapphire substrates by ICP (inductory coupled plasma) etching using Cl_2 with various stripe directions. Subsequently, undoped GaN is grown by low pressure MOCVD employing TMG (trimethylgallium) and DMHy as precursors. The growth temperatures are varied ranging from 800°C to 880°C which are lower than those using conventional NH_3. Cross-sectional observation of the regrown wafers by scanning electron microscopy (SEM) reveals that the growth only occurs from the sidewalls while virtually no growth is observed on the top of the mesa. The obtained lateral growth rate from the (11-20) facet is around 10 μm/h, which is extremely high value compared with reported lateral growth rates up to 4 $\mu m/h$[2]. Successful coalescence of the laterally grown GaN layers from adjacent grooves with the smooth top surface is also confirmed. Electron-beam diffraction pattern exhibits that the regrown GaN area has the wurtzite crystal structure. Detaild mechanism of the highly selective growth by DMHy will be discussed taking the pyrolysis of DMHy into consideration. In conclusion, highly selective MOCVD growth using DMHy with extremely high lateral growth rates is demonstrated. This maskless growth would increase the low-dislocation area without any increasing the epitaxial thickness. [1]M. Ishida *et al*, J. Cryst. Growth 221, 345 (2000). [2]A. M. Roskowski *et al*, Opto-Electron. Rev. 10,

261 (2002).

11:40 AM

Q10, Room Temperature Layer-by-Layer Epitaxial Growth of GaN on Lattice-Matched Hf (0001): *Hiroshi Fujioka*[1]; Shigeru Inoue[2]; Atsushi Kobayashi[2]; Jitsuo Ohta[1]; [1]University of Tokyo/KAST; [2]University of Tokyo

We have grown GaN films on lattice matched Hf (0001) substrates at room temperature using UHV-PLD and investigated their characteristics using RHEED, XPS, AFM, GIXR, and GIXD. Hf (0001) has been regarded as a promising candidate for GaN epitaxial growth because it offers very small lattice mismatches of 0.3% and 2.5% in the a-axis and c-axis directions, respectively. However, crystalline quality of GaN grown on Hf by conventional growth techniques has been quite poor because of serious interface reactions between GaN and Hf. We have solved this problem with the use of PLD[1, 2] which allows us to reduce the growth temperature down to room temperature (RT). We have found that stepped and terraced surfaces of Hf (0001) can be obtained by UHV annealing at 1000°C and have observed a clear streaky RHEED pattern. In-situ XPS measurements have revealed that the surface concentrations for the residual O and C are dramatically reduced by the UHV annealing. We have found that RHEED patterns of GaN grown on Hf at 700°C are spotty with rings, which is consistent with previous reports. On the other hand, a RHEED pattern for GaN grown at RT is sharp streaks, which indicates epitaxial growth of high quality GaN films. We have also found that the RHEED intensity oscillates very clearly from the initial stage of the film growth, which is indicative of the layer-by-layer growth mode. These phenomena can be attributed to the small lattice mismatch between GaN and Hf. [1]Y. Kawaguchi et al., Appl. Phys. Lett. 87, 221907 (2005). [2]J. Ohta et al., Appl. Phys. Lett. 83, 3060 (2003).

Session R: Lattice Engineered Epitaxy of III-V and IV Semiconductors

Thursday AM, June 29, 2006
Room: Conference Room 106
Location: Pennsylvania State University

Session Chairs: Sarah Olsen, University of Newcastle-upon-Tyne; Jerry M. Woodall, Purdue University

8:20 AM Student

R1, Materials Optimization for High Indium Content (In,Ga)As Channel HEMTs: *Mike Morse*[1]; [1]Duke University

Mike Morse, Inho Yoon, Changhyun Yi, April S. Brown Department of Electrical and Computer Engineering, Duke University, Durham, NC 27708 High electron mobility transistors (HEMTs) based on high Indium content (In,Ga)As channels offer potential for improved high frequency performance compared to technologies using pseudomorphic or lattice matched InGaAs due to an increasing electron velocity and mobility with increasing In fraction. Two critical issues in the design of these devices are controlling the sources of unintentional charge and accounting for the large lattice mismatch between the substrate and device layers. In this submission, we use computer simulation to assist in understanding how the surface affects the unintentional charge in the HEMT channel, and we examine the suitability of an $In_xAl_{1-x}As$ step-graded metamorphic buffer layer for device applications. For an InAs/AlSb HEMT, charge may be supplied from three sources: deep bulk levels, interface states, and surface charges. We performed self-consistent Schrodinger-Poisson simulations using Silvaco Atlas for structures with a variety of cap materials and variable deep donor concentrations. These results show that the unintentional charge found in the channel the InAs/AlSb HEMT structure is heavily dependent on the cap material for channels less than 200nm from the surface. Consistent with previously published experimental results[1], we found that using InAs as a capping material results in a lower and more controllable electron charge in the device channel. Because of the narrow bandgap of InAs and associated impact ionization related effects, there is interest in moving towards high indium content InGaAs as the channel material of choice. Nine layer step-graded metamorphic $In_xAl_{1-x}As$ buffers (x ranging from 10 to 80%) were grown on a three period 20x20nm AlAs/GaAs supperlattice on a GaAs substrates by molecular beam epitaxy (MBE). Using room temperature Hall Effect measurements, x-ray diffraction (XRD), and atomic force microscopy (AFM), we characterized samples consisting of only the $In_{0.8}Al_{0.2}As$ buffer as well as samples with additional 500µm Be doped and undoped $In_{0.8}Ga_{0.2}As$ layers. Hall measurements indicate that the $In_{0.8}Al_{0.2}As$ buffer is highly resistive, and therefore suitable to act as a pseudo-substrate for subsequent device layer growth. For our Be-doped sample, we find a hole mobility μ_h=110cm²/Vs and a hole concentration of p_b=1.95e18cm^{-3}. The undoped InGaAs exhibits an electron mobility of μ_n=6978cm²/Vs at a density of n_b=2.7e16cm^{-3}. RSM and simulation of rocking curve data indicates that there is some residual strain in the metamorphic buffer. Additionally, we do not see the crosshatch pattern in our AFM data that is typical for layers grown on fully relaxed metamorphic buffers with a superlattice as in Ref 2. Optimization of our step-graded buffer should further improve our promising Hall results. [1]A. Furukawa. Appl. Phys Lett. 62 (64) 1993 3150 [2]Ch. Heyn, J. Crys. Growth. 251 2003 832

8:40 AM Student

R2, High-Mobility 2DEG in InAlAs/InAs Heterostructures Grown on InP Using Metamorphic $InAs_yP_{1-y}$ Graded Buffers: *Yong Lin*[1]; Aaron R. Arehart[1]; Andrew M. Carlin[1]; John A. Carlin[1]; Steven A. Ringel[1]; [1]Ohio State University

Considered as a key material system for the next generation of high-speed electronics, InAs is receiving great attention because of its high electron mobility. Due to the lack of technologically-viable, lattice-matched bulk substrates for InAs device growth, metamorphic graded buffers are usually required between a conventional substrate and the device layers to accommodate the misfit strain and achieve high-quality relaxed InAs layers. In recent work, we have shown that metamorphic InAsP step-graded buffers (in which the group V sublattice is graded) on InP substrates have demonstrated superior surface morphology, lower threading dislocation density, and higher minority carrier lifetimes within overgrown double heterostructures, compared to more conventional buffers consisting of group III based grades such as InGaAs or InAlAs.[1,2] Here we have extended this work to explore properties of relaxed InAs grown on InP via InAsP buffer layers in the context of InAlAs/InAs heterostructures, by correlating mobility properties with structural properties and defect concentrations as a function of the presence of the metamorphic InAsP buffer. InAlAs/InAs heterostructures were grown by molecular beam epitaxy on InP substrates with and without $InAs_yP_{1-y}$ step-graded buffers. The entire $InAs_yP_{1-y}$ buffer thickness was 1.5 µm, and was grown at an average grading rate of 60% As/µm. To provide direct comparison, the sample without a graded buffer included a 1.5 µm thick InAs buffer layer grown directly on InP. On each buffer was subsequently grown a uniformly doped n-type ($1x10^{18}$ cm^{-3}) InAlAs/InAs heterostructure consisting of a 1 µm thick InAs layer followed by a 10 nm thick, strained $In_{0.8}Al_{0.2}As$ barrier layer. All buffer layers were unintentionally doped. High-resolution XRD results show that the heterostructures on both buffers are nearly totally relaxed; however cross-sectional TEM reveals that threading dislocations present in the heterostructures using a direct-growth InAs buffer have significantly higher density compared to heterostructures grown on the metamorphic buffer. Transport properties were investigated to determine the impact of buffers on electrical properties of heterostructures using temperature-dependent Hall measurements. In contrast to the bulk-like mobility data obtained from the direct-growth sample, an ideal two-dimensional electron gas (2DEG) temperature dependence of the electron mobility was observed in the InAlAs/InAs heterostructure grown on metamorphic $InAs_yP_{1-y}$ buffers. A very high electron mobility of 130,000 cm²/Vs at 25 K was measured for the 2DEG within the relaxed InAs layer. This extremely high mobility result based on relaxed InAs indicates the substantial potential of these virtual InAs substrates for advanced high-speed device applications. Complete details of the growth and electronic-structural property correlations will be presented. [1]M. K Hudait et al, Appl. Phys. Lett. 82, 3212 (2003). [2]Y. Lin, et al, Appl. Phys. Lett. 86, 071908 (2005).

9:00 AM Student

R3, High-Quality InP on GaAs Using Graded Buffers Grown by MOVPE (Metal Organic Vapor Phase Epitaxy): *Nate Quitoriano*[1]; Eugene A. Fitzgerald[1]; [1]Massachusetts Institute of Technology

In addition to traditional telecom applications, devices based on InP have received increased attention for high-performance electronics. InP growth on GaAs is motivated by the fact that InP wafers are smaller, more expensive, and utilize older fabrication equipment than GaAs. High-quality InP on GaAs bulk substrates has proven to be challenging, however. While a number of commercial growth foundries offer InP on GaAs for M-HEMT (Metamorphic High-Electron-Mobility Transistor) applications, the successful demonstration of InP-based, minority-carrier devices on bulk GaAs remains elusive. We demonstrate for the first time InP on GaAs suitable for minority carrier devices, exhibiting a threading dislocation density of $1.2x10^6/cm^2$. To achieve this we explored the InGaAs, InGaP, InAlAs and InGaAlAs materials systems. In each of these systems, we found that microscopic compositional inhomogeneities along the growth direction blocked dislocations leading to dislocation densities as high as $10^9/cm^2$. Using scanning-transmission electron microscopy, we determined that the composition variations were caused by surface-driven phase separation leading to Ga-rich regions. Conditions for avoiding phase separation were identified and explored. We found that we could prevent composition variations in $In_xGa_{1-x}As$ graded buffers grown at 750°C to yield low dislocation densities of $1.5x10^6/cm^2$ for $x<0.34$, accommodating ~70% of the lattice mismatch between GaAs and InP. However, further grading to 53% In is required to attain the lattice constant of InP. We have found that compositional grading in $In_yGa_{1-y}P$ ($0.8< y <1.0$) can accommodate the remaining lattice mismatch with no rise in thread density while avoiding phase separation. Consequently, to achieve high-quality InP on GaAs we started with the InGaAlAs material system and then completed the graded buffer in the InGaP system to reach InP.

9:20 AM

R4, Optical and Electrical Defect Characterization of $In_{0.49}Ga_{0.51}P$ Grown on Metamorphic SiGe Substrates: *Maria Gonzalez*[1]; Andrew Armstrong[1]; Carrie Andre[2]; Steven A. Ringel[1]; Arthur Pitera[3]; Eugene A. Fitzgerald[4]; [1]Ohio State University; [2]Akzo Nobel; [3]Contour Semiconductor; [4]Massachusetts Institute of Technology

The use of SiGe compositionally step graded buffers coupled with precise growth transitions across III-V/IV interfaces, which together accommodate mismatches between InGaP-GaAs-based materials and Si, has been established as an extremely promising approach to integrate III-V technology on Si wafers. Recently, our initial work to establish a variety of GaAs/Si devices via SiGe has been extended to include monolithic integration of more advanced III-V structures on Si that incorporate wider bandgap III-V materials, including InGaP/GaAs double junction solar cells, GaInP LEDs and visible red AlGaInP laser diodes. To date however, the impact of electronic defects that may be present within these wider bandgap III-P based materials grown on SiGe has yet to be investigated, and given the generally increased role of deep levels within larger bandgap semiconductors coupled with the presence of residual threading dislocations from the SiGe substrates, knowledge of deep level defects and their distribution is important to advance device performance and reliability. Here, we investigate deep levels within InGaP layers and p^+n diodes grown on SiGe (terminal composition is 100% Ge to form a "virtual" Ge substrate) by molecular beam epitaxy, with direct comparisons made to identical structures grown on GaAs to discern traps related to growth on the metamorphic SiGe substrate. The $In_{0.49}Ga_{0.51}P$ is nominally lattice matched to both substrates as confirmed by high resolution x-ray diffraction. Since the bandgap at this composition is ~ 1.9 eV, this precludes complete trap spectrum analysis by conventional thermal deep level transient spectroscopy (DLTS). Thus we augment DLTS with a deep level optical spectroscopy (DLOS) that has proved invaluable for similar studies of wide gap GaN. DLTS reveals the presence of three majority carrier electron traps, located at E_c-0.28 eV, E_c-0.44 eV and E_c-0.75 eV within the bandgap of the InGaP layer at similar concentrations regardless of the substrate (corroborating previous observations in GaAs/SiGe/Si layers). DLOS experiments, which enable scanning of the entire ~1.9 eV InGaP bandgap on both substrates reveal the presence of several deeper levels at E_c – 0.9 eV, 1.4 eV 1.7 eV in both cases, none of which could be detected by conventional DLTS. Interestingly, a distinct level at E_v+1.3 eV was detected but only in the InGaP/GaAs sample. Its absence in the InGaP/SiGe sample may imply the presence of a defect gettering mechanism by threading dislocations within the metamorphic structure, though this speculative conclusion and a comprehensive assessment of the properties and sources for these levels will be explained at the conference.

9:40 AM Student

R5, Lattice-Engineering for Monolithic Visible Yellow-Green Light Emitters: *Michael J. Mori*[1]; Eugene A. Fitzgerald[1]; [1]Massachusetts Institute of Technology

Low cost chip-to-chip optical interconnects may be realized on a Si platform by using monolithically integrated III-V light emitters and Si *pin* photodetectors. The absorption coefficient of Si (α_{Si}) is close to the convenient value of 10^4cm^{-1} in the wavelength range 500-600nm, thus, epitaxially integrated, direct band gap materials for emission in this range, green to yellow, are needed. The quaternary alloy AlInGaP offers promise for monolithic integration on Si due to its large direct band gap (1.9-2.2eV). The III-N materials typically have too large of a band gap for this application while their very small lattice parameters make monolithic integration on Si very difficult. Other medical, imaging, and printing applications also exist for large area monolithically integrated yellow-green emitters. We focus on AlInGaP with lattice parameters intermediate to GaP and GaAs, near 5.57 Angstroms (misfit to Si, f=-2.5%). We have engineered compositionally graded buffers at this lattice constant that will be used as device virtual substrates. Previously, 570nm AlInGaP LEDs were demonstrated on InGaP/GaP graded buffers with relatively high threading dislocation densities of about $7x10^6cm^{-2}$. These substrates were limited by III-segregation defects which escalated dislocation density (TDD). Surface roughness, which increases rapidly in InGaP at relatively low misfit (>0.1%), also escalated TDD. We have shown that by reversing the sign of strain relief (tensile instead of compressive grading) and by grading group V content of GaAsP/GaAs instead of group III in InGaP/GaP, we avoid III segregation and maintain smoother films, thus reducing the dislocation density of our virtual substrates by almost three orders of magnitude, to nearly $1x10^4cm^{-2}$. A combination of plan view TEM and etch pit density (EPD) measurements were performed obtain these measurements. Theoretical calculations of the band structure of AlInGaP strained quantum well devices on our virtual substrates indicate that light emission will be in the range 550nm to 620nm, but that a lack of a sufficient conduction band offset will limit devices at shorter wavelengths. The light emitters have been designed to port directly to a GaAs on Si platform via SiGe graded buffers using technology previously demonstrated.

10:00 AM Break

10:20 AM Student

R6, The Fabrication of Misfit Dislocation-Free Strained Si Thin Films Using Porous Si Substrates: *Jeehwan Kim*[1]; Ya-hong Xie[1]; [1]University of California at Los Angeles

Strained Si has established itself as an integral part of the high performance CMOS technology. Another important application of strained Si is for the fundamental understanding of transport physics of two-dimensional electron systems (2DES) under extreme conditions, namely, in high magnetic field at low temperature. For the latter, sample homogeneity is of extreme importance, in clear contrast to CMOS applications for which only the transconductance is important. Process induced local stress approach renders inhomogeneous stress across the sample. Global stress induced by relaxed SiGe buffer layer, on the other hand, is associated with high density of misfit dislocations that cause an undulating strain field in the 2DES leading to poor homogeneity. We report a new approach for fabricating strained Si with the objective of achieving unprecedented level of homogeneity. We employ a novel self-limiting process to fabricate thin Si films of ~500 nm thickness on microporous Si substrate of several hundred micrometer thickness. Low temperature oxidation of the porous Si substrate results in the thin Si film being strained in a controllable fashion. The process flow begins by the epitaxial growth of an intrinsic Si film on a heavily doped p-type substrate. The porous Si formation process is carried out via anodization process which proceeds from the backside of the wafer until it reaches the interface between the epilayer and the heavily doped substrate. The intrinsic film serves as an excellent anodization-stop layer as has been established by our previous experimental studies. The formation process of micro-porous

Si in heavily doped Si of hundreds of micrometers thick can stop within 10 nm upon encountering intrinsic Si with no discernable interface roughness. The anodized samples are oxidized at 500ºC in steam. The oxidation induced volume expansion in the porous Si substrate of the bilayer structure leads to tensile strain of the thin Si layer. The amount of tensile strain is controlled by the oxidation time. The biaxial strain in the layer is measured using Raman spectrometer. For the 100 nm Si layer, monotonic increase of tensile strain is observed with oxidation time until it reaches 1.04%. For the samples with increasingly thicker Si layer, the strain begins to deviate from the monotonic dependence at progressively short oxidation time. Such deviation is taken as the sign of plastic deformation of the Si film via dislocation. Some of the key technical challenges for the new approach will be discussed in detail. Our result indicates that with sufficiently thin Si film, strain values higher than 1% is achievable while completely avoiding dislocation. It is a significant step forward in sample fabrication for the transport physics research into 2DES under extreme conditions, and potentially for FET applications.

10:40 AM

R7, Novel Fabrication Process for Multi SOI Layers Using Selective Etching of SiGe in Multi Si/SiGe Layers: *Shun-Ichiro Ohmi*[1]; Tomoyuki Nakanishi[1]; Ken-Ichi Yahashi[1]; Tetsushi Sakai[1]; [1]Tokyo Institute of Technology

Novel fabrication process for multi silicon-on-insulator (SOI) layers was proposed, and a selective etching process of SiGe layers for Si/SiGe/Si/SiGe/Si(100) multi layers was investigated for 2-layer SOI formations. Si(70 nm)/$Si_{0.7}Ge_{0.3}$(10 nm)/Si(70 nm)/$Si_{0.7}Ge_{0.3}$(10 nm)/Si(150 nm) multi layers were grown on p-Si(100) substrates by UHV-CVD. The deposition temperature both for Si and $Si_{0.7}Ge_{0.3}$ layers was 550°C. The fabricated area of multi SOI layers were 0.55 µm x 4.0 µm. After the patterning and trench formation besides both sides of 0.55 µm, SiO_2 (350 nm) was deposited at 400°C by AP-CVD followed by the annealing at temperatures of 700 – 800°C for 30 min as a support for Si layers during the selective etching of $Si_{0.7}Ge_{0.3}$ layers. Then, the 2nd trench formation beside both sides of 4.0 µm was carried out, and the $Si_{0.7}Ge_{0.3}$ layers were laterally etched by the etchant of HF(50%):HNO_3(61%):H_2O. It was found that an etching rate of the upper $Si_{0.7}Ge_{0.3}$ layer is slower than that of the lower $Si_{0.7}Ge_{0.3}$ layer when the annealing temperature was 700°C. The obtained etching rate for lower $Si_{0.7}Ge_{0.3}$ layer was approximately 250 – 270 nm/min, while it was 200 nm/min for upper SiGe layer. The difference of etching rates was strongly depended on the quality of deposited SiO_2 support layer. During the selective etching of $Si_{0.7}Ge_{0.3}$ layers, SiO_2 was also etched, although its etching rate was lower than the $Si_{0.7}Ge_{0.3}$ layer, so that the support layer on top of the Si layer shrunk. The shape of the SiO_2 support layer seemed to affect the etching rate for the upper $Si_{0.7}Ge_{0.3}$ layers probably due to the strain effect. In the case of 750 – 800°C annealing, the etching of SiO_2 layer seemed to be suppressed because of the densification of the deposited SiO_2 layer. However, the etching rate of $Si_{0.7}Ge_{0.3}$ layers decreased to 170 nm/min in the case of 800°C annealing, while it was 240 nm/min in the case of 750°C annealing. Therefore, the optimum annealing temperature is considered to be 750°C. After the 750°C annealing, the etching rate of upper $Si_{0.7}Ge_{0.3}$ layer increased close to that of the lower $Si_{0.7}Ge_{0.3}$ layer, however, the difference of etching rate was still observed and it should be improved to obtain uniform multi SOI layers. The detail of the buried oxide (BOX) layer formations were also discussed at the conference.

11:00 AM

R8, Perimeter-Limited Strain in Patterned Structures of SSOI: *Albert J. Paul*[1]; [1]National Institute of Standards and Technology

Off-axis Raman spectroscopy has been used to measure the Raman Shift of a strained silicon-on-insolator(SSOI) control surface under biaxial stress and the shift of patterns formed from SSOI. Gratings and pillars were formed from 30nm thick strained silicon using interference interferometry. The gratings were 90nm wide with 100nm groves. The pillars were 80nm x 170nm. The Raman shift of the control SSOI wafer was 514.48±0.11cm^{-1}. The Raman shift of the grated structure was dependent on the polarization of the excitation laser. When the polarization of the laser was along the grated surface, the Raman shift was 516.32±0.35cm^{-1}. However, when the laser polarization was across the gratings, the Raman shift was reduced to 517.49±0.47cm^{-1}. The Raman shift of unstrained Si was 520.42±0.07cm^{-1}. The shift in the pillared structures were nearly the same as relaxed silicon. An off-axis analysis is used to determin whether the shift in the peak is due to relative shifts in the intensities of the the phonon modes or a strain relaxation due to a perimeter effect.

11:20 AM

R9, FET Mobilities in Layers Grown by Ultra-High Growth Rate CVD with High-Order Silane Precursor: *Keith H. Chung*[1]; J. C. Sturm[1]; K. K. Singh[2]; D. Carlson[2]; S. Kuppurao[2]; [1]Princeton University; [2]Applied Materials

Growth temperatures under 700°C are required for the integration of novel front-end processes in VSLI structures to avoid any dopant diffusion. In this work, we report record growth rates of device-quality epitaxial silicon grown by thermal chemical vapor deposition from 600 to 700°C. The work was enabled by a novel a high-order silane (HOS) silicon source. Growth rates of epitaxial silicon on <100> silicon substrates were 160nm/min, and 67nm/min were achieved at 650°C and 600°C respectively in a hydrogen carrier at torr. Compared to rates of 20nm/min and 5nm/min at 630°C and 600°C previously reported using a source of trisilane,[1] our work represents a factor of 10X increase at 600°C and 2.5X increase at 650°C. These growth rates are also significantly higher than the growth rates using typical silane based silicon epitaxy rates at of 5nm and 2nm/min at 650°C and 600°C respectively.[2,3] This is significant because high growth rates are desired for throughput and cost-of-ownership issues in modern single-wafer processing tools. To characterize the growth of the epitaxial layers, p-channel FET's were fabricated using a self-aligned polysilicon gate process. Approximately 200nm of epitaxy using the novel precursor was grown on blanket n-substrate wafers. FETs were well behaved for both curve-tracer and IDS vs VG characteristics. The FET thresholds on the experimental source wafers were -0.11V to -0.57V, compared to 0.05V on the control sample in n-type substrate. Hole mobilities obtained from ID vs VGS curves in the experimental devices for VGS-VT= -1V, were from 141 cm2/Vsec to 156 cm2/Vsec vs. 122 cm2/Vsec for the control devices, indicating the high quality of the epitaxy deposited with very high growth rate at low temperatures. There was no significant change in the mobility from different growth rates (~50nm/min at 600°C vs. ~150nm/min at 650°C). Subthreshold slopes were acceptable at 80meV/dec in all devices. [1]M.A. Todd et al, Applied Surface Science 224, 41-45 (2004). [2]M. Tao, Thin Solid Films 223, 201-211 (1993). [3]J. Comfort et al, Journal of the Electrochemical Society 136, 2386 (1989).

11:40 AM

R10, Late News

Session S: SiC: Growth and Interface Studies

Thursday AM, June 29, 2006
Room: Conference Room 208
Location: Pennsylvania State University

Session Chair: Michael A. Capano, Purdue University

8:20 AM

S1, Effects of Hydrogen on Physical Vapor Transport Growth and Deep Trap Concentrations in 6H SiC: *Mark Fanton*[1]; Marek Skowronski[2]; Alexander Polyakov[2]; Randal Cavalero[1]; Rodney Ray[1]; [1]Pennsylvania State University; [2]Carnegie Mellon University

The effects of hydrogen addition to the growth atmosphere during physical vapor transport (PVT) growth of 6H-SiC boules is presented. With the addition of hydrogen, the total vapor pressure of carbon species within the growth cell is significantly increased due to formation of hydrocarbons. The result is a more C-rich growth environment. Using the hydrogen assisted physical vapor transport (HPVT) process for growth of semi-insulating 6H-SiC boules results in a typical decrease in N concentration in the crystal from $9x10^{16}$ atom/cm^3 to less than $1x10^{16}$ atom/cm^3, as would be expected from site competition theory for growth under more carbon rich conditions. In addition, the concentrations of deep traps, as measured by deep level transient spectroscopy (DLTS), decrease by over a factor of ten. In particular,

the concentration of the Z1/Z2 defect is reduced from $5x10^{14}/cm^3$ to less than $1x10^{14}/cm^3$ with as little as 10% hydrogen added to the growth ambient. The concentration of hydrogen in the SiC crystal is compared to standard PVT growth by substituting deuterium for hydrogen and quantifying the concentration of deuterium in the crystal after growth by secondary ion mass spectrometry (SIMS). In addition, the deuterium concentration and the concentrations of deep traps are quantified after annealing at temperatures up to 1700°C in order to determine if the reduction in the concentration of deep traps observed in HPVT growth is accomplished by hydrogen passivation or through modification of the C/Si ratio during crystal growth.

8:40 AM Student

S2, Surface Morphology, Doping and Oxide Field of 4H-SiC C-Face Epitaxial Layer Grown by Horizontal Hot-Wall Chemical Vapor Deposition: *Kung-Yen Lee*[1]; Wenzhou Chen[1]; Michael A. Capano[1]; [1]Purdue University

Silicon carbide epitaxial layers have been grown on the carbon-face of 4H-SiC substrates using a low-pressure, hot-wall chemical vapor deposition system in different conditions. Goals of the research were to investigate n-type doping and surface morphology and oxide breakdown field of C-face epilayers. The lowest doping concentration achieved during these experiments was $6x1014cm^{-3}$, which is the lowest reported controllable n-type doping concentration. The conditions corresponding to this doping were at a pressure of 50mbar, a C/Si ratio of 4, N2 gas flow rate of 0.073sccm, and a temperature of 1600°C. The best surface morphology obtained was 0.19nm, and densities of hillocks and carrots are 0.2 and $0.8cm^{-2}$, respectively, at a temperature of 1640°C. The doping concentration and defect density of a C-face epitaxial layer are strongly dependent on pressure, temperature and the C/Si ratio. The oxide breakdown field of a C-face epilayer is less than 7MV/cm when the wet oxidation was carried out at 1150°C for 90min, followed by re-oxidation at 950°C for 2 hours and immediately annealed with NO at 1175°C. The oxide thickness is about 4700Å. The C-face oxide breakdown field can be enhanced to 8MV/cm when samples were oxidized at 950oC for 35min in the wet and oxygen ambient or 70min in the dry oxygen ambient and followed by NO anneal at 1175°C. The oxide thicknesses are about 650Å and 430Å for wet and dry oxidation, respectively. The oxide breakdown field over N-implanted region was also investigated. Samples were oxidized at 950°C in the wet oxygen ambient and followed by NO anneal at 1175°C, and the value of oxide breakdown field is about 8MV/cm. The total dose of N implantation is $1.25x1013cm^{-2}$. The root-mean-square (RMS) roughness of N-implanted region obtained by AFM is 0.6nm. However, N-implanted samples have higher leakage currents compared with non-implanted samples.

9:00 AM

S3, Chemical Vapor Deposition of Silcon Carbide Epitaxial Films and Their Characterization: Yi Chen[1]; *Govindhan Dhanaraj*[1]; Hui Chen[1]; William Vetter[1]; Hui Zhang[1]; Michael Dudley[1]; [1]Stony Brook University

Silicon carbide (SiC) is a potential semiconductor material to replace the conventionally used silicon and other related crystals in certain critical device applications. High quality substrates and epitaxial layers with very low defect densities and good surface morphology are needed for fabricating various devices. Epitaxial growth based on chemical vapor deposition (CVD) is commonly used in fabricating these device structures. Understanding the growth kinetics and defect generation is essential to increase the yield. The defects nucleated during the growth as well as the propagating micropipe dislocations from substrate to the epitaxial film need to be studied thoroughly. Even the process induced basal plane dislocation densities need to be reduced for better device performance. As the continuation of our SiC bulk and epitaxial research program, we have developed a CVD system with the aim to understand SiC growth kinetics and defect nucleation mechanisms during epitaxial deposition. Growth experiments were performed both in kinetically and thermodynamically controlled regimes. Better surface morphology was obtained in the films grown at kinetically controlled region. Epitaxial films of 6H and 4H SiC of thickness ranging from a few microns to a few hundred microns have been grown using propane and silcon tetrachloride/silane. Optimization of the growth process and improvements in the hot-zone design led to better quality homo-epitaxial layers. The grown films have been studied using Nomarski Optical Microscopy, AFM and X-ray diffraction techniques. Synchrotron white beam X-ray topographic characterization as well as chemical etching revealed lower density of basal plane dislocations of the better quality epitaxial layers grown at 5-10 microns/hr. The thicker films (100-300 microns) grown at higher rates revealed rough surface morphology. The grazing incidence white beam synchrotron X-ray topography exclusively probed the defect structure in the bulk of the 5 micron thick epilayers without affecting the surface morphology. Measurements of high resolution X-ray diffraction rocking curve widths show that in some cases the quality of the epitaxial layer can be better than the substrates. The dislocation conversions and annihilations may be occurring during the growth of the epitaxial layers. The details of substrate characterization, epitaxial growth and kinetics, and defect characterization will be presented.

9:20 AM

S4, Structural and Electrical Characterization of Carbon Nanotubes Formed on Silicon Carbide Materials by Surface Decomposition: *John Boeckl*[1]; William C. Mitchel[1]; Bill Riehl[2]; Mike Check[2]; [1]Air Force Research Laboratory; [2]Riehl-Check Industries

Carbon nanotubes (CNT's) have been formed on the surface of 4H and 6H silicon carbide (SiC) wafers during high temperature anneals (1400-1700°C) under moderate vacuum conditions (10^{-2} – 10^{-5} torr). The carbon source for the CNT's is believed to be residual carbon, from the SiC substrate, left on the surface after preferential evaporation of the Si. CNT formation is then believed to be catalyzed by low concentrations of residual oxygen in the vacuum chamber with CNT growth proceeding from the initial SiC surface into the wafer over time. No metal catalysts are required for this CNT growth method and the resulting CNT's are vertically aligned on the SiC substrate and have a high purity. Scanning electron and transmission electron microscopy along with Raman scattering measurements have confirmed the presence of both single-wall and multi-wall CNT's with a dispersion of nano particles of graphitic carbon. In this work, we extend this growth technique to include CNT growth on 3C-SiC foams, 3C-SiC nano particles, and carbon fibers that have been coated with amorphous SiC. Using scanning electron microcopy (SEM) and transmission electron microscopy (TEM) the resulting CNT structures are characterized on these novel substrates. Metal contacts were also deposited on the CNT's and I-V measurements were performed to evaluate the electrical characteristics of the CNT's and the SiC/CNT interface for use in chemical and biological sensors. We also report on the use of these materials for electrochemical impedance spectroscopy (EIS) and anodic stripping voltammetry (ASV), due to chemisorption of gases onto the CNT arrays, and the subsequent development of sensors for aqueous and vapor phase chemical detection by these techniques.

9:40 AM

S5, Late News

10:00 AM Break

10:20 AM

S6, Role of Interface Layers and Localized States in TiAl-Based Ohmic Contacts to P-Type 4H-SiC: *Min Gao*[1]; Sergey Tumakha[1]; Stefen Goss[1]; T. Onishi[2]; Susumu Tsukimoto[2]; Masanori Murakami[2]; Leonard J. Brillson[2]; [1]Ohio State University; [2]Kyoto University

Ohmic contact formation to p-type SiC is a key technology issue in the fabrication of SiC electronic devices. A leading candidate involves Ti/Al-based deposition and annealing that yield the lowest contact resistance currently available as well as high thermal stability. In order to probe the mechanism(s) responsible, we have used depth-resolved cathodoluminescence (DRCLS), Auger electron spectroscopies (AES), and secondary ion mass spectroscopy (SIMS) to investigate the roles of interfacial reaction, work function variation and localized states of Ti/Al ohmic contacts to p-type SiC on a nanometer scale. To fabricate the ohmic contacts, Ti and Al layers were deposited sequentially on p-type 4H-SiC epitaxial layers and annealed at 1000ºC for 6 min in UHV. Two sets of Ti/Al contacts were studied: Ti(100 nm)/Al(380 nm) and Ti(10 nm)/Al(38 nm).[1] AES and SIMS measurements showed a Ti-Si-C reaction layer, which was consistent with the previous transmission electron microscopy and x-ray diffraction results indicating an epitaxial Ti_3SiC_2 intermediate semiconductor layer. The plan-view AES and SIMS depth profile determined that Ti, Si, and C were the only important elements near the contact, while Al was believed to be evaporated away during the annealing and not to play an important role in either the reaction layer or

the interface. AES combined with an ultra high vacuum scanning electron microscope was also used as a scanning work function spectroscopy to study the variation of the work function across the p-SiC/Ti_3SiC_2 interface. The work function was determined by using the onset energy of secondary electron emission measured by AES. A continuous decrease in work function was observed from p-SiC to the Ti_3SiC_2 layer. Together with absence of Al, these results ruled out p-type doping of the SiC by Al indiffusion, which can cause work function increase at SiC surface. Furthermore, only a 1.1 eV decrease in work function from the p-SiC into the Ti_3SiC_2 overlayer was observed, which indicated that the work function of reaction product is intermediate between that of the p-SiC and the Ti/Al. This result is consistent with an intermediate semiconductor layer that reduces the large Schottky barrier height that would otherwise result from a large work function difference.[1,2] The DRCLS result revealed that the interfacial reaction considerably enhanced the emission intensity of a ~2.78 eV sub-band gap transition which is probably attributed to point defects in the near-interface SiC. Such interfacial defect state may further reduce the barrier for hole tunneling at the ohmic contact. Our results emphasize the role of interfacial reaction and localized states in the formation of ohmic contacts to p-SiC. [1]S. Tsukimoto, K. Nitta, T. Sakai, M. Moriyama and M. Murakami: J. Electr. Mater. 33, 460 (2004). [2]B.J. Johnson and M.A. Capano: J. Appl. Phys. 95, 5616 (2004).

10:40 AM

S7, As-Deposited Ohmic Contacts Using Ti on InN on SiC: Feroz A. Mohammad[1]; Yan Cao[1]; *Lisa M. Porter*[1]; Ariel Virshup[1]; [1]Carnegie Mellon University

Ohmic contacts to n-type SiC are typically formed by annealing Ni at temperatures above 900°C. Although annealed Ni contacts have low specific contact resistance, the high-temperature post-deposition annealing step in the standard process is undesirable because the reaction between Ni and SiC leads to broadening of the Ni-SiC interface, interface and/or surface roughening, the formation of voids, and carbon segregation at the interface and throughout the metal layer. In this study ohmic contacts to n-type 4H- and 6H-SiC were achieved without post-deposition annealing using an interlayer of epitaxial InN beneath a layer of Ti; whereas Ti contacts without an InN interlayer were not ohmic. The InN films were grown by DC reactive magnetron sputtering at 450°C, and the Ti films were deposited by electron-beam evaporation at room temperature. The films were characterized by x-ray diffraction (XRD), cross-sectional transmission electron microscopy (TEM), and Hall-effect measurements. Both XRD and TEM observations revealed that the Ti and InN films have epitaxial relationships with the underlying substrate as follows: (0001)[11-20]Ti || (0001)[11-20]InN || (0001)[11-20]6H-SiC; and the TEM images revealed relatively flat interfaces. For specific contact resistance calculations, SiC samples containing a highly-doped n-type epilayer on top of a lightly-doped epilayer to prevent current spreading into the underlying substrate were employed. The average specific contact resistances of Ti/InN on 4H-SiC (epilayer doping level = 9.8 x 10^{18} cm^{-3}) and 6H-SiC (epilayer doping level = 1.8 × 10^{19} cm^{-3}) were 1.8 × 10^{-4} and 6.7 × 10^{-5} O-cm^2, respectively. It is believed that the ohmic behavior is associated with an electron accumulation layer at the surface of InN [1]. Estimated band alignments across the Ti/InN/SiC structure are proposed to further justify the ohmic behavior. 1. K.A. Rickert, A.B. Ellis, F.J. Himpsel, H. Lu, W. Schaff, J.M. Redwing, F. Dwikusuma, and T.F. Kuech, Appl. Phys. Lett., 82, 3254 (2003).

11:00 AM Student

S8, Electronic States of Chemically Treated and/or Oxidized SiC Surfaces: *Shu Nie*[1]; R. M. Feenstra[1]; Y. Ke[2]; R. P. Devaty[2]; W. J. Choyke[2]; [1]Carnegie Mellon University; [2]University of Pittsburgh

We report on a study of electronic states at SiC surfaces that have been chemically treated and/or oxidized. The goal of the work is to determine the spectral density of states, specifically the degree of passivation of the surface by the various treatments, in order to elucidate the reported biocompatibility of SiC surfaces[1]. In particular, recent work on porous SiC prepared by photo-electrochemical (PEC) etching has indicated good biocompatibility of that material[2], which we hypothesize is due to a reduced density of midgap states for those surfaces. To test this hypothesis we have used scanning tunneling microscopy (STM) and spectroscopy (STS) to study the spectroscopy and charge transport of electronic states at both the (0001) Si-face and (000-1) C-face of p-type 4H-SiC that were PEC etched (with etching conditions to produce flat, rather than porous, surfaces). To understand the change of surface states caused by the PEC etching, we also investigated the states at n-type 6H-SiC(0001) Si-face surfaces either with their native oxides (as received) or with in situ oxidization. The oxidation is performed in an ultra-high vacuum chamber at 700°C in 1×10^{-7} Torr pressure of molecular oxygen for 4 hours, and is preceded by H-etching of the surface at 1700°C for 100 s. Auger electron spectroscopy performed as a function of oxygen exposure reveals a saturation surface coverage of about 2.1 monolayers for the Si face for this oxidation. Tunneling spectra shows that the surface of the native oxidized surface has a high density of midgap states, with characteristic states located throughout the gap. The Fermi level is found to be strongly pinned by these surface and interface states of the native-oxide surface. In contrast, STS reveals that there are many fewer midgap surface states for both the PEC-etched surface and the intentionally oxidized (preceded by H-etching) surfaces. Negligible current is detected in the band gap for those cases, so that the density of states is below our detection limit (at least 1-2 orders of magnitude below that for the native oxide surface). The current-voltage measurements in this case resemble that expected for a Schottky barrier, but measurements of current vs. tip-sample separation demonstrate conclusively that the probe-tip is not in contact with the SiC. Rather, band bending that occurs in the sample produces the observed spectra. Detailed modeling of this band bending is in progress, in an effort to more quantitatively produce an estimate of the (low) midgap state density for these surfaces. This work is supported by an ONR DURINT grant, N00014-01-1-0715. [1]C. Harder, A. Rzany, and M. Schaldach, Prog. Biomed. Res. 1, 71 (1999). [2]A. J. Rosenbloom et al., Mater. Sci. Forum Vols. 457-460, 1463 (2004).

11:20 AM Student

S9, Effect of Oxide Deposition Temperature on Interface Properties of SiC/SiO_2: *Tahir A. Khan*[1]; Mahalingam K. Balasubramanian[1]; T. Paul Chow[1]; [1]Rensselaer Polytechnic Institute

The interface between SiC/SiO_2 is widely researched in SiC MOS devices. Best reported surface field-effect mobilities are far below the bulk mobility of 4H-SiC.[1,2] In this work, we compare 4H-SiC MOS Capacitors, MOSFETs and MOS gated hall bars with SiO_2 deposited at two different temperatures and NO and CO_2 post-oxidation anneal. MOS capacitors were fabricated on n-type 4H-SiC. Samples A and C were deposited with a gate oxide stack of 30 nm thermally grown oxide and 50 nm High-temperature deposited oxide, while sample B and D has 80 nm of low-temperature deposited oxide. Post-oxidation anneal in CO_2 ambient was performed on samples A and B and in NO-ambient on samples C and D. The flatband voltages for sample A, B, C and D were 5, 1.2, 3.5, -5 V respectively. The effective fixed oxide charge (Q_{eff}) was calculated from the flatband shift of the measured samples as compared to the ideal curve. Thus for CO_2 annealing treatment, we see a reduction in Q_{eff} of almost 5 times for the low temperature oxide (-2.27x$10^{11}$$cm^{-2}$) as compared to the high temperature oxide (-1.24x$10^{12}$$cm^{-2}$). While a reversal of polarity is seen for NO annealed samples from -8.4x10^{11} to +1.43x$10^{12}$$cm^{-2}$. Thus, lowering deposition temperature leads to a negative shift of the C-V curve which is indicative of a better interface. The difference in flatband voltage of the NO and CO_2 anneal for the same oxide is also indicative of the positive fixed oxide charge (Q_f) induced by NO-anneal. MOSFETs and MOS-gated Hall bars were fabricated on p-type 4H-SiC using the same gate level processing as MOS capacitors. The highest field-effect mobility (45 cm^2/V-s) was exhibited by the sample with low temperature oxide and NO anneal. The same process had yielded the most negative flatband voltage, indicating a low concentration of Q_{it} and high concentration of Q_f. The field effect mobility measured for other samples was 6.5, 17 and 24.5 cm^2/V-s for samples A, B and C respectively. The inversion carrier mobility from Hall measurement on MOS-gated Hall bars varied from 45-60 cm^2/V-s and sheet carrier concentration (N_{eff}) was found to be higher by 50% for the low temperature oxide for both annealing ambients. For the low temperature oxide, NO anneal showed 5 times higher N_{eff} as compared to CO_2 anneal as a result of much higher Q_f. In summary, a better interface was reflected in a higher sheet carrier concentration and ultimately in a higher field-effect mobility utilizing low temperature oxide deposition. [1]Mahalingam K B, et-al, "Performance Comparison of 4H-SiC MOSFETs with Various Gate Oxide Processes", Electronic Materials Conference 2005. [2]H O Olafsson et-al, "High field effect mobility in Si face 4H-SiC MOSFET transistors",

Electronics Letters, Vol. 40, No. 8, 2004.

11:40 AM
S10, Late News

Session T: Materials and Processing for Organic Transistors

Thursday AM
June 29, 2006

Room: Conference Room 207
Location: Pennsylvania State University

Session Chairs: Alberto Salleo, Stanford University; Jon Nichols, 3M Center

8:20 AM Invited
T1, Solution-Processable Organic Conductors and Semiconductors: Viable Materials for Thin Film Electronics: *Lynn Loo*[1]; [1]University of Texas

Large-area displays based on organic materials promise low-cost fabrication, lightweight construction, mechanical flexibility and durability. To truly realize the low-cost aspects of organic electronics, however, conventional high-vacuum deposition technologies will have to be replaced by solution processing methodologies. This need has in turn driven the development of solution-processable organic semiconductors and conductors. We have focused on fabricating thin-film transistors with triethynylsilyl antradithiophene (TES ADT), a solution-processable p-type organic semiconductor. Subjecting the as-cast thin films of TES ADT to short solvent vapor annealing dramatically increases the device characteristics: we observe three orders of magnitude increase in carrier mobility and current on/off ratio, and a decrease in current hysteresis and threshold voltage. The improvement in the electrical characteristics can be directly correlated with morphological transformations during solvent vapor annealing. Our efforts in solution-processable organic conductors focus on water-dispersible polyaniline (PANI). We have fabricated bottom-contact thin-film transistors with PANI electrodes, which function as effectively as gold electrodes, when on-characteristics are concerned. Examination of the linear source-drain voltage regime suggests that PANI devices exhibit markedly less contact resistance than gold devices.

9:00 AM
T2, Acene-Based Materials for Thin-Film Transistors: *John E. Anthony*[1]; [1]University of Kentucky

The use of organic semiconductors in electronic devices holds the promise of low-cost, flexible displays, sensors and solar cells. In particular, the ability to use low-cost solution deposition methods will accelerate the adoption of organic materials in high-throughput processes. Pentacene has long reigned as the benchmark material in many organic electronic devices. However, pentacene suffers drawbacks such as poor solubility and issues with photodimerization. This talk will focus on our functionalization-based strategy to improve the solubility and stability of pentacene, an approach which also allows the manipulation of the solid-state order of the aromatic portions of the molecules. We have found that 2-dimensional electronic interactions (whether due to face-to-face or edge-to-face close contacts) are critical for the formation of useful devices, and that recent advances in the ability to synthesize high-purity materials has led to transistors with excellent performance. Newer materials have been prepared to address substrate wetting issues, electrode interface (HOMO energy level tuning) and film flexibility. Recent work with larger acenes (hexacene, heptacene) have led us to further investigate aspects of acene stability, and we have found a strong correlation between both the nature and position of functional groups on the acene backbone, and the stability of the resulting functionalized materials. Our latest findings on the stabilization of heptacene in particular will also be presented.

9:20 AM Student
T3, Pentacene Devices Fabricated by Organic Vapor Phase Deposition: *Cédric Rolin*[1]; Soeren Steudel[1]; Kris Myny[1]; David Cheyns[1]; Stijn Verlaak[1]; Jan Genoe[1]; Paul Heremans[1]; [1]IMEC

Thin films of small molecular weight organic semiconductors are typically grown by organic molecular beam deposition (OMBD), permitting a high degree of purity and good structural control. However the use of a high-vacuum process is more complex for large area substrates and reduces the throughput. On the other hand, the organic vapor phase deposition (OVPD) has been demonstrated to be an efficient and versatile technique for the growth of such thin films. The OVPD process is based on the sublimation of the small molecular weight organic material into an inert carrier gas stream in a hot-walled chamber. The gas transports the molecules to a cooled substrate where they rapidly condense to form the film. In OVPD, the functions of evaporation and condensation are spatially separated. This leads to precise control over the deposition process since the flux of impinging molecules is determined both by the sublimation temperature and by the carrier gas flow. It has been shown that OVPD improves control over doping, and is adaptable to rapid, efficient and uniform deposition of organics over large-area substrates. But the main advantage of OVPD lies in its non-vacuum character: it provides access to a larger choice of molecules with higher vapor pressures, and, overall, it allows much higher throughputs. Hence, OVPD is a low-cost process for organic thin film device preparation and it is well suited for industrial applications. The OVPD system used in this work is equipped with a showerhead that spreads the loaded carrier gas over a 2-inch diameter cooled susceptor. It appears that the system behavior and performances are strongly dependant on its architecture and geometrical characteristics. From experimental results and flow dynamics simulations, we derived a set of equations that assess our quantitative understanding of the film growth in the system. They relate the flux of impinging molecules to the different deposition parameters such as gas flow, sublimation temperature and chamber pressure.From this work, the OVPD technique has been optimized for the growth of pentacene thin films. The link between deposition conditions, thin film morphology and electrical characteristics is established with the help of imaging techniques and electrical measurements. Several devices have been fabricated (transistors, inverters, oscillators) using different substrate pretreatments (silanes and thiols, a–methyl-polystyrene) and transistor architectures (top contact, bottom contact). Besides high thin film mobilities (up to 1.35 cm^2/Vs), transistor characteristics are well behaved: The VON and VT close to 0 V in combination with a steep <0.2 V/dec subthreshold slope indicate a high purity and low trap density. These pentacene thin films deposited at pressures around 1 torr advantageously compare with the equivalent devices fabricated using OMBD.

9:40 AM Student
T4, Molecular Ordering of Solution Processed TIPS-Pentacene: *Sungkyu Park*[1]; Thomas N. Jackson[1]; John E. Anthony[2]; [1]Pennsylvania State University; [2]University of Kentucky

Most high-performance organic thin film transistors (OTFTs) reported to date have used vacuum deposited active layers, but solution-processed devices are also of interest because of their potential for low-cost manufacturing such as printed electronics and roll-to-roll processing. Most solution processed OTFTs have used polymeric organic semiconductors with relatively low mobility (typically < 0.1 cm^2/V-s) compared to vacuum deposited devices. In this work we have studied the small molecule organic semiconductor 6,13-bis(triisopropylsilylethynyl) pentacene (TIPS-pentacene). TIPS-pentacene is a functionalized pentacene with bulky organic groups added at the 6 and 13 positions of the pentacene molecule[1]. This modification provides good solubility in a range of organic solvents. TIPS-pentacene thin films deposited by drop casting from high boiling point solvents such as dichlorobenzene (b.p. 174°C), mestylene (b.p. 165°C), chlorobenzene (b.p. 138°C), and toluene (b.p. 111°C) typically have regions with good molecular ordering including molecular terraces and strong x-ray diffraction peaks. Films deposited by drop casting from lower boiling point solvents such as dichloroethane (b.p. 84°C), tetrahydrafuran (b.p. 66°C), and dichloromethane (b.p. 40°C) poor molecular ordering and less uniform thin films. Film ordering also depends on deposition technique, with spin cast and dip cast films typically less well ordered than drop cast. Using drop cast films we have fabricated bottom contact OTFTs. Self-assembled monolayers of pentafluorobenzenethiol (PFBT) and hexamethyldisilazane (HMDS) were formed on the Au source/drain electrodes and gate dielectric, respectively to modify film wetting. The active TIPS-pentacene layer was deposited from 0.5 ~ 1 wt% solutions in

several solvents. Best results were obtained form toluene and chlorobenzene with best OTFT mobility > 1.5 cm^2/V-s.

10:00 AM Break

10:20 AM Student

T5, Zinc Tetrabenzoporphyrin Organic Field-Effect Transistors: *Patrick Shea*[1]; Jerzy Kanicki[1]; Hiroko Yamada[2]; Noboru Ono[2]; [1]University of Michigan; [2]Ehime University

Zinc Tetrabenzoporphyrin (ZnTBP) is demonstrated for the first time in solution-processable organic field-effect transistors (OFETs). Precursor solutions produce polycrystalline thin-films after thermal annealing, with OFETs demonstrating field-effect mobilities exceeding 0.01 cm^2/V-s. Optical absorbance and transistor performance are discussed.

10:40 AM Student

T6, Modeling and Experiments of Organic Material Patterning by Stamping in the Fabrication of Organic Electronic Devices: *Yifang Cao*[1]; Changsoon Kim[1]; Stephen R. Forrest[1]; Winston O. Soboyejo[1]; [1]Princeton University

We present the results of computational, analytical, and experimental study of the van der Waals bonding assisted stamping process on patterned substrates used in the patterning of metal contacts on organic electronic devices. The mechanical properties of vacuum deposited, small molecular weight organic semiconductor thin films were determined using nanoindentation techniques. The measured mechanical properties were then incorporated into computational and analytical mechanics models to determine the effects of processingparameters (such as stamp modulus and thicknesses of different layers) on the ultimate pattern resolution achievable using the pressure contact (stamping) patterning technique. Experimental and computational results were found to be in good agreement. Further, a simple mechanics model combined with finite element numerical simulations, was found to successfully describe different organic material transfer modes during the stamping process over a substrate with step edges. Guided by insights provided by this model, we were able to completely transfer an organic thin film from a stamp to a patterned substrate, thereby making an array of organic light- emitting devices.

11:00 AM Student

T7, Pentacene OTFTs with Parylene Active Layer Patterning and Passivation: Lisong Zhou[1]; *Dalong Zhao*[1]; Thomas N. Jackson[1]; [1]Pennsylvania State University

Organic thin film transistors (OTFTs) are of interest for flat panel displays and other large-area electronic applications. Recently, an active matrix OLED display was demonstrated using pentacene OTFTs, with photosensitized polyvinyl alcohol (PVA) and parylene-C used to pattern and passivate the backplane[1]. However, water trapped in the PVA layer is still a threat to the OLED pixel even with the low-permeability parylene-C cover layer. As an alternative to photosensitized PVA, we have used parylene C or parylene N as a barrier layer to allow pentacene patterning with conventional photolithography. In this approach, the parylene is used to isolate the pentacene layer from the photolithography solvents that would otherwise degrade the organic semiconductor film[2]. To demonstrate the utility of parylene passivation and photo-patterning, we have fabricated patterned active layer pentacene OTFTs, including both top contact and bottom contact structures. For these test devices, heavily doped, thermally oxidized silicon was used as the substrate, gate electrode, and gate dielectric. For bottom contact OTFTs, platinum source and drain contacts were deposited by ion beam sputtering and photolithographically defined using a lift-off process, and a pentacene thin film was deposited on top of the contacts by thermal evaporation. For top contact OTFTs, evaporated gold source and drain electrodes were deposited onto a pentacene thin film. After device fabrication, 1 μm of parylene N or parylene C was deposited by vapor deposition at room temperature. For top contact devices, an ~40% mobility degradation was observed for parylene C and only small changes in mobility was observed for parylene N. For bottom contact TFTs, both parylene N and parylene C degraded the OTFTs by about 50%. Using a buffer layer of, for example, perylene, between the pentacene and parylene layers for bottom contact devices substantially reduces the mobility degradation. After parylene film deposition, conventional solvent-based photolithography was used to form photoresist structures on top of the parylene layer and the parylene and pentacene in the field area was removed by oxygen plasma dry etching. An ~10% additional degradation in mobility was observed after plasma patterning. These results demonstrate that parylene can be a useful material for OTFT patterning. [1]L. Zhou, A. Wanga, S. Wu, J. Sun, S. Park, and T. N. Jackson, "All-Organic Active Matrix OLED Flexible Display," Appl. Phys. Lett., 88, 2006.[2]D. J. Gundlach, T. N. Jackson, D. G. Schlom, and S. F. Nelson, "Solvent-induced phase transition in thermally evaporated pentacene films," Appl Phys Lett 74(22), 3302-3304, 1999.

11:20 AM

T8, All Organic Non-Volatile Switching Device Fabricated by Using Conducting Polymer Micropores: *Oleg Kirillov*[1]; John S. Suehle[1]; Lauren Cohen[2]; Wendy Wu[3]; Dean M. DeLongchamp[1]; Curt A. Richter[1]; [1]National Institute of Standards and Technology; [2]Duke University; [3]University of Texas at Austin

The use of organic polymers as materials for electronic devices has been gaining intense interest for applications such as flexible displays, smart cards, and RF ID tags. A fundamental element of any electronic system is memory. Non-volatile memory architectures such as FLASH and EEPROM have been staples in the Si microelectronics industry for several decades. All organic electronic systems will require a similar memory device to facilitate the same functionality and utility as their Si counterparts. We report an all organic bistable switching device that incorporates only a thin film of poly (3,4-ethylenedioxythiophene) with ploy(styrene sulfonic acid) (PEDOT: PSS) deposited in an insulating polymer micropore. Devices were fabricated by first evaporating 5nm of Cr followed by 100nm of Au on an oxidized Si wafer. An array of vias or pores were patterned using standard contact photolithography using photo resist or E-beam lithography using PMMA. The patterned resist also served as an organic insulating layer to isolate adjacent devices. An aqueous solution of PEDOT:PSS was spun on the wafer surface yielding a film thickness of 70 nm uniformly over the wafer. Au was thermally evaporated to make a top or gate electrode over the top of the via by using a shadow mask. Device areas ranged from .01 μm^2 to 10^4 μm^2. When electrons are injected from the gate of the device a region of negative differential resistance is observed between 0.8 and 1.4 V and hysteresis is observed as the voltage is swept back to 0 V. This behavior is not observed when electrons are injected from the substrate. Quasi-dc ramp measurements (5×10^{-5} V/s) were used to identify two conductive states that can be set by applying specific voltages across the pore. It was noted that if the voltage was allowed to go below 0.6 V during the reversed scan, the device was switched to a "high" conducting state and the device was switched to a low conducting state if the applied voltage exceeded 1.4 V. The differences between the two logic states is approximately a 10:1 change in gate current. A possible mechanism for the operation of the device is that following the reduction of the PDOT by the injection of electrons at an applied substrate potential between 1.0 - 1.4 V, the negatively charged PSS must be compensated with a positively charged ion. A positively charged species such as a proton from the oxidation of captive water (Eox = -1.23 V) in the film could satisfy charge neutrality in the device. A non-volatile electronic memory is demonstrated that exhibits a retention time to be a least several hours in duration. Over 10,000 write/read cycles have been observed.

11:40 AM

T9, Late News

Session U:
Oxide Thin Film Integration II

Thursday AM
June 29, 2006

Room: Conference Room 206
Location: Pennsylvania State University

Session Chairs: Patrick Lenahan, Pennsylvania State University; Michael Lanagan, Pennsylvania State University

8:20 AM

U1, Photocurrent-Voltage Measurements for Characterizing Oxide Charge in HfO_2 Gate Dielectrics: *Daniel Felnhofer*[1]; Evgeni Gousev[1]; Douglas A. Buchanan[2]; [1]Qualcomm MEMS Technologies; [2]University of Manitoba

The use of HfO_2 high-k dielectric for metal-oxide-semiconductor (MOS) devices has garnered much attention due to appropriate band offsets and a relatively high permittivity ($\varepsilon_{HfO2} \sim 25$). Despite these desirable properties, HfO_2 is known to have fixed and trapped charge within the dielectric. Oxide charge trapping and de-trapping within MOS devices is most readily characterized by using capacitance-voltage (C-V) or current-voltage (I-V) techniques. These techniques relate the shift in flatband voltage, ΔV_{FB}, or the shift in threshold voltage, ΔV_t, to the first moment of charge within the insulator. However, these techniques are most sensitive to charge located near the substrate due to the effect such charge has on the electric field within the silicon, and there is no separate determination of the centroid of the oxide charge distribution. To locate the charge centroid within a dielectric, a photocurrent-voltage (photo I-V) technique using internal photoemission can be used. This technique uses photons to excite electrons into the oxide conduction band from the substrate or gate (depending on the applied bias). The voltage shifts in the photocurrent response from both gate and substrate injection are related to the spatial distribution of charge within the oxide. As a result, this technique is sensitive to oxide charge within the bulk of the film. The application of the photo I-V technique to alternative high-k dielectrics provides needed information as to the spatial distribution of defects within gate stacks. For this work, MOS capacitors consisting of a semi-transparent 150Å Al electrode, a 90Å metal-organic chemical vapor deposited HfO_2 dielectric, a ~15Å intermediate SiO_x layer, and a p-type Si substrate were used to demonstrate the applicability of the photo I-V technique for high-k dielectric characterization. The MOS capacitors were stressed with the use of constant applied voltage and illumination (3.4 or 4 eV) until $1x10^{-4}$ C/cm^2 of charge was injected. For gate electron injection (i.e., negative applied bias during stressing), the effective density of trapped oxide charge, N_{eff}, was found to be ~$5x10^{12}$ cm^{-2} using the C-V technique. The calculation of the N_{eff} from the photo I-V shifts resulted in densities of ~$6x10^{12}$ cm^{-2}. The centroid of the oxide charge distribution was also determined to be between 0.19 and 0.24, indicating that a large portion of the trapped charge was located near the Al electrode. These results are indicative that oxide charge trapping at bulk HfO_2 is indeed occurring, and validates the importance of the photo I-V measurement technique for characterizing oxide trapped charge. The determination of the centroid of the oxide charge distribution, which can not be determined from traditional C-V and I-V measurements, is fundamental to understanding the trapping kinetics of HfO_2 dielectrics.

8:40 AM

U2, Internal Photoemission Studies of TaSiN and TaCN Metal Gates on SiO_2 and HfO_2: *Nhan V. Nguyen*[1]; H. Xiong[1]; J. S. Suehle[1]; E. M. Vogel[1]; [1]National Institute of Standards and Technology

As CMOS dimensions are scaled down, the traditional polysilicon gate exhibits problems such as gate depletion and boron penetration. Metal gates have been proposed to replace polysilicon to resolve these issues. One of the critical parameters in selecting an appropriate metal is its work function and the barrier threshold between the metal and the insulator. The latter quantity can be measured accurately using internal photoemission (IPE). In this report, we employed IPE to determine the energy barrier height (ϕ_0) between the Fermi level of TaSiN and TaCN metal gates and the conduction band of SiO_2 and HfO_2 insulators. The devices used in this study consisted of a 40 Å TaN / 40 Å TaSiN or 40 Å TaN / 40 Å TaCN metal deposited on 80 Å SiO_2 or 60 Å HfO_2. Various biases were applied to the metal and the photoelectrons were measured as a function of photon energies of light incident on the metal films. From the Schottky plots, the barrier heights (ϕ_0) at the flatband voltage were extracted. We found that ϕ_0's for TaCN and TaSiN are 3.52 eV and 3.35 eV on SiO_2, respectively. For the HfO_2 insulator, lower barrier heights were determined to be 2.14 eV for TaCN, and 1.93 eV for TaSiN. Consistently, on both insulators, TaCN yields a slightly larger barrier height of about 0.2 eV than that of TaSiN. These results indicate that Fermi-level pinning on HfO2 is not an issue for these metal systems.

9:00 AM Student

U3, Electron Spin Resonance and Spin Dependent Recombination Study of Deep Levels within the near Si/Dielectric Interfacial Layer of HfO2 Based Metal Oxide Silicon Field Effect Transistors: *Jason T. Ryan*[1]; Patrick Lenahan[1]; Jason Campbell[1]; Gennadi Bersuker[2]; Patrick Lysaght[2]; Wilman Tsai[3]; [1]Pennsylvania State University; [2]SEMATECH; [3]Intel

HfO2 based metal oxide silicon field effect transistors exhibit instabilities associated with defects in the HfO2, at the Si/dielectric interface or in the near Si/dielectric interfacial layer. Electron spin resonance (ESR) studies of these systems have primarily concentrated on defects at the Si/dielectric boundary or in the "bulk" of the HfO2. In this study, we combine conventional ESR measurements of simply processed blanket HfO2 dielectrics on silicon with spin dependent recombination (SDR) ESR measurements on fully processed metal gate HfO2 based transistors. Our studies include both devices and blanket samples prepared at several laboratories under a wide range of processing parameters. All measurements were performed on atomic layer deposited (ALD) HfO2 structures in which the ALD took place on very thin layers of SiO2 on silicon. The focus of our study is defects in the near Si/dielectric interfacial layer. In both conventional ESR and SDR we observe a fairly narrow line at g ˜ 2.002. In conventional ESR we observe a second line at g ˜ 2.0005. The observation of the g ˜ 2.002 signals in SDR make it certain that these defects are within a few Angstroms of the Si/dielectric interface, thus within the interfacial transition layer. The zero crossing g values and the line width, as mentioned previously, are clearly consistent with E' like defects. E' defects involve oxygen deficient silicons bonded to oxygen atoms. We find that defect densities associated with these defects is very strongly process dependent. Of particular interest, in conventional ESR measurements we find the strongest E' like signals in the simply processed blanket structures in which the ALD of HfO2 is purposely deprived of oxygen. We also find that the E' signals dominate the SDR spectrum of "high thermal budget" metal gate transistors in which a post deposition anneal of = 1000°C or higher takes place but do not observe such SDR signals in MOSFETs which have not been subjected to such high temperatures. Our results suggest most strongly that the near Si/dielectric interfacial layer is an oxygen deficient, silicon rich oxide. These observations are consistent with the recent conclusions of Bersuker et. al.1 and are also qualitatively consistent with recent statistical mechanics based arguments that high densities of oxygen vacancies are likely to be part of the interfacial layer due to differences in the enthalpy of creation of oxygen vacancies in SiO2 and HfO2.2 These oxygen vacancies are likely to be important reliability limiting defects in HfO2 based devices. [1]G. Bersuker et. al., J. J. Appl. Phys. 43 (11B), 7899-7902 (2004). [2]W. L. Scopel et. al., Appl. Phys. Lett. 84 (9), 1492-1494 (2004).

9:20 AM

U4, Photoemission and Inverse Photoemission Studies of Band Offsets in Alternative High-k Metal Oxide Semiconductor (MOS) Stacks: *Eric Bersch*[1]; Sylvie Rangan[1]; Robert Bartynski[1]; Eric Garfunkel[1]; [1]Rutgers University

The materials and electrical properties of high-k dielectrics and metal electrodes are under intense international scrutiny because of their potential to offer greatly increased performance in CMOS devices. The band offsets, that is, the relative energies of the metal Fermi level and the valence band and conduction band edges of the semiconductor and dielectric, are critical to ensure proper device performance including low leakage currents and appropriate voltage thresholds. An understanding of these relative energies, particularly the role played by the interface dipole, may enable the development of tunable band offsets at the interfaces. Using a novel instrument that combines in the same chamber valence band photoemission,

to determine occupied electronic states, with inverse photoemission, to probe the unoccupied electronic states on an equal footing, we have measured the band offsets between the layers of model hafnium silicate and nitrided hafnium silicate MOS stacks. This has been complemented with synchrotron radiation based photoemission to correlate the evolution of the valence band density of states and core level shifts. Sequential metallization has allowed us to observe the movement of the band edges as a function of metal coverage. For HfxSi1-xO2/Si, we find that the conduction band offset increases only slightly (~0.1 eV) for x=1 to x=0.4, whereas the valence band offset increases proportionally to x between the endpoint values for x=1 and x=0. We have also studied the effect of N incorporation into HfxSi1-xO2, and found nitrided films of 15 Ä thickness to have a larger CBO, a smaller VBO, and an overall smaller bandgap than their unnitrided equivalents. Aluminum and ruthenium were chosen as gate metals because of their prospective use as low and high workfunction metals in dual metal gate CMOS devices. We measured the CBO for the Al and Ru/HfxSi1-xO2 interfaces and found barriers involving Al to be 0.5 eV smaller on average, which is in reasonable agreement with the interface gap state model.

9:40 AM

U5, Growth and Characterization of Epitaxial Sc_2O_3 on Silicon by Molecular Beam Epitaxy for Alternative Gate Dielectric Applications: Lisa Friedman Edge[1]; Wei Tian[1]; Venu Vaithyanathan[1]; *Darrell G. Schlom*[1]; Dmitri Klenov[2]; Susanne Stemmer[2]; Marilyn E. Hawley[3]; [1]Pennsylvania State University; [2]University of California, Santa Barbara; [3]Los Alamos National Laboratory

The continued scaling of SiO_2 in metal-oxide-semiconductor field-effect transistors (MOSFETs) is approaching its fundamental limit and in the next few years will have to be replaced with an alternative gate dielectric if Moore's law is to continue. The higher *K* and low density of dangling bonds that an epitaxial gate dielectric could offer are attractive for future generations of MOSFETs. In this work, we investigate the growth of epitaxial Sc_2O_3 thin films on silicon by molecular beam epitaxy (MBE) directly on silicon. A major challenge in the growth of alternative gate dielectrics on silicon is the formation of excessive SiO_2 at the interface between silicon and the high-*K* gate dielectric. One technique to prevent the formation of SiO_2 is to grow the films in a low temperature / kinetically-limited oxidation regime. We have investigated the oxidation kinetics of Sc from their elemental state to fully oxidized Sc_2O_3 in the presence of oxygen using an *in situ* quartz crystal microbalance (QCM). High-resolution TEM revealed a sharp Sc_2O_3/Si interface with no discernable interfacial layer between the Sc_2O_3 thin film and silicon. Sc_2O_3 thin films grew epitaxially with the following orientation relationship (111) Sc_2O_3//(111)Si and [1-10] Sc_2O_3// [-110] Si (B-type epitaxy). Because of the considerable lattice mismatch (10.3 %), there was a high density of misfit dislocations at the interface between Sc_2O_3 and (111) silicon. The effects of substrate temperature, partial pressure of oxygen, substrate misorientation, and the method used to remove the native oxide were investigated. The films were monitored by RHEED during growth. After growth AFM, four-circle XRD, and high-resolution plan-view and cross-section TEM, including Z-contrast TEM were used to characterize the film structure and microstructure.

10:00 AM Break

10:20 AM

U6, Medium Energy Ion Scattering Study of Oxygen Diffusion-Reactions in High-k Dielectrics on Si: *Lyudmila Goncharova*[1]; Mateus Dalponte[1]; Eric Garfunkel[1]; Torgny Gustafsson[1]; Patrick Lysaght[2]; Brendan Foran[2]; Gennadi Bersuker[2]; [1]Rutgers University; [2]Sematech

Thermodynamics and kinetics of film growth during fabrication of high-k gate stacks is vital in establishing atomic level control of interfacial layers and in defect minimization. Annealing such films in oxygen-containing atmospheres potentially causes oxygen diffusion and reactions with severe consequences on device electrical properties. We have studied oxygen diffusion in, and reactions with, Hf-based dielectric films by high-resolution ion-profiling with isotopic oxygen exchange methods. Faster in-diffusion and exchange rates are observed for pure HfO_2 relative to Hf silicates. Our results indicate that atomic (not molecular) oxygen diffusion (likely via oxygen lattice exchange) is the predominant diffusion mechanism in hafnia, consistent with theoretical calculations. Oxygen exchange and incorporation is suppressed by the addition of silica and nitrogen in the hafnia framework. Compared to the as-deposited film, HfO_2 films crystallized in vacuum show an ^{18}O concentration gradient from the top surface towards the interface with the Si substrate. Both hafnium oxide and silicate films that had been exposed to a crystallization anneal in vacuum to ~800°C, show a lower degree of exchange, compared to as-deposited films with similar compositions. At least part of the suppression of oxygen exchange in Hf silicates can be attributed to SiO_2 surface segregation. The SiO_2 layer that forms at the top surface of the dielectric appears to phase separation from the hafnium silicate, blocking oxygen in-diffusion and decreasing the gas-surface molecular oxygen dissociation rate, perhaps by blocking under-coordinated Hf sites on which oxygen dissociation might otherwise have occurred. Under higher oxidation temperatures interfacial SiO_2 layer growth is apparent. Interesting that presence of nitrogen at the interface slows down, but doesn't stop interfacial layer growth, in particularly oxygen reaction with Si takes place on the Si_3N_4/Si interface with the oxygen profile going deeper into the substrate than nitrogen. Some nitrogen is lost when oxidizing at Tx>800°C, via either NO out diffusion and desorption as occurs in pure SiO_2 or a more complex lattice exchange diffusion process. Metal gate deposition and post-processing can also affect the oxygen stoichiometry and defect density by reducing or oxidizing the dielectric. We used deposition of an oxygen-gettering Ti gate on top of the high-k metal oxide to reduce and possibly to eliminate the SiO_2 interfacial layer. This multilayer diffusion is due to oxygen loss from SiO_2 through the HfO_2 layer, with dissolution of oxygen into the Ti electrode layer. This is accompanied by incorporation of Si atoms that initially constitute interfacial SiO_2 layers into the high-k layer. The mechanism of this process changes with increasing HfO_2 crystallinity, opening more permeable diffusive pathways via crystallite grain boundaries.

10:40 AM Student

U7, Characterization of n-MISFETs with Ultrathin HfO_xN_y Gate Insulator Formed by ECR-Ar/N_2 Plasma Nitridation: *Masaki Satoh*[1]; Tomoki Kurose[1]; Shun-Ichiro Ohmi[1]; [1]Tokyo Institute of Technology

Electron cyclotron resonance (ECR) -Ar/N_2 plasma nitridation of HfO_2 thin films was investigated for ultrathin HfO_xN_y gate insulator formations. HfO_xN_y thin films formed by the ECR-Ar/N_2 plasma nitridation (power: 500W, flow late: Ar/N_2 = 20/10 sccm, time: 60 s) of 1.0-nm-thick HfO_2 films (power: 500W, flow late: Ar/O_2 = 20/4 sccm) deposited on chemically oxidized Si (100) substrates were found to be effective for suppressing the interfacial layer formation during post deposition annealing (PDA) in N_2 ambient. After the 1000°C PDA for 60 s, it was found that the peak intensity of X-ray photoelectron spectra for N-N bonds and Hf-N bonds were decreased ,while Si-O bonds and Si-N bonds were increased. Therefore, HfO_xN_y films were considered to react with Si at the interface, and HfSiON interfacial layer, which have relatively high dielectric constant, was formed. A 0.7-nm-thick interfacial layer and a 2.5-nm-thick HfO_xN_y layer were observed from the cross-sectional transmission electron microscope (TEM) image for the HfO_xN_y film. The HfO_xN_y showed an EOT of 1.5 nm and a leakage current density of 1.8 x 10^{-1} A/cm^2 (at V_{FB}-1 V). Assuming that the interfacial layer as SiO_2 with the relative dielectric constant (ε_r) of 3.9, ε_r of HfO_xN_y layer was estimated to be 14. Furthermore, an EOT of 1.2 nm with a leakage current density of 5.5 x 10^{-2} A/cm^2 (at V_{FB}-1 V) was achieved by the ECR-Ar/N_2 plasma nitridation (30 s) of 0.5-nm-thick HfO_2 films followed by 1000°C PDA for 60 s. From the cross sectional TEM image for the HfO_xN_y film, the thickness of interfacial layer seemed to be retained (0.7 nm), while only the top HfO_xN_y layer was found to be thinned (1.7 nm). In this case, ε_r of the HfO_xN_y film was estimated to 16. Al gate n-channel MISFETs with these HfO_xN_y gate insulators were fabricated and their device characteristics were observed. The fabrication process was as follows. First, active area formations followed by source and drain ion implantations were carried out. Then, the HfO_xN_y gate insulators were formed followed by the Al gate electrode deposition. Finally, source and drain contact formations and Al electrode deposition were carried out. The fabricated devices showed a mobility of 240 cm^2/Vs for the MISFET with an EOT of 1.5-nm-thick gate insulator, while it was found that the mobility was degraded to 180 cm^2/Vs in case of the device with an EOT of 1.2 nm. This is probably caused by increasing of nitrogen concentration at the interface region for thinner HfO_2 layer under the same nitridation condition.

11:00 AM
U8, Late News

11:20 AM
U9, Late News

11:40 AM
U10, Late News

Session V: Non-Destructive Testing and In-Situ Monitoring and Control

Thursday AM
June 29, 2006

Room: Conference Room 108
Location: Pennsylvania State University

Session Chairs: Andrew M. Hoff, University of South Florida; Kurt G. Eyink, Air Force Research Laboratory

8:20 AM Student
V1, Surface Plasmon Resonance of Ga and In Nanoparticles Measured by *In-Situ* Spectroscopic Ellipsometry: *Pae C. Wu*[1]; Maria Losurdo[2]; Tong-Ho Kim[1]; Soojeong Choi[1]; Henry O. Everitt[1]; Jianhua Jiang[3]; April S. Brown[1]; [1]Duke University; [2]Institute of Inorganic Methodologies and of Plasmas — CNR; [3]University of Alabama, Huntsville

Coupling surface plasmon resonant structures with photonic devices can enhance emission or photon lifetime. Although Oates, *et al* recently examined the surface plasmon resonance (SPR) evolution of Ag nanoparticles via *in-situ* spectroscopic ellipsometry (SE) measurements (Nanotechnology, 16 (2005) 2606) the technique has not been widely exploited for SPR studies. Real time *in-situ* SE allows the user to monitor the metal deposition and surface plasmon resonance evolution during deposition, allowing the grower to tune the resultant nanoparticle resonance without the need for careful control of deposition conditions. Traditionally, noble metals such as Ag and Au have been studied for their surface plasmon resonant behavior. We deposited both Ga and In nanoparticles at room temperature on sapphire, SiC, and GaN substrates in a GEN-II PAMBE system equipped with an *in-situ* spectroscopic ellipsometer with a photon energy range of 1.5 to 6.5eV. The imaginary part of the pseudodielectric function (ε_i) describes the absorption of the effective medium comprised of the metal nanoparticles, the substrate and surrounding dielectric environment. SE spectra were collected during deposition and the resultant pseudodielectric spectra exhibit strong peaks which redshift with increasing deposition time. Ga nanoparticles were deposited on sapphire at varying deposition times and AFM images reveal increasing particle diameter concomitant with a red-shift of the absorption peaks. FFT image analysis of AFM data shows Ga nanoparticles of random size and distribution, which suggests the SPR peak does not originate from coherent scattering due to ordered nanoparticles. We therefore believe the strong energy dependent absorption peak present in the pseudodielectric function to be the result of incident light coupling to the surface plasmon modes of the Ga and In nanoparticles. Our work is the first demonstration, to the best of our knowledge, of the surface plasmon resonance of Ga nanoparticles. Early data for In nanoparticles grown on C-face and Si-face 4H-SiC substrates exhibit different SPR peaks for the two polarities. We observed a SPR peak shift for Ga samples that were removed from the UHV growth chamber and returned for later measurement, which may be related to oxidation effects. Annealing Ga nanoparticles at 100°C for 20 minutes redshifts the SPR for a medium deposition time sample, however AFM data shows no discernable nanoparticle size or shape change due to the anneal. Preliminary modeling of SE data points to an Al rich layer at the Ga/sapphire interface, which may contribute to the SPR redshift after annealing. The presence of a tunable Ga or In surface plasmon resonance lends itself to future work coupling GaN-based photonic devices with Ga or In nanoparticles in an all-MBE grown device.

8:40 AM Student
V2, Kinetics of Ga Adlayer Formation on Gallium Nitride (0001) Surface: *Soojeong Choi*[1]; Tong-Ho Kim[1]; Henry O. Everitt[1]; April S. Brown[1]; Maria Losurdo[2]; Giovanni Bruno[2]; Akihiro Moto[3]; [1]Duke University; [2]IMIP-CNR; [3]Innovation Core SEI, Inc

Spectroscopic ellipsometry (SE) installed on a GEN-II PAMBE machine has been shown to be an effective *in-situ real time* tool for monitoring the kinetics of gallium adlayer adsorption/desorption on the GaN(0001) surface. The deposition of Ga on a GaN template at "standard" growth temperatures of 680°C-750°C is a good imitation of the quasi-equilibrium surface state during GaN growth under Ga-rich growth conditions. The excess Ga amount on the GaN surface is known to determine the growth mode and, consequently, affects film characteristics; therefore, monitoring the kinetic of excess Ga is critical for understanding the growth mechanism, and the surface competition of Ga with other metallic component such as Al and/or In during ternary material growth, or with n- and p- type dopants. Because Ga exhibits typical metallic behavior, the Ga adlayer is very absorbent for all SE photon energies in the range 1.5eV-6.5eV. The pseudodielectric function, i.e. the optical response of the Ga-adlayer/GaN-template is sensitive to the thickness of metallic adlayer, if the thickness of adlayer is much less than the penetration depth of light. In particular, for the Ga/GaN system, the imaginary part of the pseudodielectric function has a linear relationship with adlayer thickness for thicknesses <20Å; therefore, the SE kinetic acquisition during and after Ga deposition is well suitable for direct monitoring of the adsorption/desorption of Ga atoms. In this work, we present data on the study of the Ga adsorption/desorption from a GaN(0001) template for Ga fluxes in the range 9.63E-8~1.86E^{-7} Torr, for Ga pulses in the range 5~180s and for substrate temperatures in the range 680~750°C. We observe that the Ga adlayer thickness is determined by the balance between deposition and desorption rates for low impinging flux; however, the thickness does not increase beyond a critical thickness even under higher Ga flux or long deposition time. The critical thickness of the adlayer is obtained quantitatively through a fit analysis of the spectrum measured during Ga deposition to be ~4.9Å, close to the theoretically predicted stable adlayer thickness of 2.5ML. From the decay curve of kinetic data, we obtain activation energy of 2.8eV for both the top and bottom monolayer, which is close to the activation energy of liquid Ga desorption. We also observe a desorption time delay for high Ga-fluxes and long Ga pulses. The time delay is correlated to the Ga deposition time excluding the time to form the wetting layer. This indicates the existence, in addition to the wetting layer, of a Ga reservoir, which compensates the wetting layer desorption and maintains the wetting layer thickness until it is totally depleted. A new chemical model and kinetic equation able to fit all the adsorption/desorption profiles will be presented.

9:00 AM Student
V3, Spectroscopic Ellipsometric Characterization of Metal-Free Carbon Nanotube Formation by SiC Surface Decomposition: *Jeremy Harrison*[1]; Senthil N. Sambandam[1]; John Boeckl[2]; William C. Mitchel[2]; Warren E. Collins[1]; Weijie Lu[1]; [1]Fisk University; [2]Air Force Research Laboratory

Conventional techniques for synthesizing carbon nanotubes (CNTs) involve metal catalysts which embed into the nanotubes and result in undesirable characteristics for practical applications. Development of processes to produce metal free nanotubes has been necessary and interesting. It is known that surface decomposition of SiC at high temperature and low oxygen pressure yields CNTs, which are metal-free, well-aligned, and with low structural defects. SiC is oxidized to SiO and C by residual oxygen at high temperatures. However, the mechanism of metal-free CNT growth and role of residual oxygen is unclear. In this study, CNT formations on SiC samples are investigated under vacuum from 1e-3 Torr to 1e-7 Torr and in the temperature range from 1400°C to 1700°C. The decomposed surfaces were analyzed using ex-situ spectroscopic ellipsometry technique. The spectra were analyzed by simulating the optical properties of the CNT layers on SiC based on a three layer stacking model using Bruggmann's effective medium approximation. The results demonstrate the formation of a dense layer of CNTs with a thin layer of amorphous carbon on top. The correlation of the CNT length and residual oxygen pressure has demonstrated that the CNT growth rate increases with increasing oxygen pressure and SiC is decomposed by oxidation. The growth rates observed in this study are consistent with transmission electron microscopic analysis. These results are shown to be useful in understanding the growth processes of metal free carbon nanotubes on SiC.

9:20 AM

V4, Reduced Interference Photoreflectance for Measurement of HBTs: *Eric Rehder*[1]; Peter Rice[1]; [1]Kopin Corporation

Photoreflectance (PR) is routinely used to measure optical critical points, ordering of InGaP alloys, and electric fields within devices. Its ability to measure electric fields is particularly useful in the non-destructive measurement of device structures. Production heterojunction bipolar transistors (HBTs) utilize a rough InGaAs contact layer to reduce emitter contact resistance. This rough layer strongly scatters light, which interferes with the PR measurement. Additionally, strong photoluminescence from the sample can greatly obscure the PR measurement. We have found a measurement configuration that overcomes these complications. PR measurements involve two light sources. A chopped pump laser is used to generate electron-hole pairs, which perturb electric fields in the material. The reflectivity of a probe beam is measured and the PR signal is the component collected at the chopping frequency of the pump laser. Generally these beams need to be overlapping resulting in the detection system collecting the photoluminescence and scattered light from the pump laser. Here we show that the beams can be separated for device structures incorporating PN junctions. This simple configuration physically separates the photoluminescence and light scattering from the position of the sample being probed. Separating the beams by a few millimeters is able to remove these interfering signals and recover a clear PR signal. This PR signal is maintained as the pump beam and probe are separated by tens of millimeters. A 100 mm HBT wafer was measured with the probe beam in the center and multiple measurements taken as the pump beam was moved towards the edge of the wafer. The amplitude of the PR signal decreases as the beams are separated. The results are similar to reducing the intensity of the pump laser. For comparison a sample without a PN junction was measured. This sample consisted of a GaAs wafer with a 500 nm film of n+ GaAs capped with 200 nm film of undoped GaAs. This sample exhibits a PR signal with the beams overlapped but when the beams are separated the signal vanishes. This data shows that the pump and probe beams can be separated in the PR measurement of an HBT wafer. This is not the case for structures in general. Structures without a PN junction have short carrier lifetimes and the beams must be overlapping to produce a changing electric field in the material to result in a PR signal. The PN junction of the HBT separates the carriers producing long lifetimes and allows the pump and probe beams to be widely separated. This configuration is shown to be critical for the rapid, non-destructive measurement of HBT product wafers. Similar results could be attained on device structures, which separate the photoexcited carriers such as emitters, detectors, and solar cells.

9:40 AM Student

V5, AlGaAs/GaAs Interface States by Surface Photovoltage Studies: *Clara Vargas*[1]; Gregory B. Lush[1]; [1]University of Texas at El Paso

A Kelvin probe was used to perform surface photovoltage (SPV) measurements on AlGaAs/GaAs double heterostructures (DHs) of varying doping in order to determine the energy levels of the interface electronic states and how they change with doping concentration. AlGaAs/GaAs double DHs have long been used to study device and interface properties because they are easy to build and to analyze. GaAs is of course an important semiconductor in opto-electronic applications. Knowledge of interface state energies and concentrations are very important for modeling of devices formed with AlGaAs/GaAs interfaces. This study is an attempt to evaluate the potential of the Kelvin proble as a tool for studying such interfaces. We have performed SPV studies on 0.25 micron DHs with electron concentrations from 1.3e17 to 3.8e18 per cc. The AlGaAs layers that sandwich the GaAs layers are doped to 2.0e18 per cc. The Kelvin probe is a vibrating electrode that is held over a conductive sample in order to study the surface potential. The vibration changes the distance between the probe and the surface thus changing the capacitance, causing a displacement current through the device. The potential applied to the probe is then changed to match the surface potential so that the displacement current is minimized. By shining light of varying photon energies on a semiconductor sample, the changes in surface potential due to electron and/or hole generation can be observed—this is called surface photovoltage (SPV). Band-to-band photogeneration can be observed as it changes surface potential, but excitation from interface and bulk traps can also be observed. Our SPV curves from 0.25 micron DHs showed interface states at energies 0.35, 0.46, and 0.7 eV below the conduction band and other structures we still need to study. The figures attached in the extended abstract show the SPV curves for each of the samples and the SPV and slope of SPV for one sample. Where the slopes peak is where the energy levels of the interface states are located. These samples have been studied previously using time-resolved photoluminescence to determine the bulk lifetimes and the interface recombination velocities. We wish to compare those results to the SPV results. Further studies will be performed on thicker samples in which bulk properties should be dominant. We have a matrix of 25 DHs with five DH thicknesses from 0.25 micron to 10 microns for each of five doping concentrations.

10:00 AM Break

10:20 AM

V6, Quantification of Ultra-Thin Indium MBE Layers by Low Energy X-Ray Emission Spectroscopy (LEXES): *Kurt G. Eyink*[1]; Jeremey J. Pitz[1]; David H. Tomich[1]; John A. Carlin[2]; Krishnamurthy Mahalingam[3]; Howard E. Smith[4]; C. A. Hitzman[5]; C. A. Evans[5]; [1]Air Force Research Laboratory; [2]Ohio State University; [3]Universal Technology Corporation; [4]University of Dayton; [5]Full Wafer Analysis Inc

The accurate and precise thickness measurement of ultra-thin layers grown by Molecular Beam Epitaxy (MBE) under conditions of variable and non-unity sticking is a critical technological problem. When deposition rate depends critically on the growth conditions, standard flux rate calculations are inadequate for describing deposition rate. In this work, MBE is used to produce strain-relaxed ultra-thin surface films of InAs of thicknesses from one to five monolayers. This is accomplished by simultaneously depositing In and As onto GaAs(001) for various durations under metal rich conditions, using an In beam equivalent pressure of 3x10-8 torr. Conventional ex-situ thickness measurement techniques of the InAs layer thus formed are inadequate: Energy-Dispersive X-ray analysis (EDXA) has a very large sampling volume and a concomitantly-reduced signal; X-Ray Reflectivity (XRR) was found to have inadequate sensitivity due to additional structure in the scan. Because Low Energy X-Ray Emission (LEXES) provides rapid quantitative, standard-less, high precision quantitative analysis of near surface elemental composition, its utility for addressing this problem was evaluated. LEXES, which employs an energetic electron beam to excite X-rays characteristic of the elements from the near-surface region followed by X-Ray analysis with a Wavelength Dispersive Spectrometer (WDS), was used for the quantification of InAs layers grown under both normal and non-unity sticking coefficient conditions. Comparing with TEM cross-sectional measurements, LEXES was found to be highly accurate with thickness sensitivity to the order of 1%, thus revealing a constant deposition rate. These measurements confirmed that the deposition rate was affected by non-unity sticking coefficient. This demonstrates the utility of LEXES for the general-case problem of ultra-thin layer deposition measurement, esp. compared with the destructive, labor-intensive, and time-consuming TEM method.

10:40 AM Student

V7, In-Situ Investigation of Surface Stoichiometry during $YMnO_3$, InGaN and GaN Growth by Plasma-Assisted Molecular Beam Epitaxy Using RHEED-TRAXS: *Randy P. Tompkins*[1]; Eric D. Schires[1]; Kyoungnae Lee[1]; Yewhee Chye[1]; David Lederman[1]; Thomas H. Myers[1]; [1]West Virginia University

Reflection high-energy electron diffraction total-reflection-angle x-ray spectroscopy (RHEED-TRAXS) can use high-energy electrons from the RHEED electron gun in an MBE growth system to excite x-ray fluorescence. Since the RHEED electrons just penetrate the surface, and by using a geometry that measures x-rays at the total reflection angle, RHEED-TRAXS probes the top 20 to 30 Å of material. Monitoring characteristic x-rays of selected elements using a silicon-based solid state x-ray detector (XR-100CR, Amptek) and a multi-channel analyzer (PX4 MCA, Amptek) configuration thus allows study of surface coverage of materials. Surface coverage of Ga and In during growth of GaN and InGaN was probed using this technique. Studies of the evolution of the surface layer of Ga on GaN during growth at substrate temperatures between 700°C and 750°C will be reported. RHEED-TRAXS measurements were performed during growth of InGaN by measuring the ratio of the In Lα to Ga Kα intensity. A significant surface coverage of In was observed at all temperatures investigated regardless of actual In incorporation. RHEED-TRAXS was also used to investigate surface

segregation of Mg in GaN, indicating near monolayer coverage. This is useful for studies of the suppression of surface segregation of Mg for p-type doping of GaN, as well as determining a critical Mg surface coverage for polarity inversion. A second RHEED-TRAXS assembly was constructed for use in an oxide MBE chamber at WVU. Preliminary oxide work was performed using the initial RHEED-TRAXS setup, including measurement of monolayer thick layers and determination of the critical angle of Y Lα and Mn Lα x-rays. RHEED-TRAXS measurements performed during growth of $YMnO_3$ will be discussed. Because RHEED-TRAXS has near monolayer sensitivity, it is a useful tool for determination of conditions for stoichiometric layer-by-layer growth of $YMnO_3$. This work was supported by AFOSR MURI Grant F49620-03-1-0330. *R.P. Tompkins was supported in part by a grant from the West Virginia Graduate Student Fellowships in Science, Technology, Engineering and Math (STEM) program.*

11:00 AM

V8, Composition Driven Surface Transition and Electronic Transport in $LaSrMnO_3$: *Maitri P. Warusawithana*[1]; Xiaofang Zhai[2]; Seongshik Oh[3]; Darrell G. Schlom[4]; James N. Eckstein[2]; [1]Department of Physics, University of Illinois at Urbana-Champaign; Department of Materials Science and Engineering, Pennsylvania State University; [2]Department of Physics, University of Illinois at Urbana-Champaign; [3]Department of Physics, University of Illinois at Urbana-Champaign; National Institute of Standards and Technology, Boulder; [4]Department of Materials Science and Engineering, Pennsylvania State University

Mixed-valent manganite oxides have been a focus of rigorous research due to the variety of different collective phenomena they exhibit as a function of doping. In this work we study $La_{1-x}Sr_xMnO_3$, specifically with doping, x around one third. In this doping range the ground state is ferromagnetic and exhibits a very high degree of spin polarization. The films are grown using ozone-assisted molecular-beam epitaxy, while not rotating the sample during growth. As a result of the geometry of the elemental sources a combinatorial composition spread is incorporated into the films. To discuss this further we write the chemical formula as $(La_{1-x}Sr_x)_yMnO_3$, where y is the ratio of [La]+[Sr] to [Mn]. We observe a surface transition which occurs due to a very slight change in y (less than 0.002) around y=1.000 which gives rise to 2 distinct surface morphologies. For the y>1 region atomic force microscopy images show atomically flat surfaces with unit cell terrace steps, while in the y<1 region the surface shows grains with a few Angstrom rms roughness. This sharp surface morphology transition is coupled to a collective ordering at the surface that can be observed using *in situ* reflection high energy electron diffraction (RHEED) during the growth of the film. Using RHEED feedback the boundary between the two regions can be placed somewhere in the center of the wafer. This provides a unique method of reproducibly obtaining unprecedented accuracy over the [La]+[Sr] to [Mn] ratio and enables to probe the effect of slight composition imbalances on physical properties. In this talk I will discuss the consequences of this composition spread on electronic transport and magnetic order under the formalism of the double exchange interaction.

11:20 AM Student

V9, Structural Transformations Underlying the Refractive Index Contrast for Optical Waveguides in He-Implanted Single Crystal PZN-PT: N. Tangtrakarn[1]; J. Dziedzac[1]; S. Hackney[1]; *Peter D. Moran*[1]; [1]Michigan Technological University

This work reports on the unusual structural transformations responsible for the depth dependent change in refractive index upon ion implantation and rapid thermal annealing (RTA) used to fabricate optical waveguides in PZN-PT. Single crystal bulk PZN-PT is a relaxor ferroelectric with unusually large electro-optic and piezoelectric coefficients. The goal of this work is to develop an understanding of how He ion implantation can be used to engineer the depth-dependent change in refractive index of PZN-PT for fabricating optical waveguide devices. 001-oriented 4.5%PZN-PT samples implanted with 1.0 MeV He ions for doses varying from 0.75x 1015 up to 100 x 1015 He ions /cm^2 and for 3.8 MeV He ions for doses varying from 10x1015 up to 100x1015 He ions /cm^{2}are examined. The depth-dependence of the refractive index extracted from prism-coupled optical reflectivity data is used in conjunction with high-resolution x-ray diffraction (HRXRD) Transmission Electron Microscopy (TEM) analysis, and Monte Carlo simulations of the implantation process to relate the structural transformations in single crystal PZN-PT, the optical properties of the waveguide, and the He implantation/RTA process. We relate the observed refractive index contrast to the unusually large strains observed in the implanted material, estimate the threshold implantation-deposited energy density resulting in amorphization of PZN-PT, and demonstrate that the dose-dependent impact of RTA on the optical properties of the waveguide depends critically on the difference between structural transformations that occur in amorphized or highly-strained implanted PZN-PT. These results are interpreted in terms of the physical processes resulting in the refractive index modulation and the manner in which He ion implantation can be used to fabricate optical waveguides in PZN-PT.

11:40 AM Student

V10, Pre-Oxidation Iron Contamination of Silicon and 4H-SiC Substrates: *Helen Benjamin*[1]; Elena Oborina[1]; Andrew M. Hoff[1]; [1]University of South Florida

The effects of intentional iron contamination of the substrate surface prior to oxidation of both silicon (Si) and 4H-silicon carbide (4H-SiC) materials were investigated. During device manufacturing, non-intentional iron contamination of substrates may occur from many sources. Iron contamination has been shown to reduce the reliability of thin oxides on silicon substrates, and it is now a specified contaminant in recent International Technology Roadmap for Semiconductors (ITRS) documents. The experimental process flow followed in this work for both silicon and 4H-SiC substrates included: 1) cleaning by the RCA method; 2) coating with dilute iron solutions in the range from 1ppB to 500ppB; 3) heating by a lamp assisted system; 4) cleaning by the RCA method; 5) thermal oxidation; and finally, 6) testing by non-contact corona-voltage metrology. The dielectric properties of oxides grown on both Si and 4H-SiC are compared as a function of iron contamination level. In this regard, non-contact capacitance-voltage (C-V) characteristics and the Stress-Induced Leakage Current (SILC) techniques were employed.

Session W: ZnO Growth

Thursday PM Room: Deans Hall I
June 29, 2006 Location: Pennsylvania State University

Session Chairs: Jamie D. Phillips, University of Michigan; Julia W.P. Hsu, Sandia National Laboratories

1:30 PM Student

W1, Zinc Oxide Thin Films Deposited by Laser Assisted Molecular Beam Deposition: *Meiya Li*[1]; Nehal Chokshi[2]; Robert L. DeLeon[2]; Gary Tompa[2]; Wayne A. Anderson[1]; [1]State University of New York at Buffalo; [2]AMBP Tech Corporation

Zinc oxide (ZnO) thin films are of interest for UV detectors and low-cost heterojunction solar cells. ZnO thin films were deposited by two methods. One approach utilized laser assisted molecular beam deposition (LAMBD) at room temperature (RT). The other method utilized reactive RF magnetron sputtering from a ZnO target with the substrate temperature from 25 to 400°C. Field emission scanning electron microscopy (FESEM), X-ray diffraction, X-ray photoelectron spectroscopy (XPS) analysis, and photoluminescence (PL) measurement were employed to analyze the effect of the deposition conditions and the post-deposition annealing treatment on the surface morphology, structure, chemical deposition and optical properties of ZnO thin films. Dark current-voltage (I-V), DC photo I-V, and Hall-effect measurements were employed for testing the materials and the device performance. The structural and optical properties of the films were improved with laser annealing as shown by FESEM, XPS analysis and PL measurement. Al ohmic contacts were made to both as-deposited and laser-annealed ZnO thin films. The carrier concentration and Hall-effect mobility of both as-annealed and laser-annealed samples were measured at room temperature. For one set of samples, the carrier concentration and Hall mobility were 1.68 x 10^{15} cm^{-3} and 10.6 cm^{2}V^{-1}s^{-1} for the as-deposited film; 1.12 x 10^{15} cm^{-3} and

21.9cm^{2}V^{-1}s^{-1} for the laser-annealed film, respectively. ZnO films deposited and laser-annealed under other conditions gave a Hall mobility value up to 244 cm^{2}V^{-1}s^{-1}. In some cases, the ZnO thin films were changed from n-type into p-type after laser annealing. Photoconductive behavior was clearly seen on the laser-annealed samples, with values of 2.8 x 10^{-4} Ω^{-1}. All of the non-laser and laser annealed samples showed near-band emission at ~3.3 eV. The films deposited by LAMBD showed a clear structural change from a nano-particle like film to either a micro-granular film or smooth continuous film depending upon the laser annealing power. Films were close to 1:1 Zn: O stoichiometry with minimal carbon contamination before and after laser annealing. The crystalline and stoichiometric quality of the ZnO films was improved by post-deposition annealing.

1:50 PM Student

W2, The Effect of Substrate Material and Post-Annealing on DC Sputtered ZnO: *Leo P. Schuler*[1]; Paul Miller[1]; Martin Allen[1]; Nagarajan Valanoor[1]; Roger Reeves[1]; Maan Alkaisi[1]; [1]MacDiarmid Institute

Key words: DC magnetron sputtering, multiple substrate, annealing, silicone, sapphire, fused silica glass, piezo-force microscopy (PFM), PL. The aim of this research is to optimise the PL response and piezoelectric properties of DC sputtered ZnO films by post annealing and investigate the influence of various substrates. Previous research[1] showed that DC sputtered and annealed ZnO has higher piezoelectric values and higher PL response than RF sputtered ZnO. ZnO thin films with a nominal thickness of 350 nm were deposited by DC magnetron sputtering on P-type silicone <100>, C plane sapphire and fused silica glass samples. Thermal annealing was performed at up to 1200°C in N_2 atmosphere for 30 min. The effect of annealing on the crystal quality was investigated using X-ray diffraction (XRD), photoluminescence spectra (PL), scanning electron microscopy (SEM), atomic force microscopy (AFM), and piezoelectric force measurements (PFM). In the case of ZnO deposited on Si and post-annealed at 1200°C, XRD and also SEM images showed clearly a break-down process of the ZnO coating. The Powder Diffraction File (PDF) showed a match for zinc silicate oxide (Zn_2SiO_4) which indicates the break-up of the Zn - O bonds due to the high annealing temperature (also reported in[2]). The PL response of all films improved considerably during annealing, however, the annealing temperature for maximum PL response varies between the films deposited on different substrates. We will present PL measurements for ZnO deposited on three substrates and perform detailed analysis. The influence of the interface layer on the PL response will be discussed. Piezo-force microscopy (PFM) is a variation of atomic force microscopy that is applied to investigate piezoelectric thin films at the nanometer scale. It allows determining the magnitude and phase of piezoelectric domains. This technique has been employed to investigate the converse piezoelectric effect on selected DC sputtered ZnO samples. We will present the influence of annealing trials on the domain structure. Schottky diodes were fabricated on various films and electrical measurements (I-V, C-V characteristics) as well as UV sensitivity were assessed. [1]Schuler, L.P., et al., Comparison of DC and RF sputtered Zinc Oxide Films with Post-Annealing and Dry Etching and Effect on Crystal Composition. Japanese Journal of Applied Physics, 2005. PT.1, Vol. 44(No. 10): p. 7555 - 7560. [2]Xu, X., et al., Formation mechanism of Zn_2SiO_4 crystal and amorphous SiO_2 in ZnO/Si system. Journal of Physics Condensed Matter, 2003. 15(40): p. 607-613.

2:10 PM

W3, Effect of Substrate Surface Structure and Chemistry on Microstructure and Properties of Epitaxial ZnO Thin Films Grown on Sapphire and ZnO Substrates: *Xiaoqing Pan*[1]; Haiping Sun[1]; Yanbin Chen[1]; Xinqiang Wang[2]; Akihiko Yoshikawa[2]; [1]University of Michigan; [2]Chiba University

Wurtzite ZnO is a wide band gap (3.3 eV) II-VI compound semiconductor that has many promising applications in optoelectronic devices, such as excitonic laser source. Recently, there is a growing interest to fabricate high quality single crystal ZnO films. In this talk, we present our systematic studies of the microstructure, polarity, structure and chemistry of crystal defects and interfaces of epitaxial ZnO thin films grown on both (0001) sapphire and ZnO substrates. The films were synthesized by plasma-assisted molecular beam epitaxy (MBE) and pulsed laser ablation techniques. Pretreatments of substrate surface including Ga pre-deposition or N2 pre-exposure were performed to control the microstructure, defect configuration, surface morphology, and polarity of ZnO. The microstructure of ZnO films and crystal defect structures and chemistry were systematically studied by high-resolution transmission electron microscopy (HRTEM) and analytical electron microscopy (AEM). It is found that the incorporation of Ga or N at the ZnO/sapphire interface allows to control the domain structure and polarity of ZnO. It was also found that ZnO thin films grown by plasma-assisted laser-MBE show extremely high structural quality. Interface and crystal defects including misfit dislocations and threading dislocations were also characterized. In the ZnO films grown by MBE, there is a high density of stacking faults in the films, which strongly affect the electrical and optical properties of the films.

2:30 PM

W4, Plasma-Assisted MOCVD Growth of Highly Oriented ZnO Thin Films: *Maria Losurdo*[1]; Maria M. Giangregorio[1]; Pio Capezzuto[1]; Giovanni Bruno[1]; Graziella Malandrino[2]; Ignazio Fragala[2]; [1]IMIP-CNR; [2]Universita di Catania

ZnO is a wide band gap (Eg = 3.37 eV) semiconductor material that recently has attracted much interest due to its high photocatalytic activity, and its potential applications in optoelectronics due to its strong excitonic feature and lasing properties even at room temperature, and as piezoelectric transducers, phosphors, sensors and transparent conducting films. In the past decade, most of research has been focused on the growth of ZnO thin films by techniques such as sputtering, spray pyrolysis, sol-gel, electron-beam deposition. However, the importance of MOCVD for the growth of ZnO should be re-considered, as this technique has enabled the commercial application of GaN and related materials. Therein, we present and discuss the growth process and structural and optical properties of ZnO thin films and nanostructures grown by MOCVD also plasma-assisted (PA-MOCVD) using oxygen plasma excited by 13.56MHz rf-power. A new precursor Zn(TTA)2•tmed (HTTA=2-thenoyltrifluoroacetone,TMED=N,N,N',N'-tetramethylethylendiamine) is used. Different substrates, including Si(100), 4H- and 6H-SiC(0001) and sapphire (0001), are used. These substrates are also treated in situ using various plasmas (Ar-, H2, O2,) in order to change the ZnO nanoparticles nucleation and investigate their impact on material properties. The impact of substrate temperature ranging from 300°C to 600°C and of plasma parameters (r.f. power, O2 partial pressure) on ZnO thin films is presented for both MOCVD and PA-MOCVD. X-ray diffraction (XRD) is used for investigation of deposition parameters on the structure. The surface morphologies of ZnO films is examined by atomic force microscopy (AFM). The electrical properties are studied using the 4-probe Hall measurements and electrical force microscopy. Spectroscopic ellipsometric (SE) spectra of the dielectric function acquired from 0.75 to 6.5 eV are used for investigating the optical properties (exciton of ZnO appears in dielectric function) as a function of film structure. The results show that the O2 plasma assisted growth results in growth of highly c-axis oriented ZnO films, with smoother morphologies than MOCVD and in better optical quality of ZnO films that show in the dielectric function spectra a sharp and intense exciton. In particular, from AFM analysis of roughness evolution and from XRD analysis of film crystallinity, we inferred information on the different growth dynamics characterizing PA-MOCVD and MOCVD, and the low RMS measured as a function of film thickness and the high c-axis orientation of ZnO films let us infer that a quasi-two-dimensional (2D) growth mode can be obtained by the plasma activation. We also present data on how the resulting ZnO different microstructure controls the reactivity/response of ZnO with hydrogen and nitrogen atoms.

2:50 PM Student

W5, Surface and Interface Characterization of A-Plane ZnO and $Mg_xZn_{1-x}O$ Films: *Gaurav Saraf*[1]; Jian Zhong[1]; Yicheng Lu[1]; Olga Dulub[2]; Ulrike Diebold[2]; Theo Siegrist[3]; [1]Rutgers University; [2]Tulane University; [3]Bell Laboratories

Non-polar epitaxial (11-20) and (1-100) ZnO films are important because of absence of spontaneous and piezoelectric fields compared to polar (0001) ZnO films. Presence of spontaneous and piezoelectric polarization results in spatial separation of the electrons and holes in the active layer causing a reduction of the emission efficiency undesirable for device performance. Furthermore, the non-polar ZnO films and its heterostructures with $Mg_xZn_{1-x}O$ have in-plane anisotropy, which provides unique optical, acoustic and

electrical device applications. The structural properties of these ZnO and the $Mg_xZn_{1-x}O$ films, particularly the surface and the interface quality are thus critically important for device performance. In this work we report the structural, surface and interface properties of epitaxial $Mg_xZn_{1-x}O$ and ZnO grown by Metal organic chemical vapor deposition (MOCVD) on R-sapphire substrates. The a-plane ZnO and $Mg_xZn_{1-x}O$ ($0 \le x \le 0.3$) films were grown by MOCVD in axisymmetric vertical flow rotating disc chamber. Argon was used as carrier gas and oxygen gas was used as oxidizer. Growth was done at temperatures from 450-500°C, with typical growth rate of ~500 nm/hr. X-ray diffraction (XRD) scans show that both ZnO and $Mg_xZn_{1-x}O$ films have good crystallinity and epitaxial relationship with the r-sapphire, i.e. (11-20) $Mg_xZn_{1-x}O \parallel$ (01-12) Al_2O_3 and [0001] $Mg_xZn_{1-x}O \parallel$ [0-111]Al_2O_3. The interface of both ZnO and $Mg_xZn_{1-x}O$ films on R-sapphire was found to be semi-coherent as characterized by high resolution Transmission Electron Microscopy (TEM). The $Mg_xZn_{1-x}O$ surfaces were characterized with Scanning Tunneling Microscopy (STM) in ultrahigh vacuum (UHV). After introduction into UHV, the samples were cleaned and annealed to 400 -800°C. The surface showed a characteristic wave-like morphology with needles (typically 150-400 nm wide, 10-40 nm high, and 1500 - 3000nm long). The needles run predominantly along the crystallographic c-direction with many small terraces, 15-30 nm wide and 20-40 nm long with mono-atomic step edges. The needle-like surface morphology is due to the a-plane ZnO/$Mg_xZn_{1-x}O$ dimers running parallel to the c-axis of the films and due to differential growth rates along the in-plane [0001] and [1-100] directions. The large lattice mismatch along [0001] compared to [1-100] may also affect the surface morphology. PL measurements were carried out on the ZnO and the $Mg_xZn_{1-x}O$ films to evaluate the optical properties using a 325 nm He-Cd laser. The ZnO films show a strong near-band-edge (NBE) emission around 3.31 eV with the FWHM of 114 meV. No deep level emission was observed, indicating a low defect concentration. Blue shift was observed for the $Mg_xZn_{1-x}O$ films (x ~ 9%) with NBE emission around 3.48 eV. The in-plane optical anisotropy was observed by polarized transmission measurements of a-plane $Mg_xZn_{1-x}O$ films on the R-sapphire substrate.

3:10 PM Break

3:30 PM

W6, *Three Step Growth* as a Novel Approach for the Growth of ZnO on Si(111) by MOVPE: *Takumi Moriyama*[1]; Shizuo Fujita[1]; [1]Kyoto University

ZnO on a Si substrate structure attracts attention because this offers conductive and inexpensive substrates as well as one-chip integration of multifunctional ZnO with Si devices. However, the growth of ZnO on Si is obstructed by oxidation of a Si substrate surface with oxygen source. In order to resolve this problem and to obtain higher quality ZnO epilayers, we show the potential of the novel *three step growth* procedure in metalorganic vapor phase epitaxy.We used Si(111) substrates, which were cleaned with acetone, methanol, HF and deionized water. Diethylzinc was used as the zinc source, and nitrous oxide (N_2O) gas, which has weak oxidizing ability compared with pure oxygen (O_2) gas, was used as the oxygen source. In starting the growth, to prevent the oxidation of Si surface, the Zn source was supplied earlier than the oxygen source. It has been revealed, in the growth of ZnO on A- or C-plane sapphire, that smooth films are obtained at high growth temperature and/or VI/II ratio. However, the direct growth of ZnO on Si at high temperatures (for example, >600°C) did not allow effective nucleation. It is because Si surface is easily oxidized by N_2O gas in spite of the preflow of Zn source, which may easily evaporate from the surface. Consequently, rods tended to be prepared rather than uniform films. The above results suggest the requirement of initial *nucleation layer* which is grown on Si at low temperature to completely cover the Si surface with ZnO. We have found that the ZnO, for this purpose, should be grown at 300°C, which is lower than melting point of Zn. Then the attempts were made to growth the main layer at 800°C successively, but this *two step growth* procedure resulted in segregated grains. It was considered that ZnO was evaporated at 800°C. Hence we examined the *three step growth* procedure. Firstly ZnO was grown at 300°C (15 min.) as a *nucleation layer*, then grown at 500°C (15 min.) as a *recovery layer*, and finally grown at 800°C (60 min.) as a main layer. As a result, surface morphology of ZnO film was significantly improved and got smoother. Further, the increase of VI/II ratio in the growth of the main layer, that is, from 2.8×10^4 to 1.25×10^5, effectively improved the surface morphology. From the atomic force microscope (AFM) observation, the root means square (RMS) roughness was about 6 nm, which can further be reduced by the optimization of growth conditions for the main layer and/or layer configuration. It is confirmed that the *three step growth* enables the growth of high quality ZnO films on Si substrates with preventing the oxidation of Si surface.

3:50 PM Student

W7, Growth of ZnO on Cubic Substrates by Molecular Beam Epitaxy: *Emine Cagin*[1]; Jun Yang[1]; Jamie D. Phillips[1]; Pallab Bhattacharya[1]; [1]University of Michigan

ZnO and related II-VI compound semiconductor alloys are emerging as important materials for numerous optical and electronic devices. The wurtzite structure of ZnO differs from the cubic rock-salt structure of the binary compounds CdO and MgO. The ability to integrate and alloy these binary oxides allows a wide range of bandgap engineering for device applications. Furthermore, these II-VI oxide compound semiconductor materials provide a unique opportunity for integration with ferroelectric perovskite oxide materials due to the associated chemical compatibility. Chemical incompatibility is a problem that has inhibited the success of integrating ferroelectric perovskite oxides with non-oxide semiconductor materials. In this work, the characteristics of ZnO grown on cubic substrates by molecular beam epitaxy (MBE) are presented. ZnO was grown using a two-zone zinc effusion cell to prevent source oxidation, and an RF oxygen plasma source. ZnO was grown on both MgO (001) and GaAs (001) substrates. Prior to ZnO growth, MgO substrates were thermally cleaned at 4000C and exposed to oxygen plasma. A clear MgO surface reconstruction was observed by reflection high energy electron diffraction (RHEED) during the plasma clean. Upon nucleation, the RHEED pattern transitioned from a streaky 2x1 pattern, characteristic of MgO, to a spotty pattern unlike the 2x1 ZnO Wurtzite pattern. GaAs substrates were capped with arsenic at low temperature in a separate MBE system after thermally desorbing the native oxide and observing the common (2x4) surface reconstruction. Prior to ZnO growth on these GaAs substrates, the arsenic cap was thermally removed at 4000C. Growth was initiated by exposure to zinc flux prior to turning on the oxygen plasma source. The RHEED pattern for ZnO growth indicated that the first layers of ZnO followed the GaAs 4x2 streaky pattern. After the growth of less than 100nm of ZnO, growth transitioned to the wurtzite phase as indicated by a 2x1 spotty RHEED pattern. X-ray diffraction (q-2q) measurements indicate a single ZnO crystalline orientation for growth on MgO (001) corresponds to a cubic ZnO (111) phase. X-ray diffraction (q-2q) measurements for ZnO grown on GaAs (001) indicate a predominant wurtzite (0001) ZnO orientation along with some component of the cubic (111) ZnO corresponding to the ZnO phase observed for epitaxial growth on MgO (001). The ZnO wurtzite phase (0001) observed for growth on GaAs (001) is consistent with the (0001) wurtzite orientation observed for the growth of ZnO on c-plane sapphire under similar conditions. Details of the structural, electronic, and optical properties of these epitaxial layers will be presented and discussed. This work is supported by AFOSR under contract number FA9550-04-1-0390, and the Center for Optoelectronic Nanostructured Semiconductor Technologies, a DARPA UPR award HR0011-04-1-0040.

4:10 PM Student

W8, ZnO Thin Films Produced via Reactive Pulsed Arc Molecular Beam Deposition: *Chi-Tung Chiang*[1]; Robert L. DeLeon[2]; James F. Garvey[1]; [1]University at Buffalo; [2]AMBP Tech Corporation

The structures and properties of ZnO thin films deposited on Si (100), Corning 2947 glass and plastic film substrates by pulsed arc molecular beam deposition (PAMBD) have been studied. PAMBD is an ablation technique that utilizes a high voltage electrical discharge to provide a plasma source for subsequent material ablation and oxide generation. Metal atoms are ablated from the pure metal electrodes during the arc discharge. High pressure oxygen gas is then pulsed directly into the plasma, to chemically generate the metal oxide. The resulting products are expanded and deposited onto a room temperature substrate situated within a vacuum chamber. This technique has been previously used to successfully generate metal oxide films of a wide variety of metals. In this work, ZnO thin films were grown by the PAMBD method. Some of these ZnO films were laser annealed to improve the surface morphology. The annealed and unannealed films were then characterized by scanning electron microscopy (SEM), atomic

force microscopy (AFM), X-ray photoelectron spectroscopy (XPS), X-ray diffraction (XRD), photoluminescence and ellipsometry measurements to determine the film composition, structure, growth rate, optical and electrical properties. SEM studies of ZnO films on different substrates all demonstrated that the ZnO films were dense and have columnar structures. XPS revealed highly stoichiometrical Zn and O (1:1) film composition representing chemically pure films. The refractive index ranged from 1.920 to 1.989 which is in good agreement with reported ZnO properties. By observing ZnO thin films deposited on various substrates we readily see the advantages of low temperature thin film depositions due to the rapid cooling of the metal oxide product by the molecular beam supersonic expansion. This indicates that the PAMBD process is especially suitable for deposition of these materials upon temperature-sensitive substrates.

4:30 PM Student

W9, Low Temperature Highly Conducting Boron-Doped ZnO Films by Plasma Enhanced Chemical Vapor Deposition: *Jie Sun*[1]; Diwakar Garg[2]; Thomas N. Jackson[1]; [1]Pennsylvania State University; [2]Air Products and Chemicals, Inc

Zinc oxide (ZnO) films have attracted considerable interest for large area electronic applications. Doped ZnO is both highly transparent to visible light and electrically conductive and has been used for transparent electrodes in photovoltaic devices and flat panel displays[1]. Boron-doped ZnO films deposited by atomic layer deposition (ALD) at 165°C have been reported with resistivity as low as 6.4 x 10 E-4 Ω×cm[2]. In this paper, we report on highly conductive, transparent, boron-doped ZnO films deposited on glass substrates by plasma enhanced chemical vapor deposition (PECVD). The deposition uses diethyl zinc (DEZ), carbon dioxide (CO2), and triethylborane (TEB) gas mixtures at a substrate temperature of 200°C. This is the first report of the use of TEB as a boron doping source for ZnO. TEB is much less toxic than commonly used diborane (B2H6) and may be preferable for commercial use. Optical emission spectroscopy was used for diagnosis of the deposition plasma and the PECVD deposited ZnO films were characterized by ellipsometry, X-ray diffraction (XRD), atomic force microscopy (AFM), vis-near-infrared spectrophotometry, and photoluminance (PL). Typical transmission of 100-500 nm thick films was greater than 85% over the visible range. Room temperature PL showed a free exciton transition energy of 3.39 eV with a full-width at half-maximum of 180 meV. For depositions at 200°C the ZnO films are polycrystalline with a dominant (002) orientation. PECVD deposited ZnO films with ~350 nm thickness had resistivity as low as 4 x 10 E–4 Ω×cm. To our knowledge, this is the lowest resistivity reported for a low-temperature deposited boron-doped ZnO film. Electron concentration, determined from Hall measurements, was as large as 1 x 1021 /cm[3], with mobility of 13.5 cm[2]/V×s. This work demonstrates that PECVD with DEZ-CO2 and low-toxicity TEB is a viable candidate for low-temperature highly-conducting, transparent ZnO film deposition. [1]J. J. Robbins, J. Esteban, C. Fry, and C. A. Wolden, "An investigation of the plasma chemistry involved in the synthesis of ZnO by PECVD," J. Electrochem. Soc., 150, C693-C698 (2003).[2]B. Sang, A. Yamada, M. Konagai, "Growth of Boron-doped ZnO thin films by atomic layer deposition," Solar Energy Mat. & Solar Cells, 49, 19-26, (1997).

4:50 PM

W10, Late News

Session X: MBE Growth of Group III-Nitrides

Thursday PM — Room: Deans Hall II
June 29, 2006 — Location: Pennsylvania State University

Session Chairs: Thomas H. Myers, West Virginia University; Steven M. Durbin, University of Canterbury

1:30 PM

X1, Optical Investigation of the Dependence of Luminescence Efficiency on Stokes Shift in Nanoscale Compositionally Inhomogeneous AlGaN: *Gregory A. Garrett*[1]; Anand V. Sampath[1]; H. Shen[1]; Michael Wraback[1]; [1]U.S. Army Research Laboratory

The development of efficient III-Nitride based ultraviolet emitters requires improvement in AlGaN materials that presently suffer from significant non-radiative recombination due to compositional fluctuations and large defect densities. Recently we reported on AlGaN films deposited by plasma-assisted molecular beam epitaxy that possess significantly enhanced internal quantum efficiency (~30% for a 33% AlN mole fraction alloy) as a result of self-assembled nanoscale compositional inhomogeneities (NCI). This luminescence is further characterized by an anomalously large Stokes shift (~400 meV) with respect to the band gap of the alloy. Here we report on a detailed investigation of the relationship between the magnitude of this shift and the intensity and efficiency of the photoluminescence (PL). The films investigated consisted of ~0.5-0.8 micron thick, silicon doped, 33% AlGaN deposited heteroepitaxially on c-plane sapphire substrates. Their optical properties were measured using room- and low-temperature cw-PL, PL excitation, time-resolved PL, and reflectivity techniques. Of interest is a consistent increase in PL intensity with greater Stokes shift of the NCI emission peak, a factor of 5 for a shift from 300 to 380 meV. Focusing on two samples, we examine this phenomenon with cw and time-resolved PL techniques and compare the results to a coupled rate equation model of carrier recombination dynamics. The samples had emission shifted ~350 meV and ~400 meV from a band edge absorption around 283 nm. For this pair, the sample with the larger shift was twice as bright under cw-PL excitation at 0.25 mW. Time-correlated single photon counting (TCSPC) experiments, with 25 ps resolution, reflected this showing a longer lifetime in the *brighter* sample, ~ 426 ps verses 307 ps. Further information was obtained from time-resolved PL (TRPL) by gated down-conversion with 400 fs resolution. At this resolution, the dynamics of carrier transfer from the band edge matrix to the NCI region can be seen. Contrary to expectation, for the *dimmer* sample, a faster decay in the band edge matrix was measured suggesting a more rapid transfer of carriers to a larger density of localized states that may correlate with a slightly faster rise time in the NCI emission. Comparison of the peak intensity, near time-zero, from the NCI regions corroborates this observation as the *dimmer* sample has a stronger peak signal than that of the *brighter* sample which saturates as a function of excitation pulse fluence quicker than the *dim* sample, indicating a smaller volume of NCI region. Further investigation of the correlation between Stokes shift and brightness of the emission by time-resolved and temperature dependent PL techniques may yield additional insight into the physical character of the material making up the NCI region.

1:50 PM Student

X2, The Use of Cathodoluminescence in Gallium Nitride during Growth to Determine Substrate Temperature: *Kyoungnae Lee*[1]; Eric D. Schires[1]; Thomas H. Myers[1]; [1]West Virginia University

Accurate measurement of the substrate temperature during growth of gallium nitride by molecular beam epitaxy is crucial. Typically, thermocouples are usually used to measure the temperature of the back side of block which is holding the substrate. Alternatively, pyrometers are often used. However, there is a big range of an error. In-situ cathodoluminescence (CL) occurring during reflection high energy electron diffraction is a strong candidate to determine the growth temperature. The electron beam supplied by our RHEED gun has an energy of 18 keV which was used for each measurement. CL was easily detected up to and beyond typical growth temperatures. The CL was directed into a monochromator using fiber optics. The final signal was detected with a photomultiplier tube. This technique appears quite useful to accurately and reproducibly determine substrate temperature during growth. The CL measurement at room temperature can also be used as a means to check the quality of the substrate by comparing intensities of the GaN band edge energy peak and defect peak we have observed. Also, the CL is very important to the preliminary growth of GaN and the doping studies such as Mg-doped GaN. The reproducibility of CL data and fast CL scan are strong advantages for use in the growth of GaN films. The CL could also be observed using a ccd camera. Thus, we investigated using the CL to image the sample during growth. This could be used to see temperature inhomogenaities, and potentially to map alloy composition fluctuations. We calibrated the wavelength vs. growth temperature by using narrow band-pass

interference filters. Background subtraction with blanking the e-beam could be used to remove black body radiation and other undesired sources of light. For gallium nitride, the photon energy at the growth temperature of 750°C is about 3.0eV. Using different filters, we can take a picture of e-beam on the surface of substrate for each filter and analyze the peak intensity using the line profile. We will present CL images of various samples at differing temperatures. This work was supported by the AFOSR MURI F49620-03-1-0330 monitored by Todd Steiner and Gerald Witt and by ONR Grants N00014-02-1-0974 and N00014-01-1-0571, both monitored by Colin E. C. Wood.

2:10 PM Student

X3, A New Mechanism for the Tilting of Dislocations in Oxygen Doped Gallium Nitride Layers Grown by Molecular Beam Epitaxy: *Michael E. Hawkridge*[1]; David Cherns[1]; Kyoung-Nae Lee[2]; Thomas H. Myers[2]; [1]University of Bristol; [2]West Virginia University

There are two main problems associated with the growth of gallium nitride (GaN) films. Firstly, the high dislocation densities found in the GaN layer are detrimental to device performance eg. dislocations act as non-radiative recombination centres in optical devices and as leakage paths in electronic devices. Secondly, tensile strain is produced during growth that can lead to cracking of the GaN layer upon cooling. Both strain and dislocation density can be reduced by the turning over of threading dislocations, which leads to dislocation annihilation and strain reduction. This process is normally driven by shear strain on inclined slip planes (the Matthews mechanism), but in the case of GaN devices, the slip plane (0001) is not inclined, implying no shear stress to drive such a mechanism. However, recent observations of dislocation turn over have been made in GaN epilayers doped with Be and $Al_xGa_{1-x}N$ heterostructures doped with Si. These results suggest that dopants and impurities allow the turning over mechanism to operate in GaN. Here, we examine O doped GaN grown by molecular beam epitaxy on (0001) sapphire using transmission electron microscopy. Observations on cross-sectional samples showed that threading dislocations turn over in correspondence to the introduction of an oxygen rich layer. The direction and amount of tilt is similar for all of the dislocations present at up to 20° from [0001]. After the dislocations initially turn over, their direction appears insensitive to subsequent variations in oxygen content. It was also observed that in oxygen doped samples, the surface was rough and faceted in places. Large angle convergent beam electron diffraction patterns were used to characterise the dislocations. This technique allows the magnitude and most importantly the sign of the dislocations to be found. The results showed that some dislocations act to relieve strain in the layer, whereas others turn in an opposite sense leading to an increase in strain energy. In contrast, the end of the dislocations at the surface showed a correlation with the base of the surface facets. We present an alternative explanation for dislocation tilt related purely to surface topography. It is argued that surface roughening due to the presence of oxygen during growth generates facets that the threading dislocations follow, irrespective of strain. The evidence for this mechanism will be presented and the implications for dislocation density reduction and MBE growth are discussed.

2:30 PM

X4, Unintentional Si Incorporation in GaN/AlN Interface Grown on SiC by PAMBE: *Tong-Ho Kim*[1]; Soojeong Choi[1]; Pae C. Wu[1]; Changhyun Yi[1]; April S. Brown[1]; Maria Losurdo[2]; Giovanni Bruno[2]; Akihiro Moto[3]; [1]Duke University; [2]IMIP-CNR; [3]Innovation Core SEI, Inc.

Recently, AlGaN/GaN high electron mobility transistor (HEMTs) structures grown on SiC have demonstrated very good power performance, due to the high breakdown voltage and high electron velocity in GaN. However, GaN buffers typically grown on SiC with AlN nucleation layer tend to be conductive leading to buffer leakage that degrades device DC and RF characteristics. Although intentional doping using acceptors such as Be and C during GaN buffer growth has been developed and shown to improve device performance due to compensation, study of the origin of this conductivity, including factors related to crystallinity and the possible unintentional doping by oxygen and silicon, is crucial. Herein, we present the observation and behavior of unintentional silicon incorporation during GaN buffer and AlN nucleation layer growth on SiC (0001) while using plasma assisted MBE. In particular, we investigate the influence of pretreatments of the substrate and modification of growth conditions such as substrate temperature, Al/N flux ratio during growth AlN nucleation layer, and thickness of the AlN layer. We assess Si behavior using secondary ion mass spectroscopy (SIMS). In our previous work on interfacial reactions during GaN and AlN growth on 4H- and 6H-SiC substrates, we observed Si accumulation on the surface of AlN nucleation layers grown on SiC by XPS. Furthermore, using scanning spread resistance microscopy (SSRM) and SIMS, we found that a conductive layer exists at GaN/AlN interface of a AlGaN/GaN HEMT structure grown on SiC with metal rich growth conditions. The growth temperature and Al/N flux ratio of AlN nucleation layers were varied from 580°C to 800°C and from Al-rich to N-rich, respectively. The influence of the thickness of the AlN layer and the pretreatment of substrate, using such techniques as a Ga-flash and/or nitridation on unintentional Si incorporation, was investigated. Through SIMS analysis, a Si peak was found at the GaN/AlN interface and the AlN/SiC interface in all samples grown under Al-rich growth conditions, but was absent in the sample grown under N-rich conditions. This indicates that during AlN nucleation on SiC under Al-rich growth conditions, excess Al molecules chemically react with the SiC substrate via a dissolution-precipitation process and produce precipitated Si molecules at the growth front of the AlN nucleation layer, and finally these Si atoms incorporate into the GaN layer at the GaN/AlN interface leading to GaN buffer leakage. We show that the Al/N flux is the primary factor controlling unintentional Si incorporation through the control of the chemical reaction of excess Al atoms with the SiC substrate. A lower growth temperature and thicker AlN layer, as well as pretreatments cannot effectively reduce the reaction of the excess Al with SiC during AlN nucleation and the subsequent Si corporation at the GaN/AlN interface.

2:50 PM

X5, High-Quality Nonpolar 4H-AlN Grown on 4H-SiC by Molecular-Beam Epitaxy: *Masahiro Horita*[1]; Jun Suda[1]; Tsunenobu Kimoto[1]; [1]Kyoto University

Group-III nitrides (III-N) with nonpolar orientations have attracted much attention due to its potential application for high-efficiency light-emitting devices. However, quality of III-N with nonpolar orientations is still inferior to that of well-established III-N with a conventional polar (0001) orientation. Improvement of crystalline quality of nonpolar III-N is one of challenges. We have reported growth of nonpolar AlN on 4H- and 6H-SiC substrates with nonpolar orientations, (11-20) and (1-100).[1-3] X-ray diffraction (XRD) measurements showed AlN layers grown on nonpolar 4H-SiC have high crystalline quality.[2,3] In addition, from reflection high-energy electron diffraction (RHEED), the crystalline structure of AlN was revealed to be not thermally stable wurtzite (2H) structure but 4H structure, which is the same as that of SiC substrate. We have attributed such a high crystalline quality to isopolytypic AlN/SiC interface. However, from high-resolution transmission electron microscopy (HRTEM), the 4H-AlN layers contained very high-density stacking faults (SFs). Reduction of SFs is important to apply isopolytypic AlN/SiC to device applications. In this paper, we present realization of very high-quality nonpolar 4H-AlN by controlling SiC surface condition and growth parameters of AlN. SiC (11-20) substrates were subjected to high-temperature gas etching to remove polishing damage and realize very smooth surface. AlN was grown by molecular-beam epitaxy using elemental Al and rf plasma-excited active nitrogen with optimized V/III ratio (slightly Al-rich condition). AlN layers grown with the optimized condition exhibited much superior crystalline quality in XRD measurements. Full width at half maximum (FWHM) of symmetrical (11-20) diffraction is 57 arcsec, which is better than that of previously reported 4H-AlN, 90 arcsec.[2] FWHM values for asymmetrical (11-24) and (03-30) diffractions are also excellent, 76 arcsec and 46 arcsec, respectively. From cross-sectional HRTEM, the SF density was evaluated to be 2×10^5 cm^{-1}, which is two orders of magnitude smaller than that of our previously reported 4H-AlN.[2] From plan-view TEM observation, length of stacking faults along [1-100] was found to be longer than observed area (several μm). Density of partial TD accompanied with SF is estimated to be much less than 1×10^7 cm^{-2}. The densities of SFs and dislocations are much smaller than those for nonpolar GaN on r-plane sapphire and comparable to nonpolar ELO-GaN. SFs in 4H phase (or 2H phase inclusion) may nucleate by lateral growth on (0001) side facets at rough growing surface. Using very smooth SiC surface and

optimized V/III ratio resulted in smooth growth surface, which prevents formation of SFs. [1]N. Onojima, J. Suda and H. Matsunami, Jpn. J. Appl. Phys. 41, L1348, 2002. [2]N. Onojima, J. Suda, T. Kimoto, H. Matsunami, Appl. Phys. Lett. 83, 5208, 2003. [3]R. Armitage, J. Suda, T. Kimoto, Appl. Phys. Lett. 88, 011908, 2005.

3:10 PM Break

3:30 PM Student

X6, Physical Processes during Growth of InN on GaN (0001) by Plasma-Assisted Molecular Beam Epitaxy: *Emmanouil Dimakis*[1]; Eleftherios Iliopoulos[1]; Alexandros Georgakilas[1]; [1]Microelectronics Research Group, University of Crete/Institute of Electronic Structure and Laser (IESL), Foundation for Research and Technology-Hellas (FORTH)

It is only recently that InN single crystals of decent structural quality have been heteroepitaxially grown by a limited number of research groups worldwide. The growth of InN has been investigated using sapphire or GaN as substrates. Trying to surmount the growth peculiarities of InN, each group developed it's own methodological approach using buffer layers and/or substrate temperature variations, at least in the works where the growth details are reported. In this work, we present our systematic studies on the physical processes taking place during growth of InN on GaN(0001) surfaces by molecular beam epitaxy, i.e. which they are and how they are ruled by the growth conditions used. The results were exploited to determine the growth window for high quality InN films. In addition, the results of our studies could justify the functionality of the different approaches used by other groups. It is commonly known that the growth conditions used for InN differ substantially from those used for GaN and AlN. Namely, due to the low dissociation temperature of InN, the substrate temperature has to be unusually low and the In/N flux ratio less or equal to unity. In the first part of this work, we have addressed quantitatively, using in-situ measurements, the temperature dependence of the indium-adatoms surface diffusion, the InN decomposition and the indium surface-desorption. Specifically, we observed the fast increase of the rate of these mechanisms at temperatures higher than 350°C, 450°C and 550°C, respectively. Due to the specific relation between these three characteristic temperatures, the growth of InN is limited at temperatures lower than 450°C with stoichiometric or nitrogen-rich conditions. The structure and morphology of InN is another parameter that one has to deal with. There are several works in the literature where columnar structures or films with voids on the surface are reported. In the second part of our work, we have correlated the structure and morphology with the self-regulating mechanism that takes place during the growth of InN on GaN(0001) under conditions that provide efficient indium-adatoms surface diffusion. Specifically, we observed that under nitrogen-rich conditions, the indium-adatoms diffuse along the GaN surface in order to construct InN structures with stoichiometric conditions on their top surface. In this way, the InN surface coverage, and consequently the diameter of InN structures, is being self-regulated according to the In/N flux ratio used. Two-dimensional InN films can only be obtained using stoichiometric fluxes, to avoid the creation of three-dimensional structures, and substrate temperatures close to 450°C, to ensure efficient surface diffusion of the indium-adatoms. Finally, we present how we exploit the above results to grow either InN films of high structural quality with improved electrical and optical properties, or InN quantum dots of controlled size and density.

3:50 PM

X7, Study of PA-MBE Growth of In- and N-Polar InN on SiC Substrates: *Maria Losurdo*[1]; Maria Giangregorio[1]; Giovanni Bruno[1]; Tong-Ho Kim[2]; Soojeong Choi[2]; Pae C. Wu[2]; April S. Brown[2]; [1]IMIP-CNR; [2]Duke University

InN is a very attractive material because of its outstanding material properties such as its band gap close to 0.7eV, its small effective mass, and large electron mobility. This motivates research efforts devoted to improvement of the growth process and InN film quality. So far, good quality InN has been grown using plasma-assisted molecular beam epitaxy (PAMBE) on c-plane sapphire substrate using AlN or GaN buffer layers. Little attention has been paid to the heteroepitaxial growth of InN on SiC for control of polarity. Furthermore, there is also interest in investigating the impact of hydrogen and nitrogen on InN, since both hydrogen and nitrogen vacancies can contribute to the residual n-type carrier concentration of InN. This contribution presents a study of the PAMBE growth of In- and N-polar InN directly on Si-face and C-face 6H-SiC. A two-step process consisting of deposition of a thin low-temperature InN layer, followed by its annealing and subsequent deposition of the epitaxial layer has been used. The nucleation of InN on SiC and its evolution upon annealing and during epitaxial growth is studied in real time by RHEED and spectroscopic ellipsometry. The impact of the temperature, V/III ratio and the SiC polarity on the growth kinetics, morphology, structure and optical properties of InN is discussed. It is shown that appropriate pre-treatments of the 6H-SiC yield growth of good quality In- and N-polar InN on the Si- and C-face, respectively, without the use of GaN or AlN buffer layers. This is demonstrated through an extensive characterization of films using XRD analysis of the (0002) rocking curve and pole figures showing primarily A-domains, AFM data showing very smooth morphologies, photoluminescence data indicating a very intense PL peak at 0.7 eV at room temperature, and ellipsometry showing the highest dielectric function with very sharp interband critical points so far reported for InN. As a further step, we have also investigated the InN structural, morphological, optical and electronic properties modifications upon interaction with atomic hydrogen and nitrogen produced by remote H2 and N2 plasmas, to understand any possible role of hydrogen and nitrogen in introducing and/or passivating defect states. We show that both hydrogen and nitrogen lead to indium enrichment of the InN, because of nitrogen depletion from InN through the formation of NHx and N2. Hall-effect measurements indicated an increase in the mobility upon interaction with both hydrogen and nitrogen atoms. Furthermore, hydrogen leads to strong changes in the PL, i.e, the PL band at 0.7 eV of the as-grown layer is replaced by a new PL band at energies >1.1 eV, indicating that defects due to unintentional hydrogen incorporation into InN could be one of the reason of the various value reported for the band gap.

4:10 PM Student

X8, Direct Write Composition Patterning of InGaN during Molecular Beam Epitaxy: *Xiaodong Chen*[1]; William J. Schaff[1]; [1]Cornell University

The growing surface of InGaN is exposed to a 50μm diameter pulsed 1.06μm laser beam that is directed to locations controlled by scanning mirrors. Local heating effects are observed where the laser is incident. Compositions are characterized by wavelength dispersive spectroscopy using a 6keV incident beam. There are three different In mole fractions that result from this exposure: 1) x=0.75 under exposure, 2) x=0.85 adjacent to exposure, 3) x=0.81 uniform composition away from exposed regions during a nominal 78nm deposition on a 540nm thick InGaN buffer. Thickness variation is consistent with mass transport indicating that no indium evaporates. The effect of local thermal energy is to enhance surface diffusion and not cause ablation or evaporation under the conditions studied. It is not yet known how much the presence of free carriers has on surface kinetics in comparison to simple thermal effects. A second effect of laser writing is to cause an enormous enhancement of PL efficiency. Laser written regions have 7 times higher PL intensity compared to non-written areas. There is little change in PL intensity when measured through the back of the wafer. The initial conclusion is that PL is not increasing due to increase in radiative recombination efficiency, but increases due to texturing of the surface that leads to higher extraction efficiency. Regions where exposure is halted do not show PL enhancement when thick layers are overgown. The laser exposure conditions of intensity and scanning speed are adjusted to create grayscale variations in composition with position. Composition profiles are created with grayscale images from a photograph. Composition variation is seen by backscattered electron emission due to z-contrast, while no features are visible from secondary electrons. Integrated optoelectronic components such as lenses and transmission lines are just one potential application of this technique. Direct write composition control goes beyond simply performing an effective lithography step in-situ. Lateral composition control now permits in-situ 3D fabrication of structures that can not be created by traditional 2D epitaxy followed by lithography, etching and regrowth.

4:30 PM

X9, Growth of In-Rich $in_xAl_{1-x}N$ Films on (0001) Sapphire by RF-MBE and Their Properties: *Hiroyuki Naoi*[1]; Keisuke Fujiwara[1]; Masahito Kurouchi[1]; Daisuke Muto[1]; Tsutomu Araki[1]; Hyunseok Na[1]; Yasushi Nanishi[1]; [1]Ritsumeikan University

The realization that the InN bandgap is ~ 0.7 eV rather than 1.9 eV implies that the usable light wavelength range of group III nitrides is extended from the ultraviolet and visible wavelength regions into the infrared wavelength region as well. Because AlN has the largest direct bandgap of 6.2 eV among group III nitrides, the $In_xAl_{1-x}N$ system can cover the whole range of the above mentioned wavelength regions and thus is technologically very important. While there are many potential applications for $In_xAl_{1-x}N$, this alloy system has been less studied than the $In_xGa_{1-x}N$ and $Al_xGa_{1-x}N$ systems. The literatures on $In_xAl_{1-x}N$ are indeed very few, and even the fundamental bandgaps of this alloy system have not been clarified yet. To the best of authors' knowledge, photoluminescence emission was reported only for Al-rich $In_xAl_{1-x}N$ alloys ($0.14 \leq x \leq 0.58$)[1] in the literatures. On the other hand, optical absorption data were reported for both Al-rich ($0.14 \leq x \leq 0.58$) [1] and In-rich ($0.75 \leq x \leq 1$)[2] $In_xAl_{1-x}N$ alloys. A literature demonstrating the growth of $In_xAl_{1-x}N$ alloys in the whole In composition range ($0 \leq x \leq 1$), interestingly showed the absorption edge energy approaching ~ 1.9 eV of the InN sample with increasing the In-composition[3]. The scattered data among these available literatures strongly demand fundamental studies for this alloy system. In this presentation, we have performed the growth of In-rich $In_xAl_{1-x}N$ films in the In-composition range from 1 down to 0.5 by radio-frequency molecular-beam epitaxy. The $In_xAl_{1-x}N$ films were grown directly on nitridated (0001) sapphire substrates without depositing any buffer layers in order to avoid possible unfavorable effects such as interdiffusion and strain, which could modify the optical properties of the films. It was found that the growth at temperatures close to the InN growth temperature (~530°C) was always accompanied by In-droplet formation on the $In_xAl_{1-x}N$ surface. This behavior is considerably different from that observed for In-rich $In_xGa_{1-x}N$ growth[4]. Thus a slightly reduced temperature of 460 degrees C was mainly employed for the present $In_xAl_{1-x}N$ growth. Both the photoluminescence peak energy, where available, and the optical absorption edge energy of the $In_xAl_{1-x}N$ films decreased monotonically with increasing the In composition, consistent with the InN bandgap energy of ~ 0.7 eV. The modification of both the temperature and the time for substrate nitridation from 550°C and 1 h to 300°C and 2 h respectively improved the tilt distribution in the $In_xAl_{1-x}N$ films. [1]Yamaguchi et al., Appl. Phys. Lett. 76, 876 (2000). [2]Walukiewicz et al., J. Crystal Growth 269, 119 (2004). [3]Lukitsch et al., Appl. Phys. Lett. 79, 632 (2001). [4]Kurouchi et al., phys. stat. sol. 241, 2843 (2004).

4:50 PM Student

X10, Structural, Optical and Electronic Properties of InN Grown on GaN Substrate by Molecular Beam Epitaxy: *Kejia (Albert) Wang*[1]; John Simon[1]; Jing Zhang[1]; Kai Sun[1]; Tom Kosel[1]; Alexander Mintairov[1]; James Merz[1]; Debdeep Jena[1]; [1]University of Notre Dame

Prior to 2003, the bandgap of InN was believed to be 1.9 eV,[1] but recent measurements on high quality InN have shown that the bandgap of InN is around 0.7 eV.[2,3] However, many of the structural, optical, and electronic properties of this semiconductor are still under investigation. InN has primarily been grown on sapphire substrates.[2] The growth of InN on GaN substrate has not been studied in detail. In this work, we report a study of the growth of high quality InN epitaxial films on GaN by radio frequency plasma-assisted molecular beam epitaxy (RF-MBE). The structural, optical and electronic properties are presented. To improve the film quality, a two-step growth mode is used: InN is first nucleated at a low substrate temperature (~300°C), and then an epitaxial film is grown at a higher substrate temperature (~550°C). Precise control of the III/V flux ratio and the substrate temperature are important during the growth of InN. A phase diagram is developed showing InN can be grown in two regimes: indium rich region and nitrogen rich region. Growths of InN under different conditions are presented and a growth window to obtain high quality InN is obtained. The surface morphology is characterized by AFM and the RMS of a 500nm thick InN film is about 3.7 nm. With high resolution X-ray diffraction, the FWHM of the rocking curve (0002) peak of InN is about 0.37 degree. High resolution TEM and selective area diffraction pattern show that MBE grown InN has a wurtzite crystal structure. The electrical transport is characterized by Hall measurement. High electron concentrations in the order of 1019 cm-3 and high room-temperature mobility of 1089 cm2/Vs for a 1.6μm thick InN layer are observed. Temperature dependent Hall measurement shows that the electron mobility in InN is limited by ionized donor scattering, and the mobile carriers are highly degenerate. Optical characterization by three distinct techniques: photoluminescence, absorption, and FTIR unequivocally show that the fundamental bandgap of the MBE grown InN is around 0.7 eV. [1]T. L. Tansley and C. P. Foley, "Optical band gap of indium nitride", Phys. Stat. Sol. c, 59:3241–3244, 1986. [2]K. M. Yu, Z. Liliental-Weber, W. Walukiewicz, W. Shan, III J. W. Ager, S. X. Li, R. E. Jones, E. E. Haller, Hai Lu, and William J. Schaff, "On the crystalline structure, stoichiometry and band gap of InN thin films", Appl. Phys. Lett., 86:071910, 2005. [3]Y. Nanishi, Y. Saito, T. Yamaguchi, T. Araki, T. Miyajima, and H. Naoi, "Recent development of InN RF-MBE growth and its structural and property characterization", Phys. Stat. Sol. c, 1:1487–1495, 2004.

Session Y: Epitaxy for Devices

Thursday PM — Room: Conference Room 106
June 29, 2006 — Location: Pennsylvania State University

Session Chairs: Michael Tischler, Ocis Technology; Archie L. Holmes, University of Texas

1:30 PM

Y1, Selective MBE Growth of Hexagonal Networks of GaAs Triangular Nanowires on (111)B Patterned Substrates: Isao Tamai[1]; Takahiro Tamura[1]; Taketomo Sato[1]; *Hideki Hasegawa*[1]; Tamotsu Hashizume[1]; [1]Hokkaido University

We have recently proposed a hexagonal binary decision diagram (BDD) quantum circuit architecture[1,2] for large scale integration of quantum devices. Here, quantum path-switching devices controlling flow of a single or few electrons, are formed on a hexagonal nanowire network as a directed graph for a logic function. Feasibility of this approach was demonstrated by using etched nanowire networks prepared by EB lithography and etching.[2] However, future circuits require much denser networks of nanowires with smaller wire sizes. For this, we need an epitaxy technique by which the shape, size and position of the nanowire can be controlled. In this paper, we report on successful selective MBE growth of a hexagonal network of GaAs triangular nanowires on (111)B patterned substrates for future BDD circuits. (111)B orientation is preferable, because the basic path switching BDD node device has a three-fold symmetry. Stripe patterns and hexagonal patterns of <-1-12>-oriented mesas were prepared on the substrate by EB lithography and wet etching. After growth of a GaAs buffer layer, supply of AlGaAs/GaAs/AlGaAs layers resulted in self-organized formation of an embedded trapezoidal GaAs quantum wire (QWR) with a size smaller than the initial mesa top width. Evolution of cross-section during growth was investigated by cross-sectional SEM observation of repeated QWR growth. It was found that the lateral wire width was determined by two facet boundary planes (FBP),[3] each of which is the boundary between two grown regions on the neighboring facets. From the growth experiments, basic data such as temperature and composition dependences of the FBP angle were determined, and they were fed into our growth simulator based on Nernst-Einstein equation.[3] Experiment and simulation showed excellent agreements on the trapezoidal wire shape, size and position of the QWR. As a special case, growth conditions to realize a triangular shaped wire were obtained by simulation, and subsequent growth experiments actually produced wires with desired triangular shape and size. A minimum base width of the wire of 40 nm and a further reduction seems possible. The triangular shape seems to be particularly promising for building quantum devices with tight control by a top gate. Using a hexagonal pattern, hexagonal networks of triangular nanowires were grown and a maximum node density of 1 x 107 cm-2 has been achieved. Such networks exhibited a strong and narrow PL peak whose assignment was made on the basis of spatially resolved CL measurements. Such networks seem very promising

for future high-density hexagonal BDD quantum LSIs. [1]H. Hasegawa and S. Kasai, Physica E, 10.149 (2001). [2]S. Kasai, M. Yumoto and H. Hasegawa, Solid State Electron.,.47,199(2003). [3]T. Sato, I. Tamai and H. Hasegawa, J. Vac. Sci. Technol. B 22, 2266 (2004).

1:50 PM Student

Y2, Structural and Electronic Characterization of Homoepitaxial $SrTiO_3$ Films Prepared by Molecular Beam Epitaxy: *Charles M. Brooks*[1]; Wei Tian[1]; Darrell G. Schlom[1]; Shawn Walsh[2]; Leonard J. Brillson[2]; Tassilo Heeg[3]; Jürgen Schubert[3]; [1]Pennsylvania State University; [2]Ohio State University; [3]Forschungszentrum Jülich GmbH

Homoepitaxy is a natural starting place when evaluating the suitability of a deposition technique to grow thin films of electronic materials. It brings the obvious advantages of structural and chemical compatibility, allowing modifications to the intrinsic properties of the material introduced by the growth mechanism itself to be distinguished. Although thin film techniques like molecular-beam epitaxy (MBE), off-axis sputtering, and pulsed-laser deposition (PLD) have been used for decades to grow epitaxial oxide films, and have demonstrated the ability to customize oxide layering at the level of individual atomic layers, the structural and electronic properties of homoepitaxial oxide films grown by these techniques have not been widely reported. With growing interest in utilizing functional and multifunctional oxides in device structures, it is important to assess and contrast the ability of film growth techniques to produce intrinsic oxide properties in thin films. $SrTiO_3$ is an excellent model system as it shares the perovskite structure of many multifunctional materials and can itself (through appropriate doping or strain) exhibit many multifunctionalities including superconductivity, ferroelectricity, high mobility, and a high and tunable dielectric constant. It is available as large single crystals and methods have been developed to prepare the (100) $SrTiO_3$ surface with a specific atomic termination. The homoepitaxial growth of $SrTiO_3$ by PLD at 700°C was recently reported by Ohnishi *et al.* (Appl. Phys. Lett. 87, 241919 (2005)). This careful work by a leading PLD group revealed a number of surprises. They found that the structural properties of homoepitaxial $SrTiO_3$ films are extremely sensitive to deposition conditions. Although single-phase epitaxial and fully commensurate films were easily achieved, the films had significantly extended out-of-plane lattice constants and nonstoichiometry (ranging from several percent Sr-rich to Ti-rich) except in an extremely narrow range of laser fluence. The extended lattice constants were found not to be a result of oxygen vacancies. We have studied the structural and electronic properties of homoepitaxial $SrTiO_3$ films prepared on TiO_2-terminated (100) $SrTiO_3$ by reactive MBE at a growth temperature of 650°C in a background oxygen plus ~10% ozone pressure of 5×10^{-7} Torr. In contrast to the PLD results, high-resolution x-ray diffraction (XRD) shows that extended out-of-plane lattice constants are *not* present in homoepitaxial MBE films and the structural perfection of the MBE-grown film is comparable to the underlying substrate. Nonetheless, thickness fringes are observed in XRD for the homoepitaxial $SrTiO_3$ films, indicating a difference in the density between the $SrTiO_3$ deposited by MBE and the underlying $SrTiO_3$ substrate. Cathodoluminescence results contrasting the electronic traps in homoepitaxial $SrTiO_3$ with $SrTiO_3$ single crystals will be reported, as will the effects altering the film stoichiometry and *ex situ* post annealing in oxygen.

2:10 PM Student

Y3, Asymmetric Relaxation of Semiconductor Grade $SrTiO_3$ Films: *Michael D. Biegalski*[1]; Dillon Fong[2]; Yulan Li[1]; Jeffory Haeni[1]; Long Qing Chen[1]; Reinhert Uecker[3]; Paul Reiche[3]; Jeffery Eastman[2]; Paul Fuoss[2]; Stephen Streiffer[2]; Susan Trolier-McKinstry[1]; Darrell G. Schlom[1]; [1]Pennsylvania State University; [2]Argonne National Laboratory; [3]Institute of Crystal Growth, Berlin

Using reactive MBE, strained epitaxial $SrTiO_3$ films were grown on $DyScO_3$ substrates. Films with thicknesses ranging from 50 Å to 1000 Å were prepared to determine the critical thickness. The strain state and structural perfection of these films were examined using synchrotron x-ray scattering at the Advanced Photon Source. These films have excellent crystalline quality with the narrowest rocking curve (FWHM) ever reported for any heteroepitaxial oxide film: 6.5-18 arc sec. The critical thickness of the films is between 350 Å and 500 Å. These films retain excellent crystallinity above the critical thickness, and relax very slowly. This relaxation is not similar to that shown by most oxides, but is closer to the relaxation behavior of high quality semiconductors. These films show strong in-plane orientation dependence of the relaxation due to the orthorhombic substrate. The shorter in-plane direction is almost coherent while the film relaxes along the longer in-plane direction. The dielectric properties of $SrTiO_3$ have been shown to be extremely sensitive to the strain state of the film. Although unstrained $SrTiO_3$ is not ferroelectric at any temperature, we observe these strained $SrTiO_3$ films to be ferroelectric. By inducing this transition it is possible to increase the dielectric constant to 20,000 near room temperature. Due to the sensitivity of $SrTiO_3$ to strain and the anisotropic in-plane strain states the dielectric properties of these materials have also been seen to exhibit in-plane orientation dependence.

2:30 PM Student

Y4, Structural and Magnetic Properties of MBE Grown Single Crystal Co_2MnGe on $SrTiO_3$(001), $BaTiO_3$ (001) and MgO (001) Substrates: *Swedesh Kumar Srivastava*[1]; Christoph Adelmann[1]; Darrell G. Schlom[2]; Charles Ahn[3]; Christopher J. Palmstrom[1]; [1]University of Minnesota; [2]Pennsylvania State University; [3]Yale University

There is an increasing interest in combining metallic ferromagnetic materials with semiconductors and metal oxides for novel device applications. One such application is the formation of multifunctional material heterostructures. In principle, the coupling of magnetic property of the ferromagnetic film and piezoelectric property of piezoelectric material such as $BaTiO_3$ via strain can be used for controlling magnetic properties with an electric field and vice versa. The crystal structure and chemical bonding of these dissimilar materials make heteroepitaxial growth challenging. In order to determine effects of lattice mismatch and interfacial bonding, the Heusler alloy Co_2MnGe has been grown on $SrTiO_3$ (001), $BaTiO_3$ (001), MgO (001) and GaAs(001) substrates. All bulk metal oxide substrates were prepared using ex-situ annealing in flowing O_2. For MBE grown $BaTiO_3$ film on (001) $SrTiO_3$, ex-situ annealing was not used prior to the Heusler overgrowth. AFM was used to optimize the annealing conditions so as to achieve the best surface morphology. Co_2MnGe was found to grow with a 45° in-plane rotation on the oxide surfaces resulting in a lattice mismatch of 3.84%, 1.7%, and – 3.82% for growth on $SrTiO_3$ (001), $BaTiO_3$ (001) and MgO(001), respectively. Surprisingly, the x-ray diffraction data for Co_2MnGe grown below 450°C epitaxially on $SrTiO_3$ and MgO suggest that Co_2MnGe grows in a new relaxed tetragonal phase (a = 5.72Å, c = 5.81 Å). Co_2MnGe films grown at higher temperatures grow in the expected cubic structure. X-ray diffraction also suggests that the higher the growth temperature the better is the crystal quality. The low temperature tetragonal phase, in contrast with the high temperature cubic phase, has induced perpendicular magnetocrystalline anisotropy. Substantial interfacial reactions are found for growth at 600°C on $SrTiO_3$. These results are different from Co_2MnGe growth on GaAs, where Co_2MnGe grows pseudomorphically without in-plane rotation on GaAs(001) despite the 1.6% lattice mismatch. This presentation will emphasize the influence of growth conditions and lattice mismatch on the structural and magnetic properties of Co_2MnGe/metal oxide heterostructures.

2:50 PM Student

Y5, Fabrication and Optical Modulation of Silicon-Filled Capillary Fiber: *Dong-Jin Won*[1]; Hoonsoo Kang[1]; Neil Baril[2]; Adrian Amezcua-Correa[3]; Chris. E. Finlayson[3]; Pier J.A. Sazio[3]; Venkatraman Gopalan[1]; John V. Badding[2]; [1]Materials Research Institute, Pennsylvania State University; [2]Department of Chemistry, Pennsylvania State University; [3]Optoelectronics Research Centre, University of Southampton

We have developed high pressure chemical vapor deposition (HPCVD) technique to incorporate silicon wires into capillary fibers to functionalize optical fibers. Raman scattering spectroscopy revealed that as-deposited Si films inside fibers prepared at 475°C are amorphous. Poly-Si could be induced by heating the fiber at 800°C. 1.55 μm wavelength light was successfully coupled and index-guided through 5 μm diameter Si fibers. In addition, we observed the optical modulation of guided 1.55 μm in Si-filled optical fibers based on the free-carrier plasma dispersion effect, which means the change of refractive index and absorption by the concentration variations of free-carriers of Si. In order to change the intensity of guided 1.55 μm light, we utilized photo-induced electrons and holes by illuminating green light of 532 nm onto Si wires. The Si filled fiber shows the potential of in-fiber Si

modulators for the application of optical switching.

3:10 PM Break

3:30 PM Student

Y6, MBE-Grown $Zn_xCd_{(1-x)}Se/Zn_{x'}Cd_{y'}Mg_{(1-x'-y')}Se$ Multi-Quantum Wells for Intersubband Devices: *Hong Lu*[1]; A. Shen[2]; S. K. Zhang[2]; R. R. Alfano[2]; C. Y. Song[3]; H. C. Liu[3]; M. C. Tamargo[2]; [1]City College of New York and Graduate Center of CUNY; [2]City College of New York; [3]Institute for Microstructural Sciences, National Research Council, Canada

Multi-quantum well (MQW) structures made from II-VI semiconductors have important applications in quantum well infrared photodetectors (QWIPs) and quantum cascade lasers (QCLs) due to their widely adjustable bandgaps. In particular, $Zn_xCd_{(1-x)}Se/Zn_{x'}Cd_{y'}Mg_{(1-x'-y')}Se$ is a II-VI semiconductor system recently investigated in our lab whose emission can cover the whole visible wavelength range by simply changing the QW width. Recently, contactless electroreflectance (CER) was used to determine the conduction band offset (CBO) of the $Zn_xCd_{(1-x)}Se/Zn_{x'}Cd_{y'}Mg_{(1-x'-y')}Se$ system. For a $Zn_{0.5}Cd_{0.5}Se/Zn_{0.29}Cd_{0.24}Mg_{0.47}Se$ single QW the CBO was estimated to be 590 meV[1] and for the limit composition of this lattice-matched system, $Zn_{0.5}Cd_{0.5}Se/Zn_{0.13}Mg_{0.87}Se$, the CBO was estimated to be as large as 1.12 eV[2]. In this work, a series of high quality ZnCdSe/ZnCdMgSe MQWs with different QW thicknesses have been grown on InP substrates by molecular beam epitaxy (MBE). The MQWs were characterized by a series of techniques, including X-ray diffraction (XRD), photoluminescence (PL), time-resolved PL, scanning electron microscopy (SEM), CER, and FTIR measurements. The XRD and PL experimental data show that the grown ZnCdSe/ZnCdMgSe MQWs are lattice-matched and have excellent material quality. The SEM image shows clear structure of the superlattices. Doping of the QW layers by n-type dopants to $10^{+18}/cm^3$ levels, which is needed to obtain IR absorption, has also been accomplished. Intersubband absorption in 3~5 μm range has been observed by FTIR measurements and the results agree well with the theoretical prediction. This work was supported by NSF Grant # ECS0217646, NASA Grant # NCC-1-03009, and the Institute for Ultrafast Spectroscopy and Lasers, and New York State Center for Advanced Technology for Ultrafast Photonic Materials and Applications.

3:50 PM Student

Y7, Effectiveness of SiGe Buffer Layers in Reducing Dark Current in Ge-on-Si Photodetectors: *Zhihong Huang*[1]; Ning Kong[1]; Jungwoo Oh[2]; Sanjay K. Banerjee[1]; Joe C. Campbell[3]; [1]University of Texas at Austin; [2]Sematech; [3]University of Virginia

Epitaxial growth of germanium (Ge) on silicon (Si) has found a large interest in low-cost, high-speed optical receiver applications. This material can be integrated with Si complimentary metal oxide semiconductor integrated circuit (CMOS IC) for long wavelength fiber optical communications and optical interconnects. Dark current is one of the most important parameter for photodetectors in optical receivers. Direct growth of Ge on Si generates many dislocations due to their large lattice mismatch. The large amount of dislocations will form as generation recombination centers and contribute to the dark current of photodetectors and further reduce sensitivity of the optical receivers. We report a method of utilizing silicon germanium (SiGe) as intermediate buffer layers to terminate dislocations at the heterojunction interfaces. By adjusting SiGe compositions, SiGe buffer layers will terminate threading dislocations at heterojunction interfaces, further reducing the dark current of Ge on Si photodetectors. The Ge and SiGe were grown in the ultra-high vacuum chemical vapor deposition (UHVCVD) system on n-type (001) Si wafer with resistivity in the range of 0.008-0.02 Ω-cm. Two wafers, with and without SiGe buffer layers, are compared. On the wafer with SiGe buffer layers, prior to 1μm-thick Ge grown at 600°C, one 0.18 μm-thick $Si_{0.45}Ge_{0.55}$ and one 0.30 μm-thick $Si_{0.35}Ge_{0.65}$ layer were grown at 550°C. Atomic Force Microscopy (AFM) images of the grown SiGe buffer layer show the cross hatch pattern. The final roughnesses of the Ge surface are 0.7nm - 0.9nm for both wafers. Transmission Electron Microscopy (TEM) micrographs also indicate the bend and termination of misfit dislocations at the heterojunction interfaces. Photodiodes have been fabricated on these two wafers. We have seen the dark current densities of the devices dropped from $275mA/cm^2$ to $12mA/cm^2$ at 1V reverse bias for the wafer with SiGe buffer layers. In order to further improve the effectiveness of SiGe buffer layers in reducing dark currents, we will discuss the effect of SiGe buffer layers with multiple Ge compositions and the effect of an in-situ anneal the SiGe buffer layers for 15 minutes at 750°C. By measuring dark current of the devices fabricated on these wafers, it has been shown that individually annealing the SiGe buffer layer will greatly reduce the device dark current by over one order of magnitude without degrading the quantum efficiency and speed of photodetectors, while the number of the SiGe buffer layers didn't show as much effect in reducing dark currents.

4:10 PM Student

Y8, Accurate Carbon Doping System for Low-Voltage and Low-Loss VCSELs: *Yu-Chia Chang*[1]; Chad S. Wang[1]; John E. English[2]; Larry A. Coldren[1]; [1]ECE Department, University of California, Santa Barbara; [2]Materials Department, University of California, Santa Barbara

As the performance of microprocessors keeps increasing, new interconnect architecture with higher bandwidth capacity will be required. Optical interconnects can meet this demand and vertical cavity surface emitting lasers (VCSEL) are ideal for optical interconnects because they have small footprint, can be easily made into arrays, and have higher bandwidth at lower power. However, existing VCSELs do not have the efficiency and necessary bandwidth when formed with small dimensions. The drive voltages need to be reduced without adding undue optical losses. Here we report a new wide-range carbon doping system that incorporates a temperature-controlled CBr_4 source, a variable leak valve to control the doping level, and run/vent valve switches. Low voltage, small diameter 980 nm VCSELs have been grown by molecular beam epitaxy using the improved carbon doping system. The VCSELs have three InGaAs/GaAs quantum wells and a tapered oxide aperture in the cavity. The top mirror is a 30 period carbon-doped distributed Bragg reflector (DBR) and the bottom mirror consists of a 4 period section silicon-doped DBR on top of a 3/4 wavelength n-contact layer, followed by 14 periods of undoped DBR. Because carriers have to propagate through the DBRs, these AlGaAs/GaAs interfaces have to be bandgap-engineered with special grading and doping schemes to eliminate the hetero-barriers, especially for the p-type DBRs because of the low mobility of holes. This imposes stringent requirements on the accuracy of doping in the 10^{17}~10^{18} cm^{-3} range typically used in p DBRs. On the other hand, very high doping in the 10^{20} cm^{-3} range is needed for the contact layer. The temperature of CBr_4 in our system is controlled by a custom-designed system using thermoelectric coolers (TEC). When the p-DBRs were grown, the CBr_4 temperature was kept at -25°C for better control of the doping levels. The p-contact layer was then grown at -10°C to reach 10^{20} cm^{-3} doping. With this TEC controlled approach, accurate doping and wide doping ranges can be realized simultaneously. The VCSELs grown with this carbon doping system have very low threshold voltage of 1.55 V, only 300 mV above the lower limit defined by the quasi-Fermi level separation. These devices show constant differential efficiencies of 75% from 10 μm to 1 μm aperture diameter devices, which indicates tapered oxide aperture can effectively eliminate the optical diffraction loss. With low voltage, hence low electrical dissipation, and high differential efficiency, wall-plug efficiencies are maximized. The wall-plug efficiency for 1 μm diameter devices is 33% and maximum 40% is achieved in 3.5 μm devices. The highest bandwidth achieved is 16 GHz for 2.5 μm aperture devices.

4:30 PM Student

Y9, Optically Pumped GaSb Based "Arsenic Free" Mid IR Vertical Cavity Surface Emitting Laser Design: *Ravi Kalyanam*[1]; Abdenour Amtout[1]; Ralph Dawson[1]; Phil Dowd[1]; Sanjay Krishna[1]; [1]Center for High Technology Materials

Recently there has been a growing interest in the development of semiconductor mid-infrared lasers (MWIR, 2-5 μm) for a variety of military and civilian applications. MWIR Vertical cavity surface emitting lasers (VCSEL), with their intrinsic single-mode behavior, are ideal candidates for many spectroscopic applications, such as trace gas sensing. However, most VCSEL research has been limited to telecom applications and wavelengths. We report the progress on "Arsenic free" optically pumped MWIR VCSEL designs on metamorphic InAlSb epitaxially grown on GaSb substrates. Researchers from our center have earlier demonstrated digital alloy techniques to grow metamorphic InAlSb buffer on GaSb substrate. Our group has also demonstrated optically pumped room temperature

edge-emitting lasers between 2.5-3.3 μm on such graded buffers. Despite promising advances in edge-emitting lasers, there has been little movement on VCSELs until now. The VCSEL structure in this work consists of three 0.5% compressively strained $Ga_{0.57}In_{0.43}Sb$ quantum wells (QW), each 15 nm thick, separated by 15 nm thick $Al_{0.25}Ga_{0.43}In_{0.32}Sb$ barriers in a lambda-cavity between two distributed Bragg reflectors (DBRs) comprised of $Al_{0.73}In_{0.27}Sb$/$Al_{0.25}Ga_{0.43}In_{0.32}Sb$ quarter-wave layers. The entire device structure is lattice matched to the metamorphic $Al_{0.73}In_{0.27}Sb$ buffer. As the refractive indices of these alloy compositions were not known accurately, we used a single effective oscillator model to obtain baseline refractive indices that would go in to our model to predict thickness of quarter-wave layers. To optimize the DBR, we grew several calibration samples and used reflectivity measurements and SEM to characterize them. Our initial samples revealed that the measured reflectivity spectra were blue shifted compared to design wavelengths, requiring an empirical correction to account for model inaccuracies. We optimized the active region independently, before integrating the DBR and the active region. The devices were grown using solid source molecular beam epitaxy (MBE) in a Vacuum Generators V80 reactor, on two side polished, undoped GaSb substrate (100). The device structure was grown on graded metamorphic buffer terminating with an $Al_{0.73}In_{0.27}Sb$ layer. We grew a 15 period bottom stack and a 12 period top stack, on either side of the lambda cavity. The sample showed a good matching between measured and calculated reflectivity spectra, as well as a very good agreement between the dip in the cavity resonance and the peak of gain spectrum. The device was optically pumped by a pulsed Topas optical parametric oscillator (OPO), emitting at 1.4 μm at 77K. We observed the edge emission spectrum was red shifted by about 30 nm in comparison with the 2.3 μm surface emission, which indicated the coupling of the cavity resonance. The device showed two different excitation power dependencies; above an excitation intensity of 2.5mW/cm^2 per pulse, there is a steep rise of the output power for increasing optical excitation.

4:50 PM Student
Y10, Monolithic GaSb-Based VCSEL on Si: *Ganesh Balakrishnan*[1]; Shenghong Huang[1]; Anitha Jallipalli[1]; Arezou Khoshakhlagh[1]; Manish Mehta[1]; Paul Rotella[1]; L. R. Dawson[1]; Sanjay Krishna[1]; D. L. Huffaker[1]; [1]University of New Mexico

Monolithic integration of III-V photonics with Si circuitry offers several desirable features including efficient use of the integrating platform, reduced processing complexity and better heat dissipation. The growth of III-Sbs on Si offers a unique method for achieving this objective. III-Sbs and more specifically, AlSb offers the following advantages over other III-Vs in the growth on Si - thermal expansion coefficients are well matched (a_{Si}=2.05x10^{-6}/cm^2, a_{AlSb}=2. 55x10^{-6}/cm^2), excellent III-Sb morphology can be achieved at low growth temperatures (<450°C) and most significantly, the Sb atoms show a unique mode of self-assembly on smaller lattices that results in the material system producing spontaneous 90° misfits at the epi-substrate interface. This interfacial misfit (IMF) array makes our approach to monolithic III-V growth on Si fundamentally different from the previously reported work. The IMF layer immediately relieves almost the entire strain caused by the 13% lattice mismatch in contrast to other growth modes which produce threading dislocations. This growth mode produces very low defect density (~8x10^5/cm^2) and relaxed materials growth (98%) without the use of a buffer layer. Monolithic vertical cavity surface emitting lasers (VCSELs) on Si are demonstrated under room-temperature, optically pumped conditions. The VCSEL structure is comprised of a GaSb multi-quantum well active region embedded in an Al(Ga)Sb half-wave cavity spacer layer and surrounded by AlGaSb/AlSb distributed Bragg reflectors. In this presentation, we overview the IMF growth mode, material characterization, VCSEL lasing spectra peaked at λ~1.62 μm and light-in versus light-out curves. Materials characerization includes etch-pit density analysis, transmission electron microscopy and RHEED data.

Session Z:
SiC: Characterization

Thursday PM
June 29, 2006

Room: Conference Room 208
Location: Pennsylvania State University

Session Chairs: Robert S. Okojie, NASA Glenn Research Center; Robert E. Stahlbush, Naval Research Laboratory

1:30 PM
Z1, Optical Characterization of Stacking Faults in 4H-SiC PiN Diodes: *Joshua D. Caldwell*[1]; Paul B. Klein[1]; Robert E. Stahlbush[1]; Orest J. Glembocki[1]; Kendrick X. Liu[1]; Karl D. Hobart[1]; Fritz Kub[1]; [1]Naval Research Laboratory

The effect of stacking faults, such as the Shockley (SSF), prismatic (PSF) and in-grown (IGSF), are of interest due to their affect upon the electronic behavior of SiC based devices. While the affect of SSFs is well understood, some controversy remains as to the influence of the PSFs (associated with the carrot defect)[1] and the many varieties of IGSFs that have been observed.[1-3] We present optical beam induced current (OBIC) imaging of basal plane dislocations (BPDs) associated with SSFs, PSFs and three varieties of IGSFs. In OBIC, variations in the contrast are due to the presence of current shunts (bright) or barriers (dark) or changes in the carrier lifetime. The IGSFs studied appeared as triangular areas of either bright (high current) or dark (low current) contrast. Time resolved photoluminescence indicates that none of these IGSFs influence the lifetime and therefore are shunts and barriers, respectively. It is believed that the former nucleated near the substrate/epilayer interface, whereas the latter appeared to start within the epilayer itself. In the carrot defect the IGSF is not always present. From the OBIC images, it is clear that the IGSF varies in size, indicating that nucleation may occur at different times than the PSF and many of them do not span the whole thickness of the n- drift layer. In all cases these IGSFs were observed as areas of dark contrast, while the PSF does not dramatically affect the photocurrent.[4] The OBIC images of SSFs are quire different from that of the IGSF and PSF images. The area near BPDs is dark while the body of the SSF is causes no change in the OBIC. This indicates that the BPDs are more efficient recombination centers than the SSF. In conclusion, it is clear that the many different types of SFs affect the electrical behavior differently. The behavior of IGSFs varies between samples, some acting as current paths and others providing barriers. The nucleation of the IGSF in the carrot defect was determined to differ from the PSF, which may provide insight into the defect growth mechanism. Samples provided by Cree, Inc.; ONR contract N00014-02-C-0302, monitored by Dr. H. Dietrich. [1]M. Benamara, X. Zhang, M. Skowronski *et al.*, Appl. Phys. Lett. 86, 021905 (2005). [2]M. E. Twigg, R. E. Stahlbush, P. A. Losee, *et al.*, Mater. Sci. Forum in press (2006). [3]S. Izumi, H. Tsuchida, I. Kamata, *et al.*, Appl. Phys. Lett. 86, 202108 (2005).[4]J. D. Caldwell, R. E. Stahlbush, O. Glembocki, *et al.*, J. Vac. Sci. Technol., B in press (2006).

1:50 PM
Z2, A 180 A/4.5 kV 4H-SiC PiN Diode for High Current Power Modules: *Brett A. Hull*[1]; Mrinal K. Das[1]; James T. Richmond[1]; Joseph J. Sumakeris[1]; Robert Leonard[1]; John W. Palmour[1]; Scott Leslie[2]; [1]Cree, Inc.; [2]Powerex, Inc.

A 4H-SiC PiN diode has been fabricated that blocks to 4.5 kV and conducts up to 180 A at a forward voltage (V_F) of less than 3.2 V. Under pulsed power, the diode conducted 420 A at a V_F of only 3.36 V. This single-chip 4H-SiC PiN diode, at 1.5 cm x 1.5 cm, is the largest discrete 4H-SiC power device ever reported, with over 2 times the area of the previous largest chip, a 1 cm x 1 cm, 100 A 4H-SiC thyristor.[1] The diode exhibited a leakage current of less than 0.4 μA (or less than 250 nA/cm^2) at 4.5 kV, giving a rated forward current to reverse leakage current ratio of greater than 7 x 10^8. Reverse breakdown occurred sharply near 5 kV at room temperature, but shifted out to over 6 kV when biased at 200°C. Furthermore, V_F at 180 A increased by only 0.15 V following a 50 hour constant forward DC stress at 90 A. The 180 A/4.5 kV 4H-SiC PiN diodes were fabricated on 3 inch 4H-SiC wafers cut 8° off

of the [0001] basal plane. These substrates had an extremely low micropipe density of 0.2 micropipes/cm^2, with all but one micropipe (of 10) located within 0.25 inches of the wafer edge, for an effective micropipe density of 0.03/cm^2 over the central 70% of the wafer area. The PiN diode epitaxial layers consisted of a 2.5 µm thick Al-doped (8 x 10^{18} cm^{-3}) injector layer grown on a 50 µm thick N-doped (2 x 10^{14} cm^{-3}) drift layer and were grown employing a process that significantly reduces the density of screw-type [0001] basal plane dislocations in the epitaxial films, helping to eliminate the V_F drift that is typically observed in 4H-SiC PiN diodes.[2] Diode mesas were isolated with a reactive ion etch, and the diodes were terminated with a junction termination extension. On the best wafer (of two fabricated), five of the six 180 A diodes reached the blocking specification of less than 900 µA (0.5 mA/cm^2) leakage current at 4.5 kV, and the overall lot yield was 8 diodes of 12. This phenomenal single wafer device yield of 83% (or 67% total lot yield) for a 2.25 cm^2 chip demonstrates that extremely high power, discrete SiC devices are commercially feasible with current state of the art 4H-SiC substrates, epitaxy, and device processing and is a testament to the advances in SiC materials and device fabrication technologies. This work was supported by DARPA and Sharon Beermann-Curtin through contract N00014-05-C-0202, monitored by Dr. Harry Dietrich. [1]A. K. Agarwal *et al*., *Mater. Sci. Forum*, in press (2006). [2]H. Lendenmann, *et al*., *Mater. Sci. Forum*, 353-356, 727 (2001).

2:10 PM

Z3, Improvement of PMOS Channel Properties for 4H-SiC P-IGBTs: *Mrinal K. Das*[1]; Sarah K. Haney[1]; Sei-Hyung Ryu[1]; Qingchun Zhang[1]; [1]Cree, Inc.

Advanced power conversion systems require low-loss, >10 kV semiconductor switches for successful implementation into high voltage applications. Unipolar 4H-SiC 10 kV DMOSFETs have been demonstrated with low conduction losses. However, at higher blocking voltages, the insulated gate bipolar transistor (IGBT) becomes attractive due to conductivity modulation of its thick drift layer. The conventional p-channel IGBT (p-IGBT) is favorable due to the good crystalline quality and conductivity of the n-type substrate (collector). However, the major challenge with the p-IGBT is the resistive MOS channel formed by holes. The majority of the SiC MOS effort has focused on improving the MOS electron mobility by reducing states in the upper half of the bandgap via nitridation. First generation p-IGBTs fabricated with nitrided gate oxides produced unacceptably low MOS hole mobility of 1.5 cm^2/Vs. In this paper, we present our efforts to increase the MOS hole mobility and control the threshold voltage ($|V_{TH}|$), thereby improving the p-IGBT performance. From 10 kV SiC device simulations, we determined that a mobility of 5 cm^2/Vs is needed to make the p-IGBT comparable to the DMOSFET. To achieve this goal, our first experiment identified the optimum gate oxidation process. Lateral 400 µm x 400 µm PMOSFETs were fabricated on 5E15 cm^{-3} n-type epilayers grown on 4HN substrates. A heavy aluminum dose was implanted to form source/drain regions and activated at 1650°C. A thermal gate oxide was grown followed by boron-doped poly-silicon deposition. Nickel contacts were made to the source, drain, and body. Several different thermal oxidations centering around our baseline process of 1175°C Dry O_2 + 950°C Wet O_2 + 1175°C NO were investigated. As expected, the highest hole mobility (9 cm^2/Vs) and lowest $|V_{TH}|$ (5 V) were obtained on the 1175°C Dry O_2 + 950°C Wet O_2 (Dry-Wet) process that was originally designed to reduce states in the lower half of the bandgap. Both nitridation annealing and wet oxide growth were found to be deleterious to the PMOSFET turn-on performance. Using the Dry-Wet process, our next experiment involved the fabrication of PMOSFETs on a surface structure identical to the p-IGBT. A deep, heavily doped n-type region (N-well) and a shallow, lightly doped p-type region ($|V_{TH}|$ adjust) were implanted into the channel in addition to the aforementioned process flow. Despite the presence of the heavily doped N-well, the PMOSFETs maintained an acceptably high hole mobility of 6.5 cm^2/Vs which increased to 8.2 cm^2/Vs at elevated temperatures while an adequate $|V_{TH}|$ sustained normally off behavior. This represents a substantial improvement over the first generation p-IGBT, indicating that the p-IGBT is a feasible solution to ultra high voltage switching applications. This work was supported by DARPA through Sharon Beermann-Curtin's contract N00014-05-C-0202, monitored by Dr. Harry Dietrich.

2:30 PM

Z4, Photo and Electro Luminescence Imaging of Carrot Defect in 4H-SiC Epitaxy: *Kendrick X. Liu*[1]; Robert E. Stahlbush[1]; Joshua D. Caldwell[1]; Karl D. Hobart[1]; Francis J. Kub[1]; Evan R. Glaser[1]; [1]US Naval Research Laboratory

The ability to grow high quality SiC epitaxy layers requires non-invasive techniques to monitor the layers. A technique to map whole wafers using ultraviolet photoluminescence (UV-PL) imaging is being developed. UV-PL is a non-contact technique, and post processes after the epitaxial growth can be avoided, thereby, further growth is possible. For it to be a useful technique, UV-PL must demonstrate the ability to examine various defects. UV-PL imaging of basal plane dislocations (BPDs) has been successfully demonstrated and compared to EL imaging[1]. In this report, we present the examination of carrot defects using both UV-PL and EL imaging and show that the features of the carrot defects correlate well with the model proposed by Benamara[2]. This model suggests that the underlying structure of the carrot is that of prismatic stacking faults intersecting basal plane stacking faults forming a stair-rod dislocation at the intersect. A 4H-SiC PiN diode having a metal grid was studied allowing both UV-PL and EL imaging to be performed. UV excitation was performed using the 363.8nm line of a CW argon laser. Forward voltage biasing for EL imaging was performed with probe needles on metal pads. The luminescence image was detected using a liquid nitrogen cooled CCD camera attached to a microscope. UV-PL performed with coinciding area of excitation and area of imaging showed poor contrast due to the background luminescence of dopants. However, excitation away from the area of imaging resulted in improved contrast levels similar to EL imaging. The excited carriers diffuse a significant distance enabling luminescence of the extended defects without exciting the background in their vicinity, which may originate from the heavily doped layers above and below the n- layer. Consequently, the stair-rod dislocations at the intersects of the prismatic faults and basal plane faults within the carrot defects were clearly revealed as bright straight lines extending from the tip of the carrot near the surface down toward the head of the carrot. Furthermore, dark regions bounded by dim lines (Frank partials) indicated the basal plane faults. UV-PL and EL images of carrot defects clearly revealed the major features in the simple model proposed by Benamara. However, our results also showed multiple additional dislocations within a carrot defect. Bright spots also appear at the ends of many of the dislocations. Furthermore, there are zig-zag features near the head of the carrots. In summary, we have developed a PL imaging technique and applied EL, as well as PL, imaging in the study of carrot defects. Samples provided by Cree, Inc.; ONR contract N00014-02-C-0302, monitored by Dr. H. Dietrich. [1]Liu, et al., MRS Meeting, San Francisco, April 17-21, 2006. [2]Benamara, et al., Appl. Phys. Lett. 86, 021905 (2005).

2:50 PM

Z5, Identification of a Three-Site Defect in SI 4H-SiC: *Nelson Y. Garces*[1]; William E. Carlos[1]; Evan R. Glaser[1]; Mark Fanton[2]; [1]Naval Research Laboratory; [2]Electro-Optics Center

High temperature anneals were used to study the evolution of native defects in semi-insulating 4H-SiC grown by PVT or HTCVD methods. The samples were annealed in an argon atmosphere for 30 min at temperatures from 1400°C to 2000°C. Using electron paramagnetic resonance (EPR), we observe a defect which increases significantly with annealing temperature. This spin S = 1 defect is characterized by $g^1 \sim g^2 = 2.0029$; $g^3 = 2.0038$, and a fine structure splitting D ~ 96 G whose principal axis lies in a plane perpendicular to the c-axis. Also resolved are several hyperfine interactions with the low abundant Si (A ~ 5.5 G) and C (A ~ 30 G) neighboring nuclei. A careful analysis of the intensity of these hyperfine lines allows a precise determination of the identity and the quantity of interacting nuclei. This center is diamagnetic in the ground state but can be excited into a paramagnetic triplet state by sub-bandgap light. This center quickly decays upon removal of the excitation source. There are currently two possible models. The first is a VC-CSi-VC complex which could result during annealing by the movement of an adjoining C atom onto the VSi site of the divacancy (VC–VSi) whose intensity decreases. Another possible model for this defect is that of a three-site vacancy involving a VC-VSi-VC. The angular dependence of the hyperfine interactions is being used to distinguish between the proposed models. These may be the simplest of a family of more complex and extended defects that

play a role in the semi-insulating (SI) character of SiC. A search for optical signatures associated with this defect from 0.7-3.2 eV photoluminescence (PL) studies will also be discussed.

3:10 PM Break

3:30 PM

Z6, EPR Characterization of Halide CVD 4H SiC: *Mary Ellen Zvanut*[1]; H. J. Chung[2]; A. Y. Polyakov[2]; [1]University of Alabama at Birmingham; [2]Carnegie Mellon University

Among the methods to grow silicon carbide, one promising approach for obtaining high purity substrates is the use of halide-based precursors during chemical vapor deposition. The halide CVD (HCVD) substrates used for this study were grown using different ratios of $SiCl_4$ and C_3H_8 . As the C/Si molar ratio increased from 0.065 to 0.69, the carrier concentration (N_d) decreased from 10^{18} to 10^6 cm^{-3}. The activation energy (E_a) was not measured for C/Si =0.065, but for all the others E_a increased monotonically from 0.25 to 0.85 eV. All samples were n-type. Here we report the types of point defects in 4H HCVD substrates as determined by electron paramagnetic resonance (EPR) spectroscopy measured at 4K in the dark and after illumination. The primary defect observed in the EPR spectra of samples with the highest N_d (10^{18} cm^{-3}) was substitutional nitrogen. Nitrogen was not detected in the other samples where N_d was less than 10^{15} cm^{-3},presumably due to the low signal/noise ratio. Rather, all of these samples contained at least two types of defects as determined by the g values measured with the magnetic field parallel to the c-axis. One signal with g=2.0044 is characteristic of centers containing a mixture of Si-C bonds; while a second with g=2.0027 is likely a pure C-related defect. The isotropic nature of the 2.0027 center suggests that it is a simple carbon dangling bond; however the 2.0044 center is anisotropic and may reflect one of several defects typical of high purity SiC. The two samples with largest activation energy (E_a=0.85 eV) and C/Si ratio (0.69) exhibited the EPR hyperfine pattern of the positively charged carbon vacancy. Except for substitutional nitrogen, there was no obvious correlation between the C/Si ratio and the type of centers observed in these materials. However, several interesting features should be noted. The 2.0044 center appeared only in those samples with N_d = 10^{11} cm^{-3} and E_a = 0.5 eV, and the concentration of the center is altered after illumination with light of energy greater than 0.7 eV. Both facts suggest that the 2.0044 center is a deep level defect. The observation of V_C^+ in samples with an excess of carbon in the carrier gas, C/Si=0.69, suggests that the substrate remains silicon rich despite the carbon overpressure. E_a in samples with lower C/Si ratios was below that expected for observation of V_C^+. Optical studies used to test for the presence of V_C^+ and annealing treatments which clarify the source of the anisotropic 2.0044 center will be reported to provide a thorough study of the point defects in HCVD 4H SiC, a promising method for producing high purity SiC. The work at UAB was supported by the National Science Foundation.

3:50 PM

Z7, Effect of Electron-Irradiation on Deep Centers in High-Purity Semi-Insulating 6H-SiC: *Zhaoqiang Fang*[1]; Gary C. Farlow[1]; Bruce Claflin[1]; David C. Look[1]; [1]Wright State University

Energetic-particle irradiation in conjunction with deep level transient spectroscopy (DLTS) has been used to study point-defect related traps in 6H-SiC for more than one decade. Several defect-related centers have been found in electron-irradiated, n-type 6H-SiC, and their energies range from 0.20 - 1.45 eV below the conduction band. Common designations of these centers, following Chen[1], and Balandovich[2], are ED1 (0.23 eV), E1/E2 (0.34/0.40 eV), Ei (0.50 eV), Z1/Z2 (0.62/0.64 eV), L9 (0.81 eV), L10 (1.27 eV), and L11 (1.45 eV). Most of them are believed to be related to vacancies, but the specific type of vacancy is still in doubt. For semi-insulating SiC, on the other hand, DLTS cannot be used for trap studies and so we have applied thermally stimulated current spectroscopy (TSC)[3]. The material investigated here is high-purity, semi-insulating (HPSI) 6H-SiC grown by the advanced physical vapor transport technique, and it has a conductivity activation energy of 1.1 eV, a 300-K resistivity of 1 x 10^{11} Ω-cm, and low concentrations of background shallow impurities (N and B in the low or mid-10^{15} cm^{-3} range). At least ten traps are found in the TSC spectrum of this material, and by using a heating rate of 0.3 K/s, they are peaked at 90 K, 105 K, 115 K, 150 K, 175 K, 205 K, 250 K, 265 K, 300 K, and 355 K, respectively. Some of them are associated with impurities, such as N, Ti, Al and B; others are related to point defects, such as E1/E2 and Z1/Z2, which are also observed in the electron-irradiated, conductive SiC, mentioned above. When we irradiate this HPSI SiC with 1-MeV electrons to a fluence of 4 x 10^{15} cm^{-2}, we find four new features, at 135 K, 175/185 K, 300 K, and >400 K, respectively. These new traps have activation energies of 0.24 eV, 0.33/0.35 eV, 0.62 eV, and ~1.2 eV, respectively, and are thought to be due to ED1, E1/E2, Z1/Z2, and L10. Along with the features which *emerge* due to the irradiation, others *disappear*, including features at around 145/155 K, likely related to shallow boron. Possibly the boron centers are complexing with mobile irradiation-inducted defects and becoming either deep (e.g., D centers), or neutral. Finally, a bias-related enhancement of the 175-K trap, studied earlier, becomes less prominent. In summary, we find that: i) many deep centers in as-grown HPSI 6H-SiC are indeed due to point defects and some of them can even dominate the material resistivity; and ii) electron irradiation creates some traps, and destroys others. [1]X.D. Chen et al., Phys. Rev. Lett. 92, 125504 (2004). [2]V.S. Ballandovich, Semiconductors, 33, 1188 (1999). [3]Z-Q. Fang et al., in the Proceedings of 2005-ICSCRM (in press).

4:10 PM Student

Z8, Deep Level Defects which Limit Current Gain in 4H SiC Bipolar Junction Transistors: *Corey Cochrane*[1]; Patrick Lenahan[1]; Aivars Lelis[2]; [1]Pennsylvania State University; [2]Army Research Laboratories

Progress has been made in the production of SiC bipolar junction transistors (BJTs) over the past few years; however, these devices still exhibit modest current gains. Short minority carrier lifetimes within the base are the cause of these relatively moderate current gains. Unfortunately, essentially nothing is known with certainty about the chemical and physical nature of the deep level recombination center defects responsible for the short lifetimes. In this study we use a very sensitive electron spin resonance (ESR) detection technique specifically sensitive to recombination centers in fully processed devices: spin dependent recombination (SDR). We apply SDR to fully processed 4H-SiC BJTs and directly observe the recombination defects. To the best of our knowledge, these results represent the first electron spin resonance results of any kind reported in a fully processed SiC bipolar junction transistor and provide the first direct observations of the chemical and physical nature of recombination centers in SiC bipolar junction transistors. Our observations provide insight into the physical and chemical nature of these defects and demonstrate the potential power of SDR in studies of SiC BJT problems. The devices that were utilized are npn BJTs fabricated on 4H-SiC with 15 μm thick n-type collectors doped to 4.8x1015 cm^{-3}, a 1μm thick p-type base doped to 2x1017cm^{-3} and a 1.5 μm thick n-type emitter doped to 3x1019cm^{-3}. The devices were fabricated by Cree Inc. The SDR measurements were made on homemade SDR spectrometers at X-band at room temperature. The SDR measurements were made by monitoring the collector base current in the BJTs with the junction forward biased. Our preliminary results suggest most strongly that "intrinsic" defects play very important roles in the recombination in these devices. We observe a dominant defect resonance with a g ~ 2.002 when the magnetic field vector is parallel to the crystalline c-axis and a line width of about 4 to 5 Gauss. We find semi-qualitative agreement between our SDR versus bias results and the response anticipated for recombination centers in the near base-collector junction region.

4:30 PM

Z9, Performance of SiC Field-Effect Devices at Elevated Temperature during Several Months of Continuous Operation: *Ruby N. Ghosh*[1]; Reza Loloee[1]; [1]Michigan State University

Silicon carbide is a promising candidate for electronic devices that can withstand large power dissipation and/or continuous operation at high temperature. As the native oxide of SiC is none other than SiO2 there is an interest in developing gate controlled field-effect devices. However, continuous operation in industrial applications requires a reliable gate oxide. We report on the stable operation of an array of n-MOS SiC capacitors that have been running for *four months* at 620 C. These results were obtained from several devices, with gate diameters of 500-1000 μm, on two independently fabricated chips. We initially characterized the devices as a function of temperature from 350 to 620 C, via 1 MHz capacitance - voltage (C-V) measurements. Nearly ideal C-V characteristics were obtained from accumulation into depletion. The accumulation capacitance agreed within our

experimental uncertainty with the measured oxide thickness, independently determined via spectroscopic ellipsometery, and gate area. The flat band voltage agreed well with theory. Out of the 52 capacitors on each 1 cm x 1 cm chip our yield was > 50%, including the large area (500 and 1000 μm) gates. The devices were fabricated on 6H-SiC substrates (2E16 N/cm3 epitaxial layer). The gate oxide was grown via dry oxidation at 1150 C, followed by a 900 C Ar anneal and a 2 hour 1175 C NO passivation anneal. The gate metal was 100 nm of sputtered Pt. One of the large area capacitors from each chip was chosen for long term testing as a gas sensor at 620 C. While holding the device at a constant capacitance, we subjected it to alternating pulses of oxidizing and reducing gases, and monitored the gate voltage necessary to maintain the capacitance set point, as the sensor signal. Any changes in the electrical properties of the gate insulator would be immediately observed in the device output. On the first chip a 1000 μm diameter capacitor was monitored continuously for 18 days at 620 C. No degradation in device performance was observed and the sensor signal was stable to +/- 2% over the entire time period. Note that the device was inadvertently subjected to several electric field transients due to power failures. A 500 μm capacitor on a second chip has now been operating for a cumulative time of four months at 620 C, the magnitude of the sensor signal has remained stable to +/- 6% over this period. C-V characteristics of the device taken at various times during this extended test will be presented. Our results demonstrate that n-MOS SiC capacitors have the required stability and reliability for long term operation under harsh conditions.

4:50 PM
Z10, Late News

Session AA: Organic/Inorganic Hybrid Photovoltaics

Thursday PM — Room: Conference Room 207
June 29, 2006 — Location: Pennsylvania State University

Session Chairs: Max Shtein, University of Michigan; David J. Gundlach, National Institute of Standards and Technology

1:30 PM Invited
AA1, Metal Nanostructure Enhanced Organic Solar Cells: *Peter Peumans*[1]; [1]Stanford University

The power conversion efficiency of organic solar cells is limited by a trade-off between efficient charge transport, exciton transport and light absorption. In this talk, I will present our work on approaches that combine molecular materials with inorganic nanoparticles and nanocrystals to overcome these efficiency limitations. We find that the inclusion of nanoscale metal structures into the active region of organic solar cells can be used to enhance optical absorption. If exciton quenching at the metal/organic interface is prevented using dielectric spacers, we find that light absorption can be enhanced without deleterious effects on the exciton lifetime. Moreover, we find that such metal nanostructures influence the exciton diffusion process by modifying the near-field of exciton dipoles. To fabricate multilayer structures consisting of molecular and polymer materials in combination with engineered nanoscale metal structures, we have developed an aerosol deposition tool that allows us to deposit multilayer and doped films of virtually any material without solvent orthogonality requirements. Furthermore, this tool allows us to vacuum deposit materials that cannot be sublimed such as polymers, large molecules, and metal and inorganic semiconductor nanoparticles.

2:10 PM Student
AA2, Organic Photovoltaic Cells with External Antennas: *Jonathan K. Mapel*[1]; Timothy D. Heidel[1]; Celebi Kemal[1]; Marc A. Baldo[1]; [1]Massachusetts Institute of Technology

The process of photosynthetic light conversion differs from traditional photovoltaics in the spatial organization of energy transduction events. We adapt a synthetic variant of the photosynthetic architecture to organic solar cells by introducing a synthetic light harvesting antenna which couples light energy to active layers by near field energy transfer mediated by surface plasmon polaritons. We show theoretically this process can occur with efficiencies exceeding 50% and demonstrate that transfer results in increased quantum efficiency in organic photovoltaic cells.

2:30 PM Student
AA3, A Quantum Dot Photovoltaic Device Fabricated via Microcontact Printing: *Alexi Arango*[1]; David Oertel[2]; Moungi Bawendi[2]; Vladimir Bulovic[1]; [1]Massachusetts Institute of Technology, Department of Electrical Engineering; [2]Massachusetts Institute of Technology, Department of Chemistry

We fabricate an organic-inorganic layered photovoltaic device consisting of a monolayer or multilayer of cadmium selenide (CdSe) quantum dots and the wide band gap hole transport polymer Poly(N,N'-bis(4-butylphenyl)-N,N'-bis(phenyl)benzidine (poly-TPD). The quantum dot film is deposited onto the poly-TPD layer using a non-destructive microcontact printing method. The top and bottom contacts are provided by ITO electrodes, allowing for near transparency. Current-voltage characteristics show low dark currents in reverse bias and good rectification. Excitation of the quantum dots yields a strong, saturated photoresponse, open circuit voltages of +0.5V and a fill factor of 0.4. Measurement of the locked-in photocurrent under bias reveals a strong photocurrent signal extending out to +1.5V, in excess of the built-in acceptor-donor energy level offset of ~0.8V. We attribute the photocurrent voltage depence to efficient charge extraction, low recombination rates at the heterojunction and uniform surface coverage provided by the microcontact printing method.

2:50 PM
AA4, Late News

3:10 PM Break

3:30 PM
AA5, Transparent Conducting SWNT Electrodes for Plastic Solar Cells: *Aurelien Du Pasquier*[1]; Husnu Emrah Unalan[1]; Alokik Kanwal[1]; Steve Miller[1]; Manish Chhowalla[1]; [1]Rutgers University

We describe the use of single-wall carbon nanotube (SWNT) thin films as transparent and conducting electrodes[1] for hole collection in P3HT-PCBM (poly (hexyl) thiophene- [6-6] phenyl-C61-butyric acid methyl ester) organic photovoltaics. The device layer configuration is Glass/SWNT/PEDOT: PSS/P3HT-PCBM/In-Ga. The P3HT-PCBM layers were drop-cast from a chlorobenzene solution. By adjusting the SWNT work-function with a coating of PEDOT: PSS, we show that they can form a large area, transparent and conducting hole conducting electrode. We also introduce the use of Indium-gallium eutectic cathode top-contact as a convenient replacement to evaporated aluminum[2]. We report a power conversion efficiency of 1%, a fill factor (FF) of 0.3 and a short-circuit current of 6.5 mA/cm^2 under 1000 W/m^2 polychromatic white light measured in air[3]. These values are comparatively higher than our reference cells of similar thickness (800 nm) made on ITO-PET (Indium-Tin oxide-Polyester) substrates. This is attributed to the three dimensional nature of the interface among the carbon nanotubes and the P3HT-PCBM nanocomposite. The SWNT coating thickness is controllable, and linked to its transparency and conductivity. We correlate these parameters with the performance of the solar cells. Our results indicate that transparent SWNT thin films could be a viable alternative to ITO for photovoltaic devices. Our latest results will describe flexible P3HT-PCBM solar cells using the SWNT coatings on PET substrates. [1]Zhuangchun Wu, Zhihong Chen, Xu Du, Jonathan M. Logan, Jennifer Sippel, Maria Nikolou, Katalin Kamaras, John R. Reynolds, David B. Tanner, Arthur F. Hebard, Andrew G. Rinzler Science, 305, 1273 (2004). [2]Aurelien Du Pasquier, Steve Miller and Manish Chhowalla, Solar Energy Materials and Solar Cells, in press (2005). [3]Aurelien Du Pasquier, Husnu Emrah Unalan, Alokik Kanwal and Manish Chhowalla Applied Physics Letters 87,1, (2005).

3:50 PM Student
AA6, Hybrid Conjugated Polymer/Nanostructured ZnO Photovoltaic Devices: *Dana C. Olson*[1]; Sean E. Shaheen[1]; Matthew S. White[1]; Reuben T. Collins[2]; David S. Ginley[1]; [1]National Renewable Energy Laboratory (NREL); [2]Colorado School of Mines

Conjugated polymer/nanostructured oxide semiconductor composites are promising systems for use in low cost organic photovoltaic devices.

Incorporation of a conjugated polymer into a porous oxide semiconductor can result in a bulk heterojunction device in which photogenerated charges have unimpeded transport pathways to the electrodes. These hybrid solar cells can take advantage of the high electron mobilities found in metal oxide semiconductors such as ZnO, while largely retaining the solution-based processing available to organic semiconductor devices. In addition, the morphology of the composite material can be determined in a systematic way by varying the growth conditions of the inorganic component. Here, we demonstrate solution growth of ZnO nanofibers that are vertically aligned with respect to the substrate. Once grown, the porous nanostructures are filled with a light absorbing organic semiconductor such as poly(3-hexylthiophene) (P3HT). Here we discuss fabrication and characterization of preliminary composite devices, with power conversion efficiencies of 0.5% for ZnO nanofiber/P3HT devices. The electron affinity of ZnO is reduced with a corresponding increase in the photovoltage in the device.

4:10 PM Student

AA7, Nanostructured Hybrid Solar Cells: *Vignesh Gowrishankar*[1]; Shawn R. Scully[1]; Albert T. Chan[1]; Michael D. McGehee[1]; [1]Stanford University

Hybrid solar cells seek to increase efficiencies by combining the advantages of semiconducting polymers and inorganic semiconductors. We report on the fabrication and performance of two such bilayer, hybrid systems, amorphous silicon (a-Si)/poly-3-hexylthiophene (P3HT) and a-Si/poly(2-methoxy-5-(2'-ethyl-hexyloxy)-1,4-phenylene vinylene) (MEH-PPV). These cells are compared with bilayer titania / P3HT and titania/MEH-PPV cells. The a-Si/P3HT system is found to be at least as efficient as the titania/P3HT system, despite the fact that the external quantum efficiency of the former is predicted to be more than 3 times lower than that of the latter, due to differences in the refractive indices, absorption coefficients and thicknesses of the titania and a-Si layers. By comparing the four systems of P3HT and MEH-PPV on a-Si and titania, we highlight the need for careful choice of inorganic and organic materials to make efficient hybrid solar cells, especially with regard to the bandgaps, the LUMO levels and the HOMO levels. In these four systems, upon illumination, we demonstrate that exciton-diffusion followed by forward-electron-transfer may be competing with Forster-energy-transfer followed by backward-hole-transfer for splitting excitons. The former mechanism for exciton splitting is enhanced by high exciton diffusion lengths and a suitable LUMO offset, while the latter mechanism is enhanced by large Forster radii and a suitable HOMO offset. We observe that in systems where Forster energy transfer cannot occur (e.g. titania/polymer), the LUMO offset is critical, while in systems where strong Forster energy transfer can occur (e.g. a-Si/MEH-PPV), the HOMO offset may become critical. The most efficient of these four hybrid systems is found to be a-Si/P3HT, with a power-conversion efficiency of about 0.16% (under simulated 1000 W/m^2 AM 1.5 illumination). To achieve higher efficiencies it is necessary to increase the interface area between the two semiconductors so that more excitons can be split. To effect this we use a nanostructure, in the a-Si, of pillars/ridges separated by trenches into which the P3HT is infiltrated. About 150 – 200 nm deep trenches would contain enough P3HT to absorb all the light. Trenches that are less than two exciton diffusion lengths wide would conceivably allow for maximized exciton splitting. Furthermore, the vertical walls of the trenches would allow for superior chain packing and thus higher charge carrier mobilities in the P3HT. We use techniques such as Nanosphere Lithography and Block Copolymer Lithography to create the nanopattern template on the a-Si. Liftoff followed by Reactive Ion Etching yields the required nanostructured a-Si. After melt-infiltration of the P3HT into the nanostructure, we investigate the extent of efficiency enhancement as well as potential problems present in these nanostructured hybrid solar cells.

4:30 PM Student

AA8, Investigating Charge Dynamics of Small Molecule Organic Heterojunction Interfaces in Lateral Photoconductor Devices: *John Ho*[1]; Vladimir Bulovic[1]; [1]Massachusetts Institute of Technology

We are studying charge transport and exciton dynamics in a bi-layer, small molecule organic, lateral photoconductor consisting of an absorbing layer deposited on a transport layer. The bi-layer photoconductor device structure allows us to separate the study of exciton dynamics and charge carrier dynamics. In addition we can adjust each layer independently to maximize device performance. The devices consist of a series of gold interdigitated fingers (W x L = 1500um x 4um) spaced 8um apart. The gold electrodes are photolithographically defined on glass before the organic layers are thermally evaporated. Locked-in measurements of the photocurrent spectra suggest external quantum efficiencies ranging from 10-15%. These initial experiments are aimed at determining how the carriers generated by exciton dissociation at the interface affect device parameters, such as conductivity and mobility. Ultimately we are interested in doping the absorbing layer with exciton-quenching materials to modulate the photoconduction, simulating a solid-state chemical sensor.

4:50 PM

AA9, Late News

Session BB: Oxide Thin Film Integration III

Thursday PM, June 29, 2006
Room: Conference Room 206
Location: Pennsylvania State University

Session Chairs: Darrell G. Schlom, Pennsylvania State University; Patrick Lenahan, Pennsylvania State University

1:30 PM Student

BB1, GaN MOSFET with ALD High-k Gate Dielectric: *Yanqing Wu*[1]; Peide (Peter) Ye[1]; Glen Wilk[2]; [1]Purdue University; [2]ASM America

The search for novel gate dielectrics on GaN is initiated by their relatively high gate leakage currents on GaN HEMTs which limit the performance and reliability of GaN HEMTs for high-power RF applications.[1-4] Novel device structures and gate dielectrics are needed to further drive Si CMOS integration, functional density, speed and power dissipation, and extend CMOS front-end fabrication to and beyond the 22-nm node. One emerging strategy is to use III-V compound semiconductors as conduction channels, while integrating these high mobility materials with novel dielectrics and heterogeneously integrating them on Si or SOI. GaN is a very promising material because it has high mobility, low Ion/Ioff ratio due to wide bandgap, and the demonstrated feasibility to integrate on Si.[5] The reserach on integration of ALD high-k dielectrics, such as Al2O3, on GaN is of great interest. We present experimental results, for the first time, on a GaN MOSFET using ALD Al2O3 as a gate dielectric. A 40 nm undoped AlN buffer layer, a 3 μm undoped GaN layer, and a 100 nm Si doped 5*1017/cm3 channel layer were sequentially grown by MOCVD on a 2-inch sapphire substrate. After appropriate surface pretreatment, 8 nm-30nm ALD Al2O3 was deposited at 300°C using ALD. The standard planar device fabrication process, as reported before on ALD Al2O3 GaN MOS-HEMTs,[4] was applied. The GaN MOSFET exhibits very little hysteresis in the high frequency CV measurement in the wide bias range of 15 V, demonstrating the good quality of the ALD bulk oxide and interface on GaN surface. Compared to the MESFET with the same design, the gate leakage current of MOSFET is several orders of magnitude lower at the positive bias. The channel current is 2-3 times higher than the one from MESFET, indicating the effectiveness of surface passivation with ALD Al2O3. The 1-μm gate-length MOSFET shows 200 mA/mm channel current which is about one order of magnitude higher than previously reported Gd2O3/GaN MOSFET.[6] The GaN surface mobility at Al2O3/GaN interface is also calculated from the accumulated current in the mobility region and will be compared to those from Al2O3/AlGaN/GaN, Al2O3/GaAs and Al2O3/InGaAs. These device results demonstrate that ALD is able to form high-quality high-k dielectrics on GaN and open the ways to realize reliable and scalable enhancement-mode GaN devices using ALD Al2O3 for future Si CMOS technology. [1]M.Asif Khan et al., IEEE EDL 21, 63 (2000). [2]R. Mehandra et al., APL 82, 2530 (2003). [3]T. Hashizume et al., APL 83, 2952 (2003). [4]P.D. Ye, et al., APL 86, 063501 (2005). [5]E.M. Chumbes, et al., IEDM, 397 (1999). [6]J.W. Johnson, et al., APL 77, 3230 (2000).

1:50 PM Student

BB2, CV Studies on ALD Al_2O_3/GaAs and Al_2O_3/InGaAs Interfaces for Enhancement-Mode GaAs MOSFET Application: *H. C. Lin*[1]; Yi Xuan[1]; Peide (Peter) Ye[1]; Glen Wilk[2]; [1]Purdue University; [2]ASM America

Novel device structures and gate dielectrics are needed to further drive Si CMOS integration, functional density, speed and power dissipation, and extend CMOS front-end fabrication to and beyond the 22-nm node. One emerging strategy is to use III-V compound semiconductors as conduction channels, to replace traditional Si or strained Si, while integrating these high mobility materials with novel dielectrics and heterogeneously integrating them on Si or SOI. In our previous work, we have succeeded to integrate ALD high-k dielectric Al_2O_3 on GaAs and InGaAs and demonstrated high performed depletion-mode GaAs-based MOSFETs. For VLSI or high-speed digital applications, enhancement-mode GaAs MOSFETs are real devices of interest. We present CV measurement results, for the first time, on an inversion channel enhancement-mode GaAs MOSFET using ALD Al_2O_3 as a gate dielectric. A 150 nm p-doped 5E17 /cm^3 buffer layer and a 300 nm p-doped 1E17 /cm^3 channel layer were sequentially grown by MOCVD on a 2-inch GaAs p+ substrate. After appropriate surface pretreatment, 8 nm-30nm ALD Al_2O_3 was deposited at 300°C using an ASM Pulsar2000TM ALD module. The ALD Al_2O_3 is served not only as a gate dielectric but also as an encapsulation layer. The source and drain contact regions are Si implanted and activated at 800°C by RTA. Dopant activation annealing is a very critical step which not only activates the dopant but also must preserve the smoothness of the interface at the atomic level. The ohmic contact resistance of less than 1 Ω•mm demonstrates good process on implantation and activation. The high-quality of Al_2O_3/GaAs and Al_2O_3/InGaAs interfaces after process is demonstrated by the C-V measurements on the finished devices. The 1KHz-1MHz CV curves show sharp transition from depletion region to accumulation region with negligible hysteresis. The 1KHz-1MHz frequency dispersion is less than 5%. The frequency dependent flat band shifts are observed after high temperature annealing. The strong electron inversion is also observed at CV measurements. The rough estimation of mid-gap interface trap density (Dit) is ~1E11 /cm^2-eV or better. More detailed analysis is on going. For a 30 nm-Al_2O_3 n-channel MOSFET with a gate dimension of 1 * 100 μm^2, a functional inversion-channel enhancement-mode GaAs MOSFET with a maximum drain current of 130 μA/mm is demonstrated. The low drain current could be improved by optimizing implant and annealing conditions to reduce parasitic resistance and surface scattering.

2:10 PM Student

BB3, GaAs Growth on Silicon Substrates Using a Thin (~80 Nm) Si_XGe_{1-x} Step-Graded Buffer Layer for High-k III-V MOSFET Applications: *Michael M. Oye*[1]; Davood Shahrjerdi[1]; Xiaojun Yu[2]; Sagnik Dey[1]; David Q. Kelly[1]; Shannon D. Lewis[1]; Mark A. Wistey[2]; Jeffrey B. Hurst[1]; Sachin Joshi[1]; Terry J. Mattord[1]; James S. Harris[2]; Archie L. Holmes[1]; Sanjay K. Banerjee[1]; [1]University of Texas at Austin; [2]Stanford University

The thrust to achieve high-mobility CMOS architectures on Silicon substrates can be accomplished with the integration of III-V semiconductor channels. Historically, III-V channels have been incompatible with conventional High-k gate dielectrics and the mature Silicon-based process technology. In this presentation, we will discuss our efforts in tackling two of the key compatibility issues involving High-k III-V MOSFETs on Silicon substrates: Growth of device-quality GaAs on Silicon, and improving the interface quality between a conventional High-k gate dielectric and a III-V semiconductor channel material. Our experimental procedures for the epitaxial growths involved a combination of Ultra-high Vacuum Chemical Vapor Deposition (UHVCVD) and Migration-enhanced Epitaxy (MEE). The UHVCVD growth of compressively-strained $Si_{1-x}Ge_x$ buffer layers were done on (100) silicon substrates cut 6° off-axis toward the [110] direction. The $Si_{1-x}Ge_x$ layers were step-graded using four different Ge compositions (x=0.20, 0.25, 0.40, and 1.0) to prevent defect propagation into the pure Ge layer. Instead of more commonly-used thick SiGe buffer layers, our step-graded layers allowed for a total buffer thickness of ~80 nm. These UHVCVD-grown Ge-on-Si samples were transferred to a Varian Gen-II Molecular-beam Epitaxy (MBE) system for the MEE growth of GaAs. Typically, substrate temperatures in excess of 400°C are necessary for growing device-quality GaAs. Unfortunately, we have experienced that any growth or annealing process greater than 400°C, for any length of time, led to rough (>1nm RMS) GaAs surfaces on our Ge-on-Si samples that were unsuitable for depositing thin High-k gate dielectrics. We have circumvented this limitation by growing low-temperature MEE GaAs (<400°C) with a surface roughness of ~0.9nm. The High-k gate dielectric was then deposited before any high temperature process was done. As part of the High-k gate stack fabrication process, we have also discovered that the MBE growth of a thin 1.5 nm Ge passivation layer, immediately following the GaAs growth, significantly improves the interface between the GaAs and the HfO_2. One of the key suitability tests for High-k III-V MOSFET applications is to fabricate a Metal-Oxide-Semiconductor (MOS) capacitor and measure the Capacitance-Voltage (C-V) characteristics. A minimum GaAs thickness of 30nm was required to obtain reasonable C-V data. From this, we have observed improved C-V characteristics from samples that were only RTA-annealed after the HfO_2 deposition, when compared to those samples that were also subjected to higher growth and/or annealing temperatures. We will further discuss these various conditions and present additional material characterization data.

2:30 PM

BB4, Passivation of Ge Surface Using Ceria: *Yerassimos A. Panayiotatos*[1]; Andreas Sotiropoulos[1]; Sotiria Galata[1]; Athanasios Dimoulas[1]; [1]MBE Laboratory, Institute of Materials Science, NCSR Demokritos

Metal oxide high-k dielectrics may replace SiO_2 in the gate of future nano-electronic devices. In addition, high mobility semiconductors such as Ge or III-V compounds may replace Si in the active channel to enhance device performance. The interface between high-k materials and semiconductors determines critical performance characteristics of MOS capacitors and transistors. For aggressive oxide scaling with equivalent thickness well below 1 nm, avoiding interfacial layers is highly desirable. CeO_2 is a promising high k material for this purpose. A detailed characterization of the CeO_2/Ge system has been therefore carried out. However, very often, an interfacial layer is absolutely necessary to passivate the surface. This is true for example in the case of high-k dielectrics on Ge. Cerium oxides on Ge substrates are studied as possible alternative to widely used HfO_2. CeO_2 films of various thicknesses were grown on Ge substrates (n and p type) at temperatures ranging between RT and 360°C. Also, HfO_2/CeO_2/Ge stacks with different thicknesses were also grown on Ge in order to investigate the possibility to use thin CeO_2 films as passivation layer instead of GeO_xN_y. In fact, electrical data showed that CeO_2 films deposited directly on Ge exhibit reasonable interface state density. Preliminary electrical characterization on MIS capacitors have shown that for CeO_2 films is not necessary the oxidation of Ge by a GeO_xN_y interfacial layer in order to obtain a low density of interface states. Using a variety of characterization methods we have confirmed that CeO_2 deposited directly on Ge by molecular beam deposition reacts strongly with the substrate producing thick interfacial layers which contain oxidized Ge primarily in Ge^{+3} state. Despite Ge oxidation, these layers produce MOSCAPs with improved CV characteristics, as for example very weak frequency dispersion in depletion and inversion, small hysteresis and much reduced D_{it} in the low 10^{12} $eV^{-1}cm^{-2}$ range. Knowing that Ceria is a good catalyst, spontaneous formation of GeO_x or Ce-Ge-O interfacial layers is not surprising. However, whether CeO_2-assisted catalytic oxidation of Ge plays a role in the formation of high quality passivating layers is an open question. Finally, we will show that CeO_2 appears as a promising passivation layer for Ge. However, due to the small Ge/CeO_2 barrier height, the leakage current flowing through the capacitor is too high, and CeO_2 cannot be used as such as a gate dielectric. Hence, the combination of CeO_2 (for good interface passivation) with HfO_2 (to reduce the leakage current) is potentially much interesting.

2:50 PM

BB5, Late News

3:10 PM Break

3:30 PM Student

BB6, Nonlinear Optical Probing of Polarization Dynamics in Strained Ferroelectric $SrTiO_3$ Films: *Aravind Vasudeva Rao*[1]; Sava Denev[1]; Alok Sharan[1]; Michael D. Biegalski[1]; Yulan Li[2]; Susan Trolier-McKinstry[1]; Long-Qing Chen[1]; Darrell G. Schlom[1]; Venkatraman Gopalan[1]; [1]Pennsylvania State University; [2]Los Alamos National Laboratory

$SrTiO_3$ is a material that is not normally ferroelectric at any temperature.

Recently, we have demonstrated room temperature ferroelectricity in strained $SrTiO_3$ films on (110) orthorhombic $DyScO_3$ substrate. Using optical second harmonic generation (SHG), we demonstrate that ferroelectric $SrTiO_3$ are orthorhombic with point-group symmetry of *mm2*, a ferroelectric polarization in the film growth plane in the $[110]_p$ pseudocubic direction of $SrTiO_3$, and a Curie temperature of ~320K. Using real-time SHG studies, we show domain reversal and hysterisis behavior in these films from 77-300K. Theoritical modeling of the SHG response is presented that yields quantitative measurements of nonlinear optical coefficients and birefringence as a function of temperature through the phase transition.

3:50 PM Student
BB7, Epitaxial $BiMnO_3$ Films with Reduced Twinning and the Effect of Film Composition on Ferromagnetism: *June Hyuk Lee*[1]; Yunfa Jia[1]; Tassilo Heeg[2]; Rafael S. Freitas[1]; Dmitry A. Tenne[1]; Xiaoxing Xi[1]; Venkatraman Gopalan[1]; Peter E. Schiffer[1]; Jürgen Schubert[2]; Darrell G. Schlom[1]; [1]Pennsylvania State University; [2]Institut für Schichten und Grenzflächen

The multiferroic $BiMnO_3$, which exhibits the coexistence of ferromagnetism and ferroelectricity, has attracted much attention due to its simple perovskite structure and coupling effect between two ferroic properties. This makes $BiMnO_3$ a possible candidate for spintronics devices and memory storage. We have grown epitaxial $BiMnO_3$ thin films on (100) $SrTiO_3$ and (110) $SrTiO_3$ by pulsed-laser deposition using a bismuth-rich target with composition $Bi_{1.2}MnO_z$. Despite bismuth loss during growth, single-phase epitaxial films with high structural quality can be obtained over a range of Bi_xMnO_{3-y} compositions on (100) $SrTiO_3$. The composition of the nearly single-phase epitaxial films studied varied from x=0.83 to 1.0 (± 0.05) according to Rutherford backscattering spectrometry. Magnetization measurements on all films reveal a depression of the ferromagnetic transition temperature T_c (75 K) when compared with bulk $BiMnO_3$ samples (T_c = 105 K). Remarkably, when the magnitude of the magnetization is scaled to its value at the lowest temperature, the data all collapse onto a single curve and T_c converges to 75 K. This suggests that the stoichiometry of the system is not a sensitive control parameter for the magnetic properties. Due to its lower symmetry, monoclinic $BiMnO_3$ films exhibit twinning when grown on cubic $SrTiO_3$ substrates. When grown on (100) $SrTiO_3$, there are eight twin variants and on (111) $SrTiO_3$, there are 12 twin variants. When grown on (110) $SrTiO_3$, however, only two twin variants are observed. Specifically, four-circle x-ray diffraction indicates a (11-3)-oriented $BiMnO_3$ film with in-plane twins of [-110] $BiMnO_3$ // [-110] $SrTiO_3$ and [1-10] $BiMnO_3$ // [-110] $SrTiO_3$. The rocking curve of the (11-3) peak shows a full width at half maximum (*FWHM*) of 0.079° in ω. Raman spectroscopy and second harmonic generation (*SHG*) measurements on these $BiMnO_3$ samples with reduced twinning are currently being performed.

4:10 PM
BB8, Single Nanoparticle Transistors: A New Thin Film Device: *Steve Campbell*[1]; Yongping Ding[1]; Ying Dong[1]; Ameya Bapat[1]; Sang Ho Song[1]; Julia Daneen[1]; C. Barry Carter[1]; Uwe Kortshagen[1]; [1]University of Minnesota

The need for transistors and LEDs on low temperature substrates has led to amorphous and polycrystalline devices, and more recently, organic devices. All of these suffer, to varying degrees, from similar problems including low mobility and stability. Here we present an entirely different way to approach this technology. Although this example was run on a silicon wafer, it can readily be done on other materials. Cubic, highly perfect single crystal Si nanoparticles have been produced using a constricted-mode capacitively coupled silane plasma. A typical process produces monodisperse nanoparticle with a peak in the size distribution of 35 nm and a standard deviation of 4.7 nm. Transmission electron microscopy (TEM) studies showed that the particles were primarily perfect single crystal cubes with (100) faces. The device fabrication process began with the deposition of Pt or Yb, followed by low temperature silicidation. SiO2 was deposited by on the silicided wafer and windows in the oxide were patterned. Nanoparticles were then deposited at random locations on the substrates and covered with another layer of SiO2. Outside of the windows, the particles were removed with the SiO2 wet etching and subsequent clean. Another SiO2 layer was then deposited and planarized by chemical mechanical polishing (CMP) and etched back uniformly until about 70% of the particle was above the surface of the oxide. Next a low temperature gate oxide was formed by chemical oxidation in boiling H2O2. A gate metal was then deposited. An upper insulator was deposited, planarized by CMP and etched back uniformly. The exposed gate metal on top of the particles was removed, and etched down along the faces of the particle. A thin oxide layer was deposited, planarized, and recessed back to the surface of the particle tops. A thin layer of Pt or Yb was then deposited and annealed to form the upper contact. The stack of layers was then patterned by optical lithography to expose contacts. The geometries on these masks are 1000x larger than the particle size. Devices show typical MOS behavior. PtSi contacted transistor are p-type with a Schottky barrier of 0.17 V, while YbSi contacted transistors are n-type with a Schottky barrier of 0.18 V. The drive current from these extremely small devices are quite large: 10's to 100's of nA per particle. Typical inverse subthresold slopes are ~150 mV/decade. Modeling results suggest that this short channel behavior can be eliminated with a thinner gate oxide. This work was supported by NSF through NIRT grant DMI-0304211. Facilities for this work receive partial support through NSF's NNIN program.

4:30 PM
BB9, Late News

4:50 PM
BB10, Late News

Session CC: Dilute Nitride Semiconductors

Thursday PM, June 29, 2006
Room: Conference Room 108
Location: Pennsylvania State University

Session Chairs: Charles W. Tu, University of California; Rachel S. Goldman, University of Michigan

1:30 PM
CC1, Effect of Strain on the Nitrogen Incorporation in InGaAsN Quantum Wells Grown on GaAs and InP Substrates by Metalorganic Vapor Phase Epitaxy: *Nelson Tansu*[1]; Jeng-Ya Yeh[2]; Luke J. Mawst[2]; [1]Lehigh University; [2]University of Wisconsin-Madison

Here we present the studies on the effect of quantum well (QW) strain on the nitrogen incorporation efficiency into InGaAsN QW grown by metalorganic vapor phase epitaxy (MOVPE). The comparative studies are conducted on 60-80 Å thick InGaAsN quantum wells with high-In content of approximately 30-45% grown on GaAs and InP substrates. Comparative experimental studies of photoluminescence, X-rays diffraction (XRD), and SIMS are conducted on MOVPE-grown InGaAsN quantum wells on GaAs and InP substrates, to understand the role of quantum well strain on the nitrogen incorporation efficiency. The InGaAsN QWs are designed with In-content of approximately ~ 35-40%, which results in a compressively-strained QW ($\Delta a/a$ ~ 2.5-2.8 %) when grown on a GaAs substrate and a tensile-strained QW ($\Delta a/a$ ~ - 1.0-1.5 %) when grown on a InP substrate. The N-contents in all InGaAsN QWs studied here range from ~0.5 % to ~1%. MOVPE growth of the InGaAsN QWs is conducted at growth temperature and reactor pressure of 530 C and 200 mbar, respectively. Trimethylgallium and trimethylindium are used as the group III sources, and AsH3 and U-dimethylhydrazine (U-DMHy) are used as the group V precursors. For the case of compressively-strained $In_{0.35}Ga_{0.65}AsN$ QWs on GaAs, N-content of approximately ~0.8 % is obtained by employing growth conditions with [AsH3]/III and [DMHy]/V ratios of 13.5 and 0.961, respectively. As the In-content in the compressively-strained InGaAsN QW on GaAs is increased to 40%, N-incorporation efficiency is reduced leading to lower N-content of approximately ~0.5% in the QW for identical [AsH3]/III and [DMHy]/V ratios. By employing [DMHy] / V ratio of 0.961 for the MOVPE epitaxy of tensile-strained $In_{0.4}Ga_{0.6}AsN$ QWs on InP, the N-content in the QWs is estimated from SIMS comparison as at least three orders of magnitude lower than that measured in the compressively-strained $In_{0.4}Ga_{0.6}AsN$ on GaAs with identical growth conditions. Only after increasing the [DMHy]/V ratio to 0.984, substantial nitrogen species are incorporated in the tensile QWs with 35% In-content, resulting in red shift of 100-nm in its peak luminescence

wavelength. Similar comparative experiments are also conducted for 8-nm thick $In_{0.2}Ga_{0.8}AsN$ 4-QWs with lower In-content, employing a [DMHy]/V ratios of 0.927. Despite the relatively-low In-content in $In_{0.2}Ga_{0.6}AsN$ QWs, no N-incorporation is observed for the tensile-strained QWs grown on InP. For the case of compressively-strained $In_{0.2}Ga_{0.8}AsN$ QWs on GaAs with identical In-content, evidence of N-incorporation in the QWs is clear, resulting in a red-shift of approximately 65-nm in the room temperature photoluminescence. Despite the identical In-contents and growth conditions of InGaAsN QWs, N-incorporation is significantly more efficient in the case for compressively-strained QWs (grown on GaAs) in comparison to that for tensile-strained QWs (grown on InP).

1:50 PM Student

CC2, TEM Analysis of GaInNAsSb Quantum Wells Grown and Annealed at Varied Temperatures: *Evan R. Pickett*[1]; Seth R. Bank[2]; Hopil P. Bae[1]; Homan B. Yuen[1]; Mark A. Wistey[1]; James S. Harris[1]; [1]Stanford University; [2]University of California at Santa Barbara

The substantial progress made in the dilute nitrides recently has enabled such devices as low-threshold GaAs based lasers at 1.3 and 1.55 microns. Improving these devices has required extensive effort, as the properties of the device active regions (usually GaInNAs or GaInNAsSb quantum wells (QWs) for GaAs-based dilute nitrides) are extremely sensitive to parameters such as growth temperature, nitrogen content, group V fluxes, and annealing temperature. Antimony is used as a surfactant by several groups to reduce surface roughness, minimize composition and strain modulation within the active regions, and increase nitrogen and indium incorporation. Previous studies by this group and others have examined many of the aforementioned characteristics of GaInNAs(Sb) films and devices, but none have examined the temperature-related degradation mechanisms of antimony-containing dilute nitride films. This study uses transmission electron microscopy (TEM), photoluminescence (PL), and x-ray diffraction (XRD) to examine the effect of growth and anneal temperature on the morphology and strain, chemical, and interface uniformity of antimony-containing dilute nitride QW structures. The GaInNAsSb QWs were grown on [001] GaAs substrates by molecular beam epitaxy (MBE) in a Varian Mod Gen. II reactor using effusion cells for the Group III elements and thermal crackers for As and Sb; an rf plasma cell provided reactive nitrogen. For the growth temperature study, four samples were grown with the active layer at temperatures between 420°C and 470°C. For the anneal temperature study, pieces of a single wafer grown under optimal conditions were annealed for one minute at 20-degree intervals between 680 and 820°C, with the optimal anneal temperature known to be within that range. In addition to PL and XRD, TEM using brightfield (001) diffraction conditions was used to examine film morphology and interface uniformity. Strain and chemical analyses were performed using darkfield imaging of the (002) and (220) planes. Energy dispersive x-ray spectroscopy was used for simple analysis (based against known standards) to identify phase composition. Samples were prepared via traditional polishing techniques involving mechanical thinning to ~30 microns and ion milling to electron transparency. The as-grown and optimal anneal (from PL) samples from each wafer from the growth temperature series were analyzed; for the anneal temperature series, the as-grown sample and one sample from each anneal temperature were observed. Based upon these analyses, it is proposed that properties of GaInNAs(Sb) films grown at too high a temperature degrade due to a change from 2D to 3D growth, while those annealed at too high a temperature degrade due to local phase segregation into N-rich and N-poor regions. The compositions of the different phases will be discussed.

2:10 PM Student

CC3, Relative Speed and Temperature Dependence of Constituent Processes in the Annealing of GaInNAs(Sb) and Their Implications on Device Growth and Annealing: *Hopil P. Bae*[1]; Seth Robert Bank[2]; Homan Bernard Yuen[1]; Evan R. Pickett[1]; Mark A. Wistey[1]; [1]Stanford University; [2]University of California, Santa Barbara

Dilute nitride materials have been actively researched for their potential to enable low-cost high-density GaAs-based optoelectronic devices for optical communications and interconnects in the 1.2-1.6um wavelength range. But the growth of these materials has proved very challenging, and despite many improvements and optimizations in the growth of the material, the as-grown material still has too many defects, which have to be thermally annealed to recover the material quality. Even though the annealing has become a standard process for dilute nitrides, studies of the annealing properties have been incomplete; the parameter space has not been fully and systematically explored, and most reports focused on plain QW samples rather than full laser structures. In most practical optical devices, QW growth is followed by relatively thick upper structures, such as the upper cladding in edge-emitting lasers or the top DBR in VCSELs. This cladding growth subjects the QW to hours of in-situ anneal, at a temperature lower than typical ex-situ annealing temperatures. Therefore, annealing properties of dilute-nitride devices have to be studied with consideration of this inevitable in-situ anneal. GaInNAsSb QW samples for 1.55um emission with 39% indium were grown in solid-source MBE, using an rf plasma cell for reactive nitrogen source. Samples were annealed at several temperatures ranging from 650C to 820C, and for different durations until the photoluminescence (PL) intensity started to degrade. Based on PL study, the annealing process can phenomenologically be resolved into three constituent processes: improvement of PL intensity, blueshift of peak wavelength, and eventual degradation due to overanneal. PL quality improvement and blueshift are found to proceed with roughly the same speed, reaching a saturation at roughly the same time, and they show a similar temperature dependence with an activation energy of about 3.5eV. Nearest-neighbor reconfiguration can sufficiently account for the magnitude of the blueshift, and the effect of Ga-In interdiffusion or N outdiffusion can be assumed negligible. On the other hand, the degradation process is found to be distinct from the other two processes, and to have a much steeper temperature dependence with an activation energy of about 7eV. By choosing reasonably low temperatures, the degradation can be made very slow compared to PL intensity improvement and peak blueshift, thereby opening a wide process window where annealing can be done for quality improvement without worrying about degradation. A similar experiment on a grown GaInNAs(Sb) laser structure suggests that the typical GaAs/AlGaAs growth temperature in MBE is sufficiently low for this consideration. This study shows that the improvement and degradation processes in GaInNAs(Sb) annealing can be individually identified and controlled, during both growth and ex-situ anneal. This understanding can be utilized to realize the full potential of GaInNAs(Sb) material.

2:30 PM Student

CC4, The Role of Bismuth as a Surfactant during Beryllium Doping of GaAsN Grown by Molecular Beam Epitaxy: *Ting Liu*[1]; Dimitris Korakakis[1]; Thomas H. Myers[1]; [1]West Virginia University

The large band gap bowing effect of III-V nitride alloys has made GaAsN a promising material for its use in long wavelength optoelectronic devices. However, due to the large lattice mismatch and large miscibility gap between GaAs and GaN, it is hard to get high quality GaAsN, particularly for large N concentrations. In order to reduce surface roughness caused by size mismatch as well as enhance the nitrogen incorporation, surfactant use during the growth might be an option. Currently most studies regarding this issue are related to the use of antimony as a surfactant. A recent study[1] has indicated that bismuth may dramatically alter N incorporation while acting as a surfactant. In addition, there have been few reports of p-type doping in GaAsN. Our study is focused on the use of Bi as a surfactant and to investigate beryllium doping during MBE growth. Samples are grown on (100) GaAs substrates by plasma assisted Molecular Beam Epitaxy (MBE). Atomic force microscopy (AFM), photoluminescence (PL), x-ray diffraction, Hall effect and Raman spectroscopy are used to investigation the properties of the GaAsN. The influence of bismuth on surface morphology, nitrogen incorporation, and optical properties will be discussed. Our investigation of using Be as a p-type dopant in GaAsN will be presented. This work was supported by the National Science Foundation Grant DMR - 0102753. [1]E. C. Young, S. Tixier, and T. Tiedje, J. Crystal Growth 279, 316 (2005).

2:50 PM Student

CC5, Strong Luminescence Enhancement in GaInNAsSb Quantum Wells through Variation of the Group-V Fluxes: *Seth R. Bank*[1]; Hopil P. Bae[1]; Homan B. Yuen[1]; Evan R. Pickett[1]; Mark A. Wistey[1]; Akihiro Moto[2]; James S. Harris[1]; [1]Stanford University; [2]Innovation Core SEI, Inc.

Dilute-nitride materials have received much attention recently for their promise in covering the entire 1.2-1.6 μm communications range with high-performance GaAs-based optoelectronic devices. It is well established that

low growth temperatures and high arsenic fluxes are required for single phase molecular beam epitaxial (MBE) growth of these materials. These conditions, despite improvements through the use of antimony as a surfactant and reduction in nitrogen plasma-related damage, result in many point defects that degrade laser threshold current density. Indeed, even the lowest threshold 1.5-µm GaInNAsSb lasers still show significant monomolecular recombination that comprises 30-50% of the threshold current. Reducing the number of arsenic antisites and interstitials and gallium vacancies in dilute-nitride active regions offers a great deal of promise for improving laser performance. However, there have been no investigations of dilute-nitride-antimonides in the reduced arsenic and antimony flux regimes. Samples were grown by solid-source MBE on semi-insulating (100) GaAs. Reactive nitrogen was supplied by an rf plasma cell with ions removed from the molecular beam by deflection plates at the exit aperture. The active region was a single GaInNAsSb quantum well surrounded on either side by GaNAs barriers grown at 410°C, emitting at ~1.55 µm after anneal. Flux ratios were determined from beam equivalent pressure measurements. Samples were characterized with room and low-temperature photoluminescence, high-resolution x-ray diffraction, secondary ion mass spectrometry, and transmission electron microscopy. Reduction of the arsenic flux, with all other growth parameters held constant, yielded a wide growth window of approximately identical optical properties, but slightly varying composition. Optical and structural properties degraded substantially at low arsenic fluxes, in concert with strong compositional variation. Low arsenic fluxes increase the antimony surface concentration. Due to the reactive surfactant properties of antimony, the surface diffusion length may be reduced below the optimal point, resulting in increased defects. However, reduction of both the arsenic and antimony fluxes, while maintaining a constant arsenic-to-antimony flux ratio, yielded substantially improved optical efficiency with no change in composition or emission wavelength. A fixed As/Sb flux ratio likely maintains a constant antimony surface concentration during growth, and hence, an appropriate surface diffusion length. The reduced arsenic flux then results in fewer point defects and increased luminescence. These findings yield a very promising method to further reduce long-wavelength dilute-nitride laser thresholds.

3:10 PM Break

3:30 PM Student

CC6, Influence of Nitrogen Incorporation on Electron Transport in Selectively Doped GaAsN/AlGaAs Heterostructures: *Yu Jin*[1]; Matthew Reason[1]; Xiaogang Bai[1]; Hugh Mckay[1]; Rachel S. Goldman[1]; Cagliyan Kurdak[1]; [1]University of Michigan

Dilute nitride (In)GaAs(N) alloys are useful for infrared laser diodes, high efficiency solar cells, and high performance heterojunction bipolar transistors. Typically, the electron mobility of (In)GaAs(N) alloys decreases with N incorporation, resulting in substantially lower electron mobilities than in (In)GaAs. At the present time, the precise role of N in lowering the electron mobility is not well understood. To study the nitrogen-related electron scattering effects in GaAsN, with minimal contributions from ionized impurity scattering, we have studied the transport properties of modulation-doped AlGaAs/GaAs(N) heterostructures, with Si dopants in the AlGaAs barrier layer spatially separated from the nominally undoped GaAs(N) channel layer. High quality AlGaAs/GaAs(N) heterostructures and corresponding GaAs(N) bulk-like samples with a variety of nitrogen concentrations were grown via molecular-beam epitaxy. Samples containing GaAs or GaAsN as the channel layer will be referred to as a "control sample" or "nitride sample", respectively. In all cases, the nitrogen flux was provided by a nitrogen plasma source, contained in a separately pumped chamber sealed by a pneumatic gate valve. The substitutional and interstitial nitrogen concentrations were determined using a combination of nuclear reaction analysis and Rutherford backscattering spectrometry studies of the bulk-like GaAsN films. Magnetoresistance and Hall measurements of the heterostructures were performed at 4K, using gated Van der Pauw and Hall bar geometries. Parallel resistivity, Rxx, and transverse resistivity, Rxy, were measured as a function of magnetic field up to 7 Tesla. In all heterostructures, the integer quantum Hall effect and well-resolved Shubnikov-de Haas oscillations were observed, indicating the formation of a two-dimensional electron gas (2DEG) without parallel conduction. During the measurement, the carrier density in the 2DEG channel layer was manipulated via a combination of front-gating and illumination with a GaAs light emitting diode. For the control samples, the electron mobilities were comparable to literature reports and increased with free carrier density according to µ~n^y, where y is dependent on the spacer layer thickness, typically 1~1.5.[1] This indicates that the dominant scattering mechanism is long-range ionized impurity scattering. For nitride samples, we observe a weak dependence of the electron mobility on the carrier density, and the mobility saturates for n > 1.5x10^11cm^-2, consistent with the theoretical prediction of Fahy et al.[2] These results indicate that short-range N-induced neutral scattering, rather than long-range ionized impurity scattering, is the dominant scattering source in GaAsN. The effects of varying substitutional and interstitial N concentrations on the transport properties of these GaAsN/AlGaAs heterostructures will also be discussed. [1]K. Hirakawa and H. Sakaki, Phys. Rev. B 33, 8291 (1986). [2]S. Fahy, A. Lindsay, H. Ouerdane and E.P. O'Reilly, (submitted to Phys. Rev. B) (2005).

3:50 PM Student

CC7, Growth and Fabrication of InGaNP Quantum Well Based Yellow-Red Light-Emitting Diodes: *Vladimir A. Odnoblyudov*[1]; Charles W. Tu[1]; [1]University of California, San Diego

High-brightness yellow-red light-emitting diodes (LEDs) are highly desirable for outdoor displays, car lights, traffic signals, and white light in the three-LED (red, green, and blue) approach. Currently yellow-red LEDs are fabricated from the AlInGaP/GaAs material system. We propose an alternate material system, InGaNP directly grown on a GaP(100) substrate, which would eliminate the currently used complicated and high-cost procedure of removing the light-absorbing GaAs substrate and wafer-bonding a transparent GaP substrate or a reflective layer on a carrier. Superior material properties (e.g., band offsets) of InGaNP/GaP over AlGaInP/GaAs will allow brighter, smaller and cheaper LED chips. The conduction band offset of 225 meV of the GaInNP active region emitting at 610nm is calculated to be about three times that of commercial AlInGaP LEDs (75 meV). All samples were grown in a Varian GEN II Gas Source MBE system directly on a GaP(100) substrate. Thermally cracked PH3 and RF nitrogen plasma source were used as group-V precursors. We describe growth and fabrication of LED chips emitting within the 600-650nm range, utilizing InGaNP quantum wells as an active region. Optical and structural quality of the material was examined using x-ray technique and photoluminescence measurement. LEDs with single and multiple quantum wells in the active region have been grown and fabricated. Increasing the number of quantum wells in the LED structure from 1 to 6 results in an increase of light output by a factor of 2, and shift of the saturation current from 60 mA to 90 mA. Also, AlGaP cladding layers were utilized in the LED structures for optical confinement and electrical confinement for the carriers. Optimization of the Al composition is required since AlP/GaP is a type II heterojunction, in which case there would be no confinement for electrons. A series of LED structures was grown with different aluminum concentration in the 0.5-µm-thick cladding layers: 0%, 14%, 30% and 77%. If the Al concentration is lower than 30%, the series resistance of the LED structure with AlGaP claddings increases less than 10%. If the Al concentration exceeds 50%, the series resistance increases dramatically. The optimal Al composition was found to be 14%, as it provides low series resistance and increase of the light output by 15%, as compared to a structure without AlGaP claddings. Further optimization, such as doping profiles, barrier thickness between quantum wells, and contact layer thickness of the LED structure is underway in order to maximize LED efficiency and light output.

4:10 PM

CC8, Electrical and Luminescence Properties of n- and p-Type GaPN: *Yuzo Furukawa*[1]; Hiroo Yonezu[1]; Akihiro Wakahara[1]; Sato Atsushi[1]; [1]Toyohashi University of Technology

Dilute nitrides, such as Ga(In)AsN and Ga(In)PN, are a candidate for the realization of optoelectronic integrated circuits. A $GaP_{0.98}N_{0.02}$ alloy can be lattice-matched to Si theoretically. We have already realized a lattice-matched and dislocation-free Si/GaPN/Si structure on a Si substrate by solid-source molecular beam epitaxy (MBE). Photoluminescence (PL) has been obtained from the GaPN layer. However, there are only a few reports on electrical and optical properties of n- and p-GaPN. In this study, we investigate the electrical and luminescence properties of n- and p-GaPN using Mg and S as dopants,

respectively. GaPN epitaxial layers were grown on semi-insulating GaP (100) substrates by MBE with an rf-plasma source as a nitrogen source. The growth temperature was 590°C. Magnesium and sulfur were evaporated from 6N-Mg and 6N-GaS by K-cells, respectively. The N concentration was estimated by X-ray diffraction measurement. Electrical properties were examined by Hall-effect measurements using the Van der Pauw method. Indium metal was used as an electrode by thermally alloying at 400°C under flowing-N_2 gas ambient. PL measurements were employed using the 532-nm laser as an excitation source at various temperatures. The carrier concentrations in p-GaPN:Mg and n-GaPN:S were 1.2×10^{18} and 1.8×10^{18}cm^{-3}, respectively. The N concentrations were around 0.6%. The temperature dependence of hole mobility of GaPN:Mg showed the bell shaped curve as well as p- and n-GaP. On the other hand, the electron mobility of GaPN:S seemed to be limited by ionized impurity scattering even at room temperature (RT). N atoms have a large electronegativity and favor formation of point defects in GaPN. The Fermi energy level would be close to the conduction band edge in n-GaPN. Thus the N-related point defects would trap the electrons easily, and the negatively charged point defects may act as Coulumb scattering center even at RT in n-GaPN:S. In p-GaPN:Mg, the Fermi energy level would be lower than the energy level of N-related point defects, and these defects would not act as Coulomb scattering center. PL measurements were performed at 18K. The PL intensity obviously depended on the doping condition. The peak intensity became more than 30 times lower by S doping. It was found that a number of point defects may be generated by S doping as well as N incorporation. On the other hand, the strongest luminescence was observed from the GaPN:Mg layer. Moreover, the intensity of a S and Mg codoped n-GaPN layer became around 5 times stronger, as compared with the GaPN:S. These results suggested that Mg atoms would suppress the formation of N and/or S-related point defects, which were one of the nonradiative centers, during the growth, and may induce the improvement of luminescence efficiency of GaPN.

4:30 PM

CC9, The Role of Kinetic Effects in Radiative and Non-Radiative Recombination of Optical Excitations in Dilute Nitride Heterostructures: Theory and Experiment: *Oleg Rubel*[1]; S. D. Baranovskii[1]; B. Kunert[1]; K. Hantke[1]; W. W. Rühle[1]; P. Thomas[1]; K. Volz[1]; W. Stolz[1]; [1]Philipps University Marburg

The observed non-monotonous temperature dependences of the luminescence Stokes shift and of the spectral line width evidence the essential role of disorder in the dynamics of the recombining excitations in dilute nitride semiconductor heterostructures. The spatial and energy disorder can cause a localization of photo-created excitations presumably in the form of correlated electron-hole pairs or excitons. Despite a number of experimental research in that field, the interpretation of measured photoluminescence (PL) spectra remains semi-quantitative due to lack of a theoretical basis. We present results of our theoretical and experimental study of the photoluminescence response in (GaIn)(NAs)/GaAs[1] and in novel Ga(NAsP)/GaP quantum wells, which is aimed at deriving an "easy to use" way to identify characteristics of disorder responsible for carrier localization. We show that our approach is also applicable to numerous experimental data published on this subject in the past decade. The theoretical study of the exciton dynamics is performed isung kinetic Monte-Carlo simulations of exciton hopping and recombination in the manifold of localized states[2]. We calculate the temperature-dependence of the PL peak energy and of the PL line width. A comparison between experimental spectra and theoretical calculations provides a direct estimate for the energy scale of the potential fluctuations. Proportionality factors between the disorder energy scale and measured characteristics of the PL spectra are established. The theoretical results are applied to a variety of experimental data in order to evaluate the energy scale of the band tail. In addition, we estimate the impact of annealing on the concentration of localized states and on the localization length of excitons in (GaIn)(NAs) quantum wells. In addition, the model of hopping relaxation of localized excitons[2] is extended to include non-radiative recombination of optical excitations in disordered semiconductor heterostructures. We show that the thermal quenching of the PL intensity is a consequence of an interplay between radiative and non-radiative recombination and hopping dynamics of excitations in the manifold of localized states created by the disorder potential. New experimental data on the thermal quenching of the PL intensity in (GaIn)(NAs)/GaAs and in Ga(NAsP)/GaP quantum wells are presented and compared with the theoretical results. Thus, valuable quantitative information on the energy- and spatial characteristics of disorder in the underlying materials is obtained, which also influence device characteristics for laser as well as solar cell application. [1]O. Rubel, M. Galluppi, S. D. Baranovskii, K. Volz, L. Geelhaar, H. Riechert, P. Thomas, and W. Stolz, J. Appl. Phys. 98, 063518 (2005).[2]S. D. Baranovskii, R. Eichmann, and P. Thomas, Phys. Rev. B 58, 13081 (1998).

4:50 PM Student

CC10, Bandgap Reduction and Lattice Matching in Dilute Nitride Antimonide Alloys: *Paul Jefferson*[1]; Tim Veal[1]; Louis Piper[1]; Chris McConville[1]; Brian R. Bennett[2]; Louise Buckle[3]; Tim Ashley[3]; [1]University of Warwick; [2]Naval Research Laboratory; [3]QinetiQ Ltd.

The anion substitution of dilute quantities of nitrogen into III-V semiconductor compounds is well documented to reduce the bandgap of the material from that of the host compound. Two methods used to model this phenomenon are the band anticrossing model [W. Shan *et al.*, Phys. Rev. Lett. 82 (1999) 1221] and models based on supercell calculations [P. R. C. Kent *et al.*, Semicond. Sci. Technol. 17 (2002) 851]. In both models the significant mismatch in size and electronegativity between the host anion and substitutional nitrogen is at the core of the bandgap reduction phenomenon. Though this effect has been exhaustively studied in GaAs and related materials very little work has been produced on the dilute nitride alloys of GaSb and related materials. The greater size and electronegativity mismatch between the host anion and nitrogen atoms seen in dilute nitride antimonides has been shown to result in a greater bandgap reduction than that seen in dilute nitride arsenide alloys [T. D. Veal *et al.*, Appl. Phys. Lett. 87 (2005) 132101]. The potential of such materials for the exploitation of the mid-infrared region of the electromagnetic spectrum from the bandgap of GaSb (~710 meV) and below is evident. In this work the growth of high quality GaN_xSb_{1-x} films with nitrogen incorporations less than one percent is reported. Evidence of a band anticrossing interaction between the host conduction band and the resonant electronic state resulting from the nitrogen incorporation is presented and estimates of the band anticrossing parameters E_N, the resonant nitrogen level energy, and V_{MN}, the interaction strength between the nitrogen level and the host conduction band, are given. In addition, the growth and structural characterisation of $Ga_{1-y}In_yN_xSb_{1-x}$ films lattice matched to GaSb are presented. X-ray diffraction rocking curves and reciprocal space maps verify the high crystalline quality and lattice matching of the samples. The possibility of such materials with relatively moderate quantities of indium ($y < 0.22$) and nitrogen ($x < 0.05$) being used for long wavelength applications, exploiting the 8-14 μm atmospheric transmission window, whilst maintaining a lattice match to GaSb will be discussed.

Session DD:
P-Type Doping and Electroluminescence in ZnO

Friday AM
June 30, 2006

Room: Deans Hall I
Location: Pennsylvania State University

Session Chairs: David P. Norton, University of Florida; Yicheng Lu, Rutgers University

8:20 AM Student

DD1, Band-Edge Electroluminescence from N^+-Implanted Bulk ZnO: *Hung-Ta Wang*[1]; Fan Ren[1]; Byoung Sam Kang[1]; Jau-Jiun Chen[1]; Travis Anderson[1]; Soohwan Jiang[1]; Hyun-Sik Kim[1]; Yuanjie Li[1]; David P. Norton[1]; Stephen J. Pearton[1]; [1]University of Florida

ZnO is attracting renewed interest for use in blue/UV light-emitting diodes (LEDs) with potential advantages over the III-nitride system due to the higher exciton binding energy, availability of high quality bulk substrates and ease of wet etching. Ion implantation is an attractive process for low-cost, high throughput device manufacturing and in this talk we show that N^+ implantation into bulk single-crystal ZnO substrates can be used to achieve bandedge electroluminescence (EL) in simple diode structure. $^+$ion implantation was performed at 300K with at moderate doses (1.5×10^{13}-3.5×10^{14} cm^{-2}) into nominally undoped (electron concentration of ~10^{17} cm^{-3}, electron mobility of ~190 cm^2/V s) bulk single-crystal ZnO substrates by ~300nm depth. After ion implantation, the ZnO bulk substrates were annealed in the range 600-950°C under oxygen ambient in either rapid thermal annealing (RTA) for 2mins, or conventional furnace or vacuum chamber for 45 mins. The diodes were fabricated with full backside area contacts of e-beam deposited Ti (20 nm)/Au (200nm) as n-type metal and circular front-side contacts of Ni (20nm)/Au (80nm) as p-type metal followed by 400°C annealing. The current-voltage (I-V) behavior of the diodes are characteristic of metal-insulator-semiconductor(MIS) devices and not p-n junctions and suggest the implantation creates a more resistive region in the n-ZnO in which holes are created by impact ionization during biasing, similar to the case of electroluminescence in ZnO varistors. The series resistance is only 25 Ω due to the use of the conducting ZnO substrate. Band-edge electroluminescence (EL) at 120K (~390 nm) under forward bias conditions is consisted with a small shift of band-edge photoluminescence (PL) at ~380 nm. A strong deep level-related emission peaked at > 600 nm is introduced by implantation damage means that annealing of point defects will not be complete and most of the small band-edge peak may actually come from the undamaged ZnO underneath the implanted region. We conclude that band-edge and yellow EL has been obtained from N^+-implanted bulk ZnO diodes similar to that observed in MIS diodes. Future work on acceptor implantation will focus on achieving p-type conductivity in the ZnO so that true injection LEDs may be realized.

8:40 AM Student

DD2, Photoluminescence and Electroluminescence Properties of ZnO Nanotips Grown on p-Type GaN: *Jian Zhong*[1]; Hanhong Chen[1]; Gaurav Saraf[1]; Yicheng Lu[1]; H. M. Ng[2]; C. K. Choi[3]; J. J. Song[4]; [1]Rutgers University; [2]Bell Laboratories, Lucent Technologies; [3]ZN Technology; [4]ZN Technology, University of California, San Diego

For a conventional broad area nitride LED, the quantum efficiency is often limited by the light extraction efficiency. Only ~ 4% of the internal light can be extracted, resulting from the parasitic absorption loss and the narrow escape cone. A novel approach to improve LED's external quantum efficiency is to introduce nanostructures into the LED surface. The strong surface scattering of these nanostructures will randomize the angular distribution of photons, and an enlarged equivalent escape cone for the trapped photons can be achieved. ZnO and GaN have the same wurtzite-type structure and a small in-plane mismatch (lattice mismatch ~2%). ZnO/GaN heterostructures have Type II band alignment, which benefits certain devices. We report photoluminescence (PL) and electroluminescence (EL) properties of a heterostructure p-n junction consisting of n-type ZnO nanotips direct grown on p-type GaN. Electroluminescence is observed in this heterojunction LED under forward current injection. Single crystalline ZnO nanotips are grown on a GaN/c-sapphire template at a temperature of 350-500° using MOCVD. Temperature dependent PL spectra are measured from 4.4 K to 300K under a 325 nm line He-Cd laser excitation. ZnO nanotips show sharp and prominent free excitonic emission (XA) at 4.4K, confirming their excellent optical property. Free exciton emission dominates at temperatures higher than 50K. Temperature dependent PL spectra show thermal dissociation of bound excitons at peak positions 3.369 (D0X1) and 3.364 eV (D0X2), which leads to creation of free excitons and neutral donors. Temperature dependence of PL intensities is well described with a two-channel thermal dissociation model. Based on the Arrhenius plots of PL intensities, the exciton localization energies for D0X1 and D0X2 are deduced to be 11 and 16 meV, respectively. An n-ZnO nanotips/p-GaN heterojunction light emitting diode is fabricated with a circular pattern. A thin layer of Al/Au is first deposited on ZnO nanotips mesa, serving as a transparent conductive layer. Al is then used for top ohmic contact to n-type ZnO nanotips, while Ni/Au is used for bottom ohmic contact to p-GaN. To prevent the metal particles from reaching the bottom of the ZnO nanotip, which leads to short of the junction, the interstices between ZnO nanotips are filled in using an insulator. I-V characteristics of the n-ZnO nanotips/p-GaN heterojunction LED show a junction rectifying property. A blue light emission centered at the wavelength of 406 nm is observed under the forward current injection of ~ 1mA. The EL spectrum is compared with that of PL, suggesting luminescence primarily due to electron injection into p-type GaN. The integration of ZnO nanotips with GaN shows a promising potential for UV/blue optoelectronics. This work has been supported by NSF under grant CCR-0103096, and by ARO under grant #W911NF-05-C-0023.

9:00 AM

DD3, Changes in Electrical Characteristics of p-Type Zinc Oxide Thin Films Due to Light and Gas Ambient: *Bruce Claflin*[1]; David C. Look[1]; Gene Cantwell[2]; David P. Norton[3]; [1]Semiconductor Research Center; [2]Zn Technology; [3]University of Florida

Current research aimed at the development of ZnO for electronic and optoelectronic applications such as transparent thin film transistors (TTFTs) and light-emitting diodes (LEDs) has been slowed by the challenging problem of producing stable and reliable p-type material. Recent demonstrations[1,2] of p-type behavior in N- and P-doped ZnO have been viewed with skepticism[3] due to difficulties reproducing the results in other laboratories. Furthermore, the low hole mobilities observed have led to questions about material quality. The objective of this paper is to investigate the impact that common laboratory environmental variables have on the electrical characteristics of ZnO:N thin films. Temperature-dependent Hall-effect and photo-Hall-effect measurements using blue/UV light were conducted in vacuum over the range 30–400 K on ZnO:N films prepared by molecular beam epitaxy (MBE) and by pulsed-laser deposition (PLD). Exposure to blue/UV light results in a change from weak p-type behavior in the dark to strong n-type conduction under illumination, and persistent photoconductivity (PPC) when the light source is removed. The peak electron mobility of the MBE-grown layer at low temperature is μ_n > 850 cm^2/V-s under blue/UV light. Following light exposure, the electrical properties were monitored over time as the samples were sequentially exposed to dry nitrogen (N_2) and dry oxygen (O_2) at 293 K. Dry N_2 had no effect on the electrical characteristics, but exposure to dry O_2 resulted in a steady decrease in carrier concentration and corresponding increase in resistivity. Ultimately, after sitting in dry O_2 for 12 hours, the sample returned to its original (pre-exposure) state. These O_2-induced changes persist when the sample is returned to vacuum and following Hall-effect measurements up to 400 K. Possible mechanisms for the observed changes in electrical properties involving oxygen vacancies (V_O) will be discussed since V_O is known to act as a donor. Due to the very low hole mobility and large electron mobility in these samples, n-type surface conduction can play an important[4] role, and when the surface sheet charge, n > 10^{10} cm^{-2} the sample will appear n-type. The implications of these effects on the preparation of p-type ZnO will be addressed. [1]D.C. Look, D.C. Reynolds, C.W. Litton, R.L. Jones, D.B. Eason, and G. Cantwell, Appl. Phys. Lett. 81, 1830 (2002). [2]D. K. Hwang, S. H. Kang, J. H. Lim, E. J. Yang, J. Y. Oh, J. H. Yang, and S. J. Park, Appl. Phys. Lett. 86, 222101 (2005). [3]B. K. Meyer, H. Aves, D. M. Hofmann, W. Kriegseis, D. Forster, F. Bertram, J. Christen, A. Hoffmann, M. StraBburg, M. Dworzak, U. Haboeck, A. V. Rodina, Phys. Stat. Sol. B 241,

231 (2004). [4]B. Claflin, D. C. Look, S. J. Park, G. Cantwell, J. Cryst. Growth 287, 16 (2006).

9:20 AM Student

DD4, Bi-Doped ZnO Films Grown by Molecular-Beam Epitaxy: *Faxian Xiu*[1]; Leelaprasanna J. Mandalapu[1]; Zheng Yang[1]; Jianlin Liu[1]; [1]University of California, Riverside

Substantial research is currently being conducted worldwide on ZnO material for its potential applications in optoelectronics and spintronics. Towards these applications, p-type ZnO growth is an indispensable step to realize these devices. So far group V elements such as N, P, As, and Sb, as well as group III and group V co-doping have been extensively studied for producing p-type conductivities. However, Bi, the last element in group V, has not yet been tried experimentally although Kobayashi *et al.*[1] theoretically predicted a number of years ago that Bi doping on the anion site will produce shallow acceptor levels. In this presentation, we report the growth and characterizations of Bi-doped ZnO films on Si (111) by ECR-assisted molecular-beam epitaxy. A low-temperature Bi effusion cell was used to provide Bi dopant. During growth, Bi effusion cell temperature was varied to have different doping concentrations. Room-temperature Hall effect measurements show that undoped ZnO sample has a high electron concentration of 2.7×10^{18} cm^{-3} and a low resistivity of 0.3 O cm. Bi-doped ZnO films, however, show a significant reduction of electron concentration in a range of 9.1×10^{16}-4.4×10^{17} cm^{-3} and an increased resitivity value of 2.6-4.3 O cm. Correspondingly, low-temperature photoluminescence measurements reveal a strong donor-bound exiton emission at 3.360 eV for undoped ZnO and 3.356-3.359 eV for Bi-doped ZnO films. Similar to the scenario of phosphorus-doped ZnO[2], the shifting of this peak towards lower energy may indicate the formation of acceptor states in these films. In fact, based on the first-principles calculations, Carlsson *et al.*[3] predicted that under O-rich conditions the formation of a $Bi_{Zn}+V_{Zn}+O_i$ will be a localized acceptor state and gives the grain boundary p-type character. The temperature-dependent photoluminescence measurements were also conducted to further confirm these emissions. A 3.222 eV emission-line in Bi-doped ZnO films shows an evident blue-shift with the increase of temperature, which is the typical characteristic of DAP transition[4]. Now we are using different growth conditions to explore the possibility of producing p-type conductivity by Bi doping. [1]A. Kobayashi, O. Sankey, and J. Dow, ibid, 28 (1983). [2]V. Vaithianathan, B. T. Lee, and S. S. Kim, J. of Appl. Phys. 98, 043519 (2005). [3]J. M. Carlsson, H. S. Domingos, P. D. Bristowe, and B. Hellsing, Phys. Rev. Lett. 91, 165506 (2003).[4]F. X. Xiu, Z. Yang, L. J. Mandalapu, D. T. Zhao, and J. L. Liu, Appl. Phys. Lett. 87, 252102 (2005).

9:40 AM Student

DD5, Phosphorus Bipolar Doping of ZnO Thin Films Fabricated by Pulsed Laser Deposition: *Arnold Allenic*[1]; Wei Guo[1]; Yanbin Chen[1]; Guangyuan Zhao[1]; Yong Che[2]; Zhendong Hu[2]; Bing Liu[2]; Xiaoqing Pan[1]; [1]University of Michigan; [2]IMRA America, Inc.

Phosphorus-doped ZnO (P:ZnO) thin films are fabricated on (0001) Al_2O_3 substrates by pulsed laser ablation of P_2O_5-doped ZnO targets (0.05 wt% - 1wt%). All films grow epitaxially on the sapphire substrate and will be characterized by x-ray diffraction and transmission electron microscopy. As-grown phosphorus-doped ZnO films on sapphire are n-type and more conductive than undoped ZnO. Typically, $n\sim10^{19}$ cm^{-3} and $p\sim10^{-3}$ Ω.cm, making n-type P:ZnO an excellent transparent conducting oxide for junction applications. Films grown between 400°C and 600°C and subsequently annealed in synthetic air are p-type with a hole concentration of about 5.0×10^{17} cm^{-3}, resistivity of ~43 Ω.cm and Hall mobility of ~0.3 cm^2/V.s. Photoluminescence at 10 K shows a dominant phosphorus-related recombination line at 3.3417 eV and a broad (FWHM=0.5 eV) red band peaking at 1.93 eV. More detailed PL results will be presented. Based on these results, homoepitaxial P:ZnO films are deposited on Cermet, MTI and Crystec Zn-face ZnO substrates. A p-n junction was successfully fabricated on the Cermet ZnO substrate.

10:00 AM Break

10:20 AM

DD6, ZnO Light-Emitting Diode Fabricated by Plasma-Assisted Metalorganic Chemical Vapor Deposition: *Zhizhen Ye*[1]; Weizhong Xu[1]; Yujia Zeng[1]; Liping Zhu[1]; [1]Zhejiang University

ZnO homojunction light-emitting diode was fabricated by plasma-assisted metalorganic chemical vapor deposition (MOVCD). Using NO plasma, p-type ZnO epi-layers were realized on n-type single-crystal bulk ZnO substrates. The as-grown films on glass substrates show hole concentration of 1016~1017 cm^{-1} and mobility of 1~10 cm^2V-1s-1. Room-temperature photoluminescence spectra reveal nitrogen-related emissions. The I-V characteristics of the In/Zn electrodes on the n- and p-type ZnO are reasonably linear, indicating a good Ohmic contact at both ends of the device. A typical ZnO homojunction shows rectifying behavior with a turn-on voltage of about 3 V. Electroluminescence at room temperature has been demonstrated with band-to-band emission (375 nm) at I = 40 mA and defect-related emissions in the blue-yellow spectrum range (430 - 600 nm).

10:40 AM

DD7, MOCVD Growth of ZnO and p-Type Doping: *Ming Pan*[1]; Varatharajan Rengarajan[1]; Jeff Nause[1]; [1]Cermet, Inc.

Zinc oxide is receiving considerable fascination as an ideal candidate for UV or blue light emitting and detecting applications. ZnO has wurtzite structure and a direct band gap of 3.37eV at room temperature. Furthermore, having an exciton binding energy of 60meV, much higher than that of GaN, 25meV, make it very promising for high efficiency lasing. The barrier which limits wide applications of ZnO in optoelectronics field is the difficulty to achieve p-type ZnO. Many efforts were devoted to achieve p-type ZnO with different growth technologies and dopants. In this paper, we report ZnO thin film growth and in-situ p-type doping by using metal organic chemical vapor deposition (MOCVD). A vertical, disk rotating reactor MOCVD tool with specially designed plasma system was employed for ZnO epitaxial growth, which enables a high efficiency incorporation of p-type dopant into the ZnO film. DEZn and oxygen were used as precursors for Zn and O, respectively. Different sources for nitrogen (N) dopant were investigated. N-doped ZnO films were successfully grown on sapphire, ZnO and GaN/sapphire substrates. The effects of growth parameters on the quality of the films were studied and improvements were made on the growth parameters to get high quality pure and p-doped ZnO thin films. Crystal quality of as grown doped ZnO films were characterized by X-ray diffraction. Photoluminescence was used to check the optical properties of doped ZnO. Electrical properties of the films were measured by Hall Effect.

11:00 AM

DD8, Characterization of Defects in Zinc Oxide Single Crystals: Balaji Raghothamachar[1]; *Govindhan Dhanaraj*[1]; Yi Chen[1]; Hui Chen[1]; Michael Dudley[1]; Michael J. Callahan[2]; Erik Grant[2]; Buguo Wang[3]; [1]Stony Brook University; [2]Air Force Research Laboratory; [3]Solid State Scientific Corporation

Zinc oxide (ZnO) is a direct bandgap semiconductor with an energy gap of 3.37eV. It has potential for application in emitter devices in the blue to ultraviolet region and as a substrate material for GaN based devices. It also has the highest shear modulus and most stable lattice among II-VI semiconductors because of its very small inter-atomic distances. Its large exciton binding energy (60 meV) makes it suitable for efficient UV laser applications. Also, it is a room temperature ferromagnetic semiconductor. The ZnO crystals used in our study were grown in autoclaves made of high strength steel, with a sealed platinum liner. The mineralizer solution was a mixture of Li_2CO_3, KOH, and NaOH, with the fill quantity at 80%. During growth, the nutrient zone was at 355°C with a temperature gradient of 10°C. ZnO crystals obtained from many such growth runs were characterized using synchrotron X-ray topography. ZnO crystal plates of (10-10) and (11-20) orientation, cut perpendicular to the seed, were prepared for X-ray topographic characterization. These crystal plates contained the seed crystal and the newly grown bulk crystal to reveal the growth history. Also c-cut plates were used for defect evaluation. X-ray topographs were recorded using synchrotron white beam radiation. Systematic study revealed the presence of dislocations penetrating into the bulk from the seed, dislocation refraction, growth sector boundaries, inclusions, planar inclusion defects, etc. Process induced dislocations such as dislocation loops around the seed suspension as well as slip bands could be observed. The role of edge dislocations in the growth process could also be seen. High resolution X-ray diffraction measurements reveal narrow rocking curve widths indicating high crystal

quality. Details of the X-ray defect characterization will be presented.

11:20 AM
DD9, Late News

11:40 AM
DD10, Late News

Session EE: Contacts to III-Nitrides

Friday AM
June 30, 2006

Room: Deans Hall II
Location: Pennsylvania State University

Session Chairs: Huili (Grace) Xing, University of Notre Dame; Lisa M. Porter, Carnegie Mellon University

8:20 AM Student
EE1, Comparison of Thermally Stable TiB_2, CrB_2 and W_2B_5 Based Ohmic Contacts on n-GaN: *Rohit Khanna*[1]; S. J. Pearton[1]; F. Ren[1]; I. I. Kravchenko[1]; [1]University of Florida

Three different metal borides (TiB_2, CrB_2 and W_2B_5) were examined for use in Ti/Al/boride/Ti/Au Ohmic contacts on n-type GaN and the reliability compared to the more usual Ti/Al/Ni/Au metal scheme. The minimum specific contact resistance obtained was in the range10^{-5} O.cm^2 with CrB_2 and W_2B_5 and approximately an order of magnitude lower with TiB_2. In all cases, the minimum contact resistance is achieved after annealing in the range 700-900°C. The main current transport mechanism in the contacts after this annealing is tunneling as determined by the absence of any significant measurement temperature dependence to the contact resistance. The TiB_2 and CrB_2 contacts retain smooth morphology even after annealing at 1000°C. Auger Electron Spectrosopy depth profiling indicated that formation of an interfacial TiN_X layer is likely responsible for the Ohmic nature of the contact after annealing. All three boride-based contacts show lower contact resistance than Ti/Al/Ni/Au after extended aging at 350°C.

8:40 AM Student
EE2, Reduction of Metal/GaN Barrier Height Using Nanopatterning: *Ho Gyoung Kim*[1]; Parijat Deb[1]; Timothy D. Sands[1]; [1]Purdue University

GaN is an emerging material for applications in light-emitting devices, and high power, high temperature, high frequency electronic devices. The challenges in obtaining low barrier height metal contacts for ohmic contacts to GaN have hampered the development of GaN based devices. A large variety of elemental and multicomponent metallizations have been explored for ohmic contacts to p-GaN and n-GaN. Additionally, various surface treatment techniques such as chemical etching, dry etching and laser etching have been used to reduce the ohmic contact resistance, yet specific contact resistances are still sufficiently high to impact device performance, particularly for p-GaN. In the present work, a new and inexpensive fabrication process for introducing nanoscale surface inhomogeneities on GaN surfaces is presented. Undoped 5 µm thick n-GaN films (carrier concentration of 8.81 x 10^{16} cm^{-3}) grown by hydride vapor phase epitaxy (HVPE) on c-plane sapphire substrates were patterned by reactive ion etching (RIE) using SF_6 and O_2 gases using porous anodic alumina films as masks. The porous anodic alumina masks were fabricated by two-step anodization of aluminum films, yielding 40 nm diameter pores. The average etching depth into the GaN was about 40 nm. The electrical characteristics of contacts to these nanopatterned GaN samples were compared with those of as-grown GaN samples and RIE etched GaN films without any patterning. The ohmic contact resistance was evaluated using a Ti (30 nm)/Al (110 nm) bilayer metallization. The specific contact resistivities were determined to be 7.6 x 10^{-2} Ω cm^2 for the as-grown sample, 7.4 x 10^{-3} Ω cm^2 for the RIE etched sample and 7.0 x 10^{-4} Ω cm^2 for the PAA patterned sample. Schottky metal contacts with Pt and Ni were prepared on the three samples to validate the effects of RIE and nanopatterning on electrical behavior. It was seen that there is a significant reduction in barrier height in the RIE etched sample. The effective barrier height was decreased further for the PAA patterned sample. The carrier transport at the metal-GaN interface was analyzed based on the parallel conduction model. This model predicts that the barrier height for a PAA patterned sample should be in between the barrier heights of the as-grown sample and the barrier height of the RIE etched sample. The radius of curvature of the nanoscale corrugation in the patterned interface was smaller than the depletion width (100 nm for the Pt contact and 90 nm for the Ni contact). The reduction of the depletion width at sharp corners enhanced the local tunneling current, reducing the specific contact resistivity and decreasing the effective barrier height. These results suggest that nanopatterning with PAA on GaN can significantly lower the contact resistance.

9:00 AM Student
EE3, Investigation of a Low-Temperature Cu_3Ge Ohmic Contact to *N*-GaN: *Michael L. Schuette*[1]; Wu Lu[1]; [1]Ohio State University

Analyses of a Cu_3Ge ohmic contact to *n*-GaN showed process latitude advantages, over popular Ti/Al-based contacts which involve processing temperatures in excess of 800°C, which make it a viable candidate for use in electronic or optoelectronic device processes that require small thermal budgets. In this study, XPS showed that treatment of the GaN surface by $SiCl_4$ RIE followed by an HCl solution increased the concentration of surface nitrogen vacancies (V_N), a donor-like defect, and decreased the surface oxygen content. These improvements came with no degradation in surface morphology, as evidenced by AFM. *I-V* measurements on Ge/Cu/Ge transmission-line-method test structures showed that this surface treatment played a significant role in the ohmic behavior of the contact. As shown by AES, annealing of the copper germanide contacts at 600°C caused uniform 3:1 mixing of Cu and Ge throughout the contact. More interesting is that N and Ga both diffused across the metal-semiconductor interface, leaving V_N and V_{Ga}, which, due to the donor- and acceptor-like properties of these defects, should compensate each others' efforts to move the GaN surface Fermi level toward the conduction or valence band edges. However, Ge, a donor in GaN, appeared to diffuse into the semiconductor to a greater extent than Cu, suggesting the occupation of V_{Ga} by Ge, which should increase the GaN surface *n*-doping. This mechanism, proposed by Aboelfotoh et al. for copper germanide ohmic contacts to *n*-GaAs, along with an RIE-induced nitrogen-deficient GaN surface, is believed to be responsible for heavy surface doping which would enhance electron tunneling across the metal-semiconductor interface. Finally, the phase evolution of the contact film during annealing was revealed using XRD. Although the results were complicated by the overlapping of substrate peaks with contact peaks, as well as the texture of the contact films, important observations were made. Two peaks correlating to the metastable, nonmetallic tetragonal phase of Ge, which overlapped with cubic Cu peaks, were detected from the as-deposited contact films. After annealing, the intensities of these lines decreased with the appearance of lines correlating to the highly-conductive ε_1-Cu_3Ge (orthorhombic) phase. Cubic Ge lines also emerged after annealing, one of which overlapped with an ε_1-Cu_3Ge line. Due to the bulk sensitivity of the measurements, reactions occurring at the metal-semiconductor interface which enabled the ohmic behavior of the contact were not apparent from XRD spectra. However, these phase changes, as well as general crystallization that occurred during annealing, are in part responsible for the reduction of the resistance of this contact system.

9:20 AM
EE4, Formation of High-Quality Ag Ohmic Contacts for Flip-Chip LEDs by Using Transparent Conducting Oxide Interlayers: Hyun-Gi Hong[1]; June-O Song[2]; J. Cho[3]; Y. Park[3]; J. S. Kwak[4]; *Tae-Yeon Seong*[5]; [1]Gwangju Institute of Science and Technology; [2]Georgia Institute of Technology; [3]SAIT; [4]Sunchon National University; [5]Korea University

Development of high-brightness GaN-based LEDs is of great technological importance for their application in solid-state lighting, which requires the achievement of high light extraction in LEDs. Flip-chip LEDs (FCLEDs) were shown to be effective in enhancing light extraction efficiency. Ag is the most commonly used reflectors for FCLEDs, because it has high reflectivity and gives relatively good ohmic behaviour. However, a single Ag electrode suffers from problems, such as agglomeration and the formation of interfacial voids upon annealing, which degrades the electrical and optical performances of LEDs. To solve such problems, various interlayers were introduced between Ag and p-GaN. In this work, we have used ZnO-based transparent

conducting oxide (TCO) interlayers to improve the electrical properties of Ag-based contacts to p-GaN for the fabrication of high-performance near UV-FCLEDs. For example, Mg- and Sn-doped ZnO(MZO and TZO, respectively)/Ag p-contact layer produce ohmic behavior with specific contact resistances of ~10^{-4} Ωcm^2 and reflectance of 76 – 83% at a wavelength of 405 nm when annealed at 530°C in air. It is shown that LEDs made with the TCO interlayers yield reverse leakage currents three orders of magnitude lower than that of LEDs without the interlayers. The LEDs fabricated with the TCO interlayers show higher output power as compared with the LEDs without the interlayers. Based on X-ray photoelectron spectroscopy and TEM results, possible ohmic formation mechanisms are discussed.

9:40 AM
EE5, Late News

10:00 AM Break

10:20 AM Student
EE6, Analytical Transmission Electron Microscopy (TEM) Investigation of the Structural Evolution of Ti-Based Ohmic Contacts on GaN and AlGaN/GaN at Different Annealing Temperatures: *Liang Wang*[1]; Fitih M. Mohammed[1]; Ilesanmi Adesida[1]; [1]University of Illinois at Urbana-Champaign

Understanding the ohmic contact formation mechanism is crucial for the application of GaN materials for optoelectronic and high-performance electronic devices. The mechanism could be identified only when the annealed microstructure created by the reaction between metal contacts and the GaN substrate are revealed in detail. In a standard Ti/Al-based multilayer contact, such as Ti/Al/Mo/Au, there are more than six elements participating in the reaction and even more possible reaction products. Identifying each one of the phases and their effects on contact performance by means of X-ray diffraction (XRD), Auger electron spectroscopy (AES), etc. is not possible given that the phases being analyzed are in nanometer scale and are distributed unevenly across the sample and these tools yield only average information. Alternatively, scanning TEM (STEM) is an ideal tool in investigating local microstructure and composition in a multicomponent system due to its high spatial resolution and analytical capability. In order to elucidate the ohmic formation mechanism as well as the degradation mechanism when annealed, a JEOL 2010F microscope is used to study the cross-sectional and plan view structure of Ti/Al/Mo/Au metallizations on GaN and AlGaN/GaN heterostructures annealed at different temperatures (T_a). Z-contrast images are formed in STEM mode with an electron probe diameter <1 nm. Energy dispersive X-ray spectroscopy (EDS) signals are also collected in this mode by placing electron probe on places of interest. For contacts on AlGaN/GaN, when T_a=400°C, no significant structural change is found. For T_a=600°C, Mo layer remains continuous, but it migrates outward to the surface of the metallization pushed by the in diffusion flux of Al through grain boundaries. At T_a=700°C, still no TiN forms but Mo layer breaks into particles and internal Al oxide starts to form. At an optimal temperature of 850°C, discrete TiN islands form preferentially along threading dislocations. It is hypothesized that these TiN islands create direct electrical link between the two-dimensional electron gas and metal contacts. The current transport mechanism is thus different from that reported on GaN. Our results show that the reaction pathway is completely different for contacts on GaN epilayers at 850°C. On GaN, a continuous layer of TiN formed at the interface of metal/GaN. The extraction of N from GaN triggered by TiN formation and thus the N-vacancies (which is an n-type dopant) generated in GaN at the proximity of the interface is responsible for low resistance contact formation by tunneling mechanism. A high temperature annealing of 950°C results in degradation in contact performance. The degradation mechanism is believed to be the disturbance of the 2DEG formation or reduction in its electron sheet density by abnormal TiN islands growth along dislocations at the interface.

10:40 AM Student
EE7, Low-Temperature-Annealed Mo-Based Ohmic Contacts for AlGaN/GaN Heterostructures: *Anirban Basu*[1]; Fitih M. Mohammed[1]; Liang Wang[1]; Vipan Kumar[1]; Ilesanmi Adesida[1]; [1]University of Illinois, Urbana-Champaign

AlGaN/GaN high electron mobility transistors (HEMTs), due to their high power handling capacity at high frequencies, have emerged as exceptionally promising candidates for microwave power amplifiers and next generation RF low noise applications. The realization of the full potentials of such devices requires the formation of low ohmic contact resistance after annealing at an optimal temperature. Most ohmic metallization schemes that have been reported in literature for GaN-HEMTs involve Ti/Al as the basic combination with various overlayers (e. g. Ti/Al/Ni/Au, Ti/Al/Pt/Au, Ti/Al/Mo/Au). However, high performance ohmic contacts are obtained only after annealing of these metallizations at temperatures above 750°C, which is higher than the melting point of Al (~660°C). Such high temperatures result in considerable lateral flow of the metals due to the formation of viscous AlAu4. The lateral flow increases the probability of short-circuiting between the gate and source/drain of a HEMT. Therefore, high annealing temperature may preclude the fabrication of short-channel GaN-HEMTs. Therefore, it is important to develop ohmic contact metallization that yields low contact resistances at temperatures below the Al melting point. In this work, we report our investigations on low temperature ohmic contact characteristics of a Mo/Al/Mo/Au metallization on AlGaN/GaN heterostructures annealed at temperatures ranging from 450°C to 650°C. Effects of cumulative metallization thickness have been studied by scaling the scheme from 150 nm to 70 nm. Mo is a good refractory material with a high melting point and demonstrates linear I-V characteristic on as-deposited n-GaN. Additionally, the solubility of Au in Mo is relatively low. Metal evaporation of Mo/Al/Mo/Au layers has been done in an e-beam and thermal evaporation chamber under high vacuum. Prior to metal evaporation, the AlGaN surface was bombarded in an RIE system with SiCl4 plasma at bias voltages ranging from –300 V to –500 V. Experiments have been done on two wafers from two different sources for consistency. Our investigations show that for annealing temperatures below 450°C, the annealed metallization displayed Schottky characteristics. A 70 nm thick metallization scheme after annealing at 500°C for 2 min. in a rapid thermal annealing system yielded a contact resistance of 0.40±0.05 O-mm and a specific contact resistivity of ~2.2x10-6 O-cm2. Annealing at 550°C for 2 min. yielded an optimal ohmic contact resistance of ~0.21±0.05 O-mm. These are the best ohmic contact properties that have been reported to date on GaN-HEMTs at temperatures lower than Al melting point with such thin metallization. Importance of Mo:Al ratio will be demonstrated through comparative results. Comprehensive results on contact resistance as a function of annealing temperature and time will be presented. Cross-section transmission electron microscopy analysis of the annealed microstructure will be discussed to give insights about contact formation mechanism. In addition, results on surface roughness and edge-acuity will be presented.

11:00 AM Student
EE8, Si and Ge Incorporation in Ti/Al/Mo/Au for AlGaN/GaN HEMTs: Effects on Electrical and Microstructural Properties: *Fitih M. Mohammed*[1]; Liang Wang[1]; Ilesanmi Adesida[1]; [1]University of Illinois at Urbana-Champaign

Low resistance ohmic contact formation is essential for reduction of knee voltage and resistive heating in AlGaN/GaN high electron mobility transistors (HEMTs), which present great potential for applications in microwave power amplification.[1] High performance devices for such applications require ohmic contacts with contact resistivity better than 10^{-5} Ω-cm^2.[2] Also contact metallizations need to have high thermal stability and smooth surface morphology to ensure dependable high temperature performance and to facilitate sharp edge acuity for short channel devices, respectively.[3] To this end, Selvanathan *et al*.,[4,5] have reported the formation of excellent ohmic contacts to AlGaN/GaN heterostructures using Ti/Al/Mo/Au metallization, and Gillespie *et al*.[6] have recently indicated that this scheme, in contrast to other metallization schemes, has the potential for optimization as a generic ohmic contact that is not dependent on the growth conditions of epitaxial layers. Auger electron spectroscopy and transmission electron microscopy microstructural characterizations carried out to identify ohmic contact formation mechanism of this scheme[7,8] have indicated that the high-melting point Mo third-layer is not effective as a diffusion barrier. In fact, contacts annealed at optimal conditions have been demonstrated to contain complex structures in which a thorough intermixing among the metallization layers and intermetallic grain formation in the metallization matrix is observed along with varying degree of interfacial reactions between metals and epilayer. A consequence of these complex intermetallic reactions is the formation of $AlAu_x$ phases. A review of phase diagrams of Al-Si, Au-Si, Al-

Ge and Au-Ge binary alloys[9] indicates the feasibility of low-temperature eutectic alloys formation. As such, we have explored the effect of Si and Ge incorporation in Ti/Al/Mo/Au scheme to induce the formation of Al-Au-Si and Al-Au-Ge solid solutions. Electrical characteristics of these Si and Ge-containing schemes, as well as the nature of interfacial reactions, have shown strong dependence on the content and placement of the inserted layers. While Si incorporation was found to induce a significant reduction in the contact resistance, Ge incorporation did not seem to enhance the contact performance of the Ti/Al/Mo/Au. Results from the microstructural characterizations carried out to elucidate the ohmic contact formation mechanism of Si and Ge-containing schemes will be presented along with the electrical properties of these schemes. Cases of suppression of interfacial TiN formation and activation of AlN formation reactions will be detailed. [1]Materials Science and Engineering: R 30, 55 (2000). [2]Appl. Phys. Lett. 68, 3022 (1996). [3]J. Appl. Phys. 89, 3143 (2001). [4]Physica Status Solidi A 194, 583 (2002). [5]J. Vac. Sci. and Technol. B22, 2409 (2004). [6]Solid-State Electron. 49, 670 (2005). [7]J. Vac. Sci. and Technol. B23, 2330 (2005). [8]Appl. Phys. Lett. 87, 141915 (2005). [9]H. Okamoto, "Desk Handbook: Phase Diagrams for Binary Alloys," ASM International, Materials Park, OH, USA, 2000.

11:20 AM Student

EE9, Comparison of V- and Ti-Based Ohmic Contacts to High Al-Fraction n-$Al_xGa_{1-x}N$: *Mary A. Horsey*[1]; Katherine H. A. Bogart[2]; Andrew Allerman[2]; G. S. Cargill III[3]; Alexey Nikiforov[4]; [1]Pennsylvania State University; [2]Sandia National Laboratories; [3]Lehigh University; [4]Boston University

A Ti-based multilayer metallization is typically used for ohmic contacts to n-type $Al_xGa_{1-x}N$. By optimizing the individual layer thicknesses of the contact, low specific contact resistances can be achieved with high temperature anneals. As the Al-fraction increases, we have previously reported that a multilayer V-based contact provides a lower contact resistance than the Ti-based contacts at lower optimization temperatures. Like the Ti-based contact, the V-based contact is very sensitive to layer thicknesses. Our previous V-based contacts were optimized on as-grown n-$Al_xGa_{1-x}N$. For bottom-emitting UV-LEDs, layers of semiconductor must be removed with a reactive ion etch (RIE) to make contact to the n-type region. In this work we describe how engineering the layer thicknesses can accommodate different conditions such as etched surfaces. V/Al/V/Au contacts were tested on both unetched and RIE n-$Al_xGa_{1-x}N$ with x = 0.46, 0.58 and 0.6. The RIE chemistry used was $BCl_3/Cl_2/Ar$. The contact that gave the best results on the unetched material provided poor results on the etched material. A V(13)/Al(73)/V(18)/Au(85 in nm) contact provided 3.9 x 10^{-6} Ohm-cm^2 for n-$Al_{0.46}Ga_{0.54}N$ and 1.6 x 10^{-5} Ohm-cm^2 for n-$Al_{0.6}Ga_{0.4}N$. For the etched semiconductor, to reach a specific contact resistance of 1.6 x 10^{-5} and 1 x 10^{-4} Ohm-cm^2 for x = 0.46 and 0.6 respectively, the first layer of V had to be increased to 27 nm. It was hypothesized that an increased reaction depth was needed to lower the specific contact resistance, which was consistent with our cross-sectional transmission electron microscopy (TEM) images. To understand the formation of ohmic contacts to high aluminum fraction n-$Al_xGa_{1-x}N$ in the etched and unetched conditions, it is also important to study the reaction of metal layers within the multilayer stack and their reaction with the semiconductor. Therefore, we have also performed TEM on V, Ti, and V/Al/V/Au ohmic contacts to n-$Al_xGa_{1-x}N$. The study revealed marked differences in the reaction products and reaction depth of the contacts, which help explain why different processing conditions are needed for Ti- and V-based contacts.Comparison of V- and Ti-based Ohmic Contacts to High Al-Fraction n-AlxGa1-xN.

11:40 AM

EE10, Late News

Session FF: Indium Nitride

Friday AM, June 30, 2006
Room: Conference Room 106
Location: Pennsylvania State University

Session Chairs: Joan M. Redwing, Pennsylvania State University; William J. Schaff, Cornell University

8:20 AM

FF1, Origin of the N-Type Conductivity of InN – The Role of Positively Charged Nitrogen Vacancies along Threading Dislocations: *Tim Veal*[1]; Louis Piper[1]; Chris McConville[1]; Hai Lu[2]; William J. Schaff[2]; [1]University of Warwick; [2]Cornell University

As-grown InN always exhibits n-type conductivity, with unintentional free-electron concentrations as high as 10^{21}cm^{-3}. Many theoretical and experimental studies have focussed on determining the major reason for the unintentional n-type conductivity of InN. However, no consensus has yet been reached. The traditional candidates fall into two categories: donor impurities and donor-type native defects. The impurities most commonly suggested as the primary cause of InN's n-type conductivity are oxygen and hydrogen. Amongst native defects, the nitrogen vacancy has been found from theoretical calculations to be a donor and has also been suggested as the major reason for the high n-type conductivity. Self-interstitials and anti-site defects are energetically unfavorable in InN due to the small lattice constant and the large-size mismatch between the cations and anions, respectively. More recently, surface electron accumulation has emerged as another factor contributing to the n-type conductivity in InN. The purpose of the work presented here is to investigate the relative importance of the contributions of native defects, impurities and the native surface electron accumulation to the n-type conductivity. Hall measurements from a range of high-quality InN films grown by molecular-beam epitaxy reveal a dramatic reduction of the free-electron density (from low 10^{19} cm^{-3} to low 10^{17} cm^{-3}) with increasing film thickness (from 50 to 12000 nm). This variation of free-electron density with film thickness is successfully modelled by considering a homogeneous background of donor impurities, a constant surface sheet density due to electron accumulation, and positively-charged nitrogen vacancies along threading dislocations whose density declines exponentially away from the InN/buffer layer interface. This variation of the threading dislocation density in InN thin films has been confirmed by transmission electron microscopy and follows the same trend as observed in GaN. However, in n-type GaN, negatively-charged acceptor-type gallium vacancies form along the dislocation core. In contrast, the energetic favorability of positively-charged donor-type nitrogen vacancies along dislocations in n-type InN is discussed in terms of recent density functional theory calculations and the particularly low conduction band minimum in InN. This work highlights the significance of the contribution to the n-type conductivity in InN of positively-charged nitrogen vacancies along threading dislocations. Therefore, rather than there being a single major cause of InN's n-type conductivity, native defects, impurities and electron accumulation all play a significant role. In fact, the single reason for the n-type conductivity of InN is its band structure which is responsible for the surface electron accumulation and dictates that O, H and nitrogen vacancies are all donors.

8:40 AM

FF2, Optical Properties of the In-Polarity InN/$In_{0.7}Ga_{0.3}N$ MQWs Grown by RF-MBE: *Song-Bek Che*[1]; Takuro Shinada[1]; Yoshihiro Ishitani[1]; Akihiko Yoshikawa[1]; [1]Chiba University

InN is attracting strong interest in its unique properties such narrower bandgap energy as 0.63eV compared to other III-nitride semiconductors. This indicates the potential application of InN-based III-nitrides in near-infrared photonic devices. The InN/InGaN multi-quantum wells (MQWs) structure is a candidate for an active layer of the photonic devices. It was already reported that near-infrared emission at around 1.55μm from the N-polarity InN-based MQWs by photoluminescence (PL) measurement. However, compared to the InGaN/GaN MQWs, which are generally used as an active

layer for bule-green LEDs and LDs, crystalline quality of the N-polarity InN-based MQWs is still poor and its drastic improvement is necessary when considering the realistic InN-based optical devices. In this paper, we will discuss the structural and optical properties in the In-polarity InN/$In_{0.7}Ga_{0.3}N$ MQWs by using the high-quality $In_{0.7}Ga_{0.3}N$ under- and barrier-layers, which results in the observation of RT-PL emissions at 1.55~1.62μm. We already reported the polarity dependence of In-rich InGaN ternary alloys (X_{In}>0.5) and the InN/$In_{0.7}Ga_{0.3}N$ MQWs. It was found that the drastic improvement of crystalline quality was achieved in the In-polarity growth regime despite the about 100°C lower growth temperature of the In-polarity InGaN and MQWs than that of the N-polarity ones. Recently, we succeeded in further improvement of crystalline quality of In-polarity $In_{0.72}Ga_{0.28}N$ alloys by accurately controlling their III/V ratio, which showed relatively narrower full-width at half maximum (FWHM) values of 332arcsec in (002) X-ray ω-rocking curve measurement. On the basis of these experimental results, we tried to fabricate the high-quality InN/$In_{0.7}Ga_{0.3}N$ MQWs. Here, in order to grow the In-polarity MQWs, Ga-polarity GaN template grown by MOCVD was used as a substrate. Before the MQWs growth, re-growth of GaN with its thickness about 100nm was carried out at 750°C. Then, the structure of the MQWs was grown at 450°C, which consisted of a 200 nm $In_{0.7}Ga_{0.3}N$ underlayer, InN/$In_{0.7}Ga_{0.3}N$ MQWs, and a 20nm $In_{0.7}Ga_{0.3}N$ cap layer. Thickness of the InN wells and $In_{0.7}Ga_{0.3}N$ barriers were about 0.5~1nm and 3~6nm, respectively. Here, three InN/$In_{0.7}Ga_{0.3}N$ MQWs with 5,20 and 50 periods were characterized by X-ray diffraction, PL and cathode-luminescence (CL) measurements at room temperature (RT). Clear satellite peaks were observed in these three MQWs samples, which indicate that fine periodic structures were realized even for the 5 periods MQWs. In the PL measurement at RT, emissions from the MQWs region were clearly observed in around optical communication wavelength. As for the 20 periods InN(0.8nm)/$In_{0.7}Ga_{0.3}N$ (2.7nm) MQWs, a 1.55μm emission peak was clearly observed in PL and CL measurements. These results indicate that in spite of the lower growth temperature than that of N-polarity, the In-polarity InN/InGaN MQWs would be one of good candidates for the nitride-based optical devices operating in the optical communication wavelength.

9:00 AM

FF3, In-Polar InN: Evidence of a Possible Hole Accumulation Layer: Phillip A. Anderson[1]; *Steven M. Durbin*[1]; Craig Swartz[2]; Thomas H. Myers[2]; S. J. Kim[3]; M. C. Chung[3]; Alexander N. Cartwright[3]; [1]University of Canterbury; [2]West Virginia University; [3]University at Buffalo, State University of New York

Indium nitride has a number of interesting properties beyond its low bandgap. One of these is the tendency to form a surface accumulation layer, first identified by Lu et al.[1] who observed that in plasma-assisted molecular beam epitaxy (PAMBE) grown samples the sheet carrier density did not extrapolate to zero at zero layer thickness. This phenomenon has been suggested to result from ionised donor-type surface states which pin the Fermi level well above the conduction band minimum[2]. Not surprisingly, we have observed similar behaviour in our samples also grown by plasma-assisted molecular beam epitaxy (PAMBE) on (0001) sapphire substrates, where quantitative mobility spectrum analysis (QMSA) from variable magnetic field Hall effect measurements reveals two resolvable carriers: low-mobility, high sheet carrier density electrons consistent with a surface accumulation layer, and higher mobility electrons attributed to the bulk. These samples were grown on ~300 nm thick GaN buffer layers deposited on nitrided sapphire . KOH etching reveals morphology consistent with that reported for N-polar InN. Regardless of whether a (N-polar) GaN buffer layer or nitridation step are part of the growth recipe, we have only observed N-polar InN films when using sapphire substrates. The electrical properties of these films generally show a strong dependence on the active nitrogen species used for growth, as has been reported for N-polar GaN grown by PAMBE. (111) YSZ substrates represent a better lattice match (3% mismatch compared to 9% for GaN). In contrast to the layers grown on sapphire, films grown on (111) YSZ show little dependence on plasma conditions of film electrical characteristics as measured by single-field Hall effect. KOH etching experiments also indicated these films are consistently In-polar. Both QMSA and multiple-carrier fitting (MCF) of variable field Hall effect measurements up to 12 Tesla reveal the need for three types of carriers to explain the electrical properties. The third carrier in these films is a hole having mobility in the range of 500 to 700 cm^2/Vs, and is present in the measurements over the measured temperature range of 5 to 300 K. The location of this hole layer is not clear, but is believed to be at the surface – we are currently seeking to verify this using a depth-resolved transient grating spectroscopy technique. If true, it presents the interesting possibility of realising Schottky contacts to InN, a goal frustrated to date by the presence of the surface electron accumulation in what is likely N-polar InN. [1]Hai Lu et al., Appl. Phys. Lett. 82 (2003) 1736. [2]I. Mahboob et al., Phys. Rev. B 69 (2004) 201307(R); I. Mahboob et al., Phys. Rev. Lett. 92 (2204) 036804; C.H. Swartz, et al., J. Crys. Growth 269 (2004) 29.

9:20 AM

FF4, Anisotropy of the Γ-Point Electron Effective Mass in Hexagonal InN: *Tino Hofmann*[1]; T. Chavdarov[2]; V. Darakchieva[3]; H. Lu[4]; William J. Schaff[4]; Mathias M. Schubert[1]; [1]University of Nebraska-Lincoln; [2]Universität Leipzig; [3]Linköping University; [4]Cornell University

InN has recently attracted much attention due to the availability of high-quality samples grown, e.g., by metal-organic vapor phase epitaxy, or molecular beam epitaxy. Especially the unexpected low band gap value of 0.6 to 0.7 eV has triggered new experiments, vivid debates, and many reconsiderations.[1] But still, information on fundamental material parameters such as the anisotropy of the wurtzite-structure conduction-band effective mass, its energy and strain dependencies or the experimental verification of the Γ-point electron effective mass are lacking. We report on the use of a new optical technique for measurement of the free-charge-carrier properties concentration, mobility, and effective mass in n-type wurtzite InN thin films without the need of performing electrical contacts. We are particularly interested in the connection between the carrier concentration, the band-gap value, the band-gap effective mass, its anisotropy and the influence of biaxial strain. Only few experimentally determined values on the isotropically averaged effective mass of hexagonal InN exist so far.[2,3] We employ generalized magnetooptic ellipsometry in the far-infrared spectral range [4] - which we have termed accordingly as "optical Hall effect" - and determine the effective mass parallel $m^*_{e,parallel}$ and perpendicular $m^*_{e,perp}$ to the c axis, the free electron concentration N, and parallel $\mu_{e,parallel}$ and perpendicular $\mu_{e,perp}$ optical mobility parameters in thin InN layers with different free electron concentration values N in the range between $1.75x10^{17}$ cm^{-3} to $1x10^{19}$ cm^{-3}. We avoid ambiguous data interpreation due to barrier formation in electrical contacts, required otherwise for electrical Hall effect measurements. The samples were grown by molecular beam epitaxy on sapphire substrates, and structural measurements ensure high crystal-quality of the InN layers. While our isotropically averaged effective mass values are in good agreement with recently reported values, we observe a distinctanisotropy of the effective mass, with $m^*_{e,perp} > m^*_{e,parallel}$, which is in good agreement with recent LDA band-structure calculation results.[5] Application of the simple kp scheme extrapolates the effective mass parameters for the bottom of the conduction band, and results in band gap values of 0.7eV for polarization perpendicular and 0.4eV for polarization parallel to the InN c axis, respectively. We also discuss the significant influence of biaxial strain on the effective mass parameters. References: [1]B. Monemar, P.P. Paskov, and A. Kasic, Superlattices and Microstructures 38 38 (2005); [2]A. Kasic, M. Schubert, Y. Saito, Y. Nanishi, and G. Wagner, Phys. Rev. B 65, 115206 (2002); [3]J. Wu and W. Walukiewicz, Superlattices and Microstructures 34, 63 (2003); [4]M. Schubert, T. Hofmann, and C. M. Herzinger, J. Opt. Soc. Am. A 20, 347 (2003); [5]P. Carrier and S. Wei, Journal of Applied Physics 97, 033707 (2005).

9:40 AM Student

FF5, Structural and Optical Properties of InN Layers Grown by HPCVD: *Mustafa Alevli*[1]; Goksel Durkaya[1]; Aruna Weerasekara[1]; William Fenwick[2]; Vincent Woods[2]; Ian T. Ferguson[2]; Unil Perera[1]; Nikolaus Dietz[1]; [1]Georgia State University; [2]Georgia Institute of Technology

Gaining a better understanding of the origin in the observed variations of the physical properties of Indium Nitride (InN) layers is essential for the evaluation of the potential of indium-rich group III-nitride alloys for advanced optoelectronic device applications. Indium-rich alloys, e.g. $In_x(Ga_{1-y-x}Al_y)N$, will enable the fabrication of multi-tandem solar cells, high-speed optoelectronics and solid state lasers operating in the UV to near IR spectral region. The large spectral rage covered, and the robustness of group III-nitride alloys against radiation makes this material system also of interest for many space applications. So far, the fabrication of indium rich

$(In_{1-x}Ga_x)N$ layers and heterostructures remains a challenge, primarily due to the large thermal decomposition pressures encountered in InN and indium rich group III-nitride alloys at the optimum growth temperature. In order to control and analyze the vast different partial pressures of the constituents, a novel high-pressure chemical vapor deposition (HPCVD) system has been developed with integrated real-time optical diagnostics. Our initial results on the growth of InN by HPCVD demonstrate that HPCVD is viable tool for the growth of indium rich group III-nitride alloys. It allows the growth of InN at temperatures as high as 1150 K for reactor pressures around 15 bar, which is a major step towards the fabrication of indium rich group III-nitride heterostructures by providing a closer match in the processing windows used for GaN - AlN alloys. InN is a unique material, tending to stoichiometry violation as observed in Raman modes, X-Ray diffraction (XRD) patterns and optical absorption edges. Using a combination of Raman spectroscopy and XRD, the structural properties of InN layers were analyzed as a function of the ammonia to TMI ratio for reactor pressures around 15 bar. The analysis shows that the full width half maximum (FWHM) of Raman modes improved as the ammonia to TMI ratio decreases. For NH_3 to TMI precursor ratio below 500, multiple sharp XRD peaks are observed, indicating the coexistence of InN phases in very close proximity. The optical absorption spectra shows that the onset of absorption edge that shifts from 1.8 down below to 0.7 eV as the stoichiometric ratio in the InN layers goes from nitrogen rich to indium rich. Infrared reflectance data were used to analyze the plasmon frequencies, high frequency dielectric constants (e_8), and the free carrier concentrations in these layers. The free carrier concentrations of the samples were found to be between 5E+19 and 5E+20 cm_{-3}.

10:00 AM Break

10:20 AM

FF6, Effect of the Growth Mode and Substrate Properties on the Biaxial Strain in InN (0001) Epilayers: *Eleftherios Iliopoulos*[1]; Emmanouil Dimakis[1]; Jaroslaw Domagala[2]; Katerina Tsagaraki[1]; Alexandros Georgakilas[1]; [1]Microelectronics Research Group, University of Crete, Greece, and Institute of Electronic Structure and Laser (IESL), Foundation for Research and Technology-Hellas (FORTH), Greece; [2]Institute of Physics, Polish Academy of Sciences

The dependence of the biaxial strain in InN (0001) films on the growth mode and the substrate's lattice properties has been investigated. The extended Bond method in high-resolution x-ray diffraction was used to determine the c and a lattice parameters. We compared InN samples nucleated and grown under various conditions. Three group of InN samples were grown on GaN/Al2O3 (0001) substrates. Nucleation at 400°C with stoichiometric In/N flux ratio resulted, through step-flow growth mode, in smooth InN films (samples of group A), while nucleation at 300°C under nitrogen-rich conditions resulted, through coalescence of 3D islands, in rough InN films (samples of group B). Nucleation at 400°C and 500°C under nitrogen-rich conditions resulted in porous and columnar InN structures, respectively. An additional sample was grown on GaN/6H-SiC substrate, using the same conditions as for the samples of group A. The different groups of samples exhibited different c and a lattice parameters, and a linear relation between a and c values was observed. This was attributed to different amount of built-in biaxial strain in the samples. Other types of strain, such as hydrostatic, which are related to different concentrations of point defects, can be excluded. The films of group B, which presented the lowest c and highest a values, were under tensile stress, since micro-cracks were observed on the InN surface. However, the total biaxial strain in the InN films is expected to consist of two compressive components; the misfit one that originates from the in-plane lattice mismatch between InN and GaN, and the thermal one that originates from the higher in-plane linear thermal expansion coefficient of Al2O3 than that of InN. Temperature dependent x-ray diffraction measurements confirmed that the a-lattice parameters of InN and GaN followed the thermal expansion of Al2O3. Thus, the tensile stress of the samples of group B can be correlated only with the 3D growth mode during InN nucleation. The films of group A, which presented the lowest a and highest c values, are expected to be under compressive biaxial strain. This is confirmed by the fact that the a and c values of the sample grown on SiC substrate, which has thermal expansion coefficient close to that of InN, were between the group A and the group B values. The columnar and porous samples also presented lattice parameters among those of samples of group A and group B. Based on the above results, the permitted lattice constant values of strain-free InN are estimated to be c0=5.699+-0.004Å and a0=3.535+-0.005Å. Given these values and the parameters of the regression line fit to the (c, a) data points, the biaxial strain relaxation coefficient of InN, 2C13/C33, was calculated to be equal to 0.43+-0.04.

10:40 AM

FF7, Study of Graded InGaN Buffer Layers for MOCVD Growth of Indium Nitride Thin Films: *Abhishek Jain*[1]; Xiaojun Weng[1]; Joan M. Redwing[1]; [1]Pennsylvania State University

Indium Nitride (InN) is the least studied group III-nitride semiconductor because of issues related to its growth such as a low dissociation temperature and the lack of a lattice matched substrate. Attempts to grow InN films by MOCVD on Ga-polar GaN buffer layers have typically resulted in films with high surface roughness, and poor interface adhesion has also been reported. In spite of the large lattice mismatch between InN and GaN which would be expected to give rise to a compressive growth stress in the InN layer, a tensile stress (~0.2 GPa) was previously measured during MOCVD growth of InN on GaN, which most likely originates from the initial nucleation and film coalescence process. In this study, we investigated the use of compositionally graded InGaN layers for the growth of InN on GaN. *In-situ* wafer curvature measurements were used to monitor film stress during growth. An approximately 1.5 µm thick Ga-polar GaN layer grown on (0001) sapphire by MOCVD was used as the base template for all of the growths. The effect of V/III ratio on film stress and morphology evolution was initially investigated for InGaN layers grown on GaN using a constant TMG/TMI ratio of 1.4. At a high V/III ratio (~6300), the InGaN films grew under an initial moderate compressive stress of -0.65 GPa and significant film roughening was observed beyond a critical thickness of few monolayers most likely due to V-pit formation. A reduction in the V/III ratio to ~900 resulted in reduced surface roughness and film stress (-0.25 GPa) for films up to ~200 nm in thickness. Compositionally graded InGaN layers were grown on GaN using the reduced V/III ratio conditions by varying both the growth temperature (800°C to 540°C) and the TMG/TMI ratio (1.4 to 0) continuously during deposition followed by the growth of InN. The use of graded InGaN transition layers and reduced V/III ratios resulted in reduced surface roughness compared to direct InN growth on GaN using high V/III ratios (~104). Also, while a net tensile growth stress was measured during InN growth on GaN, InN growth on the graded buffer resulted in a reduction of the net incremental growth stress to almost zero value. Transmission electron microscopy characterization is currently underway to characterize the structural properties of the films.

11:00 AM Student

FF8, Optical Properties of InN Epilayer and Self-Organized InN Quantum Dots Grown by Flow-Rate Modulated Epitaxy: *Chen-Pang Fu*[1]; Wen-Cheng Ke[1]; Wei-Kuo Chen[1]; Chin-Hau Chia[1]; Wu-Ching Chou[1]; Wen-Hao Chang[1]; Ming-Chih Lee[1]; Ching-Shun Ku[1]; [1]National Chiao Tung University

Optical properties of InN epilayers and quantum dots grown by flow-rate modulated epitaxy were investigated. The carrier dynamics in the InN epilayers was studied by time-resolved photoluminescence (PL) spectra. The increase in decay time of InN epilayer with the decrease of detection energy indicates that the emission dynamics is not only due to the radiative recombination but also the transfer process to the tailing state. The dot size and density of InN quantum dots were controlled by the growth temperature and the flow-rate. The smallest dot height and diameter were 6 nm and 70 nm, respectively. The dot density was about 10^8 cm^{-2}. We observed energy blue-shifts from 10 meV to 30 meV in the PL peak energy compared with that of the epilayer as the average dot height was reduced from 32 nm to 6 nm. The peak energy shift can be ascribed to the quantum size effect. The temperature-dependent PL measurements show that the emission peak energies of the quantum dots are insensitive to the temperature, indicating the localization of carriers in the quantum dots. The PL lineshape of InN quantum dots exhibited two features in contrast to one broad band of InN epilayer at room temperature.

11:20 AM

FF9, Low Temperature Epitaxial Growth of InN on Substrates with Small Lattice Mismatches: *Hiroshi Fujioka*[1]; Jitsuo Ohta[1]; Kazuya Mitamura[2]; Masaharu Oshima[2]; [1]University of Tokyo/KAST; [2]University of Tokyo

We have grown InN films on substrates with small lattice mismatches using UHV-PLD[1, 2] at low temperatures and investigated their characteristics using RHEED, AFM, GIXR, EBSD, and GIXD. Substrates used in this study include (Mn, Zn) Fe2O4 (111) and MgAl2O4 (111). We have found that hexagonal (0001) InN grows epitaxially on the (Mn, Zn) Fe2O4 (111) substrates even at room temperature (RT). Clear straight steps and atomically flat terraces are observed on the surface of InN grown at RT. We have found that the in-plane epitaxial relationship between RT-grown InN and the (Mn,Zn) Fe2O4 substrates is InN [11-20] // ferrite [11-2], which makes the in-plane lattice mismatch as small as 2.0%. However, we also found an 8 nm thick interfacial layer forms between the InN films and the substrates even for RT growth, which could spoil advantages of lattice matched substrates. To solve this problem, we have used MgAl2O4 substrates, which shares the same crystalline structure with (Mn, Zn) Fe2O4 and has much higher chemical stability. We have found that a MgAl2O4 substrate with an atomically flat surface can be obtained by annealing in a box made of MgAl2O4 and that epitaxial growth of high quality InN can be performed on it. GIXR measurements have revealed the thickness of the interfacial layer can be reduced greatly with the use of MgAl2O4 substrates. [1]Y. Kawaguchi et al., Appl. Phys. Lett. 87, 221907 (2005). [2]J. Ohta et al., Appl. Phys. Lett. 83, 3060 (2003).

11:40 AM

FF10, Ammonothermal Growth and Characterization of Indium Nitride Crystals: *Buguo Wang*[1]; M. J. Callahan[2]; L. Bouthillette[2]; K. Rakes[2]; M. Suscavage[2]; D. Bliss[2]; [1]Solid State Scientific; [2]Air Force Research Laboratory

Indium nitride has received increasing attention recently, not only because it has many potential applications, but also because the alloy $In_xGa_{1-x}N$ with a significant amount of InN incorporation is desired for obtaining blue light emission. In addition, reports on the InN bandgap are also controversial. Therefore, preparation of pure high quality bulk InN crystals and knowledge of its physical properties are critical. Ammonothermal growth is a promising cost effective technique for growing III-nitride crystals. We have developed the ammonothermal technique to grow thick GaN single crystals recently. If high quality InN single crystals can also be synthesized ammonothermally, nitride device performance and reliability would be enhanced, and it would be possible to understand InN physical properties more readily. This presentation will report on the synthesis of InN single crystals by the ammonothermal technique. We have successfully grown hundreds of microns of InN on polycrystalline InN and single crystal AlN seeds. Photoluminescence measurements on these crystals showed that the near bandedge emission is 1.774 eV at 2 K. Characterization of the ammonothermal InN crystals by SEM, SIMS and X-ray diffraction will also be presented. Process conditions for the synthesis and growth mechanisms will be discussed. This work was performed at AFRL Hanscom site and partially supported by AFOSR.

Session GG: Silicon and Germanium Nanowires

Friday AM
June 30, 2006

Room: Conference Room 208
Location: Pennsylvania State University

Session Chairs: Hou T. Ng, Hewlett-Packard Company; Christopher E. D. Chidsey, Stanford University

8:20 AM Student

GG1, RF Dielectric Properties of Silicon Nanowire Networks: Wenchong Hu[1]; Alexey Kovalev[1]; Sarah Dilts[1]; Yanfeng Wang[1]; Joan M. Redwing[1]; *Theresa S. Mayer*[1]; [1]Pennsylvania State University

Considerable effort is being invested into measuring the field dependent DC electrical properties of individual and 2-D arrays of silicon nanowires (SiNWs) for use as electronic and/or sensing devices. The large surface-to-volume ratio of SiNWs also makes them attractive for sensing applications that involve changes in RF dielectric properties. In this talk, we will discuss the first measurements of the RF conductivity and permittivity of dense, interconnected networks of intentionally-doped SiNWs. The SiNWs networks used in this study were synthesized by vapor-liquid-solid growth using metal catalyst nanoparticles formed by depositing a 10-nm Au thin film on a 12 mm diameter glass substrate. The nominal diameter of the NWs in the network was 80-nm, with single NW lengths exceeding 50 µm. Intentional n-type doping was introduced during VLS growth by the addition of phosphine (PH_3) to the inlet gas stream using SiH_4 as the source of silicon. Three different gas flow ratios of PH_3:SiH_4 = $1.6x10^{-3}$, $7x10^{-5}$, and $2x10^{-5}$ that correspond to a DC conductivity of approximately 1000 S/cm, 10 S/cm and 0.01 S/cm were investigated. This VLS growth process produced a dense network of SiWNs suitable for RF measurement as determined by field emission scanning electron microscopy. A cavity perturbation technique was used to measure the RF dielectric properties of as-grown and thermally annealed SiNW networks. The TE011 mode of a cylindrical cavity resonator with a frequency 7.7 GHz was used because it provided a high Q-factor (>20,000), which allowed measurements to be conducted using a small sample volume. The RF conductivity and permittivity of the SiNW networks were extracted by analyzing the frequency and Q-factor differences observed in transmission mode. Measured RF conductivity was compared with calculated values using a composite conductivity model, where the DC conductivity of individual SiNWs was included as a fitting parameter. Using this approach, we found that the RF conductivity increases with increasing dopant:SiH_4 inlet gas flow ratio. Moreover, for a given inlet gas flow ratio, the RF conductivity of the network was increased considerably by enhancing the electrical connection between individual SiNWs through high temperature annealing in forming gas.

8:40 AM Student

GG2, Nanowire Bandgap Engineering through Highly Strained Si/Ge Heterostructures: *Teresa J. Clement*[1]; J. L. Taraci[1]; A. Batwal[2]; P. Peralta[2]; Jeff Drucker[3]; S. T. Picraux[4]; [1]Department of Chemical and Materials Engineering, Arizona State University; [2]Department of Mechanical and Aerospace Engineering, Arizona State University; [3]Department of Physics and Astronomy, Arizona State University; [4]Center for Integrated Nanotechnology, Los Alamos National Laboratory

The strain in vapor-liquid-solid (VLS) grown nanowire (NW) heterostructures is measured using a novel electron microscope based 2-D mapping technique. The measured strain state of axial and core/shell heterostructure NWs quantitatively correlates with that predicted using finite element, continuum elasticity modeling. For core/shell heterostructures, the strain is partitioned between the core and shell in a proportion that depends on the core-to-shell diameter ratio. This strain partitioning provides the opportunity for strain engineering the electronic properties of the NW heterostructure. Using simple deformation potential based electronic structure modeling, we demonstrate that the bandgap of a <111> oriented Ge core may be tuned over a much larger range than that of a Si core due to the position of the conduction band valleys in the Brillouin zone. Similar analysis can be applied to strained discs in axial heterostructures to demonstrate formation of quantum dots or tunnel barriers. These NW heterostructures are grown using the VLS method from *in situ* deposited Au seed particles in a cold wall ultra high vacuum chemical vapor deposition system. Heterostructure NWs are formed by controlled variation of deposition conditions, precursor pressure and growth temperature, and precursor chemistry (di)silane or (di)germane. An optical reflectometry technique is used for *in situ* monitoring of NW growth and is used to determine *in situ* the onset of nanowire nucleation, the mean growth rate of nanowires, and the average lengths of the nanowires. The direct observation of nanowire nucleation and growth under well-defined materials and thermodynamic conditions using our optical reflectometry technique gives us the ability to quantitatively control the position of the heterojunctions along the NW and resulting structures such as quantum dots within the NWs. The *in situ* UHV evaporation of Au metal catalyst seeds is done at elevated temperature after forming an atomically clean Si surface; seeds are in intimate contact with the Si substrate, with diameters ranging from 5-50 nm, depending on desired conditions. Nanowires are then grown

at specific temperatures above the eutectic point (400-800°C) typically at a pressure of $3x10^{-3}$ Torr until the nanowires reach about 200 nm in length, as determined by glancing-angle optical reflectivity. Changing gasses at specific times during the growth allows for fabrication of different heterostructures. *Ex situ* measurements include field emission SEM and photoluminescence, as well as HRTEM and 2-D strain mapping. As nanowires advance toward a more active role in nanoscale electronics and photonics, the ability to control heterostructure growth and the resulting manipulation of the 3D structures, strain, and bandgaps as demonstrated here will become increasingly critical.

9:00 AM Student

GG3, Unintentional Background Doping of Vapor-Liquid-Solid Synthesized SiNWs: *Tsung-Ta Ho*[1]; Yanfeng Wang[1]; Kok-Keong Lew[1]; Trevor E. Clark[1]; Elizabeth C. Dickey[1]; Joan M. Redwing[1]; Theresa S. Mayer[1]; [1]Pennsylvania State University

Synthesis of silicon nanowires (SiNWs) using the vapor-liquid-solid (VLS) technique has been reported using Au nanoparticle catalysts deposited on several different growth substrates including planar oxidized silicon wafers, (111) silicon wafers, and anodic aluminum oxide (AAO) membranes. In this talk, we will present a comparison of the four-point resistivity of SiNWs grown using different dopant gas to silane (SiH_4) inlet gas flow ratios for NWs nucleated from a 1.5-nm sputtered Au thin film deposited on thermally oxidized silicon wafers with those nucleated from Au nanoparticles electrodeposited within the pores an AAO membrane. Both methods produce SiNWs with nominal 80-nm diameter. The dopant gases used in this study for p- and n-type doping of the SiNWs were trimethylboron (TMB) and phosphine (PH_3), respectively. The four point resistivity and carrier type of the SiNWs were determined using a back-gated four point test structure for SiNWs grown using TMB or PH_3 to SiH_4 gas flow ratios ranging from 0 to 1×10^{-2}. Measurements of gate-dependent conductance show that the nominally-undoped SiNWs grown from the oxidized silicon wafer and the AAO membrane both have p-type conductivity. However, the resistivity of the nominally-undoped SiNWs grown from the AAO membrane was several orders of magnitude lower than those grown from the oxidized silicon wafer. In addition, higher PH_3 gas flow ratios were required to compensate the p-type background for the SiNWs grown from the AAO membrane and produce NWs with n-type conductivity. Once the transition to n-type conduction was observed, further increases in the PH_3 to SiH_4 gas flow ratio resulted in a monotonic decrease in the SiNW resistivity. A monotonic decrease in the resistivity is also observed with increasing TMB gas flow ratios. These results show that the growth substrate plays an important role in the unintentional background doping in VLS grown SiNWs, and suggest that the AAO membrane and/or electrodeposited Au catalyst introduces additional impurities into the SiNWs. This has important implications for growth of lightly doped SiNWs in AAO membranes, which are of interest for array-based nanoelectronic or photonic device applications.

9:20 AM Student

GG4, Synthesis and X-Ray Diffraction Characterization of Heteroepitaxially Grown Germanium Nanowires: *Irene A. Goldthorpe*[1]; Joshua B. Ratchford[1]; Jacob H. Woodruff[1]; Christopher E. D. Chidsey[1]; Paul C. McIntyre[1]; [1]Stanford University

Ge nanowires (NWs) have been less extensively studied than Si NWs, however, they offer advantages such as a lower synthesis temperature and higher intrinsic carrier mobilities. In this work, epitaxial Ge NWs have been grown on single crystal Si substrates of different orientations in a cold-wall CVD reactor. To obtain arrays of wires with similar diameters, monodisperse Au nanoparticles were used as the catalysts. Because these nanoparticles are generally suspended in an aqueous solution, this presents challenges for obtaining epitaxial NW growth on Si. We will describe how sample preparations dictate the quality of the epitaxial relationship between the wires and the substrate. The epitaxial relationship was quantitatively studied by x-ray diffraction, including detailed symmetric and asymmetric diffraction scans, and x-ray pole figures. The pole figures indicated that the majority of wires were heteroepitaxial, however, evidence of twinning defects was also found, most noticeably in samples grown on Si(111) substrates where twinning occurs at the Ge/Si interface at the bases of both vertically oriented wires and wires oriented along inclined <111> directions. Since strain in NWs may affect a number of electronic properties, x-ray diffraction was used to characterize the strain state of Ge NWs. Even though the wires are believed to have a thin native oxide layer, no axial component of strain in the Ge NWs was measured by symmetric x-ray diffraction from vertical NW arrays. Heteroepitaxially depositing a Si shell around the Ge NWs may allow for the engineering of strain inside the NWs and reduce the influence of surface defects in carrier scattering by confining carriers to the NW interior. We will compare different strategies to achieve Si shell deposition and report the conditions which dictate whether three-dimensional Si islands or a continuous Si film forms around the Ge NWs.

9:40 AM Student

GG5, Structural and Field-Effect Properties of Thermally-Oxidized Silicon Nanowires: *Yanfeng Wang*[1]; Bangzhi Liu[1]; Daniel Shir[1]; Kok-Keong Lew[1]; Sarah Dilts[1]; Chad Eichfeld[1]; Joan M. Redwing[1]; Suzanne E. Mohney[1]; Theresa S. Mayer[1]; [1]Pennsylvania State University

There is considerable interest in integrating semiconductor nanowires for their application in future logic, memory, and sensor devices. Vapor-liquid-solid growth has been used successfully to synthesize p- and n-type silicon nanowires (SiNWs) of varying carrier density and with axially modulated doping profiles. Nanowire field effect devices (FETs) have been fabricated from uniformly-doped NWs that are switched using a global back gate and/or a local top gate. However, the subthreshold characteristics of these devices typically exhibit severe hysteresis and/or larger than expected subthreshold slope. This is due in part to the large unpassivated NW surface area for back-gated devices, and the poor quality interface between the NW and gate dielectric for top-gated devices. Thus, it is important to develop strategies that can improve the quality of this interface. This talk will discuss dry thermal oxidation of SiNWs to form Si/SiO_2 core-shell structures and their use in SiNW-based FETs. Oxidation experiments were conducted on 20–100 nm diameter SiNWs at temperatures of 700–900°C using either O_2 or a mixed ambient of O_2 and TCA. Transmission electron microscopy was used to measure the oxide thickness and interfacial roughness of oxidized SiNWs that were subjected to different pre-oxidation preparation processes (e.g., RCA, HF, etc.). The results of these experiments show that the oxidation rate of SiNWs is consistently faster than that observed on planar Si surfaces for both oxidation ambients, and is equal along the entire length of the SiNW. We found that the rate also depends on the starting diameter of the SiNWs for many of the conditions investigated. Pre-oxidation preparation procedures were determined to produce a smooth and uniform interface between the thermal SiO_2 shell and Si core. The field effect properties of top-gated devices fabricated by integrating nominally-undoped SiNWs with a 10nm thick SiO_2 gate dielectric shell were very stable and showed bulk switching due to field-induced depletion of the NW channel. The breakdown field strength of the SiO_2 shell determined by I-V measurement between the gate and source electrodes was ~ 8.8±0.6 MV/cm. These SiNW devices behaved as p-type FETs and had $I_{ON}/I_{OFF} \sim 10^5$, threshold voltage ~ 0 V, subthreshold slope S ~ 250 mV/dec, transconductance $g_m \sim 0.1$ µS, and maximum I_{ON} ~ 50 nA per NW. While the maximum on-state current and transconductance are limited by the barrier at the source contact to the SiNW, the subthreshold slope is considerably lower than values reported previously and hysteresis effect is significantly suppressed. The interface charge state density estimated from the subthreshold slope was ~ $(9.1\pm0.8)\times10^{12}$ $cm^{-2}eV^{-1}$. Similar stability and subthreshold slopes were observed for intentionally-doped p- and n-type SiNW-FETs. These results show that dry thermal oxidation can be used to improve the interfacial properties and stability of SiNW-FETs.

10:00 AM Break

10:20 AM Student

GG6, Growth and Passivation of Vertically Aligned Germanium Nanowires for Three Dimensional Nanoelectronics: *Hemant Adhikari*[1]; Paul C. McIntyre[1]; Christopher E. D. Chidsey[1]; [1]Stanford University

In 3-dimensional nanoelectronics, vertically aligned nanowires have been proposed to provide a solution to attain ultra high density nanoscale device arrays. Germanium nanowire (GeNW) transistors are very promising components for active device layers above a single crystal silicon substrate because of: (a) the relatively low growth temperature (<350°C) of these nanowires which is desirable for 3-dimensional integrated circuits and (b) the high intrinsic hole and electron mobilities of Ge compared to Si. In this paper, we present results of growth of vertically aligned single-crystal

germanium nanowires (GeNWs) at temperatures of 350°C or less by metal nanoparticle-catalyzed chemical vapor deposition. Single crystal Ge (111), Ge (110), Ge (001) and an epitaxially-grown Ge film on a Si (001) wafer were used to explore the epitaxial relation between the nanowires and the substrate. We have observed homoepitaxial growth of GeNWs along <111> and <110> growth orientations on these substrates. Because wires grown at higher temperatures are tapered, a two-temperature growth procedure was used to obtain epitaxial GeNWs of constant diameter. As shown by others, we also observed single crystal nanowire growth far below the bulk eutectic temperature, but intriguingly find that temperatures close to bulk eutectic are required for efficient nucleation of epitaxial nanowires on Ge substrates. Our results indicate that the range of process conditions for growth of single crystal GeNWs and those for efficient nucleation of epitaxial GeNWs on Ge surfaces are not identical. To understand the nucleation of nanowires from gold catalyst and to test whether Vapor-Liquid-Solid mechanism is actually responsible for the growth of nanowires, it is important to understand the phase equilibrium between Au nanoparticle and germanium. Capillary effects, often represented by the Gibbs-Thomson pressure, increase the free energy of the nanoparticle catalyst and the nanowire relative to their bulk values and hence cause lower the eutectic temperature. NW nucleation, where the catalyst nanoparticle is initially in contact with a flat Ge surface, and NW growth, where it is in contact with a curved GeNW, are very different situations. We have calculated the equilibrium phase diagrams for both the Au liquid nanoparticle in contact with flat Ge (nucleation) and Au liquid nanoparticle in contact with nanowire (growth) cases. These quantitative results are consistent with our experimental findings. The defect free nature of the GeNWs and their homoepitaxial relationship with the substrate has been studied by high resolution transmission electron microscope imaging and diffraction. Detailed investigation of the surface chemistry of as-grown and air-exposed GeNWs and exploration of various chemical passivation pathways is reported by the photoemission studies using a low energy synchrotron source. The control of surface composition demonstrated in this paper forms a sound basis for the deposition of high-quality gate-dielectric layers on the nanowires.

10:40 AM Student

GG7, Integrated Silicon Nanowire Diodes: *Justin B. Jackson*[1]; Sun-Gon Jun[1]; Divesh Kapoor[1]; Mark S. Miller[1]; [1]University of Utah

Integrating nanowire devices into future CMOS technologies will likely require several developments, such as controlling the nanowire growth location and the subsequent *in situ* fabrication of devices. We report here on the fabrication and characterization of integrated silicon nanowires diodes, where arrays of nanowires were grown from patterned gold catalyst arrays, processed into devices, and current-voltage measurements taken on single-nanowire diodes. Gold disk arrays were patterned using photolithography and electron beam lithography on *n*-type (100) wafers using a lift off process that left 1-nm-thick disks on silicon in windows opened in silicon dioxide layers. Nominally undoped silicon nanowires were grown using a vapor-liquid-solid mechanism in an atmospheric pressure vapor phase epitaxy system using $SiCl_4$ in a H_2 ambient at 900°C. For the catalysts defined with optical lithography, in windows of approximately 750 nm diameter, each location resulted in a dominant wire, on the order of 100 to 300 nm diameter, accompanied by several smaller diameter wires. With electron beam lithography, residues from the resist often lead to nanowire growth on the field oxide between windows. In order to fabricate a single nanowire device, thermal oxidation was used to completely oxidize the smaller diameter wires and reduce the size of the nanowire of interest. The fine, fully-oxidized nanowires were removed with a buffered HF oxide etch. Applying a spin-on-glass, ~700 nm thick, isolated the tip of the wires from the substrate, and a reactive ion etch removed the oxide from the top of the wire. Aluminum contacts were deposited and patterned on the exposed wires as well as the backside of the wafer. Annealing the aluminum created the *p*-region, nominally giving a p^+in structure. Current-voltage characteristics, taken at 300 K on single nanowire diodes from -1V to 1V, displayed rectifying behavior. Under forward bias, before series resistance becomes important above 0.4 V, the measured ideality factor is 1.2, indicating recombination currents to be small. The relatively small recombination currents suggest that gold-related impurity recombination or gross defects at the nanowire base not play dominant roles in transport. Series resistances were approximately 350 kohms for 200 nm wires and attributed to the nanowire. Under reverse bias, the saturation current increased with bias, attributed to generation. These devices provide a technology baseline for further testing the concept of integrated nanowire devices. In particular, investigations underway in our group include adding a wrap around polysilicon gate to form a transistor, reducing the nanowire diameter to the quantum point contact limit, and incorporating silicon-germanium heterostructures.

11:00 AM

GG8, Silicidation of Silicon Nanowires: *Bangzhi Liu*[1]; Suzanne E. Mohney[1]; Yanfeng Wang[1]; Theresa S. Mayer[1]; [1]Pennsylvania State University

Silicon nanowires (SiNWs) have been successfully integrated into prototype devices such as field effect transistors and biosensors. However, the ohmic contacts to the nanowires still limit the performance of many of these nanoscale devices. Improved metallizations for SiNW devices are therefore needed. In conventional microelectronics, metal silicides are used as ohmic contacts to heavily doped Si, and the reactions between metal films and silicon substrates have been the focus of many previous investigations. In our study, we have used transmission electron microscopy to compare metal silicide formation in the nanowire geometry to silicide formation in the planar geometry. We have successfully silicided SiNWs using Ni, Pd, Pt, Co and Cu. In some cases, metal silicide formation occurred readily. For example, sections of SiNWs can be converted uniformly to NiSi at 450°C. For other metals such as Pt, finding conditions for the formation of a uniform metal silicide segment was more challenging. Platinum silicide is of particular interest for ohmic contacts to p-type SiNWs because of its low Schottky barrier height to p-type Si. Therefore, a series of experiments was conducted by depositing thin Pt films on SiNWs and then annealing. The SiNWs had a nominal diameter of 80 nm and were grown by the vapor-liquid-solid technique on oxidized Si wafers. Annealing was performed between 200°C and 750°C for 30 min to 15 h. In the thin film case, Pt and Si were reported to form PtSi at a temperature as low as 200°C. However, Pt agglomerated into islands on the SiNWs when annealed at 350°C, and there was little reaction between the Pt and SiNWs. After annealing at 450°C and 550°C, PtSi islands were formed on the surface of the SiNWs, leading to a rough morphology. After annealing between 600°C and 750°C, sections of SiNWs can be converted into a platinum silicide. The silicide formed could be PtSi, α-Pt_2Si or α-$Pt_{12}Si_5$, depending on the thickness of the Pt film originally deposited. In this talk, the phase formation and morphology of the metal silicides formed during annealing are discussed with respect to the dominant diffusion species in the silicides and the geometry of the nanowires, on which surface diffusion can be important. Other factors like oxygen content in the annealing gas and stress developed during growth of the silicide may also play a role.

11:20 AM Student

GG9, Self-Assembled Nickel Silicide Nanowire Contacts and Direct Electrical Measurement: *Joondong Kim*[1]; Wayne A. Anderson[2]; [1]University at Buffalo and Pohang University of Science and Technology; [2]University at Buffalo

Nickel monosilicide (NiSi) has been intensively researched for use as a contact material of gate and source/drain in CMOS devices due to its low resistance. Metallic nanowires have been studied as nanoscale interconnects due to the low resistance as well as the tiny contact area, ideally the same as the diameter of the nanowire (NW). These merits prompt the interest in NiSi nanowires for use in nanoelectronics. The first and inevitable step of nanoelectronics integration is to form spontaneous contacts. A spontaneous NiSi NW connection across a trench was fabricated by simple optical lithography and metal lift-off. A conventional optical lithography technique was adopted to make a photoresist (PR) coated-pattern on a 200 nm SiO_2 coated wafer. Ni layer as a catalyst was formed by thermal evaporation. In metal lift-off, the Ni film above the PR was spontaneously removed leaving a Ni-coated trench pattern. Finally, buffered hydrofluoric acid (BHF) was applied to open a SiO_2 window. The Ni-patterned sample was loaded in a dc magnetron system for sputtering of Si at a substrate temperature of 575°C to form nanowire contacts across the trench by the metal-induced growth (MIG) method. A field emission scanning electron microscope (SEM) was used to observe the NB connections across a trench. The parallel propagated NW, 2.9 μm in length, formed a spontaneous connection between Ni deposited electrodes. The MIG nanowire contacts are solid with small contact area

that is the same as the diameter of the nanowire itself, about 58 nm. The electrical transport gave metallic characteristics and a low resistance of about 147.9Ω. The NB resistivity was obtained to be 10.8 μΩcm, comparable to the value for single crystalline NiSi of 10 μΩcm. One advantage of the metal-induced grown NB is in providing compatible metallic pads for electrode use with low resistance of 7Ω. The MIG pads are homogeneous to the NiSi NB to relieve an extrinsic effect caused by foreign metal use. In summary, a simple and optical lithography was adopted to make a trench, to form a nanowire contact-nanobridge. The NB was 2.9 μm in length and 58 nm in diameter. The MIG method provided a self-assembled NB across Ni silicide composed pads. The MIG NB showed a metallic transport characteristic, which is practical for use in nanoscale interconnections. The self-assembled NB formation is compatible with Si technology and is a promising nanoscale interconnection scheme.

11:40 AM
GG10, Late News

Session HH: Molecular Electronics: Devices, Materials and Contacts

Friday AM, June 30, 2006
Room: Conference Room 207
Location: Pennsylvania State University

Session Chairs: Mark C. Hersam, Northwestern University; David B. Janes, Purdue University

8:20 AM Student
HH1, Ordered Molecular Films on Semiconductors: Characterization of Ordered Organothiolate Monolayers on GaAs (100) and (110) for Molecular Electronic Applications: *Christine McGuiness*[1]; Daniel Blasini[2]; Zihua Zhu[1]; Sundararajan Uppili[1]; Andrey Shaporenko[3]; Michael Zharnikov[3]; Detlef Smilgies[4]; Nicholas Winograd[1]; David Allara[1]; [1]Pennsylvania State University; [2]Cornell University; [3]University of Heidelburg; [4]CHESS

We report the first example of translationally ordered molecular monolayers on GaAs (100) and (110) surfaces with direct molecule-semiconductor bonding. Through rigorous control of solution processing conditions, self-assembled films of organothiol molecules can chemisorb with high reproducibility. In the case of octadecanethiol (ODT) molecules, TOF-SIMs and surface sensitive HRXPS show direct S-GaAs attachment with insignificant substrate oxidation and Raman scattering indicates increases in the e-h pair recombination times. A combination of ellipsometry, liquid drop contact angles, AFM, NEXAFS, IR and XPS probes reveal a structure with conformationally ordered alkyl chains tilted on average at 14(±1)° from the surface normal with a 43(±5)° twist and a highly oleophobic, hydrophobic ambient surface. Analysis of the tilt angle and film thickness data in conjunction with GIXRD measurements show that the monolayers form a pseudo-hcp structure with a significant mismatch of the average adsorbate molecule spacings with the spacings of an intrinsic GaAs(001) surface lattice. This result suggests that formation of the monolayers is driven significantly by the molecular packing and involves some degree of reconstruction of the underlying substrate. We find evidence that the structure of the monolayers is highly dependent on chain length, moving from well ordered monolayers of long chain ODT monolayers to disorganized structures for short chain dodecanethiol monolayers and 4'4-biphenylthiol molecules. Increased oxidation of the substrate is observed as the disorder of the monolayer increases. The results show promise for the development of tailored molecular films on GaAs with applications ranging from molecular electronics to spintronics devices.

8:40 AM Student
HH2, Investigating the Stability of Organic Molecules Bound to Semiconductor Surfaces with Low Temperature UHV-STM: *Nathan L. Yoder*[1]; Nathan P. Guisinger[1]; Mark C. Hersam[1]; [1]Northwestern University

In recent years, substantial progress has been made in the emerging field of molecular electronics. Metal-molecule-metal junctions have been widely studied, although molecule-semiconductor junctions have recently received increased attention as well. The presence of the energy band gap in semiconductors provides opportunities for resonant tunneling through individual molecules, leading to interesting effects such as room temperature negative differential resistance (NDR)[1, 2]. However, the reliability of these molecular junctions is of critical importance to potential devices, and consequently warrants further investigation. Single cyclopentene molecules on silicon provide a useful test case, since the binding geometry has been studied both experimentally and theoretically. Additionally, molecules that are fully saturated upon adsorption to the silicon surface (such as cyclopentene) have been reported to be much more stable than molecules that retain some p-bonding character. In this study, a combination of experimental and theoretical tools were employed to investigate the stability of cyclopentene molecules on a degenerately doped p-type Si(100) surface. Experiments were performed using a cryogenic ultra-high vacuum scanning tunneling microscope[3]. At 80 K, cyclopentene desorbs from the surface at both positive and negative sample bias polarities over a range of tunneling currents. The desorption rate is roughly linear with tunneling current, indicating a single-electron process. The desorption yield is a strong function of bias, and has turn-on voltage of –2.5 V at negative bias and 3.5 V at positive sample bias. Electronic structure (DFT) calculations were performed in order to gain further insight into the desorption process. [1]N. P. Guisinger, M. E. Greene, R. Basu, A. S. Baluch, and M. C. Hersam, Nano Letters, 4, 55 (2004). [2]N. P. Guisinger, N. L. Yoder, and M. C. Hersam, Proc. Nat. Acad. Sci., 102, 8838 (2005).[3]E. T. Foley, N. L. Yoder, N. P. Guisinger, and M. C. Hersam, Rev. Sci. Instrum., 75, 5280 (2004).

9:00 AM Student
HH3, High Resolution Inelastic Electron Tunneling Spectroscopy of Nanoscale Crossed-Wire Molecular Junctions: *Heayoung Yoon*[1]; Lintao Cai[1]; Marco Cabassi[1]; Theresa S. Mayer[1]; [1]Pennsylvania State University

Inelastic electron tunneling spectroscopy (IETS) is a valuable in-situ spectroscopic analysis technique that can be applied in conjunction with temperature dependent transport measurements to characterize and identify the molecular species under study by measuring its vibrational fingerprint. IETS has been used previously to confirm that the measured transport properties of molecular junctions are due to the intended molecule rather than process induced artifacts. It has also been used to monitor changes in the vibrational modes of bistable molecular junctions before and after switching between low- and high-conductivity states. In the future, IETS may be used to provide insight into the issue of local heating in molecular junctions. Each of these applications of IETS requires collecting spectra with high energy resolution to resolve closely spaced vibrational features. In this talk, we will discuss the application of a new nanoscale crossed-wire molecular junction testbed comprised of lithographically-defined bottom metal contacts and self-assembled metal nanowire top contacts to study the electrical and spectroscopic properties of oligo (phenylene ethynylene) (OPE) junctions. In comparison to other testbeds, this structure offers a flexible fabrication process that permits rapid integration of junctions with different molecules and metal contacts. Immediately following fabrication, junctions comprised of top and bottom Au contacts and OPE self assembled monolayers were loaded into a variable temperature high vacuum chamber for I-V(T) and IET measurements. The junctions investigated exhibited temperature independent I-V properties (4 – 300 K), which indicates that the dominant transport mechanism is coherent tunneling. IET spectra were obtained at 4K using a standard AC modulation technique that employed a lock-in amplifier to collect directly the second harmonic signal, which is proportional to d2I/dV2. The observed IET peaks in a plot of d2I/dV2 versus V were compared to existing infrared, Raman, and high resolution electron energy loss data for OPE self-assembled monolayers. Prominent vibrations were observed at 138mV, 202mV, and 274mV and can be assigned to υ(18a), υ(8a), and C= C stretch, respectively. Additional peaks were observed at 18mV and 56mV as suggested vibrational modes of Au-S and C-S. The measurement methods used to minimize peak broadening and enhance energy resolution in these IET spectra will be presented. The authors would like to acknowledge the Tour group (Rice University) for providing the molecules used in this study.

9:20 AM

HH4, Single-Molecule Transistors to Characterize Bistability in Molecular Conduction: Zachary K. Keane[1]; David A. Corley[1]; Jacob W. Ciszek[1]; James M. Tour[1]; *Douglas Natelson*[1]; [1]Rice University

Hysteretic bistability in single molecule conduction has been a topic of interest for several years, with much speculation as to the underlying switching mechanism. One candidate mechanism that has been suggested is reduction of the molecule under large currents; another possibility is bias-induced conformational or orientational switching. Single-molecule transistors are three-terminal devices that have been used to study vibronic effects, inelastic electron tunneling, and Kondo physics. We use these devices to examine switching in BPDN, a molecule known from previous studies to exhibit conduction bistability in crossed-wire, tethered nanoparticle, STM, and mechanical break junction experiments. Gate coupling provides a means of assessing the role of redox transitions in the switching process. We report our latest results and their implications for the switching mechanism.

9:40 AM Student

HH5, Criteria for Statistical Determination of Working Devices of Microscale Via-Hole Molecular Structures: *Tae-Wook Kim*[1]; Gunuk Wang[1]; Takhee Lee[1]; [1]Gwangju Institute of Science and Technology

Due to the merits such as the use of functional molecules as a nanoscale building-block in miniaturized electronic devices for low cost, high-density, and less heat problem process, molecular electronics is currently undergoing a repaid development. Because of the robust formation of alkanethiol ($CH_3(CH_2)_{n-1}SH$) self-assembled monolayer (SAM) on Au surface, alkanethiol SAMs have been investigated extensively[1]. However, there has been little systematic work on device yield and thus average transport parameters based on statistical approach. In this presentation, we will show the charge transport through alkanethiol SAMs, the yield of mass-fabricated molecular devices (13440 devices), and criteria of determination of the working devices. The microscale M-M-M junction devices were fabricated by typical semiconductor fabrication processing. After the formation of Au bottom electrode and the deposition of SiO_2 layer, Au electrodes were exposed through the via-holes of 2 μm diameter. Three different alkanethiols (octanethiol (denoted as C8), dodecanethiol (C12), and hexadecanethiol (C16)) were self-assembled on the exposed Au surface. The top Au electrode to form M-M-M junctions was made by thermal evaporation. The evaporation was done with a shadow mask on the chips. To understand charge transport through alkanethiol in M-M-M junction, 13440 individual devices were electrically characterized by a semiconductor parameter analyzer. Among 13440 fabricated devices, 11744 devices showed electrical short. Fabrication failure and electrical open were 392 devices and 1103 devices, respectively. Among 201 working devices, C8, C12, and C16 working devices were 84, 57, and 60 devices, respectively. Thus, the device yield was found as ~1.5%. From the Simmons tunneling model[2], the optimum fitting was performed on the representative experimental data of C8, C12, and C16 and found to be $\{\phi_B = 1.01 \pm 0.01$ eV and $\alpha = 0.82 \pm 0.01\}$, $\{\phi_B = 1.20 \pm 0.04$ eV and $\alpha = 0.74 \pm 0.02\}$, and $\{\phi_B = 2.13 \pm 0.06$ eV and $\alpha = 0.54 \pm 0.01\}$, respectively. To define the working device, we considered the current densities at 1.0 V as a criterion for determination of working device. From the histograms of current densities of C8, C12, and C16, average (m) and standard deviation (σ) of current densities were determined by Gaussian distribution fitting. We took the samples within the range of ($m \pm 3$), 99.7% from the population and regarded them as statistical working devices. Interestingly, the histograms of Simmons fitting parameters of the selected C8, C12, and C16 showed Gaussian distributions and could find out the averaged α, β, and ϕ_B valves[1]. We could obtain the temperature independent tunneling behavior from the statistical working devices. [1]W. Wang, T. Lee, and M. A. Reed, Phys. Rev. B 68, 035416 (2003). [2]J. G. Simmons, J. Appl. Phys. 34, 1793 (1963).

10:00 AM Break

10:20 AM

HH6, Fundamental Studies of Vapor Deposited Metal Contacts for Molecular Electronics Devices: *Thomas A. Daniel*[1]; David Allara[1]; Masato Maitani[1]; Tim Tighe[1]; [1]Pennsylvania State University

The vacuum deposition of metal layers on organic thin films is a widely used process for many applications ranging from electronic devices to barrier coatings. Predictions of the outcome of any particular deposition are typically very difficult because of the lack of fundamental information on the complex, intertwined chemical and physical processes that can be involved in the interface formation and metal overlayer growth. As a means of building fundamental rules underlying these complex phenomena, recent efforts have focused on using the chemically and physically well-defined structures of self-assembled monolayers (SAMs) as the organic substrates. These structures not only provide model systems but have become highly relevant because of their recent applications in molecular electronic devices where vapor deposited metal contacts are used in a base electrode-molecule-metal structure for which the exact nature of the contact interface and metal morphology can profoundly affect device performance. To understand the detailed nature of metal-molecule contacts we have carried out experiments of metal atom deposition on SAMs in which the evolving interface chemistry and metal overlayer characteristics have been characterized by a combination of in-situ techniques including infrared reflection spectroscopy, XPS, AFM and CP-AFM. The talk will focus primarily on current work with Al, Ti and Au on a variety of SAMs with different terminal groups ranging from –CH3 to CO2H. Fundamental chemical and physical mechanisms of metal atom interaction with these films will be discussed and related to molecular electronics application.

10:40 AM Student

HH7, Electrical and Structural Characterization of Evaporated Contacts in Au/Molecule/GaAs Devices: *Patrick D. Carpenter*[1]; Saurabh Lodha[1]; David B. Janes[1]; Amy V. Walker[2]; [1]Purdue University; [2]Washington University in St. Louis

Recently molecular devices on semiconductors have gained considerable interest due to the relevance of semiconductors and the nanoscale dimensions of organic molecules. Semiconductors, such as GaAs, allow for stable, covalent bonds to molecular layers. However, one of the major challenges in fabricating these devices lies in obtaining a controlled and reliable contact to the molecular species. While many studies of molecular devices on metal and semiconductor substrates have characterized the molecular monolayers before deposition of top contacts, relatively few studies have characterized the interactions between the top contact and the molecular layer, or attempted to correlate these interactions to device electrical properties. Therefore, it is necessary to study and characterize the properties of the top contact in these molecular devices to determine an optimal metallization technique. The current study combines structural and electrical characterization of metal/molecule/semiconductor structures with the goal of understanding the contact interactions and their impact on device properties. Molecular devices have been fabricated in an Au/molecule/GaAs device structure using standard photolithography techniques and solution-based growth of self-assembled monolayers (SAMs).[1] After SAMs were formed on the GaAs surface, a top Au contact was formed using different evaporation conditions. Three different evaporation techniques were examined in this study. Electron beam evaporations under 77 K (liquid nitrogen) and 300 K (room temperature) conditions were used to fabricate molecular devices. Also, an indirect path, low energy evaporation technique was observed. The devices were structurally characterized using Time-of-Flight Secondary Ion Mass Spectrometry (TOF SIMS).[2] The results indicate that evaporation of the top metal contact by the indirect path, low energy evaporation technique leads to substantially less metal penetration through the molecular layer then in the direct e-beam evaporation techniques. Electrical data collected from the fabricated samples corroborates the results of the TOF SIMS experiment. When comparing the electrical data of the samples we find that the devices fabricated using the indirect path, low energy evaporation technique showed a greater increase in conductivity than the devices fabricated using the direct evaporation techniques in comparison to the Au/GaAs control sample. [1]S. Lodha, P. Carpenter and D. B. Janes, et al., *J. Appl. Phys.*, vol. 99, 24510 (2006). [2]A. V. Walker, T. B. Tighe, J. Stapleton, B. C. Haynie, S. Uppili, D. L. Allara, and N. Winograd, et al., *Appl. Phys. Lett.*, vol. 84, 4008 (2004).

11:00 AM Student

HH8, Molecule-Electrode Contact Effect on the Conductance of Single Alkanedithiols: *Xiulan Li*[1]; Joshua Hihath[1]; [1]Arizona State University

The ability to measure electron transport through single molecules not only allows us to understand the electron transport in molecules, but also is a basic requirement towards the goal of building an electronic device using

single molecules. While recent advances are impressive, it is still a nontrivial task to directly measure the conductivity of a single molecule electrically wired to two electrodes. To reliably measure the conductance of a molecule, we have developed the scanning tunneling microscopy (STM) break-junction approach with statistic analysis to measure the conductance of single molecules covalently bound to two gold electrodes. Using this method, we have studied the conduction mechanism and molecule-electrode contact effect on the conductance of single alkanedithiols. For each molecule, the conductance histogram reveals two sets of well-defined peaks, corresponding to two different conductance values. Both conductance values decrease exponentially with the molecular length with an identical decay constant, β~0.84 Å-1, but with a factor of 5 difference in the prefactor of the exponential function. The current-voltage curves of the two sets can be fit with the Simmons tunneling model. Both conductance values are independent of temperature (between -5 ºC and 60°C) and the solvent. The forces required to break the molecular junctions are the same, which is 1.5 nN. These observations lead us to believe that both are due to electron tunneling or superexchange via the bonds along the molecules but with two different molecule-electrode contact geometries. This work suggests that the conductance of a single molecule is sensitive to the microscopic details of the contacts. It also shows that although the STM break junction, together with statistical analysis, can provide reproducible data, variations in the molecule-electrode contact geometry can lead to more than one result for the conductance of single molecule.

11:20 AM Student

HH9, Scalable Molecular Electrodes at the Patterned Edge of a Metal/Insulator/Metal Junction: *Pawan Tyagi*[1]; Dong Feng[1]; Steve Holmes[1]; Bruce J. Hinds[1]; [1]University of Kentucky

Molecular electronics has great potential for being utilized in quantum computation, logic and memory circuitry in near future. Main attributes of molecular electronics are potentially simple and cost effective manufacturing through chemical synthesis and self-assembly, low power consumption, angstrom level control of device structure and the ability to tailor the electronic property of molecules. Metal break junctions and STM/AFM metal tip contact have been used for making electrical contact with molecules but are not suitable for cost effective, efficient large scale integration devices. Another common approach is to sandwich a monolayer of molecules between two metal electrodes. This is compatible with practical molecular device integration but suffer from short circuits due to diffusing of metal electrode atoms through loosely packed molecules monolayer. We have developed a novel molecular electrode design with sub-nm precision in distance between electrode in a readily scalable fabrication process. On the vertical face at the edge a multilayer pattern, we have successfully attached molecules electrochemically between two metal (M) electrodes separated by ~2nm thick alumina insulator (I). The molecule of interest is a ~3nm long, 8-metal coordination compound with thiol terminated linking functional groups. The bare tunnel junction electrodes possessed sufficiently sharp side edges and resistance greater than ~100kO. The current after molecular attachment was found to be significantly higher (>10 fold) than through the tunnel barrier of electrodes(across the plane of the insulator film). Current change is explained by Simmon's tunnel model with changes in barrier and tunnel distance that is consistant with molecular attachement. NiFe/AlOx/NiFe, Ta/AlOx/Ta and Ni/AlOx/Au systems have been used successfully for attaching molecules. The flexibility in contact materials can be easily extended for making molecular devices exhibiting classical phenomenon and new generation spintronics, opto-electronic devices. The most critical step of preparing sharp and exposed M-I-M structure for molecule attachment was carried out simply by customizing photolithography and sputtering deposition conditions. We confirmed the result by attaching molecules on sharp edge of M-I-M tunnel junction prepared by alternative method of ion beam milling, in a control experiment. To further prove the electrical contact with molecules in our electrode design, Au-AlOx-Ni electrodes were prepared. Device current due to molecule attachment disappeared and simple bare electrode current-voltage characteristics were restored after breaking the Au-molecule bond. This was achieved by substitutional chemistry only at the gold surface and can be the basis for future chemical sensors.

11:40 AM Student

HH10, From Quantum Chemistry to Molecular Electronic Circuits: *Yuhui Lu*[1]; Craig Lent[1]; [1]University of Notre Dame

Quantum-dot cellular automata (QCA) provides an alternative paradigm for the design of molecular electronics. In the QCA approach, binary information is stored in the charge configuration of single molecules, and transferred via Coulomb coupling between neighboring. Decreased resistive heating makes possible extremely high device densities without melting from the dissipated energy. Several candidate QCA molecules have been synthesized and characterized. QCA molecules have shown the switching behavior under an external field, which satisfies the basic requirement of QCA cells. Quantum chemistry ab initio techniques are also employed to study the electronic structure of candidate molecules. These calculations confirm the bistable charge configuration and possibility of information process via the intermolecular Coulomb interaction. Quantum chemistry calculations provide useful information about the single molecular QCA cell, but the study of the dynamics of QCA devices, which may involve a large number of molecules, requires more subtle techniques. We have devised a procedure to construct an effective Hamiltonian for a reduced state-space that can be scaled to describe entire QCA circuits comprised of many molecular cells. We apply this method to a model QCA molecule, the 1,10,19-eicosatriene cation. In this molecule three carbon-carbon double bonds provide extended, redox-active states that act as three quantum dots. We optimize the molecular geometry and identify the stable charge configurations using an ab initio calculation at the Hartree-Fock level. These three configurations, corresponding to charge localization on the different redox sites, can be used to represent "0", "1", and "null" states of a QCA cell. We detail the procedure for extracting the elements of the simplified Hamiltonian from the full ab initio quantum chemistry calculation. We confirm the utility of the effective Hamiltonian by comparing the calculated energy eigenstates of the simple and full molecular Hamiltonians as the QCA clocking field and signal field are varied. We model the switching dynamics of a molecular QCA circuit constructed from the QCA molecules and clocked using a sinusoidal perpendicular clocking field. From the Hamiltonian we construct a cell-level description using a coherence vector formalism based on the density matrix. The dynamics are extended to include the interaction between the molecules and the thermal environment. Both power gain at the molecular level and power dissipation can then be evaluated. We describe a well-defined hierarchical theory that connects the detailed molecular quantum chemistry to circuit-level behavior. This permits the "tuning" of molecular properties by appropriate design to achieve circuit performance. [1]H. Qi, A. Gupta, B.C. Noll, et al. J. Am. Chem. Soc., 127, 15218 (2005).

Session II: Trapping and Charge Transport in Organic Transistors

Friday AM, June 30, 2006
Room: Conference Room 206
Location: Pennsylvania State University

Session Chairs: Thomas N. Jackson, Pennsylvania State University; David J. Gundlach, National Institute of Standards and Technology

8:20 AM Invited

II1, Trapping of Majority and Minority Carriers at the Insulator-Polymer Semiconductor Interface: *David M. Taylor*[1]; Oscar Fernandez[1]; Janet Lancaster[1]; [1]University of Wales, Bangor

Two issues are emerging as key to the further development and commercialisation of organic (small molecule and polymer) electronics. The first is the widely reported threshold voltage instability which causes transistors to slowly turn off when biased to on, and turn on when biased to off. The effect has been observed in a wide range of semiconductor/insulator combinations and suggests that hole (electron) interface trapping must occur when the transistor is biased into accumulation (depletion). The second is the demonstration of n-channel behaviour, i.e. inversion, in p-type semiconductors which holds out the prospect of an organic CMOS type process. This latter effect was made possible by suitable passivation of minority electron traps at the insulator-semiconductor interface. There is a need, therefore, to develop

methods that can identify interface traps and elucidate their role in device behaviour. In this contribution we show that admittance measurements provide such a method. Initially, we will review our work on majority carrier (hole) trapping which is characterised by voltage-dependent changes in the admittance of metal-insulator-semiconductor (MIS) capacitors. We will also present the results from a photocapacitance study which reveals the behaviour of minority carriers (electrons) by tracking the relaxation in threshold-voltage-shift induced by irradiation of the MIS capacitor with light of energy greater than the semiconductor bandgap.

9:00 AM Student

II2, Trap Energy Determination by Analysis of Isothermal Gated Space-Charge-Limited Current in Organic Thin-Film Transistors: *Richard D. Yang*[1]; Xiaotian Zhou[1]; Edward T. Yu[1]; Andrew Kummel[1]; [1]University of California, San Diego

Electronic properties of trap states, and particularly trap energies, profoundly influence the device performance of organic thin-film transistors (OTFTs). Customarily, the trap energy is determined by measuring carrier mobilities over a large temperature range in vacuum. However, these measurements are very time-consuming and often perturb the OTFT device characteristics with pumping and temperature cycles. We have developed a simple method of characterizing trap energy distributions at room temperature via measurement of gate voltage controlled space-charge-limited current (SCLC). The current-voltage characteristics of thin-film transistors fabricated from p-type CuPc grown by molecular-beam epitaxy and operated in reverse mode (holes transported to grounded source electrode) are found to be dominated by SCLC at high drain bias. Scanning Kelvin probe microscopy is used to verify the existence of space-charge and trapped charges in the film at high electric field. Transistor I-V characteristics are fitted using an SCLC model with an exponential distribution of trap state energies. Using this approach, the trap energy distribution has been characterized as a function of gate voltage and film thickness at room temperature. These measurements reveal the existence of two types of trap states: bulk trap states with small activation energy (87 +/- 10 meV) and interface trap states with larger activation energy (265 +/- 30 meV). Two distinct activation energies for trapped charge release were also obtained from temperature dependent transconductance studies, with values that correlate well with those determined from the gated SCLC method, thereby validating the isothermal gated SCLC method for trap energy distribution characterization.

9:20 AM Student

II3, Measurement of Drift Velocity and Mobility of Carriers in a Polymer Thin-Film Transistor: *Debarshi Basu*[1]; Liang Wang[1]; Lawrence Dunn[1]; Ananth Dodabalapur[1]; Martin Heeney[2]; Iain McCulloch[2]; [1]University of Texas at Austin; [2]Merck Chemicals

The electrical performance of organic semiconducting polymers has improved tremendously over recent years. Their potential for use in low cost electronics and photovoltaic applications has prompted technological and scientific interest in the understanding of charge transport in these materials. The calculations of steady state mobilities from the transconductance characteristics of a transistor estimates the average velocity, but fails in generating information about the distribution of carrier velocities or the nature of dispersion created by traps. Previous work by Dunn has demonstrated the existence of fast carriers in the channel of a pentacene transistor in response to a step voltage. We have used this method to measure the drift velocity and mobility of a packet of charge injected into the channel. This work represents the first such experiment performed in a polymer transistor. Poly(2,5-bis(3-tetradecylthiophen-2-yl)thieno[3,2-b]thiophenes) (pBTTT) was used for this study because of its high field effect mobilities. Saturation region mobility of 0.8 cm^2/Vs was obtained at V_{GS} of -100 V. To study transport using the pulse method, a voltage step that ramps from zero to maximum in 10 nsec is applied to the source of a transistor. This results in a packet of charge carriers being injected into the channel. The injected carriers travel along the channel due to the longitudinal electric field ($E \sim 10^4$-10^5 V/cm) and flow out of the drain contact through a 750 Ω resistor. The delay between the arrival of current at the drain and their injection at the source is therefore a measure of the transit time of the fastest carrier. Transit time mobilities ($\mu = L^2/t\ V_{DS}$) of 0.12 cm^2/Vs are calculated at V_{DS} = -100 V. The rising edge of the output also contains information about the average velocity and the dispersion in velocities of carriers in the material. In addition, by changing the voltage of the pulse, the dependence of delay-time mobilities on the gate/drain biases can be revealed. In summary, we have made the first measurements of drift velocity and mobility in a polymer transistor. This method can be also used to explore trap states and achieve a more complete understanding of charge transport.

9:40 AM

II4, Influence of Charged Dielectrics and Adsorbed Dipoles on Organic Semiconductors in Transistor Architectures: *Howard E. Katz*[1]; Cheng Huang[1]; Kevin See[1]; Alan Becknell[2]; [1]Johns Hopkins University; [2]Applied Physics Laboratory

The anticipated advantages of organic field-effect transistors (OFETs) are low-cost processing and functionality not easily obained from silicon devices. Currents through these devices are influenced by local fields at the semiconductor interfaces as well as voltages applied from gate electrodes. Local field effects can be utilized to radically tune the input-output relationships in OFETs and to transmit information about chemical vapor adsorbance to a circuit. This seminar will cover our latest results on the creation, stability, and utilization of internal fields to enable new architectures and applications. Highlights include enhanced sensitivity to nerve gas simulants and carrier type inversion in an organic FET.

10:00 AM Break

10:20 AM Student

II5, Charge Transport as a Function of Gate Voltage and Temperature in N,N'-bis(n-octyl)-Dicyanoperylene-3,4:9,10-bis(Dicarboximide) [PDI-8CN2]: *Yeon Taek Jeong*[1]; Byungwook Yoo[1]; Brooks A. Jones[2]; Antonio Facchetti[2]; Tobin J. Marks[2]; Ananth Dodabalapur[1]; [1]University of Texas at Austin; [2]Northwestern University

Organic field-effect transistors (OFETs) have been attracting much interest because of their potential applications in active matrix displays, sensors, and electronic papers, etc. There has been remarkable progress in enhancing the performance and understanding structure-properties relationships of p-type organic semiconductors like pentacene. Like p-type, n-type organic materials are essential to realize complementary circuits. However, many factors controlling/affecting charge transport of n-channel OFETs are still not adequately understood. Variable temperature measurements for p-channel thin-film FET materials such as pentacene and polythiophene show that the field-effect mobility is both gate-voltage and temperature dependent. The data indicate that multiple trapping and release mechanism (MTR) might be a useful model in describing charge transport in organic materials. In this study, a new n-type semiconductor known as N,N'-bis(n-octyl)-dicyanoperylene-3,4:9,10-bis(dicarboximide)[PDI-8CN2] is used as the channel material. This compound is air stable and exhibits electron mobilities as large as 0.3~0.6 $cm^2/V.s$. Recently, it has been used to fabricate short channel length bottom contact transistors as well as ring oscillators with record frequencies for organic complementary circuits. In these experiments, the substrate consists of heavily doped p^+-Si with 1,000A thermally-grown SiO_2, on which the PDI-$8CN_2$ active layer and Au electrode are deposited to form either bottom or top contact OFET devices. Variable temperature electrical measurements were performed under the vacuum < 1×10^{-4} torr using liquid nitrogen as coolant. Saturation mobility μ_{sat}, V_g-dependent linear mobility μ_{lin}, and onset voltage V_o were calculated using standard MOSFET model. Our bottom and top contact devices exhibit comparable saturation mobilities of ~2×10^{-2} $cm^2/V.s$ and ~4×10^{-2} $cm^2/V.s$ at 310K, respectively. The saturation mobility increases with temperature following the Arrhenius relation $\mu_{sat} = \mu_{sat,0}$ (-Ea/kT), indicating that the charge transport mechanism is thermally-activated. The activation energies are 91.7meV and 94.9meV for bottom and top contact devices, respectively, and are temperature dependent. The $\log(\mu_{lin})$ vs. 1/T plot also shows that μ_{lin} is thermally-activated property, which increases with Vg. The bottom contact devices have higher activation energy for the same V_g indicating that the contacts influence charge transport efficiency. Intrinsic mobilities for the contact-influenced value are being extracted using the gated-four-probe technique. We have also found that there is an isokinetic point for bottom-contact devices consistent with the MTR model. The onset voltage is seen to decrease with temperature, which is an indicator that the MTR model is appropriate to describe electron transport for this material.

10:40 AM

II6, Using High-Sensitivity Electric Force Microscopy to Probe Charge Trapping in Pentacene Thin-Film Transistors: *Michael J. Jaquith*[1]; Showkat M. Yazdanian[1]; Tse Nga Ng[2]; John A. Marohn[1]; [1]Cornell University; [2]Palo Alto Research Center

The process of charge trapping in pi-conjugated organic materials remains poorly understood. Using current-voltage measurements to test theories of charge trapping is often problematic, requiring a careful disentangling of bulk and interface properties, both of which depend sensitively on temperature and electric field. We avoid these problems by measuring potential (trapped charge) and capacitance (free charge) locally with an electric force microscope (EFM). We have used EFM to study charge trapping in as-deposited polycrystalline pentacene. In films with comparatively large grains, EFM images reveal that charges trap primarily at grains near the pentacene-metal interface. By contrast, in films with small grains, EFM images show that long-lived holes traps are dispersed throughout the film. These traps, however, do not appear to be associated with grain boundaries, as is often assumed. We find that charge traps require 100's of milliseconds to form, implying that traps do not form instantaneously by the emptying of levels but instead arise from a reaction having finite activation energy. The rate depends roughly second order in charge density, which seems to indicate trapping via a bipolaron mechanism.

11:00 AM Student

II7, Charge Transport at Very High Carrier Densities in Organic Semiconductor Thin Films and Single Crystals: *Matthew J. Panzer*[1]; C. Daniel Frisbie[1]; [1]University of Minnesota

The field-effect transistor (FET) is one of the most commonly-used experimental platforms for examining the charge transport behavior of organic semiconductors. Traditional dielectric materials used to achieve electrostatic injection of charge carriers in FETs, however, possess low permittivities that limit the amount of charge one is able to induce via the field effect. For example, the maximum areal charge density that one can expect to achieve using SiO_2 as the dielectric (near breakdown field levels) is ~10^{13} charges/cm^2. Considering that many organic semiconductor materials pack with a molecular areal density on the order of 10^{14} molecules/cm^2, this means that only *~10% or fewer* of the molecules available to bear charge carriers are utilized in a SiO_2 FET. We have shown that by using a solid polymer electrolyte as an FET dielectric, areal charge densities greater than 10^{15} charges/cm^2 can be attained in a variety of organic semiconductors. Conductivity maxima at carrier densities at or above 1 charge/molecule have been observed in oligomeric, polymeric, and single-crystal organic semiconductors alike. Metallic conductivity and a nearly temperature-independent resistance ratio have been attained in poly(3-hexylthiophene) by electrostatic charge injection with a polymer electrolyte-gated FET. In spite of several drawbacks that may prohibit polymer electrolytes from finding widespread use in commercial FET applications, including slow switching speeds and chemical compatibility issues, these unique dielectric materials offer a straightforward means to achieving very high charge carrier densities in organic semiconductors. As a result, we are continuing to pursue further experiments utilizing electrolytic materials in order to gain a better understanding of the physics of carrier transport in conjugated organic materials at extremely high levels of charge injection.

11:20 AM

II8, Building Blocks for Single-Component Organic Electronics: Electrostatic Modulation and Majority Carrier Sign Inversion of Organic Semiconductors via Polarized Gates: *Cheng Huang*[1]; Howard E. Katz[1]; James E. West[1]; [1]Johns Hopkins University

We demonstrate that electrostatic induction effects from polarized gates with stored charges or oriented dipoles enable the threshold voltage shift and current modulation of organic semiconductor (OSC) thin films. This electrostatically-assisted "doping" enables quantitatively control of the doping level, to alter the carrier concentration, and to modulate the interfacial electronic properties of the OSC layer without introducing any obvious source of lattice or morphological disorder. We have successfully used excellent electret materials including charged and surface-treated silicon dioxide (SiO2) and silsesquioxane (SSQ) polymers as the dielectric layer in organic thin-film transistors (OTFTs). In addition, self-assembled monolayers (SAMs) of dipolar molecules have been utilized in the dielectric layer, with different mechanisms but similar effects compared to charged dielectrics. We present single-component OTFT unipolar inverters, comprised of only two simple OTFTs with enhancement-mode driver and depletion-mode load to implement full-swing organic logic circuits. Furthermore, it was found that as the effective surface potential increases, the OTFT gradually converts into the unipolar inversion mode, and the use of a highly charged gate dielectric realized p-type field-effect conduction in OSC that under normal device conditions only exhibits an n-type field effect. Organic field-effect transistors based on typically unipolar n-channel copper hexadecafluorophthalocyanine semiconductor thin films, deposited on a silicon dioxide quasipermanent charged electret as a gate insulator, are capable of unipolar p-channel "inversion" operation in ambient air with evaporated gold employed as the source and drain electrodes. The giant stored electric field produced by patterned, grid-controlled negative corona charging of the electret prior to semiconductor deposition electrostatically induces sufficient positive charge accumulation to fill hole traps in this normally-n material and leads to significant mobility of 0.010 cm2 V-1 s-1 for holes induced by moderate additional negative gate voltages. We demonstrate organic field-effect unipolar inversion-mode transistors and complementary logic elements employing a single OSC operable under ambient conditions. The unprecedented ability to pattern electrostatic properties prior to semiconductor and electrode deposition and to form either unipolar inverters or complementary inverters from a single, air-stable organic semiconductor material suggests alternatives for process simplification of electronic components in organic electronics.

11:40 AM

II9, High-Mobility Charge Transport in Laminated Rubrene Crystal/Polymer Field-Effect Transistors: *Jun Takeya*[1]; Koichi Yamada[2]; Kazuhito Tsukagoshi[3]; Yoshinobu Aoyagi[3]; Yasuhiro Nakazawa[1]; Yoshihiro Iwasa[4]; [1]Osaka University; [2]CRIEPI; [3]RIKEN; [4]Tohoku University

To look for prescriptions for further improving the transistor performance, detailed charge transport properties are examined of newly prepared high-mobility rubrene crystal FETs with polymeric gate dielectrics. Thin rubrene crystals are laminated on the gate insulators so that p-type normally-on devices are fabricated. The field-effect mobility defined by transconductance shows significant gate-voltage dependence with a peak around zero gate voltage, exceeding 10 cm2/Vs for some devices. Hall mobility defined by Hall effect measurement shows apparently different V_G profile with larger values on the whole, though the zero-gate peak is present. The inconsistency between the two suggests mixture of holes with different values of mobility, deviated from the simple picture of nearly equal-mobility carriers. Together with temperature dependence, possible spatial distribution of the charge mobility will be discussed to specify high-mobility region in the conduction channel of the devices.

Session JJ: Spintronic Materials

Friday AM
June 30, 2006

Room: Conference Room 108
Location: Pennsylvania State University

Session Chairs: Chris J. Palmstrom, University of Minnesota; Nitin Samarth, Pennsylvania State University

8:20 AM

JJ1, Magnetoresistance and Insulator-Metal Transition of EuO_{1-x} Thin Films Grown on (110) $YAlO_3$ and (001) Si Substrates: *Andreas Schmehl*[1]; Venu Vaithyanathan[1]; Raghava Panguluri[2]; Boris Nadgorny[2]; Marco Liberati[3]; Yves Idzerda[3]; Alexander Weber[4]; Jochen Mannhart[4]; Darrell G. Schlom[1]; [1]Pennsylvania State University; [2]Wayne State University; [3]Montana State University; [4]University of Augsburg

With its impressive electronic, magnetic, and optical properties, the ferromagnetic semiconductor EuO_{1-x} is a fascinating compound for basic studies and for possible electronic applications. In Eu-rich EuO_{1-x} single crystals the ferromagnetic transition is accompanied by an insulator–to-

metal transition with a resistivity drop of up to 13 orders of magnitude. Further, in single crystals the T_c as well as the magnitude of this transition can be shifted over a wide range by applying external magnetic fields. These dramatic property changes, together with the low charge carrier density and a reported spin polarization of about 100% in the ferromagnetic state, make EuO_{1-x} a very promising material for possible applications in spintronic devices, provided comparable properties can be achieved in thin films. To assess the properties of epitaxial EuO films, we grew Eu-rich EuO_{1-x} films by reactive-molecular beam epitaxy (MBE) and characterized their structural, magnetic, and transport properties. The films were grown either directly on (001) Si using 12 Å thick SrO buffer layers or on (110) $YAlO_3$. As EuO_{1-x} is not stable in air the films were protected with capping layers of amorphous Al_2O_3. To make electric contact with the underlying EuO_{1-x} a novel process has been developed that combines in situ ion-milling and metal deposition. The structural properties were investigated using x–ray diffraction. For both substrate types these measurements indicate (001)-oriented, single-phase films, with [110] EuO_{1-x} || [110] $YAlO_3$ and [100] EuO_{1-x} || [100] Si respectively. Rocking curve widths, measured on the EuO_{1-x} 004 reflections, show values better than 0.4° FWHM for both substrate types. Four-point transport and SQUID measurements show ferromagnetic transitions with T_cs of about 69 K and a resistivity drops at the insulator–metal transition of about seven orders of magnitude. Application of external magnetic fields up to 8 T perpendicular to the film plane suppress the resistance near T_c up to five orders of magnitude and shift the transition temperatures to ˜150 K. These samples reveal the most pronounced magnetoresistive effect reported in EuO_{1-x} films. Exposure of the samples to light leads to photo doping and thus to an increase in conductivity of about two orders of magnitude. This increase has no effect on the ferromagnetic T_c indicating a low charge carrier density in the EuO_{1-x} films. Andreev reflection measurements were performed on La-capped EuO_{1-x} films grown on Si. These measurements indicate spin polarizations of the conduction electrons exceeding 70% below T_c.

8:40 AM Student

JJ2, High Field Magnetoresistance and Hall Effect Studies of Nonmagnetic Al- and Cu-Doped (Zn,Mn)O Dilute Magnetic Semiconductors: *Theodore W. Kehl*[1]; C. J. Vera[1]; S. Manchiraju[1]; D. E. Horst[1]; K. Manivannan[1]; J. Griffiths[2]; P. K. Kahol[1]; K. Ghosh[1]; S. R. Mishra[2]; [1]Missouri State University; [2]University of Memphis

Dilute Magnetic Semiconductors (DMS) are a rare group of promising materials that utilize both electronic charge, a characteristic of semiconductor materials, and electronic spin, a characteristic of magnetic materials. Among all the DMS materials, oxide based DMS show promise of ferromagnetism (FM) at room temperature. It has been found that doping metal oxides such as (ZnO, SnO_2, TiO_2) with magnetic ions such as Fe, Co, Mn produces DMS and exhibit FM above room temperature. ZnO, a transparent opto-electronic material, is an interesting prospect for spintronics due to its unique combination of magnetic, electrical, and optical properties. The magnetic nature of Mn doped ZnO is controversial, where some groups claim the presence of high Curie temperature FMs in these films while several other groups claim the absence of FM. Additionally, ZnO doped with manganese or non magnetic metals (Al,Cu) is a DMS which shows strong exchange interaction between s-p band carriers and localized d electrons. In this paper we will present the effect of nonmagnetic doping on the high field magneto-transport properties of epitaxial thin films of Mn-doped ZnO DMS. High quality epitaxial thin films of $Zn_{0.85}Mn_{0.15}O$(ZnMnO), $Zn_{0.80}Al_{0.05}Mn_{0.15}O$ and $Zn_{0.80}Cu_{0.05}Mn_{0.15}O$ were grown on single crystal of sapphire by PLD technique using a KrF excimer laser (λ = 248 nm) under suitable epitaxial growth conditions. Both structural and physical properties of the films are sensitive to these conditions as previously observed in several oxides such as Perovskite manganites and ferroelectrics. The structural characterization was performed using XRD and Raman spectroscopy. The surface microstructure of all thin film samples were measured with AFM and SEM. XRD and Raman Spectra confirm the epitaxial growth with a strong orientation along the c-axis. With nonmagnetic dopants, Al and Cu, the position of (002) and (004) showed further shifted towards to lower angle. The increases in c values were 0.0184 A and 0.0681 A with Al and Cu dopants respectively over the original value of 5.1516 A for pure ZnMnO. The temperature and magnetic field dependence resistivity, magnetoresistance, and Hall coefficient were measured at high magnetic fields up to 15 Tesla and in a wide range of temperature from 5 K to 200 K at National High Field Magnet Laboratory, Tallahassee, FL.The observed field dependence magnetoresistance is different below and above the ferromagnetic transition temperature. The normal and anomalous contributions to the Hall effect have been extracted from the Hall measurement data. Detailed low temperature and high field magneto-transport data will be discussed in this presentation. This work was supported by the Office of Naval Research (award number N00014-03-1-0893), National Science Foundation (award number DMR- 0321187), Research Corporation (award number CC6166), and National High Field Magnet Laboratory, Tallahassee, FL.

9:00 AM

JJ3, Conduction-Band Electron Effective Mass in $Zn_{0.87}Mn_{0.13}Se$ Measured by Terahertz and Far-Infrared Magnetooptic Ellipsometry: *Tino Hofmann*[1]; K. C. Agarwal[2]; B. Daniel[2]; C. Klingshirn[2]; M. Hetterich[2]; C. M. Herzinger[3]; M. M. Schubert[1]; [1]University of Nebraska-Lincoln; [2]Universität Karlsruhe; [3]J.A.Woollam Company, Inc.

We determine the electron effective mass parameter m*=0.086±0.004 m_0 of thin film n-type low-chlorine-doped $Zn_{0.87}Mn_{0.13}Se$ with free-charge-carrier concentration $N=4.5x10^{17}$ cm^{-3} and opticalmobility μ=300±20 cm^2/(Vs) using magnetooptic generalized ellipsometry in the terahertz and far-infrared spectral domain for wavenumbers from ω=30-650 cm^{-1}. The room temperature measurements were carried out with magnetic fields up to 3 Tesla. We employ synchrotron and black-body radiation sources for the terahertz and far-infrared spectral regions, respectively. Comparison with previous experimental results from samples with considerably higher free electron density and theoretical calculations suggest that our value is sufficiently unaffected by band non-parabolicity and provides a good approximation of the Γ-point conduction band mass in $Zn_{0.87}Mn_{0.13}Se$. We further provide optical phonon mode parameters and the high-frequency dielectric constant.

9:20 AM Student

JJ4, Ferromagnetism in Fe-Implanted ZnO Films and Nanotips: *Pan Wu*[1]; Gaurav Saraf[1]; Yicheng Lu[1]; David Hill[1]; Dario Arena[2]; Robert Bartynski[1]; Leszek Wielunski[1]; Jeremy Raley[3]; Yung Kee Yeo[3]; [1]Rutgers University; [2]Brookhaven National Laboratory; [3]Air Force Institute of Technology

Transition metal (TM) doped ZnO is one of the most promising dilute magnetic semiconductors (DMS) candidates as it is predicted to be ferromagnetic above room temperature. As ZnO is a radiation-hard material, ion implantation becomes a suitable technique to introduce TM ions into ZnO without causing extensive lattice damage. Fe ions of dose 5x1016 cm-2 were implanted at 200 keV into a-plane ZnO epitaxial films on r-sapphire substrates. For comparison, Fe-ions were also implanted into c-axis oriented ZnO nanotips grown on SiO2/quartz substrates. After Fe implantation, the samples was annealed at 700°C in an oxygen flow. SEM images indicate that there are no morphological changes after implantation and post-annealing for Fe-implanted ZnO films. However, a sharpening effect on ZnO nanotips is observed after high dose Fe ion implantation, which is attributed to the competition between the surface instability created by sputtering and surface smoothening by ion-induced diffusion that determines the final surface shape. The crystallinity and epitaxial relationship of the Fe-doped ZnO films and nanotips are evaluated using x-ray diffraction (XRD). The XRD j scans show that the in-plane registry between the Fe-doped ZnO film and the r-sapphire substrate as (11-20) Zn1-xFexO || (01-12) Al2O3 and [0001] Zn1-xFexO || [0-111] Al2O3. The XRD w-rocking curve of the 40 min annealed Fe doped ZnO film demonstrates the epitaxial quality of the film with a full width at half maximum (FWHM) of ~0.45°. The XRD pattern of ZnO nanotips shows c-axis orientation in both as-implanted and annealed samples. X-ray absorption spectroscopy (XAS) spectra of Fe-ion implanted films and nanostructures show that the Fe L2,3 line shape is consistent with tetrahedral coordination, as expected for Fe ions substituting for Zn in the ZnO wurtzite lattice. SQUID measurements show that the as-implanted and post-annealed films and nanotips are ferromagnetic at room temperature. The magnetic response of Fe as-implanted ZnO nanotips is larger than Fe as-implanted ZnO films. This is due ZnO nanotips have larger surface area exposed under the impinging ions, and it is found that the ZnO nanotip surface has higher Fe concentration than the bulk. Zero field cool (ZFC) and field cool (FC) magnetization versus temperature measurements of films and nanotips show that the ferromagnetic behavior is persistent up to 400 K. The saturation magnetization reduces during annealing in both films and nanotips cases

due to redistribution of Fe ions. This work has been supported by National Science Foundation under the grants ECS-0224166.

9:40 AM Student

JJ5, Dilute Magnetic MnGe Semiconductor Using Ion Implantation of Mn into Nano-Patterned Ge: *Jingjing Chen*[1]; Kos Galatsis[1]; Kang Wang[1]; Jiayu Wang[2]; Thomas P. Russell[2]; [1]University of California, Los Angeles; [2]University of Massachusetts

Group IV Diluted Magnetic Semiconductors (DMS) such as Mn-Ge and Mn-Si hold great promise as versatile materials that may conveniently integrate potential spin devices with CMOS. With this motivation we aim to fabricate room temperature ferromagnetic Mn-Ge Device. We have employed a novel di-block copolymer nanopattern to form a mask for Mn ion implantation to periodic 20-nanometer areas on SiO_2/Ge substrates. SEM micrographs obtained show a well nanostructured pattern for the ion implantation step. Ion-implantation was performed with Mn at 40KeV and with a dose of $4.0\times 10^{15}/cm^2$, and then the samples were annealed at 400-700°C for 20min. We foresee such methods could enable consistent and reliable tailoring of Mn-Ge magnetic properties by improving uniform solubility of Mn in Ge, along with decreasing strain, lattice mismatch and defects. XRD scans taken on both n- and p-type substrate samples detected the presence of most Mn_5Ge_3 phase, which is theoretically predicted to have a T_c near room temperature. Using Superconducting Quantum Interference Device (SQUID), ferromagnetic hysteresis loops were obtained at 5K-300K on p-type substrate samples but only paramagnetic lines were found on n-type substrate samples. Such results indicate the hole-mediated ferromagnetism of the MnGe DMS materials. In addition, samples annealed at various temperatures showed the saturation magnetization reached an optimum value at 450°C of 3.4×10^{-4} emu/cm^3. The difference in the temperature-dependent remnant magnetization between the implanted n-type and p-type Ge were also observed. Our paper will discuss these results, additional material characterization and SIMS results as a function of Mn-implantation parameters and annealing conditions.

10:00 AM Break

10:20 AM

JJ6, Direct Imaging of Photo-Induced Changes in Magnetization Orientation in (Ga,Mn)As by a Scanning Magneto-Optical Microscope: *Tsuyoshi Kondo*[1]; Kenta Nomura[1]; Gaku Koizumi[1]; Hiro Munekata[1]; [1]Tokyo Institute of Technology

Optical manipulation of magnetization with relatively low excitation power has been reported in carrier-mediated ferromagnetism in III-V magnetic alloy semiconductors (MAS). Both static magneto-transport data under the circularly-polarized light and time-resolved magneto-optical signals obtained by pump-and-probe technique have led us to believe that photo-generated, spin-polarized carriers cause significant change in the orientation of magnetization in ferromagnetic (Ga,Mn)As epilayers[1, 2]. The present work reports successful, direct observation of photo-induced change in domain structures in patterned (Ga,Mn)As samples by using a home-made scanning laser magneto-optical microscope (SLMOM). The observed change shows strong dependence on circular polarization of the excitation light. A 200-nm thick (Ga,Mn)As epilayer was grown on a GaAs(001) substrate by molecular beam epitaxy at a substrate temperature of 250°C. Mn content and Curie temperature of the epilayer are [Mn] ~ 4% and T_c ~ 40K, respectively. The epilayer was processed into square mesas of 20×20 μm^2. Our SLMOM has spatial resolution of 1 μm with sensitivity of sub-milli-degree in terms of rotation power. Domain imaging was carried out by magnetic linear dichroism (MLD) at a temperature of 10K. As reported previously[3], (Ga,Mn)As shows large MLD for the incident light having linear polarization along the {110} axis, which appears to be a useful tool to detect a change in the magnitude and orientation of the in-plane magnetization. Prior to the MLD imaging, a (Ga,Mn)As mesa was first magnetized by an external field of 1000 Oe along the <100> axis. Removing the field yielded a multi-domain structure at the remanent state. After the imaging, circularly polarized white light of 700 mW/cm^2 was irradiated on the mesa for 10 sec. Irradiation with σ^- light caused no change in domain image. In contrast, irradiation with σ^+ light caused a significant change in MLD contrast, suggesting a change in overall/local magnetization orientation. Second irradiation with σ^- light resulted in the recovery of the initial magnetization condition. These cycles can be repeated many times. The magnitude of change in MLD signal seems to increase with increasing irradiation time. No change in MLD signal was observed by the irradiation with unpolarized light. This fact suggests that the light-induced heating is not responsible. Even though the mechanism is not clear at present yet, our observation gives direct evidence for photo-induced change in magnetization. The results may have a close relevance to the reported photo-induced magnetization[1]. [1]A. Oiwa *et al.*, Phys. Rev. Lett. 88 137202 (2002). [2]Y. Mitsumori *et al.*, Phys. Rev. B 69 033203 (2004). [3]A. V. Kimel *et al.*, Phys. Rev. Lett. 94 227203 (2005).

10:40 AM Student

JJ7, Electroluminescence Studies of (Ga,Mn)As-Based p-i-n Structures: *Zhiguo Ge*[1]; Raja Chakarvorty[1]; Shaoping Shen[1]; Weng-Lee Lim[1]; Xinyu Liu[1]; Jacek Furdyna[1]; Malgorzata Dobrowolska[1]; [1]University of Notre Dame

We report the observation of electroluminescence (EL) in a series of magnetic p-i-n structures grown by molecular beam epitaxy (MBE). In these samples, the ferromagnetic semiconductor (Ga,Mn)As serves as the p-type top layer, while intrinsic GaAs and Si-doped GaAs substrate play the role of the central i-layer and of the n-type bottom layer, respectively. In order to understand the mechanism of EL in such a device, we have also modified the above basic p-i-n structure by introducing an additional GaAs layer – either p-type (doped with Be), or n-type (doped with Si), or low-temperature (LT) GaAs layer – into the central i-layer. I-V characteristics were carried out to verify that all samples show good rectifying properties. Temperature- and the current-dependences of the EL spectrum were then investigated and compared. The observed significant differences among the EL spectra from these modified structures point out that the mechanism of radiative recombination in each structure is definitely affected by its energy band profile. In particular, we found that the active region from which luminescence is emitted can be tuned by the inserted layer, thus leading to the observed differences in the temperature- and current-dependences of the EL. It is well known that for a standard p-i-n structure, most of the luminescence comes from recombination in the central i-layer. In our case we observe two EL peaks, one of which we associate with Mn doping, and one with either Be, Si, or C. Experimentally, one expects all EL peaks to increase in accordance as the current increases in the device. However, in our modified p-i-p-i-n structures, the peaks associated with Mn and those corresponding to non-magnetic dopants respond differently to the applied current both in their energy position and intensity, indicating that the origin of the two recombinations is different. To understand this, numerical calculations of band diagram were carried out using a simple two-band model which simultaneously solves the Schrödinger and the Poisson equation. By introducing either an n-type or a p-type GaAs layer into the central i-layer, a potential well for capturing minority carriers is found in the central i-layer, close to the n-type bottom layer or the p-type top layer, respectively. This potential well leads to a local increase of the concentration of minority carriers, and thus increases the probability of radiative recombination in this region. Both the observed temperature- and current-dependences of the EL spectra can thus be qualitatively explained in terms of the energy band diagram described above.

11:00 AM Student

JJ8, Ferromagnetic Co_2MnGe Contacts for GaAs: Growth, Characterization, and Interface Stability: *J. L. Hilton*[1]; B. D. Schultz[1]; X. Lou[2]; P. A. Crowell[2]; C. J. Palmstrom[1]; [1]Department of Chemical Engineering and Materials Science, University of Minnesota; [2]School of Physics and Astronomy, University of Minnesota

Heusler alloys have a number of properties that make them desirable for use as contacts in semiconductor-based spintronic devices. They have Curie temperatures above room temperature, their crystal structures and lattice parameters are compatible with many compound semiconductors, and they have high spin polarization at the Fermi level. Co_2MnGe is one of the Heusler alloys that are predicted to be half-metallic, and it has been grown epitaxially on GaAs. This research investigates the growth properties, surface structure, and stability of Co_2MnGe films grown on GaAs(001) surfaces by molecular beam epitaxy. Reflection high energy electron diffraction and x-ray diffraction (XRD) indicate good crystalline quality in the films. *In-situ* x-ray photoemission spectroscopy (XPS) was used to investigate the chemistry of the interface, and shows that growth of Co_2MnGe at 175°C results in interfacial reactions that consume ~1.5 monolayers of GaAs. Growth at 250°C consumes approximately ~3 monolayers of GaAs. *In-situ* scanning

tunneling microscopy (STM) images show that the surfaces of 100Å films grown at 175°C are relatively flat with localized height variations on the order of a few monolayers, but the terrace sizes averaged less than 100Å in length. The surfaces of the films can be dramatically altered by changing the growth conditions of the film. STM images of 100Å thick films grown at 250°C show that the surfaces remained relatively flat; however, the average terrace length was found to be significantly larger than for films grown at 175°C. In order to minimize interfacial reactions and obtain atomically smooth surfaces, a template layer approach was also used to grow Co_2MnGe films where the first 25Å was grown at 175°C and the remainder of the film was grown at 250°C. XPS showed that heating the 175°C films to 250°C did not cause additional reactions, and STM showed that films grown in this manner form very flat surfaces with terrace lengths larger than those formed following growth at either 175°C or 250°C. Thicker (~1000Å) Co_2MnGe films were also grown on GaAs and post-growth annealed for times up to 12 hours at temperatures up to 450°C. Rutherford backscattering spectrometry of these samples shows that there are no significant compositional changes in the samples as a function of annealing, and XRD results suggest that the films relax as the annealing time/temperature increases. Results from *in-situ* RHEED, LEED, STM, and XPS, and *ex-situ* XRD and RBS will be combined to address the growth, characterization, and stability of epitaxial Co_2MnGe/GaAs heterostructures. Spin-LEDs will be used to measure the spin injection from Co_2MnGe contacts into GaAs-based devices. This research was supported in part by ARO, ONR, and NSF-MRSEC.

11:20 AM

JJ9, Magnetic Characterization of Fe/Tb Superlattice Grown on InAs as a Vertically Magnetized Spin Injector: *Kanji Yoh*[1]; Robert Peters[2]; Marhoun Ferhat[3]; Saori Kashiwada[1]; Werner Keune[2]; [1]Hokkaido University; [2]University of Duisburg-Essen; [3]JST

In order to realize Datta-Das spin transistor, it is crucial to achieve decent Ohmic contact resistance while maintaining high spin injection efficiency at the ferromagnet/semiconductor interface. InAs and related narrow-gap semiconductors are suitable in order to achieve high spin-orbit interaction and high spin injection efficiency while maintaining low Ohmic contact resistance at the barrier-less ferromagnet/semiconductor interface. In the course of this direction, we have been studying high efficiency spin injection in Fe/InAs spin diode structure and Fe/InGaAs spin transistor structures. For Fe grown on InAs or InGaAs with high indium content, out-of-plane direction becomes hard axis of magnetization. High magnetic field changes band structure and causes Zeeman splitting of conduction band and magnetic depopulation of valence band. In this paper, we report on Fe/Tb super lattice grown on InAs, which has easy axis of magnetization in the out-of-plane direction. The growth of Fe/Tb superlattice has been performed at room temperature under high vacuum in order to minimize interface reaction at the Fe/InAs boundary. The isotope of 57Fe was used for the initial Fe layer for the purpose of studying spin polarization in the initial Fe layer grown on InAs by Mösbauer measurement. It was shown that the initial 5 mono-layers of Fe have out-of-plane component of spin orientation of 90% in average. It is to be noted that the there exist no such "dead layer" between Fe and GaAs layer [7] and between Fe and InAs layer [8]. The magnetization characteristics of Fe/Tb superlattice grown on p-InAs substrate were measured by SQUID method. It showed strong temperature dependence. First, let's look at the Tb/Ag superlattice characteristics by SQUID analysis. The Tb layers exhibit antiferromagnetic nature below 218K. The Tb/Ag reference sample exhibits ferromagnetic characteristics at low temperature and non-ferromagnetic characteristics at room temperature as expected. However, the Fe/Tb SL exhibits ferromagnetic nature in out-of-plane orientation. Interesting temperature dependence is observed. In all temperature range from 20K to 300K, ferromagnetic nature in out-of-plane orientation is observed even though Tb itself should exhibits no ferromagnetic nature at near room temperature range. This is promising for our spin injection applications in out-of-plane magnetization set-up. The cohersive field was observed to increase from 2k-3kGauss (300K) to 5T (20K).

11:40 AM Student

JJ10, Thickness Determination of Ultra-Thin Oxide Films and the Application in Magnetic Tunnel Junctions: *Jianhua J. Yang*[1]; Chengxiang Ji[1]; Y. Austin Chang[1]; Ying Yang[1]; Feng X. Liu[2]; Bharat B. Pant[2]; Allan E. Schultz[2]; [1]University of Wisconsin-Madison; [2]Seagate Technologies

The accurate measurement of the thickness of an ultra-thin tunnel barrier oxide or nitride film (~2nm) is of critical importance in the study of tunnel barrier fabrications in magnetic tunnel junctions (MTJs), consisting of two ferromagnetic layers separated by an insulator layer, i.e. the tunnel barrier. High-resolution transmission electron microscopy (HRTEM) is one possible choice to obtain the thickness of the ultra-thin oxide. However, HRTEM cross-section sample preparation for such a thin film is very time-consuming and needs sophisticated experimental skills. In addition, artifacts such as amorphizing the unoxidized metal could be easily introduced during the process of thinning a sample by ion milling. This study demonstrates a simple method that combines surface sensitive techniques, such as X-ray photoelectron spectroscopy (XPS), with a wedge sample to determine the thickness of an ultra-thin Al oxide film. The method would also be applicable in other oxide and nitride thin film studies. The uncertainty of the measured thickness is analyzed and the factors that affect the accuracy of this measurement are also discussed. By applying this method into the optimization of the oxidation condition for the Al tunnel barrier precursor metal, a magnetic tunnel junction with high quality oxide tunnel barrier was fabricated and thus relatively high MR ratio was obtained.

Session KK: GaN Characterization

Friday PM, June 30, 2006
Room: Deans Hall II
Location: Pennsylvania State University

Session Chairs: Randall M. Feenstra, Carnegie Mellon University; Michael Wraback, U.S. Army Research Laboratory

1:30 PM

KK1, A Dynamic Micro-Analysis of Temperature Distribution and Electric Potential Distribution of AlGaN/GaN HFETs Using Micro-Raman Spectroscopy and Kelvin-Force Microscopy: *Akira Suzuki*[1]; Shin-Ichi Kamiya[2]; Masayuki Iwami[2]; Yuichi Hiroyama[2]; Tadayoshi Tsuchiya[2]; Tomoyuki Yamada[2]; Junjiroh Kikawa[2]; Ken-Ichi Kosaka[1]; Tsutomu Araki[1]; Yasushi Nanishi[1]; [1]Ritsumeikan University; [2]Advanced HF Device R&D Center, R&D Association for Future Electron Devices

Hetero-junction field effect transistors (HFETs) of AlGaN/GaN structures have extensively been studied, especially for high-frequency and high-power applications because of their excellent two-dimensional channel performance and high electrical breakdown field. For their practical use, however, device performances at high driving voltages should be analyzed and improved much more to attain no thermal destruction with less leakage currents and higher breakdown voltage. In the present study, temperature distribution and electric potential distribution of AlGaN/GaN HFETs were measured and analyzed at source-drain voltages up to around 50 V using micro-Raman spectroscopy and Kelvin-force microscopy (KFM), respectively. Sample devices were MOCVD-grown on SiC and sapphire substrates. The Al composition and thickness of AlGaN barrier layer were typically 0.25 and 30 nm, respectively. A gate electrode was Ni/Al, while source and drain electrodes Ti/Al/Nb/Au. Typical values of gate length and width were 3 micron and 40 micron, respectively. Electrical power was applied through conductive probes on the source, gate, and drain electrodes. For micro-Raman analysis of the temperature distribution, Ar laser (514.5 nm) was used, and temperature was estimated from Raman shift of E2 phonon peak, with a spatial resolution of around 1 micron. A two-dimensinal temperature distribution between the source and drain was obtained. A high temperature region was found to appear at the gate edge toward the drain. The maximum temperatures, for example, were around 290°C on sapphire and 150°C on SiC at a source-drain voltage of 40 V. For KFM analysis of the electric potential distribution, the AlGaN/GaN HFET samples were cleaved and their cross-sections were measured with a spatial resolution of around several ten nm. For a fixed gate voltage as a parameter, two-dimensional electric potential distribution was obtained with increasing source-drain voltage up to a breakdown, for example, around 40 V, which enabled us to observe the localization of electrical field

directly. Electric field was found to concentrate in the regions between the gate and drain. The change in electric potential distribution was measured with increasing source-drain voltage. A combined analysis in the present study of temperature and electric potential distributions in the micro-areas of actually working HFETs driven at high voltages (possible up to around 100 V) is a very effective tool to reveal a localization of high electric field and high thermal source, which will contribute to improve the high-power performance of AlGaN/GaN HFETs.This work was supported by the High-Power, High-Frequency Gallium Nitride Device Project of NEDO.

1:50 PM Student

KK2, Selective Quantification of AlGaN-Related Deep Levels in AlGaN/GaN Heterostructures Using Capacitance-Mode Deep Level Optical Spectroscopy: *Andrew Armstrong*[1]; Christiane Plobenz[2]; Siddharth Rajan[2]; James S. Speck[2]; Umesh K. Mishra[2]; Steven A. Ringel[1]; [1]Ohio State University; [2]University of California, Santa Barbara

Discriminating electrically active deep levels particular to the AlGaN region of an AlGaN/GaN heterostructure field effect transistor (HFET) from those associated with the GaN layer is an impediment to understanding and mitigating traps detrimental to device performance. Here we describe an approach using capacitance-mode deep level optical spectroscopy (DLOS) to quantitatively detect traps specific to the AlGaN region of an AlGaN/GaN Schottky diode with a heterostructure similar to that of an HFET device. Selectivity over the thin (~30 nm) AlGaN region compared to that of the thicker (~1000 nm) underlying GaN layer is achieved by performing measurements at 0 V bias such that the built-in polarization field depletes the AlGaN and the two-dimensional electron gas (2DEG) is accumulated. Under this condition, deep levels residing at the heterointerface or nearby GaN region wherein the 2DEG resides have no net emission rate due to the availability of free electrons for capture. Therefore, only deep levels located in the depleted region of the structure can contribute the DLOS spectra, to wit the AlGaN layer. To facilitate this study, AlGaN/GaN heterostructures were grown by plasma-assisted molecular beam epitaxy. Growth was initiated with a 45 nm AlN nucleation layer, followed by a region of GaN:C to achieve a semi-insulating buffer. Subsequently, 1 um of UID-GaN was deposited prior to the AlGaN cap growth. The AlGaN cap had 29.5% Al mole fraction with a thickness of 33 nm. Schottky diodes were processed in parallel with HFETs and served as on-wafer test devices. Electron traps at E_c–1.70, 2.23, 2.77 and 3.10 eV, a hole trap at E_v+3.36 eV and two bands of hole states were observed. Comparison of AlGaN/GaN DLOS spectra to that of bulk GaN:C demonstrate that these deep levels do not arise solely from the GaN:C layer and appear only in the presence of the AlGaN capping layer. In order to determine the trap density within the AlGaN layer, a lighted capacitance-voltage (C-V) technique was employed. Lighted C-V distinguishes between electron and hole traps, yielding collective lower bounds of 3.0×10^{11} and 4.5×10^{11} cm^{-2} for each, respectively. The lighted C-V method is similar to other frequency- or temperature-dependent C-V techniques, but here sub-bandgap illumination selectively probes electron or hole traps that are too deep to observe using traditional methods. Focus of the lighted C-V method is trained on the AlGaN layer by considering the bias region over which the 2DEG remains degenerate and thereby precludes trap emission at the heterointerface or GaN layer. The potential role of these traps in the origin of the 2DEG and AlGaN/GaN HFET device effects such as current slump and gate leakage will be considered.

2:10 PM

KK3, Anisotropic Strain in GaN Films Grown on *a*-Plane and *r*-Plane Sapphire: Effect on GaN Phonons: *V. Darakchieva*[1]; T. Paskova[2]; M. M. Schubert[3]; P. P. Paskov[1]; H. Arwin[1]; B. Monemar[1]; M. Heuken[4]; S. Figge[2]; D. Hommel[2]; B. A. Haskell[5]; P. T. Fini[5]; S. Nakamura[5]; [1]Linkoping University; [2]University of Bremen; [3]University of Nebraska; [4]Aixtron AG; [5]University of California, Santa Barbara

Recently the growth of III-nitrides on non-*c*-axis substrates has attracted considerable attention mostly because of the possibility to realize nonpolar heterostructures. Nonpolar nitrides offer a promising approach to overcome the deleterious effects that built-in electric fields along the *c*-direction have on radiative emission and wavelength. Non-polar orientations also enable polarized light emission from LEDs and higher p-type doping. Polar GaN on *a*-plane sapphire presents also technological interest because of the alignment of easy cleavage planes of the GaN and the sapphire substrate, preferable for laser cavity fabrication. In all instances of growth on non-*c*-axis substrates, the basal plane of the nitride film is expected to be anisotropically strained as a result of the different thermal expansion coefficients and lattice mismatches between film and substrate. The presence of anisotropic strain will affect all fundamental properties of the films, providing a possibility to study new effects and imposing some challenges on measurements and analyses. While the optical emission and structural properties of anisotropically strained GaN films have been widely studied, the reports on their vibrational properties are scarce. In this work we present a study of anisotropic strain and phonon modes of *c*-GaN films grown on *a*-sapphire, and *a*-GaN films grown on *r*-plane sapphire. High-resolution x-ray diffraction in symmetric, asymmetric and edge-symmetric geometries was used to determine the in-plane and out-of-plane strains in the films. The vibrational properties were studied by employing Raman scattering and generalized infrared spectroscopic ellipsometry at multiple angle of incidence and different sample geometries. We found that the strain in the growth plane of all films is compressive and the strain along the growth direction is tensile. As a result, the basal GaN plane of the *c*-oriented films is under anisotropic compression, while the nonpolar *a*-GaN films are compressed along [-1100] and extended along [11-20] directions. The estimated strain anisotropy varies in a complex manner with varying film thickness. The anisotropic distortion of the basal GaN plane was shown to lift-off the degeneracy of the phonons with E_1 symmetry. Consequently, both the E_1(TO) and E_1(LO) modes appear at different wavelengths for polarizations parallel to the GaN [-1100] and [11-20] directions, respectively. A similar splitting of the nonpolar E_2 phonon for incident polarizations parallel to the GaN [-1100] and [11-20] directions was also observed. A correlation between the different strain components and phonon frequencies allows us to determine the *c*-phonon deformation potential of GaN E_1(TO), E_1(LO) and E_2 modes for the first time. In addition, the *a*-plane GaN films allow an assessment of the A_1(TO) phonons by infrared spectroscopic ellipsometry. The *a* and *b* deformation potentials of the GaN A_1(TO) phonon were determined and discussed in the light of the existing difference between theoretical estimations and previous Raman results.

2:30 PM Student

KK4, Phase Separation and Defects in Quaternary $In_xAl_yGa_{1-X-Y}N$ Layers: *Fanyu Meng*[1]; Rao Manu[1]; Nathan Newman[1]; Subhash Mahajan[1]; [1]Department of Chemical and Materials Engineering and Center for Solid State Electronics Research, Arizona State University

We report on micro-structural analyses on phase separation and defects in quaternary $In_xAl_yGa_{1-x-y}N$ layers. The quaternary layers were grown on GaN epilayers which were nucleated and grown on sapphire by metalorganic chemical vapor deposition (MOCVD). Two non-lattice-matched layers, $In_{0.10}Al_{0.02}Ga_{0.88}N$ and $In_{0.05}Al_{0.06}Ga_{0.89}N$ were grown under 300 mBar and two lattice-matched layers, $In_{0.12}Al_{0.29}Ga_{0.59}N$ and $In_{0.06}Al_{0.18}Ga_{0.76}N$ were grown under 100 mBar. Phase separation and defects in these quaternary layers were investigated using transmission electron microscopy (TEM). Composition modulation wavelength is one important factor for studying on phase separation. Calculated modulation wavelength from sidebands in selected area diffraction patterns (SADP) is consistent with feature size in corresponding weak beam dark field (WBDF) images for every sample. The two non-lattice-matched layers have larger modulation wavelength than the two lattice-matched layers. Effects from driving force, growth pressure, and biaxial strain on phase separation were discussed. Phase separation is accelerated in quaternary layers by adding both In and Al into the growth. As practical band gap requirement restricts both In/Al incorporation, phase separation cannot be effectively suppressed by adjusting growth parameters. Compared with ternary III-nitride layers, adding one more alloying component means to add one more degree of randomness to the growth. Atomic ordering is then suppressed in the quaternary layers. Though atomic ordering isn't a dominant feature in the quaternary layers, it may occur locally in the random matrix. Dislocation density in quaternary layers depends closely on GaN buffer layer underneath, as most dislocations will thread into quaternary layers once they reach the quaternary/GaN interface. New dislocations can generate at GaN/quaternary interface as well, but such dislocations only contribute little to the total dislocation density especially when quaternary layers are close in lattice spacing with GaN epilayers. Behavior of dislocations including annihilation of nearby screw dislocations, and reactions between edge, screw and mixed

dislocations was revealed by WBDF analyses. Diffraction patterns from <11(-2)0> zone of the layers are featured with strong streaking along [0001] direction. Though <11(-2)0> and <10(-1)0> share one common [0001] direction, No streaking appears in diffraction patterns taken from <10(-1)0> zone. Using three g vectors, (0002), (11(-2)0) and (10(-1)0), WBDF analyses revealed that high density of planar defects parallel with basal planes are responsible for the streaking in the diffraction patterns. High resolution electron microscopy (HREM) images of these planar defects revealed them to be stacking faults bounded by Shockley partials.

2:50 PM

KK5, Consequences of Polarity and Related Defects on the Electrical Properties of GaN Grown by MOVPE: *Ramon Collazo*[1]; Aleks Aleksov[1]; Seiji Mita[1]; Raoul Schlesser[1]; Zlatko Sitar[1]; [1]North Carolina State University

Polar orientation in non-centrosymmetric III-nitride wurtzite semiconductors refers to the crystallographic orientation of the basal plane of the wurtzite lattice with respect to the substrate; the two polar structures are referred as the Ga-polar, and N-polar. Control of the polar orientation on a macroscopic and microscopic scale is desirable to understand and exploit the combined electrical properties of both types of polarity. We have demonstrated the growth of Ga- and N-polar thin films with the same growth rate on c-plane sapphire via MOVPE. It is based on specific surface treatments of the sapphire substrate before film deposition. N-polar films are consistently obtained after exposing a H_2-etched sapphire substrate to an ammonia atmosphere at temperatures above 900ºC. Ga-polar films are obtained either by preventing any exposure of the substrate to ammonia prior to deposition or by depositing the film on a properly annealed low temperature nucleation layer (either LT-AlN or LT-GaN) deposited on a previously ammonia annealed sapphire substrate. These conditions can be determined empirically by avoiding the occurrence of mixed-polar films, that is, films mainly single polar containing inversion domains. Inversion domains (IDs) are volumetric defects consisting of regions of opposite polar orientation than the surrounding matrix. As grown films mixed polarity are n-type, with varying carrier concentration and lower electron mobility than Ga-polar films. Ga-polar films are insulating (R_S > 20 MO/sq.) while N-polar films are n-type with carrier concentrations approaching $1x10^{19}$ cm^{-3} and electron mobility around 100 cm^2/Vs. Electron mobility around 300 cm^2/Vs can systematically be obtained with a carrier concentration of $2x10^{18}$ cm^{-3} for Si-doped Ga-polar films. In light of these characteristics, the proper nucleation layer anneal conditions are identified by obtaining the film with a dislocation density with the lowest possible twist component without introducing IDs (not crossing over into the mixed-polar process region) identified by a measurable n-type carrier concentration in the film. Two sources for the lowering of electron mobility within the mixed-polar film can be identified: an electronic potential barrier across the IDBs or an increase in the concentration of point defects within the ID. In order to identify any potential barrier across an IDB, lateral polarity junction (LPJ) devices with lithographically defined N-polar domains were grown within an n-type Ga-polar film. Results and description of the process to obtain these devices will be presented. In addition, Schottky diodes were prepared on pure Ga-polar films using Ni/Au as the Schottky contact. Rectification ratios over 7 orders of magnitude were systematically obtained for diodes prepared on this structure, which is several orders of magnitude better than results published to date.

3:10 PM Break

3:30 PM Student

KK6, Defect Reduction in GaN through Formation of 'Dislocation Clusters' at the Nanoheteroepitaxial Interface: *Mohammad Ferdous*[1]; Xinyu Sun[1]; Xin Wang[1]; Michael Fairchild[1]; Steve Hersee[1]; [1]University of New Mexico

Photoelectrochemical (PEC) etching and cross-sectional transmission electron microscopy (XTEM) were employed to measure defect density and investigate defect reduction mechanisms in n-type GaN grown by nanoheteroepitaxy (NHE) onto SiC. During PEC etching threading dislocations (TDs) are revealed as fine whiskers and the plan-view defect density can be conveniently calculated from the density of these whiskers. Defect density was examined at two etch depths, and for NHE GaN samples and planar GaN samples, grown side-by-side using metalorganic chemical vapor deposition (MOCVD). We determined that PEC etching can give reliable information on defect density and defect size and can be considered as a rapid and useful alternative to XTEM for some analyses. Defect reduction by mutual annihilation of dislocations with equal and opposite Burger's vectors was observed in the NHE samples. XTEM revealed that near the sample surface the TD areal density was 3×10^8 cm^{-2} for the NHE sample and 3×10^9 cm^{-2} for the planar GaN sample. PEC etching of both types of these samples revealed that the whisker diameter at this depth was in the range of 20 nm to 80 nm. The areal density of PEC etched whiskers agreed well with the XTEM analysis.Deeper into the epilayer, near the GaN/SiC interface region, XTEM analysis revealed that for the NHE samples defects were grouped into dense clusters, whereas in the planar samples the TDs remained randomly distributed. In the PEC etched NHE samples, the whisker diameter was approximately 200 nm to 500 in near the GaN/SiC interface. In the planar sample the whisker diameter remained in the typical value of 20 nm to 80 nm for all depths. The larger whisker features revealed by deeper PEC etching near the GaN/SiC interface therefore correspond to the dislocation clusters revealed by XTEM. Our NHE growth-mask aperture size was significantly higher, at 120 nm, than the target value of 40 nm for complete strain energy reduction in NHE theory. We conclude therefore that the 10× reduction of TD areal density in NHE samples results from the formation of the dense dislocation clusters. Specifically we propose that within these clusters there is a mutual annihilation of dislocations having equal and opposite Burger's vectors. Above this cluster typical only one TD propagates. With further reduction of the growth-mask aperture size a further reduction in dislocation density is anticipated for the NHE samples. Even for this modest (10×) reduction of defect density we observed significantly improved GaN properties in the NHE samples. The room-temperature, band-edge photoluminescence (PL) intensity was approximately 50× higher, and the electron mobility was 14× higher than for the planar GaN reference samples, indicating that at least part of the non-radiative recombination in GaN is associated with TDs.

3:50 PM Student

KK7, Influence of Arsenic Isovalent Co-Doping on the Electronic Properties of N-Type and P-Type GaN Grown by Metal-Organic Chemical Vapor Deposition: *David Gray*[1]; Michael Willemann[1]; Kai Zhang[1]; Ali Hajjiah[2]; Kevin Chern[2]; Alex Aning[1]; Louis J. Guido[3]; [1]Virginia Tech, Department of Materials Science and Engineering; [2]Virginia Tech, Department of Electrical and Computer Engineering; [3]Virginia Tech, Department of Materials Science and Engineering & Department of Electrical and Computer Engineering

Isovalent doping has been used for many years to improve the electronic, optical, and mechanical properties of compound semiconductors. This methodology may prove to be especially important for group III nitride alloys since they are defect semiconductors in the sense that concentrations of native point defects, residual chemical impurities, and threading dislocations often approach those of dopant atoms introduced intentionally during crystal growth. Such electrically active defects degrade both the majority and minority carrier properties of GaN. These issues have been addressed herein by the use of arsenic isovalent doping. Direct comparisons between n- and p-type MOCVD grown GaN samples with and without arsenic demonstrate that isovalent co-doping yields significant improvements in electronic properties. Electron transport in n-type GaN thin films is strongly influenced by a highly conductive interfacial layer, with sub-micron thickness, between the sapphire substrate and the overlying bulk layer. After correcting the measured Hall data for the contribution from this interfacial layer, the electron mobility at 300 K in our GaN:As samples approaches 1000 cm^2/Vsec with n = 10^{16} cm^{-3}. The Hall data also suggest that GaN:As exhibits a reduction in electrical compensation as compared to GaN:Si. Photoluminescence measurements at 300 K show a 10x increase in band-edge intensity for GaN:As compared with GaN:UID. In addition, the band-edge radiative efficiency is relatively independent of [As], while it decreases monotonically with [Si] after normalizing by the free electron density. The defect-mediated yellow-band (2.15 eV) and blue-band (2.8 eV) optical transitions increase with [Si]; however, co-doping with Si plus As causes a precipitous drop in intensity for these same transitions. The issue of doping efficacy in p-type GaN is considerably more complex. For GaN:Mg, the concentrations of O, H, and Mg increase monotonically with Cp_2Mg pressure, with [O] nearly 100x smaller and [H] about 5x smaller

than [Mg]. In contrast, the residual Si and C levels are independent of Cp_2Mg pressure and show no correlation with [Mg]. The most interesting trend that accompanies the addition of AsH_3 into the MOCVD ambient is a coupling between Mg concentration and As solubility. At the highest Mg doping level, the As content is 100x larger than that found in samples grown without Cp_2Mg at the same AsH_3 pressure. Recent theoretical work suggests that arsenic incorporates on gallium sites in p-type GaN forming double-donor antisite point defects, thereby making it difficult to synthesize well-conducting p-type material. Our experimental findings are not consistent with this prediction. Hall measurements on GaN:Mg+As yield hole mobility and concentration values at 300 K that are comparable to those reported in the literature for GaN:Mg.

4:10 PM
KK8, Strong Light-Matter Coupling a Room Temperature in GaN Microcavities: *Ian R. Sellers*[1]; Fabrice Semond[1]; Mathieu Leroux[1]; Jean Massies[1]; Pierre Disseix[2]; Joel Leymarie[2]; [1]Centre de Recherche sur l'Hétéro-Epitaxie et ses Applications; [2]LASMEA-Université Baisle Pascal

We present both experimental and theoretical results that demonstrate strong light-matter coupling in GaN microcavities at room-temperature. The microcavities consist of a GaN active region grown by molecular beam epitaxy on AlN/Al0.2Ga0.8N distributed Bragg reflectors (DBRs) of 7 and 12 periods respectively. The microcavity structures are completed with, in the simplest case, the deposition of a transparent aluminium mirror, and for improved finesse, with the deposition of SiN/SiO2 dielectric DBRs. The strong-coupling regime is observed with a Rabi-energy of ~50meV at room temperature. Furthermore, at low temperature, where the thermal broadening of excitons is negligible, we observe both the A and B-excitonic features of the GaN cavity and their respective anti-crossing with the photonic mode. Such results clearly indicate the high quality of our GaN material, and the large binding energy and oscillator strength of the excitons.

4:30 PM Student
KK9, Microstructural Investigation of AlN Re-Growth by MOCVD: *Xianglin Li*[1]; Ramon Collazo[1]; Rafael Dalmau[1]; Seiji Mita[1]; Zlatko Sitar[1]; [1]North Carolina State University

Metalorganic chemical vapor deposition (MOCVD) growth of homoepitaxial aluminum nitride (AlN) films was investigated. These films were grown in a vertical, cold-walled, RF-heated, low-pressure MOCVD reactor. Trimethylaluminum (TMA) and ammonia were used as the Al and N sources, respectively, and N_2 was used as the dilution and carrier gas. Substrate temperature was monitored by a single-color pyrometer; oscillations in the pyrometer signal, corresponding to interference oscillations from the growing film, were used to monitor the growth rate of the epilayers. In the first part of these experiments, 450 nm thick Al- and N-polar AlN epilayers were deposited on hydrogen-etched c-plane sapphire substrates at 1100°C. The V/III ratios for growth of Al- and N-polar layers were 400 and 1350, respectively, while the corresponding growth rates were ~1.3 and ~1.0 µm/hr. After growth, the AlN templates were removed from the reactor, exposed to air, and characterized by high-resolution x-ray diffraction (HRXRD). On- and off-axis rocking curves were used to assess the tilt and twist components of the grown films. The re-growth of AlN on the air-exposed nitride template surfaces of different polarities was subsequently studied. 450 nm thick AlN films were deposited under the same growth conditions as those for the original templates. Prior to deposition, the nitride surfaces were treated in situ to regenerate oxygen contaminated AlN surface. During deposition regular interference oscillations were observed in the pyrometer signal from the substrate. The resulting two-layer films were then characterized by HRXRD and transmission electron microscopy (TEM). On Al-polar AlN templates, HRXRD showed similar values for the on-axis rocking curve full-width at half maximum (FWHM) before and after re-growth and an improvement in the off-axis rocking curve FWHM after re-growth. On N-polar AlN templates, HRXRD showed improvements for both on-axis and off-axis rocking curves after re-growth. These results indicate that the surface treatment method employed provided surfaces suitable for homoepitaxial growth. Cross-sectional TEM characterization of the re-grown structures confirmed that there was no observable interface between the AlN template layers and the subsequently grown homoepitaxial layers. TEM also showed that the homoepitaxial AlN layers inherited the columnar structure of the AlN template layers. Microstructural characterization results of AlN epilayers and conclusions regarding the consequences for re-growth on air-exposed nitride surfaces will be presented. The role of surface preparation will also be discussed.

4:50 PM
KK10, Late News

Session LL: Compound Semiconductor Nanowires

Friday PM, June 30, 2006
Room: Conference Room 208
Location: Pennsylvania State University

Session Chair: Timothy D. Sands, Purdue University

1:30 PM
LL1, InAs Nanowire Transistors Using Solution-Grown Nanowires with Acceptor Doping: *Qingling Hang*[1]; David B. Janes[1]; Fudong Wang[2]; William Buhro[2]; [1]Purdue University; [2]Washington University in St. Louis

InAs is an excellent candidate semiconductor for high-speed circuits due to its narrow band gap (0.354 eV) and high electron mobility, which can reach 33000 cm^2/Vs in bulk material. It is also easy to form ohmic contacts with InAs due to Fermi-level pinning in the conduction band on its surface at least in the bulk form. Electrical devices based on InAs nanowires have been reported by several groups, however most of these studies concentrated on device behavior at low temperature with emphasis on single-electron transistors and supercurrent. The as-produced InAs nanowires from either chemical vapor deposition (CVD) or chemical beam epitaxy (CBE) technique present n-type conductivity. It has been observed that p-type InAs nanowires are difficult to form, possibly due to the Fermi-level pinning in the conduction band. The lack of p-type wires restricts the application of InAs nanowire devices. In this study, we have fabricated transistors using acceptor-doped InAs nanowires and studied their electrical performance. The nanowires, with nominal diameters of 20 nm, were formed using the solution-based "solution-liquid-solid" (SLS) synthesis method. This technique is superior to the above-mentioned techniques, CVD and CBE, not only from the point view of cost, but also in terms of the ease of adding dopants during nanowire growth. InAs nanowires with either Zn or Cd dopants were synthesized and used in the electrical studies. After purification, the nanowires were cast from solution on an oxidized Si wafer which had been prepatterned with contact fingers. Source and drain contacts were subsequently formed on individual InAs nanowires using electron-beam lithography. The 40-nm oxide on the heavily doped Si substrate acts as a back gate. The Cd-doped InAs nanowires exhibit ambipolar conduction properties under positive and negative biasing. The Zn-doped InAs nanowires exhibit n-channel conductivity, with on-off ratios of approximately 10^4 observed in devices with 3 micron channel lengths. The mobility extracted from the measured current-voltage characteristics for this device is around 450 cm^2/Vs. The observation of unipolar versus ambipolar conductivity in these devices, controlled by the doping species, indicates that it is possible to vary the position of the Fermi level in the InAs nanowires.

1:50 PM
LL2, Photocurrent Spectroscopy of Solution-Synthesized Nanowire-Based Photodetectors: *Huili (Grace) Xing*[1]; Xiangyang Li[2]; Amol K. Singh[1]; Debdeep Jena[1]; Masaru K. Kuno[1]; [1]University of Notre Dame; [2]Shanghai Institute of Technical Physics, Chinese Academy of Science

The primary growth technique for nanowires has been chemical vapor deposition (CVD)-based, such as the rather popular vapor-liquid-solid technique. Growth techniques utilizing solution-based synthesis, on the other hand, have a number of advantages over the CVD technique such as low cost, production scalability, ability to passivate the semiconductor surface chemically, and the ease of transfer to any substrate. One such synthetic method is the solution-liquid-solid (SLS) technique, which has been used by various groups to produce colloidal quantum dots or nanocrystals. Rudimentary photodetectors have been demonstrated using closed-packed "solids" of the

SLS-grown nanocrystals. Though photon absorption and electron-hole pair generation in nanocrystals is efficient, the extraction of carriers is difficult, involving hopping transport between the dots before being collected by the electrodes. In this work, we demonstrate photodetectors based on nanowire networks, or "quantum-wire solids". Nanowires allow band-transport along their axes, therefore potentially offering a drastic improvement over nanocrystals for the efficient collection of optically generated carriers. The quantum-wire solids are formed by drop-casting SLS grown CdSe nanowires in solution (about 20 nm in diameter and 1-5 microns long) on glass or SiO_2/Si substrates. The metal-semiconductor-metal photodetector devices are then fabricated using conventional optical lithography and metal deposition. The photodetectors are found to have very low dark currents (~ 10 nA at 5 V). Upon the illumination from room light, the resistance reduces by more than a factor of 10. The spectroscopic photoresponse of these photodetectors are measured using a xenon lamp coupled with a monochromator, and a lock-in amplifier in a photon energy range of 1.4 - 3.5 eV. We observe a sharp turn-on in the photocurrent, at 1.79 eV, near the absorption edge of the nanowires measured independently using an UV-Vis spectrophotometer. The photo responsivity (A/W) continues to increase with increasing photon energy and the second shoulder is clearly observed at 2.2 eV, the same second shoulder observed in the NW absorbance spectrum, which is ascribed to the discrete energy states rising from the strong quantum confinement in our thin NWs. The photo responsivity is estimated to be higher than 50 mA/W at a bias of 5 V at 550 nm (2.25 eV) illumination. With further increase in photon energy, the responsivity of the NW-based photodetectors shows a slow decrease, ~ 18% drop at 3.4 eV compared to that at 2.25 eV. This behavior is drastically different from a bulk semiconductor based photodetectors. To understand this behavior, the spectroscopic photoresponse under various illumination intensity, bias and time, are measured and will be presented. Since our NW-solid films are thin, ~ 100 nm, and they appear to be half transparent to bare eyes, we believe the observed photoresponsivity curve likely resembles the aborption coefficient of the NW-solids.

2:10 PM Student

LL3, Growth Mechanism and Optimization of InAs Nanowires Synthesized by OMVPE: *Shadi A. Dayeh*[1]; David Aplin[1]; Edward T. Yu[1]; Deli Wang[1]; Paul K. L. Yu[1]; [1]University of California, San Diego

Semiconductor nanowires have excited intense current research interest due to their potential applications in a wide range of electronic and photonic devices and systems. However, the detailed mechanisms of growth for many nanowire materials remain to be fully characterized and understood. We have studied the nucleation and growth, by organometallic vapor phase epitaxy (OMVPE), of InAs nanowires on both SiO_2 and InAs(111)B surfaces. Through systematic characterization of InAs nanowire morphology as a function of V/III precursor ratio, precursor flow rates, growth temperature, growth time, and the presence (or absence) and spatial arrangement of Au nanoparticles typically employed for nucleation of growth by the vapor-liquid-solid (VLS) mechanism, a number of significant insights into InAs nanowire growth by OMVPE have been developed. Specifically, we found that (1) Au nanoparticles enhance the pyrolysis of Arsine, (2) Au nanoparticles and In droplets both catalyze the growth of nanowires, (3) substrate plays an important role - Au nanoparticles initiate InAs islands and from each island multiple NWs can grow on SiO_2 surface but one per Au nanoparticle on InAs(111)B surface, (4) the nanowire growth is kinetically limited within the studied temperature range of 300-600°C, and the growth of uniform nanowires takes place at higher temperature on InAs(111)B than on SiO_2 substrate, (5) InAs nanowire growth occurs at temperatures regardless Au or Au-In nanoparticles being liquid or solid, which only stops possibly when temperatures reach the two dimensional growth (thin film deposition) region, (6) InAs nanowires decompose at elevated temperatures at which InAs thin film is normally stable. These findings are critical in the understanding of nanowire growth using OMVPE and more importantly provide guidance in design and growth of the functional nanostructures for nanoelectronics and optoelectronics. InAs nanowires grown using these approaches have been incorporated into a number of different electronic device structures; among the significant device results achieved has been the demonstration of field-effect electron mobilities as high as 6,600cm^2/V•s, the highest room-temperature mobility yet reported for any semiconductor nanowire structures.

2:30 PM

LL4, III-V Nanostructures Formed from GaP Nanowires on Si(111) Substrates: *Kouta Tateno*[1]; Hiroki Hibino[1]; Haruki Sanada[1]; Hideki Gotoh[1]; Hidetoshi Nakano[1]; [1]NTT Basic Research Laboratories

Integrating other semiconductors with silicon is promising for future optoelectronic integrated circuits. Nanowires grown by the vapor-liquid-solid method are considered to be proper structures for such integration. In this paper, we describe several nanostructures formed from GaP nanowires grown perpendicular to the Si(111) substrates. Nanowires self-arranged in lines formed from Au islands that were initially arranged at single-layer steps are also presented. These islands were spontaneously arranged under the optimum growth conditions like the temperature and the Au deposition rate. For GaP nanowires, the flow rate of PH_3, the group V source gas, is an important parameter for the wire's orientation. And the yield of the perpendicular wires and the shape of the wire critically depend on the growth temperature. Starting from the perpendicular GaP nanowires, we were able to grow InP wires and alternating GaP/InP wires.

2:50 PM

LL5, The Fabrication of Extreme Aspect Ratio Semiconductor and Metal Wires within Photonic Crystal Fibers: *Neil Baril*[1]; Don-Jin Won[1]; Thomas Scheidemantel[1]; Adrian Amezcua-Correa[2]; Chris E. Finlayson[2]; John Hayes[2]; Pier J.A. Sazio[2]; Venkatraman Gopalan[1]; John V. Badding[1]; [1]Pennsylvania State University; [2]University of Southampton

We have recently fabricated semiconducting micro- and nanowires with extreme aspect ratios in ordered arrays using microstructured optical fibers (MOF's), as templates. These systems contain the highest aspect ratio semiconducting micro- and nanowires yet produced by any method. The micro wires are over a meter in length, and the nanowires are centimeters long and ~100nm in diameter. We use versatile high-pressure CVD techniques to infiltrate the capillary holes in the MOF's with metal and semiconductor precursors. The process is capable of giving both radial and axial control over the deposition of the materials and it allows layer-by-layer deposition with control of the layer thickness. The possibilities for the fabrication of in-fiber devices are numerous. These structures combine the flexible light guiding capabilities of an optical fiber with the electronic and optical functionalities of semiconductors and have many potential applications for in-fiber sensing, light modulation, and light generation.

3:10 PM Break

3:30 PM

LL6, In Situ Electrical Annealing of Bio-Templated Nanowires: *Yan Gao*[1]; Gary Braun[1]; Chung-Yi Chiang[2]; Jing C. Zhou[3]; Norbert O. Reich[1]; Angela Belcher[2]; Bruce Dunn[3]; Evelyn Hu[1]; [1]University of California, Santa Barbara; [2]Massachusetts Institute of Technology; [3]University of California, Los Angeles

Electronic nanowires and interconnects comprise important building blocks for a nanoelectronic technology. Rapid, low-cost formation of wires of accurate dimensions and sufficient conductivity provides considerable challenges, as does the accurate placement of nanowires to nanoscale devices. As a type of 'bottom-up' technologies, biologically–templated nanowires may offer significant advantages in this regard; the regularity and size scale of bio-templates can provide control over the final nanowire dimensions and properties. We have explored the electrical measurement of different bio-templated nanowires:M13 coliphage-templated, Microtubule-templated, and DNA-templated wires. These bio-templated metal (Au, Ag and Ni) nanowires have dimensions from 20-150nm in diameter and range from 1 micron to several microns in length. Both linear and nonlinear electrical conduction were often observed in these bio-templated nanowires. The nonlinear electrical behavior may reflect the granularity of the synthesis process, correlated with gaps between metal particles along the wire. Post-synthesis annealing processes may improve the conduction of these wires, but annealing techniques must be developed that do not destroy these fragile nanowires. We have undertaken in-situ electrical annealing studies of bio-templated Au nanowires with small voltage increments and long integration times. After electrical annealing, we achieved steady-state, reproducible, improved electrical behavior of the measured nanowires. No structural changes in the wires could be observed under inspection by scanning electron microscopy and atomic force microscopy. Increase of the ambient

temperature from 100K to 300K results in an increase in some nanowire resistance. Resistance ranges from 580 Ohm to 710Ohm from 100K to 300K, which are reasonable values for the geometry of the measured wires. The repeatability of electrical measurements allows to further explore the precise mechanism of conductance in these wires, and to link the wire structure to the electrical performance.

3:50 PM Student

LL7, Contacts to Gold Nanowires in Porous Anodic Alumina Templates: *Kalapi Biswas*[1]; Yexian Qin[1]; Manuel Da'Silva[1]; Ron Reifenberger[1]; Timothy D. Sands[1]; [1]Purdue University

Nanowire array composites fabricated by electrodeposition of metal or semiconductor nanowires into porous anodic alumina (PAA) templates have potential applications in nanomagnetics, nanophotonics, thermoelectric cooling devices, interconnects for electronics, and integrated sensor arrays.. The PAA template provides structural support, feature-size definition and thermal and electrical isolation. To realize the device potential of these PAA-templated nanowire composites, it is necessary to develop contact schemes and contact resistance measurement techniques - both for arrays and for individual nanowires - that will enable the design and fabrication of integrated systems that join nanoscale functional elements with microscale contacts and interconnects. In this work using Au nanowires in PAA templates as a model system, two prototype contact schemes have been developed and explored. The first scheme, with the contact plane perpendicular to the nanowire axis, is suitable for applications in energy conversion devices that employ nanowire arrays as nanocomposite materials. The second scheme uses contacts to sectioned arrays with the contact plane parallel to the wire axis, a configuration that is amenable to the fabrication of thermally and electrically addressable sensor arrays. In both cases, microscale contact resistance may be compared with measurements of individual nanowires using conductive-tip atomic force microscopy (AFM). In the present work, the perpendicular contact process has been demonstrated with gold nanowires of diameter 50 nm that were synthesized in PAA templates by electrodeposition from a Pt back electrode. Planarization of the alumina template was achieved by mechanical polishing of the arrayed composite structure. After planarization, a uniform length of the nanowire array was exposed by selective etching of the template. The exposed nanowire tips facilitate the formation of low-resistance ohmic contacts. The structural, topographical and electrical characteristics of the exposed tip nanowire array have been studied using field-emission scanning electron microscopy (FESEM) and AFM. An electrical contact between the conducting AFM probe and the Au nanowire in the composite structure was established. The resulting I-V data showed a linear behavior with a conductance of 800±30μS. The conductance through an individual nanowire corresponded to a conductivity of 6.03±0.25 x10^6S/m, approximately an order of magnitude lower than the conductivity of bulk gold. The extension of these results to microscale contacts and to the parallel contact configuration will be discussed.

4:10 PM

LL8, Three-Dimensional Nanoscale Composition Mapping of Semiconductor Nanowires: *Lincoln J. Lauhon*[1]; Daniel E. Perea[1]; Steven J. May[1]; Jessica L. Lensch[1]; Jonathan E. Allen[1]; Bruce W. Wessels[1]; David N. Seidman[1]; [1]Northwestern University

We describe the use of local-electrode atom probe (LEAP) microscopy and pulsed-laser enhanced LEAP to map the composition individual semiconductor nanowires in three dimensions with single-atom sensitivity and sub-nanometer resolution (Perea et al, Nano Letters 6, 181 (2006)). This result is the first chemical mapping of a single semiconductor nanowire. Arrays of epitaxial InAs nanowires were grown by chemical vapor deposition on GaAs substrates patterned with gold catalyst disks. Nanowires with diameters of 10-30 nm were analyzed over lengths of hundreds of nanometers. Three-dimensional reconstructions of the atoms in the nanowire showed hexagonal faceting, indicating that the LEAP analysis accurately reproduces the cross-section and shape of the nanowires. The Au catalyst particle sitting atop a nanowire was also analyzed; tomographic slices across the nanowire diameter, when displayed in 0.5 nm increments along the growth axis, revealed an extremely abrupt catalyst-nanowire interface that is also very flat. Au atoms from the catalyst were detected within some but not all of the nanowires analyzed. Variations in Au distribution at the end of a given nanowire are attributed to changes in conditions at the end of growth. Surprisingly, oxygen and carbon were not seen in the mass spectra, which may indicate a low evaporation threshold. Preliminary measurements using a pulsed laser to induce single ion evaporation indicate that pulsed-laser LEAP microscopy is superior to the voltage-pulsed mode of operation for the analysis of brittle and non-metallic materials. Specifically, the frequency of fracture is reduced, the mass resolution is increased, and unidentified peaks in the charge-to-mass ratio spectrum are eliminated. From the pulsed laser measurements, we establish upper bounds on the amount of Au in the InAs nanowires. Recent measurements that directly compare the composition of silicon nanowires with their corresponding electrical properties will also be discussed.

4:30 PM Student

LL9, Photoluminescent Properties of ZnO/$Mg_{0.2}Zn_{0.8}O$ Coaxial Nanorod Quantum Structures: *Jinkyoung Yoo*[1]; Gyu-Chul Yi[1]; Bonghwan Chon[1]; Taiha Joo[1]; Takahashi Yatsui[2]; Motoichi Ohtsu[3]; [1]POSTECH; [2]Japan Science and Technology Agency; [3]University of Tokyo

Composition-modulated nanowire/nanorod heterostructures have great potential as building blocks for the fabrication of quantum and photonic devices. Coaxial nanorod heterostructures in which composition is modulated along their radial direction are expected to suppress surface states, hence enhancing radiative quantum efficiency and reducing thermal quenching of light emission intensity. Nevertheless, physical properties of coaxial nanowire/nanorod heterostructures have rarely been reported. Recently we developed an accurate layer thickness control method in the multishell nanowire/nanorod heterostructures, which enables us to fabricate coaxial nanorod quantum structures. Meanwhile, ZnO/$Mg_xZn_{1-x}O$ heterostructures have been considered as a promising system for photonic device applications due to a large exciton binding energy and a negligible lattice mismatch. To realize novel and functional photonic devices based on ZnO/$Mg_xZn_{1-x}O$ multishell nanorod heterostructures, an extensive understanding of the radiative recombination mechanism is required. Photoluminescence (PL) spectroscopy is a powerful and nondestructive technique for the optical characterization of semiconductor nanomaterials. Here we present on far-field and near-field PL, and time-integrated and time-resolved PL spectra of the coaxial nanorod quantum structures. ZnO/ZnO/$Mg_{0.2}Zn_{0.8}O$/ZnO/ZnO/$Mg_{0.2}Zn_{0.8}O$ multishell nanorod heterostructures were fabricated on c-sapphire and Si (100) substrates using catalyst-free metal-organic vapor phase epitaxy (MOVPE). Diethylzinc, bis-cyclopentadienyl magnesium, and oxygen were used as reactants. Catalyst-free MOVPE method enables us to control each layer thickness very precisely. ZnO/ZnO/$Mg_{0.2}Zn_{0.8}O$ multishell nanorod heterostructures were characterized by scanning electron microscopy, far-field PL, near-field PL, and time-resolved PL. Through a series of the characterizations we confirmed that composition of ZnO/ZnO/$Mg_{0.2}Zn_{0.8}O$ nanorod heterostructures were modulated along the radial direction without compositional intermixing. Far-field PL spectra of ZnO/ZnO/$Mg_{0.2}Zn_{0.8}O$ multishell nanorod heterostructures exhibited systematic blue-shift of PL emission peak as ZnO shell layer thickness decrease due to the quantum confinement effect. Near-field PL and time-resolved PL spectra of ZnO/ZnO/$Mg_{0.2}Zn_{0.8}O$ multishell nanorod heterostructures were also invesitgated.

4:50 PM Student

LL10, Transport Properties of Solution Grown Thin Film Nanowire Solids: *Amol K. Singh*[1]; Xiangyan Li[2]; Vladimir Protasenko[1]; Masaru Ken Kuno[1]; Huili (Grace) Xing[1]; Debdeep Jena[1]; [1]University of Notre Dame; [2]Shanghai Institute of Technical Physics

Nanostructured materials such as nanocrystals, nanotubes and nanowires offer the advantage of bottom up approach of making electronic and photonic devices. The use of quantum dot solids have been demonstrated in devices such as field effect transistors (FETs), photodetectors and solar cells. The performance of such devices is marred by their limited conductivity when assembled on substrates owing to hopping transport. This problem could be over come by use of assemblies of nanowires. Therefore we have investigated the transport properties of CdSe nanowires. These nanowires were grown by solution based synthesis called solution liquid solid (SLS) technique. Their diameters were about 20 nm and lengths were in 1-2 μm range. The nanowires grown by SLS technique have advantages of low cost and scalable production and an ability to passivate the surface in solution.

The thin film of CdSe nanowires were deposited on glass substrates from their colloidal suspension. These nanowires form a dense connected network which enables band transport through a major part of the solid. Metallic contacts were defined by a regular lithographic lift off technique. The current - voltage measurements under optical illumination show an increase in photoconductivity. The current under illumination was nearly 2 orders of magnitude higher than that in dark. The dark current ranged from a few nA to hundreds of nA for device lengths (separation between contacts) varying from 35 μm to 8 μm at 20 volt bias. Similarly the current under illumination ranged from hundreds of nA to 2 μA. The strong room temperature photo response of CdSe nanowires opens up avenues for their potential application in low cost photodetectors on flexible substrates. Temperature dependent current - voltage measurements were carried out from -50°C to 200°C. The competition between optical and thermal generation of charge carriers in CdSe nanowires was observed in this study. A crossover temperature exists close to 150°C above which thermally generated carriers exceed those that are optically generated. In the stress tests the dark current increased from 10 pA to 0.85 nA in 2 hours at 10 volt bias. The cause of this effect has not been resolved so far. With temperature dependent conductivity measurements we were able to estimate the band gap of the nanowire thin-film solids. A value of 2.51 eV was extracted for bandgap from low electric field, temperature dependent conductivity. This value is not in close proximity with optical band gap of 1.79 eV for these nanowires obtained from photocurrent spectroscopy but it compare favorably.

Session MM: Chemical and Biological Sensors II

Friday PM — Room: Conference Room 207
June 30, 2006 — Location: Pennsylvania State University

Session Chairs: Debdeep Jena, University of Notre Dame; Alec Talin, Sandia National Laboratories

1:30 PM

MM1, Modification of Nanoparticle-Organic Composite Electronic Materials for Improved Chemical Sensors: *Stephen W. Howell*[1]; Shawn Dirk[1]; David Wheeler[1]; Robert J. Simonson[1]; [1]Sandia National Laboratories

Molecular electronic-based chemical vapor sensors were assembled using noble metal nanoparticles and short conjugated phenylene ethynylene (PE) based molecules. Sacrificial capping ligands on the nanoparticles were replaced by tighter binding PE ligands. The films were assembled between pairs of electrodes by iteratively exposing the substrates to solutions of the nanoparticles and PE cross-linking bridging ligands. Some of the conjugated bridging molecules contained an electron deficient phenol to provide a simple platform for developing sensor applications. The phenol is calculated to have a significant change in its HOMO/LUMO gap in the presence of specific analytes. Judicious combination of nanoparticle size and ligand structure provides a film in which the organic bridging ligands dramatically affect film conductance. Specifically, π-conjugated ligands lower resistance more in films with smaller particles. Thus the sensing mechanism of these films is not based on the typical swelling mechanism but rather on the modulation of the molecular electronic structure of the conducting PE bridging ligands. For this work, interdigitated gold electrodes built on quartz substrates were utilized. A novel robotic sample preparation was employed to build nanoparticle films of different thickness on prepared electrodes. By preparing the nanoparticle films using a robot, many problems with irregularities of the deposited films were eliminated. This sample preparation system was designed with the capability to measure the resistivity of the nanoparticle films after assembly of each layer. Using such a sample preparation system is vital for developing mass-produced sensors from nanoparticle films. Initial worked focused on detecting changes in the conductance of nanoparticle films, crossed linked with PE molecules, during liquid phase exposure. A reversible change in nanoparticle film resistance was observed when exposed first to acid solution and then base solution. However, a shift in film conductance was not observed for nanoparticle control films crossed linked with octanedithiol (ODT). Extending on the liquid phase experiments, nanoparticle films cross-linked with PE and ODT were exposed simultaneously to ~ 10 ppm of DMMP (an organophosphate) vapor preconcentrated from a specialized vapor system. Our initial results show that PE linked films had a response that was several orders of magnitude larger than for films cross-linked with ODT. We believe that these results verify a molecular electronic detection mechanism and not a swelling response. This new mechanism enables selectivity for nanoparticle detection which greatly increases the scope of organic/nanoparticle films for sensor applications. Sandia is a multiprogram laboratory operated by Sandia Corporation, a Lockheed Martin Company, for the United States Department of Energy under contract DE-AC04-94AL85000.

1:50 PM

MM2, Conductance Sensor Based on Polyion Stabilized and Thiol Functionalized Double Stranded DNA Molecules: *Ajit K. Mahapatro*[1]; Kyung J. Jeong[1]; Sugata Bhattacharya[1]; Gil U. Lee[1]; David B. Janes[1]; [1]Purdue University

Sensors based on bio-functionalized systems as the active element are of great interest to basic science and technology. The ability to synthesize deoxyribonucleic acid (DNA) with sequences of choice, the unique binding properties of the purine-pyrimidine base pairs in a Watson-Crick double helix, and the capability for well ordered self assembly, make DNA a well-suited molecule for potential application in nanotechnology and bio-sensor applications. A possible readout approach involves measurement of the electrical conductivity of DNA strands bridging two narrowly spaced metallic contacts. For DNA sensors, a direct electrical readout of DNA selective binding events would enable integration of sensor elements with readout circuits. In this work, short double stranded (ds)-DNA molecules (15base pairs, ~5nm) with thiol functionalized end groups at their 3' ends, are probed by assembling them between pairs of gold electrodes in molecular scale gaps formed using a room-temperature electromigration-induced break junction technique. Electrical transport measurements are performed at ambient. In order to counterbalance the charge on the DNA strands, and therefore to allow relatively high density of DNA on the surface, the ds-DNA strands are locked with spermidine molecules. A series of fully-complementary ds-DNA sequences, in which the center sequence of 5 base pairs is changed from all-GC to all-AT pairs in steps, was studied. The all-GC strands show relatively high conductivity (~1nS at 1V). As the center sequence is varied, the conductivity is observed to decrease exponentially with the number of AT pairs. This observation is consistent with tunneling conduction due to a barrier at the AT sites. For a specific sequence, a higher conductivity was observed for the junctions in which a high salt (NaCl) concentration was present in the standard phosphate buffer solution during DNA immobilization, and is attributed to a larger number of DNA-molecules immobilized between the electrodes. This technique for measuring the single molecule conductivity in air provides an estimate of the conductivity per molecule of ds-DNAs, which provides useful insights for future electrical-based biosensors utilizing DNA interactions.

2:10 PM Student

MM3, AFM Study of Current Transport through Porphyrin Based Molecules: *Raghu Ramachandran*[1]; Kim Lewis[1]; Sathish Thiruvengadam[1]; Roy Siow[1]; Theda Daniels-Race[1]; [1]Louisiana State University

Porphyrins have recently generated great interest as a potential "electronic material" for use in functions such as sensing (i.e.-carbon monoxide), biomolecular and medical physics applications (i.e. antiviral agents) and for computer memory capability. Fundamental to the latter of these three and to the realization of molecular based electronic devices is the phenomenon of self-assembly. Transport through these molecular self assembled monolayers has been investigated by various methods. Of these only Atomic Force Microscopy has the capability to image the area of interest and then make contact to the desired molecules. AFMs are used extensively in the study and manipulation of matter at the nanoscale. In this project, the monomeric porphyrin molecule is the "matter" of interest as a potential high density and energy efficient unit. To study transport properties of molecules, a small current is passed through a conductive AFM tip into one or a small number of molecules that constitute the self assembled monolayer (SAM). This configuration, placed atop a suitable conductive substrate, reveals the charge storage and transport properties of the hybrid structure. Due to the statistical

nature of the measurements, an additional method by which to compare results of transport through the same molecule would be valuable. For this purpose we will construct two terminal tunneling electrodes fabricated by AFM lithography. Porphyrin molecules can then be immobilized between the two electrodes. AFM can be used to fabricate these electrodes by depositing 20-30nm thick tunnel junctions on an insulating substrate. These tunneling junctions can be modulated by electrodeposition. A comparison of through bond tunneling conduction mechanisms by the above two methods will be used to verify results and modeled using appropriate transmission theory. Current-Voltage curves that exhibit through bond tunneling have been observed for alkanethiol and are expected for porphyrin molecules. In addition current voltage curves would be scrutinized for switching and rectifying behavior of these molecules.

2:30 PM Student
MM4, Surface Plasmon Resonance: Sensing Chips and Applications: *Kyle Foley*[1]; Erica Forzani[1]; Nguyen H. Ly[1]; Paul Westerhoff[1]; Nongjian Tao[1]; [1]Arizona State University

Surface plasmon resonance (SPR) applications include metal-film characterization, protein discovery, food safety, medical diagnostics, and environmental analysis. Biological applications, including DNA, RNA, and antibody-antigen molecules, continue to grow in importance and focus in current SPR investigations. Our SPR device consists of a light source, collimating optics, an equilateral prism, a sensor chip, imaging optics, and a CCD camera. The sensor chip fabrication is important in creating arrays to parallelize detection to increase testing throughput. Arrays of gold sensing elements are defined on a glass substrate and modified for the detection of desired analytes, such as arsenic. An example use for the chips is a sensor for arsenic (As) detection in groundwater. The arsenic sensor allows us to discriminate between samples with and without As levels permitted by EPA (10 ppb in 2006, according to new regulations) and it is potentially useful for As level screening in groundwater. The sensor instrumentation is much simpler than the one for conventional spectroscopic and spectrometric techniques employed in As detection.

2:50 PM
MM5, Late News

3:10 PM Break

3:30 PM Student
MM6, The Functionalization of GaN and AlGaN Surfaces with Hemin for Nitric Oxide Detection: *Michael A. Garcia*[1]; Scott D. Wolter[1]; James B. Sund[1]; Tong-Ho Kim[1]; Joseph Bonaventura[1]; April S. Brown[1]; [1]Duke University

Because of its importance in biological, environmental, and defense applications, it is desirable to selectively and sensitively detect Nitric Oxide (NO) with a device that will monitor its concentration continuously.[1] One method of accomplishing this detection, pioneered by Wu and Cahen, *et. al.* with a GaAs-based sensor,[2] is to functionalize the surface of a semiconductor with a porphyrin group. Many porphyrin groups, such as hemin, react much stronger to NO than other gases such as O_2 and CO.[3] Additionally the sensitivity of the device can be enhanced by using GaN-based HFET structures, which are highly sensitive to surface charge states because of their two-dimensional electron gas (2DEG).[4] Another advantage of using a GaN-based HFET instead of a GaAs-based device is the elimination of the possibility of harmful arsenic diffusion into biological or environmental systems. Therefore with calibration and in concert with other gas sensors, a reliable NO sensor could be fabricated with a porphyrin as the functional group and a GaN-based HFET as the semiconductor material. Following similar procedures as Wu and Cahen (since the GaN surface has the same dominant native oxide, Ga_2O_3, as GaAs), XPS and FTIR analysis indicate that we have successfully functionalized GaN templates and an AlGaN HFET with several different porphyrin groups. One notable feature of the C 1s core level XPS scan is a peak at ~284eV observed for the functionalization chemistries, which is attributed to C=N bonding within the porphyrin molecule.[5] Furthermore before attempting the lengthy and costly process of microfabrication of sensor devices onto the GaN HFET, we devised a novel approach for obtaining electrical data for NO gas detection using the established van der Pauw (VDP) method for characterizing sheet resistivity.[6] Our results from this VDP experiment show that the functionalized GaN HFET samples have significant changes in sheet resistivity due to increased concentrations of NO in the controlled gaseous environment. This method seems promising for providing an initial proof of concept for NO sensors on a GaN platform. [1]E. Culotta and D. E. Koshland, Science 258, 1862 (1992). [2]D. G. Wu, D. Cahen, P. Graf, R. Naaman, A. Nitzan, and D. Shvarts, Chem. Eur. J. 7, 1743 (2001). [3]C. Rovira, K. Kunc, J. Hutter, P. Ballone, and M. Parrinello, J. Phys. Chem. A 101, 8914 (1997). [4]J. P. Ibbetson, P. T. Fini, K. D. Ness, S. P. DenBaars, J. S. Speck, and U. K. Mishra, Appl. Phys. Lett. 77, 250 (2000). [5]D. H. Karweik and N. Winograd, Inorg. Chem. 15, 2336 (1976). [6]L. J. v. d. Pauw, Philips Res. Repts. 13, 1-9 (1958).

3:50 PM
MM7, BioFETs Based on GaN/AlGaN Devices: *Kendra McCoy*[1]; Stephen J. Pearton[2]; Lloyd Whitman[1]; [1]Naval Research Laboratory; [2]University of Florida

BioFETs, Biologically modified field effect transistors (BioFETs) have the potential to directly detect biochemical interactions in aqueous solutions for a wide variety of sensing applications. In order for these devices to be useful, they must satisfy three major criteria. BioFETs must be stable in aqueous solutions across a range of pH and salt concentrations; the surfaces of these devices must be sensitive to biochemical interactions; and the devices must be able to probe specific biochemical interactions. BioFETs that we are developing and testing based on AlGaN/GaN quantum well devices can potentially satisfy all of these requirements. These charge-sensitive devices are being functionalized with receptors to stochastically sense the binding of target molecules in aqueous samples. The sensing is based on device geometries whereby the stochastic binding of individual molecules above a device will cause a detectable, transient change in conductance. It has already been demonstrated that these AlGaN/GaN quantum well devices can sense small changes in pH of electrolytic solutions. We have developed a robust method of functionalizing these devices with avidin, enabling direct immobilization of biotinylated antibody and DNA affinity probes. We will describe our characterization of these functional surfaces, and report how specific biomolecular recognition affects device capacitance and conductance. Our progress in both quantifying the number of probes added to the surface via these reactions as well as determining the ultimate sensitivity of this system will be reported.

4:10 PM
MM8, Sensing Characteristics and Mechanism of Liquid-Phase and Gas-Phase Sensors Using AlGaN/GaN Heterostructure: Takuya Kokawa[1]; Kazuo Matsuo[1]; Takeshi Kimura[1]; *Hideki Hasegawa*[1]; Tamotsu Hashizume[1]; [1]Hokkaido University

The AlGaN/GaN heterostructure is an attractive material for chemical and bio-chemical sensors because of its superb chemical stability, environment-friendly nature, feasibility of co-integration with AlGaN/GaN high electron mobility transistors (HEMTs) for sensor network applications and capability of high-temperature operation. In this paper, we investigate basic liquid-phase and gas-phase sensing characteristics of the AlGaN/GaN surface of the standard MOVPE-grown Al0.25Ga0.75N/GaN heterostructure wafer. The surface was subjected to our novel surface control process for oxygen gettering.[1] Liquid-phase sensing capability was investigated by using an open gate AlGaN/GaN HEMT structure where the AlGaN surfaceis exposed to liquid through an open window and serves as the gate. For gas-sensing experiments, hydrogen sensing characteristics were investigated by using a Pd/AlGaN/GaN Schottky diode structure. In deionized water, the open-gate HEMT device clearly showed current saturation and pinch-off behavior with respect to the saturated calomel (SCE) reference electrode. I-V characteristics were very similar to those of the standard Schottky-gate HEMT, although the gate leakage current was very much reduced in liquid. The experimental I-V curves were reproduced very well by calculation based on the gradual-channel approximation together with a field-dependent mobility, indicating excellent gate control through electrolyte/AlGaN interface. The surface potential of the device showed a good linear response vs. the pH value of the liquid with a sensitivity of 57.5mV/pH. This is close to the theoretical value of 58.9 mV/pH of the Nernstian response. Additionally, the device showed systematic threshold voltage shifts on immersion into organic polar liquids such as acetone, methanol and ethanol, with reference to the deionized water

case, indicating presence of dipole shifts. Hydrogen sensing characteristics of Pd/AlGaN/GaN Schottky diodes were investigated in vacuum. By applying the surface control process,[1] the reverse leakage currents were very much reduced and an unprecedented high H2 sensitivity was achieved where 1 Torr hydrogen caused five orders of magnitude increase of the reverse current. The Schottky C-V characteristics showed parallel shifts up to as large as 1,200 mV on H2 exposure. Transient waveforms were almost exponential for the logarithm of current, and response speed increased with increase of H2 pressure and temperature. By a detailed analysis, the sensing mechanism of the liquid- and gas- sensors was explained in terms of interface dipole formation which modifies the surface barrier height (SBH) determined by the Fermi level pinning at the charge neutrality level (Ec – 1.5 eV for AlGaN used). Apparent discrepancy between current increase and large C-V shift in hydrogen sensors is due to the fact that the current transport is not by thermionic emission, but by thermionic field emission which is much less sensitive to SBH change. [1]J. Kotani, S. Kasai, H. Hasegawa, T. Hashizume: e-Journal of Surf. Sci. & Nanotechnol., 3(2005) 433.

4:30 PM Student

MM9, Scalable Dope-Coded Biosensing Particles for Protein Detection: *Nguyen H. Ly*[1]; Nongjian Tao[1]; [1]Arizona State University

We present dope-coded biosensing particles for scalable high throughput protein detection applications. The biosensing particles (8μm in diameter and 280nm thick) are composed of biosensing/semiconducting/magnetic/adhesive layers and coded via patterned boron doping. Doping alters the local physical and electrical properties of the particles such that it supports various decoding tools, permits scalability of bit widths down to tens of nanometers, generates a large number of codes, and retains uniform particle size and shape independent of particle code for consistent protein analysis. The magnetic layer eliminates use of burdensome filters for particle extraction. Following suspension phase protein binding, the dope-coded biosensing particles are extracted with an external magnet and analyzed with an atomic force microscope (AFM). In this way, dope-coded biosensing particles undergo efficient solution phase protein capture, but are quickly recollected as a densely packed random array so that simultaneous particle decoding and protein detection may occur.

4:50 PM

MM10, Electric Field Dependence of Photoluminescence of Silica Coated CdSe/CdS Quantum Dots: *Yang Xu*[1]; Kathleen Meehan[1]; [1]Virginia Polytechnic Institute and State University

The size-tailored optical properties of semiconductor quantum dots (QDs) have drawn a great deal of attention as a reporter in biological sensing. One potential application, intracellular monitoring of biochemical changes, poses significant challenges, but will provide a wealth of data on cell function.[1] Photoluminescence quenching of functionalized QDs upon binding events[2-4] have demonstrated that the intensity of the optical emission from a functionalized QDs can be correlated to the concentration the target biochemical. Thus, it is conceivable that the concentration of specific biochemicals can be measured real-time in-vivo using functionalized quantum dots in the near future, which will enable quantification of cell response to biochemical stimuli.[5] To achieve this goal, we must understand the effect of the binding events on the photoluminescence (PL) intensity and peak wavelength. We report on preliminary results from experiments designed to shed light on the mechanisms that cause the observed changes in photoluminescence (PL) signal between the bound and unbound functionalized QDs. Colloidal CdSe/CdS core/shell QDs were first synthesized in an aqueous solution where gelatin is used as an inhibitor. The CdSe core was formed during a metathesis reaction using CdCl2 and NaSeSO3 for the source of Cd and Se, respectively. A thin CdS shell was grown on the 2nm CdSe cores by bubbling H2S into solution containing the CdSe nanoparticles and excess Cd ions. Mercaptopropyl trimethoxysilane and sodium silicate were added to the solution to form the silica coating, used to prevent photochemical degradation of the nanoparticles with an accompanying heavy metal contamination of the biological media.[6] The CdSe/CdS QDs were characterized by UV-Vis absorption and photoluminescence spectroscopy. The electrical field-dependence of the PL spectra from the silica-coated CdSe/CdS quantum dots, collected on thin films of quantum dots under an adjustable static electric field of up to 400kV/cm, was studied. Slightly enhanced photoluminescence was observed with a visible blue-shift of the PL peak with the applied electric field. A maximum energy shift of 4.50 meV was obtained at 400kV/cm. The field induced energy level shift was well fitted by a quadratic dependence on the external electric field and is attributed to the quantum confined Stark effect. Due to the complexity of the quantum dots system under investigation, a simplified calculation based upon the perturbation theory was performed to analyze the experimental results. [1]H.J. Tanke et al., Curr. Opin. Biotechnol. 16, 1 (2005). [2]C.I. Lin et al., Biosens. Bioelectron. 20, 127 (2004). [3]J.H. Kim et al., Sens. Actuat. B 102,315 (2004). [4]W.J. Jin et al., Anal. Chiminca Acta 522, 1 (2004). [5]X. Gao et al., Curr. Opin. Biotechnol. 16, 1 (2005). [6]X. Zhou et al., Appl. Surf. Sci. 242, 281 (2005).

D

E

F

G

H

I

J

K

L

M

N

O

P

T

U

V

W

X

Y

Z

Conference Room Layout

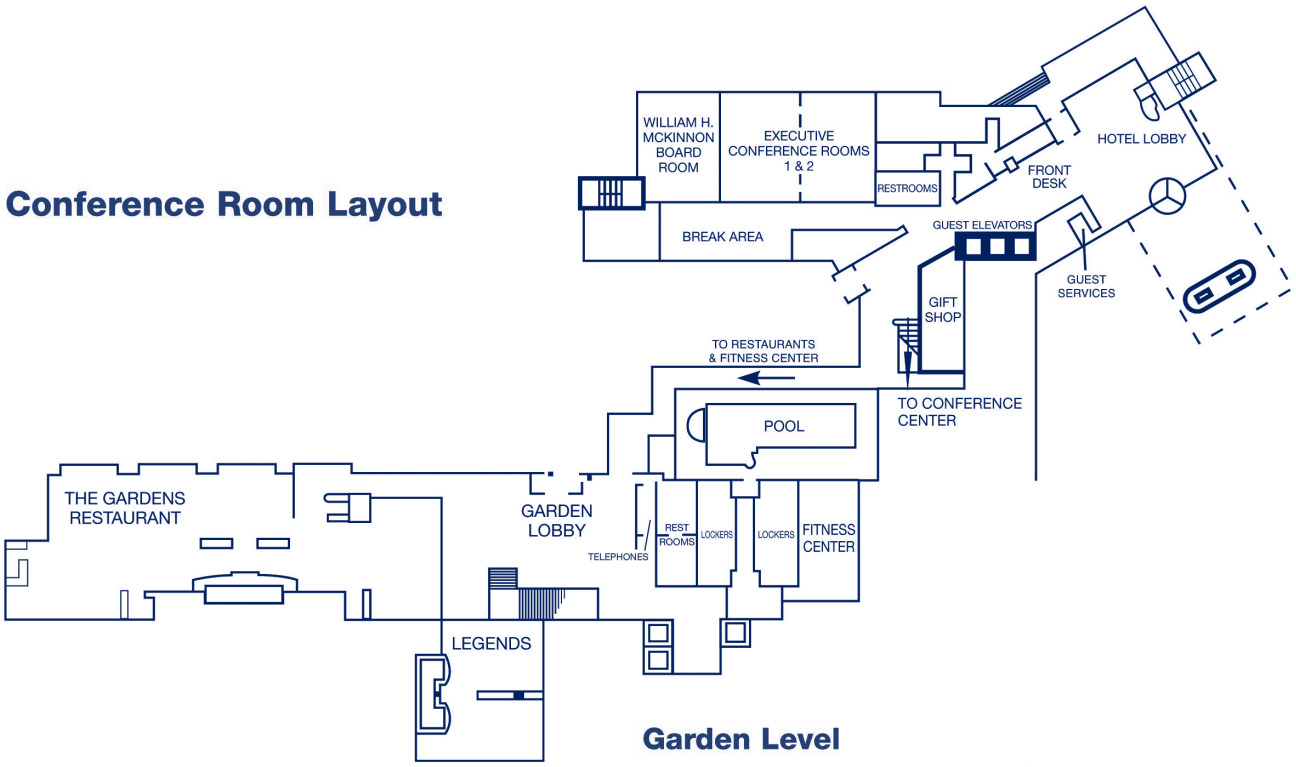

Garden Level

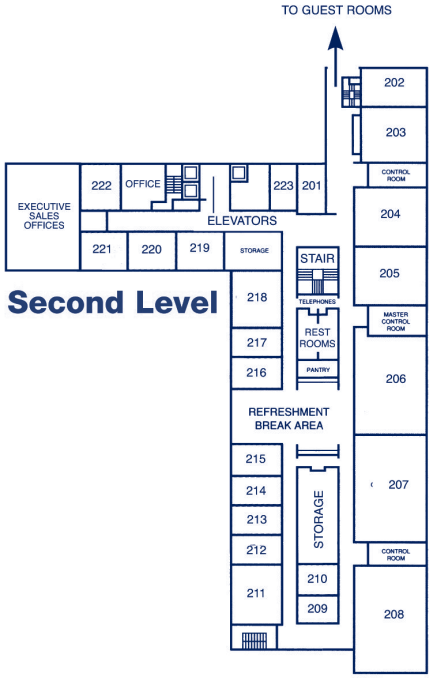

Second Level

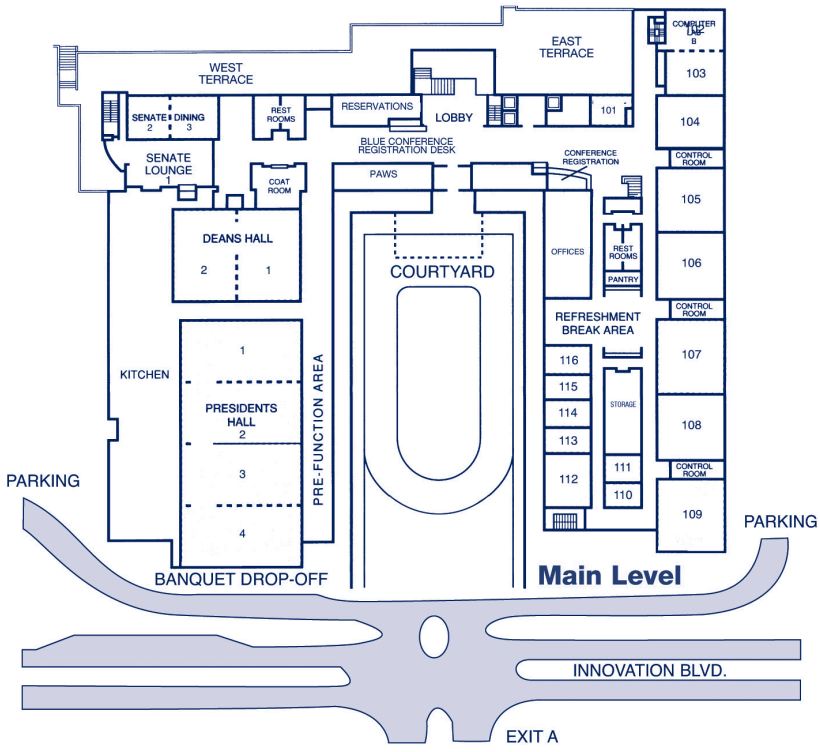

Main Level

2006 Electronics Materials Conference Grid

	Wednesday, June 28 AM	Wednesday, June 28 PM	Thursday, June 29 AM	Thursday, June 29 PM	Friday, June 30 AM	Friday, June 30 PM
Presidents Hall III & IV	EMC Plenary Lecture/Student Awards	**REGISTRATION** 3:00-5:00 PM, Tuesday, June 27, 2006, Penn Stater Conference Center Lobby 7:00 AM-5:00 PM, Wednesday, June 28, 2006, Penn Stater Conference Center Lobby 7:00 AM-4:00 PM, Thursday, June 29, 2006, Penn Stater Conference Center Lobby 7:00-10:00 AM, Friday, June 30, 2006, Penn Stater Conference Center Lobby			**EXHIBITS** Presidents Hall I & II - Main Level 9:20 AM-4:00 PM & 6:00-8:00 PM, Wednesday, June 28, 2006 10:00 AM-4:00 PM, Thursday, June 29, 2006	
106	Session C: Narrow Bandgap Semiconductors	Session I: Materials Integration: Wafer Bonding and Alternative Substrates	Session R: Lattice Engineered Epitaxy of III-V and IV Semiconductors	Session Y: Epitaxy for Devices	Session FF: Indium Nitride	
108		Session N: GaN Processing --- Session O: Semiconductors: Processing & Oxidation	Session V: Non-Destructive Testing and In-Situ Monitoring and Control	Session CC: Dilute Nitride Semiconductors	Session JJ: Spintronic Materials	
206		Session M: Oxide Thin Film Integration I	Session U: Oxide Thin Film Integration II	Session BB: Oxide Thin Film Integration III	Session II: Trapping and Charge Transport in Organic Transistors	
207	Session E: Nitride and Oxide Nanowires	Session K: Chemical and Biological Sensors I --- Session L: Contacts to Organic Thin Film Transistors	Session T: Materials and Processing for Organic Transistors	Session AA: Organic/Inorganic Hybrid Photovoltaics	Session HH: Molecular Electronics: Devices, Materials and Contacts	Session MM: Chemical and Biological Sensors II
208	Session D: Fun with Nanostructures	Session J: Nanotubes	Session S: SiC: Growth and Interface Studies	Session Z: SiC: Characterization	Session GG: Silicon and Germanium Nanowires	Session LL: Compound Semiconductor Nanowires
Deans Hall I			Session P: Device Aspects for ZnO	Session W: ZnO Growth	Session DD: P-Type Doping and Electroluminescence in ZnO	
Deans Hall II			Session Q: III-Nitride MOCVD Growth	Session X: MBE Growth of Group III-Nitrides	Session EE: Contacts to III-Nitrides	Session KK: GaN Characterization
Presidents Hall III	Session A: ZnO Nanomaterials	Session F: Directed Assembly of Nanostructures --- Session G: Quantum Dot Growth				
Presidents Hall IV	Session B: III-Nitride Optoelectronic Devices	Session H: III-Nitride Electronic Devices				